GOETHE UNIVERSITÄT FRANKFURT AM MAIN

Evolutionary transformations of the ethmoidal region in *Canis lupus familiaris* (Linné, 1758): effects of domestication on the turbinal skeleton in selected dog breeds

Dissertation

zur Erlangung des Doktorgrades

der Naturwissenschaften

vorgelegt beim Fachbereich 11 Geowissenschaften / Geographie

der Johann Wolfgang Goethe-Universität

in Frankfurt am Main

von

Franziska Wagner

Frankfurt am Main 2019

(D30)

vom Fachbereich 11 Geowissenschaften / Geographie der

Johann Wolfgang Goethe-Universität als Dissertation angenommen.

Dekan:	Prof. Dr. Georg Rümpker
Gutachter:	PD Dr. Irina Ruf
	Prof. Dr. Wolfgang Oschmann
Datum der Disputation:	05. Februar 2020

Meinen Eltern

Die Doktorarbeit wurde finanziert durch eine Projektförderung der

Deutschen Gesellschaft für Säugetierkunde, e. V.

Contents

“Our understanding of the nose,

its anatomy, function, and variation among species,

is still at an early stage”

(VAN VALKENBURGH *et al*. 2014, *Anat. Rec*. 297: 2076)

ABBREVIATIONS

ad, adult; **AE**, exterior surface area; **ALB**, area of length and breadth of snout; **AT**, turbinal surface area; **BC**, breadth of choanae; **BIF**, breadth of incisive foramina; **BLI/II**, basal length I and II; **BOR**, borzoi; **BRA**, brachycephalic; **bt**, bulla tympanica; **BZB**, bizygomatic breadth; **C**, upper canine; **CAT**, caudal aberrant turbinal(s); **CBL**, condylobasal length; **cc**, cavum cranii; **ch**, choanae; **cnp**, cupula nasi posterior; **dC**, upper deciduous canine; **dn**, ductus nasopharyngeus; **DOL**, dolichocephalic; **dP 2-4**, upper deciduous premolar 2 to 4; **ep**, epiturbinal (of ethmoturbinal I); **et**, ethmoturbinal; **EW**, Eurasian wolf (*Canis lupus lupus*); **f**, female; **fi**, foramen incisivum; **fet**, foramen ethmoidale; **fo**, fenestra olfactoria; **ft**, frontoturbinal; **GD**, Groenendael; **GLD**, Greenland dog; **GLS**, greatest length of skull; **GSD**, German shepherd; **HC**, height of choanae; **I1**, upper first incisor; **IAE**, index exterior surface area; **IAT**, index turbinal surface area; **IBL**, index length to breadth of skull; **IFB**, index facial length to length of braincase; **IOB**, interorbital breadth; **it**, interturbinal; **JAP**, Japanese chin (chin); **juv**, juvenile; **KCS**, King Charles spaniel (King spaniel); **KCSC**, Cavalier King Charles Spaniel (Cavalier); **la**, lamina anterior (of ethmoturbinal I); **lac**, lacrimal; **LBC**, length of braincase; **lc**, lamina cribrosa; **lh**, lamina horizontalis; **LIF**, length of incisive foramina; **lp**, lamina posterior (of ethmoturbinal I); **lpa**, limbus paracribrosus; **LPI/II**, length of palate I and II; **lpr**, limbus praecribrosus; **ls**, lamina semicircularis; **lt**, lamina terminalis; **ltp**, lamina transversalis posterior; **m**, male; **M1-2**, upper molar 1 and 2; **md**, mandible; **MES**, mesaticephalic; **[MfN]**, alternative labeling of mammal collection at Museum für Naturkunde Berlin, Germany; **MNHN**, Museum national d'Histoire naturelle Paris, France; **mt**, maxilloturbinal; **mx**, maxillary; **n**, nasal; **NA**, data/ information not available; **NB**, nasal width; **nc**, nasal cavity; **NHI/II**, nasal height I and II; **NLI/II**, nasal length I and II; **NMBE**, Naturhistorisches Museum der Burgergemeinde Bern, Switzerland; **nt**, nasoturbinal; **osph**, orbitosphenoid; **P1-4**, upper premolar 1 to 4; **pal**, palatine; **PEK**, pekingese; **pl**, palate; **pmx**, premaxillary; **pn**, paries nasi; **POC**, postorbital constriction; **prla**, processus anterior of lamina anterior (of ethmoturbinal I); **prlp**, processus anterior of lamina posterior (of ethmoturbinal I); **pru**, processus uncinatus; **RAT**, rostral aberrant turbinal(s); **RB**, rostral breadth; **rmx**, recessus maxillaris; **SAL**, saluki; **SDEN**, turbinal surface density; **sf**, sinus frontalis; **SH**, occipital height; **SL**, snout length; **SMF**, Senckenberg Forschungsinstitut und Naturmuseum Frankfurt, Germany; **smx**, sinus maxillaris; **sn**, septum nasi; **sprf**, septal process of frontal; **ssph**, sinus sphenoidalis; **TC**, turbinal complexity; **tn**, tectum nasi; **vo**, vomer; **WH**, whippet; **ZMB_MAM**, mammal collection of Museum für Naturkunde Berlin, Germany; **zy**, zygomatic

KURZFASSUNG

In vergangenen Jahrzehnten standen interne Schädelstrukturen der Säuger wie die Ethmoidalregion nur selten im Fokus morphologischer Studien aufgrund der Anwendung invasiver Methoden. Die Ontogenese der fetalen Nasenkapsel konnte hingegen einfacher anhand histologischen Materials untersucht werden. Seit Beginn des 21. Jahrhunderts erlauben moderne bildgebende Verfahren wie die hochauflösende Computertomographie (µCT) non-invasive Einblicke in den Säugerschädel und Visualisierungssoftware dient der virtuellen Rekonstruktion und morphometrischen Analyse des Gewebes. Am Riechmuschelskelett (Turbinalskelett) wurden bisher jedoch selten morphometrische Methoden angewendet. Außerdem wird generell entweder das Turbinalskelett als Einheit betrachtet, oder der respiratorische Bereich im Vergleich zum olfaktorischen. Die einzelnen Riechmuscheln (Turbinalien) fanden bisher in nur wenigen Studien Beachtung.

Die vorliegende Studie befasst sich mit der hochdiversen Gesichtsform des Haushundes (*Canis lupus familiaris*), die im Laufe seiner Domestikation entstanden ist. Künstliche Selektion aufgrund kontrollierter Zucht und unter menschlicher Obhut löste in prähistorischen Hunden graduell die natürliche Selektion ab. Die Folge ist eine beschleunigte Anhäufung schädlicher Mutationen an Genloci, die beispielsweise das Längenwachstum des Gesichts steuern. Gemäß veterinärmedizinischen Studien wachsen die Turbinalien kurzschnäuziger (brachyzephaler) Rassen auch nach einem verfrühten Wachstumsstopp ihrer äußeren Gesichtsknochen weiter. Diese Ergebnisse stützen sich allerdings auf CT- und MRT-Aufnahmen geringer Auflösung und ungenaue morphologische Deskriptionen. Bezüglich der Verlängerung des Gesichtsschädels dolichozephaler Rassen hatte sich bisher noch keine weitere Studie mit deren Turbinalienmorphologie befasst.

Die aktuelle Studie basiert auf vergleichender Morphologie, Morphometrie, Funktionsmorphologie und Ontogenese des Turbinalskeletts des Hundes. 32 mazerierte Schädel und vier histologische Schnittserien, die elf Rassen umfassen, decken verschiedene Schnauzenlängen (brachyzephal, mesozephal, dolichozephal; gemäß zwei Längenindices), funktionale Gruppen (Spürhund, Windhund, Begleithund/Toy), und Zuchtverläufe (antike Reinrassigkeit mit konstantem Körperbau, moderne Modezucht mit wandelndem äußerem Erscheinungsbild) ab. Die Nasenhöhle der ausgewählten Schädel wurde mittels µCT gescannt und das Turbinalskelett zu einem virtuellen 3D-Modell rekonstruiert. Der Vergleich der Rassen erfolgte in der Anzahl olfaktorischer Turbinalien, in der Morphologie aller Turbinalien und der Lamina semicircularis, sowie deren Morphometrie und Ontogenese. Basierend auf morphologischen und ontogenetischen Mustern wurde eine neue Terminologie der Interturbinalien etabliert. Die Morphometrie beinhaltet die Messung der relativen Oberflächengröße (index turbinal surface area, IAT) und die Berechnung der Oberflächendichte (surface density, SDEN) und der Turbi-

nalienkomplexität (turbinal complexity, TC). Zur Ermittlung des letztgenannten Parameters wurde eine neue morphometrische Anwendung entwickelt. Der ontogenetische Vergleich erfolgte unter Einbeziehung histologischer Schnittserien perinataler Hunde. Mazerierte Schädel dreier adulter Eurasischer Wölfe (*Canis lupus lupus*) dienten dem Außengruppenvergleich und repräsentierten als Urahn des Hundes den Grundplan, dem die Rassen gegenübergestellt wurden.

Die Ergebnisse bestätigen frühere Studien bezüglich der artspezifischen Anzahl der Fronto- und Ethmoturbinalien: der Eurasische Wolf und alle untersuchten postnatalen Hunde haben jeweils drei. Weiterhin konnten zwei Typen von Interturbinalien unterschieden werden, nämlich vier prominente Interturbinalien, die in fast jedem Individuum präsent sind und ein homologes Muster zeigen, und zusätzliche Interturbinalien mit variabler intraspezifischer Morphologie. Generell haben dolichozephale Rassen eine erhöhte Anzahl zusätzlicher Interturbinalien, sodass die Gesamtzahl olfaktorischer Turbinalien bis zu 16 im Barsoi beträgt, wohingegen viele brachyzephale Hunde aufgrund fehlender zusätzlicher Interturbinalien und eines prominenten Interturbinale lediglich neun olfaktorische Riechmuscheln besitzen. Die Betrachtung der Ontogenese konnte einen Zusammenhang des Wachstums der respiratorischen und olfaktorischen Turbinalien und der Lamina semicircularis mit dem postnatalen Wachstum des Gesichtsschädels nachweisen. Der postnatale Wachstumsstopp der Gesichtsregion brachyzephaler Rassen wirkt sich direkt auf die Ethmoidalregion aus: Die Turbinalien beider funktionalen Bereiche bilden weniger akzessorische Lamellen aus, was zu einer Reduktion der drei morphometrischen Parameter IAT, SDEN und TC führt. Der Anstieg der Werte all dieser drei Parameter mit zunehmender Verlängerung der Schnauze belegt beim Hund eine Korrelation beider Variablen im Maxilloturbinale, den olfaktorischen Turbinalien und der Lamina semicircularis. Mit Hilfe der Perinatalstadien konnten plesiomorphe Muster, die in allen Individuen vorhanden sind (z.B. Spaltung des Ethmoturbinale I in zwei Laminae, Entwicklung des Processus uncinatus), von weniger gefestigten morphologischen Merkmalen unterschieden werden, deren Reduktion vorwiegend im Zusammenhang mit Brachyzephalie erfolgt (z.B. Processus anterior der Lamina posterior des Ethmoturbinale I, caudaler Fortsatz des Frontoturbinale 1 und 2 im Frontalsinus aufgrund der Reduktion des letzteren). Der treibende Mechanismus hinter diesen und weiteren Variationen sind offensichtlich Mutationen an Genloci, die ontogenetische Prozesse steuern: der in anderen Studien bereits nachgewiesene postnatale Wachstumsstopp in den Dermalknochen des Gesichts brachyzephaler Rassen scheint in gleicher Weise die Ethmoidalregion zu beeinflussen. Die Ergebnisse der aktuellen Studie dienen als Grundlage für die Bewertung, inwiefern die Morphologie, Morphometrie und Ontogenese der knöchernen Turbinalien mit physiologischen, genetischen, neurobiologischen und phylogenetischen Mustern in Zusammenhang stehen. Des Weiteren ist der Vergleich der Wachstumsmuster des Hartgewebes zu jenen des Weichgewebes (d.h. des Nasenepithels) erforderlich.

ABSTRACT

During the last decades mammalian intracranial structures like the ethmoidal region have rarely been a focus of morphological studies, as they required invasive techniques. Contrary, the ontogeny of the fetal nasal capsule could easily be investigated based on histological material. Since the early 21st century modern imaging techniques like high-resolution computed tomography (µCT) reveal non-destructive insights into the mammalian skull. Furthermore, visualization software enables the virtual reconstruction of the tissues and additionally their morphometric analyses. However, the use of morphometric approaches on the nasal cavity is still scarce. Moreover, the turbinal skeleton is generally regarded as a unit, or the rostral respiratory part is compared to the caudal olfactory part; but the distinct olfactory turbinals have been considered only in a few studies.

The present study focuses on the highly diverse facial shape of the dog (*Canis lupus familiaris*) that evolved during domestication. Due to human-controlled breeding and care the natural selective pressure in prehistoric dogs has been replaced continually by artificial selection. As a consequence, harmful mutations on gene loci which e.g., control facial length growth got fixed within an extremely short time. According to veterinarian studies the turbinals of short snouted breeds continue their growth after the elongation of the facial bones has stopped prematurely. However, such investigations are based on low-resolution CT or MRT data and the morphological descriptions are vague. Referring to the elongation of the face in dolichocephalic breeds no former study has dealt with the detailed morphology of their turbinal skeleton so far.

The current study is based on comparative anatomical, morphometric, morphofunctional, and ontogenetic patterns of the dog's turbinal skeleton. The 32 macerated skulls and four histological serial sections represent eleven breeds which cover different snout lengths (brachycephalic, mesaticephalic, dolichocephalic; according to two length indices), functional groups (scent hound, sighthound, companion/toy), and breeding histories (ancient pure-breeding associated with an unchanged appearance, modern time fashion breeding). The nasal cavity of the selected skulls was µCT-scanned and virtual 3D models of the turbinal skeleton were reconstructed. The breeds have been compared with each other in their number of olfactory turbinals, in the morphology of all turbinals and the lamina semicircularis as well as in their morphometrics and ontogeny. Based on morphological and ontogenetic patterns a new terminology of the interturbinals was established. The morphometric data covers the measurement of the relative turbinal surface area (IAT) and the calculation of the surface density (SDEN) and the turbinal complexity (TC). For the latter parameter a new morphometric approach was developed. For the ontogenetic comparison histological serial sections of perinatal dog stages have been consulted. As the dog's ancestor macerated skulls of three adult Eurasian wolves (*Canis lupus*

lupus) function for outgroup comparison and represent the *grundplan* with which the breeds are compared.

The results support former studies concerning a species-specific number of the fronto- and ethmoturbinals: in the Eurasian wolf and all postnatal dogs under study three ethmoturbinals and three frontoturbinals are observed. Additionally, two types of interturbinals are distinguished, namely four prominent interturbinals which are present in nearly all individuals and show a homologous pattern, and a variable number of additional interturbinals which differ in their shape among the dogs. Generally, longer snouted breeds have more additional interturbinals, so the total number of olfactory turbinals is increased to a maximum of 16 in the borzoi, whereas several short snouted breeds have only nine olfactory turbinals due to the loss of additional interturbinals and one prominent interturbinal. Regarding ontogeny the growth of the respiratory and the olfactory turbinals and the lamina semicircularis is highly associated with the growth of the facial bones after birth. As the viscerocranium of brachycephalic breeds is subjected to a postnatal growth inhibition the ethmoidal region stops growing prematurely, too. The turbinals of both functional parts develop less accessory lamellae that results in the reduction of the three morphometric parameters IAT, SDEN, and TC. The increase of all these three parameters with increasing snout length proves a correlation between both variables in the maxilloturbinal, all olfactory turbinals, and the lamina semicircularis in the dog. With the help of the perinatal dog stages plesiomorphic patterns which are present in all adult specimens (e.g., separation of ethmoturbinal I into two laminae, the presence of the uncinate process) were distinguished from less established morphological traits which get preferably reduced in association with brachycephaly (e.g., the anterior process of the posterior lamina of ethmoturbinal I, the caudal processes of frontoturbinal 1 and 2 within the frontal sinus due to the latter's reduction). Obviously, the driving mechanism behind these and further variations are mutations on gene loci which control ontogenetic processes: the in other studies already described postnatal growth inhibition in the dermal bones of the midface of brachycephalic breeds seems to have a similar effect on the ethmoidal region. The results of the present study serve as basis for the evaluation how far the bony turbinals' morphology, morphometrics, and ontogeny might be associated with physiological, genetic, neurological, and phylogenetic patterns. Additionally, the growth patterns of the hard tissues need to be compared to those of the soft tissues (i.e. the nasal epithelium).

1 INTRODUCTION

The domestic dog (*Canis lupus familiaris*) is the first animal whose physical appearance is not driven by natural but by human-made selection (DRAKE & KLINGENBERG 2010, LARSON *et al.* 2012, MARCHANT *et al.* 2017). The breeding of dogs for over thousands of years for function and appearance led to at least over 400 extant breeds (SCHOENEBECK & OSTRANDER 2013, PARKER *et al.* 2017). The origin of some breeds and their relationships to each other are not easy to resolve. Phylogenetic analyses resulted in different trees (e.g., LARSON *et al.* 2012, PICKRELL & PRITCHARD 2012, FRANTZ *et al.* 2016), but only one recent study really regarded the segregation as far as the admixture across the breeds, their geographically subdivision into smaller populations over the world, and shared mutations (PARKER *et al.* 2017, **Fig. 1**).

Due to the short time scale during which new breeds evolve or existing breeds change, effects of the selective mechanisms on designated characters can be easily and comparatively fast estimated. Additionally, with its high morphological diversity the dog serves an extra-laboratory model organism for human medicine, as it helps to understand the linkage between genotype and phenotype e.g., brachycephaly and midface hypoplasia in humans (HAWORTH *et al.* 2001, DRAKE & KLINGENBERG 2010, SCHOENEBECK *et al.* 2012, MARCHANT *et al.* 2017).

1.1 Domestication in mammals

Domestication occurs in every animal that has been either caught in the wild or already born in captivity (O'REGAN & KITCHENER 2005). Under natural selection genes facilitating a phenotype's adaptation to its environment enhance its reproductive success and will become more frequent in the next generation (CAMPBELL & REECE 2009). Under human care animals are exposed to selective pressure different from the wild, as breeding is human-controlled. This artificial selection prefers individuals which habituate best to human presence and a captive environment (PRICE 1999). In both selection types mutations are an important factor which either enhance adaptation or impair it. In contrast to natural selection, artificial selection also favors mutations which may have a negative effect on an individual's fitness (FRANKHAM *et al.* 1986). Many captive species descend from a few individuals (founder effect) which may possess only a small amount of the genetic diversity of the wild population (FRANKHAM *et al.* 1986, O'REGAN & KITCHENER 2005, CAMPBELL & REECE 2009), so rare alleles will become lost in this bottleneck due to genetic drift (SOULÉ *et al.* 1986, CAMPBELL & REECE 2009). If these small populations are furthermore kept in reproductive isolation, a higher degree of inbreeding

will enhance the frequency of possible harmful recessive alleles (O'REGAN & KITCHENER 2005, CAMPBELL & REECE 2009). Gene flow between captive and wild individuals can help to minimize genetic drift and to preserve the genetic diversity among captive populations (SOULÉ *et al.* 1986).

During domestication the adaptation to human presence and a captive environment occurs on the genetic level, i.e. through genetic changes. One of the most significant changes is observed in ontogeny. Domestic animals like the dog have been selected for tameness which is associated with the behavioral persistence at a juvenile stage. This neoteny or pedomorphosis seems to have further effects on the organism's morphology and physiology on a large scale e.g., the endocrine system and fur pigmentation (PRICE 1999, TRUT 1999, CAGAN & BLASS 2016). The most common observed anatomical changes are a reduced body size and a shortening of the skull (PRICE 1999, TRUT 1999).

1.2 The origin of the dog

The dog descended from the Eurasian wolf (*Canis lupus lupus*, **Fig. 2a**) and was the first domesticated animal. The taxonomy of the dog is still debated: sometimes it is classified as a species of its own, *Canis familiaris*; but as it can still breed fertile offspring with the wolf like observed in the Czechoslovakian Wolfdog (a registered breed that resulted from a human-induced crossing between the German shepherd and the Carpathian wolf), it is mostly ranked as a subspecies, *Canis lupus familiaris* (CLUTTON-BROCK 1995, VILÀ & WAYNE 1999, WILSON & REEDER 2005, SMETANOVA *et al.* 2015). This study uses the latter taxonomic level.

In recent years many hypotheses about the origin of the dog have been established. Whereas several studies have proven an independent domestication in several regions across Asia and Europe (OVODOV *et al.* 2011, DRUZHKOVA *et al.* 2013), other authors hold the view of a single domestication event in East Asia (SAVOLAINEN *et al.* 2002), southern East Asia (WANG *et al.* 2016), or Europe (THALMANN *et al.* 2013). Beside the geography, also the determination of the beginning of domestication is difficult. The reduction of body size was one of the first changes that occurred, but in such a small extent that fossils of small wolves and early dogs are not easy to distinguish by use of morphological methods (BENECKE 1987). A canid skull found in the Goyet cave (Condroz, southern Belgium) that was dated 30,000 BC was assumed to be an ancient dog accounted for by linear measurements, as the snout of Paleolithic dogs is generally shorter and broader compared to wolves (GERMONPRÉ *et al.* 2009). In contrast, based on 3D morphometric analyses the respective skull was a wolf (DRAKE *et al.* 2015). Another skull of a canid from the Razboinichya Cave (Altai Mountains, southern Siberia) from 31,000 BC was studied by morphometric and genetic analyses, and both methods proved that it was an 'incipient' dog (OVODOV *et al.* 2011, DRUZHKOVA *et al.* 2013). Genetic studies got a large spreading

in reference to the dating of the domestication in general, because of unknown mutation rates, variable generation times, and possible bottleneck events (FREEDMAN *et al.* 2014, LINDBLAD-TOH *et al.* 2005). Therefore, the determined point in time at which wolf and dog segregated varies between 13,000 BC and up to 38,000 BC (SAVOLAINEN *et al.* 2002, FREEDMAN *et al.* 2014). In the following thousands of years the Paleolithic dog type whose size reduction in the teeth took much longer than in the skull remained nearly unchanged (GERMONPRÉ *et al.* 2009). During the Early Mesolithic the variability between primitive dogs and wolves became more obvious. Two fossil canid skulls from Star Carr (Yorkshire, GB) that date nearly 8,000 BC had a clear size difference which indicated that the smaller one was a dog. Hence, an advanced domestication over several generations was concluded (CLUTTON-BROCK & NOE-NYGAARD 1990).

Closely associated with the point in time are the reasons and the motives for domestication. The wolf is predestinated as its ecology is similar to that of humans: both species had a wide range, lived in groups with a strong hierarchy, and hunted large prey like mammoths (CLUTTON-BROCK 1984). In the Paleolithic, when men lived as hunter-gatherers on large megafauna, wolves could accompanied them on such walking-tours, ate their carcass, assisted as early hunting dogs, or helped in defending the prey from larger competitors (THALMANN *et al.* 2013, DRAKE *et al.* 2015). In the arctic Nordic dogs were initially not used to pull the sledge, but instead served as food reserve during food shortage and as pelt supplier (BREHM 1876, MOREY & AARIS-SØRENSEN 2002). If domestication took place in the Neolithic after the human settlement, wolves more likely lived as scavengers near such ancient villages (DRAKE *et al.* 2015). These pre-domesticated scavengers became domesticated to non-breed dogs which had a closer relationship with humans, and finally basic types of breeds evolved by human selection (WANG *et al.* 2016).

1.3 The forming of breeds

Some of the oldest illustrations of dogs show hunting scenes with canids which look similar to the today's Canaan dog. They are depicted on rock art in northwestern Saudi Arabia that date 7,000 BC or maybe even 8,000 BC. Most remarkably some individuals are wearing leashes proving a certain kind of control by humans, and the use of dogs for different hunting tactics (GUAGNIN *et al.* 2018). In northern Europe primitive dogs kept a 'basic' appearance with low intraspecific variation till the Iron Age (HARCOURT 1974). Contrary, Sumerian ornaments and Egyptian illustrations document the existence of greyhounds up to 5,000 BC (VOM HAGEN 1935). Beside this slender greyhound-like type a heavy mastiff-like type appeared in Egypt and Mesopotamia (YOUNG & BANNASCH 2006).

The first breeds have been listed in the *Boke of St Albans* (1486) e.g., greyhounds, mastiffs, spaniels, or terriers of which a grouping was tried in the following centuries. Members of the same breed were kept in packs within which they mated randomly. In the 18th century the sexes were separated and specifically paired for a systematical breeding to select preferred characters. This practice was also the beginning of the use of inbreeding for a faster and more pronounced fixation of favored traits. Competitions between dog owners initiated the first dog show in 1859, followed by the establishment of the Kennel Club. The first *Kennel Club Studbook* published in 1874 listed 40 different breeds whose number increased to over 400 today (PARKER *et al.* 2004, SAMPSON & BINNS 2006).

1.3.1 History of the investigated breeds

The grouping of the breeds which have been selected for this study follows the nomenclature of the Fédération Cynologique Internationale (FCI, *http://fci.be/en/Nomenclature/*). It distinguishes ten groups (Roman numeral) which are subdivided into a different number of sections (Arabic numeral).

I: Sheepdogs and cattledogs, (1) Sheepdogs

The primary function of sheepdogs was to chase robbers and wolves away, while men worked as sheepherders by themselves (BECKMANN 1895, ASH 1927a). After the extinction of the wolf on the European continent in the 17th century, in England it has already accomplished 100 years earlier, this flock guard dog changed its task to herding and keeping the flock away from the fields (BECKMANN 1895, VOM HAGEN 1935). To optimize the sheepdog for its new task, crosses between several breeds resulted in a completely working dog that can be declared as the "primitive way of breeding" (BECKMANN 1895: 101; VOM HAGEN 1935).

The German shepherd dog is a crossing between several German sheep-dog varieties (ASH 1927a) (**Fig. 2b**). At the beginning of its breeding it was just a working dog whose behavior and herding performance were preferred to appearance in form and color (BECKMANN 1895, ASH 1927a). To fix the breed's type only two or three breeding lines have been resorted. Inbreeding was avoided by fresh blood from working dogs and by the individuals' homogeneous distribution. Primarily, the selection was for courage rather than appearance, also in dog shows German shepherds were judged by obedience, sniffing performance, and braveness (ASH 1927a). Today, the breed is preferably used for police work not only because of its sensitive sense of smell, but also due to its outstanding ability to cooperate with humans (YANG *et al.* 2016).

The initial breed definition of the Belgian shepherd dog (Chien de Berger Belge) based on 117 individuals from different Belgian provinces. They were assembled in 1891, when a club for the pure-breeding of this dog was founded. Its overall characteristic is like in the German shepherd (BECKMANN 1895). The black and long-haired Groenendael is one of four varieties listed by the FCI (**Fig. 2c**).

V: Spitz and primitive types, (1) Nordic sledge dogs

In the company of humans the first dogs from Asia arrived in North America approximately 10,000 BC, but the Arctic region was uninhabited for another 7,500 years (BROWN *et al.* 2015). Skeletal remains of dogs in southwestern Greenland (Qajâ) whose morphology resembles the extant Greenland dog (**Fig. 2d**) date nearly 2,000 BC (MØHL 1986). But they occurred sporadically, and their use was for hunting and as a food reserve; until 1,000 years ago the Thule peoples arrived in the Eastern Arctic and assigned the canids a new task, namely pulling the sledge (MOREY & AARIS-SØRENSEN 2002). Together with the Canadian Eskimo dog the Greenland dog is often united to the 'Esquimaux dog' whose distribution ranges from Behring Strait to east Greenland (MARTIN 1845). Genetic studies proved an identical haplotype of these two Inuit sledge dog varieties from today with ancient dogs brought with the Thule peoples during their migration, and hence an ongoing pure breeding unaffected by the post-colonial arrival of non-native dogs (VAN ASCH *et al.* 2013, BROWN *et al.* 2013, 2015).

IX: Companion and toy dogs

Toy breeds are generally characterized as dwarfed forms and used as companion dogs. In contrast to working dogs the focus in these breeds was and still is on their physical appearance which changes continuously due to fashion trends. Mostly, the dwarf form is associated with a pug-like shortening of the face (BECKMANN 1895).

(7) English toy spaniels

The toy spaniel originated gradually from the cocker and got popular in the 16th century as so-called 'comforter' (BECKMANN 1895, VOM HAGEN 1935). The King Charles spaniel (short King spaniel) was in the ownership of Charles I. and Charles II. Old portraits of the latter, and other artworks (e.g., by Sir Edwin Henry Landseer 1845, **Fig. 2e**) show a longer snouted toy spaniel as favored in the 1830s. In the 1840s, however, the short snouted form was preferred through crossings with Chinese spaniels ('Tschins') (**Fig. 2f**). Yougatt (1845, in BECKMANN 1895) pointed out the impairment of this breeding as the spaniel's snout was too short and its eyes too big (BECKMANN 1895) (**Fig. 2g**). The return to the old type by the selection for longer snouted individuals resulted in a new breeding line established in

1928 as Cavalier King Charles spaniel (short Cavalier) (RUSBRIDGE & KNOWLER 2003, COILE 2015) (**Fig. 2h**). In the 1930s the extensive use of only six stud dogs caused a strong degree of inbreeding in the following decade (RUSBRIDGE & KNOWLER 2003). This practice was responsible for an accumulation of several welfare problems within the today's entire population (see SANDOE *et al.* 2017; RUSBRIDGE & KNOWLER 2004).

(8) Japanese chin and pekingese; (11) small molossian type dogs

As long ago as 600 BC the Chinese *Book of Odes* named the 'Shan' (long-mouthed dogs) and the 'Shejo' (short-mouthed dogs). The mention of the latter, also known as 'Lo-sze', even dates back up to 700 BC. The pekingese and the Japanese chin share the same origin, and together with the pug they are regarded as Eastern breeds, i.e. their roots are in China and Japan (ASH 1927b).

The mention of the pekingese in Japanese documents was definitely 679 AD (VOM HAGEN 1935); or probably 618 AD (ASH 1927a). The dogs were nearly exclusively kept in the holy city where they were protected and carefully bred by the imperial family with focus on a healthy and sound condition (ASH 1927b). In 1860 the first individuals arrived in England, but the European breeding just began in 1896 (**Fig. 2j, k**). The European population of the pekingese was kept in a health condition by periodical crossings with conspecifics brought from the East (VOM HAGEN 1935).

The Japanese chin (short chin) originated from small Chinese dogs which have been brought to Japan since 670 AD during the first commercial relationships between both countries (ASH 1927b). The breed got known on the island at about 800 AD, and like the pekingese it was carefully bred by its owners (ASH 1927b, VOM HAGEN 1935) (**Fig. 2m, n**).

The origin of the pug was long debated. But ASH's (1927b) hypothesis of Chinese roots is confirmed by a molecular study of PARKER *et al.* (2017). At the end of the 17th century the pug was brought to the Netherlands and its colonies and in 1689 to England (VOM HAGEN 1935). The stem sire which lived in 1864 had a longer nose than was common for this breed (BECKMANN 1895, **Fig. 2p**). In the following years the face was shortened by a long close breeding, and additionally by crossings with other breeds like the bulldog that furthermore resulted in a bigger head (BECKMANN 1895, ASH 1927b; **Fig. 2q**). As the health problems known as brachycephalic syndrome (see ch. 1.4.1 Brachycephalic syndrome (BCS) and its veterinary relevance: 14) accumulated, an initiative was founded in 2006 called 'Züchterkreis für den Retromops' (ZKR, *www.retromops.org*). The aim of its members is to return to the longer faced ancient pug type. In contrast to the Cavalier, the new 'retro pug' resulted from crossings between the pug and the Parson Russell terrier, followed by the outcrossing of the latter (ZRK, **Fig. 2r**). To date, the retro pug has been mentioned only once in scientific literature, namely

in a veterinarian study on a physical stress test in that it has been compared to the short snouted form. Of 42 short snouted pugs the half failed, whereas all seven retro pugs passed the test (MARTIN 2012).

X: Sighthounds

Dogs of the greyhound-like type appeared up to 5,000 BC in the Ancient Near East (VOM HAGEN 1935, see p. 8). NEHRING (1888) assumed that broad headed dogs were their ancestors whose heads became slenderer during domestication in the step habitat. Sighthounds evolved in open areas and were exclusively used for hunting fast animals like hares, gazelles, or antelopes by speed which requires vision as their essential sense (ASH 1927a, YOUNG & BANNASCH 2006, HOLE & WYLLIE 2007). The sighthound's reliance on vision only for chasing the prey is unique as the gray wolf and the non-sighthounds preferably orientate by scent (MARTIN 1845, ASH 1927a, HARRINGTON & ASA 2003, HALL *et al.* 2016). In the following centuries diverse sighthound breeds evolved in open treeless areas and plateaus of Africa, Asia, and Europe (BECKMANN 1894).

(1) Long-haired or fringed sighthounds

The place of origin of the sighthound is characterized by the Islam where dogs in general are regarded as being impure (BREHM 1876). However, its name *El hor* (the noble one) gives already an idea of the esteemed status of the saluki -or the sighthound in general- for the Arabs (**Fig. 2s**) (VOM HAGEN 1935). It is believed to be one of the oldest and genetically most purebred breeds (ASH 1927a, PARKER *et al.* 2004, LARSON *et al.* 2012). Illustrations which date around 4,000 BC prove the saluki's nearly unchanged appearance up to the present day (HOLE & WYLLIE 2007, **Fig. 2t**).

Told to be of a high age of several centuries, the Russian wolfhound (borzoi, **Fig. 2u**) was mentioned definitely in the 13th century (BECKMANN 1894, VOM HAGEN 1935). It is regarded as a cross-breeding between Asian or eastern greyhounds and wolf-like dogs or even the wolf itself (VOM HAGEN 1935). In its native country the symbol of Russian aristocracy became a victim of the revolution and got nearly extinct (VOM HAGEN 1935, COILE 2015).

(3) Short-haired sighthounds

The whippet (**Fig. 2w**) is a creation of the working class and used for rabbit hunting and dog racing. It can be regarded as a younger breed which resulted from a cross-breeding between the Italian greyhound and the terrier that started in 1860. In the following generations its physique manifested in favor of its greyhound ancestors resulting in a fast runner with a slender build typical for the sighthound group. The breed was recognized by the Kennel Club in 1892 (BECKMANN 1894, VOM HAGEN 1935).

1.4 Morphological variation in the dog's skull

The high morphological diversity of the dog is visible in its overall physical appearance including its skull. The different snout length types were first classified by ELLENBERGER & BAUM (1891). They defined skulls of breeds with a long and slender shape and a long face in relation to the braincase as dolichocephalic, and skulls of breeds with a short and broad shape and a short face in relation to the braincase as brachycephalic. For the mediate snout length type the term mesaticephalic became established (BREHM *et al.* 1985).

Based on the medium to long snouted wolf, shepherd dogs (e.g., collie) and sighthounds (e.g., borzoi) have a long and slender snout (YOUNG & BANNASCH 2006, SCHOENEBECK & OSTRANDER 2013). The breeding of the latter concentrated on visual skills (MARTIN 1845, ASH 1927a, HOLE & WYLLIE 2007). BREHM (1876: 592[1]) noted: "The greyhound hears and views excellent, but has in contrast a poor sense of smell, as the turbinal skeleton cannot extent sufficiently in the pointy snout, and therefore the nerve development of the respective sense can never reach the same development like in other dogs." This statement is supported by an ethological study on an odor discrimination task in that nine of ten English greyhounds failed because of lacking motivation during training phase (HALL *et al.* 2015). Another evidence for their better visual skills was provided by MCGREEVY *et al.* (2004) who observed a positive correlation between snout length and the number and distribution of retinal ganglion cells: like wolves long snouted dogs exhibit a large amount of these cells in a horizontally aligned visual streak which facilitates distance vision in open habitats. Simultaneous with greyhounds mastiffs evolved in ancient times as the first representatives of the other extreme, namely the brachycephalic head type (YOUNG & BANNASCH 2006). They are broad-headed and short snouted in favor of a strong jaw that facilitates a high bite force (MARTIN 1845). They performed duties as guardians, in combats, and for warfare; and were famous and regarded for their strength and courage (MARTIN 1845, YOUNG & BANNASCH 2006). Examples for dwarfed forms of brachycephalic dogs are the dogs of the ancient Far East like the pekingese and companions/toys like the toy spaniels (BECKMANN 1895, ASH 1927a).

A second classification refers to the dorso-basal curvature which describes the position of the palate, and hence the maxillary, to the basicranium. HOFER (1952) calls the plesiomorphic form in mammals orthocranial, in that the face forms a direct elongation of the braincase. However, in early ontogeny the cartilaginous rostrum in mammals and birds is buckled ventral to the braincase called klinorhynchic, and stretches until birth (HOFER & SPATZ 1963). In some mammal species the ventral buckling

[1] Original: „Der Windhund vernimmt und äugt vortrefflich, hat dagegen nur einen schwachen Geruchssinn, weil die Nasenmuscheln in der spitzen Schnauze sich nicht gehörig auszubreiten vermögen, und so die Nervenentwickelung des betreffenden Sinnes nie zu derselben Ausbildung gelangen kann wie bei anderen Hunden." (translation: F. Wagner).

(declination) of the palate persists in adults, furthermore a dorsal buckling (elevation) of the palate that is called airorhynchic occurs (HOFER 1952).

1.4.1 Brachycephalic syndrome (BCS) and its veterinary relevance

Initially short snouted dogs like the pug or the English and the French bulldog had a longer snout than today (see Abbildung 6 in STURZENEGGER 2011; Fig. 44G, L). Due to the upcoming domination of the cuteness factor, individuals with a short face became favored as their head shape corresponds to the scheme of childlike characteristics (STURZENEGGER 2011, O´NEIL *et al.* 2015). This breeding practice caused a still ongoing shortening of the snout of the three mentioned breeds, and other breeds like the King spaniel (see p. 10). Simultaneously, the popularity of these breeds increased (STURZENEGGER 2011, O´NEIL *et al.* 2015, LIU *et al.* 2017).

Whereas the longer headed ancient representatives had no to little health problems, the today's exaggerated creation of individuals with nearly no nose causes serious health problems including among others inspiratory stridor, heat intolerance, and asphyxia which are summarized as brachycephalic syndrome (BCS; KOCH *et al.* 2003, STURZENEGGER 2011). These symptoms result from stenotic nares and an elongated soft palate, but furthermore from a minimized nasal cavity that in turn affects directly the turbinals (OECHTERING *et al.* 2007). As a result of these health problems the nasal cavity of brachycephalic breeds has been studied by low-resolution CT scans which restrict detailed analyses of the turbinal morphology; and most veterinarians follow the problematic terminology of PAULLI (1900c; e.g., OECHTERING *et al.* 2007). These analyses are only descriptive and mostly imprecise; OECHTERING *et al.* (2007), for example, describe a pug's turbinals as thick with fewer ramifications in contrast to a German shepherd. Additionally, a displacement of the turbinals is reported, namely an expansion into the nasal meatus (rostral aberrant turbinals, RAT), and into the nasopharynx (caudal aberrant turbinals, CAT). Moreover, the viscerocranium in brachycephalic breeds is affected by a postnatal growth inhibition, whereas the turbinals are described to grow normally. Consequently, in adults the epithelia of the turbinals are compressed and in contact with each other leaving no space for the airstream (OECHTERING *et al.* 2016). However, an ethological study indicated that the olfactory sense in pugs might not be detracted compared to non-brachycephalic breeds (HALL *et al.* 2015).

1.5 The mammalian nose

The mammalian skull is of central interest for all kinds of comparative anatomical and morphofunctional studies. In adults studies on its internal structures like the turbinal skeleton within the nasal cavi-

ty usually required the destruction of the skull (e.g., ZUCKERKANDL 1887, SEYDEL 1891, PAULLI 1900a, b, c). Descriptions of the cranial morphology and ontogeny in perinatal stages based on histological serial sections are more widespread (e.g., GAUPP 1908, VOIT 1909, KUHN 1971). But using only fetal specimens restricts ontogenetic and taxonomic comparisons of the turbinal skeleton, as the ossification and differentiation of the primarily cartilaginous turbinals continue after birth to the adulthood (MAIER 1993a, RUF 2014). Nevertheless, a complete reconstruction of the turbinal ontogeny from fetal up to adult stages is still rare (e.g., ZELLER 1987, SCHRENK 1989, WAGNER & RUF 2019). Nearly since the beginning of the 21st century new techniques like high-resolution computed tomography (µCT) or magnetic resonance imaging (MRI) reveal new and especially nondestructive insights into the internal cranial structures not only of extant species, but recently also in fossils (e.g., RUF 2014, VAN VALKENBURGH *et al.* 2014b, RUF *et al.* 2014, WROE *et al.* 2018). Hence, for the first time adult specimens of various mammalian taxa can be compared systematically, and the ontogeny of the turbinal skeleton can be described up to adult stages (e.g., MAIER & RUF 2014, WAGNER & RUF 2019). In contrast, morphometric approaches on the turbinal skeleton are only sporadically used (SCHREIDER & RAABE 1981, CRAVEN *et al.* 2007, MARTINEZ *et al.* 2018, WAGNER & RUF 2019).

The second benefit of µCT data is the virtual reconstruction of selected structures as 3D models. Not only the structure's shape can be described, but furthermore measurements are possible, like surface area or volume. Nevertheless, this method is rarely distributed to date. Studies dealing with the turbinal surface area on 3D models in carnivores concentrate on the difference between the respiratory and the olfactory part, but not on the single turbinals (VAN VALKENBURGH *et al.* 2011, 2014a, GREEN *et al.* 2012). A detailed morphometric investigation of the turbinal skeleton in mammals including the surface area of the single turbinals, their surface density, and their turbinal complexity is still lacking. With the help of µCT data morphometric analyses of such characters are now possible (MARTINEZ *et al.* 2018, WAGNER & RUF 2019).

1.5.1 Morphofunctional aspects of the turbinal skeleton

The lamellae of the nasal cavity are defined in two ways: the term 'turbinal' or 'turbinate' refers just to the cartilaginous and bony structures, respectively, and the latter are preserved in the macerated skull. The turbinal stabilizes the epithelium by which it is covered, and together both build a 'concha' (OWEN 1854, MAIER 1993b).

The turbinal skeleton has a two-fold function: the maxilloturbinal and parts of the nasoturbinal are covered by respiratory mucosa for moistening, filtering, and warming the inspired air before it enters the lungs (SCHWALBE 1882, ZUCKERKANDL 1887, HILLENIUS 1992, RUF 2004). Therefore it is situat-

ed anteroventrally among the respiratory airflow (HILLENIUS 1992). The nasoturbinal serves as a bypass for conducting odorant-laden air to the fronto-, ethmo-, and interturbinals (CRAVEN *et al.* 2007). Those are covered by olfactory epithelium which contains olfactory receptor neurons as part of the sense of smell (SCHWALBE 1882, HILLENIUS 1992, SMITH *et al.* 2004). The direction of the airflow depends on the pressure with that the air is inhaled: with low pressure, the air passes the maxilloturbinal and leaves the nasal cavity through the nasopharynx without coming into contact with the olfactory epithelium; with higher pressure the airstream enters the dorso-posterior part and reaches the olfactory mucosa (DAWES 1952). During sniffing the stimulus on the olfactory receptors gets intensified (DAWES 1952, GREEN *et al.* 2012).

The basic shape of a turbinal is a single scroll; or a double scroll when two lamellae (End- oder Haupteinrollungen sensu SEYDEL 1891) are oppositely scrolled. Accessory lamellae can arise as secondary and tertiary lamellae (= epiturbinalia and epiturbinalia secundaria sensu REINBACH 1952b) with a similar scrolling that achieve the dendritic shape of the turbinal (SEYDEL 1891, PAULLI 1900a). PAULLI (1900c) describes the dog's frontoturbinals and interturbinals as double scroll, and its ethmoturbinals have secondary foldings. Regarding the maxilloturbinal the primarily shape for mammals is a double scroll (ZUCKERKANDL 1887, PAULLI 1900a). From that three further shapes derive, namely single scroll, folded (gewunden sensu WIEDEMANN 1799), and dendritic (ästig sensu WIEDEMANN 1799) (ZUCKERKANDL 1887). The latter two exhibit the largest possible surface area and the dendritic shape is a characteristic feature among canids (NEGUS 1954, SCHREIDER & RAABE 1981, VAN VALKENBURGH *et al.* 2004, CRAVEN *et al.* 2007).

1.5.2 Terminology of the turbinal skeleton

One of the first detailed descriptions of the turbinal skeleton in adult mammals originate from SCHWALBE (1882). He grouped the turbinals according to their task into the maxilloturbinal which has a respiratory function only, and the ethmoid lamellae (Ethmoidalmuscheln) which are covered by olfactory epithelium. Erroneously, SCHWALBE (1882) grouped the nasoturbinal with the latter as the most rostral ethmoid lamella despite its partly respiratory task, and he summarized it with the adjoining lamina semicircularis. Actually, the latter is not a turbinal *sensu strictu*, but represents an internal caudal growth of the nasal side wall medial to the pars intermedia (VOIT 1909, SMITH & ROSSIE 2008, MAIER & RUF 2014, RUF 2014). PAULLI (1900a, b, c) used a problematic terminology as well; indeed, he separated the nasoturbinal and the lamina semicircularis, but he grouped the latter with the endoturbinals which extend into the lumen, and contrasted them with the ectoturbinals which have a less medial extension. Anyhow, both terminologies more or less restrict the homologization of turbinals between different taxa and ontogenetic stages that is essential for evolutionary, systematic, and morpho-

functional questions. For example, 21 carnivoran species studied by PAULLI (1900c) that cover ten families of the two suborders clearly indicate that the carnivoran *grundplan* includes four endoturbinals (i.e., the lamina semicircularis and three ethmoturbinals); but the ectoturbinals vary from five up to ten as this turbinal type summarizes the frontoturbinals and the interturbinals, and the latter are highly variable in their number (MAIER & RUF 2014; see following paragraph).

Finally, histological studies on fetal stages established a third concept of nomenclature, adopted e.g., by VOIT (1909) or REINBACH (1952a, b): the therian fetal tripartite nasal capsule contains (1) in the pars anterior (pars maxillonasoturbinalis) the maxilloturbinal and dorsal to it the nasoturbinal; (2) in the pars posterior (pars ethmoturbinalis) a variable number of ethmoturbinals and interturbinals; (3) in the recessus lateralis (pars lateralis sensu REINBACH 1952a; also called pars intermedia), an also variable number of frontoturbinals and interturbinals. So far, previous studies on diverse mammalian taxa proved a species-specific number of ethmoturbinals and frontoturbinals, whereas the number of interturbinals varies between conspecifics, and even between left and right side within an individual (e.g., PAULLI 1900a, b, c; RUF 2014). In general, interturbinals interpose in later ontogeny, are smaller, and have a less medial extension (REINBACH 1952a, b). The pars intermedia is separated from the other two parts by the lamina semicircularis (VOIT 1909, SMITH & ROSSIE 2008).

The single turbinals of *Canis lupus familiaris* have been named by diverse authors e.g., ALLEN (1882) and ZUCKERKANDL (1887). As both authors use one of the problematic terminologies cited above as well, the recent study orients towards the descriptions of SCHLIEMANN (1966) who himself followed in his study on prenatal whippets the nomenclature of VOIT (1909). Despite the difficult terminology, the comprehensive work of PAULLI (1900c) is one of the most cited, so his terminology is contrasted with SCHLIEMANN (1966). SCHLIEMANN (1966) identified in the oldest prenatal whippet beside the maxilloturbinal, the nasoturbinal, and the lamina semicircularis (endoturbinal I sensu PAULLI 1900c), five frontoturbinals in the pars intermedia (ectoturbinal 1 to 5 sensu PAULLI 1900c), and two ethmoturbinals (endoturbinal II and III sensu PAULLI 1900c) with two interturbinals in the pars ethmoturbinalis. The rostral interturbinal (ectoturbinal 6 sensu PAULLI 1900c) is situated between ethmoturbinal I and II, the caudal interturbinal (endoturbinal IV sensu PAULLI 1900c) which is erroneously labeled as ethmoturbinal III in his fig. 24 (p. 528) lies caudal to ethmoturbinal II (SCHLIEMANN 1966).

1.5.3 Ontogeny of the nasal capsule

The neurocranium and the encompassed nasal capsule which shows a common *bauplan* in all therians belong to the endocranium (KUHN 1971, MAIER 1993a). It develops as a cartilaginous anlage (chondrocranium) through mesenchymal condensation (SMITH & ROSSIE 2008). The nasal capsule can be

regarded as a placeholder that stabilizes the internal structures until the dermal bones of the exocranium have developed externally through intramembranous ossification. Then, the nasal capsule gets replaced by them and partly resorbed; some cartilaginous parts ossify enchondrally, like the ethmoid, and others persist, like the nasal cartilages. Furthermore, appositional bones can arise directly from the replacement bones (KUHN 1971, MAIER 1993a,b).

Of central interest for the prospective development of the turbinals is the paries nasi or nasal side wall. It is the lateral portion of the nasal capsule; ventrally in contact with the parts of the nasal floor, dorsally fused to the nasal tectum (VOIT 1909). It is described as barrel-shaped, in a later stage as tube-shaped (SCHLIEMANN 1966); or as piriform, when the medial part of the paries that contains the pars intermedia can be externally determined by smaller bulge-like prominentiae (VOIT 1909). Internally the separation of the pars intermedia becomes more obvious. Rostrally the lamina semicircularis divides it from the pars maxillonasoturbinalis, and ethmoturbinal I gets the function as the caudal separation to the pars ethmoturbinalis (VOIT 1909, REINBACH 1952a). This generates the tripartite character of the nasal capsule (VOIT 1909, SMITH & ROSSIE 2008). The turbinals of the ethmoid bone arise as cartilaginous outgrowths on the nasal capsule and then ossify enchondrally (SEYDEL 1891, MAIER 1993a, SMITH & ROSSIE 2008). The direction in both developmental steps is from rostral to caudal, starting with ethmoturbinal I and frontoturbinal 1, respectively. The interturbinals interpose in later stages and are generally smaller (REINBACH 1952a, b, ZELLER 1983, RUF 2004, SMITH & ROSSIE 2008). Ethmoturbinals and frontoturbinals, and even larger interturbinals, can increase their surface area through so-called epiturbinals sensu REINBACH (1952b) (sekundäre Blätter sensu PAULLI 1900a), accessory lamellae which grow as non-cartilaginous appositional bone (Zuwachsknochen) (ZELLER 1989). Epiturbinals themselves again can have secondary epiturbinals (Epiturbinalia secundaria sensu REINBACH 1952b, tertiäre Blätter sensu PAULLI 1900a). The maxilloturbinal originates from the medial folding of the nasal side wall's ventral edge (VOIT 1909, SCHLIEMANN 1966). Its ossification starts on the inferior margin of the nasal side wall (SMITH & ROSSIE 2008). After the resorption of the nasal capsule the ethmoturbinals attach to the ossified laminae of the ethmoid bone, the lamina horizontalis and the lamina terminalis (ZUCKERKANDL 1887, SCHALLER 1992), the frontoturbinals to the frontal, the maxilloturbinal to the maxillary, and the nasoturbinal to the nasal (SEYDEL 1891, SMITH & ROSSIE 2008).

The turbinal skeleton of *Canis lupus familiaris* was studied by SCHLIEMANN (1966) on the basis of three different stages of prenatal whippets. The overall development of the nasal capsule in the dog does not vary from the mammal *grundplan* and agrees with the observations on e.g., the European rabbit (*Oryctolagus cuniculus*, VOIT 1909), muroid rodents (RUF 2004), dwarf lemurs and mouse lemurs (Cheirogaleidae, SMITH & ROSSIE 2008), or the aye-aye (*Daubentonia madagascariensis*, MAIER & RUF 2014).

Like all newborn mammals, dogs have a snub nose and the midface (viscerocranium) now starts to grow, together with the turbinals within the nasal cavity (MAIER 1993a, OECHTERING *et al.* 2016). The turbinals grow until they are just before coming into contact with each other still ensuring enough space between the epithelia for the airstream (OECHTERING *et al.* 2016).

1.5.4 Evolution of the turbinal skeleton

One of the upmost key achievements in mammal evolution is the change from the plesiomorphic ectothermic to an endothermic metabolism in association with homoiothermy (HILLENIUS 1992). The ability for an endothermic lifestyle is generally associated with the presence of respiratory-functioning turbinals, namely the maxilloturbinal in mammals, and analogous respiratory turbinals in birds (HILLENIUS 1994, CROMPTON *et al.* 2017). The turbinals in reptiles have olfactory function only, remain cartilaginous throughout their life, and never reach the complex form like in mammals, even in species which rely strongly on their olfactory sense (HILLENIUS 1994, HALLERMANN 1998, BERNSTEIN 1999). Nevertheless, operative respiratory epithelium is proven among some squamates, but its lower surface area and complexity compared to endotherms restrict an efficient water conservation (MURRISH & SCHMIDT-NIELSEN 1970, IWAHORI *et al.* 1987, HALLERMANN 1998).

The evidence of turbinals in the fossil record, no matter if respiratory or olfactory, is difficult: they are not only vulnerable to compressions resulting from their fragile morphology; they are supposed to have been primarily cartilaginous in non-mammaliaform cynodonts similar to extant reptiles and birds. Bony basal ridges on the lateral walls which serve as fixation for the turbinals are the only proof for their existence (HILLENIUS 1994, RUF *et al.* 2014, CROMPTON *et al.* 2017). The ossification of the entire turbinal skeleton in Mammaliaformes facilitated the increase of its surface area and complexity, especially for the maxilloturbinal (CROMPTON *et al.* 2017).

The pars maxillonasoturbinalis which houses the maxilloturbinal and the nasoturbinal, and the pars ethmoturbinalis which houses the ethmoturbinals are plesiomorphic characters among all three mammal subclasses (monotremes, marsupials, and placentals). The pars intermedia and its enclosed frontoturbinals, and the lamina semicircularis that separates the former from the pars maxillonasoturbinalis and from the pars ethmoturbinalis, are regarded as an autapomorphy of therians (GAUPP 1908, ZELLER 1989).

1.5.5 Neurobiology and genetics of the olfactory system

The gray wolf depends strongly on its olfactory sense for hunting and social communication (HALL *et al.* 2016). Dogs were and are still bred to cover different tasks of human needs. The breeds of the scent hound group serve for odor detection work (ISSEL-TARVER & RINE 1996, LESNIAK *et al.* 2008). During inspiration with high pressure the odorant-laden air is conducted by the nasoturbinal into the olfactory region which is covered by olfactory epithelium (DAWES 1952, CRAVEN *et al.* 2007). The olfactory epithelium houses olfactory sensory neurons whose dendrites project with their cilia into a mucus surface layer (PILPEL *et al.* 1998, SOKPOR *et al.* 2018). This mucosa is produced by Bowman's glands which are embedded in the olfactory epithelium, too (HAYDEN & TEELING 2014, SOKPOR *et al.* 2018). Odorant molecules are absorbed by the mucosa and then bind to the membrane of the cilia (HAYDEN & TEELING 2014). Each neuron activates only one olfactory receptor (OR) allele with an associated OR gene which in turn expresses a single type of OR protein in the cilia's membrane. This protein, however, binds a wide range of odorant molecules on its OR receptor subsequently inducing an action potential along the sensory axon to one specific glomerulus in the olfactory bulb (PILPEL *et al.* 1998). Mammals are roughly classified into two groups: canids are a member of the macrosmats which rely on a well-developed sense of smell; in contrast e.g., humans and most other primates as sight-orientated mammals are microsmats and have a weak sense of smell (ISSEL-TARVER & RINE 1996). The number of studies dealing with the OR gene in the dog (ISSEL-TARVER & RINE 1996, TACHER *et al.* 2005, ROBIN *et al.* 2009, QUIGNON *et al.* 2012) prove its popularity as an extra-laboratory model organism that results from the selection of breeds for different tasks mentioned above.

1.6 Aim of the study

Working dogs have been, and are still today, selected for fulfilling a given task (e.g., police dogs, SALGIRLI DEMIRBAS 2012). By early selection for work including hunting, guarding, scent working, and herding, and for companionship, long snouted racing dogs evolved (e.g., saluki), as far as guarding dogs (e.g., English mastiff, not in the study) which have shortened their face in favor of a higher bite force (YOUNG & BANNASCH 2006). These two ancestral groups can be regarded as being affected by artificial as well as natural selection. The saluki, for example, was bred by humans for hunting, but it also adapted naturally to an (semi-)arid habitat (ASH 1927a, YOUNG & BANNASCH 2006). But mainly since the mid-19th century humans are creating new breeds and changing existing breeds in fast motion never reachable through natural selection alone. The basic driving factors of this merely artificial selection are reproductive isolation and genetic drift caused by the use of a few popular sires (PRICE 1999, BJÖRNERFELDT *et al.* 2008, DRAKE & KLINGENBERG 2010). Due to this high inbreeding rate many breeds suffer from genetic diseases which are most common among the companion dogs which

are changing their appearance continuously due to fashion trends (BECKMANN 1895, SUTTER *et al.* 2004, YOUNG & BANNASCH 2006, ASHER *et al.* 2009, PACKER *et al.* 2015, SANDOE *et al.* 2017). The ongoing accumulation of harmful mutations combined with the morphological diversity in the dog's skull shape, makes this animal a popular model organism for genetic studies on phenotypic consequences of mutations in laboratory animals and predominantly in humans (FONDON & GARNER 2004, 2007, MARCHANT *et al.* 2017). Among the dog breeds several loci have been detected which cause the large scale variation in snout length and dorso-basal curvature (HAWORTH *et al.* 2001, SCHOENEBECK *et al.* 2012, SCHOENEBECK & OSTRANDER 2013). These studies focus on the outer morphology, whereas the dog's turbinal skeleton has mainly been of interest for general anatomic (PAULLI 1900c; macroscopic), ontogenetic (SCHLIEMANN 1966; histological) or functional (CRAVEN *et al.* 2007, 2010; physiological) studies which ignore breed differences. CT analyses of the dog's nasal cavity are nearly only restricted to the veterinarian field with the use of low-resolution data (BURK 1992a, OECHTERING *et al.* 2007). Furthermore, brachycephalic breeds like the pug have been of main interest because of the brachycephalic syndrome (HEIDENREICH *et al.* 2016, OECHTERING *et al.* 2016, see ch. 1.4.1 Brachycephalic syndrome (BCS) and its veterinary relevance: 14). As veterinarians are naturally studying living animals, the scans not only show the bony but also the soft tissue. Hence, when only referring to the 'conchae' as a whole in their descriptions, it is not evident if the two tissue types are affected in different ways by the shortening of the face or if they are associated with each other. Mesaticephalic breeds serve as representatives for the dog's basic morphological pattern (DE RYCKE *et al.* 2003: Belgian shepherd, variety not named), or for comparison to the brachycephalic type (OECHTERING *et al.* 2007: German shepherd). Dolichocephalic breeds have been CT scanned too, but only for cancerous purposes where veterinarians focused on tumor tissue; and they gave no detailed information about the involved breeds (BURK 1992b, FINCK *et al.* 2015).

By comparing the inner ear morphology (cochlea and semicircular canals) of modern dogs with dingoes, prehistoric dogs, and gray wolves no evidence for manifested domestication effects became obvious (SCHWEIZER *et al.* 2017). Facial length on the contrary, changed early in primitive dogs, although in a minimal extend at the beginning (BENECKE 1987, GERMONPRÉ *et al.* 2009, SCHOENEBECK & OSTRANDER 2013). In addition, changes in the morphology of the facial region influence directly the fetal nasal capsule and its comprised turbinals during ontogeny (MAIER 1993b). Surely, it would be justifiable to expect some variation in the turbinal morphology in these shorter snouted predomesticated dogs compared to wild gray wolves. The absent variations in the inner ear have been interpreted as being caused by highly constrained locomotion (semicircular canals) and hearing adaptations (cochlea) (SCHWEIZER *et al.* 2017). By contrast, the conspicuous changes in the head shape including the face have been promoted by the diverse functions for which already the predomesticated dogs have been used in prehistoric times.

This study is the first that analyzes the turbinal skeleton in the dog in detail by use of cross sections and virtual 3D models based on µCT data. That includes (1) the number of olfactory turbinals; (2) the turbinal morphology (i.e., its scrolling type as observed in the cross sections, its three-dimensional shape, and its position within the nasal cavity); (3) the turbinals' morphometry (i.e., surface area, surface density, and turbinal complexity). These three aspects are compared between the breeds and among the different age stages ranging from few weeks old puppies to adults. Additionally, the ontogeny of the ethmoidal region is regarded by use of morphological descriptions which are based on histological serial sections of perinatal stages. This project is also the first presenting not only morphological but also morphometric data including broad statistical analyses, further spreading over a wide range of facial shapes ranging from the long snouted and klinorhynchic Russian wolfhound to the short snouted and airorhynchic pekingese. To date, morphometric studies on the turbinal skeleton of dogs, or mammals in general, based on virtual 3D modeling are still rare and mostly restricted to measurements of surface area and volume (e.g., VAN VALKENBURGH *et al.* 2011, 2014a). On the other hand, the two derived parameters 'density' and 'complexity' are mainly determined on the basis of two-dimensional cross sections (SCHREIDER & RAABE 1981, VAN VALKENBURGH *et al.* 2004, CRAVEN *et al.* 2007). The recent use of both parameters on virtual 3D models is still scarce; beside the difficulty of a missing valid definition for the term 'complexity' (MARTINEZ *et al.* 2018, WAGNER & RUF 2019). Therefore, the dog serves as an excellent model for such morphological and morphometric analyses as it allows a detailed evaluation of the effects of mutational-like variations on intranasal structures. It also serves as a basis for further evolutionary, ontogenetic, physiological, neurobiological, and genetic studies.

In the present study the effects of domestication on the turbinal morphology in association with the creation of different breeds which cover various morphological types are investigated considering evolutionary, ontogenetic, comparative anatomical, and morphofunctional aspects. The key aspect is the time scale during which the dog has reached its outstanding intraspecific diversity. It ranges from ancient purebred dogs which remained unchanged in their appearance since thousands of generations to breeds which show a distinct transformation in their skull shape over just a few decades. The latter group contains the brachycephalic breeds, which represent an ideal model for evolutionary patterns on a short time scale.

Beside facial shape, the current study further considers the breeding history (i.e. ancient pure breeding and modern time fashion breeding) and the initial function (i.e. scent hound, sighthound, and companion/toy) as they are expected to more or less affect the ethmoidal region, too. Due to the high diversity of the dog regarding these three categories distinct variations in the morphofunctional, morphometric, and ontogenetic patterns of the turbinal skeleton among the dogs might become obvious. The following hypotheses are tested by morphological, morphometric, and ontogenetic analyses. They are based

on references about the turbinal skeleton in diverse mammalian taxa and on general information about the skull morphology, physiology, neurobiology, genetics, and ethology of dogs and gray wolves. As the dog's ancestor the Eurasian wolf functions as outgroup and represents the *grundplan* that is compared with the investigated dog specimens. In a second step, intraspecific differences between the three morphological groups and the breeds including their breeding history and initial function are highlighted. Among the given sample, the German shepherd, the Groenendael, and the Greenland dog are closest to the body size and head shape of the Eurasian wolf (BECKMANN 1895, MARTIN 1845).

1.7 Hypotheses

1) All dog breeds

The number of ethmoturbinals and frontoturbinals is phylogenetically determined and functionally constrained and consequentially species-specific. As the segregation between the Eurasian wolf and the dog has not sufficiently proceeded in time both still have the same number in these two turbinals as already described by PAULLI (1900c) and SCHLIEMANN (1966).

2) Dolichocephalic breeds I: scent hounds (German shepherd, Groenendael) and Greenland dog

(1) This head type corresponds most to its lupine ancestor in the general turbinal morphology, and more in the ancient and geographically isolated Greenland dog than in the later bred and more scent-specialized German shepherd and the Groenendael. Due to the unchanged shape of the fronto-, ethmo-, and interturbinals, the maxilloturbinal, the nasoturbinal, and the lamina semicircularis, the surface area, surface density, and turbinal complexity of the respective structures do also not vary from the Eurasian wolf.

(2) The position of the turbinals and the lamina semicircularis is equivalent to the Eurasian wolf.

(3) The maxilloturbinal in the Greenland dog as an arctic endurance runner has more accessory lamellae for a higher respiratory efficiency in a cold and arid climate. This higher amount of lamellae causes an increase in all three morphometric parameters.

3) Dolichocephalic breeds II: sighthounds (borzoi, saluki)

(1) The basic character of the sighthound group is an elongated face which offers at first view more space for the turbinals. But the simultaneous narrowing accommodates the length, and forces the olfactory turbinals and the lamina semicircularis to become simpler in their shape than in the broader snouted Eurasian wolf. Consequently, the turbinal surface area, the surface density, and the turbinal complexity have smaller values than in the dog's ancestor.

(2) The maxilloturbinal has more secondary and tertiary lamellae which provide a larger surface area, and a higher surface density and turbinal complexity than in the Eurasian wolf comparable to the Greenland dog.

(3) In order to increase the maxilloturbinal's respiratory efficiency it extends caudally and replaces ethmoturbinal I which in turn becomes rostrally shortened.

(4) As the sighthounds do not rely on olfactory performance, the frontoturbinals do not expand into the frontal sinus.

4) Brachycephalic breeds: toys (chin, pekingese, King spaniel, Cavalier, pug)

(1) Within the smaller nasal cavity the shape of the turbinals and the lamina semicircularis becomes simplified compared to the Eurasian wolf in breeds with long breeding history.

(2) The rapid nasal shortening in the modern pug prevented a proportionally adaptation in the internal nasal structures. The surface area of all turbinals, respiratory and olfactory, and of the lamina semicircularis is proportionally enlarged compared to its ancient conspecifics causing furthermore a higher surface density and turbinal complexity.

(3) The secondary elongation of the Cavalier's snout has the same effect as in the pug in reverse: its turbinal skeleton has not been able to grow simultaneously to the enlargement of the nasal cavity, so in this dog the turbinals and the lamina semicircularis are as simple in their shape as in the King spaniel. This results in a proportionally decrease in the turbinal surface area with a lower surface density and turbinal complexity.

(4) The frontal sinus is reduced or lost, and therefore the frontoturbinals have an alternative caudal ending than in the other breeds and the Eurasian wolf.

2 MATERIAL & METHODS

2.1 Specimens and linear measurements

In total, 35 macerated skulls of *Canis lupus* have been selected for the study: three adult Eurasian wolves (*Canis lupus lupus*) which represent the ancient type and serve for outgroup comparison, and 32 dogs (*Canis lupus familiaris*) of different ages covering ten breeds (**Table 1**). The pug is one example for the rapid change in snout length over a few decades driven by human selection and prewritten breed standards. Accordingly, the sample size of this breed was increased to cover individuals with changing degree in brachycephaly from the longer snouted ancient type to the shorter snouted modern type. Unfortunately, so far no collection is known having skulls of the retro pug. So, it was not possible to include it in the present study for a comparison with the ancient and the short snouted modern type. As sighthounds have not been of central interest for intranasal studies (see WAGNER & RUF 2019), the anatomy of their inner nose is almost unknown. Therefore, the borzoi was chosen as representative of the sighthound group and the number of specimens of this breed was raised as well.

Specimens labeled with [MfN] still have the inventory numbers of the former domestic animal collection (Haustiersammlung des Museum für Naturkunde Berlin). This alternative abbreviation was chosen to avoid ambiguities with specimens which have been assigned to the mammal collection of the Museum für Naturkunde Berlin (ZMB_MAM). The choice of the specimens is based on the intactness of the maxilloturbinal and the nasoturbinal visible through the nasal opening. Despite a large collection of dog skulls in some institutes much of the material was not suitable for the study due to unknown or mixed breed or destruction of the turbinal skeleton. The cranium of pug SMF 16284 was cut through the frontal sinus and the caudodorsal region of the pars intermedia. Nevertheless, this specimen was included in the study because of its long snout -even for the ancient type- and because the main focus in the pugs is more on their respiratory region. The number of investigated specimens per breed is quite heterogeneous due to limited availability of some breeds: the borzoi, for example, is represented in several collections with many individuals, whereas the Cavalier (n = 4) or the chin (n = 3) are rarely represented in the visited collections which limited the selection. Three qualified individuals of the Cavalier are of a high age (>11 years) and a kind of bone atrophy occurs on the dermal bones. Although this atrophy affects the thin turbinals as well, it is in a less extend and the µCT scans are still of suitable quality.

The age classes are divided just into juveniles (n = 4) with deciduous teeth and an erupting second dentition, and adults (n = 28) with a fully erupted second dentition (GEIGER *et al.* 2017). The juvenile German shepherd is six weeks old; the other three puppies are of unknown age. According to the den-

tition, pug MNHN 1881-47 is in the same developmental stage as the German shepherd: all deciduous teeth are erupted (dI1 to dP4), and the only tooth of the permanent dentition is P1 that is still within the alveolus on both sides. Although a general heterochrony in the dentition between the breeds needs to be taken into account, the tooth eruption is regarded to happen earlier in larger dogs, revealing an older age of the smaller pug than of the German shepherd (CORNEVIN & LESBRE 1894, in ELLENBERGER & BAUM 1906). In the borzoi both dI1 have been replaced by the two I1 which are nearly fully erupted. The remaining four incisors are erupted with their dental crone. The left dI2 is the only present deciduous incisive, but the alveoli of the right dI2 and both dI3 are still present. Probably, these three teeth got lost during the maceration process. dC and dP2 to dP4 are erupted on both sides, and P1 and M1 are visible through alveoli. Hence, the borzoi has to be older than the other two puppies. Its age is determined with the help of a table from ELLENBERGER & BAUM (1906: 206f). The data given about the eruption of the teeth of interest for the domestic dog is as follows: all deciduous teeth till six weeks of age, incisors between two to mostly five months, P1 and M1 between four to five months (ELLENBERGER & BAUM 1906: 206f). Thusly, the borzoi has to be clearly older than six weeks, but its maximum age is more difficult to determine, probably four months. The second juvenile pug (MNHN 2007-428) has a conspicuously malformed skull with a comparatively oversized mandible. Its general abnormal morphology prevents an age determination. It was just classified as a juvenile due to its skull size and the presence of deciduous teeth.

Only one specimen within the sample was difficult to classify: in pug NMBE 1051937 P1 and P2 are missing on the left and the right side, whereas all the other permanent teeth up to M2 are fully erupted, and dC and dP2 are still present on both sides. Additionally, this individual is in a heterogeneous stage regarding the fusion of its sutures (e.g., the frontonasal, interfrontal, or frontomaxillary sutures are not fused; whereas e.g., the coronal and the sagittal sutures are completely fused). SCHMIDT *et al.* (2013) determined the closure times of the spheno-occipital synchondrosis (i.e., the suture between the sphenoid and the basioccipital) in brachycephalic breeds including the pug and revealed an age of approximately twelve months. Specimen NMBE 1051937 has an open suture between these two bones. Permanent teeth erupt until six months of age in the dog, and later in smaller dogs (ELLENBERGER & BAUM 1906). Persistent deciduous teeth are frequently found in small dog breeds (HENNET 1997), also in this sample (modern pug NMBE 1052345, dP2 left; ancient pug [MfN] 1845, dC; King spaniel NMBE 1051948, dP2 right; chin ZMB_MAM 7436, dC; pekingese NMBE 1051965, dP2 left). In contrast to pug NMBE 1051937, all these listed individuals have fused sutures. Persistent deciduous teeth are not present in any of the larger dogs (borzoi, saluki, German shepherd, Groenendael, Greenland dog). The µCT scan shows that the two missing premolars in pug NMBE 1051937 have not developed. It is considered to be subadult and grouped with the adults.

The skulls of the juveniles and the adults were measured with two analog, high steel calipers (160mm/ 0.05mm; 550mm/0.1mm). 22 variables have been defined which are presented in **Table 2** and illustrated in **Fig. 3**. The measurements were taken three times and then averaged (**Table S1**, Supplementary material); characters measured on both sides (LIF, BIF; see **Table eS1**, electronic Supplementary material) are summarized. In senior individuals like borzoi NMBE 1051180 the nearly completely fusion of the sutures made some measurements difficult. But the well preserved turbinal skeleton of the respective specimen was still suitable for the morphological description; and the three repeats had a low standard deviation (SD) in all measurements (<1.0mm) except one character (CBL, mean = 228.4mm, SD = 1.415mm).

The skulls are grouped in two ways (**Table 1**):

1) Morphology: the morphological description is based on the breeds as grouped by the FCI and already used in the introduction. Furthermore, to ensure a better overview for comparison and discussion, breeds of similar head shape have been summarized into different snout length categories: the brachycephalic to mesaticephalic group includes the chin, the pekingese, and the King spaniel; and also the pug and the Cavalier. Though mesaticephalic in their head shape, the two ancient pugs [MfN] 2657 and ZMB_MAM 30980 are grouped with their shorter snouted modern conspecifics for simplification. The same method was used for the also medium snouted Cavalier for a less complicate comparison of evolutionary transformations with its short-faced ancestor, the King spaniel; the mesaticephalic to dolichocephalic Greenland dog was classified with the other larger dog specimens of borzoi, saluki, German shepherd, and Groenendael which represent the dolichocephalic group. The latter was further separated into the scent hounds/ Nordic sledge dogs (German shepherd, Groenendael, Greenland dog), and the sighthounds (borzoi, saluki).

2) Morphometry: in order to elucidate functional constraints the specimens were classified according to the three snout length types based on two indices by ELLENBERGER & BAUM (1891: 74): a) index between breadth to length of skull ($IBL=BZB*GLS^{-1}$); b) index between facial length to length of braincase ($IFB=NLII*LBC^{-1}$) (**Table 2**, **Fig. 4**).

Four histological series of different perinatal stages of a whippet in coronal section have been investigated to elucidate the homology of ambiguous turbinals (**Table 3**). Three serial sections represent prenatal stages which have been fixated after Stieve, embedded in celloidin and colored with AZAN (SCHLIEMANN 1966: 504). About the handling method of the fourth whippet, a neonate, no information is available. Maybe it is the specimen mentioned in SCHLIEMANN (1987), but the only information given there is that it is embedded in celloidin as well. The histological material was studied and photographed with the KEYENCE VHX-5000 digital microscope at the Centrum für Naturkunde,

Universität Hamburg, Germany. As the morphological description and comparison did not require all slices of the series, selected slices were photographed which are available in the electronic Supplementary material.

2.2 µCT scanning and virtual 3D modeling

The skulls have been scanned with three different µCT devices: GE phoenix x|ray v|tome|x s housed at the Institut für Geowissenschaften und Meteorologie at the Rheinische Friedrich-Wilhelms-Universität Bonn, Germany; GE phoenix|x-ray nanotom 180 s housed at the Institut für Geowissenschaften at the Goethe-Universität, Frankfurt am Main, Germany; and TomoScope HV500 (Werth Messtechnik GmbH) housed at Fraunhofer Anwendungszentrum CTMT in Deggendorf, Germany. The isotropic voxel size (resolution), current, voltage and timing of the scans are given in **Table 1**.

The turbinal skeleton of one Eurasian wolf, the three juveniles and 17 adult dog specimens has been reconstructed in AMIRA 5.4.0 and AVIZO 9.0.1 (Thermo Fisher Scientific FEI) as virtual 3D models with the manual segmentation tool (**Table 1**). If more than one specimen of a breed was scanned, the one with the most complete turbinal skeleton and the best contrast of the scan was chosen. In general, only one side -the most intact- has been reconstructed as this method is very time-consuming. Whereas larger skulls have a slight asymmetry, it is pronounced in nearly all brachycephalic individuals; therefore in selected specimens both sides have been edited. The 3D models of the first segmented individuals (juvenile German shepherd, one pekingese, two pugs, and one borzoi, right side) were reconstructed with surface smoothing. To avoid gaps, the lines were drawn thicker than the original lamellae of the turbinals actually are. The other 16 dogs (including the left side of the above mentioned borzoi) and the Eurasian wolf were segmented with thinner lines resembling the turbinals' original diameter, and without surface smoothing. Only these specimens were involved in the morphometric analyses, while the smoothed models still supported the descriptions of the turbinals' position within the nasal cavity. In AMIRA 5.4.0 and AVIZO 9.0.1 snapshots were taken of the reconstructed turbinal skeleton within the transparent nasal cavity in lateral, medial, and dorsal view to illustrate the position of all turbinals. Of the reconstructed specimens beside the illustrations in the text-figures (**Figs. 8–42**) further µCT cross sections and the virtual 3D model in dorsal view are available in the electronic supplementary material.

During the selection of the specimens the completeness of the turbinal skeleton could be only controlled based on the skull's intactness and by viewing through the nasal opening, as the most exposed rostral lamellae (primarily of the maxilloturbinal) are mostly affected by destructions. Logically, the more caudal structures deep within the nasal cavity could not be checked before the µCT scanning.

Consequently, in some specimens (e.g., the juvenile borzoi, Cavalier NMBE 1059207) either one or even both sides had caudally partly broken turbinals within the olfactory recess. Other issues were scan artefacts and residual tissue resulting from incomplete maceration and treatment with dermestids, respectively. For example, the entire turbinal skeleton of the saluki is covered by dry shred tissue; indeed its morphology could be described, but it was not suitable for the reconstruction of a 3D model. In the Eurasian wolf ZMB_MAM 93307 an artefact overlaps with the ventral lamina of the lamina semicircularis that prevented the reconstruction of the uncinate process. Hidden lead balls in borzoi NMBE 1051166 and Eurasian wolf ZMB_MAM 93308 eliminated the contrast in the scan. However, at least in the latter the contrast could be enhanced in VG StudioMAX 2.2 (Volume Graphics), but not in the borzoi.

2.3 Morphological analysis: terminology of the turbinal's shape

The comparative morphological description is based on the µCT cross sections as this is the only way for a detailed view into the turbinals' complex inner structure, whereas the position of the turbinals within the nasal cavity can be better described based on the reconstructed virtual 3D models. The perinatal and juvenile stages serve for the comparison to and validation of the terminology of the dog's turbinal skeleton presented by PAULLI (1900c) and SCHLIEMANN (1966). Then, the turbinals of the adult specimens have been homologized with the young stages (**Table 5**). Among the adults the Eurasian wolf serves as the representative of the *grundplan*, so its turbinal morphology is described first and each dog breed is compared to it.

For the description of the turbinals' morphology their shape patterns were defined as follows:

Single scroll sensu ZUCKERKANDL (1887) consists of a proximal 'base' (Basal-/ Ursprungslamelle sensu SEYDEL 1891) that is attached to a bony structure, and a distal 'scrolling' (Einrollungen sensu SEYDEL 1891).

Double scroll sensu ZUCKERKANDL (1887) with two oppositely scrolled lamellae. Thus, in this study a new mediate structure, the 'stem' is added between the base and the first distal separation of the lamellae, which are furthermore defined as 'lamellae of first degree'.

Multiple scrolls have further outgrowths, the 'lamellae of second degree' (sekundäre Blätter sensu PAULLI 1900A; epiturbinalia sensu REINBACH 1952B).

Dendritic (ästig sensu WIEDEMANN 1799) is the most complicated shape with a higher level of outgrowths (tertiäre Blätter sensu PAULLI 1900A; epiturbinalia secundaria sensu REINBACH 1952b). The term is basically used to define one shape type of the maxilloturbinal (e.g., in canids, WIEDEMANN 1799, VAN VALKENBURGH *et al.* 2004).

A special morphological character is observed in the lamina semicircularis and ethmoturbinal I which both consist of two laminae. Ethmoturbinal I has the anterior lamina (pars anterior) and the posterior lamina (pars posterior) (e.g., KUHN 1971, ZELLER 1983). The lamina semicircularis has a dorsal lamina and a ventral lamina (e.g., WAGNER & RUF 2019). Otherwise, the additional outgrowths in the multiple scrolled and dendritic shapes are just summarized as accessory lamellae for reasons of simplification. The transition between the four shape patterns is fluently, and a complex turbinal can change between them during its topography.

As from the not segmented specimens no morphometric data is at hand, the packing of their turbinals' lamellae is interpreted descriptively and depends on the observer's personal view. To segregate these estimations from the definitive measurements the turbinals are characterized as having either a 'complicated' shape or a 'simplified' and 'loose' shape, respectively. 'Complex' in turn refers only to the interpretation of the morphometric data.

2.4 Terminology of interturbinals

It is an appointed standard in scientific literature that ethmoturbinals and frontoturbinals are numbered according to their development from rostral to caudal. Regarding the interturbinals no such standard is given due to enormous intraspecific and individual (right vs. left side) variations in their number and position (PAULLI 1900a, b, c, RUF 2014). However, in two histological cross sections of their fetal aye-aye (*Daubentonia madagascariensis*) MAIER & RUF (2014: see their fig. 4) numbered the three interturbinals in the pars intermedia the same way like the frontoturbinals, starting with interturbinal 1 lateral to the lamina semicircularis.

The descriptions of the first scans in the current study suggest that two types of interturbinals occur in the dog's nasal cavity: some are larger, have a homologous morphology and topography among the dog specimens, and seem to be generally present in all individuals. Furthermore, smaller interturbinals with a less uniform morphology and topography are more heterogeneously distributed in both, intraspecifically and between left and right side within an individual. The large amount of interturbinals in *Canis lupus* especially within the pars intermedia (see table 4 in WAGNER & RUF 2019) required the establishment of a new terminology for the differentiation between these two interturbinal types to prevent ambiguity errors. In the first publication of some results from this study the larger interturbi-

nals are named ‘prominent interturbinals’, and the smaller interturbinals ‘additional interturbinals’ (WAGNER & RUF 2019). In the recent study, the three oldest perinatal whippet stages serve for the differentiation between the two interturbinal types and as basis for the description of the juveniles and the adult dogs and Eurasian wolves. Initially, in both types the interturbinals were distinguished only based on their position between the frontoturbinals and ethmoturbinals (WAGNER & RUF 2019). However, the evaluation of the large data presented here necessitates the adoption of a numbering system at least for the prominent interturbinals to avoid confusions when comparing these turbinals between the specimens. Consequently, similar to the frontoturbinals and ethmoturbinals in this study with the use of the perinatal whippets the prominent interturbinals are ontogenetically sorted by Greek letters (interturbinal α etc.). In contrast to the fronto- and ethmoturbinals, no differentiation is made between prominent interturbinals within the pars intermedia and the pars ethmoturbinalis, but in both recesses they are summarized. As the additional interturbinals are heterogeneously distributed within the pars intermedia and the pars ethmoturbinalis and not really homologous to each other between the specimens, they are simply counted.

2.5 Morphometric analyses

The morphological descriptions are supported by morphometric analyses of the shape by using Microsoft Excel 2010 and R 3.3.0 (R Core Team 2016). The surface area of the segmented structures was measured in AMIRA 5.4.0. In order to compare the surface area of the turbinals (AT, **Table eS2**, electronic Supplementary material) between the specimens, it was formed to an index (IAT, **Table 4**) with the area of the length and breadth of the snout (ALB=LPII*IOB, **Table 2**):

$$IAT=AT*ALB^{-1}$$

In a second step the surface density was computed by surrounding every single lamella by an exterior surface area. For this, after the segmentation the cross sections of the reconstructed turbinal skeleton have been opened in AMIRA 5.4.0. Slice per slice, the outer edges of every turbinal and the entire turbinal skeleton have been outlined by a straight line to get the shortest contour. A similar method was already used by SCHREIDER & RAABE (1981), who studied the nasal-pharyngeal airway in beagles based on silicone rubber. The authors measured the area and perimeter of the airway in single cross sections, but they did not bring them into an arithmetical correlation. This was realized by VAN VALKENBURGH *et al.* (2004) by the index between the volume of the bony turbinal and the nasal cavity. Nevertheless, similar to SCHREIDER & RAABE (1981) they worked with 2D cross sections as well. This study used 3D measurements through reconstructing the slices of the surrounded turbinals to a

second 3D model for the calculation of the exterior surface area (AE, **Table eS2**, electronic Supplementary material). For uniformity with AT, this value was standardized as well (**Table 4**):

$IAE=AE*ALB^{-1}$

The surface density (SDEN) defines the compression of a turbinal's lamellae and hence its surface area within the surrounding space. It is the index between IAT and IAE:

$SDEN=IAT*IAE^{-1}$

With the use of the ANOVA a correlation between IAT and IAE was tested in R 3.3.0 in the first segmented dogs and in the Eurasian wolf (WAGNER & RUF 2019). The segmentation of the shorter snouted breeds (e.g., the pekingese) validated this significance and furthermore its independence from snout length (three examples are illustrated in **Fig. 5**):

$IAT=a*IAE^{m}$, [*a* and *m* are given in the ANOVA]

This function was used to define a new morphometric approach named turbinal complexity (TC). It was presented in the first publication that emerged from this study (WAGNER & RUF 2019). The term 'complexity' has already been used by SCHREIDER & RAABE (1981), but just as a qualitative parameter and without an applicable definition. CRAVEN *et al.* (2007) used two parameters, the *airway perimeter* (*P*) and the *cross-sectional area* (A_C), to calculate the complexity as the slope between logA_C and log*P* called *fractal dimension of the airway perimeter* (*D*). They also worked with single cross sections like SCHREIDER & RAABE (1981), whereas in this study the slope of the power function on IAT is based on the 3D models. To calculate TC from IAT, the power function first has been inversed:

$IAE=(IAT*a^{-1})^{1/m}$

Then, the slope was calculated by the derivation of the function:

$IAE'=(am)^{-1}*(IAT*a^{-1})^{(1/m)-1}$

To get the values of the original function, the derived function has been inversed a second time:

$TC=am*(IAT*a^{-1})^{-(1/m)+1}$

TC describes the degree of the growth of IAT in correlation to IAE, i.e. in a steep curve IAT increases faster to IAE than in a more flat curve, resulting in a more complex structure of the lamellae. TC only serves for a comparison of the turbinals between specimens.

The body measurements (height at the withers and body mass) of the represented breeds were added to the linear measurements and morphometric data which have been collected in the current study. They

are adapted from the American Kennel Club (AKC, *https://www.akc.org/*) breed standards and presented in **Table S2** (Supplementary material). As the original data is given in inch and pound, it was converted into the metric system which is given in the table, too. Only the Greenland dog is missing as it is not a registered breed in the AKC; and the FCI lists its body mass, but not its size. In the larger breeds the sexes are separated in body size and/or in body mass by the Kennel Clubs, whereas in the toy breeds the sexes are summarized. In specimens with noted sex in the larger breeds the mean of the measurements for males or females was noted; in the smaller breeds the males were given a higher mass than the females; in specimens with unknown sex the mean of the breed was used. The skulls of the ancient pugs and of one borzoi date from the 19th century (**Table 1**). Because of the continuous change of the breed standards that involves body dimensions as well (e.g., STURZENEGGER 2011), data adopted from BECKMANN (1894, 1895) that closely approximates this time period was assigned to the respective specimens. The data used for the correlation test with the ANOVA in R 3.3.0 is listed in **Table S3** (Supplementary material).

In order to illustrate the specimens in the plots in Excel 2010 and R 3.3.0 they are lined up based on IFB which was preferred over IBL as it directly refers to the snout length. Not only the single specimens have been compared with each other in their definite snout length, but they furthermore have been summarized within the three snout length groups in IFB and IBL. To compare the three groups with each other, in R 3.3.0 the TukeyHSD test was used. This test serves for the indication of the significant difference between the short, medium, and long snouted dogs in IAT, SDEN, and TC on a 95% confidence interval. The ANOVA shows the standard error, the degrees of freedom, the adjusted r^2, the F-value, and the p-value which are all listed in the respective tables. The TukeyHSD test only gives the p-value.

3 RESULTS

3.1 Morphological description of the turbinal skeleton

3.1.1 Comparative morphology of early ontogenetic stages

Prenatal stages

A detailed ontogenetic description of the whole skull including the nasal capsule of the three prenatal whippets is presented by SCHLIEMANN (1966). The present description focuses on reinterpretations and so far undescribed ontogenetic patterns of the morphology and topography of the single turbinals. As in 'whippet A' no turbinals have developed yet (**Tables 5, 6**; **Fig. S1**, Supplementary material), only 'whippet B' and 'whippet C' are regarded (**Fig. 6**). Though housed in Prof. Schliemann's collection as well, the neonate stage is not known to have been morphologically described in a published article so far. Even if it seems to be obviously the specimen mentioned in SCHLIEMANN (1987, see ch. 2.1 Specimens and linear measurements: 27) this neonate whippet has not been described in similar detail like the three prenatal stages in SCHLIEMANN (1966).

'Whippet B' has seven olfactory turbinals, namely three frontoturbinals, three ethmoturbinals, and an interturbinal between ethmoturbinal I and II (**Tables 5, 6**; **Fig. 6**B–D). It is the first developing prominent interturbinal (WAGNER & RUF 2019) and hence labeled as interturbinal α. The number of olfactory turbinals has increased in 'whippet C' by two interturbinals. The interturbinal ventral to frontoturbinal 3 is the second prominent interturbinal, named interturbinal β (**Fig. 6**F), a further interturbinal between interturbinal α and ethmoturbinal II is regarded as additional interturbinal (**Tables 5**, **6; Fig. 6**G). An outgrowth dorsal on the stem of ethmoturbinal I foreshadowed by an epithelial bulge in 'whippet B' (**Fig. 6**B) is interpreted as an epiturbinal (**Fig. 6**F).

Neonate stage

The complete nasal capsule and its enclosed turbinals are still cartilaginous in the neonate whippet (**Fig. 7**). The number of the fronto- and ethmoturbinals and of the interturbinals within the pars ethmoturbinalis has not changed compared to 'whippet C'. Within the pars intermedia two additional ridges on the nasal side wall indicate the growth of two further prominent interturbinals (interturbinal γ between frontoturbinal 1 and 2, and interturbinal δ medial to frontoturbinal 1), so the total number of olfactory turbinals within the ethmoidal region is eleven (**Tables 5, 6**; **Fig. 7**C–G). The posterior lamina of ethmoturbinal I and ethmoturbinal II and III are single scrolled (**Fig. 7**G–M). All other turbinals

including the epiturbinal and the anterior lamina of ethmoturbinal I are increasing their complicate structure and develop their basic double scrolled shape giving them a fungiform appearance in cross section (**Fig. 7**F–L). The maxilloturbinal has further diversified and reminds of the folded stage sensu ZUCKERKANDL (1887) yet (**Fig. 7**A). Its ventral lamella is curling laterally and has nearly the same size as the dorsal lamella. The rostral tip of the nasoturbinal is separated from the nasal capsule and hence forms a process (**Fig. 7**A). Caudally, it is fused to the lamina semicircularis, but in some serial sections a thin suture is visible between them. Neither the lamina semicircularis nor the lamina horizontalis show any difference to the latest fetal stage (**Fig. 7**B–K). The posterior lamina of ethmoturbinal I is now expanding rostrally and forms the anterior process medial to the anterior process of the anterior lamina of ethmoturbinal I (**Fig. 7**E). The epiturbinal of ethmoturbinal I runs onto the lamina horizontalis rostrally to which it is fused (**Fig. 7**F–J). In contrast to the prenatal stages, interturbinal α and the stem of ethmoturbinal II are beginning to fuse together and to the lamina horizontalis rostrally. (**Fig. 7**F, G). Then, this interturbinal runs caudodorsally along the lamina horizontalis onto the stem of ethmoturbinal I and fuses to it as indicated in 'whippet B' and 'whippet C' (**Fig. 7**H–K). The second interturbinal of the pars ethmoturbinalis starts between the lamina horizontalis and ethmoturbinal II and runs onto the lamina horizontalis caudally (**Fig. 7**H–L). Interturbinal β merges into the nasal side wall, ethmoturbinal II and III end on the transition between the paries and the lamina cribrosa; ethmoturbinal I, the three frontoturbinals, and interturbinal γ and δ fuse to the cartilaginous lamina cribrosa (**Fig. 7**G–M).

Juvenile Stage

In the three healthy juvenile dogs the caudal part of the nasal septum has become ossified as far as the lamina terminalis that fuses caudally together with the medially positioned osseous vomer (**Figs. 8–10**). The cartilaginous bars which enclosed the fila olfactoria in the neonate whippet have completely ossified as well and united to the lamina cribrosa. Some of the now ossified turbinals are attached with their base to the dermal bones; the maxilloturbinal to the maxillary, the nasoturbinal to the nasal, and the turbinals of the pars intermedia to the frontal. The turbinals of the pars ethmoturbinalis are connected with the ossified lamina horizontalis rostrally; caudal to it they shift to the palatine and to the orbitosphenoid. The three juveniles are comparable to the three oldest perinatal whippet stages in the number of frontoturbinals and ethmoturbinals. The younger puppies (German shepherd, pug) have a less number of interturbinals in both, the pars intermedia and the pars ethmoturbinalis compared to the neonate whippet (**Table 6**, see pp. 37, 39). The turbinal number within the olfactory recess in these two juveniles resembles 'whippet B'. However, within the pars intermedia the borzoi has a higher amount of additional interturbinals compared to the whippets and the other two juveniles, namely one

to two. Its number of interturbinals within the pars ethmoturbinalis is identical to the neonate whippet, so in sum it has twelve to thirteen olfactory turbinals (**Table 6**).

The turbinals of the borzoi are larger and their lamellae are denser than in the two younger dogs in the µCT cross sections reflecting its older age. That is also visible in the virtual 3D models in which the elongated snout of the dolichocephalic borzoi is in considerable contrast to the still more snub-nosed German shepherd and especially to the pug. The borzoi's turbinals are elongated and frontoturbinal 1 and 2 extend caudally into the frontal sinus resulting, together with the also caudally extending ethmoturbinal II and III, in a concave caudal shape of its turbinal skeleton in medial view (**Fig. 10**B, C). The two mentioned ethmoturbinals show the same posterior position in the German shepherd and in the pug. Frontoturbinal 1 and 2, however, show a distinct pattern due to the incomplete development of the frontal sinus in the two younger puppies (see p. 37). The two frontoturbinals are not extending caudally in the same degree like in the borzoi (**Figs. 8, 9**, in both B, C). The in medial view concave shaped nasoturbinal in the juvenile pug is associated with a slightly dorsally pointing tip of its nasal bone. Its snout is already showing the airorhynchic characteristic of brachycephalic breeds that affects the anterior process of the anterior lamina of ethmoturbinal I and the position of the maxilloturbinal which are both more dorsally situated than in the borzoi and in the German shepherd.

All juvenile dogs have a well-developed **maxilloturbinal** showing the two opposing scrolled lamellae of first degree in cross section (**Figs. 8–10**, in all D, E). The ventral lamella has a dendritic shape and is laterally scrolled as foreshadowed by the neonate whippet. In the German shepherd and the borzoi the dorsal lamella is dendritic, too. In the pug the dorsal lamella is double scrolled and the maxilloturbinal leaves a larger space to the palate and to the nasal septum compared to the other two juveniles. In the young borzoi the maxilloturbinal is laterally compressed due to the development of the canines of the second dentition. The **nasoturbinal** is straight to medioventrally curved in cross section and its suture to the lamina semicircularis has completely disappeared in all three individuals resulting in a continuous bony plate. The nasoturbinal is a conspicuously thick lamella on the pug's right side, but on the left side it is as thin as in the other individuals (**Fig. 9**D).

The **lamina semicircularis** has two laminae and the straight (pug) to single scrolled (German shepherd, borzoi) ventral lamina ends as uncinate process within the maxillary sinus (**Figs. 8**C, G**; 9**C**;** **10**C, H). The dorsal lamina is double scrolled in the borzoi (**Fig. 10**G), in the other two puppies it is a simpler single scroll (**Fig. 8**G). In all three specimens the lamina semicircularis fuses to the lamina cribrosa caudally. The borzoi has a small and straight accessory lamella dorsally on the stem of the lamina semicircularis to which it fuses caudally. In anterior direction it runs onto the frontal and merges into it.

In all three juveniles the **three frontoturbinals** show the basic scrolling type and resemble each other in their general topography. Frontoturbinal 1 is rostrally attached to the maxillary in the borzoi and the German shepherd (**Figs. 8**G; **10**G). Frontoturbinal 2 and 3, and in the pug furthermore frontoturbinal 1 (**Fig. 9**F), are additionally continuous with the lamina semicircularis in all three individuals (**Figs. 8**H; **9**G; **10**H). The frontoturbinals are primary double scrolls, but variations occur in their rostral part. In the borzoi frontoturbinal 1 is the simplest turbinal as it forms a double scroll on its rostral end, whereas the other two frontoturbinals tend to be multiple scrolls. In the German shepherd frontoturbinal 1 and 2 are dendritic anteriorly, and frontoturbinal 3 is less complicated with a straight tip. The pug has the simplest frontoturbinals in total, with a straight frontoturbinal 1 and 2 rostrally, and two separated single scrolls in frontoturbinal 3 which merge caudally and form a double scroll. In all specimens the frontoturbinals run onto the frontal caudally, but they show different endings. The borzoi has a well-developed frontal sinus in which frontoturbinal 1 and 2 end as processes in separate chambers, while frontoturbinal 3 fuses to the lamina cribrosa (**Fig. 10**N–P). In the two younger dogs the frontal sinus is nascent, and its chambers are slightly indicated yet (**Figs. 8**M, N; **9**K, L). Additionally, in the German shepherd the lamina cribrosa seems to be mainly cartilaginous, as only fragments persist after the maceration process (**Fig. 8**L, M). In the pug the ossification of the lamina cribrosa is more advanced as its net-like structure is more pronounced in the cross sections of the µCT scans (**Fig. 9**L). However, in this dog it is not immediately obvious if frontoturbinal 1 and 2 are merging with a septum of the developing frontal sinus, or into the lamina cribrosa. Maybe both younger specimens show an intermediate pattern. The caudal end of frontoturbinal 3 in the German shepherd and the pug is similar to that in the borzoi.

Within the pars intermedia the borzoi has all three **prominent interturbinals**, whereas the German shepherd is lacking interturbinal δ, and in the pug interturbinal γ is absent. Both younger puppies have no additional interturbinals, in the borzoi an additional interturbinal is present ventral to interturbinal β, and on the left side between frontoturbinal 2 and 3 (**Table 5**). **Interturbinal δ** is well-developed in the juvenile borzoi in which it is rostrally fixed to the nasal-frontal suture (**Fig. 10**B, H–L). It forms a single scroll and runs caudomedially onto the septal process of the frontal to which it fuses rostral to the lamina cribrosa. In the pug a short, small, and low ridge on the nasal can be regarded as an early anlage of interturbinal δ. **Interturbinal γ** is attached to the frontal to which it fuses rostrally. It is straight in the borzoi, but a small single scroll in the German shepherd. Interturbinal γ stretches caudally into the lumen to form a septum of the frontal sinus in the borzoi (**Fig. 10**L–P). Due to the not yet developed sinus, in the German shepherd interturbinal γ ends posteriorly on the frontal. The anterior end of **interturbinal β** merges into the lamina horizontalis in the German shepherd, in the borzoi it fuses to frontoturbinal 3 on the right side and to ethmoturbinal I on the left side. In the pug interturbinal β merges rostrally into the fusion between ethmoturbinal I and the lamina horizontalis and is in its most anterior part connected with frontoturbinal 3. In the two younger dogs interturbinal β

is straight and complicates to a double scroll posteriorly that shifts to the frontal and ends on the lamina cribrosa (**Figs. 8**J–M; **9**H–L). On the right side in the borzoi this prominent interturbinal is a double scroll and runs onto the frontal, too. Caudoventral to interturbinal β a single scrolled additional interturbinal fuses to the lamina horizontalis anteriorly. Caudal to the lamina horizontalis it runs onto the frontal and touches the stem of interturbinal β for a short distance. These two mentioned interturbinals fuse to the lamina cribrosa whereby the smaller ventral additional interturbinal approaches the stem of ethmoturbinal I. On the borzoi's left side one multiple scrolled lamella that ends on the lamina horizontalis rostrally separates caudally into a dorsal single scrolled and a ventral double scrolled lamella. The dorsal one shifts onto the frontal. The ventral lamella is fixed to the suture between the frontal and the lamina horizontalis before running onto the frontal caudal to the lamina horizontalis. Both lamellae end on the lamina cribrosa. In comparison to the right side, the dorsal lamella is homologous to interturbinal β. The ventral lamella is similar to the additional interturbinal on the borzoi's right side, as it approaches the stem of ethmoturbinal I caudally, too (**Fig. 10**L). The additional interturbinal between frontoturbinal 2 and 3 on the borzoi's left side fuses rostrally to the stem of frontoturbinal 2, forms a straight shape, and runs onto the frontal until it merges into the lamina cribrosa.

Within the **pars ethmoturbinalis** the variations between the turbinals are as minor as within the pars intermedia. The anterior lamina and the posterior lamina of ethmoturbinal I form anterior processes (**Figs. 8**B, G; **9**B, F; **10**B, F). The anterior process of the anterior lamina of ethmoturbinal I overlays the caudodorsal end of the maxilloturbinal (**Figs. 8–10**; in all B). Both anterior processes of ethmoturbinal I are dendritic in the borzoi, slightly dendritic in the pug, and bulbous-like in the German shepherd. The two laminae fuse together to one stem on the lamina horizontalis where the anterior lamina of ethmoturbinal I forms a double scroll in all three dogs, and the posterior lamina of ethmoturbinal I a single scroll (German shepherd, **Fig. 8**J), double scroll (borzoi, **Fig. 10**H, J), and multiple scrolls (pug, **Fig. 9**H). An epiturbinal which is homologous to the one present at the same position in 'whippet C' and the neonate, namely on the dorsal side of the stem of ethmoturbinal I, complicates to a double scroll in the borzoi (**Fig. 10**J–L) and the German shepherd (**Fig. 8**J–L), whereas in the pug it remains a simpler single scroll (**Fig. 9**J–L). The borzoi has a second epiturbinal-like lamella that is continuous rostrally with the lamina horizontalis and runs as a double scroll proximal to the epiturbinal onto the stem of ethmoturbinal I (**Fig. 10**L). This second lamella merges into the stem posteriorly. In all three puppies ethmoturbinal I fuses to the lamina cribrosa caudally. The rostral process of ethmoturbinal II medial to the two anterior processes of ethmoturbinal I has the same shape as the latter, namely dendritic (borzoi, **Fig. 10**G) or bulbous-like and pneumatic (German shepherd). In the pug this turbinal forms a simpler straight process. Rostrally, ethmoturbinal II attaches to ethmoturbinal I and then runs onto the lamina horizontalis forming multiple scrolls, and caudal to the lamina horizontalis onto the palatine in all three juveniles. In the German shepherd it ends here on the lamina cribrosa. In the other two juveniles ethmoturbinal II projects more caudally onto the orbitosphenoid and then ends

on the lamina cribrosa (borzoi) or as a process within the sphenoid sinus (pug). Ethmoturbinal III emerges rostrally as a straight lamella from the lamina horizontalis; in the pug it is additionally continuous with ethmoturbinal II (right side), or with the lamina terminalis (left side). Ethmoturbinal III forms a single scroll in the German shepherd, but it complicates to a double scroll in the two other puppies. Caudal to the lamina horizontalis it shifts to the palatine, in the borzoi and in the pug furthermore to the orbitosphenoid, and ends as a process within the sphenoid sinus in all juveniles.

Like in the perinatal stages interturbinals within the pars ethmoturbinalis are present between ethmoturbinal I and II. The stem of **interturbinal α** emerges rostrally from ethmoturbinal II in the pug (**Fig. 9**H). The borzoi has a single scrolled (**Fig. 10**G) and the German shepherd a bulbous-like rostral process. In all three specimens interturbinal α becomes a double scroll during its course from ethmoturbinal II along the lamina horizontalis to the stem of ethmoturbinal I, and fuses to the lamina cribrosa caudally (e.g., borzoi, **Fig. 10**H–N). In the borzoi the second interturbinal ventral to interturbinal α present on both sides is fused to the stem of ethmoturbinal II rostrally. It forms a double scroll, runs dorsal to the lamina horizontalis onto the frontal and ends on the lamina cribrosa.

The skull of the juvenile pug MNHN 2007-428 (**Fig. 11**) is conspicuously malformed with a comparatively oversized mandible causing an underbite, and a narrow interorbital breadth. Most interestingly for this study its rostrum is extremely shortened with a flattened front (**Fig. 11**A–C). No external nasal opening is visible. The µCT scan reveals further intracranial abnormalities. Within the dermal bones smaller cavities occur which show no external openings, neither for a nasal opening as already observed on the outer skull. The incisive foramen is unpaired and covered by residual tissue (**Fig. 11**D, E). It continues caudally into the nasopharyngeal duct dorsal to the palate (**Fig. 11**F–K). Both the incisive foramen and the nasopharyngeal duct have no connection to the rudimentary nasal cavity that houses a reduced nasal septum (**Fig. 11**G). Caudally, the lamina cribrosa is absent, and the completely enclosed nasal cavity is separated from the brain cavity by the ossified cupula nasi posterior (**Fig. 11**H–L). The nasopharyngeal duct opens into the choanae caudally (**Fig. 11**L). The morphology of the cranial cavity gives evidence for a lost connection between the rudimentary nasal cavity and the olfactory bulb or even a complete absence of the latter at all (**Fig. 11**L, M).

3.1.2 Comparative morphology of adult stages

In the following subchapters the morphology of the turbinal skeleton is described for all breeds involved in this study. First, the Eurasian wolf (*Canis lupus lupus*) is described as it represents the dog's ancestor. Afterwards, the single breeds are compared to this plesiomorphic morphotype according to

the listing by the FCI already used in the introduction. Finally, a comparison between the adult dogs follows with consideration on the breeds and the snout length types.

Eurasian wolf (Canis lupus lupus)

The maxilloturbinal and the nasoturbinal are the only structures lying within the respiratory pathway, whereas the olfactory turbinals are located caudodorsal to it, and dorsal to the lamina terminalis (**Fig. 13**B, C, G–J). The three investigated Eurasian wolves have three frontoturbinals, three ethmoturbinals, and two interturbinals within the pars ethmoturbinalis (**Figs. 12–14**). The number of interturbinals within the pars intermedia ranges from three (ZMB_MAM 93308, right side) to seven (ZMB_MAM 815, left side), resulting in a total number of eleven up to fifteen olfactory turbinals (**Table 6**). Caudally the turbinal skeleton has a concave shape in medial and lateral view caused by the caudal extension of frontoturbinal 1 and 2 into the frontal sinus as far as of ethmoturbinal III into the sphenoid sinus, so that all these three turbinals extent far beyond the lamina cribrosa (**Fig. 12**J).

In all three specimens of the Eurasian wolf the **maxilloturbinal** shows a double scrolled type in cross section (**Fig. 13**D). The laterally scrolled ventral lamella and the dorsal lamella unite on one stem that is attached to the maxillary. Both have a strongly pronounced dendritic shape and completely fill the pars maxillonasoturbinalis. The caudal part of the maxilloturbinal is overlaid by the anterior process of the anterior lamina of ethmoturbinal I, visible in the 3D model of ZMB_MAM 93307 (**Fig. 13**B). The stem of the maxilloturbinal takes a ventral course along the maxillary, so it ends rostral to the opening of the nasopharyngeal duct which is dorsally enclosed by the vomer and more posteriorly further by the lamina terminalis (**Fig. 13**F, G). The simply built **nasoturbinal** reaches nearly as far rostrally as the nasal bone to which it is attached in its entire length. Its free medial margin points ventrally into the lumen. Caudally, the nasoturbinal is continuous with the lamina semicircularis.

The **lamina semicircularis** has two laminae (**Fig. 14**C). The ventral lamina has a single scrolled shape and ends as the uncinate process within the maxillary sinus ventrolateral to the lamina horizontalis. The dorsal lamina forms a double scroll in ZMB_MAM 93308 and multiple scrolls in ZMB_MAM 815 and ZMB_MAM 93307 (**Fig. 13**F), and ends caudally on the lamina cribrosa. In all three specimens a small accessory lamella that becomes double scrolled in ZMB_MAM 93307 is attached proximally to the dorsal side of the stem to which it fuses caudally. In rostral direction it runs dorsally onto the frontal and merges into it (**Fig. 13**F).

The basic shape of the three frontoturbinals is a double scroll whose two opposing lamellae of first degree complicate in different degrees in all three wolves (**Table 5**; **Fig. 13**G, H). Rostrally the turbinals complicate to dendritic and the base of frontoturbinal 1 and 2 is attached to the maxillary (**Fig.**

14D). Caudally, the shape of all frontoturbinals changes via multiple to double scroll. The stem of **frontoturbinal 1** is rostrally continuous with the lamina horizontalis in the three individuals. This fusion is also observed in **frontoturbinal 2** in ZMB_MAM 815, whereas in the other two Eurasian wolves its stem merges anteriorly into the lamina semicircularis and further forms a rostral process (**Fig. 14**C). Both frontoturbinals run caudally along the frontal onto a septum of the frontal sinus and extend as processes into the latter, each in a separate chamber (**Fig. 14**H). **Frontoturbinal 3** starts rostrally on the lamina horizontalis. It runs onto the frontal caudally, too (**Fig. 13**G). The base of frontoturbinal 3 is attached to the frontal in its entire length in ZMB_MAM 93308. It fuses to the lamina cribrosa in all specimens and has a less caudal extension than the other two frontoturbinals (**Fig. 13**B, C).

Within the pars intermedia three larger prominent interturbinals are present which are very similar in their morphology and topography between all three specimens, also with regard to the dogs' ontogeny (see ch. 3.1.1 Comparative morphology of early ontogenetic stages: 34). Thus, they are considered to be homologous to the whippets (**Table 5**, see also WAGNER & RUF 2019). Beside the three prominent interturbinals smaller additional interturbinals which have a variable morphology and topography are present on two positions: medial to interturbinal δ on at least one side in all three Eurasian wolves, and dorsal to ethmoturbinal I in one individual (**Table 5**, see below). The rostral tip of **interturbinal δ** is attached to the nasal but on the left side in ZMB_MAM 93308 to the frontal. It has a diverse shape (single scroll in ZMB_MAM 93308, double scroll in ZMB_MAM 815, multiple scrolls in ZMB_MAM 93307). The interturbinal runs caudomedially onto the septal process of the frontal (**Fig. 13**G). Hence, it has a more horizontal position in medial view instead of following the forehead's inclination like observed in frontoturbinal 1 and 2 (**Fig. 13**B). Interturbinal δ merges into the frontal rostral to the lamina cribrosa (**Fig. 14**F). **Interturbinal γ** is rostrally attached to the frontal ventral to the frontal sinus (**Fig. 13**H). On the left side in ZMB_MAM 815 its anterior tip extends rostral to the sinus. Forming a straight lamella interturbinal γ ends as a septum of the frontal sinus lateral to frontoturbinal 1 in all individuals (**Fig. 13**J). **Interturbinal β** is rostrally fused to the lamina horizontalis; on the right side in ZMB_MAM 815 it is additionally continuous with the epiturbinal of ethmoturbinal I. Caudal to the lamina horizontalis it runs onto the frontal (**Fig. 12**G, H). In ZMB_MAM 815 interturbinal β forms multiple scrolls, and in ZMB_MAM 93307 it starts dendritic rostrally and changes via multiple scrolls to a double scroll. In ZMB_MAM 93308 a dorsal single scroll merges with a ventral double scroll to the multiple scrolled interturbinal β (**Fig. 14**D). It is nearly as long as frontoturbinal 3 (**Fig. 13**C) and ends on the lamina cribrosa in the three specimens. In ZMB_MAM 93308 (left side) the base of the additional interturbinal medial to interturbinal δ is attached to the nasal; in ZMB_MAM 93307 this interturbinal extends less rostrally and is connected with the septal process of the frontal. On the left side in ZMB_MAM 815 three serially positioned and morphologically identical interturbinals fuse to the nasal anteriorly, form single scrolls caudally, and run ventrally next

to the lamina semicircularis, where they end. The second additional interturbinal which is fixed to the lamina horizontalis dorsal to ethmoturbinal I in ZMB_MAM 815 is extremely narrowed (**Table 5**). On the left side this straight lamella fuses to the stem of ethmoturbinal I whereas its base is still attached to the lamina horizontalis; on the right side it changes to single scroll and its caudal end fuses to the lamina horizontalis.

Within the pars ethmoturbinalis three ethmoturbinals are present in the three Eurasian wolves (**Table 5**). **Ethmoturbinal I** has two rostrally extending laminae, the anterior lamina and caudomedial to it the posterior lamina of which each continues into a dendritic anterior process (**Fig. 13**B, D). Caudally, the posterior lamina of ethmoturbinal I shifts ventral to the anterior lamina of ethmoturbinal I, and then both fuse together on one stem that is attached to the lamina horizontalis (**Fig. 13**F, G). Both form multiple scrolls on the stem and change to double scrolls caudally; in ZMB_MAM 93308 the posterior lamina of ethmoturbinal I is double scrolled in its entire length. On the right side in ZMB_MAM 815 a short gap arises between the anterior and the posterior lamina of ethmoturbinal I, because both are attached to the lamina horizontalis as separated laminae. Proximally on the stem of ethmoturbinal I a multiple scrolled epiturbinal arises (**Fig. 12**F, G).The epiturbinal sectionally separates from ethmoturbinal I on the right side in ZMB_MAM 815. It runs onto the lamina horizontalis on which interturbinal β merges into the epiturbinal. In ZMB_MAM 93308 it is vice versa and caudal to its separation from interturbinal β the epiturbinal runs back onto the stem of ethmoturbinal I. During its distal course along the stem the epiturbinal separates into two lamellae. Two Eurasian wolf specimens have a second epiturbinal-like lamella proximal to the first one. In ZMB_MAM 93307 it is double scrolled, in ZMB_MAM 93308 short and low. The lamella fuses into the stem of ethmoturbinal I caudally. In all three specimens ethmoturbinal I merges into the lamina cribrosa. **Ethmoturbinal II** forms multiple scrolls on the lamina horizontalis and merges rostrally into ethmoturbinal I (**Fig. 14**C, D). It has a dendritic rostral process caudomedial to the two anterior processes of ethmoturbinal I (**Fig. 13**B, E). Caudal to the lamina horizontalis ethmoturbinal II curves along the palatine to the orbitosphenoid. During this course it simplifies to a double scroll and ends slightly caudal to ethmoturbinal I on the lamina cribrosa (**Fig. 13**H). **Ethmoturbinal III** varies from the other two ethmoturbinals in lacking a rostral process but ends as a straight lamella either on the stem of ethmoturbinal II with a caudal shift to the lamina horizontalis (ZMB_MAM 815, ZMB_MAM 93308, **Fig. 14**D, E), or directly on the latter (ZMB_MAM 93307, **Fig. 13**F). Ethmoturbinal III is double scrolled in ZMB_MAM 93308 and multiple scrolled in the other two Eurasian wolves. Like ethmoturbinal II it runs caudal to the lamina horizontalis onto the palatine and the orbitosphenoid and ends as an inflated process within the sphenoid sinus extending the most posterior within the pars ethmoturbinalis (**Fig. 14**J).

The two interturbinals within the pars ethmoturbinalis are positioned between ethmoturbinal I and II (**Table 5**). **Interturbinal α** extends rostrally with a dendritic process identical to ethmoturbinal I

and II, and forms caudally multiple scrolls (**Fig. 13**E). The base of this interturbinal is attached to the stem of ethmoturbinal II and curves along the lamina horizontalis to the stem of ethmoturbinal I in posterior direction (**Fig. 12**E–G). Interturbinal α ends on the lamina cribrosa (**Fig. 13**J). Its pattern is the same in all three Eurasian wolves. The second and less pronounced interturbinal caudoventral to the first one is fused to the lamina horizontalis rostrally (**Fig. 12**F) and on the right side in ZMB_MAM 93307 continuous with the stem of ethmoturbinal II. The second interturbinal is generally a straight lamella but can form a single scroll like observed in ZMB_MAM 93308. Caudal to the lamina horizontalis the second interturbinal is attached to the palatine in ZMB_MAM 93308 (**Fig. 14**F), and to the frontal in all Eurasian wolf specimens where it comes into contact with ethmoturbinal I in ZMB_MAM 93307 (right side) and ZMB_MAM 93308 (left side). On the left side in ZMB_MAM 815 the second interturbinal extends more caudally, so that its base moreover touches the orbitosphenoid. The interturbinal fuses to the lamina cribrosa.

Domestic Dogs (*Canis lupus familiaris*)

The number of the fronto- and ethmoturbinals is identical to the wolf among all sampled dog specimens, namely three ethmoturbinals and three frontoturbinals. Further, all individuals have one prominent interturbinal within the pars ethmoturbinalis (interturbinal α), and two prominent interturbinals within the pars intermedia (interturbinal β and δ). Interturbinal γ is lacking in some dogs, and the additional interturbinals vary in their presence and distribution (see detailed descriptions below).

SHEEPDOGS (German shepherd and Groenendael)

In general, differences to the turbinal skeleton of the Eurasian wolf are more common in the Groenendael (**Fig. 17**) than in the two adult German shepherds (**Figs. 15, 16**), and refer predominantly to the turbinals' rostral end and their overall shape. The position and shape of the turbinals in the 3D models of the two German shepherds is in accordance with Eurasian wolf ZMB_MAM 93307 due to their generally similar skull shape (**Figs. 13**A**, 15**A). The higher forehead in the two German shepherds compared to the reconstructed Eurasian wolf specimen causes a bulge-like dorsal extension in frontoturbinal 1 and 2 (**Figs. 15**B, C; **16**B, C).

The **pars maxillonasoturbinalis** does not differ from the pattern observed in the Eurasian wolf (**Fig. 15**B–D). The ventral lamina of the **lamina semicircularis** forms a short uncinate process in the Groenendael's left nasal cavity (**Fig. 17**D), whereas on the right side the uncinate process ends rostromedial to the lamina horizontalis in the transition area between the maxillary sinus and the pars intermedia. In the two German shepherds the 3D models prove a more pronounced uncinate process

than in the segmented Eurasian wolf specimen (**Figs. 15**C, **16**C). The dorsal lamina is dendritic in the Groenendael; in the two German shepherds it is double scrolled more agreeing with the Eurasian wolf which is double to multiple scrolled. The accessory lamella is rostrally attached to the septal process of the frontal in the Groenendael and the German shepherds, and in the Eurasian wolf to the frontal bone. In all six individuals this lamella is running onto the stem of the lamina semicircularis and fusing to it.

Frontoturbinal 1 extends rostrally onto the maxillary in German shepherd MNHN 1985-1274 (**Fig. 15**E), in the Groenendael it is additionally continuous with the lamina semicircularis (right side) and with the lamina horizontalis (left side), respectively. In German shepherd MNHN 1985-1274 frontoturbinal 1 has a straight rostral process and forms multiple scrolls caudally, whereas in the other two group members and in the Eurasian wolf it starts with a dendritic process and simplifies caudally. In the Groenendael the attachment and rostral fusion of **frontoturbinal 2** is equivalent to frontoturbinal 1 on both sides. In German shepherd MNHN 1985-1274 (right side) frontoturbinal 2 is continuous with frontoturbinal 3 rostrally. Whereas in all the other five specimens **frontoturbinal 3** is connected rostrally with the lamina horizontalis, in the Groenendael it additionally merges with the epiturbinal of ethmoturbinal I.

Interturbinal δ shows no difference to the Eurasian wolf. It protrudes more rostrally in German shepherd SMF 93607 (**Fig. 16**F). **Interturbinal γ** projects onto the frontal anteriorly in both German shepherds (in SMF 93607 on the right side), like in Eurasian wolf ZMB_MAM 815 (right side). Although the Groenendael has a well-developed frontal sinus with a septum between frontoturbinal 1 and 2, this septum merges rostrally into a thick bony ridge on the frontal ventral to the sinus. This fused structure is not regarded as a turbinal (**Fig. 17**G, H). In German shepherd MNHN 1985-1274 interturbinal γ is markedly expanding caudodorsally, even beyond frontoturbinal 1 and 2 (**Fig. 15**B, C). Between frontoturbinal 3 and ethmoturbinal I differences in the position of the interturbinals are observed. The three dogs have a very similar **interturbinal β** like the Eurasian wolf. In the Groenendael it separates rostrally into two single scrolled lamellae: the medial one fuses to the lamina horizontalis and to ethmoturbinal I, like in German shepherd SMF 93607 and Eurasian wolf ZMB_MAM 815; the lateral lamella fuses to the lamina horizontalis, as observed in the other specimens. These two lamellae unite to a double scroll caudally (**Fig. 17**F). Both German shepherds have an additional interturbinal dorsal to interturbinal β. It ends rostrally on the frontal in MNHN 1985-1274 and on the right side in SMF 93607 and on the left side in the latter on the suture to the frontal and then runs onto this bone. The additional interturbinal is straight to slightly curved (SMF 93607) or single scrolled (MNHN 1985-1274) and fuses in both specimens to the frontal rostral to the lamina cribrosa (**Fig. 16**L, M). This interturbinal can hardly be homologized with the additional interturbinal

in Eurasian wolf ZMB_MAM 815, as it shows a completely different pattern; not to mention that in the wolf this interturbinal is situated ventral to interturbinal β (**Table 5**).

The double scrolled posterior lamina of ethmoturbinal I separates for a short way into a medial single scroll and a lateral double scroll in the Groenendael (**Fig. 17**E). In the other five specimens the posterior lamina of ethmoturbinal I is continuously multiple scrolled. German shepherd SMF 93607 has a shortened anterior process of the anterior lamina of ethmoturbinal I that overlays the caudal end of the maxilloturbinal (**Fig. 16**B). The second German shepherd reflects more the morphology of the Eurasian wolf in this character (**Fig. 15**B). The epiturbinal of ethmoturbinal I in German shepherd SMF 93607 forms two single scrolls rostrally (**Fig. 16**K) that unite and form multiple scrolls. In the Groenendael the separation occurs sectionally and is comparable to Eurasian wolf ZMB_MAM 93308, also regarding the form of these lamellae as two single scrolls (**Fig. 17**F). Both then fuse to a double scroll. A second epiturbinal-like lamella on the stem of ethmoturbinal I is present on the left side in the Groenendael and forms a single scroll. The rostral process of **ethmoturbinal II** is less extended in both German shepherds (**Figs. 15**B, **16**B). In the Groenendael this turbinal runs onto the frontal caudal to the lamina horizontalis; on the left side it is furthermore attached to the stem of ethmoturbinal I for a short distance (**Fig. 17**F). In the two German shepherds and in the Eurasian wolf ethmoturbinal II runs onto the palatine. More caudally, in all six specimens this turbinal is fixed to the orbitosphenoid (**Fig. 15**J). In **ethmoturbinal III** variations towards the Eurasian wolf are observed in its caudal end. In German shepherd MNHN 1985-1274 (right side) and the Groenendael (right side) it is continuous with the lamina terminalis on the stem of ethmoturbinal II. On the left side in the mentioned German shepherd specimen and in SMF 93607 ethmoturbinal III arises from the transition between the lamina terminalis and the lamina horizontalis.

Interturbinal α differs in the Groenendael from the Eurasian wolf in its rostral process which is a simpler scroll that complicates up to dendritic on the left side. Apart from that, interturbinal α remains a single scroll until its fusion to the lamina cribrosa (**Fig. 17**G). The second additional interturbinal is present in the two German shepherds. Rostrally it merges into the stem of ethmoturbinal II resembling Eurasian wolf ZMB_MAM 93307; on the left side in SMF 93607 it is further continuous with the lamina horizontalis. MNHN 1985-1274 differs in the interturbinal's topography through running from ethmoturbinal II onto the frontal (**Fig. 15**H). The topography in SMF 93607 and the caudal end in both German shepherds are homologous to the Eurasian wolf.

NORDIC SLEDGE DOGS (Greenland dog)

Like the German shepherd and the Groenendael the Greenland dog represents the morphology of its ancestor (**Fig. 18**). The **maxilloturbinal**, the **nasoturbinal**, and the **lamina semicircularis** exactly resemble the descriptions of the Eurasian wolf.

No differences are observed in **frontoturbinal 1 and 2**, whereas **frontoturbinal 3** is additionally continuous with ethmoturbinal I rostrally. The number of interturbinals within the pars intermedia has increased in the Greenland dog to seven and is comparable to the highest number among the wolf sample observed on the left side in ZMB_MAM 815 (**Table 6**). Like the Eurasian wolf the Greenland dog has an additional interturbinal lateral to the lamina semicircularis and dorsal to ethmoturbinal I. Two additional interturbinals which are absent in the Eurasian wolf are present on both sides between frontoturbinal 2 and 3 and dorsal to interturbinal β (**Table 5**). **Interturbinal δ** shows no variations and has a simpler single scrolled shape corresponding with Eurasian wolf ZMB_MAM 93308 (**Fig. 18**G). **Interturbinal γ** is fused to the frontal anterior to the frontal sinus, like on the left side in Eurasian wolf ZMB_MAM 815. In its caudal course it is homologous to the ancestral pattern. **Interturbinal β** has two separated lamellae rostrally: the medial lamella arises from the epiturbinal of ethmoturbinal I on the right side and is on the left side additionally attached to the lamina horizontalis; the lateral lamella arises anteriorly from the lamina horizontalis on both sides. These two single scrolls unite to multiple scrolls which directly change to a double scroll (**Fig. 18**G). Like in the Eurasian wolf interturbinal β runs onto the frontal and fuses to the lamina cribrosa. The additional interturbinal next to the lamina semicircularis is small and straight rostrally and caudally fused to the medial septum of the nasal, like in wolf ZMB_MAM 93308. The additional interturbinal ventral to interturbinal β is comparable to Eurasian wolf ZMB_MAM 815 in its position and straight shape (**Fig. 18**H). In the Greenland dog this interturbinal merges rostrally into the stem of ethmoturbinal I on the left side and into the frontal on the right side, and fuses on both sides to the frontal rostral to the lamina cribrosa. The two further additional interturbinals are attached to the frontal in their entire length and form a single scroll between frontoturbinal 2 and 3 (**Fig. 18**H), and a small straight lamella dorsal to interturbinal β.

All **three ethmoturbinals** and **interturbinal α** are like in the Eurasian wolf, too. The posterior lamina of ethmoturbinal I is a simpler double scroll equivalent to wolf ZMB_MAM 93308. The epiturbinal of ethmoturbinal I runs rostrally onto the lamina horizontalis instead staying on the stem of ethmoturbinal I throughout as observed in all three Eurasian wolf specimens (**Fig. 18**E, F). Posteriorly, it runs onto the stem of ethmoturbinal I with a more complex dendritic shape. A second epiturbinal-like lamella is lacking in the Greenland dog. An additional interturbinal caudoventral to interturbinal α differs in its rostral attachment on the left side, namely to the frontal. It complicates to a double scroll differing from the simpler straight up to single scrolled shape in the Eurasian wolf (**Fig. 18**H). The

additional interturbinal fuses to the frontal, while in the ancient pattern it extends more posteriorly into the lamina cribrosa.

The position of the turbinals inside the nasal cavity and their form cannot be described as this Greenland dog specimen was not virtually segmented. But the cross sections suggest that they should not differ in a large extent from the Eurasian wolf.

ENGLISH TOY SPANIELS (King spaniel and Cavalier)

All four spaniel specimens show a conspicuous asymmetry within their nasal cavity (**Figs. 19–22**). The bony part of the nasal septum has a convex shape to the left side in King spaniel NMBE 1051945 and Cavalier NMBE 1062998, and to the right side in the other two skulls. Considering the overall morphology, ethmoturbinal II seems the least affected by the rostral shortening of the face in the reconstructed King spaniel NMBE 1051945 (**Fig. 19**B, C). The other turbinals show a strong rostrocaudal shortening. Compared to the segmented King spaniel and to the Eurasian wolf the segmented Cavalier NMBE 1062998 (**Fig. 22**B–E) more or less resembles an intermediate stage. Its face is clearly longer than the King spaniel's, but nevertheless brachycephalic with a steep forehead. The caudal extensions of frontoturbinal 1 and 2 result in the posterior concave shape of the turbinal skeleton in lateral and medial view similar to the Eurasian wolf.

In cross section in both spaniel breeds the **maxilloturbinal** is of double scrolled basic type, but its dendritic shape is less pronounced, especially in both King spaniels: in NMBE 1051945 (**Fig. 19**) the laterally scrolled ventral lamella is slightly dendritic, loose, and has less accessory lamellae in comparison to the Eurasian wolf (**Fig. 19**D). Its dorsal lamella complicates to double scroll. In the other King spaniel (NMBE 1051948, **Fig. 20**) the lateral scroll in the dendritic ventral lamella is not identifiable, and the dorsal lamella is more or less straight with small crest-like outgrowths (**Fig. 20**B). In both spaniel specimens the lamellae of the maxilloturbinal do not fill the complete pars maxillonasoturbinalis but are leaving a distinct space to the nasal septum and to the palate. The maxilloturbinal in King spaniel NMBE 1051945 shows a thin rostrodorsal and a caudoventral process in the virtual 3D model (**Fig. 19**B, C). It differs from the compact and regular shape in the Eurasian wolf more properly represented by Cavalier NMBE 1062998 (**Fig. 22**). In both Cavaliers the shape of the ventral lamella and the general extension of the maxilloturbinal are similar to the Eurasian wolf (**Fig. 22**D–J). The nasal septum's convex shape to the right side in Cavalier NMBE 1059207 induces in the dorsal lamella a dendritic shape on the left side and a smaller size with a less dendritic shape on the right side (**Fig. 21**B). In Cavalier NMBE 1062998 it is vice versa, namely a simpler multiple scroll in the maxilloturbinal's dorsal lamella on the right side, whereas it more complicates to dendritic on the left side. On the left side within the same specimen in the intermediate section of the maxilloturbinal its two lamellae are attached to the maxillary separately. The **nasoturbinal** is generally straight to curved in all

four specimens. In King spaniel NMBE 1051945 it is small and short, and even a suture to the caudally attaching lamina semicircularis is observed. In Cavalier NMBE 1062998 the nasoturbinal is longer and dorsally curved on its rostral end following the snout's airorhynchic shape which affects the nasal (**Fig. 22**G). In both Cavaliers (in NMBE 1062998 on the right side) the nasoturbinal separates on its distal end into two low crests.

The **lamina semicircularis** has two laminae (**Fig. 22**K) which are broken on the right side in King spaniel NMBE 1051945. The shape of the ventral lamina is identical to the Eurasian wolf in both Cavaliers, whereas in the two King spaniels it complicates to a double scroll. A dorsoventral depression of the pars maxillonasoturbinalis in NMBE 1051948 causes the shift of the ventral lamina caudolateral to the root of the canine (**Fig. 20**B). Furthermore, this lamina connects with the lamina horizontalis in this specimen, but nonetheless forms the uncinate process within the maxillary sinus like in the other three English toy spaniels (**Fig. 20**C). The dorsal lamina is a conspicuously simpler single scroll in the four individuals, though it complicates to a double scroll on the intact left side in King spaniel NMBE 1051945. The lamina semicircularis ends caudally on the lamina cribrosa comparable to the Eurasian wolf. An accessory lamella is present in King spaniel NMBE 1051945 on the left side and in Cavalier NMBE 1059207 on the right side. In the King spaniel it is attached to the frontal rostrally, and curves as a short small lamella along the stem of the lamina semicircularis. In the Cavalier the accessory lamella is continuous with the nasal rostrally, while its base is attached to the lamina semicircularis. It ends on the stem of the lamina semicircularis in both specimens.

Frontoturbinal 1 is attached anteriorly to the frontal in King spaniel NMBE 1051945 (**Fig. 19**D), and to the maxillary in King spaniel NMBE 1051948 and Cavalier NMBE 1059207 (**Fig. 21**C). In Cavalier NMBE 1062998 the suture between the maxillary and the frontal is not visible in the µCT scans. In the short snouted spaniel breed frontoturbinal 1 is connected with the fused lamina semicircularis and lamina horizontalis rostrally. In NMBE 1051945 frontoturbinal 1 is the first structure that separates from this threefold connection (**Fig. 19**D), whereas in NMBE 1051948 the lamina semicircularis separates first (**Fig. 20**C) and then more caudally frontoturbinal 1 separates from the lamina horizontalis. The two Cavaliers are similar to NMBE 1051948. The shape of frontoturbinal 1 differs between the four individuals: in King spaniel NMBE 1051945 it forms a double scroll to multiple scrolls, in NMBE 1051948 the basic type is difficult to identify as it builds some smaller rostral and caudal processes within the pars intermedia. In Cavalier NMBE 1059207 frontoturbinal 1 is slightly dendritic rostrally, whereas in its conspecific a rostral single scroll complicates to dendritic. Posteriorly, frontoturbinal 1 is attached to the frontal. The rostral end of **frontoturbinal 2** reflects more the Eurasian wolf. It is connected distally with the lamina horizontalis, and on its base with the frontal in King spaniel NMBE 1051945 (**Fig. 19**D, E) or with the maxillary in King spaniel NMBE 1051948 (**Fig. 20**C) and Cavalier NMBE 1059207. It forms a double scroll in both King spaniels, in the Cava-

liers it complicates in NMBE 1062998 to multiple scrolls for a short distance with a straight rostral end, and to multiple scrolls to slightly dendritic in NMBE 1059207. With some exceptions, frontoturbinal 2 shows the same topography and caudal end like frontoturbinal 1 in the four specimens. In King spaniel NMBE 1051945 the stem fuses to the lamina cribrosa whereas the distal end forms a caudal process within the pars intermedia (**Fig. 19**F). On the left side the mentioned process passes onto frontoturbinal 3. In King spaniel NMBE 1051948 frontoturbinal 1 and 2 fuse separately to a septum of the reduced frontal sinus. Frontoturbinal 2 differs on the right side in forming a process within the pars intermedia similar to NMBE 1051945. In both Cavaliers frontoturbinal 1 and 2 extend as processes into two separate chambers of the frontal sinus (**Fig. 22**N, P). In Cavalier NMBE 1059207 frontoturbinal 2 is broken caudally (**Fig. 21**F). The homologous caudal end of frontoturbinal 1 and 2 is reflected in the 3D models: the complete loss of the frontal sinus causes their posterior reduction in King spaniel NMBE 1051945 (**Fig. 19**B, C). In the Cavalier frontoturbinal 1 and 2 extent farer caudally, but additionally farer dorsally compared to the Eurasian wolf resulting from the breed's steep forehead (**Fig. 22**B–G). The rostral end of **frontoturbinal 3** varies in Cavalier NMBE 1062998 from the Eurasian wolf: on the left side it ends on the frontal near the lamina horizontalis, on the right side it fuses to the lamina horizontalis but is furthermore continuous with the epiturbinal of ethmoturbinal I. In Cavalier NMBE 1059207 the base of frontoturbinal 3 is attached rostrally to the lamina horizontalis, whereas its stem separates from the frontal in caudal direction. In its posterior course interturbinal β separates from frontoturbinal 3 on the right side in NMBE 1059207, and on the left side the epiturbinal of ethmoturbinal I (**Fig. 21**D) and interturbinal β. In all English toy spaniels frontoturbinal 3 has a double scrolled shape and runs onto the frontal. In Cavalier NMBE 1062998 it fuses with a lamella which is attached to the lamina horizontalis. Frontoturbinal 3 shows different caudal endings: in King spaniel NMBE 1051945 it is homologous to frontoturbinal 1 and 2, namely a fusion of the stem to the lamina cribrosa -on the left side frontoturbinal 3 merges additionally with interturbinal β- while the distal end forms a process within the pars intermedia (**Fig. 19**H); in King spaniel NMBE 1051948 frontoturbinal 3 forms a process within the pars intermedia, and in the Cavaliers it merges into the lamina cribrosa.

King spaniel NMBE 1051945 is lacking interturbinal γ on both sides, as in this individual the frontal sinus is extremely reduced. Otherwise, all prominent interturbinals are present in all four specimens. Dorsal to ethmoturbinal I an additional interturbinal is observed on the left side in the mentioned King spaniel specimen and on the right side in each of the two Cavaliers. In contrast to the Eurasian wolf, further additional interturbinals are located between frontoturbinal 2 and 3 on both sides in two individuals. King spaniel NMBE 1051948 has one interturbinal, and Cavalier NMBE 1059207 has one interturbinal on the right side and two on the left side (**Table 5**). The total number of interturbinals within the pars intermedia is three to five in the Cavaliers and two to four in the King spaniels, and in the former closer to the Eurasian wolf (**Table 6**). **Interturbinal δ** is rostrally attached to the nasal

in all English toy spaniels, is straight in King spaniel NMBE 1051945 and single scrolled in King spaniel NMBE 1051948 and Cavalier NMBE 1059207 and NMBE 1062998 (left side), and runs caudally onto the frontal. On the right side in Cavalier NMBE 1062998 the interturbinal forms a double scroll which separates into two straight lamellae caudally. Interturbinal δ fuses to the frontal rostral to the lamina cribrosa, but persists dorsal to the septal process of the frontal in the two King spaniels (**Fig. 20**C), while in the two Cavaliers it shifts to the septal process (**Fig. 21**E). **Interturbinal γ** merges rostrally into the frontal on the right side in King spaniel NMBE 1051948 and is a part of a bony bulbous process, and then runs onto the frontal as a straight lamella on the left side. Caudally in the same specimen interturbinal γ fuses to the lamina cribrosa on the right side, or it forms a septum within the small frontal sinus on the left side. In both Cavaliers instead interturbinal γ has the same morphological pattern as in the Eurasian wolf due to their well-developed frontal sinus (**Fig. 22**L–N). The stem of **interturbinal β** is fixed rostrally to the lamina horizontalis in all specimens according to the Eurasian wolf (**Fig. 19**F). Like in the two Eurasian wolves ZMB_MAM 93307 and ZMB_MAM 93308 it has anteriorly no further connection on the left side in Cavalier NMBE 1062998. On the left side in King spaniel NMBE 1051948 interturbinal β forms a rostral process within the pars intermedia and is on its most anterior end attached to the lamina horizontalis and caudally to the frontal. While fixed to the lamina horizontalis on the left side in King spaniel NMBE 1051945 (**Fig. 19**G) and on the right side in NMBE 1051948 interturbinal β fuses rostrally to the epiturbinal of ethmoturbinal I like in Eurasian wolf ZMB_MAM 815 (right side). On the left side in Cavalier NMBE 1059207 interturbinal β merges into frontoturbinal 3. A rostral separation of interturbinal β into two lamellae is observed on the right side in all three, King spaniel NMBE 1051945, and Cavalier NMBE 1059207 and NMBE 1062998, and with a similar pattern: a medial lamella on the lamina horizontalis is continuous rostrally with the epiturbinal of ethmoturbinal I, a lateral lamella ends on the lamina horizontalis and is in Cavalier NMBE 1059207 additionally fused to frontoturbinal 3. Interturbinal β complicates to a double scroll in all individuals, on the right side in Cavalier NMBE 1059207 it is slightly dendritic rostrally. It runs onto the frontal in all four specimens and on the right side in Cavalier NMBE 1062998 interturbinal β unites on one stem with frontoturbinal 3 (**Fig. 22**N). Interturbinal β ends on the lamina cribrosa except King spaniel NMBE 1051945 in which it fuses to frontoturbinal 3 on the left side (on the right side it is caudally broken). The additional interturbinal between frontoturbinal 2 and 3 forms in King spaniel NMBE 1051948 a bulbous rostral process which separates into two single scrolls caudally (**Fig. 20**C). The dorsal lamella runs onto the stem of frontoturbinal 2 and fuses to it, the ventral lamella fuses to the frontal. The additional interturbinal next to frontoturbinal 2 on the left side in Cavalier NMBE 1059207 is continuous with the stem of frontoturbinal 2 rostrally and runs onto the frontal. The second additional interturbinal located next to frontoturbinal 3 and the single additional interturbinal on the right side in the Cavalier specimen are attached to the frontal in their entire length (**Fig. 21**E). All three additional interturbinals at this position in this individual are small and narrow

and fuse to the frontal caudally. The additional interturbinal caudodorsal to ethmoturbinal I merges into the lamina horizontalis rostrally in the three specimens in which it is present. In Cavalier NMBE 1062998 its distal tip is fused to interturbinal β (**Fig. 22**G). The shape of the additional interturbinal is single scrolled in Cavalier NMBE 1059207, and double scrolled in King spaniel NMBE 1051945 and the other Cavalier. It runs onto the frontal caudally; in the King spaniel it is located on the suture between the lamina horizontalis and the frontal. In its caudal end the additional interturbinal forms a process within the pars intermedia in Cavalier NMBE 1062998 or fuses to the frontal rostral to the lamina cribrosa in Cavalier NMBE 1059207. Both types of ending are present in the King spaniel in which the distal end forms a process whereas the stem passes onto the frontal.

Ethmoturbinal I forms two anterior processes in all four English toy spaniels, but they are broken rostrally on the right side in King spaniel NMBE 1051945. Except the right side in King spaniel NMBE 1051948 in which the straight anterior process of the posterior lamina of ethmoturbinal I lies rostroventral to the bulbous anterior process of the anterior lamina of ethmoturbinal I, all individuals and the mentioned King spaniel's left side correspond to the Eurasian wolf in the position of both processes to each other. They are simpler in their form and slightly dendritic in both Cavaliers and on the left side in King spaniel NMBE 1051948. The anterior lamina of ethmoturbinal I on the intact left side in King spaniel NMBE 1051945 has a similar dendritic anterior process, its posterior lamina of ethmoturbinal I forms a straight anterior process. The anterior lamina of ethmoturbinal I is double scrolled in all individuals, the posterior lamina of ethmoturbinal I shows a greater variation and is straight on the right side in King spaniel NMBE 1051945, single scrolled on the left side in King spaniel NMBE 1051948 (**Fig. 20**D–F) and in Cavalier NMBE 1059207, and dendritic in the other Cavalier. In King spaniel NMBE 1051945 the posterior lamina of ethmoturbinal I merges with ethmoturbinal II rostrally (**Fig. 19**G). The posterior lamina of ethmoturbinal I in Cavalier NMBE 1062998 has a strongly aberrant anterior process whose ventrally displaced knob-like distal end is directly positioned caudal to the maxilloturbinal (**Fig. 22**F, J, K). Ethmoturbinal I has in its entire length a concave notch on its dorsal side at the same height where both lamellae unite. The epiturbinal is present in all four English toy spaniels. In contrast to the Eurasian wolf it passes onto the lamina horizontalis rostrally where it is either continuous with interturbinal β represented in King spaniel NMBE 1051945 and on the left side in Cavalier NMBE 1062998 or with frontoturbinal 3 and more caudally with interturbinal β like on the right side in Cavalier NMBE 1062998. After shifting to the stem of ethmoturbinal I, the epiturbinal runs distally forming a single scroll in both King spaniels and on the right side in Cavalier NMBE 1062998 (**Fig. 22**L–P) and a double scroll in Cavalier NMBE 1059207 and on the left side in NMBE 1062998. A second epiturbinal-like lamella is absent. The caudal end of ethmoturbinal I differs in King spaniel NMBE 1051945 from the ancestral pattern: it forms a process which ends within the pars ethmoturbinalis, caudolateral to it a second lamella fuses to the lamina cribrosa, and a third lamella caudomedial to the two former fuses to the frontal. **Ethmoturbinal II** shows some variations in

the four toy spaniels to the Eurasian wolf: King spaniel NMBE 1051945 has a long thin and straight rostral process that fuses to the anterior process of the anterior lamina of ethmoturbinal I (**Fig. 19**F); and it protrudes nearly as far rostrally as observed in the virtual 3D model (**Fig. 19**B, C). On the right side in the other King spaniel NMBE 1051948 a dendritic rostral process is present caudomedial to its stem which is fused to ethmoturbinal I on the lamina horizontalis. In Cavalier NMBE 1062998 the straight rostral process of ethmoturbinal II lies caudoventral (left side) and caudomedial (right side) to the anterior process of the posterior lamina of ethmoturbinal I. Within the same Cavalier specimen, the stem of ethmoturbinal II unites with the rostral process after it has separated caudally from ethmoturbinal I (**Fig. 22**D, F, K, L). The other Cavalier specimen has no rostral process; here the stem of ethmoturbinal II separates caudally together with ethmoturbinal III from the lamina terminalis (**Fig. 21**F). In King spaniel NMBE 1051948 ethmoturbinal II forms a double scroll and in the other three toy spaniels it shows multiple scrolls. During its caudal course it is connected with the lamina horizontalis in Cavalier NMBE 1062998 and additionally with the lamina terminalis in NMBE 1059207 and both King spaniels. The topography of ethmoturbinal II differs in King spaniel NMBE 1051948 as it connects with the lamina cribrosa before moving onto the orbitosphenoid and ending as a process within the sphenoid sinus. The other three individuals resemble the Eurasian wolf: ethmoturbinal II curves caudal to the lamina horizontalis along the palatine to the orbitosphenoid. In King spaniel NMBE 1051945 ethmoturbinal II fuses to the orbitosphenoid, and in the two Cavaliers it follows the pattern observed in the Eurasian wolf. On the left side in Cavalier NMBE 1062998 **ethmoturbinal III** ends on the lamina horizontalis rostrally identical to the Eurasian wolf. It is additionally continuous with the stem of ethmoturbinal II on both sides in this specimen. In the other Cavalier NMBE 1059207 ethmoturbinal III is fused rostrally to ethmoturbinal II on the lamina terminalis on the left side, or it merges into the lamina terminalis as a separate turbinal on the right side. In the two King spaniels the stem of ethmoturbinal III is attached to the lamina terminalis, and specimen NMBE 1051948 has a rostral process on the left side. Ethmoturbinal III forms a single scroll in both King spaniels, runs onto the orbitosphenoid (in NMBE 1051945 it is furthermore attached to the palatine for a short way), and forms a far caudally displaced process within the sphenoid sinus (e.g., NMBE 1051945, **Fig. 19**B, C). On the right side in NMBE 1051945 the caudal end of ethmoturbinal III varies in fusing to the orbitosphenoid. In the two Cavaliers ethmoturbinal III complicates to a double scroll more approaching the ancestral shape. Its course and caudal end are similar to the Eurasian wolf (**Fig. 22**Q) without a caudal displacement which is observed in the segmented King spaniel (**Fig. 22**D–G). On the left side in Cavalier NMBE 1059207 ethmoturbinal III differs from the Eurasian wolf in fusing caudally to the wall of the orbitosphenoid similar to King spaniel NMBE 1051948.

Interturbinal α forms a tip-like rostral process in King spaniel NMBE 1051945 (**Fig. 19**H), and a small slightly dendritic rostral process on the left side in Cavalier NMBE 1062998. On the right side in the mentioned Cavalier specimen a rostral process is absent and interturbinal α is fused to the stem of

ethmoturbinal II. In Cavalier NMBE 1059207 and in King spaniel NMBE 1051948 interturbinal α merges rostrally into the lamina terminalis and is in the King spaniel specimen continuous with the posterior lamina of ethmoturbinal I on the right side, and with ethmoturbinal II on the left side. Interturbinal α is single scrolled in King spaniel NMBE 1051948 and double scrolled in the other three specimens. The four spaniels are similar to the Eurasian wolf regarding the course of interturbinal α except King spaniel NMBE 1051948 (right side) in which it curves along ethmoturbinal II directly to ethmoturbinal I without touching the lamina horizontalis. Interturbinal α forms a caudal process within the ethmoturbinal recess in all specimens, but on the left side in King spaniel NMBE 1051948 it fuses to the lamina cribrosa without a process. All four specimens have a second interturbinal within the pars ethmoturbinalis caudoventral to the prominent interturbinal (**Table 5**) that merges rostrally into the lamina horizontalis; on the left side in Cavalier NMBE 1062998 it is additionally continuous with ethmoturbinal I. This additional interturbinal is small in King spaniel NMBE 1051945 (**Fig. 19**J) and Cavalier NMBE 1062998, but single scrolled in the other two specimens. It stays on the lamina horizontalis and fuses to it posteriorly in King spaniel NMBE 1051945. On the right side in Cavalier NMBE 1062998 the additional interturbinal ends on the stem of ethmoturbinal II, whereas on the left side it runs onto the frontal into which it merges. The additional interturbinal extends farer caudally in Cavalier NMBE 1059207 and King spaniel NMBE 1051948, and fuses to the orbitosphenoid in the King spaniel and on the Cavalier's right side, and to the palatine on the Cavalier's left side.

JAPANESE CHIN AND PEKINGESE

The reconstructed turbinal skeleton is denser and apparently more complicate in pekingese NMBE 1051962 (**Fig. 23**) and chin NMBE 1051951 (**Fig. 27**) than in pekingese SMF 35611 (**Fig. 24**). Due to the reduction of the frontal sinus (see p. 55) frontoturbinal 1 and 2 are caudally shortened in the three segmented specimens compared to Eurasian wolf ZMB_MAM 93307. Chin NMBE 1051951 and pekingese NMBE 1051962 have a convex dorsal shape in ethmoturbinal I, the chin in the anterior process of the anterior lamina of ethmoturbinal I (**Fig. 27**B), and the pekingese in the anterior process of both the anterior and the posterior lamina of ethmoturbinal I (**Fig. 23**B). Ethmoturbinal II and III are markedly displaced dorsally in pekingese SMF 35611 and chin NMBE 1051951, whereas in pekingese NMBE 1051962 ethmoturbinal III is affected.

The **maxilloturbinal** shows the basic double scrolled type in cross section in all individuals except pekingese SMF 35611 in which it is a straight branchless lamella which has two short crests distally. This straight lamella leaves a lot of open space within the pars maxillonasoturbinalis and keeps a considerable distance to the olfactory turbinals. The maxilloturbinal follows a steep rostrodorsal to caudoventral course in this pekingese (**Fig. 24B–G**). The basic lateral scroll in the ventral lamella is identifiable in chin NMBE 1051951 (**Fig. 27**D) in combination with a slightly dendritic shape, and in

pekingese NMBE 1051965 (**Fig. 25**) in combination with multiple scrolls. In chin ZMB_MAM 7436 (**Fig. 26**) the ventral lamella is scrolled medially and slightly dendritic on the left side and more or less single scrolled on the right side. The bony lamellae have a lot of gaps in pekingese NMBE 1051962 (**Fig. 23**D). The dorsal lamella shows no uniform shape and is straight in pekingese NMBE 1051965, single to double scrolled in chin NMBE 1051951, and slightly dendritic in pekingese NMBE 1051962 and chin ZMB_MAM 7436 (right side). On the left side in ZMB_MAM 7436 the dorsal lamella separates caudally into a lateral single scroll and a medial double scroll. Accessory lamellae which are observed in the cross sections prove the maxilloturbinal's denser and apparently more complicated morphology in the 3D model of pekingese NMBE 1051962 (**Fig. 23**E) and chin NMBE 1051951 (**Fig. 27**D) compared to pekingese SMF 35611. However, these accessory lamellae show a loose arrangement in both specimens and leave a lot of space to the surrounding bones (maxillary, nasal septum, palate). The maxilloturbinal of pekingese NMBE 1051962 is more shortened rostrocaudally than in chin NMBE 1051951 (**Figs. 23**B, C; **27**B, C). No bony **nasoturbinal** is observed in pekingese NMBE 1051965 and on the right side in pekingese SMF 35611. In the other individuals and on the left side in SMF 35611 the nasoturbinal is reduced to a small and short rostral tip attached to the lamina semicircularis with no visible suture (e.g., chin NMBE 1051951, **Fig. 27**B–D).

The **lamina semicircularis** resembles the Eurasian wolf in the presence of the two laminae and the uncinate process. The ventral lamina forms a single scroll in chin ZMB_MAM 7436 and in the other four individuals it is straight. The uncinate process points into the maxillary sinus, except pekingese SMF 35611 in which it ends rostral to the maxillary sinus and to the frontoturbinal recess medioventral (left side) or lateroventral (right side) to the lamina horizontalis. Both laminae do not unite on the right side in this specimen (**Fig. 24**B–E). The dorsal lamina is as simplified as the ventral one in both breeds: the straight shape is present in chin NMBE 1051951 and pekingese SMF 35611, the single scrolled shape in chin ZMB_MAM 7436 and pekingese NMBE 1051962 and NMBE 1051965. In pekingese NMBE 1051962 both laminae are shifted towards each other, so the ventral lamina is positioned rostrally and the dorsal lamina follows caudally. The caudal end of the dorsal lamina differs in pekingese NMBE 1051965 from the ancestral pattern in forming a process within the ethmoidal recess. Chin ZMB_MAM 7436 shows both patterns, a fusion to the lamina cribrosa corresponding with the Eurasian wolf plus a caudal process within the ethmoidal recess. None of the two breeds has the small dorsal accessory lamella proximal on the stem of the lamina semicircularis as observed in the Eurasian wolf.

Frontoturbinal 1 merges rostrally into the maxillary and is continuous with the lamina horizontalis in pekingese NMBE 1051962 (**Fig. 23**F) like in the Eurasian wolf, or with the fused lamina horizontalis and lamina semicircularis in both chins. In the other two pekingese (NMBE 1051965, SMF 35611) the stem of frontoturbinal 1 fuses to the maxillary and its distal margin ends as rostral process

rostromedial to the stem on the right side in NMBE 1051965 and caudomedial to the stem in SMF 35611 and on the left side in NMBE 1051965 (**Fig. 25**C). In its rostral beginning the in cross section distal end of frontoturbinal 1 is fused with the lamina semicircularis on the right side in pekingese SMF 35611 (**Fig. 24**C, D). Its shape is a single scroll in pekingese NMBE 1051965, a double scroll in chin ZMB_MAM 7436 and pekingese NMBE 1051962 and SMF 35611, and multiple scrolls in chin NMBE 1051951. Caudally frontoturbinal 1 runs onto the frontal in all specimens, but not onto a septum of the frontal sinus like in the Eurasian wolf due to the reduction of the sinus. The two chins and pekingese NMBE 1051962 (**Fig. 23**K, L) have a small frontal sinus in which frontoturbinal 1 ends as a process, albeit in chin ZMB_MAM 7436 it additionally fuses to the lamina cribrosa representing an intermediate stage. The frontal sinus is completely reduced in pekingese NMBE 1051965 and SMF 35611; hence frontoturbinal 1 merges into the lamina cribrosa and furthermore forms a caudal process within the pars intermedia in NMBE 1051965. **Frontoturbinal 2** has the same rostral fusion as frontoturbinal 1 in chin NMBE 1051951 and pekingese NMBE 1051962. A difference is observed in pekingese NMBE 1051965, namely two short rostral processes anterolateral and anteromedial to the stem (**Fig. 25**C, D), and in chin ZMB_MAM 7436 in which frontoturbinal 2 is fused to the lamina semicircularis only. In pekingese SMF 35611 frontoturbinal 2 varies in being beside its attachment to the maxillary additionally continuous with the lamina horizontalis. In the same specimen a rostral process is positioned caudomedial to the stem on the left side and caudolateral to the stem on the right side. Frontoturbinal 2 is double scrolled in all individuals and like frontoturbinal 1 it is attached to the frontal caudally. It merges into the lamina cribrosa in pekingese SMF 35611 (**Fig. 24**H) and the two chins, but in chin ZMB_MAM 7436 the fusion occurs within the reduced frontal sinus. Pekingese NMBE 1051962 has a process within the small frontal sinus, and in pekingese NMBE 1051965 frontoturbinal 2 runs onto the lamina cribrosa and shows a process within the pars intermedia. According to the Eurasian wolf, **frontoturbinal 3** merges rostrally into the lamina horizontalis; in chin NMBE 1051951 on the transition to the frontal on the right side and to the maxillary on left side. It forms a double scroll in four individuals, but pekingese NMBE 1051965 has a single scroll on the right side and a straight lamella on the left side and on both sides frontoturbinal 3 forms several rostral and caudal processes within the pars intermedia. In the mentioned pekingese specimen frontoturbinal 3 is attached to the lamina horizontalis in its entire length though it runs onto the frontal for a short way (**Fig. 25**E), and ends on the lamina horizontalis. Like in the Eurasian wolf in the other four dogs frontoturbinal 3 runs onto the frontal and ends on the lamina cribrosa.

All individuals in both breeds have, if any, the three prominent interturbinals within the pars intermedia, but no additional interturbinals (**Table 5**). **Interturbinal δ** corresponds in its rostral fusion to the Eurasian wolf but is simplified to a straight lamella in both chins and pekingese NMBE 1051962 (**Fig. 23**H–K) and to a single scroll in the other two pekingese. Interturbinal δ shifts to the frontal caudally, and in chin ZMB_MAM 7436 to the septal process of the frontal. It fuses to the lamina cribrosa

in both chins and pekingese SMF 35611. In the other two pekingese interturbinal δ extends less posteriorly and instead ends on the frontal in NMBE 1051965, and on the septal process of the frontal in NMBE 1051962. **Interturbinal γ** is reduced to a straight, small, and thickened lamella tending to be crest-like e.g., in chin ZMB_MAM 7436 (**Fig. 26**D). In both chins it is attached rostrally to the frontal and ends as a septum of the extremely reduced frontal sinus (e.g., NMBE 1051951, **Fig. 27**H). The rostral end of interturbinal γ is identical to the chins in pekingese SMF 35611, but it fuses to the lamina cribrosa caudally. In this individual a suture to the frontal proves to regard this ridge still as a turbinal. Although on the left side in pekingese NMBE 1051962 a suture to the frontal is observed too, the respective structure is a thick crest. Its morphology resembles the shape on the other side and in pekingese NMBE 1051965 in which the structure is fused with the bone. Hence, this bony septum is no longer defined as a turbinal in the two named pekingese. **Interturbinal β** is more like in the Eurasian wolf, though it is a simpler double scroll: in both chins and in pekingese SMF 35611 and NMBE 1051965 (left side) it merges into the lamina horizontalis rostrally and runs onto the frontal. A variation is an additional rostral fusion to ethmoturbinal I in two pekingese, either to its epiturbinal in NMBE 1051962 and NMBE 1051965, in each on the right side, or to its stem on the left side in NMBE 1051962. Caudally in pekingese NMBE 1051965 interturbinal β fuses as a straight lamella to the frontal on the left side, whereas on the right side it separates as a double scroll into a lateral lamella that ends on the transition between the lamina horizontalis and the frontal, and into a medial lamella that forms a process within the pars intermedia.

The most obvious difference in **ethmoturbinal I** to the Eurasian wolf is its less complicate shape in the chin and the pekingese. Both anterior processes are absent on the right side in pekingese SMF 35611and the anterior lamina and the posterior lamina are not distinguishable. Instead, ethmoturbinal I is attached to the lamina cribrosa rostrodorsally and to the lamina horizontalis caudoventrally (**Fig. 24**H, J). Due to the rostral shortening of ethmoturbinal I in this specimen it is less affected by the palate's elevation (**Fig. 24**B). On the left side in pekingese SMF 35611 and in the other four individuals the two laminae of ethmoturbinal I are present and unite on the lamina horizontalis. The anterior lamina of ethmoturbinal I has a slightly dendritic anterior process in pekingese NMBE 1051965 and on the left side in SMF 35611, and a straight anterior process in the two chins (e.g., NMBE 1051951, **Fig. 27**D), and pekingese NMBE 1051962. The anterior lamina of ethmoturbinal I forms a double scroll on the lamina horizontalis (e.g., chin ZMB_MAM 7436, **Fig. 26**E), except the left side in pekingese SMF 35611 in which it is a simpler single scroll. Pekingese NMBE 1051962 is lacking the anterior process of the posterior lamina of ethmoturbinal I. Instead, the latter merges rostrally into the anterior lamina of ethmoturbinal I (**Fig. 23**E–G). The shape of the anterior process of the posterior lamina of ethmoturbinal I present in the other four specimens including the left side in pekingese SMF 35611 is identical to the anterior lamina of ethmoturbinal I within each specimen. More caudally, the posterior lamina of ethmoturbinal I is single scrolled in chin ZMB_MAM 7436 and on the left side in pekingese

NMBE 1051965 (**Fig.25**E, F), and double scrolled on the right side in NMBE 1051965 and in chin NMBE 1051951. The double scroll in the posterior lamina of ethmoturbinal I on the left side in pekingese SMF 35611 is indicated by two small distal ridges. A lamella which forms a bulbous rostral process dorsolateral to ethmoturbinal I and attaches to its stem as a double scroll on the left side in SMF 35611 is identical to the topography described in the Eurasian wolf's epiturbinal (**Fig. 24**J, K). The epiturbinal in the four other specimens merges into the stem of ethmoturbinal I rostrally. It is straight in pekingese NMBE 1051965, separates caudally into two single scrolls in pekingese NMBE 1051962, and complicates to a double scroll in both chins. Ethmoturbinal I fuses to the lamina cribrosa caudally. **Ethmoturbinal II** is lacking a rostral process in pekingese SMF 35611. In chin ZMB_MAM 7436 the rostral process is displaced rostroventral to the lamina terminalis. A similar dislocation is observed on the right side in chin NMBE 1051951 in which the process additionally extends into the pars maxillonasoturbinalis (**Fig. 27**E–G). On the left side in the mentioned chin and in pekingese NMBE 1051962 and NMBE 1051965 the rostral process of ethmoturbinal II is located within the ethmoturbinal recess dorsal to the lamina terminalis. The process in these two pekingese is small and tip-like. The stem of ethmoturbinal II merges rostrally into the lamina terminalis in the two pekingese NMBE 1051965 and SMF 35611 (left side). On the right side in pekingese SMF 35611 and in NMBE 1051962 and the two chins the stem is attached with its base to the lamina horizontalis and continuous with the lamina terminalis. In all five specimens ethmoturbinal II forms multiple scrolls and runs onto the lamina horizontalis, and caudal to it onto the palatine and the orbitosphenoid (e.g., chin ZMB_MAM 7436, **Fig. 26**F–H). Whereas in the Eurasian wolf ethmoturbinal II ends on the lamina cribrosa within the pars ethmoturbinalis, in the two chins and the three pekingese it extends into the orbitosphenoid; either as a process into the sphenoid sinus as observed in chin ZMB_MAM 7436 and pekingese NMBE 1051962, SMF 35611 and on the right side in NMBE 1051965, or it merges into the orbitosphenoid like in chin NMBE 1051951 and on the left side in pekingese NMBE 1051965. **Ethmoturbinal III** varies from the pattern which is described in the Eurasian wolf in its rostral end: it fuses as a straight lamella to the lamina terminalis (e.g., pekingese NMBE 1051962, **Fig. 23**K) except chin NMBE 1051951 in which ethmoturbinal III is attached rostrally to the lamina horizontalis and continuous with the lamina terminalis (**Fig. 27**K). It forms a single scroll on the left side in chin ZMB_MAM 7436 and in pekingese NMBE 1051965 and SMF 35611, and a double scroll in chin NMBE 1051951 and on the right side in ZMB_MAM 7436 and pekingese NMBE 1051962. Ethmoturbinal III has different attachments in its caudal course. In chin NMBE 1051951 it runs onto the lamina horizontalis and caudal to it along the palatine onto the orbitosphenoid; in pekingese NMBE 1051965 it curves along the lamina terminalis to the orbitosphenoid, and in chin ZMB_MAM 7436 and pekingese NMBE 1051962 and SMF 35611 it is attached to the palatine for a short distance before it shifts to the orbitosphenoid. The caudal end of ethmoturbinal III resembles the Eurasian wolf (e.g., pekingese SMF 35611, **Fig. 24**N).

Interturbinal α is present in all five individuals, but both chins (e.g., NMBE 1051951, **Fig. 27**C) and pekingese SMF 35611 have an additional interturbinal ventral to the prominent one (**Table 5**). Interturbinal α has no rostral process in any of the specimens, but like in the Eurasian wolf its stem runs rostrally onto ethmoturbinal II in four of them. Pekingese NMBE 1051962 shows a variation, as interturbinal α reaches slightly more rostrally than ethmoturbinal II and has a similar rostral connection with the lamina horizontalis and the lamina terminalis (**Fig. 23**H). The interturbinal's shape complicates to double scroll, in pekingese NMBE 1051965 it is single scrolled. As in pekingese NMBE 1051962 interturbinal α fuses onto the lamina horizontalis rostrally, it has no connection with ethmoturbinal II, but with ethmoturbinal I caudally. The other four individuals are comparable to the Eurasian wolf in the interturbinal's topography; and its caudal end does not differ from the ancestral pattern in any of the five specimens. The additional interturbinal in the two chins merges into the lamina horizontalis anteriorly, runs as a straight to curved lamella onto the palatine, and fuses to the lamina cribrosa in NMBE 1051951 and to the palatine in ZMB_MAM 7436. The single scrolled additional interturbinal in pekingese SMF 35611 (not depicted in the given cross sections) has no free margin in its entire length. Consequently, it cannot be determined which side is the base and which side the initially free distal end. On the right side this 'double bases' are fused to the lamina horizontalis rostrally and the dorsal one runs onto the frontal; on the left side the dorsal end is attached to the frontal in its entire course. On both sides in the pekingese specimen the additional interturbinal fuses to the frontal caudally.

SMALL MOLOSSIAN TYPE DOGS (pug)

The shortening of the pugs' snout affects the pars intermedia mainly in its caudal part through a proportionally caudodorsal extension of frontoturbinal 1 and 2. Within the pars ethmoturbinalis the highest variation from the Eurasian wolf is in the rostral part (**Fig. 28**B, C). All three ethmoturbinals and interturbinal α are shortened, combined with a rostral reduction of ethmoturbinal I and II, and a lesser caudal displacement of ethmoturbinal II and III (**Figs. 28–35**). In lateral view the caudal shape of the turbinal skeleton looks like the curve of a power function: the frontoturbinals end nearly vertical to each other, the ethmoturbinals are placed caudoventral to each other (**Fig. 34**B). In both modern individuals (NMBE 1051937, NMBE 1052345) the maxilloturbinal is affected by the palate's elevation and shows an oblique orientation. In the ancient pugs the maxilloturbinal is -in different intensity- rostrocaudally shortened in comparison to the Eurasian wolf (e.g., [MfN] 2620, **Fig. 32**B, C). The overlap by the anterior process of the anterior lamina of ethmoturbinal I is shorter than in the Eurasian wolf as well (see p. 63). The frontoturbinals do not vary in their shape and position within the turbinal skeleton compared to the Eurasian wolf. Like frontoturbinal 1 frontoturbinal 2 follows a rostroventral to caudodorsal course and extends more caudally than frontoturbinal 1 (e.g., ancient specimen [MfN]

2657, **Fig. 34**B, M). As the forehead in the brachycephalic breed is generally steeper than in the Eurasian wolf, both frontoturbinals follow the shape of the frontal bone they are fixed to. Frontoturbinal 3, however, is less affected by the shortening of the snout. Compared to the segmented Eurasian wolf specimen, interturbinal β is not markedly shortened (e.g., in the ancient types SMF 16284 and [MfN] 2620, **Fig. 32**C). In all pugs both anterior processes of ethmoturbinal I protrude rostrodorsally. The anterior process of the anterior lamina of ethmoturbinal I is located medial to the maxilloturbinal. This position is more homologous with the anterior process of the posterior lamina of ethmoturbinal I in the Eurasian wolf whose anterior process of the anterior lamina of ethmoturbinal I expands additionally dorsal to the maxilloturbinal. Except for the modern type NMBE 1051937 (see p. 63) in all pugs the olfactory turbinals are situated dorsal to the lamina terminalis, whereas the maxilloturbinal is positioned within the respiratory pathway.

In the µCT cross sections all adult pugs show the double scrolled type in their **maxilloturbinal** (e.g., [MfN] 1845, **Fig. 31**D, E). The two modern types NMBE 1051937 and NMBE 1052345 are lacking the lateral scroll in their ventral lamella; instead in NMBE 1051937 its dendritic ventral lamella is more or less straight (**Figs. 28**D**; 29**F, G). The basic form (a dendritic lateral scroll which is described in the Eurasian wolf) is observed in the six ancient types except [MfN] 2657 which more tends to a double scroll; nevertheless, the lateral scroll in the ventral lamella is pronounced in this specimen (**Fig. 34**D). The shape of the dorsal lamella is single scrolled in the modern type NMBE 1052345 and the ancient types [MfN] 2657 and [MfN] 2630 (left side), double scrolled in the modern type NMBE 1051937, and dendritic on the right side in [MfN] 2630 and the ancient types SMF 16284, [MfN] 1845, [MfN] 2620 and ZMB_MAM 30980. The maxilloturbinal's secondary and tertiary lamellae leave some space to the maxillary and the nasal septum in both modern types and the ancient type [MfN] 2657. In the others, especially SMF 16284 (**Fig. 30**D), the space is closer. In the modern pug NMBE 1051937 both lamellae are shifted towards each other; the ventral lamella is situated rostrally, and the dorsal lamella follows caudally (**Fig. 28**B, C). On the left side in the second modern type NMBE 1052345 the ventral and the dorsal lamella are fixed as separated lamellae to the maxillary rostrally and unite caudally. This leads to a process-like shape of the dorsal lamella in lateral view of the virtual 3D model (**Fig. 29**D, E). The **nasoturbinal** is a straight up to curved lamella in cross sectional view. In the ancient pug [MfN] 1845 no nasoturbinal is observed on the left side (**Fig. 31**B–E) and on the left side in the modern type NMBE 1052345 it is reduced to a rostral tip of the lamina semicircularis. The ancient type SMF 16284 has a thickened nasoturbinal on the right side, whereas on the left side the nasoturbinal is as thin as in the Eurasian wolf, but shortened rostrally. In the modern individual NMBE 1051937 the nasoturbinal is a short ventral ridge on the lamina semicircularis. The caudal fusion of the nasoturbinal with the lamina semicircularis does not differ from that in the Eurasian wolf.

The **lamina semicircularis** shows the greatest variation in the modern pug NMBE 1052345 whose ventral lamina lies rostrally and the dorsal lamina follows caudally (**Fig. 29**G, H). Both laminae are straight, but the uncinate process and the caudal connection with the lamina cribrosa are present (**Fig. 29**B–E). In the other seven pugs the position of the two laminae towards each other, the dorsal lamina's caudal end, and the ventral lamina's pattern are comparable to the Eurasian wolf. In the modern type NMBE 1051937 and the ancient individual [MfN] 2657 the ventral lamina is straight. The dorsal lamina is simpler built than in the Eurasian wolf and complicates in the ancient pug ZMB_MAM 30980 to double scroll, in all other individuals it is single scrolled. A small accessory lamella dorsal on the stem of the lamina semicircularis is present in the ancient type [MfN] 2630. It fuses to the stem caudally and runs onto the medial septum of the nasal rostrally.

On its rostral end **frontoturbinal 1** fuses to the maxillary and is additionally continuous with the lamina semicircularis (ancient types SMF 16284, [MfN] 1845, ZMB_MAM 30980) or like in the Eurasian wolf with the lamina horizontalis (ancient types [MfN] 2620, [MfN] 2630, [MfN] 2657, and both modern types). Generally, this turbinal has a straight rostral end, but is double scrolled in the ancient type SMF 16284, multiple scrolled in the ancient type [MfN] 2657, and dendritic in the ancient pug [MfN] 1845. Frontoturbinal 1 changes to a double scroll caudally, in the ancient type ZMB_MAM 30980 to multiple scrolls, and runs onto the frontal in all pugs. Frontoturbinal 1 fuses to the lamina cribrosa in the modern type NMBE 1052345 (**Fig. 29**H); in the other sampled skulls it enters the more or less strongly reduced frontal sinus and either forms a process (e.g., the second modern type NMBE 1051937, **Fig. 28**K, L) or fuses to one of the sinus' septa (e.g., on the right side in the ancient pug [MfN] 2630). The variation in the modern pug NMBE 1052345 has no effect on the caudal extension of frontoturbinal 1 compared to its conspecifics (**Fig. 29**B, D vs. e.g., ancient individual [MfN] 2620, **Fig. 32**B). Like in the Eurasian wolf ZMB_MAM 815 **frontoturbinal 2** is rostrally attached to the maxillary and fused to the lamina horizontalis in all individuals except the right side of the ancient type [MfN] 2620 that shows a fusion to the lamina semicircularis, and the right side of the ancient type [MfN] 2630 in which frontoturbinal 2 is attached to the frontal and fused to frontoturbinal 1 (**Fig. 33**J, K). Frontoturbinal 2 ends anteriorly as a straight lamella and becomes double scrolled posteriorly (ancient types [MfN] 2620, SMF 16284, both modern types) or multiple scrolled ([MfN] 2630, ZMB_MAM 30980). In the two ancient pugs [MfN] 1845 and [MfN] 2657 frontoturbinal 2 is multiple scrolled in its rostral beginning and simplifies caudally to a double scroll. Its topography and caudal end are like in frontoturbinal 1: in the modern type NMBE 1052345 it merges into the lamina cribrosa, in NMBE 1051937 and all ancient pugs it forms a process within the frontal sinus or merges with its septum. **Frontoturbinal 3** is fused to the lamina horizontalis rostrally like in the Eurasian wolf. In two specimens of the ancient type frontoturbinal 3 is continuous with the lamina horizontalis and attached to the frontal on the right side in [MfN] 1845, and to the maxillary on the left side in [MfN] 2657, respectively. Additionally, in these two specimens a short rostral process is present, but in

[MfN] 2657 just on the right side. In the two ancient pugs ZMB_MAM 30980 (**Fig. 35**C) and SMF 16284 two lamellae unite on the lamina horizontalis and form the double scrolled frontoturbinal 3; in the latter specimen the medial lamella is continuous with ethmoturbinal I rostrally. On the right side in the ancient representative [MfN] 2657 frontoturbinal 3 ends rostrally with multiple scrolls similar to frontoturbinal 1 and 2. Posteriorly, frontoturbinal 3 simplifies to a double scroll on both sides in this specimen. In the ancient pug [MfN] 1845 a double scroll simplifies caudally to a single scroll (**Fig. 31**H–L). Frontoturbinal 3 remains double scrolled on the left side in both the modern pug NMBE 1051937 and the ancient specimen [MfN] 2657. A rostrocaudal complication from a straight to a double scrolled lamella is observed on the right side in NMBE 1051937, in its modern conspecific NMBE 1052345, and on the left side in the ancient pug [MfN] 2620. In the ancient individual [MfN] 2630 a single scroll becomes double scrolled, and on the right side in the ancient specimen [MfN] 2620 a double scroll forms multiple scrolls caudally. Whereas the general topography of frontoturbinal 3 does not vary from frontoturbinal 1 and 2, it fuses caudally to the lamina cribrosa in all specimens. Frontoturbinal 3 is variably shortened in its length; in one pug stronger (e.g., the ancient type [MfN] 1845, **Fig. 31**C), in the others slighter (e.g., both ancient pugs SMF 16284 and ZMB_MAM 30980, **Fig. 35**C).

Regarding the prominent interturbinals within the frontoturbinal recess interturbinal δ and β are present in all pugs, but interturbinal γ just in the two ancient specimens [MfN] 2620 and ZMB_MAM 30980 (**Table 5**). In the ancient pug SMF 16284 the frontal and the turbinals attached to it are caudally destroyed between the lamina semicircularis and frontoturbinal 2 due to the sawn forehead. On its right side the rostral part of interturbinal δ is present. On the left side of the asymmetric skull the nasal cavity extends more dorsally and is consequently stronger affected by the destruction. A fragmented lamella that seems homologous to interturbinal δ (see below) is not fixed to a bone. The presence of interturbinal γ cannot be verified on that side in this specimen. The ancient pug [MfN] 2630 has one additional interturbinal between frontoturbinal 2 and 3 on the right side. Other additional interturbinals are observed between frontoturbinal 3 and ethmoturbinal I in two ancient types, namely one on the left side in ZMB_MAM 30980 dorsal to interturbinal β, and one on both sides of interturbinal β on the right side in [MfN] 2657. The rostral end of **interturbinal δ** is attached to the nasal in the modern pug NMBE 1052345 and the ancient types [MfN] 2630, [MfN] 2657, and ZMB_MAM 30980, or to its suture, either next to the maxillary like in the modern type NMBE 1051937 and the ancient type [MfN] 1845, or next to the frontal as observed in the ancient pugs [MfN] 2620 and SMF 16284 (right side). The shape of interturbinal δ is a single scroll which is also identified in the fragmented lamella on the left side in the ancient pug SMF 16284 (see above). Exceptions are the right side in the modern type NMBE 1051937 which has a simpler straight lamella, and the two ancient pugs, [MfN] 2630 and ZMB_MAM 30980 which have a double scroll. On the left side in the ancient representative [MfN] 1845 a short lamella separates from interturbinal δ. In its caudomedial course onto the frontal and its

fusion to the septal process of the frontal interturbinal δ resembles the pattern observed in the Eurasian wolf (e.g., ancient specimen ZMB_MAM 30980, **Fig. 35**J). In the ancient pug [MfN] 2630 it differs in that it fuses to the frontal rostral to the lamina cribrosa. The three-dimensional shape of interturbinal δ shows a strong variation between the ancient types in medial view: in ZMB_MAM 30980 it is long and slender (**Fig. 35**D), whereas in [MfN] 1845 it is shortened in its length and simultaneously broadened venterodorsally causing a more or less triangle shape (**Fig. 31**B). In the modern pug NMBE 1052345 interturbinal δ is extremely shortened and its anterior end is oriented dorsally; it has a rostrodorsal buckling and a small caudoventral process-like ending on the left and the right side of the nasal cavity (**Fig. 29**B, D). **Interturbinal γ**, that has a prominent characteristic in the Eurasian wolf, is small, straight, and reduced in the two ancient types [MfN] 2620 and ZMB_MAM 30980 (**Figs. 32**C, J; **35B, C, K–M**). On the right side in [MfN] 2620 it is a bony crest. Despite its reduced size interturbinal γ forms a septum of the frontal sinus in these two specimens. In the other ancient pugs ([MfN] 1845, [MfN] 2630, [MfN] 2657) and the two modern types the frontal sinus is too small to identify an associated interturbinal. The presence of interturbinal γ in the pug with the sawn skull, SMF 16284 is speculative. **Interturbinal β** ends rostrally on the lamina horizontalis in the modern types NMBE 1052345 and NMBE 1051937 (right side), and the ancient types SMF 16284 (right side) and [MfN] 2657 (left side). Additionally, interturbinal β is continuous with frontoturbinal 3 on the left side in the modern pug NMBE 1051937 and the ancient specimens SMF 16284 (left side), [MfN] 2630 (left side), [MfN] 2657 (right side), and ZMB_MAM 30980, or with ethmoturbinal I in the ancient pug [MfN] 1845. On the right side in the ancient pug [MfN] 2630 the double scrolled interturbinal β is separated into a medial lamella which merges into ethmoturbinal I and frontoturbinal 3 rostrally, and a lateral lamella which merges into the lamina horizontalis. In the ancient pug [MfN] 2620 interturbinal β starts rostrally with two lamellae too, which unite on the lamina horizontalis. In this specimen, the ventral lamella is continuous with ethmoturbinal I on the lamina horizontalis, the dorsal lamella arises from the lamina horizontalis without further fusions. Rostrally, interturbinal β is a straight lamella in the modern pugs NMBE 1051937 (right side) and NMBE 1052345, and in the ancient pugs [MfN] 2620 and ZMB_MAM 30980 (**Fig. 35**G), and single scrolled on the left side in NMBE 1051937, and on the left side in both ancient types SMF 16284 and [MfN] 2630. Caudally, in all pugs interturbinal β changes to a double scroll. In the ancient pugs [MfN] 2657 and on the right side in SMF 16284 it is double scrolled in its entire length. Interturbinal β simplifies caudally from a double to a single scroll in the ancient specimen [MfN] 1845. Its general topography and caudal end are identical to the Eurasian wolf among the entire sample. Among the shorter snouted pugs of ancient and modern type interturbinal β is obliquely oriented parallel to the airorhynchic palate and has a convex dorsal shape (e.g., in the ancient specimen [MfN] 2630, **Fig. 33**E). The additional interturbinal between frontoturbinal 2 and 3 present on the right side in the ancient pug [MfN] 2630 is attached to the frontal in its entire length and fuses to it rostral to the lamina cribrosa. It forms a single scroll and becomes crest-like cau-

dally. Between frontoturbinal 3 and ethmoturbinal I two types of additional interturbinals are observed in two ancient pugs. The one ventral to frontoturbinal 3 merges anteriorly into the lamina horizontalis in [MfN] 2657 and merges into the stem of frontoturbinal 3 on the right side in ZMB_MAM 30980. Caudally, the additional interturbinal forms a double scroll and shifts to the frontal on which it ends. The second additional interturbinal dorsolateral to ethmoturbinal I on the right side in [MfN] 2657 is rostrally continuous with interturbinal β on the lamina horizontalis, forms posteriorly a double scroll and runs onto the frontal on which it fuses to the lamina cribrosa.

The dorsal orientation of the anterior process of both the anterior and the posterior lamina of **ethmoturbinal I** is variably pronounced in the 3D models. In the modern pug NMBE 1051937 both laminae of ethmoturbinal I on the left side and the anterior lamina of ethmoturbinal I on the right side are extending nearly rectangular in medial view. In the two ancient types ZMB_MAM 30980 and [MfN] 2657 the rostrodorsal curvature of the anterior and the posterior lamina of ethmoturbinal I is the slightest developed among the pug sample (**Fig. 34**B). The anterior process of the posterior lamina of ethmoturbinal I on the right side in the modern pug NMBE 1051937 extends nearly vertically ventral and forms a knob-like ending (**Fig. 28**B, C, E, F). Together with the rostral process of ethmoturbinal II it is displaced caudal to the maxilloturbinal, and rostral to the lamina terminalis and to the nasopharyngeal duct. Consequently, both processes are located within the respiratory pathway. On the left side in the modern pug NMBE 1052345 a deep dorsal notch in the medial part of ethmoturbinal I constricts the anterior process of its anterior lamina (**Fig. 29**D). The anterior process of the anterior lamina of ethmoturbinal I extends rostrally in different intensities (e.g., ancient pug [MfN] 1845, **Fig. 31**B, D, E). In the ancient representative [MfN] 2620 the anterior process of the anterior lamina of ethmoturbinal I is a slender tip (**Fig. 32**B); on the right side in the modern type NMBE 1052345 ethmoturbinal I extends as far rostrally as the maxilloturbinal covering nearly the half of the latter in medial view (**Fig. 29**B). In contrast, in the ancient pug [MfN] 2657 a gap between both turbinals is observed (**Fig. 34**B, C). In the six ancient pugs the anterior process is present in both laminae of ethmoturbinal I and they are at least slightly dendritic. The anterior processes of the two modern pugs differ between the two specimens and from the ancient type. The anterior lamina of ethmoturbinal I forms a dendritic anterior process in NMBE 1051937. The anterior lamina of ethmoturbinal I on the left side in NMBE 1052345 extends rostrally with a straight process, the anterior process of the posterior lamina of ethmoturbinal I is completely reduced (**Fig. 29**D, J, K). On the right side in NMBE 1052345 the anterior process of the anterior lamina of ethmoturbinal I is slightly dendritic, the anterior process of the posterior lamina of ethmoturbinal I remains a straight lamella (**Fig. 29**H). Caudal to the fusion of both laminae on the lamina horizontalis the anterior lamina of ethmoturbinal I forms a double scroll among the entire pug sample (e.g., the ancient representative ZMB_MAM 30980, **Fig. 35**H). The posterior lamina of ethmoturbinal I is single scrolled rostrally in the two ancient types SMF 16284 and [MfN] 2620, and fuses to a double scroll with an epiturbinal-like lamella (e.g., SMF 16284, **Fig. 30**H–K). The single scrolled

posterior lamina of ethmoturbinal I in the ancient pug [MfN] 2657 complicates to a double scroll without any fusions. In the modern pug NMBE 1051937 (right side) and the ancient pugs [MfN] 1845, [MfN] 2630 (right side), [MfN] 2657 (**Fig. 34**K, L), and ZMB_MAM 30980 (right side) the double scrolled posterior lamina of ethmoturbinal I caudally separates into two single scrolls on the stem of ethmoturbinal I. One ancient individual, ZMB_MAM 30980, is lacking an epiturbinal dorsally on the stem of ethmoturbinal I. The modern type NMBE 1052345 has a short and straight, the ancient type [MfN] 1845 a straight to curved, the ancient specimen SMF 16284 (left side) a single scrolled, and the ancient type [MfN] 2657 a double scrolled epiturbinal. The epiturbinal of ethmoturbinal I becomes single scrolled caudally through a separation from a double scrolled lamella on the right side in the ancient type SMF 16284 and the modern specimen NMBE 1051937, and vice versa in the two ancient types [MfN] 2620 and [MfN] 2630, namely double scrolled caudally through fusing with a further lamella. Two ancient types have a second epiturbinal-like lamella proximal to the first one on the stem of ethmoturbinal I. In SMF 16284 it is short and crest-like, and in [MfN] 1845 it is present on the right side and straight. Ethmoturbinal I fuses to the lamina cribrosa with a dorsal curvature (e.g., [MfN] 2620, **Fig. 32**B, K, L). The shortening of the breed's snout affects the rostral part of **ethmoturbinal II** in different degrees. Ethmoturbinal II is lacking the rostral process on the left side in each of the two modern pugs and in the ancient type [MfN] 2657. Within the ancient representatives, ZMB_MAM 30980 resembles most the Eurasian wolf; SMF 16284 and [MfN] 1845 show a rostral shortening and a caudal shift. In [MfN] 2620 the rostral reduction of ethmoturbinal II results in a clear gap to the maxilloturbinal, and in the modern pug NMBE 1051937 the rostral process of ethmoturbinal II extends ventrally with a knob-like tip similar to the anterior process of the posterior lamina of ethmoturbinal I. In the modern pugs the stem of ethmoturbinal II merges into the lamina horizontalis rostrally and in NMBE 1051937 it is additionally continuous with the lamina terminalis (**Fig. 28**G). In the ancient specimen [MfN] 2657 ethmoturbinal II runs anteriorly onto ethmoturbinal I (**Fig. 34**H). In the other ancient pugs and on the right side in both modern specimens a rostral process of ethmoturbinal II is positioned medial to ethmoturbinal I. It is straight in the two modern pugs and the ancient individual [MfN] 2630, single scrolled in the ancient skull [MfN] 2620, and slightly dendritic in the ancient pugs SMF 16284, [MfN] 1845, and ZMB_MAM 30980. In all investigated pugs ethmoturbinal II forms multiple scrolls and curves caudal to the lamina horizontalis along the palatine to the orbitosphenoid (e.g., [MfN] 2620, **Fig. 32**K–M). In the ancient specimen [MfN] 1845 ethmoturbinal II is additionally attached to the lamina terminalis before running onto the lamina horizontalis. On the left side in the ancient type ZMB_MAM 30980 ethmoturbinal II runs from ethmoturbinal I directly onto the palatine with no contact to the lamina horizontalis. It ends as a process within the sphenoid sinus; in the ancient pug [MfN] 2657 ethmoturbinal II fuses to the orbitosphenoid. Rostrally, **Ethmoturbinal III** runs as a straight lamella onto the lamina horizontalis on the right side in both modern types (e.g., NMBE 1051937, **Fig. 28**K), and on both sides in the ancient specimen [MfN] 2630. It is additionally continuous with the stem of ethmoturbinal II on the left side in the modern type NMBE 1052345 and in the

ancient pug SMF 16284, and with the lamina terminalis in the ancient representative ZMB_MAM 30980. On the left side in the modern pug NMBE 1051937 and the ancient pug [MfN] 2657 (**Fig. 34**M) ethmoturbinal III fuses rostrally only to the lamina terminalis. In two ancient specimens ethmoturbinal III merges into ethmoturbinal II, in [MfN] 2620 into its stem (**Fig. 32**H), and in [MfN] 1845 more proximal on the fusion between ethmoturbinal II and the lamina terminalis. Ethmoturbinal III is the least complex, namely single scrolled, in the modern specimen NMBE 1051937, on the left side in NMBE 1052345, and in the two ancient types SMF 16284 and [MfN] 2630. A more complicate double scroll is observed on the right side in the modern pug NMBE 1052345 and the ancient representatives [MfN] 1845, [MfN] 2620, [MfN] 2657, ZMB_MAM 30980. Ethmoturbinal III runs along the lamina terminalis in the modern specimens NMBE 1051937 (right side) and NMBE 1052345 (left side), and in the ancient pug [MfN] 1845, and along the lamina horizontalis in the two ancient pugs [MfN] 2620 and [MfN] 2657 (left side). Caudally, ethmoturbinal III curves along the palatine to the orbitosphenoid in all specimens and forms a process within the sphenoid sinus (e.g., ancient type [MfN] 2620, **Fig. 32**N). Its caudal extension is slightly (e.g., ancient type [MfN] 2620, **Fig. 32**B) or stronger pronounced (e.g., ancient pug SMF 16284, **Fig. 30**B).

Only in the ancient type [MfN] 2657 **interturbinal α** has a rostral process (**Fig. 34**J). In the modern pug NMBE 1052345 it ends on the lamina horizontalis rostrally and on the right side it is additionally continuous with ethmoturbinal II. In the other pugs interturbinal α merges with ethmoturbinal II. It is double scrolled among the entire pug sample. Three pug specimens vary in the topography of interturbinal α from the Eurasian wolf in which it runs from ethmoturbinal II via the lamina semicircularis onto the stem of ethmoturbinal I: in the modern pug NMBE 1052345 (left side) interturbinal α does not touch ethmoturbinal II. In the ancient type [MfN] 1845 (left side) interturbinal α approaches the stem of ethmoturbinal I without merging into it, but it is attached to the palatine caudal to the lamina horizontalis. In the ancient pug ZMB_MAM 30980 (left side) interturbinal α runs from ethmoturbinal II directly onto the stem of ethmoturbinal I where both fuse. In all specimens interturbinal α merges into the lamina cribrosa (e.g., ancient type ZMB_MAM 30980, **Fig. 35**M) except for the modern pug NMBE 1052345 in which interturbinal α forms a caudal process within the sphenoid sinus. This process appears in the reconstructed 3D model with a conspicuously convex ventral shape (**Fig. 29**C, D). In lateral view interturbinal α is shortened in the two modern specimens, whereas e.g., in the ancient type SMF 16284 it is elongated and thus more similar to the Eurasian wolf (**Fig. 30**B, C). An additional interturbinal within the pars ethmoturbinalis is present ventral to interturbinal α in one pug, namely the ancient specimen [MfN] 2657 (**Table 5**; **Fig. 34**B, C, N). Rostrally, this interturbinal fuses to the lamina horizontalis on the right side and to the stem of ethmoturbinal II on the left side. Both patterns are also represented in the Eurasian wolf. The additional interturbinal forms a single scroll and runs onto the orbitosphenoid caudal to the lamina horizontalis (right side) or from ethmoturbinal II

along the palatine onto the orbitosphenoid (left side). The fusion of the additional interturbinal is identical to the pattern observed in the Eurasian wolf.

LONG-HAIRED OR FRINGED SIGHTHOUNDS (saluki and borzoi)

The two segmented borzois resemble Eurasian wolf ZMB_MAM 93307 in the morphology of their turbinal skeleton. Within the **pars maxillonasoturbinalis** no variation is observed in the borzois (**Figs. 36–41**) and the saluki (**Fig. 42**) compared to the Eurasian wolf. Also similar to their ancestor in both breeds the lamina semicircularis has two laminae. All three ethmoturbinals are as long as in the Eurasian wolf. None of them is significantly reduced rostrally or displaced by the maxilloturbinal (**Figs. 36**B, C; **40**B, C). Interturbinal α does not vary in its shape from the ancestral pattern either. Within the pars intermedia, the caudal process of both frontoturbinal 1 and 2 has a slight ventral buckling caused by the declination of the borzoi's face which is more pronounced in specimen NMBE 1051164 (**Fig. 36**B, C). Frontoturbinal 3 is lesser affected by the breed's klinorhynchic head shape, as it is shorter posteriorly.

In [MfN] 1403 the nasoturbinal overlays the rostral tip of the anterior process of the anterior lamina of ethmoturbinal I in medial view (**Fig. 40**B). The ventral lamina of the **lamina semicircularis** differs in its form in borzoi [MfN] 7374 in being double (to multiple) scrolled and having an additional uncinate process-like structure within the pars intermedia caudal to the uncinate process. A similar additional process is present in the saluki. In contrast to Eurasian wolf ZMB_MAM 93307 and borzoi [MfN] 1403, in borzoi NMBE 1051164 a well-developed uncinate process is observed in the 3D model (**Fig. 36**C) that is comparable to the two non-segmented Eurasian wolves according to the µCT cross sections. The uncinate process in borzoi NMBE 1051180 ends on the right side rostromedial to the lamina horizontalis in the confluent area between the maxillary sinus and the pars intermedia, and on the left side lateral to the lamina horizontalis within the maxillary sinus. The dorsal lamella of the lamina semicircularis has in borzoi NMBE 1051164 a dendritic shape (**Fig. 36**H), whereas in [MfN] 1403 it is a simpler single (**Fig. 40**F) to double scroll. The small accessory lamella dorsal on the stem of the lamina semicircularis is absent on the left side in borzoi [MfN] 1403, and in the saluki it is present on the left side on which it extends rostrally onto the medial septum of the nasal. Borzoi [MfN] 7374 has increased the number of accessory lamellae to two on the right side and three on the left side.

Frontoturbinal 1 ends rostrally on the maxillary; it is not connected to the lamina horizontalis like in the Eurasian wolf (**Fig. 39**D). Rostrally, its shape is a single scroll that caudally complicates to dendritic in borzoi NMBE 1051164 (**Fig. 38**E). In borzoi [MfN] 1403 frontoturbinal 1 is rostrally a less complicate double scroll. **Frontoturbinal 2** fuses to the lamina horizontalis in the two borzois NMBE 1051164 and [MfN] 7374 and contacts the maxillary more caudally (**Fig. 41**D). In contrast, in

the four other borzois NMBE 1051166, NMBE 1051180, NMBE 1052706, and [MfN] 1403 (**Fig. 40**F) and in the saluki frontoturbinal 2 resembles Eurasian wolf ZMB_MAM 815: it is attached to the maxillary and fuses to the lamina horizontalis rostrally. Frontoturbinal 2 is multiple scrolled anteriorly in borzoi [MfN] 1403. In its caudal course it runs from the maxillary onto the frontal in all specimens. In borzoi NMBE 1051164, [MfN] 1403 (left side), and [MfN] 7374 frontoturbinal 2 runs onto the septal process of the frontal for a short distance, whereas in the saluki it persists on this process caudally. Like frontoturbinal 1 frontoturbinal 2 forms a process within the frontal sinus in a separate chamber. **Frontoturbinal 3** varies in borzoi NMBE 1051164 and in the saluki from the Eurasian wolf. In the borzoi its anterior end is continuous with the epiturbinal of ethmoturbinal I on the lamina horizontalis. On this borzoi's left side a further lamella that ends on the lamina horizontalis merges with frontoturbinal 3, and then both run onto the frontal. On the right side, frontoturbinal 3 fuses with a similar further lamella on the frontal. Frontoturbinal 3 is rostrally single scrolled and complicates more caudally to dendritic in borzoi NMBE 1051164. In the saluki frontoturbinal 3 is continuous with frontoturbinal 2 on the lamina horizontalis rostrally. On the left side in this specimen a medial single scrolled lamella unites on the lamina horizontalis with a lateral double scrolled lamella that runs off the frontal to form the dendritic shaped frontoturbinal 3. On the right side in the saluki frontoturbinal 3 does not separate into two lamellae but is double scrolled rostrally and complicates to dendritic caudally. In the topography and caudal end of frontoturbinal 3 all sighthounds correspond to the Eurasian wolf.

The borzois have an enlarged number of interturbinals within the pars intermedia compared to the Eurasian wolf (three to seven) that ranges from four in [MfN] 1403 and on the right side in NMBE 1051180, to a maximum of eight on the right side in NMBE 1051166 (**Table 6**). The saluki has the three prominent interturbinals, but is lacking additional interturbinals. Beside the three prominent ones, additional interturbinals are present at each position between the lamina semicircularis and ethmoturbinal I, namely medial and lateral to interturbinal δ, lateral to interturbinal γ, between frontoturbinal 2 and 3, and dorsal and ventral to interturbinal β, whereas in the Eurasian wolf additional interturbinals are restricted medial to interturbinal δ and ventral to interturbinal β (**Table 5**). One additional interturbinal medial to interturbinal δ is observed on both sides in NMBE 1051164, NMBE 1052706 and on the left side in NMBE 1051166. On the right side of the latter specimen the number of additional interturbinals is increased to three. Lateral to interturbinal δ one additional interturbinal is present in NMBE 1051164 and on the left side in NMBE 1051180. [MfN] 1403 (right side) and [MfN] 7374 have an additional interturbinal between interturbinal γ and frontoturbinal 2. Between frontoturbinal 2 and 3 NMBE 1051166 has two additional interturbinals on each side, but NMBE 1051180, NMBE 1052706 (right side), and [MfN] 7374 have one at this position. One additional interturbinal between frontoturbinal 3 and ethmoturbinal I is present in NMBE 1052706 dorsal, and in [MfN] 1403 (left side) ventral to interturbinal β.

Interturbinal δ is rostrally attached to the suture between the nasal and the frontal in borzoi NMBE 1051164, NMBE 1051166 (right side), NMBE 1052706 (associated with a fusion of two lamellae), [MfN] 1403 (**Fig. 40**F), and the saluki (left side). In borzoi [MfN] 7374 interturbinal δ is rostrally attached to the nasal, like in the Eurasian wolf, and additionally continuous with the dorsal lamina of the lamina semicircularis. Borzoi NMBE 1051180 corresponds to the Eurasian wolf, as NMBE 1051166 on the left side and the saluki on the right side. In borzoi [MfN] 7374 two single scrolled lamellae separate from the multiple scrolled interturbinal δ and curve caudolaterally. In the saluki interturbinal δ curves along the nasal to the nasal-frontal suture and follows this suture in caudomedial direction. It merges together with an additional interturbinal lateral to it on the right side in borzoi NMBE 1051164 (see below) but both separate more caudally. In two specimens **interturbinal γ** differs from the Eurasian wolf by merging into frontoturbinal 1 rostrally: the interturbinal ends on the stem of frontoturbinal 1 in NMBE 1051164 (**Fig. 36**M, N), in the saluki it is rostrally emerging from a folding of the stem of frontoturbinal 1 (**Fig. 42**G). Interturbinal γ complicates caudally to a double scroll in NMBE 1051164, and in NMBE 1052706 and [MfN] 7374 it then becomes a straight lamella. The topography and the caudal end resemble the Eurasian wolf in all borzois and the saluki. **Interturbinal β** differs in its rostral end from the Eurasian wolf in some characters. In two borzois it is continuous with ethmoturbinal I, in NMBE 1051164 and on the left side in [MfN] 1403 with the epiturbinal of ethmoturbinal I, and on the right side in [MfN] 1403 with its stem. In three other borzois interturbinal β merges rostrally into the lamina horizontalis with different additional fusions: on the left side in NMBE 1052706 it is fused to frontoturbinal 3, in NMBE 1051180 to the epiturbinal of ethmoturbinal I, and in NMBE 1051166 interturbinal β is continuous with both structures mentioned before. The saluki has a short rostral process that is caudally attached to the epiturbinal of ethmoturbinal I, whereas its stem is rostrally attached to the lamina horizontalis. The caudal course of interturbinal β differs on the left side in borzoi NMBE 1051164 from the Eurasian wolf as it runs from the epiturbinal of ethmoturbinal I along the lamina horizontalis and caudal to it onto the frontal where it fuses with a further lamella. Then, interturbinal β attaches to the stem of frontoturbinal 3 and then shifts back to the frontal. Variations to the Eurasian wolf regarding the shape and position of the three prominent interturbinals within the pars intermedia are not observed.

Four types of additional interturbinals are present between the lamina semicircularis and frontoturbinal 1; three are positioned medial and one lateral to interturbinal δ. The first additional interturbinal next to the lamina semicircularis is similar to the additional interturbinal present in the Eurasian wolf. A variation is observed in its topography in borzoi NMBE 1051164, as it runs from the medial septum of the nasal onto the septal process of the frontal. The second and third additional interturbinals at this position are present in two borzois, but not in the Eurasian wolf. The second one in NMBE 1051166 and NMBE 1052706 is continuous rostrally with the lamina semicircularis on the nasal, runs

dorsocaudally as a single scroll in NMBE 1052706 (in the other borzoi the low contrast of the scan hampers the determination of its shape, see **Fig. 37**B–G), and fuses to the nasal. The third small and short additional interturbinal in NMBE 1051166 ends rostrally on the medial septum of the nasal and shows the same topography and ending like the second additional interturbinal. The additional interturbinal between interturbinal δ and frontoturbinal 1 merges anteriorly into the nasal in NMBE 1051164 and into the suture between the nasal and the frontal in NMBE 1051180, and forms a single scroll in both borzois. In NMBE 1051164 the additional interturbinal runs onto the frontal caudolaterally, on the right side it merges into interturbinal δ, and ends on the frontal caudally. In NMBE 1051180 the additional interturbinal separates into two straight lamellae posteriorly, of which the medial one runs slightly medially, and the lateral one laterally, probably onto the frontal. The doubt regarding the attachment of the lateral lamella in this specimen refers to the invisibility of the suture between the nasal and the frontal in the caudal part of the face. Independently from each other both the medial and the lateral lamella fuse to the frontal, as they are extending more caudally than the nasal when considering the nasal's caudal end in the other borzoi specimens. The additional interturbinal between interturbinal γ and frontoturbinal 2 that is present in borzoi [MfN] 1403 and [MfN] 7374 fuses to the frontal anteriorly and is straight to single scrolled. In [MfN] 1403 this additional interturbinal runs onto the septum of the frontal sinus and fuses to it posteriorly, whereas in [MfN] 7374 it is attached to the frontal in its entire length. Borzoi NMBE 1051166 has two additional interturbinals between frontoturbinal 2 and 3 and three other borzois have one. The additional interturbinal next to frontoturbinal 2 in NMBE 1051166 is similar to the one which is present in [MfN] 7374. The former specimen has a single scroll on the frontal, and the latter specimen has a straight lamella that runs along the lamina horizontalis onto the frontal. In both specimens this additional interturbinal fuses to this bone. The second additional interturbinal next to frontoturbinal 3 in NMBE 1051166 resembles the additional interturbinal in NMBE 1051180 and NMBE 1052706. In all three specimens it fuses to frontoturbinal 3 rostrally and runs caudodorsally onto the frontal. In NMBE 1051166 and NMBE 1052706 the additional interturbinal fuses to the frontal, whereas in NMBE 1051180 it additionally runs onto frontoturbinal 2 and fuses to its stem. The shape is a single scroll in NMBE 1052706, and a simple straight lamella in NMBE 1051180. In NMBE 1051166 the shape of the additional interturbinal is not identifiable due to the low contrast of the µCT scan. Dorsal to interturbinal β, NMBE 1052706 has a single to double scrolled additional interturbinal. It is attached to the frontal in its entire length. Borzoi [MfN] 1403 has a double scrolled additional interturbinal ventral to interturbinal β (**Fig. 40**G). It is similar to the additional interturbinal in Eurasian wolf ZMB_MAM 815 in its rostral end on the lamina horizontalis. It runs onto the frontal caudal to the lamina horizontalis to approach and touch the stem of ethmoturbinal I, but the additional interturbinal fuses to the frontal rostral to the lamina cribrosa.

Ethmoturbinal I differs from the Eurasian wolf in four of the borzois in the morphology of its epiturbinal. Borzoi NMBE 1051166 and the right side in [MfN] 1403 exactly resemble the Eurasian wolf. On the right side in the saluki the epiturbinal merges into the stem of ethmoturbinal I rostrally, but it is additionally attached to the lamina horizontalis for a short distance (**Fig. 42**E). On the right side in borzoi NMBE 1051180 the epiturbinal ends anteriorly on the frontal, and on the left side in the saluki and in borzoi NMBE 1051164, NMBE 1052706, on the left side in [MfN] 1403, and in [MfN] 7374 on the lamina horizontalis. Caudally, the epiturbinal shifts to the stem of ethmoturbinal I. On the left side in borzoi NMBE 1051180 the epiturbinal is continuous with the lamina horizontalis on the stem of ethmoturbinal I. The epiturbinal's shape complicates to dendritic in [MfN] 7374, whereas in the other specimens it is a simpler double scroll. On the left side in NMBE 1051164 the double scrolled epiturbinal merges with a second lamella and forms multiple scrolls. Similar to the epiturbinal a second epiturbinal-like lamella is rostrally attached to the lamina horizontalis on the right side in NMBE 1051164, in [MfN] 7374, and on the left side in NMBE 1052706. On the right side of the last mentioned specimen the lamella is fixed to the transition between the lamina horizontalis and the stem of ethmoturbinal I. Then, it runs onto the stem of ethmoturbinal I in all specimens on which it ends. A second epiturbinal-like lamella is absent in the saluki and in borzoi [MfN] 1403, NMBE 1051164 (left side), and NMBE 1051180 (right side). The anterior lamina and the posterior lamina of ethmoturbinal I vary in two borzois: the anterior lamina of ethmoturbinal I forms a caudodorsal process induced by the lamina semicircularis in [MfN] 1403, and in NMBE 1051164 the posterior lamina of ethmoturbinal I separates into a lateral single scroll and a medial double scroll (**Fig. 36**K). With respect to **ethmoturbinal II** both breeds correspond to the Eurasian wolf except borzoi [MfN] 1403. On the left side in this specimen ethmoturbinal II runs caudally onto the frontal between the palatine and the orbitosphenoid, and is fused to the stem of ethmoturbinal I for a short distance. **Ethmoturbinal III** is rostrally continuous with the lamina horizontalis and the lamina terminalis on the right side in the saluki. In borzoi NMBE 1051164 it runs along the stem of ethmoturbinal II directly onto the palatine without touching the lamina horizontalis.

Interturbinal α is double scrolled in borzoi NMBE 1051180, NMBE 1052706, and [MfN] 1403, whereas in the saluki it varies to a more complicate dendritic shape. On the left side in borzoi NMBE 1052706 interturbinal α is not attached to the lamina horizontalis. The additional interturbinal differs among the entire sample from the Eurasian wolf in its anterior origin, topography, and caudal end. Rostrally, it is fixed to the stem of ethmoturbinal II (e.g., borzoi [MfN] 7374, **Fig. 41**E) except for the saluki and borzoi [MfN] 1403. On the right side in the saluki the additional interturbinal is like in the Eurasian wolf; on the left side it does not extend far rostrally to touch the lamina horizontalis and ends on the frontal like in borzoi [MfN] 1403. The additional interturbinal is as simple built as in the Eurasian wolf, namely straight (e.g., borzoi [MfN] 7374, **Fig. 41**F) to single scrolled. On the left side in borzoi NMBE 1051164 it complicates to a double scroll. The additional interturbinal runs along the

lamina horizontalis onto the frontal in borzoi NMBE 1051164, NMBE 1051180, NMBE 1052706 and on the right side in the saluki, and onto the palate in borzoi NMBE 1051166. In borzoi [MfN] 1403, [MfN] 7374 and on the left side in the saluki the additional interturbinal does not touch the lamina horizontalis. It stays on the frontal in its entire length in borzoi [MfN] 1403 and the saluki. In borzoi [MfN] 7374 the additional interturbinal runs from ethmoturbinal II directly onto the frontal on both sides and on the right side a third interturbinal (or more precisely the second additional interturbinal) shifts to the palatine. The additional interturbinal fuses to the lamina cribrosa in borzoi NMBE 1051164, NMBE 1051180, [MfN] 7374, and the saluki, and on the left side in the two borzois NMBE 1051166 and NMBE 1052706. In borzoi [MfN] 1403 and on the right side in the three borzois NMBE 1051166, NMBE 1052706, and [MfN] 7374 the additional interturbinal runs back onto the stem of ethmoturbinal II and fuses to it.

Comparison

In the Eurasian wolf and in the dolichocephalic breeds the respiratory and the olfactory pathway are clearly separated from each other by the lamina terminalis as illustrated by the example of Eurasian wolf ZMB_MAM 93307 and borzoi NMBE 1051164 (**Fig. 43**). More anteriorly, an overlap between the maxilloturbinal and the anterior process of the anterior lamina of ethmoturbinal I becomes apparent. In contrast, displaced rostral parts of ethmoturbinal I and II in some brachycephalic to mesaticephalic dogs are positioned within the respiratory pathway as visible on the sagittal sections on the example of the modern pug NMBE 1051937 and Cavalier NMBE 1062998 (**Fig. 43**).

All adult dogs have the same number of fronto- and ethmoturbinals like the Eurasian wolf, namely three frontoturbinals and three ethmoturbinals (**Table 6**). The number of interturbinals within the pars intermedia ranges from two in the Groenendael and some smaller toy breeds (e.g., pekingese NMBE 1051962) up to eight on the right side in borzoi NMBE 1051166. Together with the Groenendael the saluki has a lower number of interturbinals (three) within the pars intermedia compared to the other large and dolichocephalic breeds (German shepherd, Greenland dog, borzoi) which have on average a higher number of interturbinals (four to eight) than the smaller toy breeds (two to five). Within the pars ethmoturbinalis the variation is conspicuously smaller with one to two interturbinals among the sample; one specimen, borzoi [MfN] 7374 has three interturbinals on its right side. Resulting from the high variation of interturbinals within the pars intermedia the total number of olfactory turbinals varies between nine (e.g., Groenendael, some toy breeds like Pekingese NMBE 1051962 mentioned above) up to a maximum of seventeen on the right side in borzoi NMBE 1051166.

A general comparison proves a homology of the turbinal skeleton's overall morphology and its position within the nasal cavity of the long snouted breeds (borzoi, German shepherd) with the Eurasian

wolf (**Fig. 44**A–F). The mesaticephalic ancient pug (ZMB_MAM 30980) does also not vary in a great extent, although its forehead is significantly steeper than in the Eurasian wolf (**Fig. 44**G, H). That is also observed in the medium snouted Cavalier (NMBE 1062998), whose turbinal skeleton is more shortened in its length compared to the mentioned pug specimen (**Fig. 44**J, K). But the greatest difference to the Eurasian wolf is in the three most extreme brachycephalic breeds: the modern pug (NMBE 1052345), the King spaniel (NMBE 1051945), and the pekingese (NMBE 1051962) (**Fig. 44**L–R).

The overall morphology of the **maxilloturbinal** corresponds to the Eurasian wolf in the adult specimens of the borzoi and the saluki, the German shepherd and the Groenendael, and the Greenland dog. The Cavaliers and the ancient pugs except [MfN] 2657 (see below), do not differ from the dog's ancestor either. In the other short to medium snouted breeds some variations occur in the maxilloturbinal: the double scrolled basic type is absent in pekingese SMF 35611, in which the maxilloturbinal is a straight lamella. The initially lateral scroll in the ventral lamella becomes straight in some individuals e.g., the modern pug NMBE 1051937, and the primarily dendritic shape is simplified (e.g., multiple scrolls in pekingese NMBE 1051965). The dorsal lamella is simplified, too, to slightly dendritic at most, and both lamellae are not completely filling the space of the pars maxillonasoturbinalis. Interestingly, the longer snouted ancient pug [MfN] 2657 resembles the short snouted dogs. A variation in the **nasoturbinal** is its rostral shortening in extreme brachycephalic specimens (e.g., chin ZMB_MAM 7436, modern pug NMBE 1051937) to a small rostral tip of the lamina semicircularis.

The **lamina semicircularis** is similar to the ancestral pattern in the long snouted dogs, whereas in the medium to short snouted specimens the shape of both the ventral and the dorsal lamina is simplified. Two specimens have an additional uncinate process-like structure which is associated with a multiple scrolled ventral lamina in borzoi [MfN] 7374 and with a single scrolled ventral lamina in the saluki. Both King spaniels have a double scrolled ventral lamina, but they are missing a second uncinate process-like structure. A small accessory lamella proximal on the stem of the lamina semicircularis is common in the dolichocephalic group, and absent in the shorter snouted group.

All **three frontoturbinals** show nearly the same pattern and vary in a small extend from the Eurasian wolf. Their rostral fusions are different among the breeds: in the borzois and in the saluki frontoturbinal 1 is rostrally attached to the maxillary; in the other breeds its distal end is additionally continuous with the lamina semicircularis or like in the Eurasian wolf with the lamina horizontalis in cross sectional view. Frontoturbinal 2 exhibits on its rostral end an intraspecific variation within the Eurasian wolf; and frontoturbinal 3 shows a randomly distributed distal connection with the lamina horizontalis, ethmoturbinal I, or frontoturbinal 2 among the dogs. The type, topography, and caudal end of the three frontoturbinals are comparable to the Eurasian wolf in the borzoi, the saluki, the German shepherd, the Groenendael, and the Greenland dog. The medium to short snouted dogs (Cavalier, ancient pug) have a simplified shape that is in some individuals similar to the Eurasian wolf in its

highest complication. In all brachycephalic dogs (chin, pekingese, King spaniel, modern pug) all three frontoturbinals curve caudally to the frontal. Frontoturbinal 3 which is not affected by a minimized frontal sinus has the same caudal end like in the Eurasian wolf in all snout types. Variations occur in frontoturbinal 1 and 2. In dogs with an at least rather developed frontal sinus both end as processes within it, whereas in individuals with a small or even completely reduced sinus frontoturbinal 1 and 2 fuse to the lamina cribrosa or to a septum of the sinus.

The **three prominent interturbinals** within the pars intermedia differ slightly from the Eurasian wolf. The rostral end of interturbinal δ shows smaller variations among the dogs e.g., an attachment to the suture between the nasal and the frontal that is observed in borzoi NMBE 1051164 and the ancient pug [MfN] 2620. The shape, topography, and caudal end in all three prominent interturbinals and the rostral end in interturbinal γ and β are identical between the Eurasian wolf and borzoi, saluki, German shepherd, Groenendael, and Greenland dog. In the brachycephalic to mesaticephalic breeds the shape of all three prominent interturbinals is simplified similar to the frontoturbinals. Their topography corresponds to the Eurasian wolf, as does the caudal end of interturbinal γ and β. Interturbinal δ varies within the brachycephalic to mesaticephalic group from the Eurasian wolf in fusing to the lamina cribrosa or to the frontal caudally.

The dolichocephalic dogs (borzoi, saluki, German shepherd, Groenendael, and Greenland dog) show no considerable variations to the Eurasian wolf in all **three ethmoturbinals**. Smaller differences are in the basically multiple scrolled epiturbinal of ethmoturbinal I which is double scrolled in the saluki and dendritic in the Greenland dog. Except ancient pug ZMB_MAM 30980 all brachycephalic to mesaticephalic breeds have a simpler (to double scrolled) but nevertheless large and well-developed epiturbinal. A greater variation in the short to medium snouted individuals is observed in the two laminae of ethmoturbinal I and their anterior processes: the two Cavaliers and the ancient pugs exclusive [MfN] 2657, resemble the Eurasian wolf with at least slightly dendritic anterior processes in ethmoturbinal I. In the other brachycephalic breeds (chin, King spaniel, pekingese, modern pug) both anterior processes are simpler, sometimes straight (e.g., in both chins). In two pekingese (SMF 35611, NMBE 1051962) and one modern pug (NMBE 1052345) the anterior and posterior lamina of ethmoturbinal I show a reduced anterior process. Within most individuals both anterior processes have an identical shape. An exception is e.g., King spaniel NMBE 1051945 whose anterior process of the anterior lamina of ethmoturbinal I is slightly dendritic, whereas the posterior lamina of ethmoturbinal I has a simpler straight anterior process. The anterior lamina and posterior lamina of ethmoturbinal I are simpler in their shape in the short to medium snouted breeds, too, namely double scrolled at most. The separation of the double scrolled posterior lamina of ethmoturbinal I into two single scrolls, or the reverse, is exclusively present in six of the eight adult pugs among the brachycephalic to mesaticephalic breeds. The second epiturbinal-like lamella on ethmoturbinal I is generally present in long snouted

breeds and absent in short snouted breeds. The caudal end of ethmoturbinal I has not changed in brachycephalic to mesaticephalic dogs. Ethmoturbinal II represents the plesiomorphic pattern in its rostral fusion in nearly all pugs; in the other brachycephalic to mesaticephalic dogs it varies without a breed-specific pattern. The type and topography of ethmoturbinal II do not differ from the Eurasian wolf in any short to medium snouted individual, as does its caudal end in both Cavaliers. In the other brachycephalic to mesaticephalic specimens ethmoturbinal II differs in its caudal end in extending into the sphenoid sinus. Ethmoturbinal III is rostrally rarely connected with the lamina terminalis in the long snouted dogs. This fusion is present more frequently among the short to medium snouted individuals, in which the morphology of ethmoturbinal III is simplified. Its topography and caudal end show no variation towards the Eurasian wolf.

Variations in **interturbinal α** occur in the brachycephalic to mesaticephalic individuals, but not in the dolichocephalic breeds. A rostral process is rare, and reduced if present (e.g., King spaniel NMBE 1051945). Instead, interturbinal α fuses to ethmoturbinal II or the lamina horizontalis or it is continuous with ethmoturbinal II on the lamina horizontalis. The shape of interturbinal α is less complicate like in the ethmoturbinals, and variations in its topography do not depend on the breed. Sometimes interturbinal α fuses to the lamina cribrosa e.g., in the ancient pug [MfN] 1845.

3.2 Morphometric analyses

3.2.1 Snout length groups based on IFB and IBL

Regarding the adult dogs (n = 27, excluding the destroyed ancient pug SMF 16284, **Table 1**) including the Eurasian wolves (n = 3) IFB and IBL (ELLENBERGER & BAUM 1891, **Fig. 4**) are highly correlated with each other ($r^2 = 0.914$; $p \approx 0$; **Table S4**, Supplementary material). However, the grouping of the skulls including the juveniles (n = 3) is not homogeneous within all specimens as the measurements overlap between the indices (**Fig. S2**, Supplementary material): 23 individuals belong to a distinct snout length type (7 brachycephalic, 3 mesaticephalic, 13 dolichocephalic), but ten individuals are heterogeneously distributed (7 brachycephalic/mesaticephalic, 3 mesaticephalic/dolichocephalic) (**Table 1**).

The three pekingese and both King spaniels are extremely brachycephalic in both indices. They even exceed the maximum value of ELLENBERGER & BAUM (1891: IFB, 0.3 to 0.36; IBL, 0.84 to 0.9). Pekingese NMBE 1051965 has the most extreme values in both with 0.15 (IFB) and 1.09 (IBL), respectively. One of the two modern pugs (NMBE 1052345) is also brachycephalic in both indices; the second modern pug (NMBE 1051937) is mesaticephalic in IBL and brachycephalic in IFB, like the juve-

nile and three adults of its ancient conspecifics. Two pugs of the ancient type (ZMB_MAM 30980, [MfN] 2657) are mesaticephalic. In contrast to the King spaniels the two Cavaliers are mesaticephalic except IFB in NMBE 1062998 whose value corresponds to the brachycephalic type.

All borzois (including the juvenile), the saluki, both German shepherds and the Groenendael are dolichocephalic, but they exceed ELLENBERGER & BAUM's (1891: IFB, 0.6 to 0.7; IBL, 0.6 to 0.65) defined maximum values as well: borzoi [MfN] 1403 has an IFB of 0.75, and borzoi NMBE 1051164 has an IBL of 0.4. The Greenland dog which is dolichocephalic in IBL can be grouped with the long snouted breeds, as its IFB (0.59) is extremely close to the referenced lower limit. The Eurasian wolf can be regarded as long snouted, too; only specimen ZMB_MAM 93307 is medium snouted in IFB.

3.2.2 Turbinal surface area (IAT) vs. exterior turbinal surface area (IAE)

The correlation between IAT and IAE that was significant between the long snouted dogs (WAGNER & RUF 2019) and the short snouted individuals which have been reconstructed at the beginning of the project (**Fig. 5**) was furthermore tested in the dog skulls which have been segmented in AMIRA 5.4.0 during the following months. In all of them the ANOVA confirmed the correlation regardless of snout length and age (**Table S5**, Supplementary material). Hence, in sum for each of the 16 dog individuals (n = 18, as in two of them both sides were reconstructed) under study and the Eurasian wolf the dependence of IAT on IAE is verified. The specimens are summarized in **Fig. 45**; their ablines are separately illustrated in **Fig. 46**. For the single plots of the remaining specimens beside the three depicted examples in **Fig. 5** (Eurasian wolf, borzoi, and pekingese) see **Fig. S3** (Supplementary material).

3.2.3 Turbinal surface area (IAT/AT)

The highest total IAT is observed in the Eurasian wolf (14.586), then in both adult borzois (14.124, NMBE 1051164; 10.910, [MfN] 1403) and in the German shepherds (10.874, SMF 93607; 9.748, MNHN 1985-1274) (**Table 4**; **Figs. 47**, **48**). Together with the borzoi puppy (8.872) the dolichocephalic individuals show distinct higher values than the two mesaticephalic ancient pugs (6.285, ZMB_MAM 30980; 4.207, [MfN] 2657). The latter pug has a smaller total IAT than the slightly brachycephalic Cavalier (5.064, left side; 5.700, right side); the other short snouted dogs have smaller values, up to the modern pug NMBE 1052345 with a value of 1.485 (left side).

As a general pattern independent from age the maxilloturbinal has the largest IAT followed by ethmoturbinal I in longer snouted dogs up to an IFB of 0.34 (pug [MfN] 2620), in dogs with a shorter snout

it is vice versa. Exceptions are pug [MfN] 2657 in which ethmoturbinal I is larger (0.792; 0.453, maxilloturbinal), and the chin with a slightly higher value in the maxilloturbinal (0.382; 0.341, ethmoturbinal I). In the pekingese both turbinals are exceeded by the lamina semicircularis (0.328) and by frontoturbinal 2 (0.381). With respect to the pars ethmoturbinalis in all specimens including the puppies and the Eurasian wolf ethmoturbinal I has the largest IAT, followed by ethmoturbinal II and III. Interturbinal α has smaller values; even though in some of the extreme short snouted specimens (modern pugs NMBE 1051937 and NMBE 1052345, left side; King spaniel) it exceeds ethmoturbinal III. Within the pars intermedia all frontoturbinals in all ontogenetic stages and the outgroup are larger in IAT than the interturbinals. An association between the presence of the frontal sinus and the caudal end of the first two frontoturbinals within it and the size order between these two turbinals cannot be proven. In summary, frontoturbinal 2 has higher values than frontoturbinal 1, and frontoturbinal 3 is the third largest in all individuals. Only in the King spaniel (frontal sinus lost) and in borzoi NMBE 1051164 frontoturbinal 2 is exceeded by frontoturbinal 1; in the ancient pug [MfN] 1845 they are close to each other (0.306, frontoturbinal 1; 0.305, frontoturbinal 2; small frontal sinus present). Another specimen with a completely lost frontal sinus is the modern pug NMBE 1052345 in which again frontoturbinal 2 is the largest. In the chin frontoturbinal 1 ends within the frontal sinus, whereas the larger frontoturbinal 2 does not. Generally, the three prominent interturbinals in the pars intermedia are larger than the nasoturbinal. Exceptions are the ancient pugs [MfN] 2620, [MfN] 2657, and ZMB_MAM 30980, German shepherd SMF 93607, all three borzois, and the Eurasian wolf in which the nasoturbinal is larger than interturbinal δ (e.g., pug [MfN] 2620), interturbinal γ (e.g., German shepherd), or both (e.g., Eurasian wolf).

The Eurasian wolf has the highest values in IAT within the pars ethmoturbinalis (2.847, ethmoturbinal I; 1.693, ethmoturbinal II; 0.931, ethmoturbinal III) including interturbinal α (0.684) (**Table 4**; **Figs. 47**, **48**). Regarding the maxilloturbinal it equals borzoi NMBE 1051164 (3.725; 3.672, Eurasian wolf), which has higher values in frontoturbinal 1 (1.822) and 2 (1.475); the size of frontoturbinal 1 in the Eurasian wolf (1.059) is similar to the second borzoi (1.087, [MfN] 1403) and to German shepherd MNHN 1985-1274 (1.061). Frontoturbinal 3 is the largest in the Eurasian wolf (0.860).

Both juveniles nearly exactly correspond to the Eurasian wolf in the size order of their turbinals: the maxilloturbinal has the highest value followed by ethmoturbinal I (in the pug it is vice versa), then ethmoturbinal II, frontoturbinal 2, frontoturbinal 1, ethmoturbinal III, and frontoturbinal 3. The maxilloturbinal and ethmoturbinal I are clearly distinct from ethmoturbinal II in IAT. In the young pug interturbinal α (0.126) has a higher value than frontoturbinal 3 (0.096), whereas in the Eurasian wolf and in the borzoi puppy all interturbinals have a lesser IAT than the ethmoturbinals and the frontoturbinals. Interturbinal α is larger than all interturbinals in the pars intermedia in the two juveniles and the Eurasian wolf.

Among the dolichocephalic dogs to which the juvenile borzoi belongs borzoi [MfN] 1403 (2.440) is exceeded by German shepherd SMF 93607 (2.895) in the IAT of its maxilloturbinal. Borzoi NMBE 1051164 has distinct higher values in frontoturbinal 1 and 2 than the second borzoi and both German shepherds; frontoturbinal 3 is less distinct between the four specimens. Ethmoturbinal I is the largest in both adult borzois (2.187, NMBE 1051164; 2.013, [MfN] 1403) and nearly equal between both adult German shepherds (1.588, SMF 93607; 1.576, MNHN 1985-1274). German shepherd SMF 93607 has a higher IAT in ethmoturbinal II (1.122) than both adult borzois (1.061, NMBE 1051164; 1.013, [MfN] 1403), but the differences are quite small. Borzoi NMBE 1051164 has the highest value in ethmoturbinal III (0.737), whereas its conspecific (0.588) closely corresponds to German shepherd SMF 93607 (0.642) and the juvenile borzoi (0.620). The interturbinals in both compartments are also not showing a uniform pattern, but vary in their IAT between the dolichocephalic breeds and specimens.

The two mesaticephalic ancient pugs ([MfN] 2657, ZMB_MAM 30980) are not considerably distinctive from the brachycephalic specimens, even though they have a large distance in their IFB to both the short snouted and the long snouted dogs (**Fig. 48**). Both modern pugs (0.525, NMBE 1051937; 0.319, right side; 0.202, left side, NMBE 1052345) have a smaller or nearly similar surface area in the maxilloturbinal than their ancient conspecifics (0.614, [MfN] 1845; 0.785, [MfN] 2620; 1.367, ZMB_MAM 30980); although the ancient pug [MfN] 2657 has a notably small IAT in this turbinal as well (0.453). Ethmoturbinal I is smaller in the modern pug NMBE 1052345 (0.435, right side; 0.296, left side), whereas the second modern specimen NMBE 1051937 (0.724) corresponds more closely to the ancient breed-type. Ethmoturbinal II and III increase with snout length within the breed as does interturbinal α, with a slight decline of the latter in the ancient pug [MfN] 2620. The difference between frontoturbinal 1 and 2 are the highest in the two mesaticephalic ancient pugs ([MfN] 2657, ZMB_MAM 30980) and the short snouted modern pug NMBE 1051937. In contrast to frontoturbinal 1 frontoturbinal 2 and 3 increase linearly with snout length; they are at least more or less equal among the pug specimens. The juvenile ancient pug has already a longer snout in IFB (and IBL) than the two adult modern individuals. Its values are comparable to the adult modern type NMBE 1052345.

The Cavalier which is close to the medium snouted group in IFB (0.35; lower limit 0.36, ELLENBERGER & BAUM 1891) is similar to the two mesaticephalic ancient pugs in its values. The brachycephalic King spaniel, however, resembles the other short snouted dogs (**Fig. 48**). It has the smallest maxilloturbinal within the entire sample (0.186); its frontoturbinals equal the values of the two ancient pugs [MfN] 1845 and [MfN] 2620, whereas its ethmoturbinals correspond more to the chin, the pekingese, and to the modern pugs. The pekingese exceeds the chin in all turbinals except ethmoturbinal I (0.310, pekingese; 0.341, chin). Regarding the frontoturbinals the two mentioned specimens have a larger IAT than the modern pug NMBE 1052345, whereas the values of the second

modern pug NMBE 1051937, the pekingese, and the chin vary compared to each other (**Table 4**; **Fig. 47**). Within the pars ethmoturbinalis the chin and the pekingese exceed the two modern pugs only in ethmoturbinal III (0.147, pekingese; 0.121, chin; 0.065, left side and 0.110, right side, NMBE 1052345; 0.106, NMBE 1051937). In the two other ethmoturbinals and in interturbinal α the modern pug NMBE 1051937 has the highest values within these four mentioned specimens.

In two short snouted specimens, namely in the modern pug NMBE 1052345 and in the Cavalier, a conspicuous asymmetry is observed in the µCT scans, so both sides of the nasal cavity were reconstructed. This strong asymmetry is proven in the maxilloturbinal in both specimens (0.202, left side and 0.319, right side, pug; 0.931, left side and 1.366, right side, Cavalier). Furthermore, the pug shows strong differences in all three ethmoturbinals, the Cavalier in frontoturbinal 2 and 3, and in ethmoturbinal I.

Regarding the three compartments the proportion of AT does not correlate with IBL and IFB in the pars ethmoturbinalis and the pars intermedia (for details see **Table S6**, Supplementary material). The pars maxillonasoturbinalis that mainly consists of the maxilloturbinal shows a positive correlation with snout length ($p = 0.0018$, IFB; $p = 0.0009$, IBL), with the highest proportion in German shepherd SMF 93607 (27.7%) and borzoi NMBE 1051164 (27.4%), and the smallest in the King spaniel (8.1%) (**Fig. 49**; **Table S7**, Supplementary material). The lamina semicircularis is negatively correlated with facial length ($p = 0.0007$, IFB; $p = 0.0015$, IBL), spreading between 4.8% in the Eurasian wolf up to 13.7% in the pekingese. The pars intermedia has a larger proportion in AT than the pars ethmoturbinalis in the three most extreme brachycephalic specimens (pekingese, King spaniel, chin), but also in the long snouted German shepherd MNHN 1985-1274 and borzoi NMBE 1051164. The highest difference between the larger pars ethmoturbinalis and the pars intermedia is exclusively observed among the pugs, no matter if modern (43.2% : 30.9%, NMBE 1052345, right side; 44.4% : 26.8%, NMBE 1051937) or ancient type (41.4% : 30.5%, [MfN] 1845; 39.5% : 26.5%, [MfN] 2620; 39.4% : 30.5%, ZMB_MAM 30980). They closely correspond to the Eurasian wolf (42.5% : 26.6%) and both juvenile dogs (48.5% : 23.9%, pug; 40.4% : 25.0%, borzoi). In the two other pugs the difference is less (37.8% : 36.7%, left side, modern type NMBE 1052345; 40.1% : 37.9%, ancient type [MfN] 2657). The large AT of the maxilloturbinal in the dolichocephalic group affects the proportion of both the pars intermedia and the pars ethmoturbinalis.

In a further ANOVA the total AT and the AT of the respiratory surface area (maxilloturbinal) is tested against the relative (IFB) and the absolute nasal length (NLII), respectively. In the four variables a positive correlation is proven (**Table S8**, Supplementary material). Additionally, the AT of the maxilloturbinal increases linearly with body mass ($n = 15$; $r^2 = 0.8586$; $p < 10^{-6}$; see **Tables S1, S9**; and **Fig. S4**, Supplementary material). In the two German shepherds the variation towards the abline is smaller than in the two borzois, of which one's AT lies under, the second's AT above the line. The brachyce-

phalic breeds show a heterogeneous pattern. The chin has a comparatively large AT in its maxilloturbinal compared to body mass, as has the Cavalier. Both plot above the abline, together with ancient pug ZMB_MAM 30980. The other ancient pugs [MfN] 1845, [MfN] 2620, and [MfN] 2657, the King spaniel, and the pekingese are near the abline. The two modern pugs have a conspicuously small AT in their maxilloturbinal with regard to body mass.

3.2.4 Turbinal surface density (SDEN)

In general, within an individual its entire turbinal skeleton is denser than regarding the single turbinals. The values of SDEN are listed in **Table S10** (Supplementary material). Exceptions are observed in five specimens. The total SDEN is exceeded by ethmoturbinal I in the King spaniel (1.901 and 1.813), and by the maxilloturbinal in both German shepherds (4.011 and 3.893, MNHN 1985-1274; 4.183 and 4.143, SMF 93607) and the modern pug NMBE 1052345 (1.508 and 1.428, left side). On the same side in the last mentioned specimen the total SDEN is additionally close to three olfactory turbinals (1.458, frontoturbinal 2; 1.453, frontoturbinal 3; 1.402, ethmoturbinal I). In the ancient pug [MfN] 2657 four turbinals (1.956, ethmoturbinal I; 1.939, frontoturbinal 3; 1.865, frontoturbinal 1; 1.838, frontoturbinal 2) are denser than the specimen's entire turbinal skeleton (1.774).

Among the sample the Eurasian wolf has the highest SDEN in frontoturbinal 1 (2.440), frontoturbinal 3 (2.766), and ethmoturbinal II (2.615). The other values of the Eurasian wolf are similar to the long snouted dogs, though the wolf is mesaticephalic in IFB (**Fig. 50**). Its total SDEN (4.765) is only exceeded by borzoi NMBE 1051164 (4.959).

Although all turbinals are increasing their SDEN with snout length (**Fig. 51**), the strongest increase of the value is observed in the maxilloturbinal. It has the second lowest SDEN in the pekingese (1.037), but with an increasing IFB it exceeds the other turbinals and has the highest value among all specimens in borzoi NMBE 1051164 (4.496). In three specimens the SDEN of the maxilloturbinal is even higher than the total SDEN of the turbinal skeleton (see above). The nasoturbinal has a value of nearly 1 in all individuals, up to a maximum of 1.162 in the chin.

Within the pars intermedia the three dogs with the longest snout (German shepherd SMF 93607, both borzois) have the highest SDEN in frontoturbinal 3, followed by frontoturbinal 2 and 1. The same order is observed in two brachycephalic specimens: in the ancient pug [MfN] 2620 (1.735, frontoturbinal 3; 1.726, frontoturbinal 2; 1.626, frontoturbinal 1), and the King spaniel (1.447, frontoturbinal 3; 1.304, frontoturbinal 2; 1.200, frontoturbinal 1). Frontoturbinal 1 is also the least dense in the four most extreme brachycephalic individuals (pekingese, King spaniel, chin, and modern Pug NMBE 1052345), the order in the density between the other two frontoturbinals varies in these specimens.

Within the pars intermedia the largest distance between the highest and the lowest value is observed in the specimens with the longest snout (both borzois, German shepherd SMF 93607), and in the specimens with the shortest snout (modern pug NMBE 1052345, right side; chin, King spaniel, and pekingese). Generally, all interturbinals in the pars intermedia have a smaller SDEN than the frontoturbinals. Among the former, interturbinal β has the highest value except in the chin in which interturbinal γ is slightly denser (1.363 and 1.384, respectively). Interturbinal β exceeds the least dense frontoturbinal in borzoi NMBE 1051164 (2.423; 2.300, frontoturbinal 1), German shepherd MNHN 1985-1274 (2.066; 1.964, frontoturbinal 1), the two modern pugs NMBE 1051937 (1.640; 1.580, frontoturbinal 3) and NMBE 1052345 (right side, 1.459; 1.295, frontoturbinal 1), and the pekingese (1.499; 1.423, frontoturbinal 1).

The pars ethmoturbinalis has the highest SDEN in ethmoturbinal I exclusive three brachycephalic specimens: in the pekingese (1.441) and the modern pug NMBE 1051937 (1.446) it has the lowest SDEN within the pars ethmoturbinalis, and in the Cavalier (right side) its value is between the other two ethmoturbinals and the interturbinals. In the modern pug NMBE 1051937 ethmoturbinal II and III are less dense than interturbinal α as well; this pattern is also observed in the second modern pug (NMBE 1052345, on both sides), and in the chin. In the pekingese interturbinal α (1.470) closely resembles ethmoturbinal I and III (1.441 and 1.451). In the other specimens the three ethmoturbinals have a higher SDEN than all interturbinals.

Borzoi NMBE 1051164 has the highest values in the maxilloturbinal and within the pars lateralis. Also its ethmoturbinal I is the densest among all specimens including the Eurasian wolf. The borzoi's ethmoturbinal II (2.145) is exceeded by German shepherd SMF 93607 (2.213), and by the juvenile borzoi (2.292); and its ethmoturbinal III (2.177) slightly by the second borzoi [MfN] 1403 (2.226). Within the dolichocephalic group and the Eurasian wolf interturbinal α has nearly an identical SDEN (1.698, German shepherd SMF 93607; up to 1.797, Borzoi [MfN] 1403); only German shepherd MNHN 1985-1274 (1.482) differs from that range.

Among the pugs, the SDEN of the maxilloturbinal in the ancient and medium snouted [MfN] 2657 (1.598) fits more with the two modern specimens (1.508, left side, 1.622, right side, NMBE 1052345; 1.608, NMBE 1051937), whereas in its ancient conspecifics inclusive the juvenile the value for the maxilloturbinal is higher (at least 1.796, juvenile pug). Frontoturbinal 2 of the two modern individuals corresponds more or less to the ancient ones, whereas frontoturbinal 1 and 3 and the three ethmoturbinals have a lower SDEN. The interturbinals in both compartments show no difference between the short snouted and the slightly longer snouted pugs. But the modern pug NMBE 1051937 has a conspicuously high SDEN in interturbinal α and β.

3.2.5 Turbinal complexity (TC)

In all its turbinals the Eurasian wolf most closely corresponds to German shepherd SMF 93607 (**Fig. 52**). The detailed TC values are given in **Table S11** (Supplementary material). The differences between the two specimens are best visible in the pars ethmoturbinalis in that the Eurasian wolf has a higher TC in the three ethmoturbinals and in interturbinal α. The Eurasian wolf is mostly less complex in its turbinal skeleton than the two adult borzois, or at least similar to the lesser complex borzoi [MfN] 1403 (e.g., ethmoturbinal III: 2.588, Eurasian wolf; 2.522, [MfN] 1403; 2.747, NMBE 1051164). Compared to the other dogs including the two juveniles, the Eurasian wolf has a higher TC in its turbinals.

Borzoi NMBE 1051164 has the highest values in all turbinals, and together with the second adult borzoi they have in general the most complex turbinal skeleton; the latter specimen is in some values similar to the Eurasian wolf and German shepherd SMF 93607 (frontoturbinal 3, ethmoturbinal II), or slightly less complex than these two (interturbinal β). The juvenile borzoi falls between both German shepherds; within the pars intermedia its frontoturbinals and interturbinal β and δ have lower values.

The pug with the longest snout in IFB (ancient type ZMB_MAM 30980) is comparable to the dolichocephalic group, especially to German shepherd MNHN 1985-1274, but clearly distinct from the second mesaticephalic ancient pug ([MfN] 2657) and the entire brachycephalic group (**Fig. 53**). In its total TC (4.172) ancient pug ZMB_MAM 30980 even exceeds the above mentioned German shepherd (4.004). It is almost similar to the juvenile borzoi (4.143), and slightly below the value of the Eurasian wolf (4.267). The second highest TC among the pugs is observed in the shorter snouted ancient type [MfN] 1845. The two modern pugs (NMBE 1052345, NMBE 1051937) have a less complex turbinal skeleton compared to the adult ancient individuals. The values of interturbinal δ in NMBE 1052345 (1.296, right side) and NMBE 1051937 (1.291) are close to the ancient pug ZMB_MAM 30980 (1.220). Furthermore, NMBE 1051937 resembles the ancient specimen [MfN] 2620 in interturbinal α (1.640, NMBE 1051937; 1.611, [MfN] 2620) and interturbinal β (1.586, NMBE 1051937; 1.554, [MfN] 2620). The juvenile pug is almost in accordance with the modern individual NMBE 1051937; considering the slight difference in TC between both specimens, the juvenile has in general higher values within the pars ethmoturbinalis and lower values within the pars intermedia.

The pekingese nearly corresponds to the chin, with a greater difference in the nasoturbinal (1.286, pekingese; 1.396, chin) and in interturbinal δ (1.286, pekingese; 1.396, chin). The TC in the single turbinals of these two individuals is similar to the modern pug NMBE 1052345 (right side), and higher than in the King spaniel. The modern pug NMBE 1052345 has on its left side the lowest values in all turbinals among the entire dog sample except interturbinal β which is lower in the King spaniel, even though not markedly (1.249, NMBE 1052345; 1.243, King spaniel).

3.2.6 Correlation with morphometric data

The ANOVA has proven a significant positive correlation between the relative snout length (IFB and IBL) and the morphometric parameters (IAT, SDEN, and TC) of the entire turbinal skeleton among the entire sample of adult dog specimens (**Table S12**, Supplementary material). The correlation also counts for each olfactory turbinal (ethmoturbinal, frontoturbinal, and prominent interturbinal) as well as for the lamina semicircularis and the maxilloturbinal (**Table S13**, Supplementary material). The smaller additional interturbinals are excluded from this detailed analyses due to limited sample size (**Table 5**) and the difficulty to homologize them morphologically among the specimens. The significance spreads between $p = 0.0067$ (SDEN in interturbinal α for IBL), up to $p < 10^{-9}$ (IAT in the nasoturbinal for IFB). Only the SDEN of the nasoturbinal shows no significance in both indices ($p = 0.9594$, IFB; $p = 0.8220$, IBL; see ch. 3.2.4 Turbinal surface density (SDEN): 79).

Beside the individuals the three snout length groups in both IFB and IBL have been compared to each other in IAT, SDEN, and TC (adult dogs; **Table S14**, Supplementary material). As only one Eurasian wolf specimen was segmented, it was excluded from the data analyses. However, apart from that it is included in the boxplot as representative of the outgroup and closest to the dolichocephalic group (**Fig. 54**). The TukeyHSD test reveals that in all six plots the difference between the brachycephalic and the dolichocephalic group is highly significant ($p < 10^{-5}$). All three groups are distinct in their TC in IBL. According to three additional highly significant values (TC in IFB, IAT and SDEN in IBL) the mesaticephalic group differs more from the dolichocephalic group than from the brachycephalic group. Simultaneously, in three variables (IAT in both facial length indices, SDEN in IFB) the mesaticephalic and the brachycephalic group show no significant separation ($p > 0.17$). In general, in all three morphometric parameters the dogs are more distinguishable from each other in their head shape when they are grouped according to IBL instead of IFB.

4 DISCUSSION

4.1 The *grundplan* of *Canis lupus lupus* and *Canis lupus familiaris*

4.1.1 The number of olfactory turbinals

In all investigated dog specimens the number of ethmoturbinals and frontoturbinals is identical with the Eurasian wolf, namely three in both turbinal types. This pattern supports observations of a species-specific number of these turbinals in other mammalian taxa like lagomorphs (RUF 2014) or didelphids (MACRINI 2014). MACRINI (2012) found a variation in the number of ectoturbinals in one specimen of the southern marsupial mole (*Notoryctes typhlops*), namely two on the left side and three on the right side. However, the ectoturbinals not only refer to the frontoturbinals but also to the interturbinals as already pointed out e.g., by SMITH & ROSSIE (2008). MACRINI's (2012) terminology was examined on basis of the µCT cross sections of the respective specimen available on DigiMorph (*http://www.digimorph.org/specimens/Notoryctes_typhlops/*, last access June 22nd 2019). To the author's knowledge the third ectoturbinal on the right side in *Notoryctes typhlops* is an interturbinal ventral to frontoturbinal 2. Neither the narrowing nor the shortening of the snout altered the number of the fronto- and ethmoturbinals, and this proves a phylogenetic or ontogenetic predetermination for *Canis lupus familiaris* as well.

Beside the ethmoturbinals and the frontoturbinals interturbinals are present in the nasal cavity of wolves and dogs as well. In the present study the interturbinals have been subdivided into two groups. Interturbinals are reported to exhibit a heterogeneous presence and distribution within a species and even between left and right side within individuals (RUF 2014, WAGNER & RUF 2019). RUF (2014) named this type of interturbinals additional interturbinals. Nevertheless, other interturbinals have been proven to correspond to the pattern of the ethmoturbinals and frontoturbinals, namely a species-specific presence and distribution (WAGNER & RUF 2019). In their study of the dogs WAGNER & RUF (2019) introduced them as the second interturbinal-type, called prominent interturbinals. The Eurasian wolves and the dogs have four of them, one within the pars ethmoturbinalis between ethmoturbinal I and II, and three within the pars intermedia (medial to frontoturbinal 1, between frontoturbinal 1 and 2, and ventral to frontoturbinal 3).

The determined number of the ethmoturbinals, frontoturbinals, and prominent interturbinals (except interturbinal γ) among all dog breeds reflects the short time scale in which the different snout types evolved when comparing the dog specimens at hand with the varying snout lengths among other mammal taxa (e.g., HARCOURT 1974). For example, feliforms have generally a reduced number of

olfactory turbinals within the pars intermedia compared to the supposed carnivoran *grundplan* (see p. 86). The domestic cat (*Felis catus*) has three frontoturbinals and one interturbinal (PAULLI 1900c). The African lion (*Panthera leo*) has three frontoturbinals and no interturbinal (pers. obs.). Also in primates the pars intermedia is smaller and houses one to two frontoturbinals and no interturbinal (MAIER 1993a, SMITH & ROSSIE 2008). *Daubentonia madagascariensis* varies in having three frontoturbinals and three interturbinals (MAIER 1993a, MAIER & RUF 2014). Within primates the change to a primary visual orientation also affected the pars ethmoturbinalis in reducing the number of three ethmoturbinals and one interturbinal in strepsirrhines (e.g., *Microcebus murinus*) to one or two ethmoturbinals in simiiforms (Cebidae, Aotidae, Cercopithecidae, Hylobatidae) (MAIER 1993a).

Nevertheless, a significant difference between wild living mammal species which evolved through natural selection over millions of years (e.g., Canidae, WANG & TEDFORD 2008), and dog breeds which developed in a short time scale through domestication is proven: in the short snouted dogs the plesiomorphic number of ethmoturbinals, frontoturbinals, and prominent interturbinals for *Canis lupus* is forced to develop within the restricted nasal cavity. Longer snouted caniforms have an enlarged number of fronto- and interturbinals compared to feliforms. For example, the South American coati (*Nasua nasua*) has four frontoturbinals with two interturbinals, and the brown bear (*Ursus arctos*) has four frontoturbinals and four interturbinals (PAULLI 1900c). Similar to the brachycephalic breeds in the long snouted dogs the number of ethmoturbinals, frontoturbinals, and prominent interturbinals has not changed either.

Among the dog breeds the number of additional interturbinals shows a high intraspecific variation within the pars intermedia, but not within the pars ethmoturbinalis. Both the elongation and the shortening of the snout altered the number of additional interturbinals, but not as expected. Generally, the number is reduced in the brachycephalic breeds as expected, but on the contrary not in the narrowed snout of the visual oriented sighthounds. The analysis of the juvenile borzoi, its six adult conspecifics, and the adult saluki clearly contradicts BREHM's (1876) hypothesis that sighthounds have less olfactory turbinals within their slender snout (see citation ch. 1.4 Morphological variation in the dog's skull: 13). Instead, the borzoi and the saluki are similar to the German shepherd (WAGNER & RUF 2019) and the Greenland dog. On average, these breeds have a higher number of additional interturbinals within the pars intermedia compared to the Eurasian wolf. Furthermore, in the four mentioned breeds the additional interturbinals are distributed between all frontoturbinals, but in the Eurasian wolves they are only present medial to frontoturbinal 1 and ventral to interturbinal β.

The overall comparison of the effect of a changing facial length on the turbinal number presumes an obvious difference between the dog's short-term artificial selection and the natural selection over millions of years in other mammal taxa (LEONARD *et al.* 2006, WANG & TEDFORD 2008, WESTHEIDE & RIEGER 2010). During the evolution of wild species, the number of all turbinals changes (PAULLI

1900a, b, c, MAIER 1993a, MACRINI 2012, RUF 2014), whereas in the dog only the additional interturbinals vary. This pattern proves that this type of turbinal is the least genetically determined, so it is first affected by morphological changes within the nasal cavity, obviously on an intraspecific level. On the example of the dog this morphological change refers to the postnatal facial growth which is inhibited in brachycephalic breeds and accelerated in dolichocephalic breeds (OECHTERING *et al.* 2016). Furthermore, the positive correlation of the number of additional interturbinals with snout length is not associated with the specific selection of a breed for scent working or for hunting by sight (e.g., ROBIN *et al.* 2009). However, the reason for the reduced number of additional interturbinals and the loss of interturbinal γ in the long snouted Groenendael specimen remains speculative, as the olfactory performance of the breed does not seem to be less developed compared to other scent hounds (see ch. 4.4.2 Olfactory performance: 110).

4.1.1.1 Perspectives of the establishment of a mammal turbinal formula

For mammals or especially placentals no general plesiomorphic 'turbinal formula' comparable to the common placental dental formula is given so far (MACRINI 2014, VAN VALKENBURGH *et al.* 2014b). The number of ethmoturbinals in mammals generally spreads between three and five (STARCK 1982). Their plesiomorph number is three (SCHRENK 1989), although according to MACRINI (2014) marsupials primary have four ethmoturbinals. A further basic pattern is the presence of an interturbinal between ethmoturbinal I and II in placentals (SCHRENK 1989, RUF 2004, 2014), and between ethmoturbinal II and III in marsupials (MACRINI 2014). Regarding the pars intermedia a mammal *grundplan* for the number of its frontoturbinals and interturbinals cannot be defined. First, many authors still summarize the frontoturbinals and the interturbinals according to the nomenclature of PAULLI (1900a, b, c). Second, according to SMITH & ROSSIE (2008) and MACRINI (2012) frontoturbinals are difficult to homologize between species and among higher taxa. SMITH & ROSSIE (2008) emphasize that e.g., the single frontoturbinal of the gray mouse lemur (*Microcebus murinus*) may not be homologous to the first frontoturbinal of non-primates.

4.1.1.2 The turbinal number of the carnivoran *grundplan*

Data about the turbinal number and terminology of the fully-grown turbinal skeleton in other members of the genus *Canis*, the family Canidae, or the order Carnivora are rare, as recent studies on the turbinal skeleton mainly focus on the morphofunction and no details on single turbinals are given (e.g., VAN VALKENBURGH *et al.* 2011, 2014a). The only detailed description in which the single turbinals are named is given by PAULLI (1900c) who investigated beside the dog one further canid, namely the

Arctic fox (*Vulpes lagopus*) which he said to correspond to *Canis lupus familiaris* in its turbinal skeleton. PAULLI (1900c) investigated eleven additional caniforms covering Ursidae, Procyonidae, Mustelidae, Mephitidae, and Phocidae; the eight species of feliforms belong to Viverridae, Herpestidae, Hyaenidae, and Felidae. PAULLI's (1900c) descriptions reveal that the carnivoran *grundplan* of the pars ethmoturbinalis includes three ethmoturbinals with one prominent interturbinal between ethmoturbinal I and II. These four turbinals are present in all twenty-one carnivoran species PAULLI (1900c) investigated. Consequently, the order represents the presumed ancestral placental pattern cited above. Among the caniforms two species have four ethmoturbinals (harbor seal, *Phoca vitulina*, and gray seal, *Halichoerus grypus*), and two species have five ethmoturbinals (South American coati, *Nasua nasua*, crab-eating raccoon, *Procyon cancrivorus*). Further interturbinals within the pars ethmoturbinalis are present in species of both carnivoran superfamilies (PAULLI 1900c). As the ectoturbinals refer to the frontoturbinals and to the interturbinals (e.g., SMITH & ROSSIE 2008), it is difficult to distinguish between these two types on the basis of both PAULLI's (1900c) descriptions in the text and his figures. Another difficulty is that PAULLI (1900c) depicted the nasal cavity of nearly all species of the caniforms, but of the feliforms just the domestic cat (*Felis catus*) and the lion (*Panthera leo*). For the remaining feliforms the exact determination of the frontoturbinals and the interturbinals based on PAULLI's (1900c) text notes alone is vague. It can be said that within the pars intermedia carnivorans basically have five ectoturbinals whose number can be raised in caniforms and reduced in feliforms. Most probably, these ectoturbinals represent one interturbinal medial to frontoturbinal 1 in caniforms, maybe also in feliforms, three frontoturbinals in both superfamilies, and either a second interturbinal or a fourth frontoturbinal in caniforms. According to PAULLI's (1900c) illustrations the most caudal ectoturbinal in the caniforms seems to be more likely frontoturbinal 4 than a further interturbinal as supposed in the dog in the current study (interturbinal β). In sum, *Canis lupus* obviously represents the carnivoran or even placental *grundplan* pattern at least in its pars ethmoturbinalis. Regarding the pars intermedia the comprehensive descriptions of PAULLI (1900c) cannot assist in the elucidation if the dog represents the carnivoran plesiomorphic pattern. Therefor further investigations on the identification of the turbinals –especially the differentiation between fronto- and interturbinals– in different carnivorans and other mammal orders are required.

4.1.1.3 A new approach for the terminology of interturbinals

As the prominent interturbinals are showing the same pattern like the frontoturbinals and the ethmoturbinals, namely a species-specific presence and distribution, it is valid to include this type in the *grundplan* of each mammal species as well. This method is already realized for interturbinal α which is included in the placental *grundplan* (see ch. 4.1.1.1 Perspectives of the establishment of a mammal turbinal formula: 85). As the frontal sinus is a plesiomorphic character at least within the species *Ca-*

nis lupus (CURTIS & VAN VALKENBURGH 2014), its associated septum-forming interturbinal γ is assigned to the prominent interturbinals despite its absence in some brachycephalic breeds (see **Table 5**, and ch. 4.3.2 Influence of dermal bone growth on intranasal structures: 101). Despite the uncertainty concerning the naming of interturbinal β (frontoturbinal 4 sensu SCHLIEMANN 1966) in *Canis lupus* the four prominent interturbinals are numbered from α to δ. Two different options were possible for the order, namely either following the rostrocaudal order parallel to the fronto- and ethmoturbinals as used by MAIER & RUF (2014: see their fig. 4C); or following the developmental order homologous to the fronto- and ethmoturbinals but in reverse direction, namely from ventral to dorsal. Finally, the second choice was preferred, as the ontogeny was given a higher priority and additionally seems to be unlinked between the prominent interturbinals and the fronto- and ethmoturbinals. According to the difference in the ontogenetic development between the prominent and the additional interturbinals (see ch. 4.1.2 Developmental patterns of the olfactory region in the dog: 91) the second interturbinal between interturbinal α and ethmoturbinal II should be more likely grouped with the prominent interturbinals. Even if it is smaller and less complicate, its presence in all three Eurasian wolves could support the reinterpretation. However, the additional interturbinals which mainly cause the variation in the number of olfactory turbinals among the dogs are separated from the prominent ones and not numbered.

4.1.1.4 Re-evaluation of the turbinal terminology in the dog

Although diverse authors like ALLEN (1882) or ZUCKERKANDL (1887) already present a terminology of the turbinal skeleton in the dog and other mammal species, PAULLI (1900a, b, c) is one of the most regarded and cited authors in recent literature (e.g., MILLER *et al.* 1964), as his comprehensive work "still has to serve as a major source of information" (MAIER 1993b: 176). However, PAULLI (1900c) and other authors studied postnatal stages, whereas SCHLIEMANN (1966) identified the turbinals based on prenatal dog stages and hence regarded their developmental patterns. As the histological material of these prenatal dogs was investigated in the present study for the re-evaluation, beside PAULLI (1900c) also SCHLIEMANN's (1966) naming of the olfactory turbinals is used as reference. Additionally, SCHLIEMANN (1966) differs from PAULLI (1900c) and the above named authors as he refers to the nomenclature used by VOIT (1909). Whereas SCHLIEMANN (1966) gives information about the sizes of the three prenatal whippets, PAULLI (1900c) just noted that the dog individuals he used were of different ages, breeds, and body sizes. In the present study more ontogenetic stages were available, namely beside the three prenatal whippets handled by SCHLIEMANN (1966) the neonate whippet and three juvenile dogs of different breeds. Based on these additional ontogenetic stages the terminology of the olfactory turbinals, and of the lamina semicircularis, has been re-evaluated in comparison to PAULLI (1900c) and SCHLIEMANN (1966) the following way (from medial to lateral):

PAULLI (1900c)	SCHLIEMANN (1966)	Present study
endoturbinal I	lamina semicircularis	lamina semicircularis
ectoturbinal 1	-absent-	interturbinal δ
ectoturbinal 2	frontoturbinal 1	frontoturbinal 1
-not named-	-not named-	interturbinal γ
ectoturbinal 3	frontoturbinal 2	frontoturbinal 2
ectoturbinal 4	frontoturbinal 3	frontoturbinal 3
ectoturbinal 5	frontoturbinal 4	interturbinal β
-not named-	frontoturbinal 5	epiturbinal (etI)
endoturbinal II	ethmoturbinal I	ethmoturbinal I
ectoturbinal 6	interturbinal	interturbinal α
-not named-	epiturbinal (etII)	interturbinal
endoturbinal III	ethmoturbinal II	ethmoturbinal II
endoturbinal IV	interturbinal/ethmoturbinal III*	ethmoturbinal III

* SCHLIEMANN (1966) names the turbinal in the text (p. 528) and in figure 15 interturbinal, whereas in figure 14 he labels it as ethmoturbinal III.

The re-interpretation closely resembles SCHLIEMANN (1966). Concerning the terminology of PAULLI (1900c) and several other authors, the three ethmoturbinals and the lamina semicircularis correspond to the four endoturbinals, and the three frontoturbinals and three of the four interturbinals to the six ectoturbinals. There is no doubt about the renaming of frontoturbinal 5 sensu SCHLIEMANN (1966) and of the epiturbinal of ethmoturbinal II sensu SCHLIEMANN (1966) in 'whippet C'. The attachment of the epiturbinal to ethmoturbinal I in its entire length corresponds exactly to REINBACH's (1952b: 57) definition of epiturbinals "that grow out the wall of the turbinals [i.e., fronto- and ethmoturbinals] […] and hence are attached to them." (translation: FW). In the investigated juvenile and adult dogs the epiturbinal runs rostrally onto the lamina horizontalis. All turbinals of the pars intermedia are attached with their base to the frontal caudal to the lamina horizontalis in all specimens and ontogenetic stages in this study. Contrary to REINBACH's (1952b) definition of epiturbinals in 'whippet C' the additional interturbinal ventral to interturbinal α is rostrally connected with the lamina horizontalis and just fuses in its caudal end to ethmoturbinal II. This topography is also observed for the second additional interturbinal in the pars ethmoturbinalis present in borzoi NMBE 1052706 or in Cavalier NMBE 1062998, for example. In fact, ethmoturbinal II has an epiturbinal-like lamella on the dorsal side of its stem, but in no dog specimen or ontogenetic stage a connection with the lamina horizontalis was observed. SCHLIEMANN's (1966) terminology of the most caudal turbinal within the pars ethmoturbinalis remains unclear, but according to the results from this study there is no doubt that it has to be ethmotur-

binal III which forms the caudal process within the sphenoid sinus in adult dogs as reported e.g., by ZUCKERKANDL (1887, 'fünfter medialer Riechwulst') and PAULLI (1900c, 'endoturbinal IV').

The only turbinal that is difficult to identify is frontoturbinal 4 sensu SCHLIEMANN (1966). Interturbinals differ from frontoturbinals (and ethmoturbinals) in that they are smaller und develop later in ontogeny and in between the latter (VOIT 1909, REINBACH 1952b, RUF 2004, SMITH & ROSSIE 2008). The developmental order cannot serve as a decision support, as the respective turbinal could be either the last developing frontoturbinal or the first developing interturbinal within the pars intermedia. The second character, namely the size of interturbinal β, is associated with the shape. It reflects the morphological pattern of the three frontoturbinals as a double scroll in the neonate. Hence, this shape differs conspicuously from the other two short, straight, and smaller prominent interturbinals, interturbinal γ and δ. A size reduction among the ethmo- and frontoturbinals from the most anterior to the posterior turbinal is obviously a general pattern which is described in many mammals e.g., in *Dasypus novemcinctus* (REINBACH 1952a). The morphometric analyses of the juvenile and adult dogs in this study prove these morphological observations. In most of the specimens the IAT and the SDEN of interturbinal β fall between the values of the frontoturbinals and the prominent interturbinals, but they are predominantly closer to the former. In contrast to the neonate whippet, in the adult individuals an intermediate stage can also be observed in the shape comparison between all turbinals. The first three frontoturbinals are dendritic in the Eurasian wolf and in the dolichocephalic adult dogs (borzoi, saluki, German shepherd, Groenendael, and Greenland dog). Interturbinal δ complicates to multiple scrolls and interturbinal γ is simplified as it caudally continues into the septum of the frontal sinus. Interturbinal β is mostly multiple scrolled in the dolichocephalic dogs according to interturbinal δ, but can complicate to dendritic in the Eurasian wolf corresponding to the three frontoturbinals. However, in sum neither the ontogenetic nor the morphologic and morphometric characters give clear evidence about the intermediate stage of interturbinal β. Hence, either it is the smaller, looser, and simpler last developing frontoturbinal 4, or the larger, denser, and more complicate first developing prominent interturbinal within the pars intermedia. The decisive reason for the renaming is a more unsophisticated character of interturbinals, namely their less medial extension combined with the overlapping by the fronto- and ethmoturbinals in medial view of the turbinal skeleton, in the case of interturbinal β by ethmoturbinal I (PAULLI 1900a, SMITH & ROSSIE 2008, RUF *et al.* 2015). In conclusion, on the basis of the data in this study frontoturbinal 4 sensu SCHLIEMANN (1966) is tentatively renamed as interturbinal β.

4.1.1.5 The dog's plesiomorphic turbinal pattern as observed in *Canis lupus lupus*

The *grundplan* pattern of the turbinal skeleton of the dog is defined based on the Eurasian wolf as the dog's ancestor to which the breeds in the present study are compared. All subspecies of the gray wolf

including the dog are macrosmats which furthermore depend on a high respiratory efficiency (PETERSON & CIUCCI 2003, HALL *et al.* 2016). The breeds investigated in this study cover a wide array of breeding history, function for humans, and head shapes. All of these components have more or less effects on the respiratory and olfactory part of the turbinal skeleton, and are sometimes affecting each other.

The current study proves that several of the already described species-specific characters in dogs and gray wolves are plesiomorphic among canids and belong to the *grundplan* of *Canis lupus* (**Table 7**): (1) the maxilloturbinal has a highly complex dendritic shape (SCHREIDER & RAABE 1981, VAN VALKENBURGH *et al.* 2004, CRAVEN *et al.* 2007); (2) the respiratory and the olfactory region are spatially separated (DAWES 1952, VAN VALKENBURGH *et al.* 2014a); (3) the frontoturbinals and the ethmoturbinals complicate to multiple scrolls; (4) when a frontal sinus is present (see ch. 4.3.2 Influence of dermal bone growth on intranasal structures: 101), frontoturbinal 1 and 2 expand caudally into it, and each of them into a separate chamber (PAULLI 1900c); (3) ethmoturbinal III expands caudally into the sphenoid sinus (PAULLI 1900c, MILLER *et al.* 1964); (4) interturbinal γ continues in its caudal end into the septum of the frontal sinus (only proven for the dog and the Eurasian wolf so far, WAGNER & RUF 2019).

4.1.2 Developmental patterns of the olfactory region in the dog

Within eutherians the lamina semicircularis and the ethmoturbinals develop earlier than the frontoturbinals (e.g., in muroid rodents, RUF 2004; the mouse lemurs, *Microcebus myoxinus* and *Microcebus murinus*, SMITH & ROSSIE 2008). Concerning the lamina semicircularis alone this developmental pattern is observed in the youngest ‘whippet A’, in that it is the first structure emerging as a small ridge on the nasal side wall (SCHLIEMANN 1966, and pers. obs.). Unfortunately, an earlier emergence of the ethmoturbinals compared to the frontoturbinals could not be verified in the available stages of the whippet. However, the pattern is observed in another histological serial section of a prenatal dog of unknown breed described by OLMSTEAD (1911). In this specimen the nasal capsule’s tripartite shape has diversified, but only ethmoturbinal I and II are developed, together with the lamina semicircularis (OLMSTEAD 1911).

The turbinals of neonate mammals have a simplified shape which starts to complicate during postnatal life (SMITH *et al.* 2016). Despite an increasing complexity, several ontogenetic patterns of the olfactory region that refer to its morphology and are observed in the perinatal whippets are also present in all adult dogs independent from snout length (**Table 7**): (1) ethmoturbinal I is separated into the anterior lamina and the posterior lamina. These two laminae emerge in the prenatal ‘whippet B’; (2) on the

turbinals epiturbinals are developing prenatally and postnatally. The most pronounced is the epiturbinal dorsal on the stem of ethmoturbinal I that is present as epithelial bulge in ‘whippet B’. This epiturbinal is absent in one specimen, the ancient pug ZMB_MAM 30980. These two patterns are generally present in therians (e.g., nine-banded armadillo, *Dasypus novemcinctus*, REINBACH 1952a, b; aye-aye, *Daubentonia madagascariensis*, MAIER & RUF 2014) and in monotremes (KUHN 1971, ZELLER 1989). Further patterns refer to therians only: (3) the frontoturbinals have a double scrolled basic shape which is observed in the neonate stage (PAULLI 1900a); (4) the uncinate process of the lamina semicircularis present in ‘whippet B’ is described in marsupials and in several eutherians like primates (e.g., *Daubentonia madagascariensis* and *Homo sapiens*, MAIER & RUF 2014), lagomorphs (e.g., *Oryctolagus cuniculus*, VOIT 1909, RUF 2014), or cingulates (pichi, *Zaedyus pichiy caurinus* = *Zaedyus minutus*, REINBACH 1955). The apparently absence of the uncinate process in the Eurasian wolf ZMB_MAM 93307 is caused by its covering by residual tissue which prevented its segmentation in the µCT cross sections.

A pattern which has not been described in mammals to date is the timing of development of the two interturbinal types in the dog. Similar to the fronto- and ethmoturbinals interturbinals which correspond to the prominent ones in the present study develop during prenatal ontogeny (SCHLIEMANN 1966 and pers. obs., WAGNER & RUF 2019; furthermore e.g., *Oryctolagus cuniculus*, VOIT 1909 and RUF 2014, *Caluromys philander*, MACRINI 2014; *Daubentonia madagascariensis*, MAIER & RUF 2014; *Ptilocerus lowii* and *Tupaia* sp., RUF *et al.* 2015). The additional interturbinals have been observed to arise mainly during postnatal life (SCHLIEMANN 1966 and pers. obs., WAGNER & RUF 2019). Two exceptions occurred: the interturbinal ventral to interturbinal α that has been grouped with the additional interturbinals is present in ‘whippet C’; and interturbinal δ is lacking in the juvenile German shepherd. The absence of this prominent interturbinal in the German shepherd specimen could be due to a variable or a heterochronic pattern. No exact data about the heterochronic skull development between the dog breeds was available and in all three juvenile dog specimens the growth and complication of the turbinal skeleton is still ongoing. As interturbinal δ is present in the neonate whippet, the other two juveniles, and all adult dogs including the two German shepherds, in the juvenile German shepherd the assumption of a delayed development due to a heterochronic effect is preferred.

4.1.3 Respiratory turbinals: the developmental pattern of the maxilloturbinal

ZUCKERKANDL (1887) defined four shape types of the maxilloturbinal in mammals that he adopted and enhanced from WIEDEMANN (1799). These types are linked with each other in an ontogenetic order reflected by the perinatal whippets. The common shape in mammals is a double scroll which is formed by a dorsal and a ventral lamella like described in ‘whippet B’ (ZUCKERKANDL 1887,

SCHLIEMANN 1966, and pers. obs.), and further e.g., in *Oryctolagus cuniculus* (VOIT 1909), *Dasypus novemcinctus* (REINBACH 1952a), *Tachyglossus aculeatus* (KUHN 1971), *Cheirogaleus medius* (SMITH & ROSSIE 2008), and *Daubentonia madagascariensis* (MAIER & RUF 2014). Even in the dog a double scrolled maxilloturbinal is species-specifically determined as it is pronounced in all studied specimens no matter how short a breed's snout has become (**Table 7**). The two more enhanced shape types (see below) still exhibit this basilar type in their shape e.g., in the canids through a dorsal and a ventral laterally scrolled main lamella (VAN VALKENBURGH *et al.* 2004, CRAVEN *et al.* 2007). An exception among the entire sample is pekingese SMF 35611 whose maxilloturbinal consists just of the stem which is fixed to the maxillary. However, the double scroll is indicated by a low dorsal and ventral ridge whose distal parts most likely persisted cartilaginous and consequently dissolved during maceration process. Similarly, the short nasoturbinal of all brachycephalic breeds is just its ossified caudal part. Generally, the anterior parts of the mammal nasal capsule including the cupula nasi anterior and the rostral part of the nasal septum, the maxilloturbinal, and the nasoturbinal persist as cartilage to the adulthood (STARCK 1979, MAIER 2002, RUF *et al.* 2015, HUPPI *et al.* 2018). Other short snouted dog specimens whose maxilloturbinal has rostrally an incomplete structure have a mixture of ossified and cartilaginous tissue (e.g., pekingese NMBE 1051962, pug NMBE 1051937). In the second ontogenetic step the maxilloturbinal develops an infolding on its medial side similar to the folded type represented by 'whippet C' (ZUCKERKANDL 1887). The most advanced is the dendritic shape already described in canids by WIEDEMANN (1799) and following authors (e.g., ZUCKERKANDL 1887) that is observed in the neonate whippet. The fast development of the dendritic shape until birth proves the importance of the respiratory organ for the dog in general (OECHTERING *et al.* 2016), whereas the olfactory turbinals are conspicuously more simple lamellae (SCHLIEMANN 1966, and pers. obs.). The single scroll as the fourth shape type is not represented in the investigated whippet stages. The separate development of this type from the basic double scroll that is completely unlinked to the folded and the dendritic type is proven in some Lemuriformes. The Coquerel's Sifaka (*Propithecus coquereli*) has a single scroll during its entire development and hence differs from the more complicate double scroll of the Ring-tailed Lemur (*Lemur catta*), four species of *Eulemur* (Red-collared Lemur *E. collaris*, Black Lemur *E. macaco macaco* and *E.macaco flavifrons*, Mongoose Lemur *E. mongoz*, and Brown Lemur *E. fulvus*), and the Gray Bamboo Lemur (*Hapalemur griseus*) (ZUCKERKANDL 1887, SMITH *et al.* 2016). According to ZUCKERKANDL (1887) the single scroll in adult stages evolves through the loss of the dorsal lamella like in *Propithecus coquereli* (SMITH *et al.* 2016: see their figs. 3, 9). Though, in muroid rodents the ventral lamella is reduced (RUF 2004). Some mammals with an extremely small dorsal lamella in their double scrolled maxilloturbinal represent an intermediate state e.g., felids (VAN VALKENBURGH *et al.* 2004: see their figs. 2, 9). Obviously, the dorsal lamella of the maxilloturbinal seems to be less genetically determined in its morphology in mammals in general. The same pattern is observed in the brachycephalic breeds, as the size and shape similarity between the dorsal and the ventral lamella is lower than in the dolichocephalic dogs. This means that the dorsal lamella is stronger affected by the

shortening of the snout in the dog by simplifying to a straight lamella whereas the ventral lamella is at least slightly dendritic. Maybe the difference is caused by the maxilloturbinal's rostrodorsal orientation parallel to the elevation of the hard palate as observed in the 3D models (e.g., chin NMBE 1051951). That would provide more space for the ventral lamella to the detriment of the dorsal lamella. However, this hypothesis cannot be verified descriptively in both the µCT cross-sections and the 3D models. Probably the use of geometric morphometrics can help here. Nevertheless, the general position of the maxilloturbinal within the nasal cavity has not markedly changed in brachycephalic breeds and neither in the sighthounds. In the borzoi and in the saluki the maxilloturbinal does not expand caudally and hence it does not displace the anterior lamina of ethmoturbinal I. Among the dolichocephalic breeds, the maxilloturbinal has a conspicuous dendritic shape in all specimens. Morphological comparisons by the use of the µCT cross-sections alone cannot elucidate a higher complication of the maxilloturbinal in the two investigated sighthound breeds in comparison to the German shepherd, the Groenendael, and the Greenland dog. Therefore, morphometric analyses on basis of segmented 3D models are needed to evaluate possible variations, as demonstrated here on the examples of the borzois and the German shepherds. Nevertheless, independent from measurements it can be noted that all the long snouted breeds represented here correspond to the Eurasian wolf in their morphology.

4.2 Morphometric aspects of the turbinal skeleton among dog breeds

4.2.1 IAT, SDEN, and TC of the maxilloturbinal

The maxilloturbinal shows a highly variable morphology among the dog sample, ranging from a dendritic shape with a large surface area (IAT), and high surface density (SDEN) and turbinal complexity (TC) in dolichocephalic breeds to the conspicuous simplification with low values in the three respective parameters in brachycephalic breeds. This correlation between shape and morphometrics within a species supports former studies that the dendritic shape is the most complex for the maxilloturbinal and hence serves the best respiratory efficiency (WIEDEMANN 1799, SCHREIDER & RAABE 1981, VAN VALKENBURGH *et al.* 2004). VAN VALKENBURGH *et al.* (2004) proved a positive correlation between a species' maxilloturbinal bone volume and its body mass in canids and felids. Two variables are hampering the comparison of the results: VAN VALKENBURGH *et al.* (2004) used 2D measurements of volume, this study used 3D measurements of surface area. A further obstacle is the correlation with body mass (VAN VALKENBURGH *et al.* 2004) versus skull dimensions (current study). The six adult borzois which have been investigated in the present study have a higher IFB and in total a longer face and overall skull than the two adult German shepherds. Regarding body dimensions, the racing dog is taller and naturally lighter:

		IFB[a]	CBL (mm)[b]	BLII (mm)[b]	SL (mm)[b]	Height (cm)[AKC]	Mass (g)[AKC]
BOR (n=6)	♂	≥0.68	≥217.9	≥199.8	≥122.7	≥71.1	34,019 – 47,627
	♀					≥ 66.0	27,216 – 38,555
GSD (n=2)	♂	≤0.66	≤199.0	≤183.6	≤107.2	61.0 – 66.0	29,484 – 40,823
	♀					55.9 – 61.0	22,680 – 31,751

a) see **Table 1**; **b)** see **Table S1** (Supplementary material), sexes are combined; abbreviations: p. 1; AKC = American Kennel Club breed standards; height = height at withers.

More similar to the present study is a positive correlation between skull length and the surface area and the complexity of the respiratory turbinals (maxilloturbinal plus nasoturbinal) that is proven among 55 species of a rodent subfamily, the Murinae (MARTINEZ *et al.* 2018).

In contrast to the volume, between the maxilloturbinal's packing (i.e., density) and body size, habitat, and activity pattern VAN VALKENBURGH *et al.* (2004) could not prove a correlation in their sampled carnivores. They conclude that the shape of the maxilloturbinal is phylogenetically predetermined, and that its solidified morphology might impede an adaptation to environmental changes that instead happens faster in a species' fur, body dimensions, and behavior (VAN VALKENBURGH *et al.* 2004). Contrary, MARTINEZ *et al.* (2018) prove an influence of the diet on the respiratory surface area, as vermivorous murine rodents have smaller respiratory turbinals than carnivorous and omnivorous members of this subfamily (see ch. 4.4.1 Respiratory efficiency: 105). The conspicuous decrease in IAT, SDEN, and TC in brachycephalic breeds proves the morphological analyses which reveal the premature growth stop of the maxilloturbinal's surface area (see ch. 4.3.2 Influence of dermal bone growth on intranasal structures: 103). The positive correlation between AT (in the entire turbinal skeleton and in the maxilloturbinal alone) with relative (IFB) and absolute snout length (NLII) gives rise to the question, if this growth pattern also appears in wild canid species. The evolution of the intranasal structures of wild canids under natural selection on a larger time scale could be affected by factors which are diminished in the dog breeds under almost exclusively artificial selection (DRAKE & KLINGENBERG 2010). VAN VALKENBURGH *et al.* (2014a, see their table 1) investigated ten canid species covering the genera *Canis*, *Lycaon*, *Nyctereutes*, *Otocyon*, *Speothos*, *Urocyon*, and *Vulpes* by µCT. The surface measurements of the respiratory and the olfactory region in the respective specimens correlated with body mass, but unfortunately they were not tested with skull dimensions (VAN VALKENBURGH *et al.* 2014a). A further issue is the smaller variation of snout length among wild canids or even carnivorans which do not cover the diversity observed in the domestic dog, especially in extreme brachycephaly (DRAKE & KLINGENBERG 2010, see also their fig. 3). The steep decrease of IAT in the maxilloturbinal with increasing brachycephaly among the dog sample even culminates in a conspicuously larger IAT of ethmoturbinal I in both modern pug specimens and in the King spaniel. To better understand the

mechanisms of turbinal growth and for including the actual results into a larger evolutionary context the domestic dog needs to be compared with shorter and longer snouted wild canids on the basis of length dimensions of the skull.

4.2.2 IAT, SDEN, and TC of the olfactory region

On the basis of morphometric analyses on sighthounds, German shepherds, and Eurasian wolves two patterns regarding the development of the two olfactory parts within the nasal capsule and of the lamina semicircularis in eutherians have been observed: first, the juvenile borzoi has a conspicuously larger proportion of AT within the pars ethmoturbinalis compared to the pars intermedia; in three adult dogs under study (two borzois, one German shepherd) the difference is smaller or even reversed. Considering the nearly exact resemblance of the juvenile borzoi's proportions to the Eurasian wolf a recapitulation of the ancestral stage within the domestic dog is assumed. Second, in the young borzoi the IAT of the lamina semicircularis is higher than in all three frontoturbinals, whereas in the adult dogs and in the Eurasian wolf frontoturbinal 1 and 2, sometimes also frontoturbinal 3, have a higher IAT. Combined with the ontogenetic observations in this study and on other mammal species (see ch. 4.1.2 Developmental patterns of the olfactory region in the dog: 90) an earlier growth of the lamina semicircularis and the ethmoturbinals is proven, whereas the frontoturbinals enlarge their AT mainly during later ontogeny (WAGNER & RUF 2019). In both cases the juvenile pug and the second adult German shepherd (SMF 93607) fit into the pattern. The higher juvenile-like ratio in the AT of the pars ethmoturbinalis in nearly all adult pugs supports the hypothesis regarding the persistence of short snouted dogs at a premature ontogenetic stage (GEIGER & HAUSSMAN 2016, OECHTERING *et al.* 2016). However, the other short snouted breeds (pekingese, King spaniel, chin) correspond to the Cavalier and the long snouted dogs. The possible reason for this heterogeneity among the toy breeds represented here cannot be elucidated with the current data analyses and the small sample size of pekingese, King spaniel, and chin. A suitable interpretation requires different ontogenetic stages of all respective breeds and probably volume measurements of the ethmoidal region. The IAT varies between the lamina semicircularis and the frontoturbinals among all adult brachycephalic to mesaticephalic dogs independent from the breed. Hence, the ratio between the pars ethmoturbinalis and the pars intermedia is not associated with the IAT between the lamina semicircularis and the frontoturbinals (e.g., in the ancient pug [MfN] 1845 the pars intermedia has a smaller proportion in AT, but the frontoturbinals have a higher IAT than the lamina semicircularis). The values in IAT and the proportions of AT of the lamina semicircularis prove that this structure is the least affected by the shortening of the snout. The morphometric data correspond to the uniform morphology of the lamina semicircularis among the different facial length types. The reason might be its different ontogenetic origin, as the lamina semicircularis is not a

turbinal, and its early development (SCHLIEMANN 1966, and pers. obs., RUF 2004, 2014, SMITH & ROSSIE 2008).

Based on the similar morphology, a large IAT, and a high SDEN and TC in the Groenendael and the Greenland dog can be assumed by the two reconstructed German shepherd specimens. Similar to the morphology the morphometric analyses in the borzoi clearly disprove BREHM's (1876) statement regarding the restricted space for the olfactory turbinals within the sighthound's narrowed snout. The borzoi's ethmoturbinals, frontoturbinals, and prominent interturbinals have a distinct large IAT, and a high SDEN and TC. The similar shape between the two investigated sighthound breeds justifies a comparable large, dense, and complex olfactory turbinal skeleton in the saluki. Hence, the ancient purebred saluki refutes an influence of northern dogs on the olfactory turbinals of the younger and initially mixed-bred borzoi (ASH 1927a, VOM HAGEN 1935). Due to their extremely small IAT and low SDEN and TC, the unexpected high number of additional interturbinals in the borzoi does not support a great enhancement of its olfactory ability. The higher value of IAT of frontoturbinal 1 compared to frontoturbinal 2 in borzoi NMBE 1051164 is probably caused by segmentation difficulties: as the turbinals in sighthounds are delicate, the transition between the stem of frontoturbinal 1 and the septum of the frontal sinus to that it is attached is not clearly visible in the segmented specimen. The same problem occurred in frontoturbinal 1 of the German shepherd MNHN 1985-1274. Furthermore, the caudal fusion of interturbinal γ was difficult to reconstruct in this specimen, resulting in its conspicuously high IAT.

4.2.3 Evaluation of the turbinal complexity (TC) as a new morphometric approach

Although several studies used morphometric methods for a mathematical estimation of the shape of the turbinals (SCHREIDER & RAABE 1981, CRAVEN *et al.* 2007) or other anatomical structures (e.g., the baculum, GARDINER *et al.* 2018), no definition for the term 'complexity' has established so far (MARTINEZ *et al.* 2018, WAGNER & RUF 2019).

The TC in the present study is a self-devised new morphometric approach which serves as an indicator for the degree of a turbinal's folding: the higher AT increases within a given AE the higher the complexity of a turbinal is. That means a turbinal has (1) more accessory lamellae (higher AT), (2) a denser packing in its lamellae (higher SDEN), or (3) both.

The formula results from statistical analyses with the use of the ANOVA whose application requires a sufficient sample size of the turbinals. All dogs including the juveniles and the brachycephalic ones have a minimum number of n=12 (maxilloturbinal, nasoturbinal, lamina semicircularis, and 9^{+} olfactory turbinals). But the lower the sample size is the weaker is the significance of statistical analyses.

Some mammal species may have a too low number of turbinals for an expressive correlation between AT and AE, like the leporid *Romerolagus diazi* (six turbinals + the lamina semicircularis, RUF 2014), or *Homo sapiens* (five turbinals + the lamina semicircularis; SCHWALBE 1882, MAIER & RUF 2014). In such examples a correlation in the ANOVA should not be tested within each individual separately, but on population- or species-level. Due to the generally lower intraspecific morphological diversity among other mammals compared to the dog (O´NEIL *et al.* 2015), individuals can be rather grouped to enlarge the overall sample size of the turbinals.

The TC was first introduced on the example of the borzoi in comparison to the German shepherd and the Eurasian wolf, all of which are long snouted (WAGNER & RUF 2019). During the subsequent segmentation and analyses of the brachycephalic to mesaticephalic breeds a strong influence of AT became apparent: despite the standardization of AT with snout length and breadth, the differences in IAT are still enormous e.g., in the maxilloturbinal: its maximum value (3.725, borzoi NMBE 1051164) is twentyfold higher than its minimum value (0.186, King spaniel). This high variation causes contrarieties in the illustration and interpretation of the values of TC. The nasoturbinal, for example, is a straight to slightly curved lamella with a SDEN of about 1 in all specimens. Hence, it is expected to have the lowest TC not only within each individual but especially among all dogs under study. But because of the abline's steep curve in the dolichocephalic individuals the TC of their nasoturbinal (e.g., German shepherd SMF 93607, 1.796) surpasses all turbinals of the brachycephalic breeds (e.g., ethmoturbinal I in the chin, 1.555). The values of the given example do not match with an expected higher TC in the chin's ethmoturbinal I which has two double scrolled laminae compared to the German shepherd's slightly curved nasoturbinal. On the contrary, the high variation in AT/IAT makes the domestic dog the ideal model to improve the approach of the alignment in the respective measurements among the sample. Then, also TC will be optimized for comparisons of the intranasal complexity between species and higher taxa among functional groups (microsmatic versus macrosmatic), morphological groups (body size, body mass, and snout length), ethological groups (activity pattern), physiological groups (mobility, metabolism), climatic adaptations (arid versus humid), and habitats (terrestrial, semi-aquatic, aquatic). A suitable comparison of the TC between samples with extremely divergent AT/IAT requires a modification of the presented formula by inclusion of a further standardization factor or by integration in IAT.

In the next step the ANOVA needs to be tested on other mammal species to approve the formula's validity. All 16 dog specimens and the Eurasian wolf whose turbinal skeletons have been segmented, measured, and statistically tested fitted into the correlation. The sample size should be high enough to assume a general correlation between AT and AE. But to date this can be only proven for *Canis lupus*; a transfer to other mammalian taxa without any verification is not justifiable. So, beside the alignment of IAT the validation of the new approach on a large dataset which covers different species across the

phylogenetic tree would be the second challenge for prospective morphometric analyses on the mammalian turbinal skeleton.

4.3 Skull shape: dermal bone growth in the domestic dog

4.3.1 Growth patterns of the viscerocranium among brachycephalic and dolichocephalic breeds

Long and short snouted dogs separated in ancient times (YOUNG & BANNASCH 2006, see ch. 1.3 The forming of breeds: 8). Whereas sighthounds are still used and bred for coursing, either for hunting or just for sports, brachycephaly in its present exaggerated form occurs generally among small breeds which serve for companion and fashion (BECKMANN 1895, DRAKE & KLINGENBERG 2010, COILE 2015). Although small companion dogs already appeared in ancient times e.g., during the Roman era their radiation just began during the Victorian era (HARCOURT 1974, PARKER *et al.* 2004, BOYKO *et al.* 2010). Many modern breeds emerged from a small gene pool by close breeding (SUTTER *et al.* 2004, BJÖRNERFELDT *et al.* 2008, SCHOENEBECK & OSTRANDER 2013). These founder effects which are caused by isolation lead to genetic drift; therefore, they may be transferable to the evolution of new species in the wild on a larger time scale (DARWIN 1859, DRAKE & KLINGENBERG 2010). By contrast, the crucial selection pressure on dog breeds is no longer driven by nature, but artificially by the breed standards prewritten by the diverse Kennel Clubs for their registered members (PARKER *et al.* 2004). As a result, evolutionary processes like the creation of different phenotypes resulting from mutations and genetic variation can be observed on the high diversity of dog breeds on a short time scale (DRAKE & KLINGENBERG 2010). The crucial factors during dog domestication were at last deactivated natural selection and human care for extraordinary creatures which otherwise would not be able to survive in the wild (DRAKE & KLINGENBERG 2010, MARCHANT *et al.* 2017, SANDOE *et al.* 2017).

Beside the morphology, the absent elongation and caudal extension of the maxilloturbinal in the borzoi could be explained by the shape of the dermal bones in which the elongation of the sighthound's face might not have changed its proportions (DRAKE & KLINGENBERG 2010). Contrary, SIEGEL & MOONEY (1990, in OECHTERING *et al.* 2016) suggest an elongation of the dog's face in the maxillary alone. For brachycephalic breeds exact information about a possible change of their facial proportions is given neither, just that the shortening affects the viscerocranium (OECHTERING *et al.* 2016). This part of the cranium includes the premaxilla, the maxilla, the nasal, and the bones of the nasal cavity, and further the palatine, the zygomatic, the lacrimal, the pterygoid, and the mandible (see table 3 in MILLER *et al.* 1964). Maybe the hypothesis cited and advocated by OECHTERING *et al.* (2016) refers to the evolution of the dog on the species-level, whereas within the breeds the proportions remain stable as changes in the cranial development affect the whole skull with its single dermal bones (DRAKE &

KLINGENBERG 2010). A verification requires more precise analysis of proportions based on finer scaled measurements through sub-divisions of the snout, as done by the use of geometric morphometrics by DRAKE & KLINGENBERG (2010), FONDON & GARNER (2007), SCHOENEBECK *et al.* (2012), and MARCHANT *et al.* (2017). The three latter studies combined their morphometric data with genetic analyses to detect the gene loci which affect the head shapes among the dog breeds.

All members of the caniforms exhibit a longer snout compared to their sister taxon, the feliforms (VAN VALKENBURGH *et al.* 2014a). The deactivated natural selective pressure due to human-controlled dog breeding promoted the emergence of extremely brachycephalic forms which even outperform short snouted feliforms (DRAKE & KLINGENBERG 2010). HAWORTH *et al.* (2001) genotyped different dogs and localized a point mutation (homozygous and heterozygous) in form of a T396 allele on the Treacher Collins Syndrome gene (*TCOF1*) in five brachycephalic breeds. Whereas in the study of HAWORTH *et al.* (2001, see their table 4) all four dolichocephalic and eight of eleven mesaticephalic breeds carry the homozygous C396 allele which expresses proline at position 117 (Pro117), in short snouted dogs a substitution to serine (Ser117) occurred. This mutation is believed to have evolved just once during dog domestication that separated long and short snouted dogs (HAWORTH *et al.* 2001). A sequence analysis of Quantitative Trait Loci (QTL) proves a positive correlation between single nucleotide polymorphism (SNP) frequency on two derived alleles on the canine chromosomes CFA1 and CFA5 and the degree of brachycephaly (BOYKO *et al.* 2010). Short faced breeds also display a missense mutation in the bone morphogenetic protein 3 (*BMP3*) on CFA32 (SCHOENEBECK *et al.* 2012). Similarly associated with brachycephaly is a dysfunction on the SPARC-related modular calcium binding gene (*SMOC2*) located at the basement membrane protein 40 (BM-40) that controls cellular growth factors in the bone and further tissues (GÖHRING *et al.* 1998, MARCHANT *et al.* 2017). All these studies prove the caniform ancestral state of the mesaticephalic to dolichocephalic head type, whereas the evolution of the brachycephalic head type bases on mutations which accumulated among several gene loci.

Beside point mutations, tandem repeats are believed to have an effect on skull shape, too. Tandem repeats are two or more serial duplications of nucleotids in the DNA sequence (BENSON 1999). They occur for example on the canine runt-related transcription factor (*Runx-2*) regulator gene whose allele encodes the antagonistic working polyglutamines (Q; transcription driving) and polyalanines (A; transcription repressing) (FONDON & GARNER 2004). The length ratio (Q/A) between these two amino acids controls the activity of the allele: the higher the amount of alanine repeats (or the lower the amount of glutamine repeats) the weaker is the transcribed *Runx-2* protein. This reduces the transcription activation of target genes which induce osteoblast differentiation during ontogeny (FONDON & GARNER 2004, 2007). In association with the studies reviewed above, the greater length of polygluta-

mine tandem repeats reflects the canids' plesiomorphic condition and the shifted ratio in favor of the polyalanines the apomorphic condition among short snouted dogs.

With its diverse skull morphology the dog serves as a favorite model organism for comparisons of mutations either to other laboratory animals (e.g., mouse, HAWORTH *et al.* 2001; zebra fish, SCHOENEBECK *et al.* 2012) or to humans (HAWORTH *et al.* 2001, MARCHANT *et al.* 2017). Obviously, brachycephalic breeds are preferred for genetic analyses of pathologies in the cranial development as their skull shape extends far beyond the natural variation within the carnivoran order (DRAKE & KLINGENBERG 2010, SCHOENEBECK & OSTRANDER 2013). Contrary, the facial elongation of dolichocephalic breeds does not conspicuously surpass the maximal snout length in wild canids (DRAKE & KLINGENBERG 2010). Hence, mutations on DNA sequences which affect facial length growth might easier to be found in extreme brachycephalic breeds than in long snouted breeds. Furthermore, short snouted dogs are important model organisms with respect to human genetic defects (SCHOENEBECK & OSTRANDER 2013, MARCHANT *et al.* 2017). Brachycephaly also occurs in humans and manifests in growth zone defects during cranial development similar to short faced dogs (SCHOENEBECK & OSTRANDER 2013). The diverse genetic mutations in short snouted dogs cause the postnatal growth inhibition in their viscerocranium e.g., through the restriction of osteoblast differentiation causing hypoplasia, or through an early syntosis (FONDON & GARNER 2004, SCHOENEBECK *et al.* 2012, SCHOENEBECK & OSTRANDER 2013, OECHTERING *et al.* 2016). Medium to long snouted breeds obviously do not suffer from genetic defects in their skull shape. The young malformed pug (MNHN 2007-428) obviously suffered from a genetic defect, but unfortunately nothing is known about its syndrome[2] and the cause and year of its death. No literature is available to the author dealing with such kind of pathologic cranial morphology in the dog or other mammals, or even in human medicine.

4.3.2 Influence of dermal bone growth on intranasal structures

The morphological and morphometric differences among the dog breeds may be related some kind of pathologic changes in the brachycephalic specimens (see ch. 4.4.1.1 Brachycephalic breeds in the veterinary medicine: 107). But when including the whippets into the comparison as illustrated in **Table 7** it becomes evident that the deviations from the Eurasian wolf and the medium to long snouted breeds are instead similarities to perinatal stages. Although the dog's skull length is already prenatally determined by several gene loci, until birth dogs of all facial length types have a similar snub-nose (GEIGER & HAUSSMAN 2016, OECHTERING *et al.* 2016). The morphological differences in facial length growth

[2] Pers. commun. Jessica Lorenz, ENT assistant medical director, Tierklinik Hofheim, Katharina-Kemmler-Str. 7, 65719 Hofheim, Germany; via email, Dec. 13th 2018.

between long and short snouted dogs emerge mainly during postnatal ontogeny (OECHTERING *et al.* 2016). This allows the comparison of the adult brachycephalic dogs with the perinatally short snouted dolichocephalic whippets in the present study. Due to the postnatal growth inhibition the brachycephalic breeds represented in this study resemble the perinatal ontogenetic stage (OECHTERING *et al.* 2016). The following similarities between the whippets and the brachycephalic adult dogs prove this conclusion: (1) the olfactory turbinals have a simplified shape like in the neonate whippet and become more complicate after birth in non-brachycephalic breeds; (2) the anterior process of the anterior lamina of ethmoturbinal I grows earlier (first presence in 'whippet B') than the anterior process of the posterior lamina of ethmoturbinal I (first presence in the neonate whippet); (3) interturbinal α has no rostral process until the neonate stage, but in the two younger stages it merges rostrally into the lamina horizontalis and in the neonate stage additionally into the stem of ethmoturbinal II; (4) the frontal sinus is absent in the whippets and still developing in the six weeks old German shepherd. Hence, frontoturbinal 1 and 2 extend within the pars intermedia and fuse to the lamina cribrosa and prenatally with the limbus praecribrosus or limbus paracribrosus; (5) the septum-forming interturbinal γ forms a crest in the neonate whippet. Associated with the heterogeneous development of the frontal sinus in brachycephalic adult dogs its associated crest-like interturbinal γ is variably reduced or even absent.

All these characters are frequently observed among the sampled brachycephalic specimens and indicate clearly that in some characters their turbinal skeleton in fact persists at an early ontogenetic stage. This result corresponds to former studies on the external cranial bones of dogs (mainly the viscerocranium) that prove that short snouted breeds are arrested at a juvenile stage (OECHTERING *et al.* 2016). Also the growth of the maxilloturbinal stops prematurely in short faced dogs proven by its less complicate shape as consequence of fewer accessory lamellae, and in its incomplete ossification which leaves gaps in the bone after maceration (see pekingese NMBE 1051962 or pug NMBE 1051937). However, the persistence at different ontogenetic stages (e.g., in the neonate whippet the posterior lamina of ethmoturbinal I has an anterior process, but not in the adult pekingese NMBE 1051962) again proves a heterochronic pattern of the turbinal skeleton's development in the dog.

The ethmoidal region of the German shepherd, the Groenendael, and the Greenland dog exhibits no considerable differences to the Eurasian wolf. Also within the olfactory region of the borzoi and the saluki all turbinals, no matter if fronto- and ethmoturbinals or prominent interturbinals, correspond in their topography, shape, and general morphology to the ancestral stage (**Table 7**). In contrast to the shortening and the elevation in brachycephalic specimens, the narrowing in the sighthound's snout and the additional declination in the borzoi's face have no considerable effect on the overall shape of its turbinal skeleton. It looks like in the Eurasian wolf, and accordingly like in the two segmented adult German shepherds. Only frontoturbinal 1 and 2 seem to be affected by the reduced space within the

slender nasal cavity in that they reach more caudally into the frontal sinus which appears more inflated.

The frontal sinus and the frontal bone are apparently associated in their growth in carnivorans (CURTIS & VAN VALKENBURGH 2014, CURTIS *et al.* 2015). To evaluate if the borzoi has in fact a larger frontal sinus than the Eurasian wolf and long snouted non-sighthounds morphometric data is required (e.g., CURTIS & VAN VALKENBURGH 2014, CURTIS *et al.* 2015). The function of the frontal sinus is still investigated, but it is supposed to be multi-functional (see CURTIS *et al.* 2015). For the slightly built racing dog the most likely advantage of an inflated frontal sinus mentioned by CURTIS & VAN VALKENBURGH (2014) could be weight reduction. Additionally, as the borzoi initially served for wolf, bear, and deer hunting, a large frontal sinus might assist for stress distribution while gripping the prey (ASH 1927b, CURTIS & VAN VALKENBURGH 2014). The absence of the frontal sinus in some brachycephalic dog breeds can be regarded as an artificially evolved apomorphy within the species *Canis lupus*. An intraspecific correlation between body size and sinus size (PAULLI 1900c) cannot be discussed, as among the present sample all small body-sized dogs are brachycephalic, and the larger sized dogs are dolichocephalic. Hence, a correlation between sinus size and body size which is unlinked to snout length cannot be tested on the basis of the available breeds. However, the loss of the frontal sinus due to reduced space in dependence on a specific skull morphology is no uncommon phenomenon among mammals. Some small to medium-sized carnivorans have lost or reduced their frontal sinus, too. The kinkajou (*Potos flavus*) is an example for a species that lost its frontal sinus as consequence of an adaptation as a nocturnal frugivore (CURTIS *et al.* 2015). Convergent to primates -and human created brachycephalic dogs- it evolved a shortened snout and forward oriented eyes which leave no space for the pneumatization of the frontal (PAULLI 1900c, MCGREEVY *et al.* 2004, CURTIS *et al.* 2015). Although its frontal sinus and the septum between frontoturbinal 1 and 2 are as well-developed as in the other longer snouted breeds, the Groenendael has a reduced interturbinal γ. Weather this pattern is breed-specific or an individual variation cannot be estimated on basis of the limited sample in this study.

Regarding ontogeny a genetic linkage of the growth between the dermal bones and the internal turbinal skeleton becomes clearly obvious. A proof of this hypothesis is noted by SCHOENEBECK *et al.* (2012: 4): “Distortion of the skull, as observed among brachycephalic and dolichocephalic dog breeds, affects bones presumably derived from endochondral and intramembraneous ossification.” The former refers to the cartilaginous turbinals, the latter to the dermal bones and to the turbinals’ appositional bones. This theory would also explain the complicate shape, the large IAT, and the high SDEN and TC of the olfactory turbinals in the sight-oriented borzoi that so far left a puzzling pattern (WAGNER & RUF 2019). The skull length in sighthounds implies a faster and/or continued growth linked with a complication of the turbinals beyond the mesaticephalic snout type; but it still correlates with IFB.

That is on the one hand demonstrated by the morphometric data, but on the other hand by the sighthounds' lesser surpassing of the carnivoran facial length variation (DRAKE & KLINGENBERG 2010). On the contrary, in short snouted dogs the facial bones and the turbinals persist at an infantile stage. The examples of the breeds in the present study clearly demonstrate some kind of genetically determined 'freezing' at a specified ontogenetic stage that affects the growth of both, the facial length and the turbinal skeleton. But this genetic linkage in the development between the two bony structures further proves that the growth patterns in the turbinal skeleton in brachycephalic and dolichocephalic dogs might be reversible. This refutes the hypothesis that the turbinal morphology of the Cavalier is similar to the King spaniel due to the short time scale in which this more medium snouted dog has been bred. This means, the intraspecific growth of the turbinal skeleton is less determined by phylogeny, but rather by the individual's ontogeny, as suggested by MAIER (1993b). The correlation between IAT, SDEN, and TC and snout length -or more exactly the facial length growth- furthermore suggests that physiology, like the breeding for smelling performance in scent hounds, does not seem to influence the morphology of the bony turbinals; at least on species-level. This may furthermore explain the high values in the three parameters in the olfactory turbinals among the primarily visually orientated sighthounds.

4.3.3 Ontogenetic growth: bone versus epithelium

The genetic studies summarized in chapter 4.3.1 Growth patterns of the viscerocranium among brachycephalic and dolichocephalic breeds (p. 99) combined blood samples from living animals and tissue samples of frozen individuals with measurements on macerated skulls within each breed. The analyses only focused on the genetic influence on dermal bone growth, but not on the growth of the soft tissue.

The chondrocranium, including its later developing replacement bones and appositional bones, and the dermatocranium derive from the neural crest. The neural crest cells originate from the ectoderm during the segregation of the neural tube from the epidermis. The olfactory epithelium with its multipotent cells, however, emerges from the neural crest as well, but furthermore from a second ectodermal derivate, namely the olfactory/nasal placode (FORNI *et al.* 2011). During ontogeny the olfactory epithelium differentiates into three multicellular compartments: the basal layer contains the multipotent horizontal basal cells which produce globose basal cells. The latter either differentiate to olfactory sensory cells (mature or immature) in the medium layer, or they generate non-neuronal Bowman's glands, microvillar cells, or cell sustentacular cells. All these three types are found in the apical layer. The cell development in the olfactory epithelium is controlled by other transcription factors than the chondroblast and osteoblast differentiation in the cartilage and the bone (SOKPOR *et al.* 2018). Hence, an unlinked development of soft and hard tissue can be assumed that leads to the question how far the genes

which are responsible for epithelial growth might have -or have not- been affected by the dog's change of skull shape.

This uncertainty is of particular importance for extreme brachycephalic breeds, especially in veterinary medicine. In the literature it is not immediately obvious, if the authors are referring to the hard and/or the soft tissue when talking about 'conchae' and 'turbinates', respectively. STURZENEGGER (2011) emphasized that the problems arising with brachycephaly are not exclusively related to the bony elements, namely the aberrant turbinals in the nasal opening and in the nasopharyngeal duct. The µCT scans of the nasal cavity of the two macerated modern pugs of this study support the hypothesis that the impairments in brachycephalic breeds are caused by the continuing growth of the soft tissue which follows the ancient mesaticephalic pattern after the simultaneous growth inhibition of the bone (LIU *et al.* 2015). This means that the thickness of the (respiratory and olfactory) epithelium could be like in medium snouted dogs e.g., the German shepherd. But as small brachycephalic dogs have a manifold smaller volume in their nasal cavity this epithelium obstructs the airway though the bony turbinals have an extremely reduced IAT and SDEN. The observed disequilibrium between both tissue types in brachycephalic breeds proves that beside the displaced bony aberrant turbinals the nasal cavity becomes restricted by the comparatively thickened soft tissue, as is the case with the pharynx concerning the relatively elongated soft palate (LIU *et al.* 2017).

4.4 Functional morphology of the turbinal skeleton in the wolf and the dog

4.4.1 Respiratory efficiency

Before local exterminations over the last decades the gray wolf (*Canis lupus*) was cosmopolitically distributed over the northern hemisphere and occupied diverse habitats ranging from deserts to the polar region (MECH 1974, FULLER *et al.* 2003). It is a cursorial hunter which preferably chases large ungulates over great distances (PETERSON & CIUCCI 2003). Obviously, the extremely complex and dense shape and the enlarged surface area of the maxilloturbinal are associated with an enormously efficient respiratory achievement in this highly mobile and adaptive species (HILLENIUS 1992, FULLER *et al.* 2003, VAN VALKENBURGH *et al.* 2004). As the dendritic form is already the most complex for a turbinal and serves the highest surface area (WIEDEMANN 1799, SCHREIDER & RAABE 1981, VAN VALKENBURGH *et al.* 2004), the sighthound cannot or rather has just no need to change the basic shape in its maxilloturbinal. However, the time scale in that sighthounds evolved as fast runners was maybe too short for considerable adaptations to a hot and arid climate (ASH 1927a, HOLE & WYLLIE 2007). Whereas the saluki is an ancient breed which adapted to a semiarid to arid habitat, the clearly younger northern borzoi breed resulted from crossings dating back at least to the late Middle Ages

(VOM HAGEN 1935, HOLE & WYLLIE 2007). Even after its establishment as a breed, during the 19th century a high inbreeding rate resulted in a strong population decline in the borzoi, so it was hybridized with the Scottish deerhound, another sighthound breed to enhance its genetic diversity (ASH 1927a). Hence, the choice of sighthound breed might be of particular importance here. Nevertheless, the morphometric data prove a larger IAT and a higher SDEN of the respiratory functioning maxilloturbinal in the borzoi in comparison to e.g., the scent orientated German shepherd – most likely through the increased growth of secondary and tertiary lamellae. Although these results refer to intraspecific variations, they correspond to a further study by VAN VALKENBURGH *et al.* (2011) on the maxilloturbinal's surface area between terrestrial and aquatic carnivorans: they proved a positive correlation to snout length, as far as to body mass and nasal chamber volume; and in all these three variables the surface density is higher in aquatic carnivores which rely more on heat and water preservation in the cold and saline sea. As an increasing body mass facilitates heat storage, it is inversely correlated with the proportional surface area of the maxilloturbinal (VAN VALKENBURGH *et al.* 2011). Among the dog breeds, however, the proportional surface area of the maxilloturbinal (AT_{mt}) increases with body mass (**Table S9**; **Fig. S4**; Supplementary material). But the unambiguously interlinking between body mass and snout length in the selected breeds has to be kept in mind, as in this study all small toy breeds are brachycephalic to mesaticephalic, and the larger German shepherd and the borzoi are dolichocephalic. For a more precise evaluation how far maxilloturbinal surface area is indeed associated with body mass in the dog independent from snout length, data of large short snouted breeds (e.g., boxer or bullmastiff) and of small medium to long snouted breeds (e.g., Italian greyhound or papillon) need to be included in the present sample. The dependence on a high thermoregulatory efficiency in aquatic carnivorans forced their maxilloturbinal to enlarge its surface area to the detriment of the olfactory surface area. That was demonstrated in the nearly reversed ratio between both mucosal types in comparison to terrestrial carnivorans (VAN VALKENBURGH *et al.* 2011). The opposite process can occur too, as observed on the example of the vermivorous murine rodents. The corresponding species depend on a good sense of smell to find their prey under various layers of earth. The reduction of the respiratory surface area to the advantage of an increased olfactory surface area in worm-eating rodents is enabled by their less important need for heat and moisture conservation as residents of a tropical habitat (MARTINEZ *et al.* 2018).

In both segmented borzoi specimens, however, no shift in the proportional surface areas compared to the two segmented German shepherds became obvious. That might be due to the shorter adaptation process and/or a species-specific genetic determination. The inconsistencies in habitat adaptation between the two studies of VAN VALKENBURGH *et al.* (2004, 2011) are argued by the authors in that bone volume and bone surface area do not need to correlate with each other (VAN VALKENBURGH *et al.* 2004). In sum, within the dog or even a functional group like the sighthounds the morphometric data on surface area might be of central relevance here, not the morphological description of the shape.

And this holds especially true for the maxilloturbinal, as the degree of its highly dendritic shape cannot be evaluated just descriptively.

Contrary to the postulated hypothesis (see p. 24), the borzoi's maxilloturbinal does not extend caudally to replace ethmoturbinal I. Two morphological characters can explain the absent replacement: first, the rostral part of ethmoturbinal I is reported to be covered by respiratory epithelium as well. This is proven on the basis of histological material which allows the differentiation between both epithelial types in the goat (*Capra hircus*, KUMAR *et al.* 1993), the horse (*Equus caballus*, KUMAR *et al.* 2000), muroid rodents (RUF 2004), strepsirrhine primates (SMITH *et al.* 2004, 2007), and the gray short-tailed opossum (*Monodelphis domestica*, ROWE *et al.* 2005), for example. Airflow experiments support the physiological studies as e.g., in the domestic cat (*Felis catus*) and in the bobcat (*Lynx rufus*) the rostral tip of ethmoturbinal I is positioned within the respiratory pathway (PANG *et al.* 2016). In a more recent study CRAVEN *et al.* (2007) reconstructed the nasal airflow in a Labrador retriever virtually, but they just differentiate between the maxilloturbinal and the ethmoturbinal region. Such division prevents an estimation of a potentially respiratory function of the rostral tip of ethmoturbinal I. However, a parallelization between short snouted felids and primary long snouted canids is refuted by VAN VALKENBURGH *et al.* (2014a) who proved a spatial separation between the maxilloturbinal and the fronto- and ethmoturbinals in Caniformia by views on different sagittal sections. The scan of an arctic fox (*Vulpes lagopus*, see fig. 3A in VAN VALKENBURGH *et al.* 2014a) is similar to the µCT scans of the Eurasian wolf (ZMB_MAM 93307) and the adult borzoi (NMBE 1051164, **Fig. 43**E–H) from the present study: the fronto- and ethmoturbinals are positioned dorsal to the lamina terminalis and the maxilloturbinal rostral to the nasopharyngeal duct. Corresponding to the sagittal sections airflow experiments on fresh material of dogs (breeds not named) revealed a non-contact of low-pressure breathing air with the ethmoturbinals (DAWES 1952). Obviously, in Caniformia the rostral part of the ethmoturbinals is not covered by respiratory epithelium and hence does not assist the maxilloturbinal in respiration. Hence, the second explanation refers to the location and expansion of the maxilloturbinal that is associated with the lamina terminalis: to replace ethmoturbinal I the maxilloturbinal would be forced to expand dorsal to the lamina terminalis into the olfactory recess; and accordingly off the respiratory pathway that would limit its respiratory function. Similar to felids in brachycephalic to mesaticephalic breeds ethmoturbinal I is rostrally expanding into the respiratory pathway. Assuming a species-specific distribution of olfactory epithelium on the fronto- and ethmoturbinals this shifted rostral process of ethmoturbinal I is neither expected to assist in respiration (SMITH *et al.* 2004, 2007). Future studies on airflow experiments in the dog should involve different breeds of various snout types and additionally regard possible subunits on a turbinal where required, like for example the anterior process of the anterior lamina of ethmoturbinal I. The use of geometric morphometrics can assist in investigating the position of the maxilloturbinal in relation to the rostral expansion and proportion of

the lamina terminalis between long and short snouted dogs. In this regard, the height and breadth of the nasopharyngeal duct should be considered as well.

Concerning the adaptation of the respiratory system to running in an arid environment, the Greenland dog functions as the high northern pendant to the southern saluki – despite the difference that the former is an endurance runner and the latter a sprinter (BANNISTER 1869, HOLE & WYLLIE 2007). A further similarity is their ancient history and their breeding in geographic isolation in spite of reported hybridizations of the Greenland dog with wild gray wolves (MARTIN 1845, BREHM 1876, ASH 1927a, BROWN *et al.* 2015). It needs to be discussed, if the Greenland dog has a comparatively higher AT in its maxilloturbinal than the shepherd dog and especially the Eurasian wolf as well. This ambiguity cannot be evaluated here for some reasons. First, the sample size is too small with just one specimen of the Greenland dog whose turbinal skeleton has not been virtually reconstructed yet; second, even though the Eurasian wolf is the dog's (including all sledge dog varieties) ancestor, it might not be suitable for morphological comparisons of the maxilloturbinal due to its adaptation to more temperate habitats (SILLERO-ZUBIRI 2009). For the evaluation of respiratory adaptations to an artic habitat, the Greenland dog has to be compared with wolf subspecies which inhabit a similar climatic zone like the arctic wolf (*Canis lupus arctos*, Canadian High Arctic) or the timber wolf (*Canis lupus occidentalis*, Alaska, NW Canada) (SILLERO-ZUBIRI 2009, VAN ASCH *et al.* 2013); third, the turbinal morphology of the gray wolf (*Canis lupus*) and consequently the variation between its subspecies and the different climatic zones they adapted to is nearly unknown. Greenland dogs and gray wolves are endurance runners which travel large distances e.g., for finding prey (BANNISTER 1869, PETERSON & CIUCCI 2003). It will be difficult to estimate how morphofunctional differences in the maxilloturbinal to the Eurasian wolf and simultaneous similarities to arctic gray wolves may evolved: they could either be convergent due to the Greenland dog's secondary adaptation, or they could be caused by occasionally hybridizations of 'Esquimaux dogs' (Greenland dog and Canadian Eskimo dog) with arctic wolves (MARTIN 1845, CLUTTON-BROCK *et al.* 1994). Nevertheless, the µCT data of the single individual at hand gives evidence that the Greenland dog's respiratory region should be as complex as in the two segmented borzois.

4.4.1.1 Brachycephalic breeds in the veterinary medicine

According to the reports by veterinarians the respiratory airway in brachycephalic dogs is obstructed by aberrant turbinals (rostral, RAT; caudal, CAT) and by constricted lamellae (OECHTERING *et al.* 2007, 2016, PACKER *et al.* 2015, HEIDENREICH *et al.* 2016). Regarding aberrant turbinals one of the two modern pugs (NMBE 1051937) might be such a candidate. Both the µCT sagittal sections and the virtual 3D model clearly show that the anterior process of the posterior lamina of ethmoturbinal I and

the rostral process of ethmoturbinal II are strongly oriented ventrally, so they are positioned between the maxilloturbinal and the nasopharyngeal duct within the respiratory pathway. The anterior process of the anterior lamina of ethmoturbinal I also expands far rostrally to the anterior end of the maxilloturbinal. Therefore, it is consistent to interpret these abnormalities as RAT and CAT. HEIDENREICH *et al.* (2016) concluded that the pug is more often affected by CAT. In the second modern pug (NMBE 1052345) no such aberrations are detected, although on the right side of its nasal cavity the anterior process of the anterior lamina of ethmoturbinal I reaches far rostrally as well and might also restrict the respiratory airflow as a RAT. Of course, two modern pugs are not a sufficient sample size for an evaluation. But as one seems to have RAT and CAT and the second RAT, these two individuals give evidence how such aberrant turbinals appear in macerated skulls. Veterinarians describe and depict the turbinal skeleton in living individuals including the covering soft tissue (see for example the illustration of the aberrant turbinals in a French bulldog in fig. 7 in LIU *et al.* 2017).

The second impairment refers to the constricted airflow by thickened lamellae which are in contact with each other (PACKER *et al.* 2015). This hypothesis is not proven in the bony tissue of the two modern pugs, but exactly the opposite. The own morphological observations correspond to OECHTERING *et al.*'s (2007) report of a lesser branching shape of the turbinals. The morphometric data of the recent study further support the descriptive analyses by the low values of IAT, SDEN, and TC. The stopped bone growth at an early postnatal stage in the turbinal skeleton occurs simultaneously in the dermal bones (OECHTERING *et al.* 2016). This result agrees with the statement of SCHOENEBECK *et al.* (2012) that brachycephaly (and dolichocephaly as well) affects dermal and endochondral bones similarly (see citation in ch. 4.3.2 Influence of dermal bone growth on intranasal structures: 102).

Unfortunately, veterinarian studies on respiratory difficulties in the dog focus nearly on just three breeds: the pug and the English and French bulldog (LIU *et al.* 2015, HEIDENREICH *et al.* 2016, OECHTERING *et al.* 2016). These dogs enjoy an increasing popularity and e.g., in the UK they belong to the ten most favorite breeds (OECHTERING *et al.* 2007, LIU *et al.* 2017). The other brachycephalic breeds in the present study (chin, pekingese, King spaniel) are less considered in such studies (PACKER *et al.* 2012). One reason might be their less popularity and consequently lower number and distribution of individuals. Hence, naturally their percentage among dogs which suffer from breathing difficulties is small, so veterinarians pay less attention to them. COILE (2015) listed for the pekingese an elongated soft palate and stenotic nares as health concerns, but interestingly no respiratory difficulties for the chin and the King spaniel. However, whereas in the Cavalier the brachycephalic obstructive airway syndrome (BOAS) is less common, the chin and the pekingese have a similar risk to suffer from this restriction as the pug and the two bulldog breeds named above (PACKER *et al.* 2015). Hence, the hypothesized adaptation of the chin and the pekingese to the shortened snout due to a longer consistent evolution and more responsible breeding can be refused (ASH 1927b). Given that the examined

specimens of these two breeds date from modern times they are similarly affected by the breeding practices of the Kennel Clubs (PARKER *et al.* 2004). Dogs which lived prior to the establishment of the Kennel Clubs and their inbreeding enhancing stud books are supposed to more resemble the ancestral morphology in their skull including its intranasal structures. That might also refer to the King spaniel whose roots date back at least to the 16th century (BECKMANN 1895). Intranasal studies by the use of µCT or MRT in which chin, pekingese, and both English toy spaniel breeds are of interest are not available in scientific literature so far. The present study proves the presence of CAT in one pekingese (ethmoturbinal I) and in each of the two chins (ethmoturbinal II). Furthermore, aberrant turbinals are not restricted to extreme brachycephalic dogs. Similar to the modern pug specimen one slightly brachycephalic Cavalier has a conspicuously enlarged CAT formed by the posterior lamina of ethmoturbinal I. Regarding the similar affection by BCS and the aberrant morphology of the turbinal skeleton it would be interesting to compare the turbinal epithelia of the less regarded breeds (chin, pekingese, English toy spaniels) with the modern pug.

Maybe some differences in the intensity of BCS among brachycephalic breeds refer to the maxilloturbinal's respiratory task. During rest at low ambient temperatures the thermoregulation in dogs occurs nearly exclusively on their inner nose, i.e. on the respiratory mucosa. During exercise or in a hot environment a dog starts panting in which the airflow additionally passes through the opened mouth to enhance the increased respiratory requirements (GOLDBERG *et al.* 1981, MACKENSEN *et al.* 2017). During an endotherms' postnatal growth its respiratory epithelium enlarges its surface area proportionally to body size to compensate the associated increasing metabolic rate (SMITH *et al.* 2016). The maxilloturbinal's premature growth inhibition reduces its thermoregulatory effectiveness due to the minimized surface area and the shortened way over which the breathing air passes (VAN VALKENBURGH *et al.* 2004, OECHTERING *et al.* 2016). If this restriction is too high, short snouted dogs are even panting during rest and at lower ambient temperatures compared to longer snouted breeds in order to achieve the required respiratory capacity (MACKENSEN *et al.* 2017). As juveniles brachycephalic breeds have fewer problems with BCS as their already smaller maxilloturbinal surface area is still able to ensure its respiratory performance. But only as long as the body size or rather the body mass and its associated metabolic rate do not surpass the epithelium's capacity. Then, the breathing difficulties are beginning to accumulate; in the pug and the English and French bulldog at an age of about twelve months (PACKER *et al.* 2015). With regard to the metabolic rate an additional worsening physiologic parameter is overweight (MACKENSEN *et al.* 2017). Despite their similar body size the pug and the pekingese are much heavier than the King spaniel and the chin according to the breed standards of the American Kennel Club (AKC; **Table S2**, Supplementary material). The breed-specific corpulence of the pug (and the English and French bulldog, LIU *et al.* 2017; see also the AKC breed standards) might be one of the most relevant causes for its higher suffering from breathing-related health problems, mainly stress and heat intolerance. That is further proven in the strong shift of the

relation between the maxilloturbinal's AT and the body mass in favor of the latter (**Fig. S4**, Supplementary material): with a similar AT, the modern pug is more massive than the pekingese, the King spaniel, and especially the chin. This raises the question, if the lower body mass in the three breeds enables the maxilloturbinal a more effective compensation of its minimized surface area. The ancient pugs and the similarly longer snouted Cavaliers also have a larger respiratory surface area with a simultaneously lower body mass than the ancient pug's corpulent present-day conspecifics. A thickened neck which is associated with breed-specific obesity further depresses the airways through adipose tissue (PACKER *et al.* 2015).

4.4.2 Olfactory performance

The gray wolf was naturally selected for an excellent sense of smell (PETERSON & CIUCCI 2003). Its olfactory turbinal skeleton is large and complex and completely fills the olfactory recess including the sphenoid sinus and the rostral parts of the frontal sinus. Its Eurasian subspecies bequeathed this trait to its domesticated descendants of which some have then been selected for this keen sense and evolved as sniffer dogs (ISSEL-TARVER & RINE 1996, HALL *et al.* 2016). They are employed in numerous fields of activities and perform a high variety of duties which include not only drug or explosive detection for police or the finding of missing people, but even early cancer diagnosis or warning of hypoglycernia for diabetics, for example (LESNIAK *et al.* 2008, ROONEY *et al.* 2013, AMUNDSEN *et al.* 2014, YANG *et al.* 2016). Regarding police work, the German shepherd is the typical scent hound candidate (HALL *et al.* 2015, YANG *et al.* 2016). This is supported by the morphology and morphometry of the olfactory turbinal skeleton of the two adult specimens in this study, namely in their complicate turbinals which have a large IAT, and a high SDEN and TC. However, recently the Belgian Malinois, another member of the four Belgian shepherd varieties (FCI), is the most preferred breed for police work, mainly for ethological reasons (SALGIRLI DEMIRBAS 2012). Unfortunately, no information about the use of the Groenendael in this working field is available. The specimen in the actual study has a reduced number of olfactory turbinals compared to the other large sized dog specimens (German shepherd, Greenland dog). As interbreeding between the four Belgian shepherd varieties is forbidden by the FCI (the AKC even lists them as single breeds), a first explanation might be a decades-long selection for different tasks in the Groenendael and the Malinois; with a lacking focus on sensitivity in sniffing in the Groenendael (VASALLO 2016). This provisional hypothesis is refused by two cancer detection studies: in the first, one Groenendael and three other dogs (Border collie, hard hair dachshund, and Rottweiler) did not significantly differ in their cancer detection performance (see Table V in AMUNDSEN *et al.* 2014). In the second study both a Groenendael and a Malinois had a sensitivity and specificity of 100% after sniffing trials of different cancer types (YOEL *et al.* 2015). As the sampled Groenendael specimen was not virtually reconstructed and measured, a possible correlation between

its reduced interturbinal number, the IAT and SDEN of its olfactory region, and their potentially effects on the smell performance in this Belgian shepherd variety cannot be evaluated yet.

The single Greenland dog specimen in the current study has a higher number of additional interturbinals than the Eurasian wolf and the German shepherd. Beside pulling the sledge over large distances with high power the Greenland dog is reported to have an outstanding scent ability qualifying it for hunting as well (MARTIN 1845, BANNISTER 1869). Probably its high smell performance is associated with its arctic home. Gray wolves generally use sight and scent for prey detection in open habitats (PETERSON & CIUCCI 2003). Two large herbivore species are living in the Alaskan and Canadian tundra, the caribou (*Rangifer tarandus*) and the muskoxen (*Ovibos moschatus*) whose biomass is up to 18kg*km^{-2}, whereas in some regions of African savannas the biomass of large grazers is a thousand times higher (KLEIN 1970). According to HALL *et al.* (2016) this low abundance of large prey forces northern predators like the arctic wolf or the timber wolf to rely stronger on olfaction than on vision. A higher smelling performance may distinguish these populations from their conspecifics of temperate zones (GITTLEMAN & HARVEY 1982). Data about possible subspecies or habitat differences in the olfactory turbinal morphology and the resulting smell performance of *Canis lupus* is not given in the literature. And studies on home range sizes in mammals mostly focus on species-level and not on intraspecific variations (GITTLEMAN & HARVEY 1982). In an olfactory experiment HALL *et al.* (2016) report a more sensitive sense of smell in the arctic fox (*Vulpes lagopus*) in contrast to its temperate close relative, the red fox (*Vulpes vulpes*). Similar to the maxilloturbinal the olfactory turbinal skeleton needs to be compared between the wolf subspecies (Eurasian wolf versus arctic and timber wolf), then probably the Greenland dog can be plotted into this dataset to evaluate its olfactory performance. If similarities to the Nordic wolf subspecies occur, also with regard to the olfactory part it will be difficult to differentiate between homology due to hybridization and convergent evolution as result of the breed's secondary adaptation to the arctic region.

All brachycephalic breeds included in the current study are members of the companion or toy dog group. In contrast to scent hounds and sighthounds which have been selected for work, toy breeds are preferentially bred for appearance and breeders focus on actual fashion trends (BECKMANN 1895, ISSEL-TARVER & RINE 1996, PACKER *et al.* 2012). The pug is considered as a dwarfed form of the molossian type (BECKMANN 1895, ASH 1927b, FCI). This group has been selected for fighting and the simultaneous disregarding of the smelling performance in its members diminished this sense (MARTIN 1845). Contrary, YOUNG & BANNASCH (2006) report the descent of scent hounds from mastiffs which had a sensitive nose. Although brachycephalic breeds exhibit a ventral shift of the main olfactory bulb (MOB), a potential negative effect on smelling performance has not been examined to date (ROBERTS *et al.* 2010). However, the morphology of this "primary brain center of the olfactory system" (BARON *et al.* 1983: 551) is associated with feeding and social behavior among Chrysochloridae, Tenrecidae,

Eulipotyphla, and Primates: sight and acoustic oriented species of these taxa have a small MOB (BARON *et al.* 1983). Nevertheless, a shortened snout allows a higher bite force which is needed for fighting or defending the owners and their home (YOUNG & BANNASCH 2006). This phenotype has been naturally selected in felids; especially larger species require a powerful jaw closing as they need to kill prey more massive than themselves (SLATER & VAN VALKENBURGH 2009). As an adaptation to the shortened face, ethmoturbinal I extends into the respiratory recess whereby its most rostral process assists the minimized maxilloturbinal in its respiratory task (VAN VALKENBURGH *et al.* 2014a, PANG *et al.* 2016). This functional shift of the rostral part of ethmoturbinal I is associated with a reduction of the overall olfactory surface area. The decrease of the olfactory mucosa is compensated by the felids' stronger relay on vision than on olfaction during foraging (VAN VALKENBURGH *et al.* 2014a). Unlike feliforms the reduction of snout length in selected dogs did not enhance their sense of sight, but exactly the opposite. Contrasting the wolf and the longer snouted dogs (see ch. 1.4 Morphological variation in the dog's skull: 13) in short snouted breeds the retinal ganglion cells are less in number and thus accumulated within an area centralis. Especially for brachycephalic toy dogs like the pug this physiologic modification is supposed to have caused the behavioral change from the running predator to the human face oriented companion (MCGREEVY *et al.* 2004). With this background HALL *et al.* (2015) have chosen one representative of each of the three groups, namely the German shepherd, the English greyhound, and the pug for a study on olfactory performance. Surprisingly, the short snouted companion-serving pugs (n = 10) passed the test with better results than the German shepherds (n = 10) (HALL *et al.* 2015). This contradiction leaves several open questions about the correlation between olfactory efficiency and snout length and particularly the special selection of scent hounds for odor detection employment. The lacking interest of the greyhounds (n = 10) did not refer to the sniffing exercise *per se*, they rather refused to take a visible treat lying on pine shavings in a bin. One pug and nine greyhounds failed this initial motivation test and were excluded prior to the basic study. The reason for their absent motivation is not discussed, as this visual test had to correspond to the sighthound's nature (HALL *et al.* 2015). Sighthounds correspond to the gray wolf in the arrangement of the retinal ganglion cells and hence to the behavior of a running predator (MCGREEVY *et al.* 2004).

4.4.3 Physiology, neurobiology, and genetics

The elements on which the scent ability of mammals depends are physiology, i.e. the size and thickness of the olfactory epithelium, neurobiology, i.e. the number, density, and capacity of olfactory receptors (OR) on the epithelium, and genetics, i.e. the OR gene repertoire including the level of polymorphism and the ratio between functional genes and pseudogenes resulting from single nucleotide polymorphism (SNP) (SMITH *et al.* 2004, QUIGNON *et al.* 2012).

The variation in olfactory surface area (OSA) is up to 16-fold between breeds (ISSEL-TARVER & RINE 1996). Indeed, the differentiation between respiratory and olfactory surfaces and their distribution on the bony turbinal sublayer can be studied only histologically (e.g., SMITH *et al.* 2004, 2007, MAIER & RUF 2014). The maxilloturbinal is solely covered by respiratory epithelium, but the ethmoturbinals and obviously even the frontoturbinals can serve both functions (SCHWALBE 1882, SCHRENK 1989, ROWE *et al.* 2005, SMITH *et al.* 2016). Two patterns for the distribution of both epithelial types could probably serve an explanation for the equal olfactory performance in the brachycephalic pug compared to the scent working German shepherd (HALL *et al.* 2015). First, SMITH *et al.* (2014) compared the distribution of respiratory and olfactory mucosa between the two primate suborders strepsirrhines and haplorrhines: generally, the latter have a reduced midface length and fewer olfactory turbinals compared to their sister taxon. Contrary to most expectations, the overall olfactory epithelium size of two haplorrhine pygmy marmosets (*Callithrix jacchus*, *Cebuella = Callithrix pygmea*) is not significantly reduced compared to the strepsirrhine gray mouse lemur (*Microcebus murinus*) (SMITH *et al.* 2014). According to SMITH *et al.* (2014) marmosets compensate the reduction of the bony turbinals by a more rostral extension of the olfactory mucosa and its redistribution on further structures e.g., along the nasal septum. This enlargement of the olfactory surface area achieves a diminished reduction of olfactory performance in haplorrhines than was previously hypothesized (SMITH *et al.* 2014). Probably a convergent redistribution of olfactory mucosa has occurred during the dog's shortening of the snout. On the contrary, felids altered the distribution in favor of respiratory epithelium on the rostral part of ethmoturbinal I (VAN VALKENBURGH *et al.* 2014a). Second, the distribution of respiratory and olfactory epithelium varies not only between taxa, but also during ontogeny. Neonate primates have a larger portion of olfactory mucosa on ethmoturbinal I, and after birth the rostral growth of the respective turbinal shifts the proportion of its surfaces in favor of the respiratory epithelium (SMITH *et al.* 2004, 2007). The pug's comparatively good smelling performance could possibly result from its persistence at the neonate stage in the proportions of respiratory versus olfactory mucosae. Then, similar to the hard tissue the soft tissue with its associated physiologic qualities is affected by the premature stop in its development. Only histological studies of different aged individuals can help to evaluate not only the epithelial thickness (see ch. 4.4.1.1 Brachycephalic breeds in the veterinary medicine: 108), but also how olfactory surfaces are distributed among different ontogenetic stages in brachycephalic breeds versus mesaticephalic breeds.

The density and distribution of the olfactory sensory neurons (OSN) with their associated ORs on the epithelial surface may be of greater importance for a species olfactory ability (SMITH *et al.* 2004, VAN VALKENBURGH *et al.* 2014a). Each OSN has one active allele on its OR gene that transcribes one OR protein carrying the receptor. Each receptor recognizes different odorant molecules and each odorant molecule, in turn, can bind on different receptors (PILPEL *et al.* 1998). VAN VALKENBURGH *et al.* (2011) divide the smelling performance into three components: acuity (diversity of odorant molecule

detection), discrimination (distinction between odorant molecules), and sensitivity (concentration of odorant molecules). ISSEL-TARVER & RINE (1996) assume an influence of OSN number on the sensitivity. A reduction of OSN number may either influence the diversity or the density of OR receptors on the mucosa. If diversity decreases with a smaller epithelium, the acuity will be affected, as the receptors for a certain odorant molecule get completely lost; so the molecule will no longer be perceived. A reduction of OSN density might have direct consequences on the sensitivity due to the need of a higher concentration of odorant molecules. Discrimination would be less affected in both: with lower diversity less odorant molecules can be distinguished on the remaining receptors at low concentrations; and with lower density all odorant molecules can be distinguished, but need a higher concentration. Referring to VAN VALKENBURGH *et al.* (2011) two of the three components are not (sensitivity) and less (discrimination) affected by a minimized turbinal or epithelial surface area. The authors' consequential assumption that a reduction of turbinal surface area results in an increased OSN density is supported by the sensitive sense of smell in aquatic carnivorans despite their smaller olfactory surface area compared to terrestrial species of this order (VAN VALKENBURGH *et al.* 2011). Their hypothesis could explain the high olfactory performance in the pug despite its smaller olfactory turbinal surface area compared to the German shepherd, because HALL *et al.* (2015) tested discrimination (anise extract versus mineral oil) and sensitivity (dilution of the anise extract). Acuity, however, was not part of the latter study, but VAN VALKENBURGH *et al.* (2011) assume that at least this is the component which depends on olfactory surface area.

Strongly linked with the OSNs is the lamina cribrosa. In carnivorans its foramina serve as proxy for the olfactory epithelial area and the density of its neurons. The surface area of the lamina cribrosa correlates highly with the cross-sectional area of its foramina, and both again are associated with the olfactory surface area of the turbinal skeleton (BIRD *et al.* 2014). The inclusion of OR genes in different mammalian taxa proves a linkage of the surface area of the lamina cribrosa with the total number of OR genes and with functional OR genes (BIRD *et al.* 2018). How far similar correlations can be presumed for the single dog breeds which underwent a strong bottleneck with a high mutation rate and genetic drift needs to be investigated (DRAKE & KLINGENBERG 2010, BIRD *et al.* 2018).

The next level following OSNs are their OR genes on which polymorphism is the crucial factor for smelling performance (TACHER *et al.* 2005). Because of its breeding for scent, sight, and companionship diverse studies dealt with the linkage between genotype and olfactory ability in the dog. ISSEL-TARVER & RINE (1996) studied four subfamilies of the OR gene family among 26 breeds including the borzoi, the saluki, and the pug. The number of subfamilies is expected to influence acuity, and the number of genes among the single subfamilies seems to correlate with discrimination (KAY *et al.* 2004). The three functional groups of dogs do not differ in the gene number among the subfamilies which indicates that discrimination ability does not depend on the breed and its classification (ISSEL-

TARVER & RINE 1996). ROBIN *et al.* (2009) refer to single nucleotide polymorphisms (SNPs) which are abundant in some breeds and absent in others. Although the authors assume an influence on the smelling capacities, the exact degree remains unknown so far. Pseudogenes which result from SNPs are another factor that needs to be considered, as their antagonistic intact OR genes alone cannot serve a reliable indicator for gene expression which influences sensitivity (KAY *et al.* 2004). The ratio of pseudogenes was higher in a dog compared to a wolf (ZHANG *et al.* 2011). However, ZHANG *et al.* (2011) sampled these two individuals only and further did not note the dog's breed. But this information is important as even among the dog breeds the number and ratio of pseudogenes vary (TACHER *et al.* 2005). Among primates a shifted ratio from intact OR genes to pseudogenes diminished the olfactory ability (KAY *et al.* 2004). Although a similar correlation in the dogs' OR has not been proven so far an identical effect on the breeds' olfactory performance seems obvious (TACHER *et al.* 2005). In sum, differences between the breeds occur in the allele number, the polymorphism, and the number and rate of pseudogenes (TACHER *et al.* 2005, ROBIN *et al.* 2009, QUIGNON *et al.* 2012). The randomness of variations independent from a breed's affiliation to a special group (e.g., scent hounds versus toys) indicates that "it is not yet possible to explain the different olfactory capacities of the different dog breeds." (QUIGNON *et al.* 2012: 140). Maybe the differences on breed-level are just the result of the overall occurring genetic drift as consequence of inbreeding and reproductive isolation (see e.g., SUTTER *et al.* 2004, VAYSSE *et al.* 2011). Nevertheless, polymorphisms and SNPs definitively have an effect on smelling performance, even if not among functional groups or breeds, but among individuals. LESNIAK *et al.* (2008) compared OR genes of police dogs (e.g., German shepherds, Labrador retrievers). Similarly to HALL *et al.* (2015) they tested discrimination (target odor versus four decoys) and sensitivity (treat under one to five layers of lignin). In combination with genetic analyses two genes were decoded whose SNPs have a negative influence on discrimination, but not on sensitivity (LESNIAK *et al.* 2008). It has to be noted that for their interpretation of discrimination LESNIAK *et al.* (2008) ranked the dogs just according to their values on the test; it does not automatically imply an underdeveloped discrimination ability in low-ranked individuals. Based on this study YANG *et al.* (2016) genotyped 48 German shepherds in police employ. The individuals differ in their discrimination ability as consequence of the SNP rate, and in their sensitivity according to the level of polymorphism (YANG *et al.* 2016).

In sum, the diverse genetic studies suggest the following overall conclusion: if mutations in the OR gene reduce the diversity of binding positions for a certain odorant molecule on the transcribed OR protein in general, this odorant molecule could still bind on other proteins. Hence, the acuity would not be affected (LESNIAK *et al.* 2008). Polymorphism would rely on a higher concentration of odorant molecules to compensate the lower presence of OR receptors. An accumulation of pseudogenes through SNPs could reduce the binding potential of similar odorant molecules and hence the discrimination ability (YANG *et al.* 2016). Thus, the acuity seems to depend on OSN diversity that in turn cor-

relates with epithelial or turbinal surface area, whereas sensitivity and discrimination depend on the OR protein (VAN VALKENBURGH *et al.* 2011, YANG *et al.* 2016). That means the quantity of smelling performance is the first level functioning on mucosal size which again depends on snout length and is consequently breed-specific. The quality of odorant molecule perception is the second level that functions on the OR and varies among the individuals independent from breed – and consequently from snout length.

4.4.4 Ethology

It is possible that OR genes are not the most important indicators for a scent hound's work performance. The sampled sniffer dogs and German shepherds in police employ exhibited a high frequency of unfavorable discrimination lessening alleles (LESNIAK *et al.* 2008, YANG *et al.* 2016). In both studies the authors then took a closer look at further possible parameters, since dogs are not only chosen for their olfactory performance, but also for their behavior "due to the fact that the recruitment system for candidates for police dogs is based mainly on the behavioral aspects and the dog's training potential" (LESNIAK *et al.* 2008: 526). Required and selected behavioral aspects include among others courage and boldness, nerve stability, motivation, and cooperation which are essential for an employment as a working dog (WILSSON & SUNDGREN 1997, SVARTBERG 2002, ADAMKIEWICZ *et al.* 2013). Potential sniffing dogs need to deal with environmental distractions, long and potentially unsuccessful searching phases, and stress; and for a successful qualification the relationship to their handler might be even the most important criterion (LESNIAK *et al.* 2008, YANG *et al.* 2016). To ensure this desired personality police dogs are specifically bred in distinct breeding lines which are separated from the show dog bloodline (SALGIRLI DEMIRBAS 2012). German shepherds, Labrador retrievers, or Malinois might belong to the most recruited breeds for odor detection services (LESNIAK *et al.* 2008, SALGIRLI DEMIRBAS 2012, ADAMKIEWICZ *et al.* 2013). But an acute sense of smell is not exclusive to these breeds as proven in diverse studies e.g., with the giant schnauzer (HORVATH *et al.* 2013) or the Groenendael, the border collie, the dachshund, and the Rottweiler (AMUNDSEN *et al.* 2014, YOEL *et al.* 2015). Whether a special breed serves a suitable scent worker has to be searched in its behavior and health, and less in its smelling efficiency (WILSSON & SUNDGREN 1997, SALGIRLI DEMIRBAS 2012, ADAMKIEWICZ *et al.* 2013). Consequently, the selective pressure on the OR genes in scent hounds is lower than formerly expected. This promotes a higher variability in the genotypes and explains the increased ratio of unfavorable smelling impairing alleles in the studied police dogs (DARWIN 1859, LESNIAK *et al.* 2008, YANG *et al.* 2016).

HALL *et al.* (2015) recruited untrained pet dogs for their test on smelling performance. Maybe the reason for the lacking interest for participation of the English greyhound has to be searched in the breed's

temperament: the pug is told to be really extroverted and the German shepherd to be diligent, loyal towards its family, and distant towards strangers (COILE 2015). The English greyhound is characterized as being "reserved with strangers, very sensitive, and sometimes timid" (COILE 2015: 89). Unfortunately, the recruiting system for the candidates focused on health, thoroughbred, and inexperience towards scent tests; and no information is noted about the individuals' personality (HALL *et al.* 2015). It could be possible that the English greyhounds were just unconfident of the unfamiliar situation during testing phase. The orientation with its eyes is not a new evolutionary acquisition of the sighthound group. Instead, the visual sense is already as important as scent for free-living gray wolves for orientation and chasing their prey (HALL *et al.* 2016). Instead, the sighthounds changed to merely visual hunters as since their first appearance the breeding focused exclusively on this sense (ASH 1927a). The gray wolf uses scent to find the naturally widespread prey, and sight for chasing it after detection (HALL *et al.* 2016). When the sighthounds evolved the 'first phase', the searching of prey by sniffing has been omitted within the first generations (ASH 1927a, PETERSON & CIUCCI 2003, HALL *et al.* 2016). The physiological results of MCGREEVY *et al.* (2004) support the ethological studies and the greyhounds have the same arrangement of the retinal ganglion cells like gray wolves.

5 SUMMARY

In the present pilot study the turbinal skeleton of the domestic dog (*Canis lupus familiaris*) has been investigated. Based on the Eurasian wolf (*Canis lupus lupus*) as the dog's ancestor and representative of the *grundplan* the eleven chosen breeds cover different facial lengths (brachycephalic, mesaticephalic, dolichocephalic), functional groups (scent hound, sighthound, toy/companion), and breeding histories (ancient pure breeding, modern time fashion breeding). The turbinal skeleton has been compared within these three categories in the number of olfactory turbinals and in the morphology, morphometrics, and ontogeny of the olfactory and respiratory turbinals and the lamina semicircularis. The data is based on high-resolution computed tomography (μCT) cross sections, virtual 3D models, and morphometric analyses (index turbinal surface area, IAT; surface density, SDEN; turbinal complexity, TC) of macerated skulls (28 adult and 4 juvenile dogs, 3 adult Eurasian wolves), and on histological serial sections of perinatal dogs (4 ontogenetic stages). The following results can be declared so far:

All dog breeds

The former assertions regarding the species-specific number of ethmoturbinals and frontoturbinals are proven (e.g., PAULLI 1900a, b, c; RUF 2014). Contrasting SCHLIEMANN (1966) the Eurasian wolf has three instead of two ethmoturbinals and three instead of five frontoturbinals invariably found in all studied individuals of the domestic dog regardless of a breed's function, historical age, and head shape. This conformance indicates a too short time scale in that the dog was domesticated for considerable changes. Furthermore, the *grundplan* of *Canis lupus* includes four larger prominent interturbinals between ethmoturbinal I and II (interturbinal α), between ethmoturbinal I and frontoturbinal 3 (interturbinal β; frontoturbinal 4 sensu SCHLIEMANN 1966), between frontoturbinal 1 and 2 (interturbinal γ), and medial to frontoturbinal 1 (interturbinal δ). The further two terminological differences to SCHLIEMANN (1966) refer to ethmoturbinal III (interturbinal sensu SCHLIEMANN 1966) and to the epiturbinal of ethmoturbinal I (frontoturbinal 5 sensu SCHLIEMANN 1966). The only variation in the *grundplan* occurs in interturbinal γ. As its caudal part continues into a septum of the frontal sinus its development and morphology are associated with the latter. The sinus in turn is a plesiomorphic structure of the genus *Canis* (CURTIS & VAN VALKENBURGH 2014), consequently interturbinal γ was integrated into the *grundplan* of *Canis lupus*. However, the reduction of the frontal sinus in association with the loss of its prominent interturbinal in the deformed skull of brachycephalic breeds can be regarded as some kind of 'human-made apomorphy' within the dog. Beside interturbinal γ brachycephalic breeds have a reduced number of additional interturbinals, and hence in total less olfactory tur-

binals (9 to 13). Within the dolichocephalic breeds the Groenendael shows the highest deviation from the *grundplan* in missing any and all additional interturbinals and the septal forming interturbinal γ, although it has a well-developed frontal sinus similar to the German shepherd. The latter is in accordance with the Eurasian wolf regarding the number of olfactory turbinals (12 to 13; Eurasian wolf 11 to 15), whereas the Greenland dog has an increased number of olfactory turbinals (15) due to additional interturbinals within the pars intermedia, but without exceeding the ancestral stage. The slender snout of the sighthounds has not reduced the number of interturbinals. In fact, although extremely small and simplified, the borzoi has more additional interturbinals in the pars intermedia than the Eurasian wolf and the scent hounds (total number of olfactory turbinals: 11 to 16).

The example of *Canis lupus familiaris* clearly indicates that also some interturbinals follow the *grundplan* and consequently need to be involved into the general mammalian turbinal formula as well. However, only a sufficient sample size of a species can ensure the differentiation between homologous (i.e. prominent) and variable (i.e. additional) interturbinals.

Dolichocephalic breeds I: scent hounds (German shepherd, Groenendael) and Greenland dog

(1) No morphological variations can be observed within the olfactory region including the lamina semicircularis between these three breeds and the *grundplan*. The selection for scent has not altered the IAT, the SDEN, or the TC in the bony tissue of the two German shepherds. They are rather reduced in comparison to the reconstructed Eurasian wolf specimen. As the turbinal morphology of the Groenendael and the Greenland dog corresponds to the German shepherd, variations in the three morphometric parameters cannot be expected in these two breeds either.

(2) According to the shape the position of the turbinals and the lamina semicircularis within the nasal cavity has not changed either. Also in this case the Groenendael and the Greenland dog can be considered to be identical with the German shepherd.

(3) The maxilloturbinal keeps its strong dendritic type with a large amount of secondary and tertiary lamellae. As the turbinal skeleton of the Greenland dog has not been virtually segmented yet, a larger and more complex respiratory surface area in this breed cannot be validated based on descriptive comparison alone, so it remains speculative.

In sum, with different evolutionary histories both groups show the *grundplan* in their turbinal skeleton: the indigenous Greenland dog persists in the plesiomorphic stage through millennia-long pure breeding and occasional hybridization with Nordic wolves, whereas the modern shepherd dogs regained the plesiomorphic condition most likely through some kind of backcrossing with different

breed varieties (MARTIN 1845, BECKMANN 1895, ASH 1927a, VAN ASCH *et al.* 2013, BROWN *et al.* 2015).

Dolichocephalic breeds II: sighthounds (borzoi, saluki)

Within the sighthound group two types of breeds are represented here: the saluki has been selected in the Near East for hunting fast prey (hares, gazelles etc.), and remained purebred since about 4,000 years (HOLE & WYLLIE 2007). On the other side, the initially mixed bred borzoi has markedly younger roots dating back at least to the Late Middle Ages (13th century) (VOM HAGEN 1935). The borzoi's first use was for wolf-hunting (BECKMANN 1894). Independent from influences by its northern dog ancestors the borzoi has the same sighthound-like skull shape as the saluki. And both correspond to each other in the morphology of their intranasal skeleton.

(1) The loss of scent ability in sighthounds that was postulated by BREHM (1876: 592) has been supported by one ethological study on English greyhounds (HALL *et al.* 2015). However, neither in the borzoi nor in the saluki the morphology and morphometry of their olfactory turbinal skeleton including the lamina semicircularis gives any evidence for a reduced sense of smell compared to non-sighthounds. Though the snout is narrowed, all olfactory turbinals of borzoi and saluki show the basic double scrolled shape that complicates to multiple scrolls (ethmoturbinals) up to dendritic (frontoturbinals), as described for the *grundplan*. The two reconstructed borzois prove the morphological descriptions through high values in IAT, SDEN, and TC.

(2) The complicate dendritic shape of the maxilloturbinal in the borzoi verifies a highly efficient respiratory capacity in the anterior part of the nasal cavity. This physiological trait is of special importance for sprinters living in a hot and dry environment like the saluki (HILLENIUS 1992, HOLE & WYLLIE 2007). But based on descriptive comparisons alone a higher amount of secondary and tertiary lamellae in saluki and borzoi compared to the represented long snouted non-sighthounds cannot be estimated. The Eurasian wolf, both shepherd breeds, and the Greenland dog have the same highly dendritic shape in the maxilloturbinal like the two sighthound breeds. Admittedly, IAT, SDEN, and TC have increased in the borzoi, but both segmented individuals resemble the proven correlation with snout length in *Canis lupus familiaris*.

(3) The maxilloturbinal does not extend far caudally and it does also not replace ethmoturbinal I. The reason could be that a) the rostral tip of the anterior lamina of ethmoturbinal I could have a respiratory function as well. Than it would not make sense to replace one structure with an-

other that fulfills the same task; b) the position of the lamina terminalis that separates the nasopharyngeal duct from the overlying olfactory part of the nasal cavity has not changed with snout elongation. This means that for replacing any of the olfactory turbinals the maxilloturbinal would be forced to extend dorsal to the lamina terminalis into the olfactory recess; and hence consequently off the respiratory pathway.

(4) Contrasting the hypothesis of a reduced smell performance, frontoturbinal 1 and 2 are expanding into the frontal sinus that, although measurements have not been taken, seems to be larger than in non-sighthounds. This development might be caused by the correlation between facial length and turbinal surface area: the turbinals are not affected in their growth by the reduced space of the slender snout. Indeed, in association with the ongoing facial length growth they are even forced to growth more caudally into the frontal sinus.

Brachycephalic breeds: toys (chin, pekingese, English toy spaniels, pug)

In contrast to the scent hounds the specimens which represent the brachycephalic type in this study show a conspicuous aberration within their nasal cavity. This is mostly due to their overall skull shape which affects the shape and topography of the olfactory turbinals, but not their position within the nasal cavity *per se*: the shortening of the snout reduces the frontoturbinals caudally as they cannot expand into the minimized frontal sinus anymore. The palate's elevation constricts the space for the ethmoturbinals, so their rostral processes are shortened. The reduction of interturbinal γ to a crest-like shape makes its identification difficult in some specimens. However, the individuals with a longer snout, namely the ancient pugs and the Cavaliers, roughly correspond to the *grundplan*, although one of the mesaticephalic pugs corresponds more to the shorter snouted types in its morphology and morphometric data.

(1) In the ancient breeds (pekingese, chin, ancient pug, King spaniel) the fronto-, ethmo-, and interturbinals are generally simplified with less secondary or tertiary lamellae, but they retain the basic double scrolled shape that sometimes complicates to multiple scrolls. Also the lamina semicircularis does not vary concerning the development of the two laminae. The maxilloturbinal keeps its double scrolled shape, but has a minimized number of accessory lamellae causing a less pronounced dendritic shape. In this context, cartilaginous parts of the rostral turbinals that got lost during maceration process cannot be excluded (SMITH *et al.* 2016). The IAT, the SDEN, and the TC have in fact declined in the respective specimens which are regarded as being more ancient and more carefully bred (e.g., pekingese and chin, ASH 1927b). The morphometric data corresponds to the simplified shape, so an adaptation of the turbinal skeleton to the shorter snout in these ancient breeds is assumed.

(2) A kind of disequilibrium in terms of the 'relative conchal hypertrophy' (OECHTERING *et al.* 2016) could not be validated in the modern pug's bony tissue alone. All three morphometric parameters correlate with relative snout length independent of the breed and its age and evolutionary history. This implies that in all turbinals and the lamina semicircularis the values of IAT, SDEN, and TC are smaller in the shorter snouted modern type of the pug. Regarding aberrant turbinals, one modern pug developed CAT, but contradicting veterinarian studies (e.g., OECHTERING *et al.* 2016) not only ethmoturbinal I (posterior lamina) is involved, but also ethmoturbinal II. Both modern pugs have RAT built by the anterior process of the anterior lamina of ethmoturbinal I. Surprisingly, aberrant turbinals are not a phenomenon only observed in pugs (or English and French bulldogs, see table 1 in OECHTERING *et al.* 2007), but in other brachycephalic breeds as well. In this study CAT are present in the pekingese, the chin, and even in the slightly longer snouted Cavalier.

(3) The dependence on snout length which is observed in the above named toy breeds holds also true for both English toy spaniels. The Cavalier has a larger IAT, and a higher SDEN and TC than the extreme brachycephalic King spaniel. The more complicate shape in the Cavalier's turbinals compared to its short snouted ancestor is stronger pronounced in the maxilloturbinal than in the olfactory turbinals and the lamina semicircularis.

(4) In specimens whose frontal sinus is too small to house frontoturbinal 1 and 2 the respective turbinals stay within the frontoturbinal recess and pass caudally onto the lamina cribrosa. Hence, they are showing the same pattern like frontoturbinal 3 in the *grundplan* and in all other dogs.

The use of the dog as a model organism proves the following basic characters which are valid for the mammal class:

(1) The theory regarding the genetically manifested species-specific number of the fronto- and ethmoturbinals was confirmed (e.g., RUF 2014) – even within a restricted space of a dog's shortened or slender snout. The only reference naming the single turbinals for some other carnivoran species is PAULLI (1900C). Due to his use of the problematic terminology the comparison with the nomenclature used in the present study is not certain. Nevertheless, according to PAULLI's (1900c) results it can be assumed that at least within the pars ethmoturbinalis *Canis lupus* corresponds to the carnivoran *grundplan* with three ethmoturbinals and one prominent interturbinal. Within the pars intermedia most probably five ectoturbinals represent the order's *grundplan*, presumably referring to the dog's three frontoturbinals and interturbinal β and δ.

(2) The growth of the bony turbinals is genetically linked with the growth of the dermal bones: both stop at a specific ontogenetic stage. The most extreme dolichocephalic breeds, namely the sighthound group, have even in their olfactory turbinals a larger surface area than the slightly dolichocephalic scent hounds. In brachycephalic breeds the turbinal growth stops at an early ontogenetic stage as observed in the viscerocranium causing a reduced turbinal surface area.

(3) Characters appearing in short snouted dogs are already present in perinatal stages. This includes:

   a. the uncinate process of the lamina semicircularis

   b. the separation of ethmoturbinal I into two laminae, namely the anterior lamina and the posterior lamina; with a rostral pointing anterior process in the former. The anterior process of the posterior lamina, however, is beginning its rostral growing at the neonate stage and is absent in some adult brachycephalic breeds

   c. the presence of the epiturbinal dorsoproximal on ethmoturbinal I

   d. the basic double scrolled shape in the maxilloturbinal and in the frontoturbinals

(4) Only macerated skulls of adult dogs have been objects of this study. The ‘relative conchal hypertrophy’, i.e. the ongoing growth of the turbinals after the elongation of the face has stopped prematurely (e.g., OECHTERING *et al*. 2016), could be not supported. In fact, the bony turbinals of brachycephalic breeds have even a smaller relative surface area and surface density compared to longer snouted breeds.

(5) The influence of the bony turbinals varies between the respiratory and the olfactory epithelium:

   a. The surface area of the respiratory system directly depends on the size of its bony sublayer covered by the thermoregulatory functioning mucosa. Although turbinal growth is linked with skull growth, breeds with a stronger rely on their respiratory capacity like the sighthounds and the Greenland dog seem to have more accessory lamellae. These provide the maxilloturbinal a denser and more complex shape and hence a higher thermoregulatory efficiency. In brachycephalic breeds the development of accessory lamellae stops prematurely, whereas body mass increases up to the adulthood. This disproportion reduces the thermoregulatory efficiency and causes heat intolerance (PACKER *et al.* 2015).

b. Brachycephalic breeds have a well sense of smell compared to scent hounds despite their extremely reduced olfactory surface area. Simultaneously, sight-oriented greyhounds seem to have a reduced sense of smell despite a large surface area in their fronto- and ethmoturbinals. Both groups support the hypothesis that smelling performance does not depend on the bony turbinals (SMITH *et al.* 2004; opposite view VAN VALKENBURGH *et al.* 2011).

With its high morphological diversity the domestic dog serves as an ideal model organism in different scientific fields, covering biology (evolution, DRAKE & KLINGENBERG 2010; genetics, FONDON & GARNER 2004, BOYKO *et al.* 2010; ontogeny and morphology, SCHOENEBECK *et al.* 2012, GEIGER & HAUSSMAN 2016) and human medicine, namely pathology (MARCHANT *et al.* 2017). The dog's head shape is strongly affected by human-induced inbreeding events and reproductive isolation. Both result in radiation and bottleneck effects through genetic drift. The morphological variation got exaggerated as a consequence of inactivated natural selection which got replaced due to human care which facilitates usually fitness-reducing mutations (FONDON & GARNER 2004, PARKER *et al.* 2004, SUTTER *et al.* 2004, GERMONPRÉ *et al.* 2009, BOYKO *et al.* 2010, DRAKE & KLINGENBERG 2010). The turbinal skeleton is genetically linked with dermal bone growth and hence shows a rapid variation in its morphology over a short time scale as well. The numerous dog breeds which differ in snout length and function in our society can serve as a basis for fundamental intranasal studies and reflect to which degree the developmental patterns of the turbinal skeleton are related to associated structures: although the bony turbinals are not a direct indicator for smelling performance in general (SMITH *et al.* 2004), our understanding of the linkage between turbinal growth and morphology and related biological disciplines is still at the beginning. That includes among others the comparison with olfactory performance under genetic, physiological, and neurobiological influence (i.e., olfactory sensory neurons, olfactory receptor genes; ISSEL-TARVER & RINE 1996, VAN VALKENBURGH *et al.* 2011), the ethology of scent ability (HALL *et al.* 2015), or the morphofunctional association with other bony structures (e.g., the lamina cribrosa, BIRD *et al.* 2018) or organs (e.g., the olfactory bulb, ROBERTS *et al.* 2010).

6 OUTLOOK

The current study offers a unique and so far unrepresented database that can be enhanced with the collection of further data including the increase of the sample size of already integrated breeds and the inclusion of new breeds. However, only specimens of modern breeds have been studied so far. Due to the breeding barriers prewritten by the Kennel Clubs' studbooks small populations of pedigree dogs get separated by reproductive isolation. The genetic drift gets fastened through bottleneck events caused by the use of a few popular sires (PARKER *et al.* 2004, BJÖRNERFELDT *et al.* 2008). The resulting genetic mutations exhibit a high influence e.g., on bone growth (DRAKE & KLINGENBERG 2010). Accordingly, the present study has proven several variations in the morphology and ontogeny of the turbinal skeleton of the modern dog to its ancestor, the Eurasian wolf. But a more precise reconstruction of morphological changes in the turbinal skeleton requires the inclusion of dogs which represent an intermediate stage, like the subfossil dogs which are housed at the Naturhistorisches Museum der Burgergemeinde Bern, Switzerland. These specimens represent an early stage of domestication and their diverse gene pool furthermore contrasts with the reproductive barriers and the resulting high degree of inbreeding in modern breeds (PARKER *et al.* 2004, GERMONPRÉ *et al.* 2009). Nevertheless, the respective prehistoric specimens exhibit a markedly intraspecific variation in skull size and shape (I. Ruf, pers. comm.). Additionally, the Museum of Zoology at the University of Cambridge, UK houses skulls of ancient Egyptian dogs which date from 2,500 BC (pers. obs.). Both the prehistoric and the ancient dogs can serve as a transitional stage between the naturally evolved wild gray wolf and the nearly exclusively artificially selected modern dog breeds. Therefore, in a subsequent project a more precise reconstruction of the natural and artificial domestication events which underlay morphological changes of the face and the turbinal skeleton should be accomplished.

The evolutionary background of the changes in intranasal morphology under natural selection can help veterinarians to improve the health of dog breeds which suffer from the brachycephalic syndrome like the pug or the English and the French bulldog (PACKER *et al.* 2015). Therefore, among modern dogs low-resolution CT data of affected individuals can be combined with µCT scans of macerated skulls. Further, these modern short snouted representatives can be contrasted with conspecifics of the longer snouted ancient and retro types which have no breathing difficulties. The pugs which lived over 100 years ago can help in the evaluation, if the retro pug has returned to the old type, or if its turbinal morphology has completely changed and adapted to different selective pressures.

Another point of discussion in which the pug also takes part refers to the olfactory performance. The short snouted toy breed does not have a less sensitivity and discrimination ability compared to a typical scent hound (HALL *et al.* 2015). Based on the hypotheses that epithelial surface area instead seems

to affect acuity (VAN VALKENBURGH *et al.* 2011) further studies on smelling performance in dogs should now concentrate on odorant diversity between breeds of different snout lengths. Then, based on the example of the breeds involved in HALL *et al.* (2015) it can be surely proven that the German shepherd might detect a larger amount of odorant molecules than the pug.

In the current study it was tried to cover the diverse biological disciplines evolution, physiology, genetic, ethology, and neurobiology when comparing the morphological, morphometric, and ontogenetic results between the chosen breeds for integrating them into this larger interdisciplinary context. Some ambiguities could be resolved, whereas other still remained e.g., how far a shortened snout and the consequently smaller turbinal skeleton are associated with smelling performance, or if the growth of the soft tissue is similarly affected by a changed facial length. The crosslink with these fields through cooperations with the respective experts offers possibilities to answer the remaining questions. These results would also improve our understanding of general physiological, neurobiological, evolutionary, ontogenetic, phylogenetic, and genetic influences on the turbinal skeleton in mammals.

ZUSAMMENFASSUNG

Das Riechmuschelskelett (Turbinalskelett) rückt seit einigen Jahren immer stärker in den Fokus biologischer Studien aufgrund der Verfügbarkeit non-invasiver moderner bildgebender Verfahren wie hochauflösende Computertomographie (µCT, siehe VAN VALKENBURGH *et al.* 2014b). Das Turbinalskelett der Säuger erfüllt in der Nasenhöhle eine zweifache Funktion: Das rostral innerhalb der Pars maxillonasoturbinalis gelegene Maxilloturbinale und Teile des Nasoturbinale dienen der Respiration; die Atemluft wird vor Eintritt in die Lungen befeuchtet, auf Körpertemperatur reguliert und gefiltert. Die eigentlichen Riechmuscheln, die die Reichschleimhaut mit Geruchsrezeptoren tragen, liegen im caudalen Bereich der Nasenhöhle. Innerhalb dessen wird die Pars intermedia, die Frontoturbinalien enthält, durch die Lamina semicircularis von der Pars ethmoturbinalis, die Ethmoturbinalien beherbergt, getrennt. Die Anzahl an Fronto- und Ethmoturbinalien ist artspezifisch. Zwischen ihnen entwickeln sich kleinere und in ihrer Präsenz heterogene Interturbinalien (MAIER & RUF 2014).

Die folgende Pilotstudie befasst sich mit dem Turbinalskelett des Haushundes (*Canis lupus familiaris*). Er ist das erste Tier, dessen äußeres Erscheinungsbild nicht durch natürliche, sondern menschengemachte Selektion geformt wurde (DRAKE & KLINGENBERG 2010, LARSON *et al.* 2012, MARCHANT *et al.* 2017). Die seit Jahrtausenden anhaltende Zucht nach Funktion und Aussehen führte zur Entwicklung von heute über 400 Rassen, deren breites Spektrum an Körper- und besonders Schädelformen unter Säugern einzigartig ist (SCHOENEBECK & OSTRANDER 2013, PARKER *et al.* 2017). Aufgrund der kurzen Zeitspanne, innerhalb derer neue Rassen entstehen und bestehende sich verändern, können die Auswirkungen selektiver Mechanismen ausgewählter Merkmale einfach und vergleichsweise schnell beobachtet werden. Aus diesem Grund und wegen seiner hohen morphologischen Diversität dient der Hund in der Humanmedizin als außerlaboratorischer Modelorganismus, anhand dessen sich Genotyp-Phänotyp Beziehungen, wie Brachyzephalie und Gesichtshypoplasie, auf den Menschen übertragen lassen (HAWORTH *et al.* 2001, DRAKE & KLINGENBERG 2010, SCHOENEBECK *et al.* 2012, MARCHANT *et al.* 2017). Angefangen mit der Entstehung zweier Basistypen, dem dolichozephalen (langschnäuzigen) Windhund und dem brachyzephalen (kurzschnäuzigen) Mastiff im antiken Nahen Osten, entstanden in den folgenden Jahrhunderten diverse Rassen, die unterschiedliche Funktionen erfüllten (z. B. Jagd-, Schutz-, oder Spürhunde; YOUNG & BANNASCH 2006). Seit Mitte des 19. Jahrhunderts erschaffen Züchter neue Rassen und ändern bestehende Rassen im Zeitraffer, was natürliche Selektion allein nicht erreichen kann. Vielmehr wird letztere nun durch jene künstliche Selektion ersetzt, die Gendrift durch Reproduktionsbarrieren und Flaschenhalseffekte begünstigt (PRICE 1999, BJÖRNERFELDT *et al.* 2008, DRAKE & KLINGENBERG 2010). Die Verwendung von Inzucht zur schnelleren Fixierung bevorzugter Merkmale erhöht jedoch auch die Allelfrequenz schädlicher Mutationen

an Genloci, die beispielsweise das Längenwachstum des Gesichts steuern (BECKMANN 1895, HAWORTH *et al.* 2001, SUTTER *et al.* 2004, YOUNG & BANNASCH 2006, ASHER *et al.* 2009, SCHOENEBECK *et al.* 2012, SCHOENEBECK & OSTRANDER 2013, PACKER *et al.* 2015, SANDOE *et al.* 2017). Obwohl kurzschnäuzige Hunde keine moderne Erscheinung sind –ihre Existenz ist beispielsweise in China bereits im 1. Jahrtausend v. Chr. belegt– erfolgte die extreme Verkürzung des Gesichts, wie man sie heutzutage beispielsweise beim Mops sieht, erst innerhalb der letzten Jahrzehnte (STURZENEGGER 2011, ASH 1927b). Die gesundheitlichen Beschwerden, wie Atemgeräusche (inspiratorischer Stridor), Hitzeempfindlichkeit und Atemnot, werden als brachyzephales Syndrom zusammengefasst (KOCH *et al.* 2003, OECHTERING *et al.* 2007). An diesem sollen auch die proportional vergrößerten Turbinalien beteiligt sein, die nach dem verfrühten Wachstumsstopp der Gesichtsschädellänge weiterwachsen und die Luftwege innerhalb der verkleinerten Nasenhöhle blockieren (‚Relative conchale Hypertrophie', OECHTERING *et al.* 2016). Aus diesem Grund wurden die Nasenhöhle und das Turbinalskelett brachyzephaler Rassen bereits in diversen veterinärmedizinischen Studien mittels CT oder Magnetresonanztomographie (MRT) untersucht (z. B. HEIDENREICH *et al.* 2016, OECHTERING *et al.* 2016). Die Deskriptionen stützen sich allerdings auf Aufnahmen geringer Auflösung und sind unpräzise. Aufnahmen des Turbinalskeletts von Rassen mittlerer Schnauzenlänge (mesozephal) dienten bisher lediglich als Vergleichsmaterial (Deutscher Schäferhund, OECHTERING *et al.* 2007), oder zur Rekonstruktion des morphologischen Grundplans (Belgischer Schäferhund, DE RYCKE *et al.* 2003). Die Nasenhöhle dolichozephaler Rassen stand ausschließlich in der Krebsforschung im Fokus, ohne Hinweise auf die verwendeten Rassen (BURK 1992b, FINCK *et al.* 2015).

Während die äußeren Schädelstrukturen und die genetischen Faktoren ihrer Entwicklung hinreichend zwischen verschiedenen Rassen untersucht wurden (z. B. HAWORTH *et al.* 2001, FONDON & GARNER 2004, 2007, SCHOENEBECK *et al.* 2012, SCHOENEBECK & OSTRANDER 2013), beschränken sich Studien am Turbinalskelett des Hundes auf allgemeine anatomische (PAULLI 1900c, makroskopisch), ontogenetische (OLMSTEAD 1911, SCHLIEMANN 1966; histologisch) oder funktionelle (CRAVEN *et al.* 2007, 2010; physiologisch) Fragestellungen ohne Berücksichtigung potenzieller Rasseunterschiede.

Basierend auf dem Eurasischen Wolf (*Canis lupus lupus*) als Urahn des Hundes und Repräsentant des Grundplans decken die elf hier vertretenen Rassen verschiedene Gesichtsschädellängen (brachyzephal, mesozephal, dolichozephal), Zuchtverläufe (antike Reinrassigkeit, moderne Modezucht), und funktionale Gruppen (Spürhund, Windhund, Gesellschaftshund/Toy) ab. Es wird ein Einfluss aller drei Kategorien auf die Entwicklungsmuster des Turbinalskeletts erwartet, der sich aufgrund ihrer hohen Diversität deutlich in der Anzahl der olfaktorischen Turbinalien und der Morphologie, Morphometrie und Ontogenese der respiratorischen und olfaktorischen Turbinalien sowie der Lamina semicircularis widerspiegelt. Die Daten basieren zum einen auf µCT-Schnittbildern mazerierter Schädel (28 adulte und 4 juvenile Hunde, 3 adulte Wölfe) einschließlich virtueller Rekonstruktion von 3D-Modellen und

morphometrischer Analysen, zum anderen auf histologischen Schnittserien perinataler Hunde (4 ontogenetische Stadien). Die morphometrischen Analysen beziehen die Messung der relativen Oberflächengröße (index turbial surface area, IAT), sowie die Berechnung der Oberflächendichte (surface density, SDEN) und der Turbinalienkomplexität (turbinal complexity, TC) ein. In der vorliegenden Studie werden erstmals detaillierte morphologische und ontogenetische Untersuchungen am Turbinalskelett des Hundes durchgeführt, die nicht nur die Schädelform, sondern auch die Geschichte jeder Rasse und ihre ursprüngliche Funktion berücksichtigen. Ferner werden verstärkt morphometrische Methoden angewandt, die in früheren Studien nicht die einzelnen olfaktorischen Turbinalien berücksichtigten, sondern den olfaktorischen Part als Einheit betrachteten (z. B. VAN VALKENBURGH *et al.* 2011, 2014a). Zur Ermittlung der Komplexität der Turbinalien wurde eine neue morphometrische Anwendung entwickelt. Die aufgestellten und im Folgenden gelisteten Hypothesen stützen sich auf Literaturangaben über das Turbinalskelett diverser Säugertaxa sowie auf generelle Informationen über die Schädelmorphologie, Physiologie und Ethologie von Hund und Wolf.

1) Alle Rassen

Die Anzahl der Fronto- und Ethmoturbinalien ist phylogenetisch und funktionell determiniert und folglich artspezifisch. Da die Trennung zwischen Hund und Eurasischem Wolf noch nicht ausreichend fortgeschritten ist, haben beide dieselbe Anzahl an Fronto- und Ethmoturbinalien, die bereits von PAULLI (1900c) und SCHLIEMANN (1966) benannt wurden.

2) Dolichozephale Rassen I: Spürhunde (Deutscher Schäferhund, Groenendael) und Grönlandhund

(1) Dieser Schädeltyp steht seinem Wolfsvorfahr in der generellen Turbinalienmorphologie am nächsten, und stärker im ursprünglichen und geographisch isolierten Grönlandhund als in den später gezüchteten und eher geruchsspezialisierten Deutschen Schäferhund und Groenendael. Da die Form der Fronto-, Ethmo- und Interturbinalien, des Maxilloturbinale, des Nasoturbinale und der Lamina semicircularis nicht vom Eurasischen Wolf abweicht; stimmen Oberflächengröße, Oberflächendichte und Turbinalienkomplexität der betreffenden Strukturen ebenso mit dem Grundplan überein.

(2) Die Position der Turbinalien und der Lamina semicircularis innerhalb der Nasenhöhle entspricht dem Eurasischen Wolf.

(3) Das Maxilloturbinale des Grönlandhundes als arktischer Ausdauerläufer besitzt mehr akzessorische Lamellen um eine höhere respiratorische Effizienz im kaltariden Klima zu gewährleisten. Diese größere Anzahl zeigt sich auch in der Erhöhung aller drei morphometrischer Parameter.

3) Dolichozephale Rassen II: Windhunde (Barsoi, Saluki)

(1) Das Grundmerkmal der Windhunde ist ein verlängertes Gesicht, das den Turbinalien mehr Raum zu bieten scheint. Doch die gleichzeitige Verschmälerung hebt die Länge auf und zwingt die olfaktorischen Turbinalien und die Lamina semicircularis zu einer Vereinfachung ihrer Form im Vergleich zum Eurasischen Wolf mit breiterer Schnauze. Folglich weisen Oberflächengröße, Oberflächendichte, und Turbinalienkomplexität geringer Werte auf als der Grundplan.

(2) Das Maxilloturbinale hat mehr sekundäre und tertiäre Lamellen, die, vergleichbar dem Grönlandhund, eine größere Oberfläche, Oberflächendichte und Turbinalienkomplexität gewährleisten als im Eurasischen Wolf.

(3) Um die respiratorische Leistung weiter zu steigern, breitet sich das Maxilloturbinale nach caudal aus und verdrängt Ethmoturbinale I, das rostral verkürzt wird.

(4) Da der Geruchssinn in Windhunden eine untergeordnete Rolle spielt, breiten sich die Frontoturbinalien nicht in den Frontalsinus aus.

4) Brachyzephale Rassen: Toys (Chin, Pekinese, King Spaniel, Cavalier, Mops)

(1) Innerhalb der verkleinerten Nasenhöhle ist in Rassen höheren historischen Alters die Form der Turbinalien und der Lamina semicircularis vereinfacht im Vergleich zum Eurasischen Wolf.

(2) Die rapide Verkürzung der Schnauze im modernen Mops verhinderte eine proportionale Anpassung in der Morphologie der Ethmoidalregion. Die Oberfläche der Turbinalien, sowohl respiratorisch als auch olfaktorisch, und der Lamina semicircularis ist proportional vergrößert im Vergleich zum Urmops, was gleichzeitig zu einer erhöhten Oberflächendichte und Turbinalienkomplexität führt.

(3) Die sekundäre Verlängerung der Schnauze des Cavaliers zeigt die umgekehrten Effekte zum Mops: Sein Turbinalskelett war nicht in der Lage, entsprechend der schnellen Vergrößerung der Nasenhöhle zu wachsen, sodass die Turbinalien und die Lamina semicircularis in dieser Rasse

genauso einfach gebaut sind wie im King Spaniel. Die Folge ist eine Verringerung ihrer relativen Oberflächengröße, Oberflächendichte und Turbinalienkomplexität.

(4) Ist der Frontalsinus reduziert oder fehlt, variiert das caudale Ende der Frontoturbinalien im Vergleich zu den anderen Rassen und dem Eurasischen Wolf.

Folgende Ergebnisse dieser Studie können basierend auf den aufgestellten Hypothesen festgehalten werden:

Alle Hunderassen

Die bereits aufgestellte Annahme einer artspezifischen Anzahl an Fronto- und Ethmoturbinalien wurde bestätigt (u.a. PAULLI 1900a, b, c; RUF 2014). Im Gegensatz zu SCHLIEMANNs (1966) Deskriptionen besitzt der Eurasische Wolf drei statt zwei Ethmoturbinalien, und drei statt fünf Frontoturbinalien, die unabhängig der Funktion, des historischen Alters und der Form des Gesichtsschädels in allen Rassen vorhanden sind. Diese Konformität belegt, dass die Zeitspanne der Domestikation des Hundes zu kurz war, um hinreichende Abweichungen vom Eurasischen Wolf zu bewirken. Des Weiteren beinhaltet der Grundplan der Art *Canis lupus* vier größere prominente Interturbinalien (WAGNER & RUF 2019) zwischen Ethmoturbinale I und II (Interturbinale α), zwischen Ethmoturbinale I und Frontoturbinale 3 (Interturbinale β; Frontoturbinale 4 sensu SCHLIEMANN 1966), zwischen Frontoturbinale 1 und 2 (Interturbinale γ), und medial zu Frontoturbinale 1 (Interturbinale δ). Die übrigen zwei Differenzen in der Terminologie zu SCHLIEMANN (1966) beziehen sich auf das Ethmoturbinale III (Interturbinale sensu SCHLIEMANN 1966) und das Epiturbinale des Ethmoturbinale I (Frontoturbinale 5 sensu SCHLIEMANN 1966). Die einzige Variation zum Grundplan tritt in Interturbinale γ auf: Da es in seinem caudalen Bereich in ein Septum des Frontalsinus übergeht, sind seine Entwicklung und Morphologie mit jenem assoziiert. Der Sinus wiederum stellt eine plesiomorphe Struktur der Gattung *Canis* dar (CURTIS & VAN VALKENBURGH 2014), weshalb Interturbinale γ in dieser Studie in den Grundplan von *Canis lupus* integriert wurde. Hingegen ist in brachyzephalen Rassen die starke Reduktion des Frontalsinus in Verbindung mit Verlust seines prominenten Interturbinale, resultierend aus der extremen Deformation des Schädels, als eine Art ‚menschenverursachte Apomorphie' aufzufassen. Überdies besitzen brachyzephale Rassen eine reduzierte Anzahl zusätzlicher Interturbinalien, was die Gesamtzahl ihrer olfaktorischen Turbinalien verringert (9 bis 13). Innerhalb der dolichozephalen Hunde weist der Groenendael die höchste Abweichung vom Grundplan auf, da ihm sämtliche zusätzlichen Interturbinalien und das Septum-formende Interturbinale γ fehlen. Widersprüchlicher Weise ist die Ausprägung des Frontalsinus jenes Individuums der des Deutschen Schäferhundes vergleichbar. Letzterer stimmt in der Anzahl

olfaktorischer Turbinalien mit dem Eurasischen Wolf überein (12 bis 13; Eurasischer Wolf 11 bis 15), während der Grönlandhund aufgrund einer erhöhten Anzahl zusätzlicher Interturbinalien in der Pars intermedia eine höhere Zahl olfaktorischer Turbinalien besitzt (15), ohne jedoch den Grundplan zu übertreffen. Die Verschmälerung der Schnauze der Windhunde hat nicht zu einer Abnahme in der Anzahl an Interturbinalien geführt. Tatsächlich besitzt der Russische Windhund (Barsoi) mehr zusätzliche Interturbinalien in der Pars intermedia als die Spürhunde, auch wenn sie extrem klein und vereinfacht sind (Gesamtzahl olfaktorischer Turbinalien 11 bis 16). Das Beispiel von *Canis lupus familiaris* macht deutlich, dass auch einige Interturbinalien einem Grundmuster folgen und entsprechend in die allgemeine Turbinalienformel der Säuger integriert werden sollten. Allerdings kann nur eine ausreichende Stichprobengröße einer Spezies die Differenzierung zwischen homologen (d.h. prominenten) und variablen (d.h. zusätzlichen) Interturbinalien gewährleisten.

Dolichozephale Rassen I: Spürhunde (Deutscher Schäferhund, Groenendael) und Grönlandhund

(1) Morphologische Variationen in der olfaktorischen Region inklusive der Lamina semicircularis der drei Rassen zum Grundplan konnten nicht beobachtet werden. Die Selektion des Riechvermögens hat die Werte für IAT, SDEN und TC in den Knochenstrukturen der beiden virtuell rekonstruierten Deutschen Schäferhunde nicht verändert. Sie sind im Vergleich zum Eurasischen Wolf sogar verringert. Da die Turbinalienmorphologie des Groenendaels und des Grönlandhundes der des Schäferhundes entspricht, können auch in diesen beiden nichtsegmentierten Rassen keine Veränderungen in den morphometrischen Parametern ihrer olfaktorischen Turbinalien angenommen werden.
(2) Gleichsam mit der Form ist die Position der einzelnen Turbinalien und der Lamina semicircularis innerhalb der Nasenhöhle identisch geblieben. Auch in diesem Falle gilt eine Übereinstimmung des Grönlandhundes und des Groenendaels mit dem Deutschen Schäferhund als wahrscheinlich
(3) Das Maxilloturbinale behält seine stark dendritische Form mit einer hohen Zahl sekundärer und tertiärer Lamellen bei. Da das Turbinalskelett des Grönlandhundes bisher nicht virtuell rekonstruiert wurde, kann eine größere und komplexere Oberfläche in dieser Rasse allein auf Grundlage deskriptiver Vergleiche nicht bestätigt werden; die Hypothese bleibt spekulativ.

Insgesamt weisen beide Gruppen trotz unterschiedlicher evolutiver Hintergründe in ihrer Ethmoidalregion den Grundplan auf: der indigene Grönlandhund ist aufgrund jahrtausendlanger Reinrassigkeit und sporadischer Hybridisierung mit nordischen Wölfen in einem plesiomorphen Stadium verblieben, während beide modernen Schäferhundrassen höchstwahrscheinlich durch eine Art Rückkreuzung ver-

schiedener Rassevariation den plesiomorphen Zustand wiedererlangt haben (MARTIN 1845, BECKMANN 1895, ASH 1927a, VAN ASCH *et al*. 2013, BROWN *et al*. 2015).

Dolichozephale Rassen II: Windhunde (Barsoi, Saluki)

In dieser Studie sind zwei Typen von Windhunden vertreten: Der Saluki wurde im (semi-)ariden Klima des Nahen Osten für die Jagd schneller Beutetiere (Hasen, Gazellen etc.) selektiert und seine reinrassige Zucht erfolgt seit etwa 4000 Jahren (HOLE & WYLLIE 2007). Die Wurzeln des durch Kreuzung verschiedener Rassen entstandenen und deutlich jüngeren Barsois reichen mindestens bis ins Mittelalter zurück (13. Jahrhundert) (VOM HAGEN 1935). Seine erste Verwendung war die Wolfsjagd (BECKMANN 1894). Unabhängig möglicher Einflüsse seiner nordischen Ahnen besitzt der Barsoi dieselbe Windhund-typische Schädelform wie der Saluki. Und beide entsprechen einander in der Morphologie ihrer Ethmoidalregion.

(1) In einer ethologischen Studie wurde am Beispiel des English Greyhound die von BREHM (1876: 592) postulierte Reduktion des Geruchssinns des Windhundes bestätigt (HALL *et al*. 2015). Allerdings lassen weder Barsoi noch Saluki in der Morphologie ihres olfaktorischen Turbinalskeletts und der Lamina semicircularis einen gegenüber nicht-Windhunden reduzierten Geruchssinn erkennen. Obwohl die Schnauze verschmälert ist, weisen die olfaktorischen Turbinalien beider Rassen die grundlegende doppelt eingerollte Form auf, die sich zur multiplen Einrollung (Ethmoturbinalien) oder sogar zur dendritischen Form (Frontoturbinalien) verkompliziert, so wie im Grundplan beschrieben. Beide virtuell rekonstruierte Barsois belegen die morphologischen Deskriptionen durch im Vergleich zum Eurasischen Wolf höhere Werte in IAT, SDEN und TC.

(2) Der extrem komplizierte dendritische Bau des Maxilloturbinale gibt Hinweise auf eine hoch effiziente respiratorische Leistung im rostralen Bereich der Nasenhöhle. Dieses physiologische Merkmal ist von besonderer Wichtigkeit für Sprinter, die einen heißariden Lebensraum bewohnen, wie den Saluki (HILLENIUS 1992, HOLE & WYLLIE 2007). Allerdings kann eine höhere Anzahl sekundärer und tertiärer Lamellen in Saluki und Barsoi gegenüber den hier repräsentierten dolichozephalen nicht-Windhunden anhand deskriptiver Vergleiche allein nicht bestätigt werden. Sowohl Eurasischer Wolf als auch beide Schäferhundrassen und der Grönlandhund haben dieselbe stark dendritische Form wie die beiden Windhundrassen. Zwar sind die Werte in IAT, SDEN und TC im Maxilloturbinale des Barsois erhöht, doch beide segmentierten Individuen befinden sich innerhalb der in *Canis lupus familiaris* festgestellten Korrelation zur Schnauzenlänge.

(3) Das Maxilloturbinale breitet sich nicht nach caudal aus und verdrängt auch nicht Ethmoturbinale I. Der Grund könnte darin liegen dass a) die rostrale Spitze der Lamina anterior des Ethmoturbinale I ebenfalls eine respiratorische Funktion hat. In diesem Falle wäre es nicht sinnvoll, diese Struktur durch eine Struktur gleicher Funktion zu ersetzen; b) die Position der Lamina terminalis, die den Nasengang vom aufliegendem olfaktorischen Bereich der Nasenhöhle trennt, hat sich mit Verlängerung der Schnauze nicht verändert. Das bedeutet, dass sich das Maxilloturbinale für eine Verdrängung eines olfaktorischen Turbinale dorsal der Lamina terminalis in den olfaktorischen Bereich verlagern müsste; und sich folglich widersprüchlich seiner Funktion außerhalb des respiratorischen Luftstroms befände.

(4) Entgegen der Hypothese bezüglich des verringerten Geruchssinns reichen Frontoturbinale 1 und 2 in den Frontalsinus hinein, der, obwohl keine Messungen durchgeführt wurden, größer zu sein scheint als in nicht-Windhunden. Diese Entwicklung könnte in der Korrelation zwischen Gesichtsschädellänge und Turbinalienoberfläche begründet sein: die Turbinalien werden nicht durch den verkleinerten Raum der schmalen Schnauze in ihrem Wachstum gehemmt, sondern sind aufgrund ihres Zusammenhangs mit dem anhaltenden Längenwachstum des Gesichts sogar gezwungen noch stärker in den Frontalsinus auszuweichen.

Brachyzephale Rassen: Toys (Chin, Pekinese, Englische Zwergspaniels, Mops)

Im Gegensatz zu den Spürhunden weisen die Vertreter des brachyzephalen Typs in der aktuellen Studie eine deutliche Abweichung ihrer Ethmoidalregion auf. Diese steht größtenteils im Zusammenhang mit der Schädelform als Ganzes, welche zwar die Togographie der olfaktorischen Turbinalien, jedoch nicht ihre Position innerhalb der Nasenhöhle *per se* beeinflusst: Die Verkürzung der Schnauze reduziert die Frontoturbinalien im caudalen Bereich, da sie nicht mehr in den minimierten Frontalsinus hineinragen können. Die Elevation des Gaumens, d.h. seine rostrodorsale Schrägstellung in Bezug zur Schädelbasis, verengt den Raum für die Ethmoturbinalien, weshalb deren rostrale Processus verkürzt werden. Die Rückbildung des Interturbinale γ zu einer leistenartigen Struktur erschwert in manchen Schädeln seine Identifizierung. Dennoch entsprechen die Individuen mit längerer Schnauze, Urmops und Cavalier, annähernd dem Grundplan, obwohl die Morphologie und Morphometrie einer der mesozephalen Möpse wiederum eher dem kurzschnäuzigen Typ gleicht.

(1) In den antiken Rassen (Pekinese, Chin, Urmops und King Spaniel) sind die Fronto- und Ethmoturbinalien und die Interturbinalien generell vereinfacht aufgrund weniger sekundärer und tertiärer Lamellen. Dennoch behalten sie den doppelt eingerollten Typ bei, der sich teilweise zur multiplen Einrollung kompliziert. Auch die Lamina semicircularis weicht bezüglich der

Bildung beider Laminae nicht ab. Das Maxilloturbinale behält seine doppelt eingerollte Form, doch die reduzierte Anzahl akzessorischer Lamellen bewirkt eine geringere Ausprägung seiner dendritischen Gestalt. Diesbezüglich kann nicht ausgeschlossen werden, dass sich während der Mazeration rostrale zeitlebens knorpelige Anteile des Turbinale aufgelöst haben (SMITH et al. 2016). IAT, SDEN und TC sind in Rassen, die auf eine längere und verantwortungsvollere Zucht zurückgehen (z.B. Pekinese und Chin, ASH 1927b) in der Tat verringert. Die morphometrischen Daten decken sich mit der vereinfachten Form, sodass in diesen antiken Rassen eine Anpassung des Turbinalskeletts an die Verkürzung der Schnauze angenommen werden kann.

(2) Ein Ungleichgewicht unter dem Aspekt der ‚relativen conchalen Hyopetrophie' (OECHTERING *et al*. 2016) konnte im modernen Mops anhand des knöchernen Gewebes allein nicht bestätigt werden. Alle drei morphometrischen Parameter korrelieren mit der relativen Schnauzenlänge unabhängig der Rasse und ihres historischen Alters und ihrer evolutiven Hintergründe. In Bezug auf die Verlagerung von Turbinalien besitzt ein moderner Mops caudal aberrante Turbinalien (CAT), doch entgegen veterinärmedizinischer Studien (z.B. OECHTERING *et al*. 2016) ist nicht nur Ethmoturbinale I (Lamina posterior) beteiligt, sondern auch Ethmoturbinale II. Beide in dieser Studie vertretenen modernen Möpse haben rostral aberrante Turbinalien (RAT), welche durch die Lamina anterior des Ethmoturbinale I gebildet werden. Überraschenderweise treten aberrante Turbinalien nicht nur beim Mops (und Englischer und Französischer Bulldogge, siehe Tabelle 1 in OECHTERING *et al.* 2007) auf, sondern auch in weiteren brachyzephalen Rassen. In der aktuellen Studie wurden CAT in Pekinese und Chin, und sogar im etwas längerschnäuzigem Cavalier nachgewiesen.

(3) Die Abhängigkeit von der Schnauzenlänge, die in den bisher genannten Toy-Rassen bestätigt wurde, gilt ebenfalls für beide Englischen Zwergspaniels. Der Cavalier hat höhere Werte in IAT, SDEN und TC als der extrem brachyzephale King Spaniel. Der kompliziertere Bau der Turbinalien des Cavaliers im Vergleich zu seinem kurzschnäuzigen Vorfahr ist stärker im Maxilloturbinale ausgeprägt als in den olfaktorischen Turbinalien und der Lamina semicircularis.

(4) In Individuen, in deren verkleinerten Frontalsinus Frontoturbinale 1 und 2 nicht länger hineinragen können, verbleiben beide genannten Turbinalien innerhalb der Pars intermedia und fusionieren caudal mit der Lamina cribrosa. Somit entsprechen sie dem Muster des Frontoturbinale 3 im Grundplan und allen anderen Hunden.

Durch die Verwendung des Hundes als Modellorganismus konnten folgende grundlegende Merkmale für die Klasse der Säugetiere validiert werden:

(1) Die Theorie bezüglich einer genetisch manifestierten artspezifischen Anzahl der Fronto- und Ethmoturbinalien wurde bestätigt (z. B. RUF 2014) – unabhängig des beengten Raumes einer verkürzten oder verschmälerten Schnauze einer Rasse. Die einzige Referenz, die eine Terminologie der einzelnen Turbinalien weiterer Carnivora-Arten angibt, stammt von PAULLI (1900c). Seine Verwendung einer problematischen Terminologie erschwert einen Vergleich mit der Nomenklatur, an der sich die hier vorliegende Studie orientiert. Dennoch kann in Hinblick auf PAULLIS (1900c) Ergebnissen postuliert werden, dass *Canis lupus* zumindest in der Pars ethmoturbinalis den Grundplan der Carnivora von drei Ethmoturbinalien und einem prominenten Interturbinale aufweist. Die Pars intermedia besitzt im Grundplan dieser Säugerordnung höchstwahrscheinlich fünf Ektoturbinalien sensu PAULLI (1900c), welche im Hund den drei Frontoturbinalien und zwei prominenten Interturbinalien (Interturbinale β und δ) entsprechen.

(2) Das Wachstum der knöchernen Turbinalien ist genetisch gekoppelt mit dem Wachstum der Dermalknochen: in beiden endet es in einem spezifischen ontogenetischem Stadium. Entsprechend weisen die olfaktorischen Turbinalien der Rassen mit dem höchsten Grad der Dolichozephalie, der Windhunde, eine größere Oberfläche auf als diejenigen der mäßig langschnäuzigen Spürhunde. Wie bereits in diversen anderen Studien im Gesichtsbereich beobachtet (z. B. OECHTERING *et al*. 2016), stoppt das Turbinalienwachstum in brachyzephalen Rassen zu einem früheren ontogenetischen Zeitpunkt, was die reduzierte Oberflächengröße der Turbinalien begründet.

(3) Merkmale, die in brachyzephalen Rassen präsent sind, treten bereits in Perinatalstadien auf. Dazu zählen:

   a. der Processus uncinatus der Lamina semicircularis
   b. die Spaltung des Ethmoturbinale I in zwei Laminae, Lamina anterior und Lamina posterior; erstere besitzt einen nach rostral weisendem Processus anterior. Die rostrale Verlängerung des Processus anterior der Lamina posterior hingegen beginnt im neonaten Stadium und ist in manchen adulten brachyzephalen Hunden abwesend.
   c. die Entwicklung des Epiturbinale dorsoproximal an Ethmoturbinale I
   d. die doppelt eingerollte Grundform des Maxilloturbinale und der Frontoturbinalien.

(4) Von den erwachsenen Hunden wurden in dieser Studie lediglich mazerierte Schädel untersucht. Die beschriebene ‚relative chonchale Hypertrophy' (OECHTERING *et al*. 2016) kann nicht belegt werden. Stattdessen weisen die knöchernen Turbinalien brachyzephaler Rassen

gegenüber Hunden mit längerer Schnauze sogar eine Verringerung ihrer relativen Oberflächengröße und Oberflächendichte auf.

(5) Der Einfluss der knöchernen Turbinalien variiert zwischen respiratorischem und olfaktorischem Epithel:

a. Die Oberfläche des respiratorischen Systems ist von der Größe der knöchernen Struktur abhängig, die mit thermoregulatorischer Schleimhaut bedeckt ist. Obwohl das Turbinalienwachstum mit dem Schädelwachstum gekoppelt ist, scheinen sich mehr akzessorische Lamellen auszubilden in Rassen wie diversen Windhunden und Grönlandhund, die auf eine höhere respiratorische Effizienz angewiesen sind. Die erhöhte Anzahl jener Lamellen gewährleistet eine größere Oberfläche, sowie eine höhere Dichte und Komplexität des Maxilloturbinale und folglich eine gesteigerte thermoregulatorische Effizienz. In brachyzephalen Rassen stoppt das Wachstum akzessorischer Lamellen vorzeitig, während die Körpermasse noch bis ins Erwachsenenalter zunimmt. Dieses Ungleichgewicht verringert die respiratorische Leistung und führt zu Hitzeintoleranz (PACKER *et al*. 2015).
b. Sowohl der trotz reduzierter Oberflächengröße wohlentwickelte Geruchssinn brachyzephaler Rassen im Vergleich zu Spürhunden, als auch der postulierte reduzierte Geruchsinn der Windhunde trotz erhöhter Oberflächengröße olfaktorischer Turbinalien scheint darauf hinzudeuten, dass die knöchernen Turbinalien keinen Einfluss auf das Riechvermögen haben (SMITH *et al*. 2004, Widerspruch in VAN VALKENBURGH *et al*. 2011).

Das Turbinalskelett ist genetisch gekoppelt mit dem Wachstum der Dermalknochen und zeigt folglich über einen kurzen evolutiven Zeitraum eine ähnlich schnelle Variation in seiner Morphologie wie der Gesichtsschädel. Diese Ergebnisse können nun als Basis für weiterführende Studien in anderen Forschungsfeldern dienen (Evolution, DRAKE & KLINGENBERG 2010; Genetik, FONDON & GARNER 2004, BOYKO *et al*. 2010; Ontogenese und Morphologie, SCHOENEBECK *et al*. 2012, GEIGER & HAUSSMANN 2016; Physiologie und Neurobiologie, ISSEL-TARVER & RINE 1996, TACHER *et al*. 2005). Sie bieten die Möglichkeit, Zusammenhänge der Muster zwischen dem knöchernen Turbinalskelett und der Genetik, Physiologie und Neurobiologie (z.B. olfaktorische Sensorneuronen, olfaktorische Rezeptorgene; ROBIN *et al*. 2009, VAN VALKENBURGH *et al.* 2011), Ethologie und Geruchswahrnehmung (HALL *et al.* 2015), oder Morphologie (knöcherne Strukturen wie Lamina cribrosa, BIRD *et al.* 2018; andere Organe wie der Riechkolben, ROBERTS *et al.* 2010) zu finden. Auch wenn nach derzeitigem Standpunkt im Allgemeinen die knöchernen Turbinalien kein direkter Anzeiger der Geruchsleistung darzustellen scheinen (SMITH *et al.* 2004), steht unser Verständnis des Gesamtkomplexes dieses Sinnesorgans noch immer am Anfang.

REFERENCES

Adamkiewicz E, Jezierski T, Walczak M, Gorecka-Bruzda A, Sobczynska M, Prokopczyk M, Ensminger J (2013): Traits of drug and explosives detection in dogs of two breeds as evaluated by their handlers and trainers. *Anim. Sci. Pap. Rep.* 31: 205-217.

AKC - American Kennel Club, *https://www.akc.org/*; last access: 2019/09/16.

Allen H (1882): On a revision of the ethmoid bone in the Mammalia, with special reference to the description of this bone and of the sense of smelling in the Cheiroptera. *Bull. Mus. Comp. Zool.* 10: 135-164.

Amundsen T, Sundstrøm S, Buvik T, Gederaas OA, Haaverstad R (2014): Can dogs smell lung cancer? First study using exhaled breath and urine screening in unselected patients with suspected lung cancer. *Acta Oncol.* 53: 307-315.

Ash EC (1927a): *Dogs: their History and Development* I. London: Ernest Benn Limited.

Ash EC (1927b): *Dogs: their History and Development* II. London: Ernest Benn Limited.

Asher L, Diesel G, Summers JF, McGreevy PD, Collins LM (2009): Inherited defects in pedigree dogs. Part 1: disorders related to breed standards. *Vet. J.* 182: 402-411.

Bannister HM (1869): The Esquimaux Dog. *Am. Nat.* 3: 522-530.

Baron G, Frahm HD, Bhatnagar KP, Stephan H (1983): Comparison of brain structure volumes in Insectivora and Primates. III. Main olfactory bulb (MOB). *J. Hirnforsch.* 24: 551-568.

Beckmann L (1894): *Geschichte und Beschreibung der Rassen des Hundes* I. Braunschweig: Druck und Verlag von Friedrich Bieweg und Sohn.

Beckmann L (1895): *Geschichte und Beschreibung der Rassen des Hundes* II. Braunschweig: Druck und Verlag von Friedrich Bieweg und Sohn.

Benecke N (1987): Studies on early dog remains from Northern Europe. *J. Archaeol. Sci.* 14: 31-49.

Benson G (1999): Tandem repeats finder: a program to analyze DNA sequences. *Nucleic Acids Res.* 27: 573-580.

Bernstein P (1999): Morphology of the nasal capsule of *Heloderma suspectum* with comments on the systematic position of helodermatids (Squamata : Helodermatidae). *Acta Zool.* 80: 219-230.

Bird DJ, Amirkhanian A, Pang B, Van Valkenburgh B (2014): Quantifying the cribriform plate: influences of allometry, function, and phylogeny in Carnivora. *Anat. Rec.* 297: 2080-2092.

Bird DJ, Murphy WJ, Fox-Rosales L, Hamid I, Eagle RA, Van Valkenburgh B (2018): Olfaction written in bone: cribriform plate size parallels olfactory receptor gene repertoires in Mammalia. *Proc. Biol. Sci.* 285: 20180100.

Björnerfeldt S, Hailer F, Nord M, Vilà C (2008): Assortative mating and fragmentation within dog breeds. *BMC Evol. Biol.* 8: 28.

Boyko AR, Quignon P, Li L, Schoenebeck JJ, Degenhardt JD, Lohmueller KE, Zhao K, Brisbin A, Parker HG, vonHoldt BM, Cargill M, Auton A, Reynolds A, Elkahloun AG, Castelhano M, Mosher DS, Sutter NB, Johnson GS, Novembre J, Hubisz MJ, Siepel A, Wayne RK, Bustamante CD, Ostrander EA (2010): A simple genetic architecture underlies morphological variation in dogs. *PLoS Biol.* 8: e1000451.

Brehm A (1876): Die Säugethiere 1: Affen und Halbaffen, Flatterthiere, Raubthiere. In Brehm AE [ed.]: *Brehms Thierleben. Allgemeine Kunde des Thierreichs* I. Leipzig: Bibliographisches Institut.

Brehm H, Loeffler K, Komeyli H (1985): Schädelformen beim Hund. *Anat. Histol. Embryol.* 14: 324-331.

Brown SK, Darwent CM, Sacks BN (2013): Ancient DNA evidence for genetic continuity in arctic dogs. *J. Archaeol. Sci.* 40: 1279-1288.

Brown SK, Darwent CM, Wictum EJ, Sacks BN (2015): Using multiple markers to elucidate the ancient, historical and modern relationships among North American Arctic dog breeds. *Heredity* 115: 488-495.

Burk RL (1992a): Computed Tomographic Anatomy of the Canine Nasal Passages. *Vet. Radiol. Ultrasound* 33: 170-176.

Burk RL (1992b): Computed tomographic imaging of nasal disease in 100 dogs. *Vet. Radiol. Ultrasound* 33: 177-180.

Cagan A, Blass T (2016): Identification of genomic variants putatively targeted by selection during dog domestication. *BMC Evol. Biol.* 16: 10.

Campbell NA, Reece JB (2009): *Biologie*. München: Pearson Studium.

Clutton-Brock J (1984): Dog. In Mason I [ed.]: *Evolution of domesticated animals*: 198-211. London: Longman.

Clutton-Brock J (1995): Origins of the dog: domestication and early history. In Serpell J [ed.]: *The domestic dog. Its evolution, behaviour, and interactions with people*: 7-20. Cambridge: Cambridge University Press.

Clutton-Brock J, Kitchener A, Lynch J (1994): Changes in the skull morphology of the Arctic wolf, *Canis lupus arctos*, during the twentieth century. *J. Zool., Lond.* 233: 19-36.

Clutton-Brock J, Noe-Nygaard N (1990): New Osteological and C-Isotope Evidence on Mesolithic Dogs: Companions to Hunters and Fishers at Star Carr, Seamer Carr and Kongemose. *J. Archaeol. Sci.* 17: 643-653.

Coile D (2015): *Encyclopedia of Dog Breeds*. New York: Barron's Educational Series, Inc.

Craven BA, Neuberger T, Paterson EG, Webb AG, Josephson EM, Morrison EE, Settles GS (2007): Reconstruction and morphometric analysis of the nasal airway of the dog (*Canis familiaris*) and implications regarding olfactory airflow. *Anat. Rec.* 290: 1325-1340.

Craven BA, Paterson EG, Settles GS (2010): The fluid dynamics of canine olfaction: unique nasal airflow patterns as an explanation of macrosmia. *J. Roy. Soc. Interface* 7: 933-943.

Crompton AW, Owerkowicz T, Bhullar BAS, Musinsky C (2017): Structure of the Nasal Region of Non-Mammalian Cynodonts and Mammaliaforms: Speculations on the Evolution of Mammalian Endothermy. *J. Vertebr. Paleontol.* 37: e1269116.

Curtis AA, Lai G, Wei F, Van Valkenburgh B (2015): Repeated loss of frontal sinuses in arctoid carnivorans. *J. Morphol.* 276: 22-32.

Curtis AA, Van Valkenburgh B (2014): Beyond the sniffer: frontal sinuses in Carnivora. *Anat. Rec.* 297: 2047-2064.

Darwin C (1859): *On the origin of species by means of natural selection, or the preservation of favoured races in the struggle for life*. London: John Murray, Albemarle Street.

Dawes J (1952): The course of the nasal airstreams. *J. Laryngol. Otol.* 66: 583-593.

De Rycke LM, Saunders JH, Gielen IM, van Bree HJ, Simoens PJ (2003): Magnetic resonance imaging, computed tomography, and cross-sectional views of the anatomy of normal nasal cavities and paranasal sinuses in mesaticephalic dogs. *Am. J. Vet. Res.* 64: 1093-1098.

Drake AG, Coquerelle M, Colombeau G (2015): 3D morphometric analysis of fossil canid skulls contradicts the suggested domestication of dogs during the late Paleolithic. *Sci. Rep.* 5: 8299.

Drake AG, Klingenberg CP (2010): Large-scale diversification of skull shape in domestic dogs: disparity and modularity. *Am. Nat.* 175: 289-301.

Druzhkova AS, Thalmann O, Trifonov VA, Leonard JA, Vorobieva NV, Ovodov ND, Graphodatsky AS, Wayne RK (2013): Ancient DNA Analysis Affirms the Canid from Altai as a Primitive Dog. *PLoS ONE* 8: e57754.

Ellenberger W, Baum H (1891): *Systematische und topographische Anatomie des Hundes*. Berlin, Hamburg: Paul Parey.

Ellenberger W, Baum H (1906): *Handbuch der vergleichenden Anatomie der Haustiere*. Berlin: August Hirschwald.

FCI - Fédération Cynologique Internationale, *http://www.fci.be/en/*; last access: 2019/09/16.

Finck M, Ponce F, Guilbaud L, Chervier C, Floch F, Cadore JL, Chuzel T, Hugonnard M (2015): Computed tomography or rhinoscopy as the first-line procedure for suspected nasal tumor: a pilot study. *Canadian Vet. J.* 56: 185-192.

Fondon JW, 3rd, Garner HR (2004): Molecular origins of rapid and continuous morphological evolution. *Proc. Natl. Acad. Sci. U S A* 101: 18058-18063.

Fondon JW, 3rd, Garner HR (2007): Detection of length-dependent effects of tandem repeat alleles by 3-D geometric decomposition of craniofacial variation. *Dev. Genes Evol.* 217: 79-85.

Forni PE, Taylor-Burds C, Melvin VS, Williams T, Wray S (2011): Neural crest and ectodermal cells intermix in the nasal placode to give rise to GnRH-1 neurons, sensory neurons, and olfactory ensheathing cells. *J. Neurosci.* 31: 6915-6927.

Frankham R, Hemmer H, Ryder OA, Cothran EG, Soulé ME, Murray ND, Snyder M (1986): Selection in Captive Populations. *Zoo. Biol.* 5: 127-138.

Frantz LA, Mullin VE, Pionnier-Capitan M, Lebrasseur O, Ollivier M, Perri A, Linderholm A, Mattiangeli V, Teasdale MD, Dimopoulos EA, Tresset A, Duffraisse M, McCormick F, Bartosiewicz L, Gál E, Nyerges EA, Sablin MV, Bréhard S, Mashkour M, Bălăşescu A, Gillet B, Hughes S, Chassaing O, Hitte C, Vigne JD, Dobney K, Hanni C, Bradley DG, Larson G (2016): Genomic and archaeological evidence suggest a dual origin of domestic dogs. *Science* 352: 1228-1231.

Freedman AH, Gronau I, Schweizer RM, Ortega-Del Vecchyo D, Han E, Silva PM, Galaverni M, Fan Z, Marx P, Lorente-Galdos B, Beale H, Ramirez O, Hormozdiari F, Alkan C, Vilà C, Squire K, Geffen E, Kusak J, Boyko AR, Parker HG, Lee C, Tadigotla V, Wilton A, Siepel A, Bustamante CD, Harkins TT, Nelson SF, Ostrander EA, Marques-Bonet T, Wayne RK, Novembre J (2014): Genome sequencing highlights the dynamic early history of dogs. *PLoS Genet.* 10: e1004016.

Fuller TK, Mech LD, Cochrane JF (2003): Wolf Population Dynamics. In Mech L, Boitani L [eds.]: *Wolves. Behavior, Ecology, and Conservation*: 161-191. Chicago: The University of Chicago Press.

Gardiner JD, Behnsen J, Brassey CA (2018): Alpha shapes: determining 3D shape complexity across morphologically diverse structures. *BMC evolutionary biology* 18: 184.

Gaupp E (1908): Zur Entwicklunsgeschichte und vergleichenden Morphologie des Schädels von *Echidna aculeata* var. *typica*. In Semon R [ed.]: *Zoologische Forschungsreisen in Australien und dem Malayischen Archipel VI*: 539-788. Jena: Fischer.

Geiger M, Evin A, Sánchez-Villagra MR, Gascho D, Mainini C, Zollikofer CPE (2017): Neomorphosis and heterochrony of skull shape in dog domestication. *Sci. Rep.* 7: 13443.

Geiger M, Haussman S (2016): Cranial Suture Closure in Domestic Dog Breeds and Its Relationships to Skull Morphology. *Anat. Rec.* 299: 412-420.

Germonpré M, Sablin MV, Stevens RE, Hedges REM, Hofreiter M, Stiller M, Després VR (2009): Fossil dogs and wolves from Palaeolithic sites in Belgium, the Ukraine and Russia: osteometry, ancient DNA and stable isotopes. *J. Archaeol. Sci.* 36: 473-490.

Gittleman J, Harvey P (1982): Carnivore home-range size, metabolic needs and ecology. *Behav. Ecol. Sociobiol.* 10: 57-63.

Göhring W, Sasaki T, Heldin C, Timpl R (1998): Mapping of the binding of platelet-derived growth factor to distinct domains of the basement membrane proteins BM-40 and perlecan and distinction from the BM-40 collagen-binding epitope. *Eur. J. Biochem.* 255: 60-66.

Goldberg MB, Langman VA, Taylor CR (1981): Panting in dogs: paths of air flow in response to heat and exercise. *Respir. Physiol.* 43: 327-338.

Green PA, Van Valkenburgh B, Pang B, Bird D, Rowe T, Curtis A (2012): Respiratory and olfactory turbinal size in canid and arctoid carnivorans. *J. Anat.* 221: 609-621.

Guagnin M, Perri AR, Petraglia MD (2018): Pre-Neolithic evidence for dog-assisted hunting strategies in Arabia. *J. Anthropol. Archaeol.* 49: 225-236.

Hall NJ, Glenn K, Smith DW, Wynne CD (2015): Performance of Pugs, German Shepherds, and Greyhounds (*Canis lupus familiaris*) on an odor-discrimination task. *J. Comp. Psychol.* 129: 237-246.

Hall NJ, Protopopova A, Wynne CDL (2016): Olfaction in Wild Canids and Russian Canid Hybrids. In Jezierski T, Ensminger J, Papet LE [eds.]: *Canine Olfaction Science and Law*: 57-66. Boca Raton: CRC Press.

Hallermann J (1998): The ethmoidal region of *Dibamus taylori* (Squamata: Dibamidae), with a phylogenetic hypothesis on dibamid relationships within Squamata. *Zool. J. Linn. Soc.* 122: 385-426.

Harcourt RA (1974): The Dog in Prehistoric and Early Historic Britain. *J. Archaeol. Sci.* 1: 151-175.

Harrington F, Asa C (2003): Wolf Communication. In Mech L, Boitani L [eds.]: *Wolves. Behavior, Ecology, and Conservation*: 66-103. Chicago: The University of Chicago Press.

Haworth KE, Islam I, Breen M, Putt W, Makrinou E, Binns M, Hopkinson D, Edwards Y (2001): Canine *TCOF1*; cloning, chromosome assignment and genetic analysis in dogs with different head types. *Mamm. Genome* 12: 622-629.

Hayden S, Teeling EC (2014): The molecular biology of vertebrate olfaction. *Anat. Rec.* 297: 2216-2226.

Heidenreich D, Gradner G, Kneissl S, Dupre G (2016): Nasopharyngeal Dimensions From Computed Tomography of Pugs and French Bulldogs With Brachycephalic Airway Syndrome. *Vet. Surg.* 45: 83-90.

Hennet P (1997): The persistence of deciduous teeth in dogs and cats and its consequences. *Prat. Med. Chir. Anim.* 32: 69-76.

Hillenius WJ (1992): The evolution of nasal turbinates and mammalian endothermy. *Paleobiology* 18: 17-29.

Hillenius WJ (1994): Turbinates in therapsids - evidence for late permian origins of mammalian endothermy. *Evolution* 48: 207-229.

Hofer H (1952): Der Gestaltwandel des Schädels der Säugetiere und Vögel, mit besonderer Berücksichtigung der Knickungstypen und der Schädelbasis. *Verh. Anat. Ges.* 50: 102-113.

Hofer H, Spatz W (1963): Studien zum Problem des Gestaltwandels des Schädels der Säugetiere, insbesondere der Primaten: II. Über die Kyphosen fetaler und neonater Primatenschädel. *Z. Morphol. Anthropol.* 53: 29-52.

Hole F, Wyllie C (2007): The oldest depictions of canines and a possible early breed of dog in Iran. *Paléorient* 33: 175-185.

Horvath G, Andersson H, Nemes S (2013): Cancer odor in the blood of ovarian cancer patients: a retrospective study of detection by dogs during treatment, 3 and 6 months afterward. *Bmc Cancer* 13: 396.

Huppi E, Sanchez-Villagra MR, Tzika AC, Werneburg I (2018): Ontogeny and phylogeny of the mammalian chondrocranium: the cupula nasi anterior and associated structures of the anterior head region. *Zool Lett* 4: https://doi.org/10.1186/s40851-40018-40112-40850.

Issel-Tarver L, Rine J (1996): Organization and expression of canine olfactory receptor genes. *Proc. Natl. Acad. Sci. U S A* 93: 10897-10902.

Iwahori N, Kiyota E, Nakamura K (1987): Olfactory and respiratory epithelia in the snake, *Elaphe quadrivirgata*. *Okajimas Folia Anat. Jpn.* 64: 183-191.

Kay RF, Campbell VM, Rossie JB, Colbert MW, Rowe TB (2004): Olfactory fossa of *Tremacebus harringtoni* (platyrrhini, early Miocene, Sacanana, Argentina): implications for activity pattern. *Anat. Rec. A Discov. Mol. Cell. Evol. Biol.* 281: 1157-1172.

Klein D (1970): Tundra ranges north of the boreal forest. *J. Range Manage.* 23: 8-14.

Koch DA, Arnold S, Hubler M, Montavon PM (2003): Brachycephalic syndrome in dogs. *Comp. Cont. Educ. Pract.* 25: 48-54.

Kuhn H-J (1971): Die Entwicklung und Morphologie des Schädels von *Tachyglossus aculeatus*. *Abh. senckenb. naturforsch. Ges.* 528: 1-224.

Kumar P, Kumar S, Singh Y (1993): Histological Studies on the Nasal Ethmoturbinates of Goats. *Small Rumin. Res.* 11: 85-92.

Kumar P, Timoney JF, Southgate HH, Sheoran AS (2000): Light and scanning electron microscopic studies of the nasal turbinates of the horse. *Anat. Histol. Embryol.* 29: 103-109.

Larson G, Karlsson EK, Perri A, Webster MT, Ho SYW, Peters J, Stahl PW, Piper PJ, Lingaas F, Fredholm M, Comstock KE, Modiano JF, Schelling C, Agoulnik AI, Leegwater PA, Dobney K, Vigne J-D, Vilà C, Andersson L, Lindblad-Toh K (2012): Rethinking dog domestication by integrating genetics, archeology, and biogeography. *Proc. Natl. Acad. Sci. U S A* 109: 8878-8883.

Leonard JA, Vilà C, Wayne RK (2006): From Wild Wolf to Domestic Dog. In Ostrander E, Giger U, Lindblad-Toh K [eds.]: *The Dog and its Genome*: 95-117. New York: Cold Springer Harbor Laboratory Press.

Lesniak A, Walczak M, Jezierski T, Sacharczuk M, Gawkowski M, Jaszczak K (2008): Canine olfactory receptor gene polymorphism and its relation to odor detection performance by sniffer dogs. *J. Hered.* 99: 518-527.

Lindblad-Toh K, Wade CM, Mikkelsen TS, Karlsson EK, Jaffe DB, Kamal M, Clamp M, Chang JL, Kulbokas EJ, 3rd, Zody MC, Mauceli E, Xie X, Breen M, Wayne RK, Ostrander EA, Ponting CP, Galibert F, Smith DR, DeJong PJ, Kirkness E, Alvarez P, Biagi T, Brockman W, Butler J, Chin CW, Cook A, Cuff J, Daly MJ, DeCaprio D, Gnerre S, Grabherr M, Kellis M, Kleber M, Bardeleben C, Goodstadt L, Heger A, Hitte C, Kim L, Koepfli KP, Parker HG, Pollinger JP, Searle SM, Sutter NB, Thomas R, Webber C, Baldwin J, Abebe A, Abouelleil A, Aftuck L, Ait-Zahra M, Aldredge T, Allen N, An P, Anderson S, Antoine C, Arachchi H, Aslam A, Ayotte L, Bachantsang P, Barry A, Bayul T, Benamara M, Berlin A, Bessette D, Blitshteyn B, Bloom T, Blye J, Boguslavskiy L, Bonnet C, Boukhgalter B, Brown A, Cahill P, Calixte N, Camarata J, Cheshatsang Y, Chu J, Citroen M, Collymore A, Cooke P, Dawoe T, Daza R, Decktor K, DeGray S, Dhargay N, Dooley K, Dooley K, Dorje P, Dorjee K, Dorris L, Duffey N, Dupes A, Egbiremolen O, Elong R, Falk J, Farina A, Faro S, Ferguson D, Ferreira P, Fisher S, FitzGerald M, Foley K, Foley C,

Franke A, Friedrich D, Gage D, Garber M, Gearin G, Giannoukos G, Goode T, Goyette A, Graham J, Grandbois E, Gyaltsen K, Hafez N, Hagopian D, Hagos B, Hall J, Healy C, Hegarty R, Honan T, Horn A, Houde N, Hughes L, Hunnicutt L, Husby M, Jester B, Jones C, Kamat A, Kanga B, Kells C, Khazanovich D, Kieu AC, Kisner P, Kumar M, Lance K, Landers T, Lara M, Lee W, Leger JP, Lennon N, Leuper L, LeVine S, Liu J, Liu X, Lokyitsang Y, Lokyitsang T, Lui A, Macdonald J, Major J, Marabella R, Maru K, Matthews C, McDonough S, Mehta T, Meldrim J, Melnikov A, Meneus L, Mihalev A, Mihova T, Miller K, Mittelman R, Mlenga V, Mulrain L, Munson G, Navidi A, Naylor J, Nguyen T, Nguyen N, Nguyen C, Nguyen T, Nicol R, Norbu N, Norbu C, Novod N, Nyima T, Olandt P, O'Neill B, O'Neill K, Osman S, Oyono L, Patti C, Perrin D, Phunkhang P, Pierre F, Priest M, Rachupka A, Raghuraman S, Rameau R, Ray V, Raymond C, Rege F, Rise C, Rogers J, Rogov P, Sahalie J, Settipalli S, Sharpe T, Shea T, Sheehan M, Sherpa N, Shi J, Shih D, Sloan J, Smith C, Sparrow T, Stalker J, Stange-Thomann N, Stavropoulos S, Stone C, Stone S, Sykes S, Tchuinga P, Tenzing P, Tesfaye S, Thoulutsang D, Thoulutsang Y, Topham K, Topping I, Tsamla T, Vassiliev H, Venkataraman V, Vo A, Wangchuk T, Wangdi T, Weiand M, Wilkinson J, Wilson A, Yadav S, Yang S, Yang X, Young G, Yu Q, Zainoun J, Zembek L, Zimmer A, Lander ES (2005): Genome sequence, comparative analysis and haplotype structure of the domestic dog. *Nature* 438: 803-819.

Liu NC, Sargan DR, Adams VJ, Ladlow JF (2015): Characterisation of Brachycephalic Obstructive Airway Syndrome in French Bulldogs Using Whole-Body Barometric Plethysmography. *PLoS ONE* 10: e0130741.

Liu NC, Troconis EL, Kalmar L, Price DJ, Wright HE, Adams VJ, Sargan DR, Ladlow JF (2017): Conformational risk factors of brachycephalic obstructive airway syndrome (BOAS) in pugs, French bulldogs, and bulldogs. *PloS ONE* 12: e0181928.

Mackensen H, Furler-Mihali A, Moritz J, Rickert D, Cermak R (2017): Beurteilung von brachyzephalen Hunderassen hinsichtlich Qualzuchtmerkmale am Beispiel des Mops. Ein Merkblatt zum Erkennen von tierschutzrelevanten Merkmalen. *Dt. TÄBl.* 7/2017: 910-915.

Macrini TE (2012): Comparative Morphology of the Internal Nasal Skeleton of Adult Marsupials Based on X-Ray Computed Tomography. *B. Am. Mus. Nat. Hist.* 365: 1-91.

Macrini TE (2014): Development of the ethmoid in *Caluromys philander* (Didelphidae, Marsupialia) with a discussion on the homology of the turbinal elements in marsupials. *Anat. Rec.* 297: 2007-2017.

Maier W (1993a): Cranial morphology of the Therian common ancestor, as suggested by the adaptations of neonate marsupials. In Szalay F, Novacek M, McKenna M [eds.]: *Mammal Phylogeny*: 165-181. New York: Springer.

Maier W (1993b): Zur evolutiven und funktionellen Morphologie des Gesichtsschädels der Primaten. *Z. Morph. Anthropol.* 79: 279-299.

Maier W (2002): Zur funktionellen Morphologie der rostralen Nasenknorpel bei Soriciden. *Mamm. Biol.* 67: 1-17.

Maier W, Ruf I (2014): Morphology of the nasal capsule of primates - with special reference to *Daubentonia* and *Homo*. *Anat. Rec.* 297: 1985-2006.

Marchant TW, Johnson EJ, McTeir L, Johnson CI, Gow A, Liuti T, Kuehn D, Svenson K, Bermingham ML, Drogemuller M, Nussbaumer M, Davey MG, Argyle DJ, Powell RM, Guilherme S, Lang J, Ter Haar G, Leeb T, Schwarz T, Mellanby RJ, Clements DN, Schoenebeck JJ (2017): Canine Brachycephaly Is Associated with a Retrotransposon-Mediated Missplicing of SMOC2. *Curr. Biol.* 27: 1573-1584.

Martin WCL (1845): *The history of the dog: its origin, physical and moral characteristics, and its principal varieties*. London: Charles Knight & Co.

Martin VM (2012): *Aussagekraft eines Belastungstests für Möpse bezüglich mit dem brachyzephalen Atemnotsyndrom assoziierter Probleme*. Dissertation, Ludwig-Maximilians-Universität München, München.

Martinez Q, Lebrun R, Achmadi AS, Esselstyn JA, Evans AR, Heaney LR, Miguez RP, Rowe KC, Fabre PH (2018): Convergent evolution of an extreme dietary specialisation, the olfactory system of worm-eating rodents. *Sci. Rep.* 8: 17806.

Mazák JH (2010): Geographical variation and phylogenetics of modern lions based on craniometric data. *J. Zool.* 281: 194-209.

McGreevy P, Grassi TD, Harman AM (2004): A strong correlation exists between the distribution of retinal ganglion cells and nose length in the dog. *Brain Behav. Evol.* 63: 13-22.

Mech LD (1974): *Canis lupus*. *Mamm. Species* 37: 1-6.

Miller M, Christiansen G, Evans H (1964): *Anatomy of the Dog*. Philadelphia: W. B. Saunders Company.

Møhl J (1986): Dog remains from a paleoeskimo settlement in West Greenland. *Arct. Anthropol.* 23: 81-89.

Morey DF, Aaris-Sørensen K (2002): Paleoeskimo dogs of the Eastern Arctic. *Arctic* 55: 44-56.

Murrish DE, Schmidt-Nielsen K (1970): Exhaled air temperature and water conservation in lizards. *Respir. Physiol.* 10: 151-158.

Negus, VE (1954): *Introduction to the comparative anatomy of the nose and paranasal sinuses*. Hunterian Lecture delivered at the Royal College of Surgeons of England on 20th May 1954.

Nehring A (1888): Zur Abstammung der Hunde-Rassen. *Zool. Jahrb.* 3: 51-58.

Niethammer J, Krapp F (1978): Bd. 1, Rodentia: Sciuridae, Castoridae, Gliridae, Muridae. In Niethammer J, Krapp F [eds.]: *Handbuch der Säugetiere Europas* I. Wiebelsheim: AULA.

Oechtering TH, Oechtering GU, Noller C (2007): Structural characteristics of the nose in brachycephalic dog breeds analysed by computed tomography. *Tieraerztl. Prax. K. H.* 35: 177-187.

Oechtering GU, Pohl S, Schlueter C, Lippert JP, Alef M, Kiefer I, Ludewig E, Schuenemann R (2016): A Novel Approach to Brachycephalic Syndrome. 1. Evaluation of Anatomical Intranasal Airway Obstruction. *Vet. Surg.* 45: 165-172.

Olmstead MP (1911): Das Primordialcranium eines Hundeembryo. Ein Beitrag zur Morphologie des Säugetierschädels. *Anat. Hefte* 43: 335-375.

O´Neil DG, Jackson C, Guy JH, Church DB, McGreevy PD, Thomson PC, Brodbelt DC (2015): Epidemiological associations between brachycephaly and upper respiratory tract disorders in dogs attending veterinary practices in England. *Genet. Epidemiol.* 2: 10.

O'Regan HJ, Kitchener AC (2005): The effects of captivity on the morphology of captive, domesticated and feral mammals. *Mammal Rev.* 35: 215-230.

Ovodov ND, Crockford SJ, Kuzmin YV, Higham TF, Hodgins GW, van der Plicht J (2011): A 33,000-year-old incipient dog from the Altai Mountains of Siberia: evidence of the earliest domestication disrupted by the Last Glacial Maximum. *PLoS ONE* 6: e22821.

Owen R (1854): *The principal forms of the skeleton and of the teeth*. Philadelphia: Blanchard and Lea.

Packer RMA, Hendricks A, Burn CC (2012): Do dog owners perceive the clinical signs related to conformational inherited disorders as 'normal' for the breed? A potential constraint to improving canine welfare. *Anim. Welfare* 21: 81-93.

Packer RMA, Hendricks A, Tivers MS, Burn CC (2015): Impact of Facial Conformation on Canine Health: Brachycephalic Obstructive Airway Syndrome. *PLoS ONE* 10: e0137496.

Pang B, Yee KK, Lischka FW, Rawson NE, Haskins ME, Wysocki CJ, Craven BA, Van Valkenburgh B (2016): The influence of nasal airflow on respiratory and olfactory epithelial distribution in felids. *J. Exp. Biol.* 219: 1866-1874.

Parker HG, Dreger DL, Rimbault M, Davis BW, Mullen AB, Carpintero-Ramirez G, Ostrander EA (2017): Genomic Analyses Reveal the Influence of Geographic Origin, Migration, and Hybridization on Modern Dog Breed Development. *Cell Rep.* 19: 697-708.

Parker HG, Kim LV, Sutter NB, Carlson S, Lorentzen TD, Malek TB, Johnson GS, DeFrance HB, Ostrander EA, Kruglyak L (2004): Genetic structure of the purebred domestic dog. *Science* 304: 1160-1164.

Paulli S (1900a): Über die Pneumaticität des Schädels bei den Säugetieren. Eine morphologische Studie. I. Über den Bau des Siebbeins. Über die Morphologie des Siebbeins und die Pneumaticität bei den Monotremen und den Marsupialiern. *Morphol. Jb.* 28: 147-178.

Paulli S (1900b): Über die Pneumaticität des Schädels bei den Säugetieren. Eine morphologische Studie. II. Über die Morphologie des Siebbeins und der Pneumaticität bei den Ungulaten und Prosbosciden. *Morphol. Jb.* 28: 179-251.

Paulli S (1900c): Über die Pneumaticität des Schädels bei den Säugetieren. Eine morphologische Studie. III. Über die Morphologie des Siebbeins und die Pneumaticität bei den Insectivoren, Hyracoideen, Chiropteren, Carnivoren, Pinnipeden, Edentaten, Rodentiern, Prosimiern und Primaten, nebst einer zusammenfassenden Übersicht über die Morphologie des Siebbeins und die der Pneumaticität des Schädels bei den Säugetieren. *Morphol. Jb.* 28: 483-564.

Peterson RO, Ciucci P (2003): The Wolf as a Carnivore. In Mech L, Boitani L [eds.]: *Wolves. Behavior, Ecology, and Conservation*: 104-130. Chicago: The University of Chicago Press.

Pickrell JK, Pritchard JK (2012): Inference of population splits and mixtures from genome-wide allele frequency data. *PLoS Genet.* 8: e1002967.

Pilpel Y, Sosinsky A, Lancet D (1998): Molecular biology of olfactory receptors. *Essays Biochem.* 33: 93-104.

Price EO (1999): Behavioral development in animals undergoing domestication. *Appl. Anim. Behav. Sci.* 65: 245-271.

Quignon P, Rimbault M, Robin S, Galibert F (2012): Genetics of canine olfaction and receptor diversity. *Mamm. Genome* 23: 132-143.

Reinbach W (1952a): Zur Entwicklung des Primordialcraniums von *Dasypus novemcinctus* LINNÉ (*Tatusia novemcinctus* LESSON) I. *Z. Morphol. Anthropol.* 44: 375-444.

Reinbach W (1952b): Zur Entwicklung des Primordialcraniums von *Dasypus novemcinctus* LINNÉ (*Tatusia novemcinctus* LESSON) II. *Z. Morphol. Anthropol.* 45: 1-72.

Reinbach W (1955): Das Cranium eines Embryos des Gürteltieres *Zaedyus minutus* (65mm Sch.St.). *Morphol. Jb.* 95: 79-141.

Roberts T, McGreevy P, Valenzuela M (2010): Human induced rotation and reorganization of the brain of domestic dogs. *PLoS ONE* 5: e11946.

Robin S, Tacher S, Rimbault M, Vaysse A, Dréano S, André C, Hitte C, Galibert F (2009): Genetic diversity of canine olfactory receptors. *BMC genomics* 10: 21.

Rooney NJ, Morant S, Guest C (2013): Investigation into the Value of Trained Glycaemia Alert Dogs to Clients with Type I Diabetes. *Plos ONE* 8: e69921.

Rowe TB, Eiting TP, Macrini TE, Ketcham RA (2005): Organization of the Olfactory and Respiratory Skeleton in the Nose of the Gray Short-Tailed Opossum *Monodelphis domestica*. *J. Mamm. Evol.* 12: 303-336.

Ruf I (2004): *Vergleichend-ontogenetische Untersuchungen an der Ethmoidalregion der Muroidea (Rodentia, Mammalia). Ein Beitrag zur Morphologie und Systematik der Nagetiere*. Dissertation, Eberhard-Karls-Universität Tübingen, Tübingen.

R Core Team (2016): *R: A language and environment for statistical computing*. Vienna, Austria: R Foundation for Statistical Computing.

Ruf I (2014): Comparative anatomy and systematic implications of the turbinal skeleton in Lagomorpha (Mammalia). *Anat. Rec.* 297: 2031-2046.

Ruf I, Janßen S, Zeller U (2015): The ethmoidal region of the skull of *Ptilocerus lowii* (Ptiloceridae, Scandentia, Mammalia) - a contribution to the reconstruction of the cranial morphotype of primates. *Primate Biol.* 2: 89-110.

Ruf I, Maier W, Rodrigues PG, Schultz CL (2014): Nasal Anatomy of the Non-mammaliaform Cynodont *Brasilitherium riograndensis* (Eucynodontia, Therapsida) Reveals New Insight into Mammalian Evolution. *Anat. Rec.* 297: 2018-2030.

Rusbridge C, Knowler SP (2003): Hereditary aspects of occipital bone hypoplasia and syringomyelia (Chiari-like malformation) in cavalier King Charles spaniels. *Vet. Rec.* 153: 107-112.

Rusbridge C, Knowler SP (2004): Inheritance of occipital bone hypoplasia (Chiari-like malformation) in cavalier King Charles spaniels. *J. Vet. Intern. Med.* 18: 673-678.

Salgirli Demirbas Y (2012): Evaluation of body postures of Belgian Malinois dogs during a police dog training in Germany. *Ankara Üniv. Vet. Fak. Derg.* 59: 241-246.

Sampson J, Binns MM (2006): The Kennel Club and the Early History of Dog Shows. In Ostrander E, Giger U, Lindblad-Toh K [eds]: *The Dog and its Genome*: 19-30. New York: Cold Springer Harbor Laboratory Press.

Sandoe P, Kondrup SV, Bennett PC, Forkman B, Meyer I, Proschowsky HF, Serpell JA, Lund TB (2017): Why do people buy dogs with potential welfare problems related to extreme conformation and inherited disease? A representative study of Danish owners of four small dog breeds. *PLoS ONE* 12: e0172091.

Savolainen P, Zhang YP, Luo J, Lundeberg J, Leitner T (2002): Genetic evidence for an East Asian origin of domestic dogs. *Science* 298: 1610-1613.

Schaller O (1992): *Illustrated Veterinary Anatomical Nomenclature*. Stuttgart: Ferdinand Enke Verlag.

Schliemann H (1987): The Solum nasi of the mammalian chondrocranium with special reference to the Carnivora. In Kuhn H-J, Zeller U [eds.]: *Morphogenesis of the Mammalian skull (Mammalia depicta 13)*: 91-103. Hamburg: Parey.

Schliemann H (1966): Zur Morphologie und Entwicklung des Craniums von *Canis lupus* f. *familiaris* L. *Morphol. Jb.* 109: 501-603.

Schmidt MJ, Volk H, Klingler M, Failing K, Kramer M, Ondreka N (2013): Comparison of closure times for cranial base synchondroses in mesaticephalic, brachycephalic, and Cavalier King Charles Spaniel dogs. *Veterinary radiology & ultrasound : the official journal of the American College of Veterinary Radiology and the International Veterinary Radiology Association* 54: 497-503.

Schoenebeck JJ, Hutchinson SA, Byers A, Beale HC, Carrington B, Faden DL, Rimbault M, Decker B, Kidd JM, Sood R, Boyko AR, Fondon JW, 3rd, Wayne RK, Bustamante CD, Ciruna B, Ostrander EA (2012): Variation of BMP3 contributes to dog breed skull diversity. *PLoS Genet.* 8: e1002849.

Schoenebeck JJ, Ostrander EA (2013): The genetics of canine skull shape variation. *Genetics* 193: 317-325.

Schreider JP, Raabe OG (1981): Anatomy of the nasal-pharyngeal airway of experimental animals. *Anat. Rec.* 200: 195-205.

Schrenk F (1989): Zur Schädelentwicklung von *Ctenodactylus gundi* (Rothmann 1776) (Mammalia: Rodentia). *Cour. Forsch.-Inst. Senckenberg* 108: 1-241.

Schwalbe G (1882): Ueber die Nasenmuscheln der Säugethiere und des Menschen. *Sitzungsberichte der physikalisch-ökonomischen Gesellschaft zu Königsberg* 23: 3-6.

Schweizer AV, Lebrun R, Wilson LAB, Costeur L, Schmelzle T, Sánchez-Villagra MR (2017): Size Variation under Domestication: Conservatism in the inner ear shape of wolves, dogs and dingoes. *Sci. Rep.* 7: 13330.

Seydel O (1891): Ueber die Nasenhöhle der höheren Säugethiere und des Menschen. *Morphol. Jb.* 17: 44-99.

Sillero-Zubiri C (2009): Family Canidae (dogs). In Wilson DE, Mittermeier RA [eds.]: *Handbook of the Mammals of the World* 1, Carnivores: 352-446. Barcelona: Lynx Edicions.

Slater G, Van Valkenburgh B (2009): Allometry and performance: the evolution of skull form and function in felids. *J. Evol. Biol.* 22: 2278-2287.

Smetanova M, Cerna Bolfikova B, Randi E, Caniglia R, Fabbri E, Galaverni M, Kutal M, Hulva P (2015): From Wolves to Dogs, and Back: Genetic Composition of the Czechoslovakian Wolfdog. *PloS ONE* 10: e0143807.

Smith TD, Bhatnagar KP, Rossie JB, Docherty BA, Burrows AM, Cooper GM, Mooney MP, Siegel MI (2007): Scaling of the first ethmoturbinal in nocturnal strepsirrhines: olfactory and respiratory surfaces. *Anat. Rec.* 290: 215-237.

Smith TD, Bhatnagar KP, Tuladhar P, Burrows AM (2004): Distribution of olfactory epithelium in the primate nasal cavity: are microsmia and macrosmia valid morphological concepts? *Anat. Rec.* 281: 1173-1181.

Smith TD, Eiting TP, Bonar CJ, Craven BA (2014): Nasal morphometry in marmosets: loss and redistribution of olfactory surface area. *Anat. Rec.* 297: 2093-2104.

Smith TD, Martell MC, Rossie JB, Bonar CJ, Deleon VB (2016): Ontogeny and Microanatomy of the Nasal Turbinals in Lemuriformes. *Anat. Rec.* 299: 1492-1510.

Smith TD, Rossie JB (2008): Nasal fossa of mouse and dwarf lemurs (Primates, Cheirogaleidae). *Anat. Rec.* 291: 895-915.

Sokpor G, Abbas E, Rosenbusch J, Staiger JF, Tuoc T (2018): Transcriptional and Epigenetic Control of Mammalian Olfactory Epithelium Development. *Mol. Neurobiol.* 55: 8306-8327.

Soulé M, Gilpin M, Conway W, Foose T (1986): The Millennium Ark - How Long a Voyage, How Many Staterooms, How Many Passengers. *Zoo Biol.* 5: 101-113.

Starck D (1979): Das Skeletsystem. Allgemeines, Skeletsubstanzen, Skelet der Wirbeltiere einschließlich Lokomotionstypen. In Starck D [ed.]: *Vergleichende Anatomie der Wirbeltiere* II. Berlin: Springer.

Starck D (1982): Organe des aktiven Bewegungsapparates, der Koordination, der Umweltbeziehung, des Stoffwechsels und der Fortpflanzung. In Starck D [ed.]: *Vergleichende Anatomie der Wirbeltiere* III. Berlin: Springer.

Sturzenegger N (2011): *Veränderungen des Gesichts-/ Gehirnschädelverhältnisses (S-Index) ausgewählter brachycephaler Hunderassen im Verlaufe der letzten 100 Jahre*. Dissertation, Universität Zürich, Zürich.

Sutter NB, Eberle MA, Parker HG, Pullar BJ, Kirkness EF, Kruglyak L, Ostrander EA (2004): Extensive and breed-specific linkage disequilibrium in *Canis familiaris*. *Genome Res.* 14: 2388-2396.

Svartberg K (2002): Shyness-boldness predicts performance in working dogs. *Appl. Anim. Behav. Sci.* 79: 157-174.

Tacher S, Quignon P, Rimbault M, Dreano S, Andre C, Galibert F (2005): Olfactory receptor sequence polymorphism within and between breeds of dogs. *J. Hered.* 96: 812-816.

Thalmann O, Shapiro B, Cui P, Schuenemann VJ, Sawyer SK, Greenfield DL, Germonpré MB, Sablin MV, López-Giráldez F, Domingo-Roura X, Napierala H, Uerpmann HP, Loponte DM, Acosta AA, Giemsch L, Schmitz RW, Worthington B, Buikstra JE, Druzhkova A, Graphodatsky AS, Ovodov ND, Wahlberg N, Freedman AH, Schweizer RM, Koepfli KP, Leonard JA, Meyer M, Krause J, Pääbo S, Green RE, Wayne RK (2013): Complete mitochondrial genomes of ancient canids suggest a European origin of domestic dogs. *Science* 342: 871-874.

Trut LN (1999): Early canid domestication: The farm-fox experiment. *Am. Sci.* 87: 160-169.

van Asch B, Zhang AB, Oskarsson MC, Klutsch CF, Amorim A, Savolainen P (2013): Pre-Columbian origins of Native American dog breeds, with only limited replacement by European dogs, confirmed by mtDNA analysis. *Proc. Royal Soc. B* 280: 20131142.

Van Valkenburgh B, Curtis A, Samuels JX, Bird D, Fulkerson B, Meachen-Samuels J, Slater GJ (2011): Aquatic adaptations in the nose of carnivorans: evidence from the turbinates. *J. Anat.* 218: 298-310.

Van Valkenburgh B, Pang B, Bird D, Curtis A, Yee K, Wysocki C, Craven BA (2014a): Respiratory and olfactory turbinals in feliform and caniform carnivorans: the influence of snout length. *Anat. Rec.* 297: 2065-2079.

Van Valkenburgh B, Smith TD, Craven BA (2014b): Tour of a labyrinth: exploring the vertebrate nose. *Anat. Rec.* 297: 1975-1984.

Van Valkenburgh B, Theodor J, Friscia A, Pollack A, Rowe T (2004): Respiratory turbinates of canids and felids: a quantitative comparison. *J. Zool.* 264: 281-293.

Vasallo L (2016): Behavioral differences among Belgian Shepherd Dogs varieties. *Dog Behavior* 2: 15-19.

Vaysse A, Ratnakumar A, Derrien T, Axelsson E, Rosengren Pielberg G, Sigurdsson S, Fall T, Seppälä EH, Hansen MS, Lawley CT, Karlsson EK, The LUPA Consortium, Bannasch D, Vilà C, Lohi H, Galibert F, Fredholm M, Häggström J, Hedhammar Å, André C, Lindblad-Toh K, Hitte C, Webster MT (2011): Identification of genomic regions associated with phenotypic variation between dog breeds using selection mapping. *PLoS Genet.* 7: e1002316.

Vilà C, Wayne RK (1999): Hybridization between wolves and dogs. *Conserv. Biol.* 13: 195-198.

Voit M (1909): Das Primordialcranium des Kaninchens unter Berücksichtigung der Deckknochen. Ein Beitrag zur Morphologie des Säugetierschädels. *Anat. Hefte* 38: 425-616.

vom Hagen A (1935): *Die Hunderassen. Ein Handbuch für Hundeliebhaber und Züchter*. Potsdam: Akademische Verlagsgesellschaft Athenaion M.B.H.

Wagner F (2014): *Taxonomy within the genus Otocyon Müller, 1836 (Carnivora: Canidae) based on craniometric and craniological characters and zoogeographic data*. Master's thesis, Philipps-Universität Marburg, Marburg.

Wagner F, Ruf I (2019): Who nose the borzoi? Turbinal skeleton in a dolichocephalic dog breed (*Canis lupus familiaris*). *Mamm. Biol.* 94: 106-119.

Wang X, Tedford R (2008): *Dogs. Their fossil relatives and evolutionary history*. New York: Columbia University Press.

Wang GD, Zhai W, Yang HC, Wang L, Zhong L, Liu YH, Fan RX, Yin TT, Zhu CL, Poyarkov AD, Irwin DM, Hytonen MK, Lohi H, Wu CI, Savolainen P, Zhang YP (2016): Out of southern East Asia: the natural history of domestic dogs across the world. *Cell research* 26: 21-33.

Westheide W, Rieger R (2010): Wirbel- oder Schädeltiere. In Westheide W, Rieger R [eds.]: *Spezielle Zoologie* 2. Heidelberg: Springer.

Wiedemann C (1799): *Harwood's System der vergleichenden Anatomie und Physiologie*. Berlin: G. C. Nauksche Buchhandlung.

Wilson D, Reeder D (2005): *Mammal Species of the World. A Taxonomic and Geographic Reference*. Johns Hopkins University Press.

Wilsson E, Sundgren P-E (1997): The use of a behaviour test for the selection of dogs for service and breeding, I: Method of testing and evaluating test results in the adult dog, demands on different kinds of service dogs, sex and breed differences. *Appl. Anim. Behav. Sci.* 53: 279-295.

Wroe S, Parr WCH, Ledogar JA, Bourke J, Evans SP, Fiorenza L, Benazzi S, Hublin JJ, Stringer C, Kullmer O, Curry M, Rae TC, Yokley TR (2018): Computer simulations show that Neanderthal facial morphology represents adaptation to cold and high energy demands, but not heavy biting. *P. Roy. Soc. B-Biol. Sci.* 285: 20180085.

Yang M, Geng GJ, Zhang W, Cui L, Zhang HX, Zheng JL (2016): SNP genotypes of olfactory receptor genes associated with olfactory ability in German Shepherd dogs. *Anim. Genet.* 47: 240-244.

Yoel U, Gopas J, Ozer J, Peleg R, Shvartzman P (2015): Canine Scent Detection of Volatile Elements, Characteristic of Malignant Cells, in Cell Cultures. *Isr. Med. Assoc. J.* 17: 567-570.

Young A, Bannasch D (2006): Morphological Variation in the Dog. In Ostrander E, Giger U, Lindblad-Toh K [eds.]: *The Dog and its Genome*: 47-65. New York: Cold Springer Harbor Laboratory Press.

Zeller U (1983): *Zur Ontogenese und Morphologie des Craniums von Tupaia belangeri (Tupaiidae, Scandentia, Mammalia)*. Dissertation, Georg-August-Universität zu Göttingen, Göttingen.

Zeller U (1987): Morphogenesis of the mammalian skull with special reference to *Tupaia*. In Kuhn H-J, Zeller U [eds.]: *Morphogenesis of the Mammalian skull (Mammalia depicta 13)*: 17-50. Hamburg: Parey.

Zeller U (1989): Die Entwicklung und Morphologie des Schädels von *Ornithorhynchus anatinus* (Mammalia: Protheria: Monotremata). *Abh. Senckenberg. Naturforsch. Ges.* 545: 1-188.

Zhang H-H, Wei Q-G, Zhang H-X, Chen L (2011): Comparison of the fraction of olfactory receptor pseudogenes in wolf (*Canis lupus*) with domestic dog (*Canis familiaris*). *J. Forestry Res.* 22: 275-280.

ZKR - Züchterkreis für den Retromops, *https://www.retromops.org*; last access: 2019/09/30.

Zuckerkandl E (1887): *Das periphere Geruchsorgan der Säugethiere. Eine vergleichend antatomische Studie*. Stuttgart: Enke.

PICTURE CREDITS

Fig. 1a PARKER *et al*. (2017), *Cell Rep*. 19: 697-708, Figure 1, modified.

Fig. 1b PARKER *et al*. (2017), *Cell Rep*. 19: 697-708, Figure 4, modified.

Fig. 2b German shepherd
https://s3.amazonaws.com/cdn-origin-etr.akc.org/wp-content/uploads/2017/11/12213218/German-Shepherd-on-White-00.jpg; modified, last access 2019/09/16.

German shepherd, head
https://s3.amazonaws.com/cdn-origin-etr.akc.org/wp-content/uploads/2017/11/12233022/German-Shepherd-Dog-On-White-08.jpg; modified, last access 2019/09/16.

Fig. 2c Groenendael
https://s3.amazonaws.com/cdn-origin-etr.akc.org/wp-content/uploads/2017/11/13000641/Belgian-Sheepdog-On-White-01.jpg; modified, last access 2019/09/16.

Groenendael, head
https://s3.amazonaws.com/cdn-origin-etr.akc.org/wp-content/uploads/2017/11/13000638/Belgian-Sheepdog-On-White-02.jpg; modified, last access 2019/09/16.

Fig. 2d Greenland dog
https://www.skk.se/en/NKU-home/nordic-dog-breeds/denmark/greenland-dog/; modified, last access 2019/09/16.

Fig. 2e *The Cavalier's Pets* (by Sir E. H. Landseer, 1845)
https://artuk.org/discover/artworks/king-charles-spaniels-the-cavaliers-pets-199742/search/actor:landseer-edwin-henry-18021873/page/6; modified, last access 2019/09/16.

Fig. 2f King spaniel (ancient type, head)
BECKMANN (1895): *Geschichte und Beschreibung der Rassen des Hundes* II. Brauschweig: Druck und Verlag von Friedrich Bieweg und Sohn; Tafel 79, modified.

Fig. 2g King spaniel
https://s3.amazonaws.com/cdn-origin-etr.akc.org/wp-content/uploads/2017/11/12233456/English-Toy-Spaniel-On-White-03.jpg; modified, last access 2019/09/16.

King spaniel, head
https://s3.amazonaws.com/cdn-origin-etr.akc.org/wp-content/uploads/2017/11/12233500/English-Toy-Spaniel-On-White-02.jpg; modified, last access 2019/09/16.

Fig. 2h Cavalier, head
COILE (2015): *Encyclopedia of Dog Breeds*. New York: Barron's Educational Series, Inc; p. 251, modified.

Fig. 2j Pekingese
ASH (1927b): *Dogs: their History and Development* II. London: Ernest Benn Limited; Plate 138, modified.

Fig. 2k Pekingese (modern type)
https://s3.amazonaws.com/cdn-origin-etr.akc.org/wp-content/uploads/2017/11/12225945/Pekingese-On-White-01.jpg; modified, last access 2019/09/16.

Pekingese, head
https://s3.amazonaws.com/cdn-origin-etr.akc.org/wp-content/uploads/2017/11/12225941/Pekingese-On-White-02.jpg; modified, last access 2019/09/16.

Fig. 2m Chin
https://s3.amazonaws.com/cdn-origin-etr.akc.org/wp-content/uploads/2017/11/12210831/Japanese-Chin-on-White-02.jpg.jpg; modified, last access 2019/09/16.

Fig. 2n Chin, head
VOM HAGEN (1935): *Die Hunderassen. Ein Handbuch für Hundeliebhaber und Züchter*. Potsdam: Akademische Verlagsgesellschaft Athenaion M.B.H.; p. 61, Fig. 240, modified.

Fig. 2p Pug, ancient type
BECKMANN (1895): *Geschichte und Beschreibung der Rassen des Hundes* II. Brauschweig: Druck und Verlag von Friedrich Bieweg und Sohn; Tafel 78, modified.

Fig. 2q Pug, modern type
https://s3.amazonaws.com/cdn-origin-etr.akc.org/wp-content/uploads/2017/11/12225358/Pug-On-White-01.jpg; modified, last access 2019/09/16.

Pug, modern type, head
https://s3.amazonaws.com/cdn-origin-etr.akc.org/wp-content/uploads/2017/11/12225356/Pug-On-White-02.jpg; modified, last access 2019/09/16.

Fig. 2r Pug, retro type, head
https://image.jimcdn.com/app/cms/image/transf/dimension=455x10000:format=jpg/path/s0ec3240e4131113e/image/i365aedd30ef35ca9/version/1488997754/image.jpg; modified, last access 2019/09/16.

Fig. 2s Saluki
https://s3.amazonaws.com/cdn-origin-etr.akc.org/wp-content/uploads/2017/11/14185322/AKC-121716-139.jpg; modified, last access 2019/09/16.

Saluki, head
https://s3.amazonaws.com/cdn-origin-etr.akc.org/wp-content/uploads/2017/11/08144047/Saluki.profile.jpg; modified, last access 2019/09/16.

Fig. 2t Bowl from late Susa
HOLE & WYLLIE (2007): *Paléorient* 33: 175-185; Fig. 2.4, modified.

Fig. 2u Borzoi
https://s3.amazonaws.com/cdn-origin-etr.akc.org/wp-content/uploads/2017/11/01132030/Borzoi-On-White-031.jpg; modified, last access 2019/09/16.

Borzoi, head
https://s3.amazonaws.com/cdn-origin-etr.akc.org/wp-content/uploads/2017/11/12235843/Borzoi-On-White-02.jpg; modified, last access 2019/09/16.

Fig. 2w Whippet
https://s3.amazonaws.com/cdn-origin-etr.akc.org/wp-content/uploads/2017/11/12223025/Whippet-On-White-01.jpg; modified, last access 2019/09/16.

APPENDIX: TABLES

Table 1: List of investigated specimens of *Canis lupus lupus* and *Canis lupus familiaris*. The breeds are grouped based on the Fédération Cynologique Internationale (FCI). For the morphometric analyses the specimens are grouped into the three snout length types (ELLENBERGER & BAUM 1891). Furthermore, the scan parameters (resolution = isotropic voxel size) and the side (L, left; R, right) that has been segmented in AMIRA 5.4.0 are given. For information about the µCT devices (DEG = Deggendorf, BN = Bonn, F = Frankfurt am Main) see ch. 2.2 µCT scanning and virtual 3D modeling: 28. Abbreviations: 1.

Inventory number	Breed	Age	Sex	Year of inventory	IFB[type]	IBL[type]
Eurasian wolf (*Canis lupus lupus*); outgroup						
ZMB_MAM 815	EW	adult	f	NA	0.70 [DOL]	0.53 [DOL]
ZMB_MAM 93307	EW	adult	NA	1910	0.58 [MES]	0.50 [DOL]
ZMB_MAM 93308	EW	adult	f	1914	0.63 [DOL]	0.56 [DOL]
I: Sheepdogs and Cattledogs						
48.1	GSD	juvenile	NA	NA	0.42 [MES]	0.60 [DOL]
MNHN 1985-1274	GSD	adult	f	≤1985	0.60 [DOL]	0.52 [DOL]
SMF 93607	GSD	adult	m	1904	0.66 [DOL]	0.53 [DOL]
MNHN 1985-1216	GD	adult	m	≤1985	0.61 [DOL]	0.52 [DOL]
V: Spitz and primitive types						
MNHN 1947-78	GLD	adult	m	≤1947	0.59 [MES]	0.55 [DOL]
IX: Companion and toy dogs						
NMBE 1051945	KCS	adult	m	1959	0.21 [BRA]	0.90 [BRA]
NMBE 1051948	KCS	adult	f	1979	0.19 [BRA]	0.89 [BRA]
NMBE 1059207	KCSC	adult	f	2006	0.53 [MES]	0.70 [MES]
NMBE 1062998	KCSC	adult	m	2010	0.35 [BRA]	0.76 [MES]
NMBE 1051962	PEK	adult	m	1962	0.20 [BRA]	0.93 [BRA]
NMBE 1051965	PEK	adult	m	1976	0.15 [BRA]	1.09 [BRA]
SMF 35611	PEK	adult	NA	NA	0.21 [BRA]	0.84 [BRA]

Table 1 (continued)

CT device	Resolution (mm)	Current (µA)	Voltage (kV)	Timing (ms)	Side	Notes	Breed	Inventory number
							Eurasian wolf (*Canis lupus lupus*); outgroup	
DEG	0.089757	300	180	285	-	Origin: Lapland	EW	ZMB_MAM 815
DEG	0.089757	300	180	285	R	Origin: Romania	EW	ZMB_MAM 93307
BN	0.147545	150	110	667	-	Origin: Bosnia and Herzegovina	EW	ZMB_MAM 93308
							I: Sheepdogs and Cattledogs	
F	0.029596	40	100	1500	L, R	Six weeks old; Pers. Coll. W. Maier	GSD	48.1
BN	0.141289	170	190	667	R		GSD	MNHN 1985-1274
BN	0.149425	130	150	667	R		GSD	SMF 93607
BN	0.150301	170	190	1000	-		GD	MNHN 1985-1216
							V: Spitz and primitive types	
BN	0.141705	160	170	667	-		GLD	MNHN 1947-78
							IX: Companion and toy dogs	
BN	0.053870	120	120	667	L	Age: 1 year	KCS	NMBE 1051945
BN	0.062318	120	120	667	-		KCS	NMBE 1051948
BN	0.073043	120	120	667	-	Age: 12.3 years	KCSC	NMBE 1059207
BN	0.074643	130	130	667	L, R	Age: 11.6 years	KCSC	NMBE 1062998
BN	0.061444	170	190	667	R		PEK	NMBE 1051962
BN	0.048005	130	130	667	-		PEK	NMBE 1051965
F	0.023750	60	90	1500	L, R		PEK	SMF 35611

Table 1 (continued)

Inventory number	Breed	Age	Sex	Year of inventory	IFB[type]	IBL[type]
IX: Companion and toy dogs (continued)						
NMBE 1051951	JAP	adult	NA	NA	0.25 [BRA]	0.83 [MES]
ZMB_MAM 7436	JAP	adult	m	>1883	0.20 [BRA]	0.85 [BRA]
MNHN 2007-428	PUG	juvenile	NA	≤2007	NA	0.78 [MES]
MNHN 1881-47	PUG	juvenile	NA	≤1881	0.30 [BRA]	0.70 [MES]
NMBE 1051937	PUG	adult	m	1992	0.27 [BRA]	0.83 [MES]
NMBE 1052345	PUG	adult	m	1998	0.26 [BRA]	0.88 [BRA]
SMF 16284	PUG	adult	NA	1904	NA	NA
[MfN] 1845	PUG	adult	NA	<1883	0.32 [BRA]	0.74 [MES]
[MfN] 2620	PUG	adult	NA	<1883	0.34 [BRA]	0.75 [MES]
[MfN] 2630	PUG	adult	f	<1883	0.30 [BRA]	0.75 [MES]
[MfN] 2657	PUG	adult	f	<1883	0.46 [MES]	0.69 [MES]
ZMB_MAM 30980	PUG	adult	NA	>1883	0.48 [MES]	0.75 [MES]
X: Sighthounds						
[MfN] 2709	SAL	adult	m	<1883	0.65 [DOL]	0.53 [DOL]
SMF 16303	BOR	juvenile	NA	1908	0.64 [DOL]	0.44 [DOL]
NMBE 1051164	BOR	adult	m	1976	0.70 [DOL]	0.39 [DOL]
NMBE 1051166	BOR	adult	f	1980	0.72 [DOL]	0.40 [DOL]
NMBE 1051180	BOR	adult	f	1992	0.68 [DOL]	0.38 [DOL]
NMBE 1052706	BOR	adult	f	1991	0.71 [DOL]	0.42 [DOL]
[MfN] 1403	BOR	adult	m	1870	0.75 [DOL]	0.44 [DOL]
[MfN] 7374	BOR	adult	m	>1883	0.68 [DOL]	0.39 [DOL]

Table 1 (continued)

CT device	Resolution (mm)	Current (µA)	Voltage (kV)	Timing (ms)	Side	Notes	Breed	Inventory number
							IX: Companion and toy dogs (continued)	
BN	0.054133	170	190	667	L		JAP	NMBE 1051951
BN	0.060168	130	130	667	-		JAP	ZMB_MAM 7436
BN	0.044896	160	170	667	-	Skull deformed, rudimentary nasal cavity	PUG	MNHN 2007-428
BN	0.054176	160	170	500	L		PUG	MNHN 1881-47
BN	0.054969	170	190	667	R		PUG	NMBE 1051937
BN	0.056488	170	190	667	L, R		PUG	NMBE 1052345
F	0.027692	100	110	750	R	Cranium sawn through frontal sinus	PUG	SMF 16284
BN	0.069422	130	140	667	R		PUG	[MfN] 1845
F	0.030000	100	110	1000	L		PUG	[MfN] 2620
F	0.027049	100	120	750	L, R		PUG	[MfN] 2630
BN	0.086096	120	120	667	R		PUG	[MfN] 2657
BN	0.086245	180	200	500	R		PUG	ZMB_MAM 30980
								X: Sighthounds
BN	0.124329	130	150	667	-	"Syrischer Windhund; Libanon"	SAL	[MfN] 2709
BN	0.118445	180	200	500	L		BOR	SMF 16303
BN	0.202628	180	200	500	L, R		BOR	NMBE 1051164
BN	0.188933	180	200	500	-		BOR	NMBE 1051166
BN	0.193641	180	200	500	-		BOR	NMBE 1051180
BN	0.184468	180	200	500	-		BOR	NMBE 1052706
BN	0.180031	180	200	500	L		BOR	[MfN] 1403
DEG	0.060801	300	220	2000	-		BOR	[MfN] 7374

Table 2: Definitions of the characters for the linear measurements on the skulls of *Canis lupus lupus* and *Canis lupus familiaris*. The measurements are illustrated in Fig. 3.

Abbr.	Name	Definition
CBL	Condylobasal length	Length from prosthion to condylion [M]
GLS	Greatest length of skull	Greatest distance between prosthion and opisthocranion [E&B,M]
BLI	Basal length I	Length from prosthion to basion [M]
BLII	Basal length II	Length from inside incisor alveolus to basion [M]
NLI	Nasal length I	The greatest length of nasal bones measured straight line [M]
NLII	Nasal length II	From the rostral (= Incisura nasalis) to the caudal end of the nasal suture [E&B]
SL	Snout length	From prosthion to the caudal end of the nasals [B]
LBC	Length of braincase	From the caudal tip of the nasals to opisthocranion [E&B]
LPI	Length of palate I	From inside incisor alveolus to the caudal end of the palatine suture [W]
LPII	Length of palate II	From the rostral end of the incisive foramina to the caudal end of the palatine suture
LIF	Length of incisive foramina	Greatest length on both sides [N&K]
BZB	Bizygomatic breadth	Greatest breadth of zygomatics [E&B,M]
RB	Rostral breadth	The greatest breadth across maxillae above canines [M]
NB	Nasal width	Greatest breadth on the inner edges of the nose [R]
BIF	Breadth of incisive foramina	Greatest width on both sides [R]
IOB	Interorbital breadth	The smallest distance between inner edges of orbits [M]
POC	Postorbital constriction	Greatest breadth of the postorbital processes [W]
BC	Breadth of choanae	Greatest distance between the processes of the palatine [R]
SH	Occipital height	Distance from basion to the tip of occiput [M]
NHI	Nasal height I	From prosthion to the rostral end of the internasal suture [R]
NHII	Nasal height II	Between the rostral edges of the incisive foramina to the rostral end of the internasal suture [R]
HC	Height of choanae	From basilar to the caudal end of the palatine suture [R]

References: B = BREHM *et al.* (1985); E&B = ELLENBERGER & BAUM (1891); N&K = NIETHAMMER & KRAPP (1978); M = MAZÁK (2010); R = PD Dr. I. Ruf (unpublished); W = WAGNER (2014)

Table 3: Histological serial sections of the perinatal whippet stages in coronal view. The material is housed at the Centrum für Naturkunde, Universität Hamburg, Germany. About the neonate whippet no information was available (NA).

Specimen	Age	Year	CRL (mm)	Slice thickness (µm)	Fixation	Coloration	Enbedding	Notes
'Whippet A'	prenatal	≤1966	17.5	25	Stieve	AZAN	Celloidin	SCHLIEMANN (1966)
'Whippet B'	prenatal	≤1966	39.0	25	Stieve	AZAN	Celloidin	SCHLIEMANN (1966)
'Whippet C'	prenatal	≤1966	59.0	25	Stieve	AZAN	Celloidin	SCHLIEMANN (1966)
'Whippet neonatus / I'	neonate	NA	NA	NA	NA	NA	Celloidin	SCHLIEMANN (year unknown, probably 1987)

Table 4: Index turbinal surface area (IAT) and index exterior surface area (IAE) in the turbinal skeleton of the specimens of *Canis lupus lupus* and *Canis lupus familiaris* that have been reconstructed in AMIRA 5.4.0. In two specimens both sides (L, left; R, right) have been reconstructed. Cells with '-' refer to absent turbinals. Abbreviations: 1. The raw data of turbinal surface area (AT) and exterior surface area (AE) which have been measured in AMIRA 5.4.0 is given in Table eS2 (electronic Supplementary material).

	PUG (juvenile) MNHN 1881-47		**BOR** (juvenile) SMF 16303		**EW** ZMB_MAM 93307		**GSD** MNHN 1985-1274		**GSD** SMF93607	
	IAT	IAE	IAT	IAE	IAT	IAE	IAT	IAE	IAT	IAE
mt	0.343	0.191	2.135	0.642	3.672	0.917	2.341	0.583	2.895	0.692
nt	0.021	0.021	0.125	0.121	0.128	0.124	0.085	0.084	0.117	0.111
ls	0.196	0.154	0.809	0.517	0.700	0.556	0.542	0.415	0.615	0.412
it	-	-	-	-	0.004	0.004	-	-	0.007	0.007
itδ	-	-	0.035	0.033	0.086	0.063	0.098	0.075	0.161	0.114
it	-	-	-	-	-	-	-	-	-	-
ft1	0.160	0.108	0.684	0.346	1.059	0.434	1.061	0.540	0.945	0.454
itγ	-	-	0.104	0.101	0.072	0.066	0.259	0.245	0.058	0.057
ft2	0.169	0.128	0.715	0.349	1.296	0.552	1.081	0.499	1.169	0.513
it	-	-	0.013	0.013	-	-	-	-	-	-
ft3	0.096	0.076	0.340	0.179	0.860	0.311	0.570	0.291	0.669	0.262
it	-	-	-	-	-	-	0.011	0.011	0.020	0.019
itβ	0.061	0.051	0.145	0.095	0.503	0.210	0.366	0.177	0.390	0.187
it	-	-	0.179	0.129	-	-	-	-	-	-
etI	0.483	0.270	1.625	0.692	2.847	1.088	1.576	0.649	1.588	0.630
itα	0.126	0.099	0.328	0.191	0.684	0.383	0.329	0.222	0.455	0.268
it	-	-	-	-	-	-	-	-	-	-
it	-	-	0.034	0.031	0.051	0.051	0.053	0.047	0.021	0.021
etII	0.242	0.184	0.981	0.428	1.693	0.647	0.832	0.415	1.122	0.507
etIII	0.135	0.088	0.620	0.320	0.931	0.480	0.544	0.295	0.642	0.323
Total	2.033	1.052	8.872	2.529	14.586	3.061	9.748	2.504	10.874	2.623

Table 4 (continued)

	KCS NMBE 1051945		**KCSC** NMBE 1062998, R		**KCSC** NMBE 1062998, L		**PEK** NMBE 1051962		**JAP** NMBE 1051951	
	IAT	IAE	IAT	IAE	IAT	IAE	IAT	IAE	IAT	IAE
mt	0.186	0.154	1.366	0.554	0.931	0.461	0.305	0.294	0.382	0.227
nt	0.003	0.003	0.055	0.055	0.041	0.041	0.008	0.008	0.019	0.016
ls	0.240	0.276	0.454	0.360	0.403	0.349	0.328	0.292	0.283	0.271
it	-	-	-	-	-	-	-	-	-	-
itδ	0.016	0.016	0.061	0.054	0.049	0.045	0.027	0.027	0.064	0.055
it	-	-	-	-	-	-	-	-	-	-
ft1	0.335	0.279	0.544	0.294	0.561	0.292	0.238	0.168	0.227	0.158
itγ	-	-	0.078	0.078	-	-	-	-	0.020	0.014
ft2	0.303	0.232	0.594	0.334	0.669	0.350	0.381	0.221	0.250	0.145
it	-	-	-	-	-	-	-	-	-	-
ft3	0.226	0.156	0.248	0.132	0.328	0.167	0.177	0.109	0.151	0.103
it	-	-	-	-	-	-	-	-	-	-
itβ	0.046	0.043	0.170	0.099	0.171	0.111	0.092	0.061	0.069	0.051
it	0.048	0.047	0.106	0.068	-	-	-	0.000	-	-
etI	0.481	0.253	0.992	0.614	0.851	0.416	0.310	0.215	0.341	0.227
itα	0.124	0.108	0.245	0.154	0.258	0.158	0.122	0.083	0.086	0.060
it	-	-	0.004	0.004	-	-	-	-	-	-
it	-	-	-	-	0.004	0.004	-	-	0.005	0.005
etII	0.234	0.145	0.498	0.280	0.504	0.268	0.263	0.162	0.192	0.147
etIII	0.093	0.060	0.287	0.165	0.293	0.158	0.147	0.102	0.121	0.092
Total	2.335	1.288	5.700	2.063	5.064	1.889	2.398	1.289	2.210	1.063

Table 4 (continued)

	PUG NMBE 1051937		**PUG** NMBE 1052345, R		**PUG** NMBE 1052345, L		**PUG** [MfN] 1845		**PUG** [MfN] 2620	
	IAT	IAE	IAT	IAE	IAT	IAE	IAT	IAE	IAT	IAE
mt	0.525	0.327	0.319	0.197	0.202	0.134	0.614	0.309	0.785	0.403
nt	0.010	0.010	0.031	0.031	0.010	0.010	0.046	0.046	0.057	0.057
ls	0.317	0.264	0.174	0.192	0.167	0.199	0.297	0.274	0.372	0.294
it	-	-	-	-	-	-	-	-	-	-
itδ	0.015	0.015	0.042	0.042	0.033	0.033	0.050	0.048	0.034	0.032
it	-	-	-	-	-	-	-	-	-	-
ft1	0.188	0.116	0.184	0.142	0.163	0.119	0.306	0.165	0.267	0.164
itγ	-	-	-	-	-	-	-	-	0.005	0.005
ft2	0.283	0.153	0.210	0.124	0.179	0.123	0.305	0.164	0.308	0.178
it	-	-	-	-	-	-	-	-	-	-
ft3	0.181	0.115	0.119	0.077	0.110	0.076	0.245	0.146	0.226	0.130
it	-	-	-	-	-	-	-	-	-	-
itβ	0.123	0.075	0.068	0.047	0.060	0.044	0.133	0.095	0.090	0.069
it	-	-	-	-	-	-	-	-	0.014	0.012
etI	0.724	0.501	0.435	0.280	0.296	0.211	0.639	0.334	0.642	0.337
itα	0.174	0.098	0.099	0.073	0.071	0.057	0.165	0.108	0.119	0.085
it	-	-	-	-	-	-	-	-	-	-
it	-	-	-	-	-	-	-	-	-	-
etII	0.306	0.196	0.227	0.177	0.129	0.121	0.416	0.237	0.423	0.260
etIII	0.106	0.070	0.110	0.086	0.065	0.064	0.188	0.115	0.226	0.135
Total	2.954	1.555	2.017	1.149	1.485	1.040	3.405	1.300	3.568	1.553

Table 4 (continued)

	PUG [MfN] 2657		**PUG** ZMB_MAM 30980		**BOR** NMBE 1051164		**BOR** [MfN] 1403	
	IAT	IAE	IAT	IAE	IAT	IAE	IAT	IAE
mt	0.453	0.284	1.367	0.532	3.725	0.829	2.440	0.691
nt	0.084	0.084	0.082	0.082	0.140	0.136	0.130	0.129
ls	0.389	0.316	0.439	0.308	0.981	0.516	0.870	0.523
it	-	-	-	-	0.029	0.028	-	-
itδ	0.028	0.026	0.033	0.032	0.249	0.129	0.163	0.127
it	-	-	-	-	0.010	0.010	-	-
ft1	0.386	0.207	0.536	0.273	1.822	0.792	1.087	0.512
itγ	-	-	0.054	0.054	0.086	0.086	0.077	0.077
ft2	0.609	0.332	0.645	0.355	1.475	0.598	1.169	0.548
it	-	-	-	-	-	-	-	-
ft3	0.380	0.196	0.399	0.217	0.685	0.265	0.598	0.241
it	0.008	0.007	-	-	-	-	-	-
itβ	0.185	0.114	0.251	0.162	0.391	0.161	0.292	0.148
it	-	-	-	-	-	-	0.045	0.037
etI	0.792	0.405	1.041	0.514	2.187	0.755	2.013	0.814
itα	0.200	0.131	0.295	0.187	0.474	0.269	0.426	0.237
it	-	-	-	-	-	-	-	-
it	0.024	0.021	-	-	0.071	0.052	-	-
etII	0.438	0.258	0.711	0.391	1.061	0.495	1.013	0.497
etIII	0.232	0.144	0.431	0.251	0.737	0.338	0.588	0.264
Total	4.207	1.617	6.285	2.190	14.124	2.848	10.910	2.773

Table 5: Distribution and total number of the turbinals (lamina semicircularis excluded) on each side (L, left; R, right) of the nasal cavity in the specimens of *Canis lupus familiaris* and *Canis lupus lupus* under study. The cells indicate the presence and number (1, 2, 3) or the absence (-) of the respective turbinal. Abbreviations: 1.

Specimen	Breed	Side	mt	nt	ls	it	itδ	it	ft1	itγ	it	ft2
Perinatal and juvenile stages												
'whippet A'	WH	L	-	-	-	-	-	-	-	-	-	-
		R	-	-	-	-	-	-	-	-	-	-
'whippet B'	WH	L	1	1	1	-	-	-	1	-	-	1
		R	1	1	1	-	-	-	1	-	-	1
'whippet C'	WH	L	1	1	1	-	-	-	1	-	-	1
		R	1	1	1	-	-	-	1	-	-	1
'neonate whippet'	WH	L	1	1	1	-	1	-	1	1	-	1
		R	1	1	1	-	1	-	1	1	-	1
48.1	GSD	L	1	1	1	-	-	-	1	1	-	1
		R	1	1	1	-	-	-	1	1	-	1
MNHN 1881-47	PUG	L	1	1	1	-	1	-	1	-	-	1
		R	1	1	1	-	1	-	1	-	-	1
SMF 16303	BOR	L	1	1	1	-	1	-	1	1	-	1
		R	1	1	1	-	1	-	1	1	-	1
MNHN 2007-428	PUG	L	-	-	-	-	-	-	-	-	-	-
		R	-	-	-	-	-	-	-	-	-	-
Eurasian wolf (*Canis lupus lupus*)												
ZMB_MAM 815	EW	L	1	1	1	3	1	-	1	1	-	1
		R	1	1	1	-	1	-	1	1	-	1
ZMB_MAM 93307	EW	L	1	1	1	1	1	-	1	1	-	1
		R	1	1	1	1	1	-	1	1	-	1
ZMB_MAM 93308	EW	L	1	1	1	1	1	-	1	1	-	1
		R	1	1	1	-	1	-	1	1	-	1
I: Sheepdogs and Cattledogs												
MNHN 1985-1274	GSD	L	1	1	1	-	1	-	1	1	-	1
		R	1	1	1	-	1	-	1	1	-	1
SMF 93607	GSD	L	1	1	1	-	1	-	1	1	-	1
		R	1	1	1	-	1	-	1	1	-	1
MNHN 1985-1216	GD	L	1	1	1	-	1	-	1	-	-	1
		R	1	1	1	-	1	-	1	-	-	1

Table 5 (continued)

it	ft3	it	itβ	it	etI	itα	it	etII	etIII	Total	Side	Breed	Specimen
													Perinatal and juvenile stages
-	-	-	-	-	-	-	-	-	-	**0**	L	WH	'whippet A'
-	-	-	-	-	-	-	-	-	-	**0**	R		
-	1	-	-	-	1	1	-	1	1	**9**	L	WH	'whippet B'
-	1	-	-	-	1	1	-	1	1	**9**	R		
-	1	-	1	-	1	1	1	1	1	**11**	L	WH	'whippet C'
-	1	-	1	-	1	1	1	1	1	**11**	R		
-	1	-	1	-	1	1	1	1	1	**13**	L	WH	'neonate whippet'
-	1	-	1	-	1	1	1	1	1	**13**	R		
-	1	-	1	-	1	1	-	1	1	**11**	L	GSD	48.1
-	1	-	1	-	1	1	-	1	1	**11**	R		
-	1	-	1	-	1	1	-	1	1	**11**	L	PUG	MNHN 1881-47
-	1	-	1	-	1	1	-	1	1	**11**	R		
1	1	-	1	1	1	1	1	1	1	**15**	L	BOR	SMF 16303
-	1	-	1	1	1	1	1	1	1	**14**	R		
-	-	-	-	-	-	-	-	-	-	**0**	L	PUG	MNHN 2007-428
-	-	-	-	-	-	-	-	-	-	**0**	R		
													Eurasian wolf (*Canis lupus lupus*)
-	1	-	1	1	1	1	1	1	1	**17**	L	EW	ZMB_MAM 815
-	1	-	1	1	1	1	1	1	1	**14**	R		
-	1	-	1	-	1	1	1	1	1	**14**	L	EW	ZMB_MAM 93307
-	1	-	1	-	1	1	1	1	1	**14**	R		
-	1	-	1	-	1	1	1	1	1	**14**	L	EW	ZMB_MAM 93308
-	1	-	1	-	1	1	1	1	1	**13**	R		
													I: Sheepdogs and Cattledogs
1	1	1	1	-	1	1	1	1	1	**15**	L	GSD	MNHN 1985-1274
-	1	1	1	-	1	1	1	1	1	**14**	R		
1	1	1	1	-	1	1	1	1	1	**15**	L	GSD	SMF 93607
-	1	1	1	-	1	1	1	1	1	**14**	R		
-	1	-	1	-	1	1	-	1	1	**11**	L	GD	MNHN 1985-1216
-	1	-	1	-	1	1	-	1	1	**11**	R		

Table 5 (continued)

Specimen	Breed	Side	mt	nt	ls	it	itδ	it	ft1	itγ	it	ft2
V: Spitz and primitive types												
MNHN 1947-78	GLD	L	1	1	1	1	1	-	1	1	-	1
		R	1	1	1	1	1	-	1	1	-	1
IX: Companion and toy dogs												
NMBE 1051945	KCS	L	1	1	1	-	1	-	1	-	-	1
		R	1	1	1	-	1	-	1	-	-	1
NMBE 1051948	KCS	L	1	1	1	-	1	-	1	1	-	1
		R	1	1	1	-	1	-	1	1	-	1
NMBE 1059207	KCSC	L	1	1	1	-	1	-	1	1	-	1
		R	1	1	1	-	1	-	1	1	-	1
NMBE 1062998	KCSC	L	1	1	1	-	1	-	1	1	-	1
		R	1	1	1	-	1	-	1	1	-	1
NMBE 1051962	PEK	L	1	1	1	-	1	-	1	-	-	1
		R	1	1	1	-	1	-	1	-	-	1
NMBE 1051965	PEK	L	1		1	-	1	-	1	-	-	1
		R	1		1	-	1	-	1	-	-	1
SMF 35611	PEK	L	1		1	-	1	-	1	1	-	1
		R	1	1	1	-	1	-	1	1	-	1
NMBE 1051951	JAP	L	1	1	1	-	1	-	1	1	-	1
		R	1	1	1	-	1	-	1	1	-	1
ZMB_MAM 7436	JAP	L	1	1	1	-	1	-	1	1	-	1
		R	1	1	1	-	1	-	1	1	-	1
NMBE 1051937	PUG	L	1	1	1	-	1	-	1	-	-	1
		R	1	1	1	-	1	-	1	-	-	1
NMBE 1052345	PUG	L	1	1	1	-	1	-	1	-	-	1
		R	1	1	1	-	1	-	1	-	-	1
SMF 16284	PUG	L	1	1	1	NA	NA	NA	1	NA	NA	1
		R	1	1	1	NA	1	NA	1	NA	NA	1

Table 5 (continued)

it	ft3	it	itβ	it	etI	itα	it	etII	etIII	Total	Side	Breed	Specimen
													V: Spitz and primitive types
1	1	1	1	1	1	1	1	1	1	**17**	L	GLD	MNHN 1947-78
1	1	1	1	1	1	1	1	1	1	**17**	R		
													IX: Companion and toy dogs
-	1	-	1	1	1	1	1	1	1	**13**	L	KCS	NMBE 1051945
-	1	-	1	NA	1	1	-	1	1	**11**	R		
1	1	-	1	-	1	1	-	1	1	**13**	L	KCS	NMBE 1051948
1	1	-	1	-	1	1	1	1	1	**14**	R		
2	1	-	1	-	1	1	1	1	1	**15**	L	KCSC	NMBE 1059207
1	1	-	1	1	1	1	1	1	1	**15**	R		
-	1	-	1	-	1	1	1	1	1	**13**	L	KCSC	NMBE 1062998
-	1	-	1	1	1	1	1	1	1	**14**	R		
-	1	-	1	-	1	1	-	1	1	**11**	L	PEK	NMBE 1051962
-	1	-	1	-	1	1	-	1	1	**11**	R		
-	1	-	1	-	1	1	-	1	1	**10**	L	PEK	NMBE 1051965
-	1	-	1	-	1	1	-	1	1	**10**	R		
-	1	-	1	-	1	1	1	1	1	**12**	L	PEK	SMF 35611
-	1	-	1	-	1	1	1	1	1	**13**	R		
-	1	-	1	-	1	1	1	1	1	**13**	L	JAP	NMBE 1051951
-	1	-	1	-	1	1	1	1	1	**13**	R		
-	1	-	1	-	1	1	-	1	1	**12**	L	JAP	ZMB_MAM 7436
-	1	-	1	-	1	1	1	1	1	**13**	R		
-	1	-	1	-	1	1	-	1	1	**11**	L	PUG	NMBE 1051937
-	1	-	1	-	1	1	-	1	1	**11**	R		
-	1	-	1	-	1	1	-	1	1	**11**	L	PUG	NMBE 1052345
-	1	-	1	-	1	1	-	1	1	**11**	R		
-	1	-	1	-	1	1	-	1	1	**10**	L	PUG	SMF 16284
-	1	-	1	-	1	1	-	1	1	**11**	R		

Table 5 (continued)

Specimen	Breed	Side	mt	nt	ls	it	itδ	it	ft1	itγ	it	ft2
IX: Companion and toy dogs (continued)												
[MfN] 1845	PUG	L	1	1	1	-	1	-	1	-	-	1
		R	1	1	1	-	1	-	1	-	-	1
[MfN] 2620	PUG	L	1	1	1	-	1	-	1	1	-	1
		R	1	1	1	-	1	-	1	1	-	1
[MfN] 2630	PUG	L	1	1	1	-	1	-	1	-	-	1
		R	1	1	1	-	1	-	1	-	-	1
[MfN] 2657	PUG	L	1	1	1	-	1	-	1	-	-	1
		R	1	1	1	-	1	-	1	-	-	1
ZMB_MAM 30980	PUG	L	1	1	1	-	1	-	1	1	-	1
		R	1	1	1	-	1	-	1	1	-	1
X: Sighthounds												
[MfN] 2709	SAL	L	1	1	1	-	1	-	1	1	-	1
		R	1	1	1	-	1	-	1	1	-	1
NMBE 1051164	BOR	L	1	1	1	1	1	1	1	1	-	1
		R	1	1	1	1	1	1	1	1	-	1
NMBE 1051166	BOR	L	1	1	1	1	1	-	1	1	-	1
		R	1	1	1	3	1	-	1	1	-	1
NMBE 1051180	BOR	L	1	1	1	-	1	1	1	1	-	1
		R	1	1	1	-	1	-	1	1	-	1
NMBE 1052706	BOR	L	1	1	1	1	1	-	1	1	-	1
		R	1	1	1	1	1	-	1	1	-	1
[MfN] 1403	BOR	L	1	1	1	-	1	-	1	1	-	1
		R	1	1	1	-	1	-	1	1	1	1
[MfN] 7374	BOR	L	1	1	1	-	1	-	1	1	1	1
		R	1	1	1	-	1	-	1	1	1	1

Table 5 (continued)

it	ft3	it	itβ	it	etI	itα	it	etII	etIII	Total	Side	Breed	Specimen
													IX: Companion and toy dogs (continued)
-	1	-	1	-	1	1	-	1	1	**11**	L	PUG	[MfN] 1845
-	1	-	1	-	1	1	-	1	1	**11**	R		
-	1	-	1	-	1	1	-	1	1	**12**	L	PUG	[MfN] 2620
-	1	-	1	-	1	1	-	1	1	**12**	R		
-	1	-	1	-	1	1	-	1	1	**11**	L	PUG	[MfN] 2630
1	1	-	1	-	1	1	-	1	1	**12**	R		
-	1	-	1	-	1	1	1	1	1	**12**	L	PUG	[MfN] 2657
-	1	1	1	1	1	1	1	1	1	**14**	R		
-	1	1	1	-	1	1	-	1	1	**13**	L	PUG	ZMB_MAM 30980
-	1	-	1	-	1	1	-	1	1	**12**	R		
													X: Sighthounds
-	1	-	1	-	1	1	1	1	1	**13**	L	SAL	[MfN] 2709
-	1	-	1	-	1	1	1	1	1	**13**	R		
-	1	-	1	-	1	1	1	1	1	**15**	L	BOR	NMBE 1051164
-	1	-	1	-	1	1	1	1	1	**15**	R		
2	1	-	1	-	1	1	1	1	1	**16**	L	BOR	NMBE 1051166
2	1	-	1	-	1	1	1	1	1	**18**	R		
1	1	-	1	-	1	1	1	1	1	**15**	L	BOR	NMBE 1051180
1	1	-	1	-	1	1	1	1	1	**14**	R		
-	1	1	1	-	1	1	1	1	1	**15**	L	BOR	NMBE 1052706
1	1	1	1	-	1	1	1	1	1	**16**	R		
-	1	-	1	1	1	1	-	1	1	**13**	L	BOR	[MfN] 1403
-	1	-	1	-	1	1	1	1	1	**14**	R		
1	1	-	1	-	1	1	1	1	1	**15**	L	BOR	[MfN] 7374
1	1	-	1	-	1	1	2	1	1	**16**	R		

Table 6: Summarized and total number of olfactory turbinals in all specimens of *Canis lupus familiaris* and *Canis lupus lupus* from Table 5.

			Pars intermedia		Pars ethmoturbinalis		
Specimen	**Breed**	**Side**	**ft**	**it**	**et**	**it**	**Total**
Neonate and juvenile stages							
'whippet A'	WH	L	0	0	0	0	**0**
		R	0	0	0	0	**0**
'whippet B'	WH	L	3	0	3	1	**7**
		R	3	0	3	1	**7**
'whippet C'	WH	L	3	1	3	2	**9**
		R	3	1	3	2	**9**
'neonate whippet'	WH	L	3	3	3	2	**11**
		R	3	3	3	2	**11**
48.1	GSD	L	3	2	3	1	**9**
		R	3	2	3	1	**9**
MNHN 1881-47	PUG	L	3	2	3	1	**9**
		R	3	2	3	1	**9**
SMF 16303	BOR	L	3	5	3	2	**13**
		R	3	4	3	2	**12**
MNHN 2007-428	PUG	L	0	0	0	0	**0**
		R	0	0	0	0	**0**
Eurasian wolf (*Canis lupus lupus*)							
ZMB_MAM 815	EW	L	3	7	3	2	**15**
		R	3	4	3	2	**12**
ZMB_MAM 93307	EW	L	3	4	3	2	**12**
		R	3	4	3	2	**12**
ZMB_MAM 93308	EW	L	3	4	3	2	**12**
		R	3	3	3	2	**11**

Table 6 (continued)

			Pars intermedia		Pars ethmoturbinalis		
Specimen	**Breed**	**Side**	**ft**	**it**	**et**	**it**	**Total**
I: Sheepdogs and Cattledogs							
MNHN 1985-1274	GSD	L	3	5	3	2	**13**
		R	3	4	3	2	**12**
SMF 93607	GSD	L	3	5	3	2	**13**
		R	3	4	3	2	**12**
MNHN 1985-1216	GD	L	3	2	3	1	**9**
		R	3	2	3	1	**9**
V: Spitz and primitive types							
MNHN 1947-78	GLD	L	3	7	3	2	**15**
		R	3	7	3	2	**15**
X: Companion and toy dogs							
NMBE 1051945	KCS	L	3	3	3	2	**11**
		R	3	2	3	1	**9**
NMBE 1051948	KCS	L	3	4	3	1	**11**
		R	3	4	3	2	**12**
NMBE 1059207	KCSC	L	3	5	3	2	**13**
		R	3	5	3	2	**13**
NMBE 1062998	KCSC	L	3	3	3	2	**11**
		R	3	4	3	2	**12**
NMBE 1051962	PEK	L	3	2	3	1	**9**
		R	3	2	3	1	**9**
NMBE 1051965	PEK	L	3	2	3	1	**9**
		R	3	2	3	1	**9**
SMF 35611	PEK	L	3	3	3	2	**11**
		R	3	3	3	2	**11**
NMBE 1051951	JAP	L	3	3	3	2	**11**
		R	3	3	3	2	**11**
ZMB 7436	JAP	L	3	3	3	1	**10**
		R	3	3	3	2	**11**
NMBE 1051937	PUG	L	3	2	3	1	**9**
		R	3	2	3	1	**9**
NMBE 1052345	PUG	L	3	2	3	1	**9**
		R	3	2	3	1	**9**

Table 6 (continued)

			Pars intermedia		Pars ethmoturbinalis		
Specimen	**Breed**	**Side**	**ft**	**it**	**et**	**it**	**Total**
IX: Companion and toy dogs (continued)							
SMF 16284	PUG	L	3	1	3	1	**8**
		R	3	2	3	1	**9**
[MfN] 1845	PUG	L	3	2	3	1	**9**
		R	3	2	3	1	**9**
[MfN] 2620	PUG	L	3	3	3	1	**10**
		R	3	3	3	1	**10**
[MfN] 2630	PUG	L	3	2	3	1	**9**
		R	3	3	3	1	**10**
[MfN] 2657	PUG	L	3	2	3	2	**10**
		R	3	4	3	2	**12**
ZMB_MAM 30980	PUG	L	3	4	3	1	**11**
		R	3	3	3	1	**10**
X: Sighthounds							
[MfN] 2709	SAL	L	3	3	3	2	**11**
		R	3	3	3	2	**11**
NMBE 1051164	BOR	L	3	5	3	2	**13**
		R	3	5	3	2	**13**
NMBE 1051166	BOR	L	3	6	3	2	**14**
		R	3	8	3	2	**16**
NMBE 1051180	BOR	L	3	5	3	2	**13**
		R	3	4	3	2	**12**
NMBE 1052706	BOR	L	3	5	3	2	**13**
		R	3	6	3	2	**14**
[MfN] 1403	BOR	L	3	4	3	1	**11**
		R	3	4	3	2	**12**
[MfN] 7374	BOR	L	3	5	3	2	**13**
		R	3	5	3	3	**14**

Table 7: Summarized morphological characters in the turbinal skeleton of *Canis lupus*. As the dog's (*Canis lupus familiaris*) ancestor the **Eurasian wolf** (*Canis lupus lupus*, n=3) represents the ***grundplan*** to which the breeds are compared. The grouping bases on the two indices facial length to length of braincase and length to breadth of skull (IFB, IBL, ELLENBERGER & BAUM 1891, see **Table 1**). The **dolichocephalic (DOL**, n=11**)** breeds include the sighthounds **borzoi** and **saluki**; the scent hounds **German shepherd** and **Groenendael**; and the **Greenland dog**. Two of the ancient pugs which are mesaticephalic are grouped with their brachycephalic conspecifics to avoid a separation within the breed. For the same reason, the also mesaticephalic Cavalier is grouped with its short snouted ancestor, the King spaniel. Consequently, in this table the second group combines the **brachycephalic to mesaticephalic (BRA/MES**, n=17**)** breeds to which **pug, King spaniel, Cavalier, chin,** and **pekingese** belong. Additionally, the **ontogenetic** patterns of the turbinal skeleton are described based on the histological serial sections of the three oldest **perinatal stages** of the whippets (**'whippet B'**, **'whippet C'**, and the **neonate**). To avoid intricacies in the distinction of the ontogenetic stages, the three juveniles (German shepherd, pug, and borzoi) are excluded. Of the olfactory recess, besides the fronto-and ethmoturbinals only the prominent interturbinals are listed. The smaller additional interturbinals are not represented due to their heterochronic presence and morphology.

MAXILLOTURBINAL (MT)

	Perinatal stages (WH-B,C; neonate)	***grundplan*** (Eurasian wolf)	**DOL** (BOR, GD, GLD, GSD, SAL)	**BRA/MES** (JAP, KCS, KCSC, PEK, PUG)
Basic type	**Double scroll**	**Double scroll**	**≙ *grundplan***	**≙ *grundplan*** (straight n=1)
Ventral lamella	**Crest-like** (WH-B, C) **Initiation dendritic shape, lateral scroll** (neonate)	**Dendritic, lateral scroll**	**≙ *grundplan***	**≙ *grundplan*** (n=10) **≙ *perinatal*** (max. slightly dendritic n=5; reduction of lateral scroll n=3)
Dorsal lamella	**Crest-like** (WH-B, C) **Dendritic** (neonate)	**Dendritic**	**≙ *grundplan***	**± *grundplan*** (n=5) **≙ *perinatal*** (n=11)
Space of nasal cavity	**Open**	**Closed**	**≙ *grundplan***	**≙ *grundplan*** (n=7) **≙ *perinatal*** (n=10)
Topography	**Caudoventrally**	**Caudoventrally**	**≙ *grundplan***	**≙ *grundplan***

NASOTURBINAL (NT)

	Perinatal stages (WH-B,C; neonate)	***grundplan*** (Eurasian wolf)	**DOL** (BOR, GD, GLD, GSD, SAL)	**BRA/MES** (JAP, KCS, KCSC, PEK, PUG)
Shape	**Straight**	**Straight to medioventrally curved**	**≙ *grundplan***	**≙ *grundplan***
End	**Pointed,** no connection with ls (WH B, C) **Beginning fusion to ls** (neonate)	**Continuous with ls; no suture visible**	**≙ *grundplan***	**≙ *grundplan*** **Reduction** (rostral tip of ls in extreme brachycephalic individuals)

LAMINA SEMICIRCULARIS (LS)

	Perinatal stages (WH-B,C; neonate)	***grundplan*** (Eurasian wolf)	**DOL** (BOR, GD, GLD, GSD, SAL)	**BRA/MES** (JAP, KCS, KCSC, PEK, PUG)
Ventral lamina	**Straight; uncinate process in maxillary sinus**	**Single scroll; uncinate process in maxillary sinus**	**≙ *grundplan*** (uncinate process absent in one BOR; alternate position uncinate process n=2; double scroll + 2nd process n=2)	**≙ *grundplan*** (n=8) **≙ *perinatal*** (straight n=7)// **Complication** (double scroll n=2)
Dorsal lamina	**Absent** (WH-B, C) **Single scroll, merging caudally into lamina cribrosa** (neonate)	**Double to multiple scrolls; merging caudally into lamina cribrosa**	**≙ *grundplan***	**≙ *perinatal*** **≙ *grundplan*** (double scroll n = 2)
Accessory lamella	**Absent**	**Dorsal to ls onto frontal; straight to double scroll; shift to stem of ls and merging into it**	**≙ *grundplan*** (absent in GLD)	**≙ *perinatal*** **≙ *grundplan*** (one PUG, dorsal to ls onto nasal)

FRONTOTURBINAL 1 (FT1)

	Perinatal stages (WH-B,C; neonate)	***grundplan*** (Eurasian wolf)	**DOL** (BOR, GD, GLD, GSD, SAL)	**BRA/MES** (JAP, KCS, KCSC, PEK, PUG)
Rostral end	**Paries & continuous with lamina horizontalis**	**Maxillary & continuous with lamina horizontalis**	**Maxillary** (BOR, SAL)// **maxillary & continuous with ls/lamina horizontalis**	**Maxillary & continuous with ls/lamina horizontalis**
Shape	**Straight** (WH-B/ C) **Initial double scroll** (WH-C) **Double scroll** (neonate)	**Rostrally dendritic → caudally multiple scrolls**	**≙ *grundplan***	**≙ *perinatal*** **≙ *grundplan*** (rostrally dendritic n=4; caudally multiple scrolls n=3)
Topography	**Onto paries**	**Onto frontal → septum of frontal sinus**	**≙ *grundplan***	**Onto frontal** (frontal sinus minimized to reduced)
Caudal end	**Transition limbus praecribrosus and limbus paracribrostralus** (WH-B) **Limbus paracribrostralus** (WH-C) **Lamina cribrosa** (neonate)	**Process in frontal sinus**	**≙ *grundplan***	**≙ *grundplan*** **≙ *perinatal*** (lamina cribrosa// septum) (fluent degrees in reduction of frontal sinus; no pattern between breed and size of frontal sinus)

FRONTOTURBINAL 2 (FT2)

	Perinatal stages (WH-B,C; neonate)	***grundplan*** (Eurasian wolf)	**DOL** (BOR, GD, GLD, GSD, SAL)	**BRA/MES** (JAP, KCS, KCSC, PEK, PUG)
Rostral end	**Paries & continuous with lamina horizontalis, no rostral process**	**Maxillary & continuous with** (1) **ls with rostral process** (2) **lamina horizontalis without rostral process**	**≙ *grundplan***	**≙ *grundplan***
Shape	**Straight** (WH-B/ C) **Initial double scroll** (WH-C) **Double scroll** (neonate)	**Rostrally dendritic → caudally multiple scrolls**	**≙ *grundplan***	**≙ *perinatal*** (n=11); **≙ *grundplan*** (n=6)
Topography	**Onto paries**	**Onto frontal → septum of frontal sinus**	**≙ *grundplan*** (n=2) **Onto frontal** (others)	**Onto frontal** (frontal sinus reduced to lost)
Caudal end	**Limbus paracribrosus** (WH-B, C) **Lamina cribrosa** (neonate)	**Process in frontal sinus**	**≙ *grundplan***	**≙ *grundplan*** **≙ *perinatal*** (lamina cribrosa// septum of frontal sinus) (fluent degrees of reduction of frontal sinus; no pattern between breed and size of frontal sinus)

FRONTOTURBINAL 3 (FT3)

	Perinatal stages (WH-B,C; neonate)	***grundplan*** (Eurasian wolf)	**DOL** (BOR, GD, GLD, GSD, SAL)	**BRA/MES** (JAP, KCS, KCSC, PEK, PUG)
Rostral end	**Paries & continuous with lamina horizontalis** (WH-B) **Lamina horizontalis** (WH-C, neonate)	**Lamina horizontalis**// **Frontal & continuous with lamina horizontalis**	**Lamina horizontalis**// **Lamina horizontalis & continuous with etl**	**≙ *perinatal*** (WH-C, neonate)
Shape	**Crest-like** (WH-B) **Straight** (WH-C) **Double scroll** (neonate)	**Rostrally dendritic → caudally multiple**	**≙ *grundplan***	**≙ *perinatal*** (max. double scroll)
Topography	**Onto paries**	**Onto frontal**	**≙ *grundplan***	**≙ *grundplan*** (one PEK ontp lamina horizontalis)
Caudal end	**Paries** (WH-B, C) **Lamina cribrosa** (neonate)	**Lamina cribrosa**	**≙ *grundplan***	**≙ *grundplan***

INTERTURBINAL α (itα) [Pars ethmoturbinalis]

	Perinatal stages (WH-B,C; neonate)	***grundplan*** (Eurasian wolf)	**DOL** (BOR, GD, GLD, GSD, SAL)	**BRA/MES** (JAP, KCS, KCSC, PEK, PUG)
Rostral end	**Lamina horizontalis**	**Rostral process, dendritic**	**≙ *grundplan***	**≙ *grundplan*** (n = 2) **EtII// lamina horizontalis & continuous with etII** (one PEK onto lamina terminalis, rostral to etII)
Shape	**Crest-like** (WH-B) **Straight** (WH-C) **Double scroll** (neonate)	**Multiple scrolls**	**≙ *grundplan*** (double scroll n=5)	**≙ *perinatal*** (max. double scroll)
Topography	**Approaches stem etI** (WH-B) **Onto stem etI** (WH-C, neonate)	**EtII → lamina horizontalis → etI**	**≙ *grundplan***	**≙ *grundplan*** **No touch lamina horizontalis** (one PUG) **or etII** (one PEK)
Caudal end	**Lamina horizontalis and/or etI** (WH-B) **EtI** (WH-C; neonate)	**Lamina cribrosa**	**≙ *grundplan***	**± *grundplan*** (process in pars ethmoturbinalis or sphenoid sinus n=5)

INTERTURBINAL β (itβ) [Pars intermedia]

	Perinatal stages (WH-C, neonate)	***grundplan*** (Eurasian wolf)	**DOL** (BOR, GD, GLD, GSD, SAL)	**BRA/MES** (JAP, KCS, KCSC, PEK, PUG)
Rostral end	**Lamina horizontalis**	**Lamina horizontalis**	**≙ *grundplan*** (continuous with ft3 and/ or etI n=7)	**≙ *grundplan*** (continuous with ft3 and/ or etI n=8)
Shape	**Crest-like**	**Multiple scrolls to dendritic**	**Max. multiple scrolls**	**Simplification** (double scroll) (one PEK straight)
Topography	**Onto paries**	**Caudal to lamina horizon-Talis onto frontal**	**≙ *grundplan***	**≙ *grundplan***
Caudal end	**Paries**	**Lamina cribrosa**	**≙ *grundplan***	**≙ *grundplan***

INTERTURBINAL γ (itγ) [Pars intermedia]

	Perinatal stages (neonate)	***grundplan*** (Eurasian wolf)	**DOL** (BOR, GD, GLD, GSD, SAL)	**BRA/MES** (JAP, KCS, KCSC, PEK, PUG) (present n=8)
Rostral end	**Paries**	**Frontal ventral to frontal sinus** (n=2)// **frontal rostral to frontal sinus**	**≙ *grundplan*** (rostral to frontal sinus n=6; stem ft1 n=2)	**≙ *grundplan*** (in all rostral to frontal sinus)
Shape	**Crest-like**	**Straight, well developed**	**≙ *grundplan*** (rostral end max. single scroll)	**≙ *perinatal***
Topography	**None**	**None// onto septum**	**≙ *grundplan***	**≙ *perinatal***
Caudal end	**Lamina cribrosa**	**As septum of frontal sinus**	**≙ *grundplan***	**≙ *grundplan*** **≙ *perinatal*** (one PEK)

INTERTURBINAL δ (itδ) [Pars intermedia]

	Perinatal stages (neonate)	***grundplan*** (Eurasian wolf)	**DOL** (BOR, GD, GLD, GSD, SAL)	**BRA/MES** (JAP, KCS, KCSC, PEK, PUG)
Rostral end	**Paries**	**Nasal** (n=2)// **frontal**	**Nasal// suture nasal-frontal**	**Nasal// suture nasal-frontal/ nasal-maxillary** (n=4)
Shape	**Crest-like**	**Variable** (single to multiple scrolls)	**≙ *grundplan***	**Simplification** (straight to single scroll) (double scroll n=2)
Topography	**Medially**	**Medially**	**≙ *grundplan***	**≙ *grundplan***
Caudal end	**Lamina cribrosa**	**Septal process of frontal (rostral to lamina cribrosa)**	**≙ *grundplan***	**≙ *grundplan*** **≙ *perinatal*** (n=3) **frontal** (n=4)

ETHMOTURBINAL I (ETI)

	Perinatal stages (WH-B,C; neonate)	***grundplan*** (Eurasian wolf)	**DOL** (BOR, GD, GLD, GSD, SAL)	**BRA/MES** (JAP, KCS, KCSC, PEK, PUG)
Process	**Process of lamina anterior; straight, bulbous-like** (WH-B, C) **Process of lamina anterior beginning complication; mediocaudally process of lamina posterior, straight** (neonate)	**Rostral process of lamina anterior; mediocaudally process of lamina posterior; both dendritic**	**≙ *grundplan***	**± *grundplan*** (min. slightly dendritic n=8) **Simplification** (straight to slightly dendritic n=9) **Reduction process** (process of lamina anterior and/ or process of lamina posterior n=2) Shape identical within specimen (n=12)
Fusion	**One stem on lamina horizontalis**	**One stem on lamina horizontalis**	**≙ *grundplan***	**≙ *grundplan***
Lamina anterior	**Beginning double scroll** (WH-B, C) **Double scroll** (neonate)	**Multiple scrolls**	**≙ *grundplan***	**≙ *perinatal*** (double scroll)
Lamina posterior	**Outgrowth lamina anterior, straight** (WH-B, C) **Single scroll** (neonate)	**Shift ventral to lamina anterior; max. multiple scrolls**	**≙ *grundplan***	**Simplification** (max. double scroll) (partly dendritic one KCSC) where process of lamina posterior absent: **Outgrowth lamina anterior// lamina horizontalis** **Separation of double scroll// fusion of single scroll with epiturbinal to double scroll** (PUGs, not all)
Epi-turbinal	**Onto stem, moving distally; epithelial bulge** (WH-B) **crest-like** (WH-C) **double scroll** (neonate)	**Dorsoproximal on stem; moving distally; max. multiple scrolls**	**≙ *grundplan*** (up to dendritic; SAL double scroll)	**≙ *perinatal*, Well developed** (large surface area) (absent in one PUG)
2nd 'epi-turbinal'	**Absence**	**Proximal to 1st, small, max. double scroll**	**≙ *grundplan*** (BOR, GD) **≙ *perinatal*** (GLD, GSD, SAL)	**≙ *perinatal*** (presence in one PUG)
Caudal end	**Paries** (WH-B & C) **Lamina cribrosa**(neonate)	**Lamina cribrosa**	**≙ *grundplan***	**≙ *grundplan*** (pars ethmoturbinalis & lamina cribrosa & frontal one KCS)

ETHMOTURBINAL II (ETII)

	Perinatal stages (WH-B,C; neonate)	***grundplan*** (Eurasian wolf)	**DOL** (BOR, GD, GLD, GSD, SAL)	**BRA/MES** (JAP, KCS, KCSC, PEK, PUG)
Rostral end	**Rostral process, straight**	**Rostral process, dendritic; medial to process of lamina posterior**	**≙ *grundplan***	**Simplification** (ancient PUG; max. slightly dendritic; absence of process n=2) **No pattern; high variability** (others including modern PUG)
Shape	**Single scroll**	**Multiple scrolls**	**≙ *grundplan***	**≙ *grundplan***
Topography	**Lamina horizontalis → caudal to it paries**	**EtI → lamina horizontalis → caudal to it palatine → orbitosphenoid**	**≙ *grundplan***	**≙ *grundplan*** (additionally onto lamina terminalis n=5)
Caudal end	**Paries** (WH-B, C) **Lamina cribrosa & paries** (neonate)	**Lamina cribrosa**	**≙ *grundplan***	**Sphenoid sinus** **≙ *grundplan*** (KCSC)

ETHMOTURBINAL III (ETIII)

	Perinatal stages (WH-B,C; neonate)	***grundplan*** (Eurasian wolf)	**DOL** (BOR, GD, GLD, GSD, SAL)	**BRA/MES** (JAP, KCS, KCSC, PEK, PUG)
Rostral end	**Paries** (WH-B, C) **Lamina horizontalis next to stem etII** (neonate)	**Straight lamella on stem etII// lamina horizontalis**	**≙ *grundplan*** (additionally fusion to lamina terminalis one GSD)	**± *grundplan*** (fusion to lamina terminalis n=10)
Shape	**Crest-like** (WH-B) **Straight** (WH-C) **Single scroll** (neonate)	**Double to multiple scrolls**	**≙ *grundplan***	**≙ *perinatal*** (max. double scroll)
Topography	**None** (WH-B & C) **Caudal to lamina horizontalis onto paries** (neonate)	**(Stem etII →) lamina horizontalis → caudal to it palatine → orbitosphenoid**	**≙ *grundplan***	**≙ *grundplan***
Caudal end	**Paries** (WH-B & C) **Lamina cribrosa & paries** (neonate)	**Process in sphenoid sinus**	**≙ *grundplan***	**≙ *grundplan***

APPENDIX: FIGURES

A Akita/Asian spitz
B Shih tzu/Asian toy
C Icelandic sheepdog/Nordic spitz
D (Miniature) schnauzer; Pomeranian/small spitz; Brussels griffon/toy spitz
E Puli/Hungarian
F (Standard) poodle
G Chihuahua/American toy; Rat terrier/American terrier
H (Miniature) pinscher
J (Irish) terrier
L Saluki/Mediterranean
M Basset hound/scent hound
N (American cocker) spaniel
P (Golden) retriever
Q German shorthaired pointer/pointer setter
R Briard/continental herder
S Shetland sheepdog/UK rural
T Rottweiler/drover
U Saint Bernard/alpine
W English/European mastiff

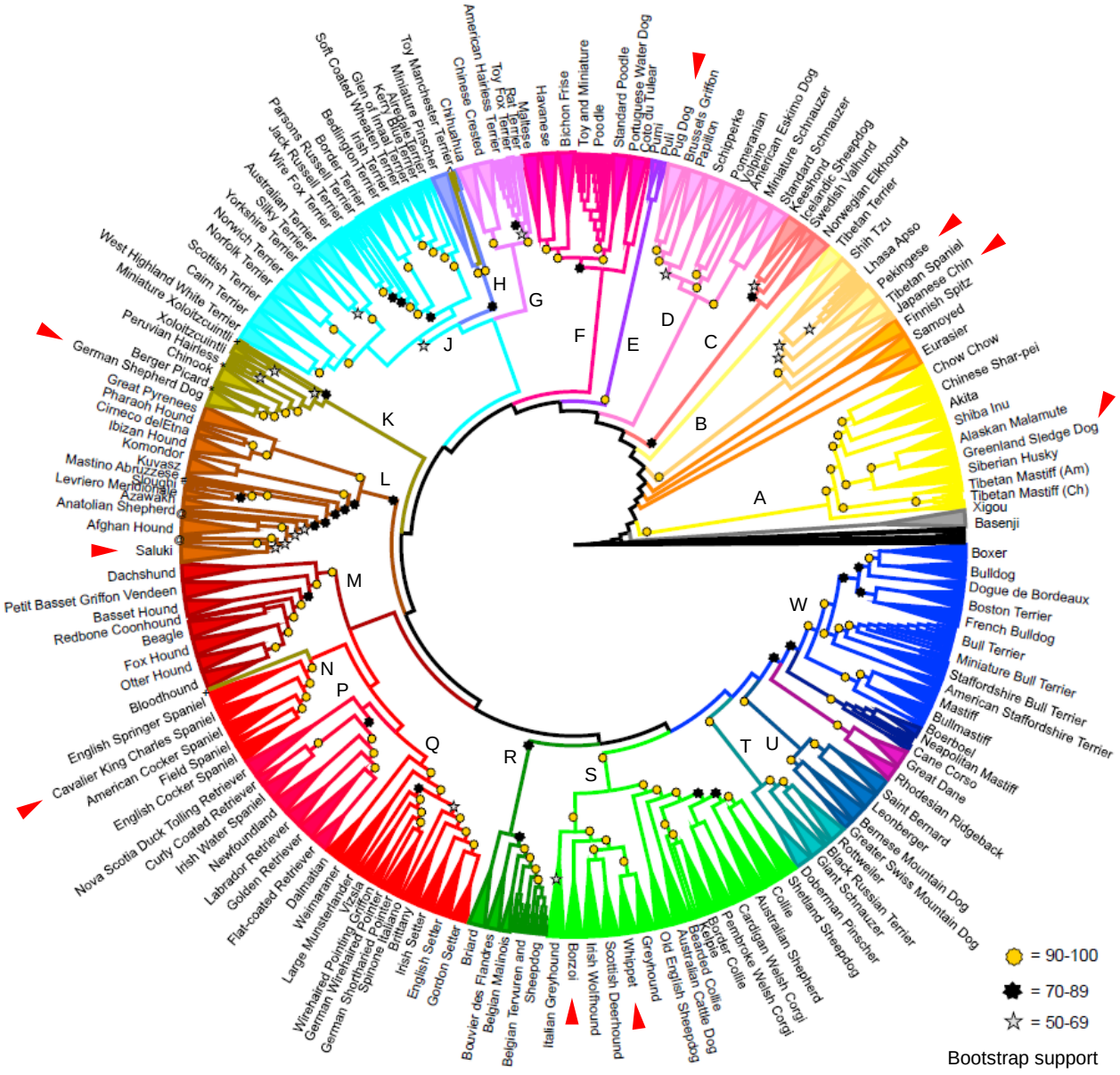

Fig. 1a: Neighbour joining cladogramm showing the genetic relationships among 161 dog breeds which are classified into 23 clades. Breeds which are represented in the present study are marked with red arrows (adopted from PARKER *et al*. 2017, figure 1).

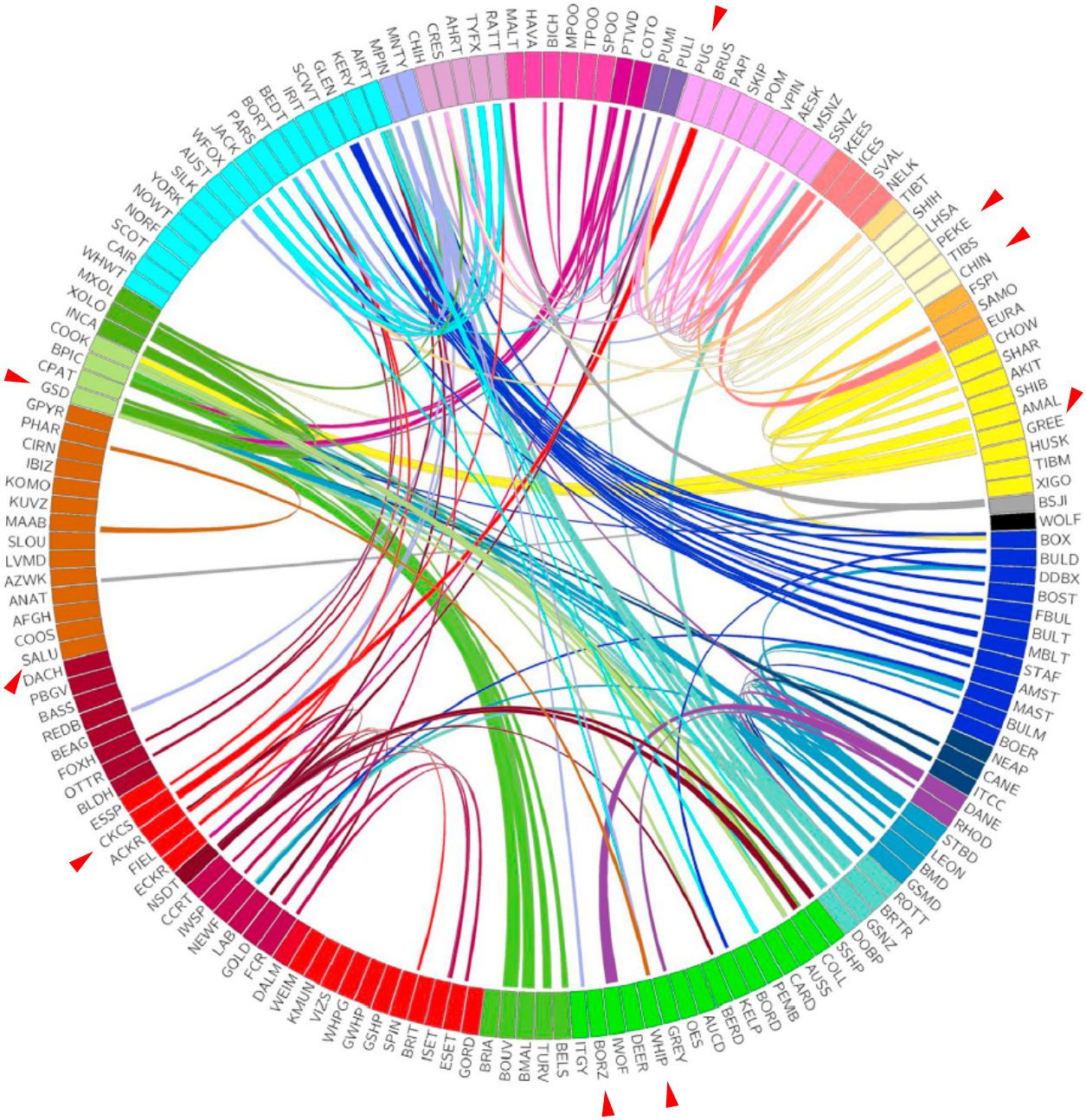

GREE	Greenland dog
CHIN	Japanese chin
PEKE	pekingese
GSD	German shepherd
SALU	saluki
CKCS	Cavalier King Charles spaniel
BORZ	borzoi
WHIP	whippet

Fig. 1b: Circus plot showing the shared haplotypes among the 161 dog breeds from the neighbour joining cladogramm in Fig. 1a. The colors refer to this colorcode. Breeds which are represented in the present study are marked with red arrows (adopted from PARKER *et al*. 2017, figure 4).

Fig. 2: Pictures of the Eurasian wolf (*Canis lupus lupus*, outgroup) and of the dog breeds (*Canis lupus familiaris*) which have been chosen for the present study. Differing from the descriptive order in the introduction, the long snouted breeds are grouped together, and the medium to short snouted toys (see following page). AKC, © American Kennel Club; NKU, © Nordic Kennel Union; ZKR, © Züchterkreis für den Retromops; FW, own photographs. Not to scale.

Fig. 2 (continued; toy/companion dogs)

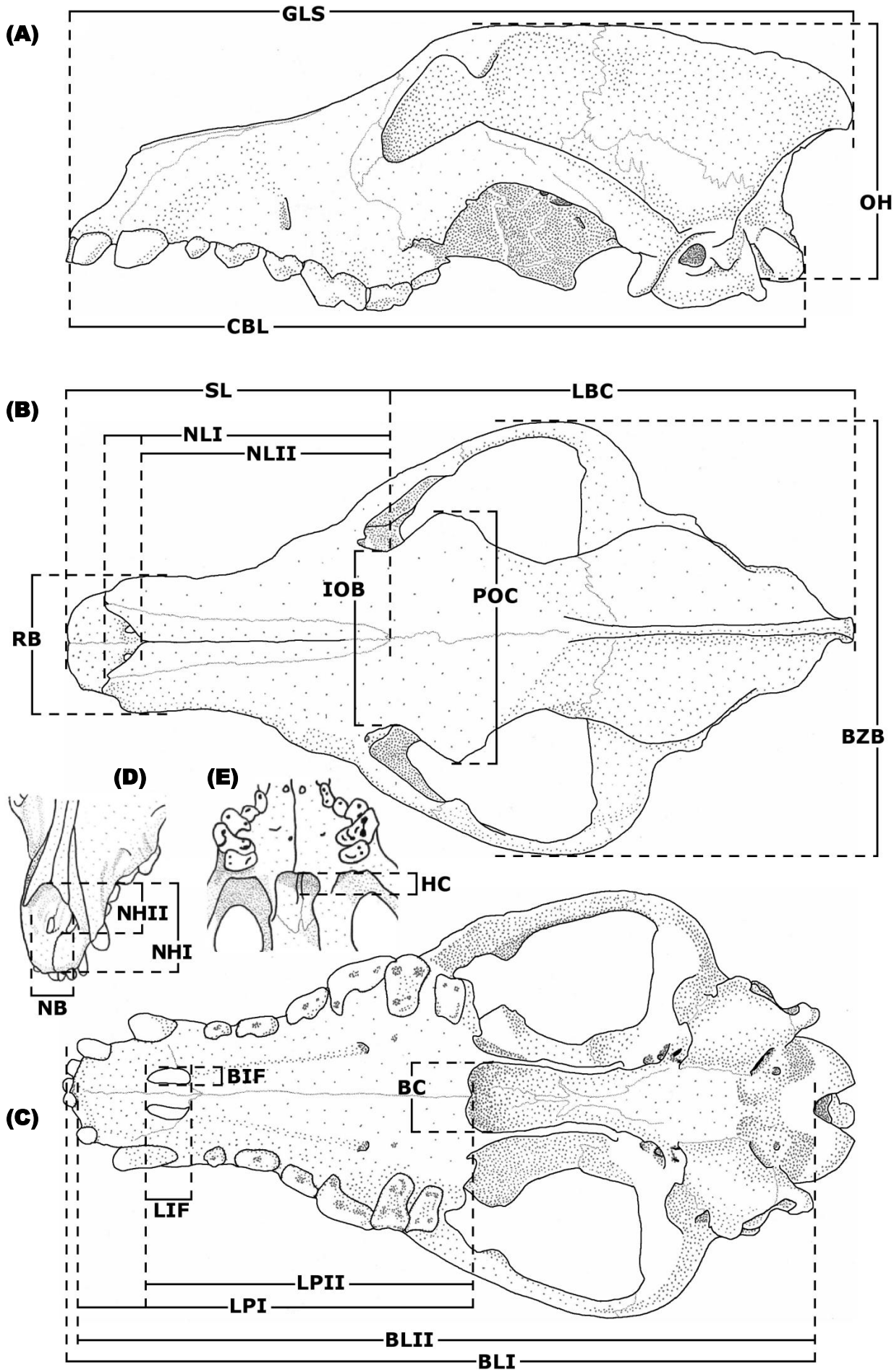

Fig. 3: Skull of an adult Eurasian wolf (*Canis lupus lupus*, SMF 53501) in (A) lateral, (B) dorsal, and (C) ventral view as far as (D) the rostrum in dorsolateral view and (E) the choanae in caudoventral view illustrating the measurements which are defined in Table 2. Sketches are adopted from own photographs.

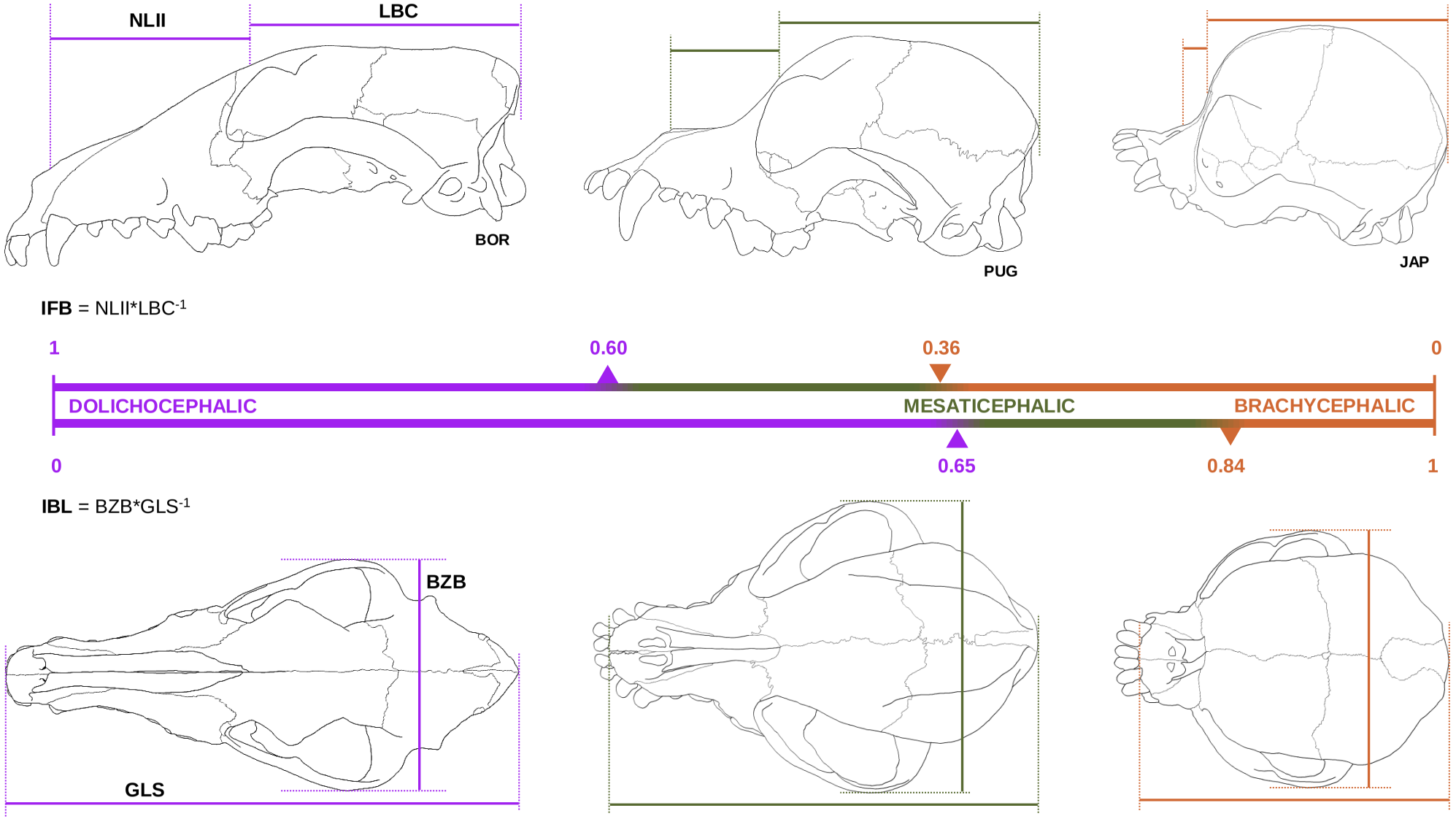

Fig. 4: Classification of the selected breeds into the three snout length types based on the two indices index facial length to length of braincase (IFB) and index length to breadth of skull (IBL) (ELLENBERGER & BAUM 1891). [specimens: **BOR, borzoi** [MfN] 1403; **pug** [MfN] 2657; **JAP, Japanese chin** ZMB_MAM 7436]. The definitions of the measurements are listed in Table 2.

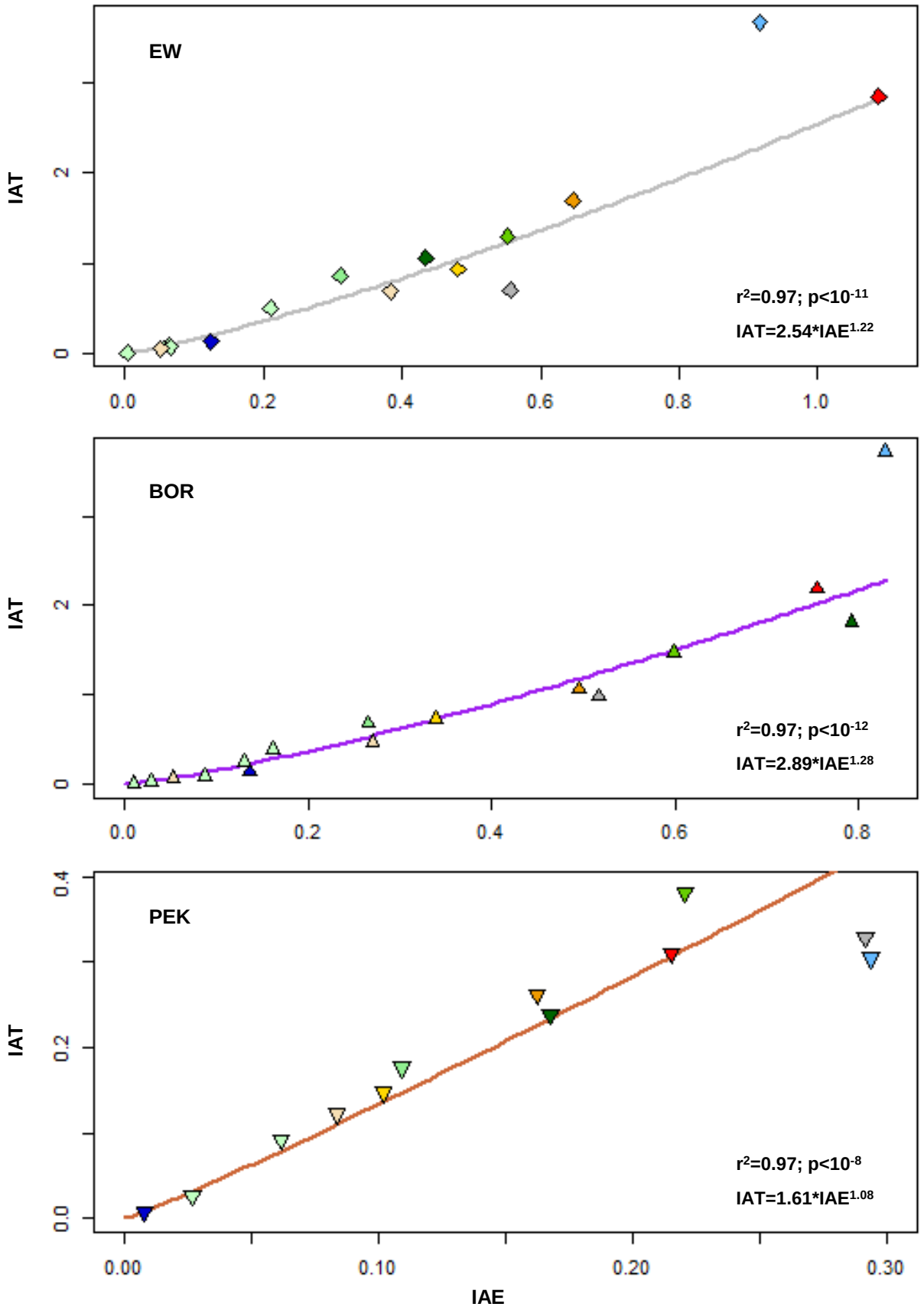

Fig. 5: Scatter plots illustratingthe correlation between index turbinal surface area (IAT) and index exterior surface area (IAE) between the turbinals including the lamina semicircularis on the example of three specimens of *Canis lupus*: **EW, Eurasian wolf** (*Canis lupus lupus*; ZMB_MAM 93307; outgroup); **BOR, borzoi** (*Canis lupus familiaris*; NMBE 1051164; dolichocephalic); **PEK, pekingese** (*Canis lupus familiaris*; NMBE 1051962; brachycephalic). The positive correlation describes a power function given in the plot, as far as the adjusted r^2- and the p-value resulting from the ANOVA in R 3.3.0. The colors of the ablines refer to their summarized illustration in Fig. 46. The plots of the other specimens are illustrated in Fig. S3 (Supplementary material). For the values of the ANOVA see Table S5 (Supplementary material). Abbreviations: 1; colors of the points refer to the turbinal color code.

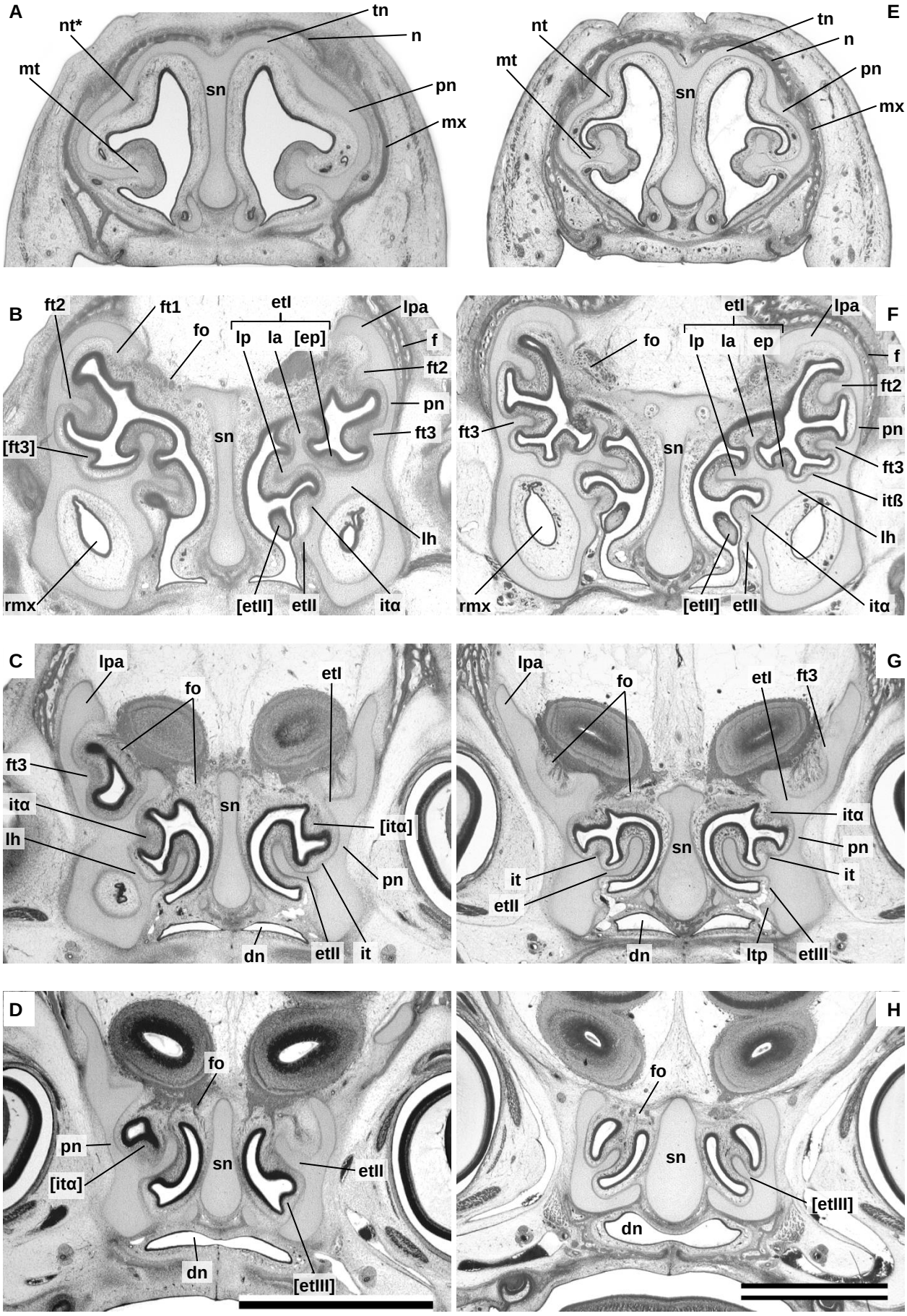

Fig. 6: Histological serial sections of the ethmoidal region of two prenatal whippets (*Canis lupus familiaris*, SCHLIEMANN 1966) from rostral to caudal in coronal view: **A–D)** 'whippet B'; **E–H)** 'whippet C'. **A, E)** pars maxillonasoturbinalis, **B, C, F)** pars ethmoturbinalis and pars intermedia; **D, G, H)** pars ethmoturbinalis. Turbinals which are present as epithelial bulge are in brackets; the nasoturbinal (nt*) in 'whippet B' is developing through mesenchymal condensation. Abbreviations: 1; scale bars: 2mm.

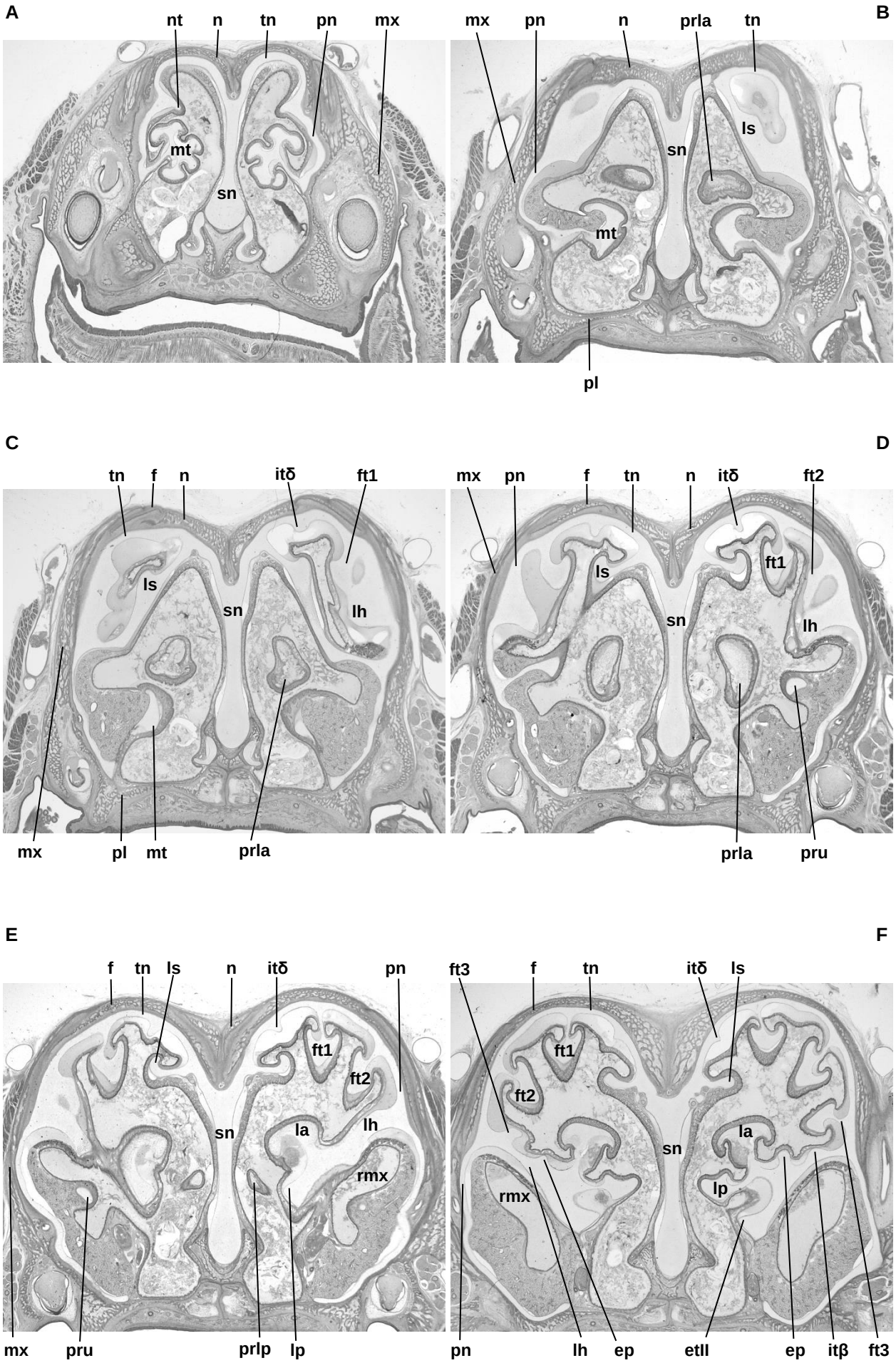

Fig. 7 (description: next page)

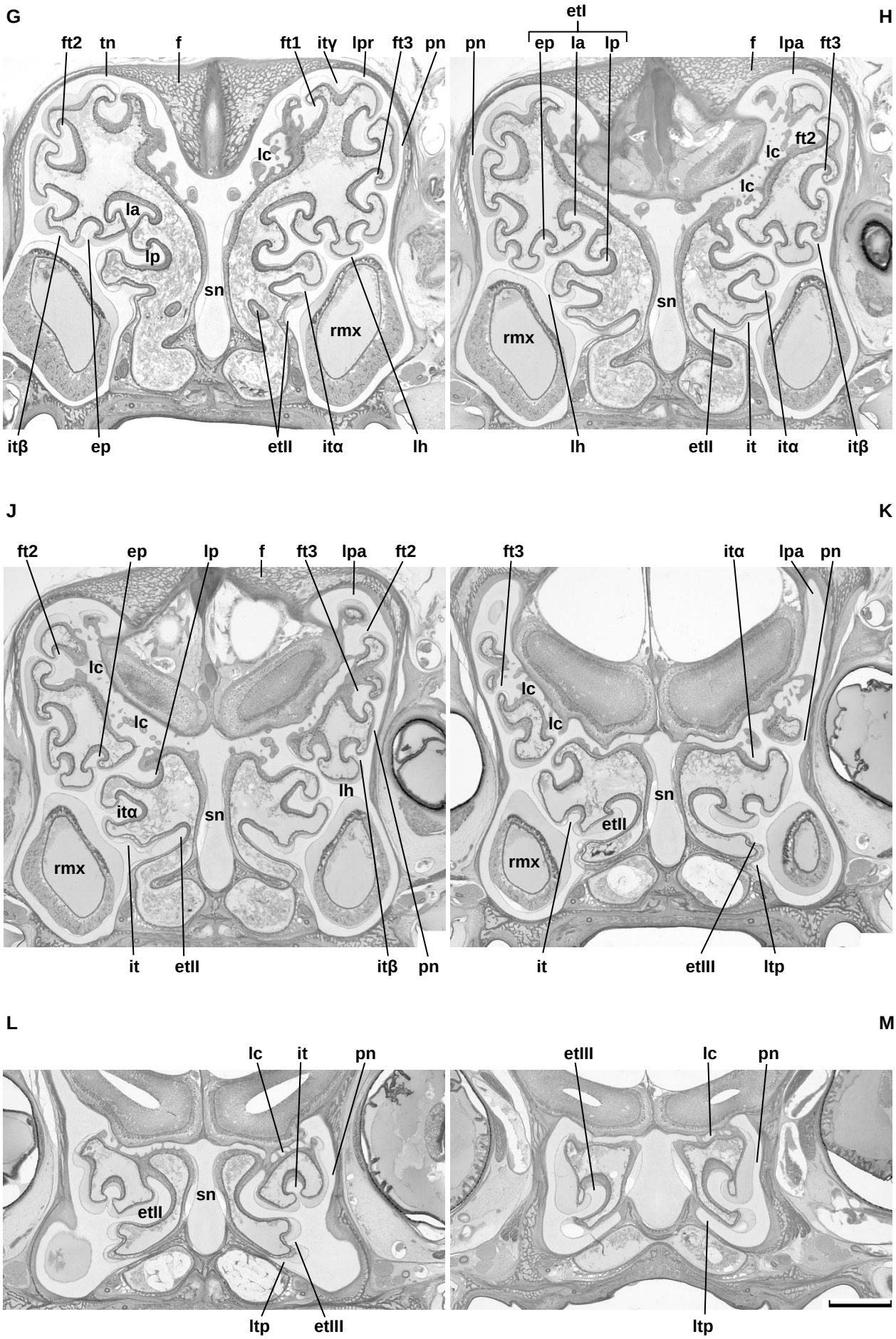

Fig. 7: Histological serial sections of the ethmoidal region of a neonate whippet (*Canis lupus familiaris*, SCHLIEMANN, year unknown); coronal sections from rostral to caudal. **A, B)** pars maxillonasoturbinalis; **C–K)** pars ethmoturbinalis and pars intermedia; **L, M)** pars ethmoturbinalis. Abbreviations: 1; scale bar: 2mm.

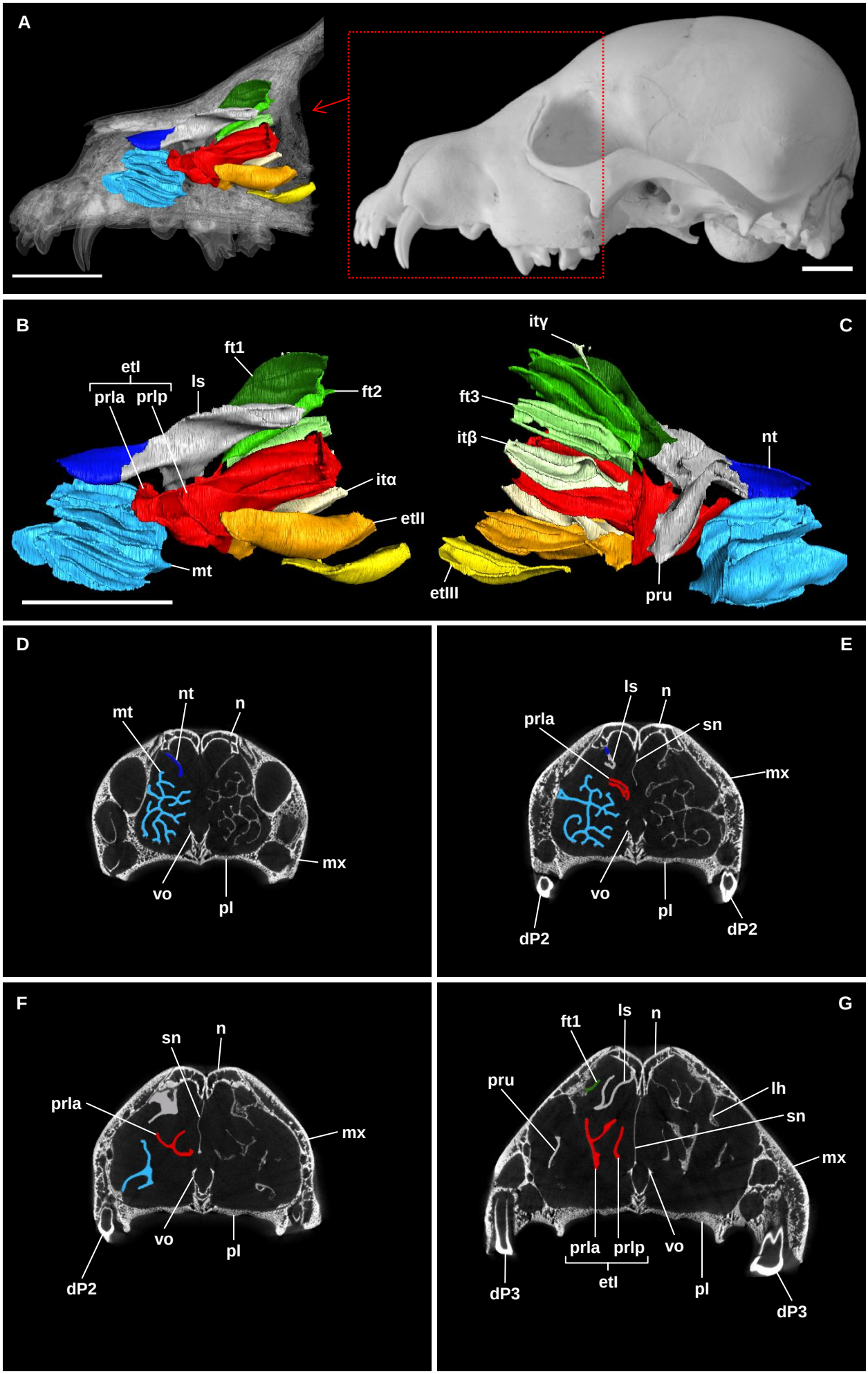

Fig. 8 (description: next page)

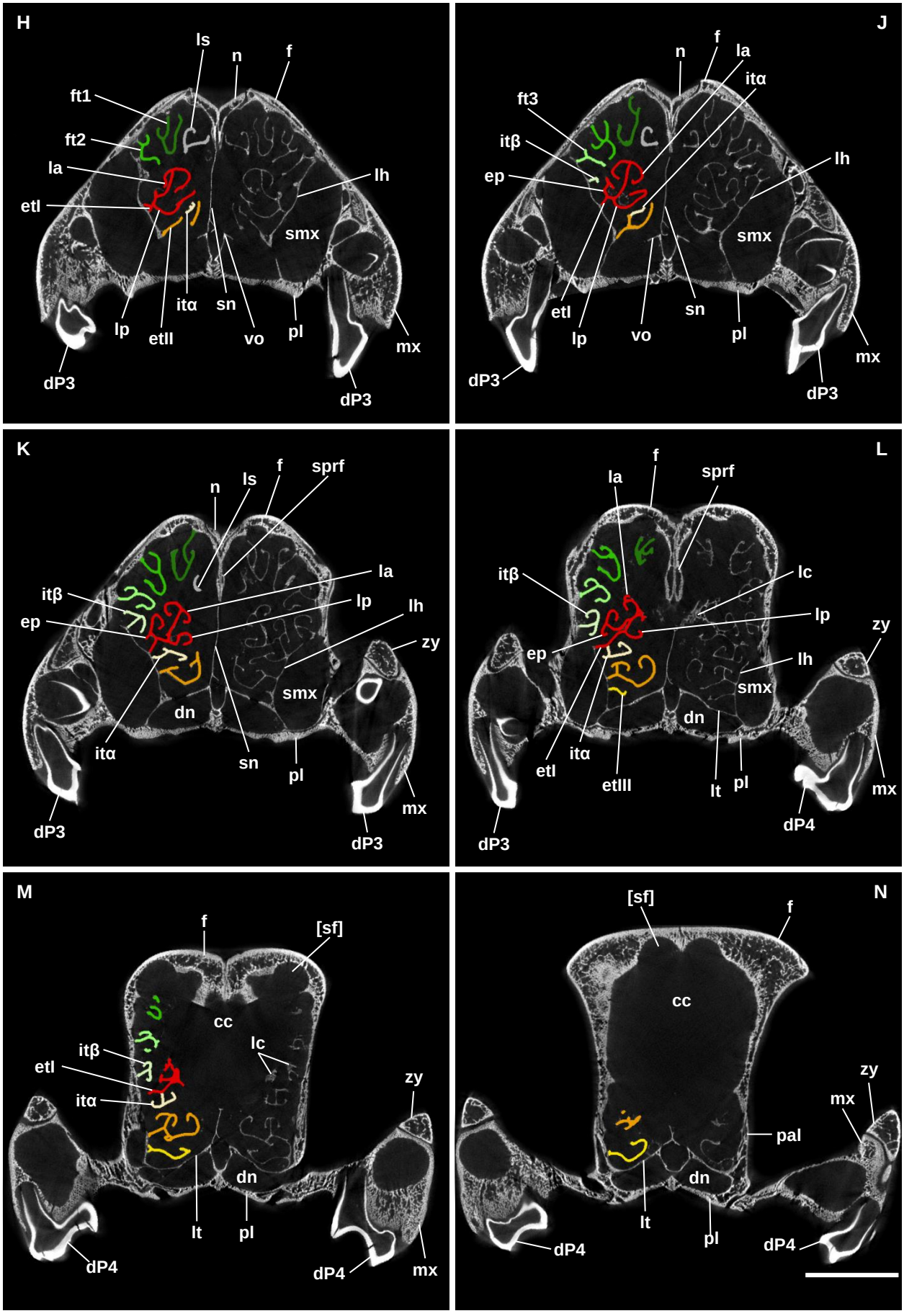

Fig. 8: Juvenile German shepherd, six weeks old (48.1, pers. coll. W. Maier): **A)** virtual 3D model showing the position of the turbinal skeleton within the transparent nasal cavity in medial view (left side, mirrored); next to it the skull in lateral view showing the region of interest; **B)** virtual 3D model of the turbinal skeleton in medial and **C)** in lateral view (both mirrored); **D)–N)** µCT cross sections of the ethmoidal region from rostral to caudal in caudal view, the turbinals are highlighted on one side. [sf] = incipient recesses of the developing frontal sinus. Scale bars: 10mm; Abbreviations: 1; colors refer to the turbinal color code.

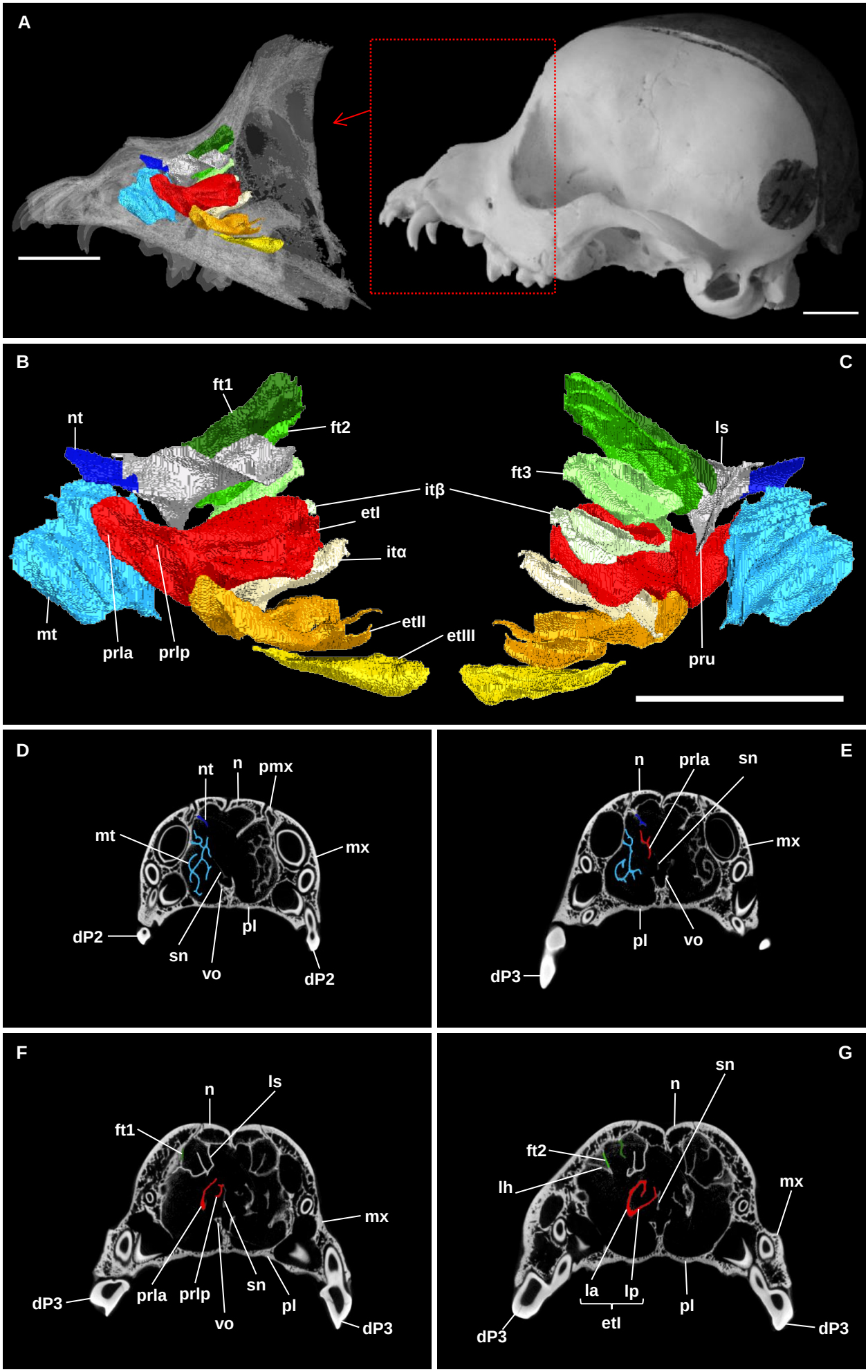

Fig. 9 (description: next page)

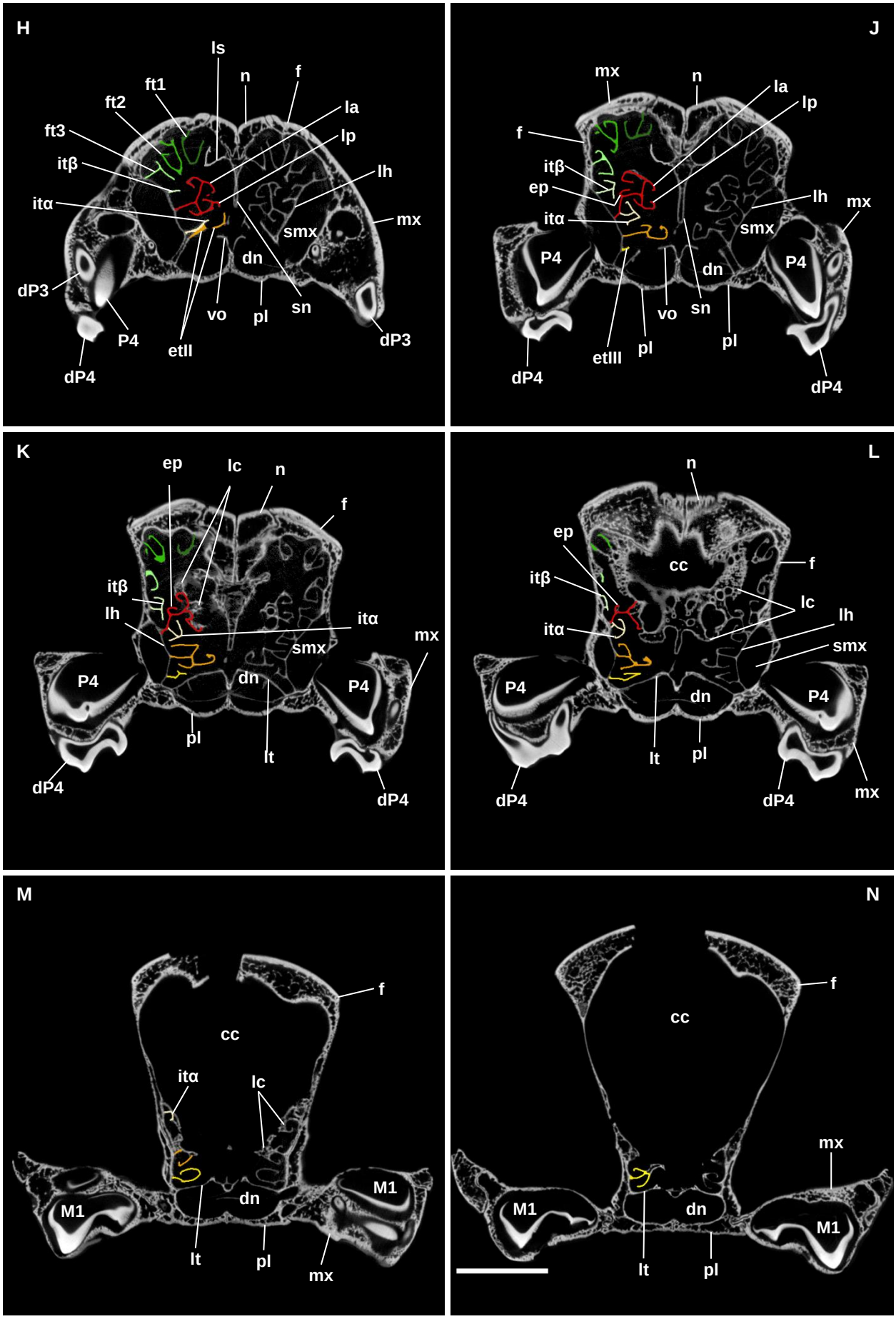

Fig. 9: Juvenile pug (MNHN 1881-47, age unknown): **A)** virtual 3D model showing the position of the turbinal skeleton within the transparent nasal cavity in medial view (left side, mirrored); next to it the skull in lateral view showing the region of interest; **B)** virtual 3D model of the turbinal skeleton in medial and **C)** in lateral view (both mirrored); **D)–N)** µCT cross sections of the ethmoidal region from rostral to caudal in caudal view, the turbinals are highlighted on one side. Scale bars: 10mm; Abbreviations: 1; colors refer to the turbinal color code.

FIGURES

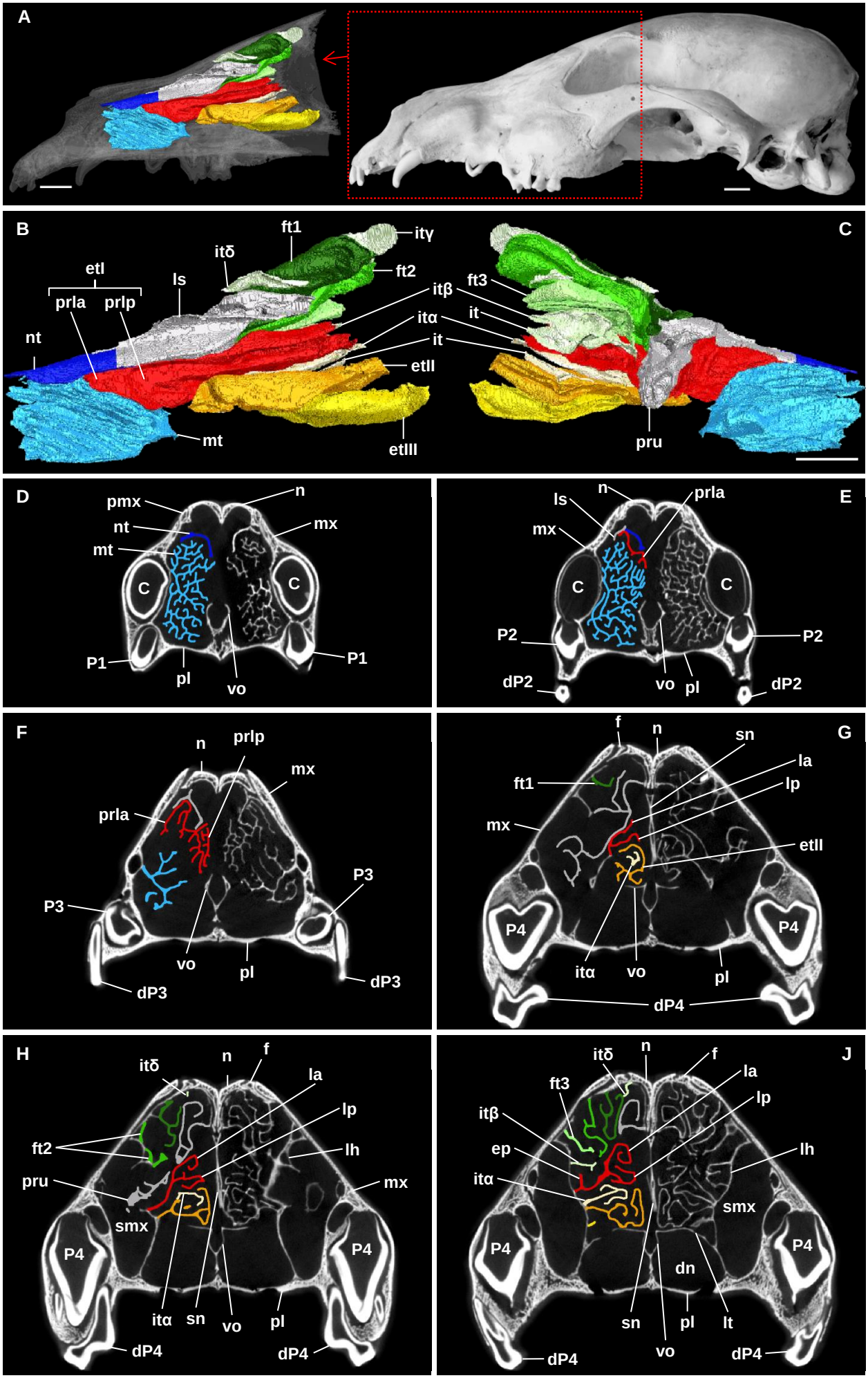

Fig. 10 (description: next page)

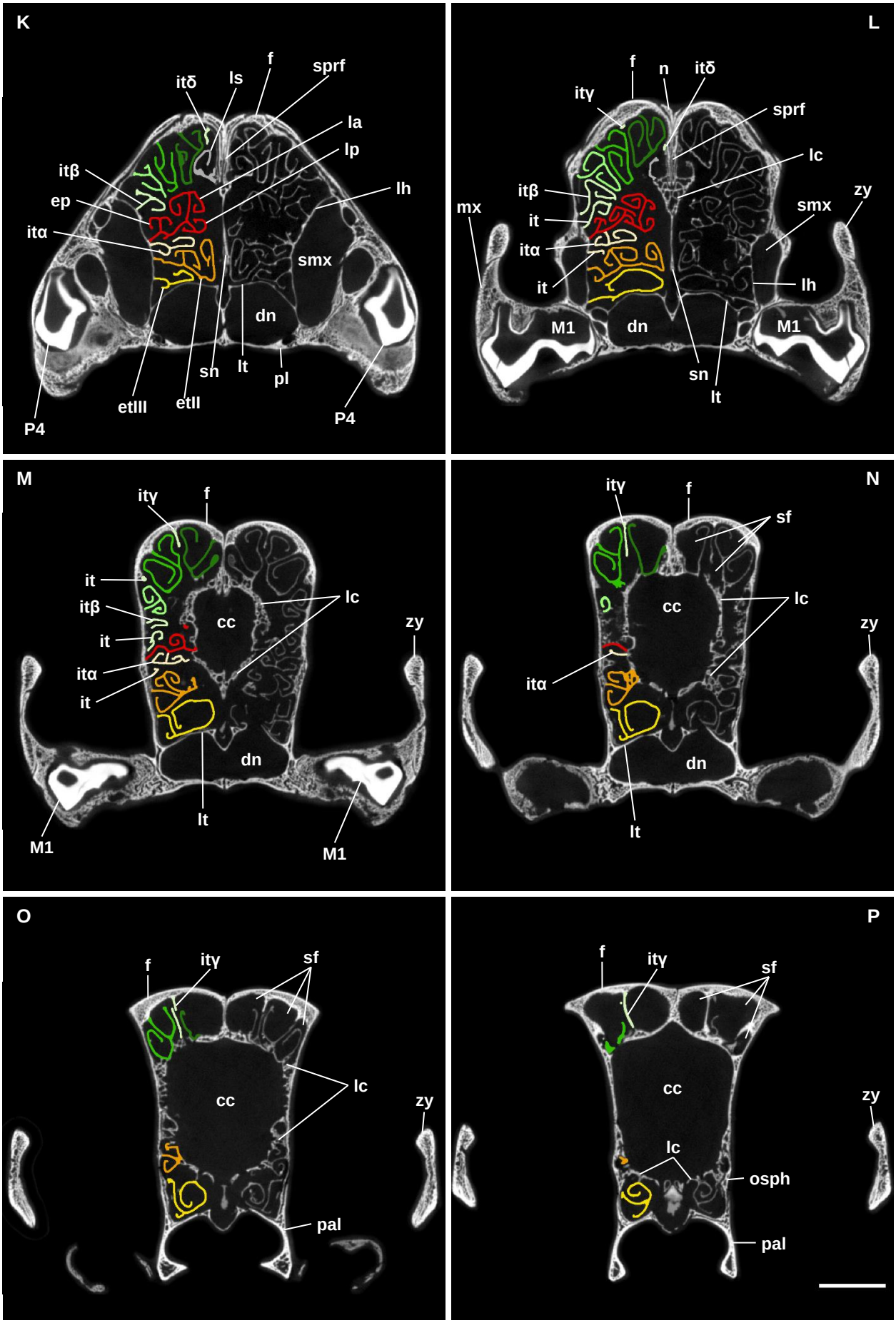

Fig. 10: Juvenile borzoi (SMF 16303, age unknown): **A)** virtual 3D model showing the position of the turbinal skeleton within the transparent nasal cavity in medial view (left side, mirrored); next to it the skull in lateral view showing the region of interest; **B)** virtual 3D model of the turbinal skeleton in medial and **C)** in lateral view (both mirrored); **D)–P)** µCT cross sections of the ethmoidal region from rostral to caudal in caudal view, the turbinals are highlighted on one side. Scale bars: 10mm; Abbreviations: 1; colors refer to the turbinal color code.

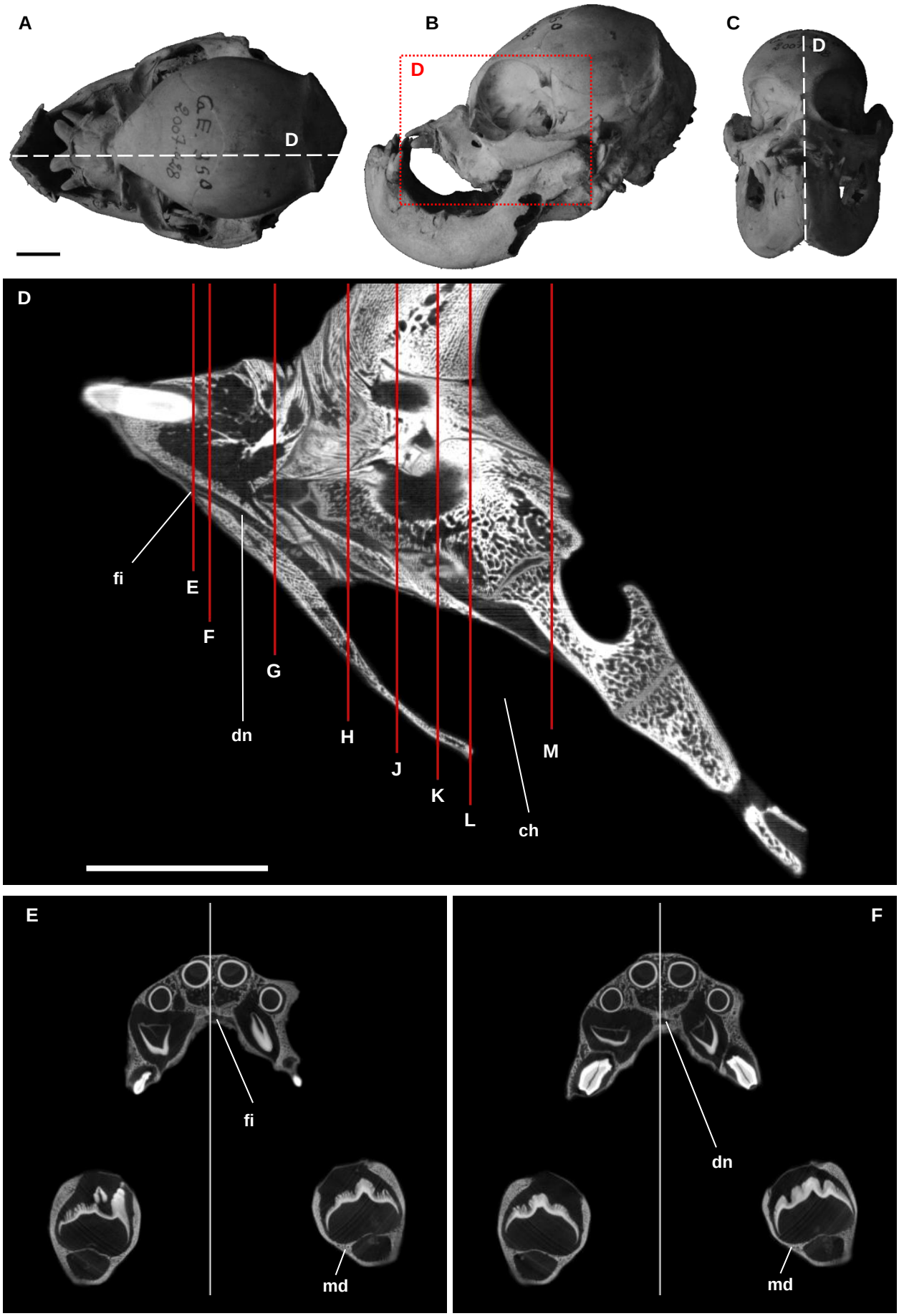

Fig. 11: Juvenile pug (MNHN 2007-428, age unknown), **A)** skull in dorsal, **B)** lateral, **C)** rostral view; marked is the region of the sagittal section from D. **D)** µCT sagittal section, lateral view; the cross sections from E–L are marked; **E–M)** µCT cross sections from rostral to caudal in caudal view, the sagittal section from D is marked. This individual has an extremely deformed skull: a nasal opening is lacking; the unpaired incisive foramen (fi) is covered by residual tissue;... (continued on next page)

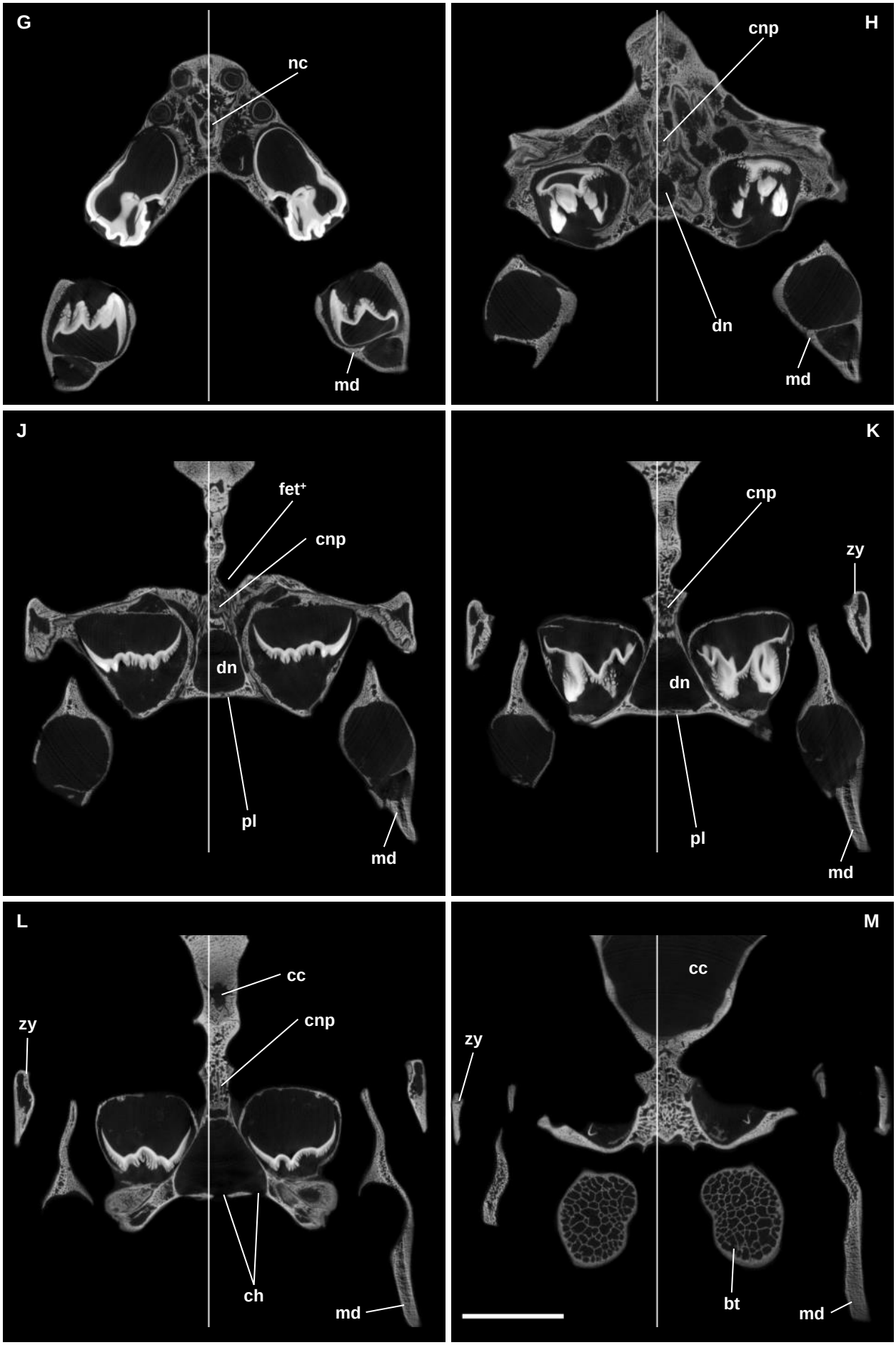

Fig. 11 (continued): ... the rudimentary nasal cavity (nc) has no external connections and the nasal septum is reduced; one ethmoid foramen (fet) for the caudal nasal nerve is present. Generally, *Canis lupus familiaris* has two ethmoid foramina (SCHALLER 1992: 14f; but pekingese SMF 35611 also has just one formamen on ist left side). Scale bars: 10mm; Abbreviations: 1.

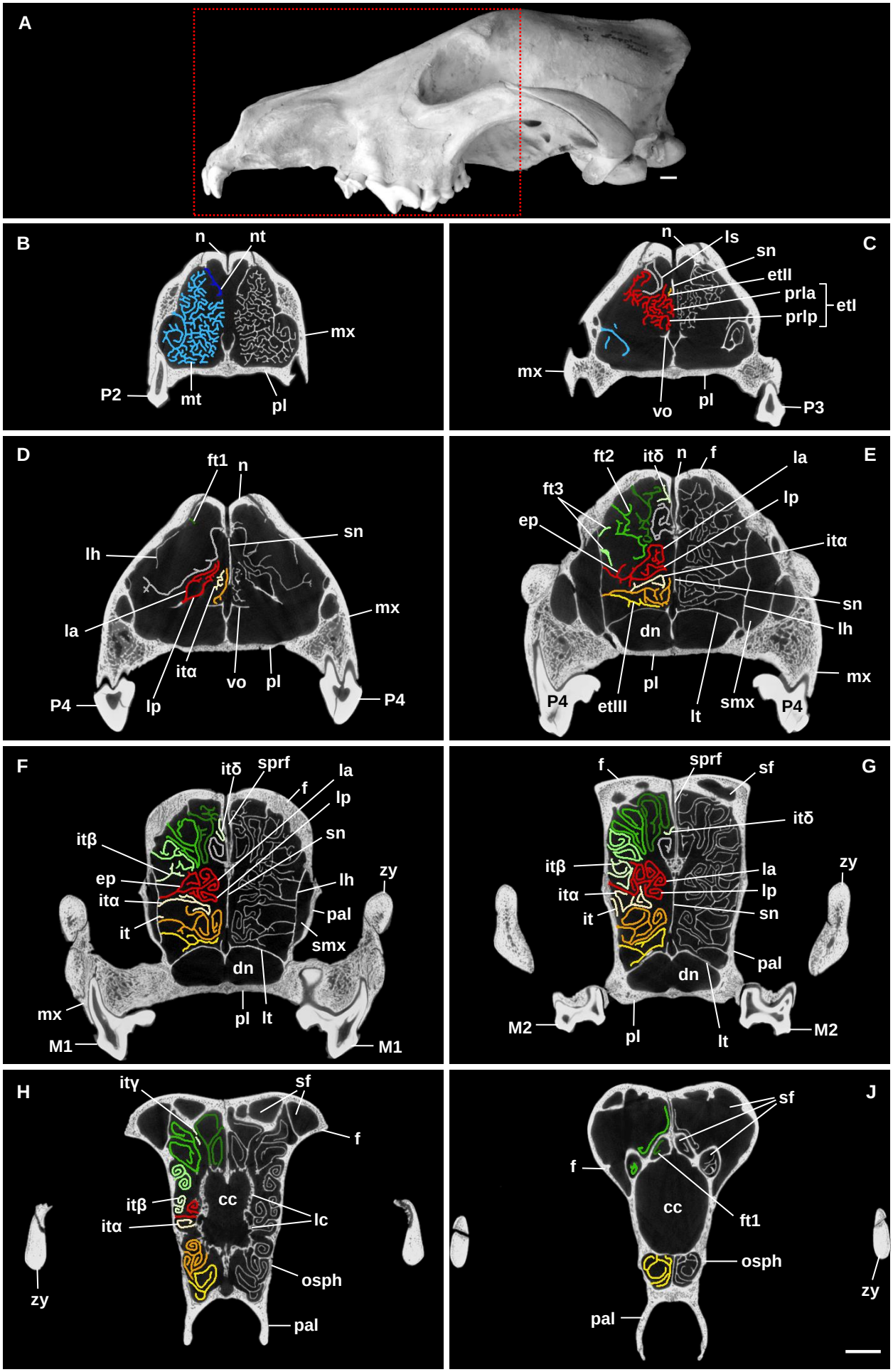

Fig. 12: Eurasian wolf (*Canis lupus lupus*, ZMB_MAM 815): **A)** skull in lateral view showing the region of interest; **B)–J)** µCT cross sections of the ethmoidal region from rostral to caudal in rostral view, the turbinals are highlighted on one side. Scale bars: 10mm; Abbreviations: 1; colors refer to the turbinal color code.

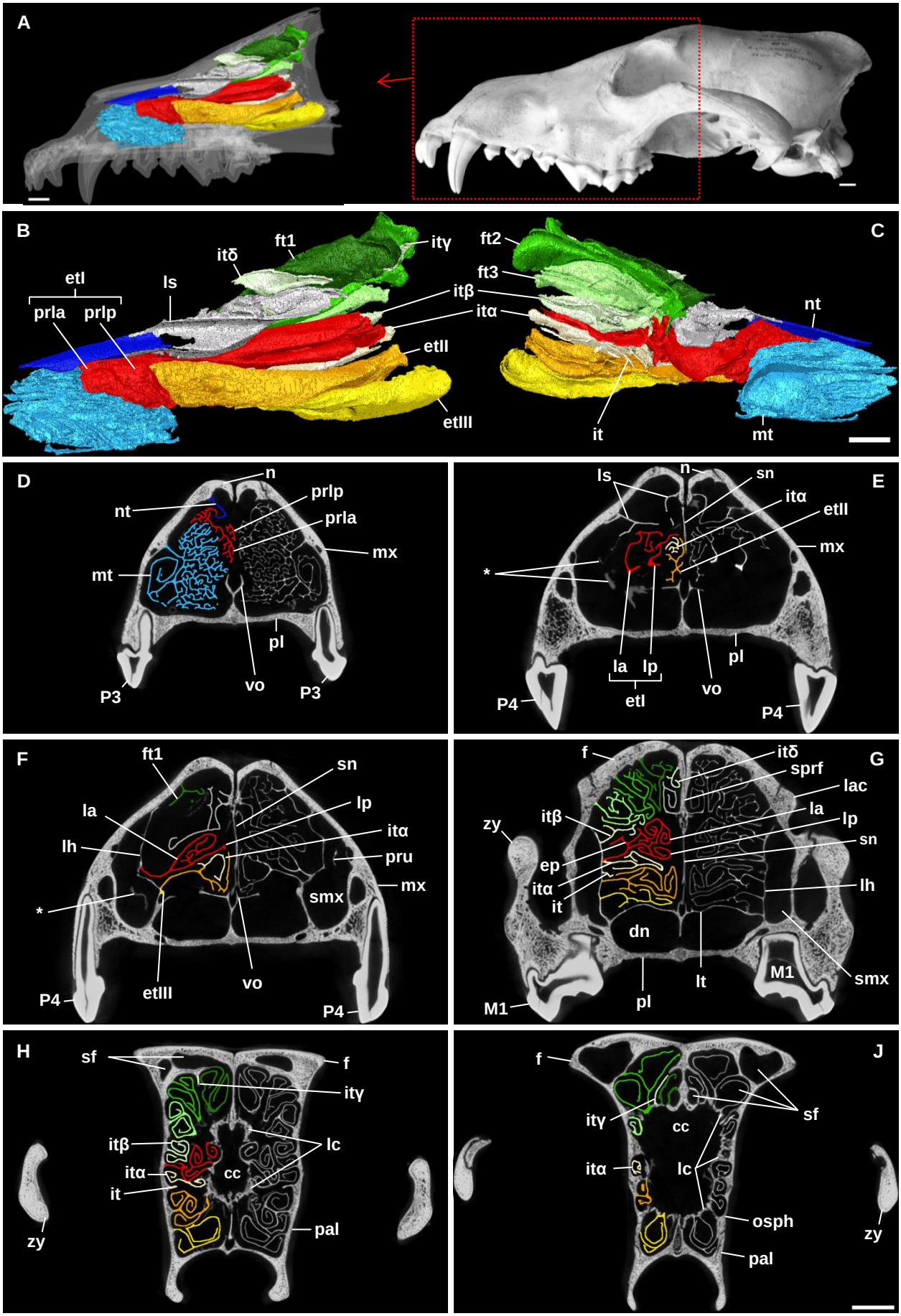

Fig. 13: Eurasian wolf (*Canis lupus lupus*, ZMB_MAM 93307): **A)** virtual 3D model showing the position of the turbinal skeleton within the transparent nasal cavity in medial view (right side); next to it the skull in lateral view showing the region of interest; **B)** virtual 3D model of the turbinal skeleton in medial and **C)** in lateral view; **D)–J)** µCT cross sections of the ethmoidal region from rostral to caudal in rostral view, the turbinals are highlighted on one side. Scale bars: 10mm; Abbreviations: 1; colors refer to the turbinal color code. *on the right side the uncinate process could not be segmented because of covering residual tissue.

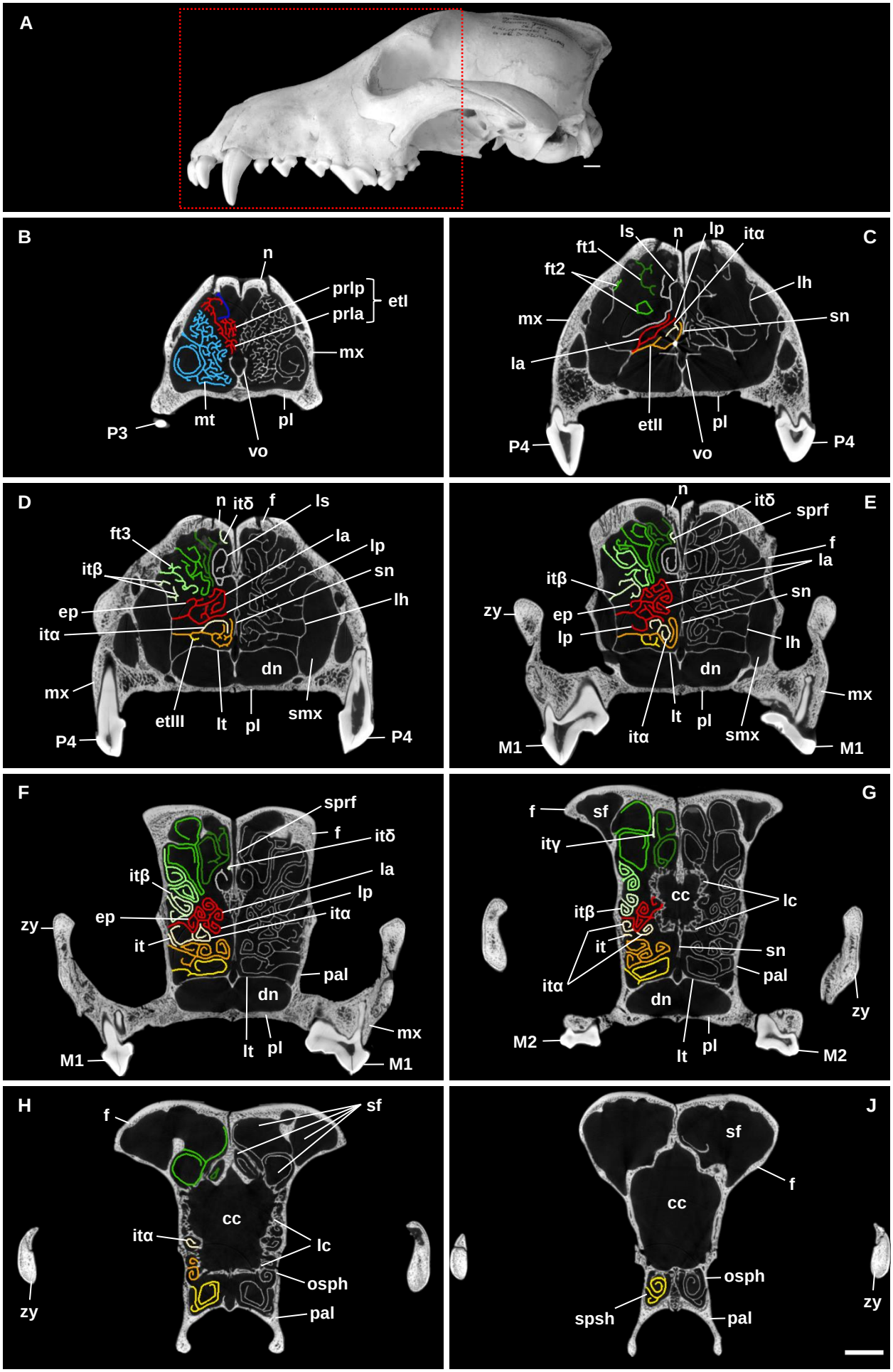

Fig. 14: Eurasian wolf (*Canis lupus lupus*, ZMB_MAM 93308): **A)** skull in lateral view showing the region of interest; **B)–J)** µCT cross sections of the ethmoidal region from rostral to caudal in caudal view, the turbinals are highlighted on one side. Scale bars: 10mm; Abbreviations: 1; colors refer to the turbinal color code.

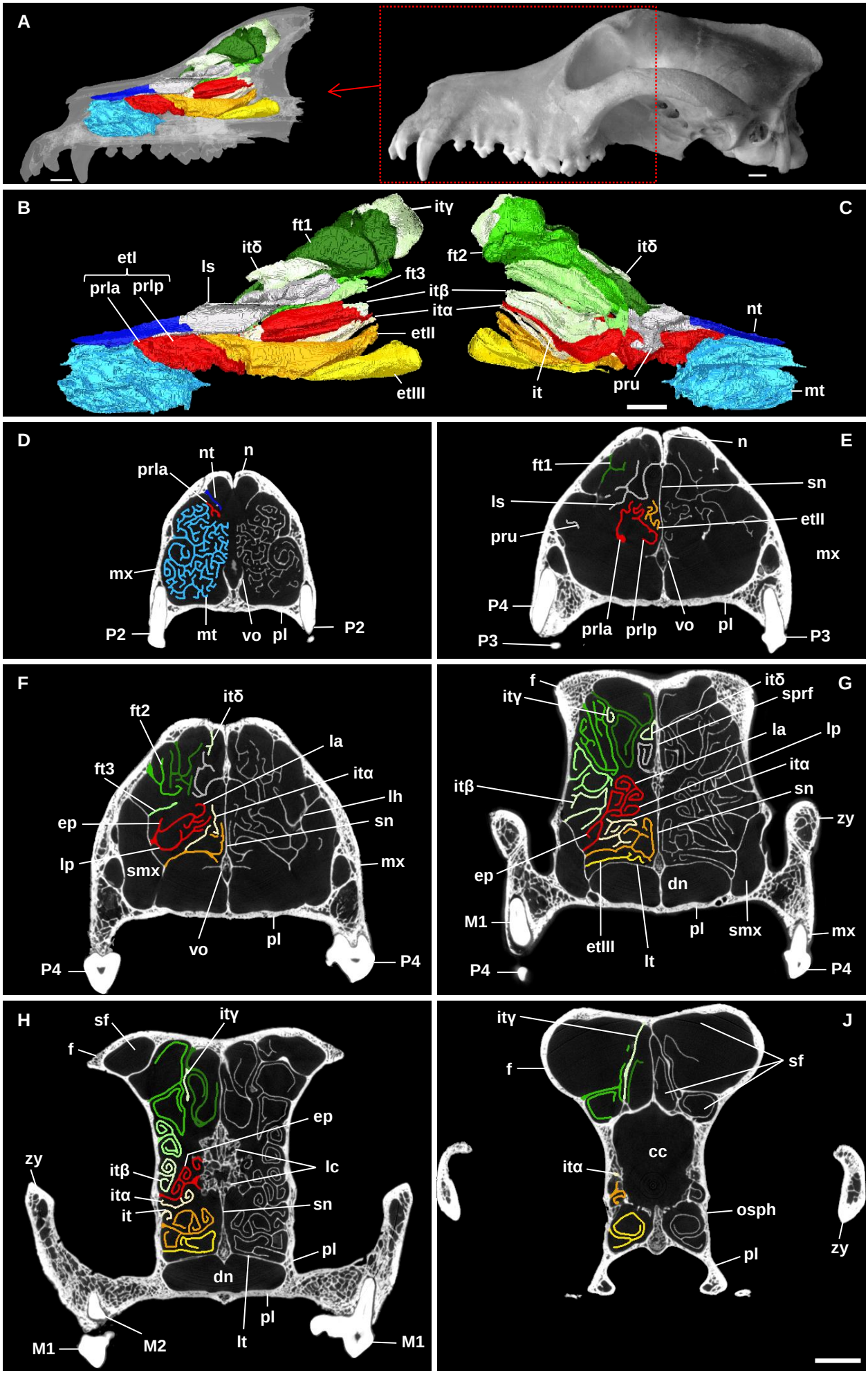

Fig. 15 (description: next page)

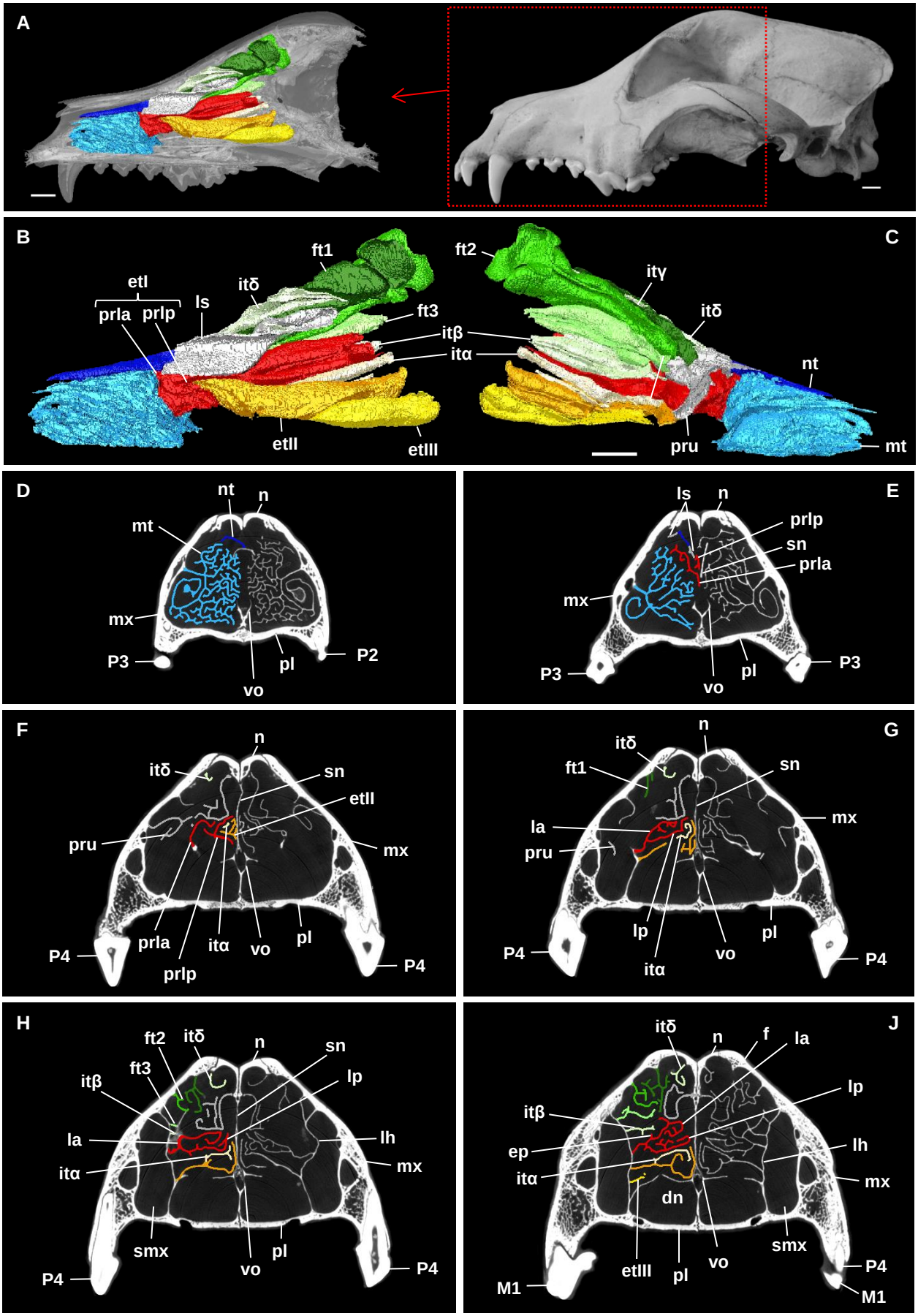

Fig. 16 (description: next page)

◄◄ foregoing page: **Fig. 15:** Adult German shepherd (MNHN 1985-1274): **A)** virtual 3D model showing the position of the turbinal skeleton within the transparent nasal cavity in medial view (right side); next to it the skull in lateral view showing the region of interest; **B)** virtual 3D model of the turbinal skeleton in medial and **C)** in lateral view; **D)–J)** µCT cross sections of the ethmoidal region from rostral to caudal in rostral view, the turbinals are highlighted on one side. Scale bars: 10mm; Abbreviations: 1; colors refer to the turbinal color code.

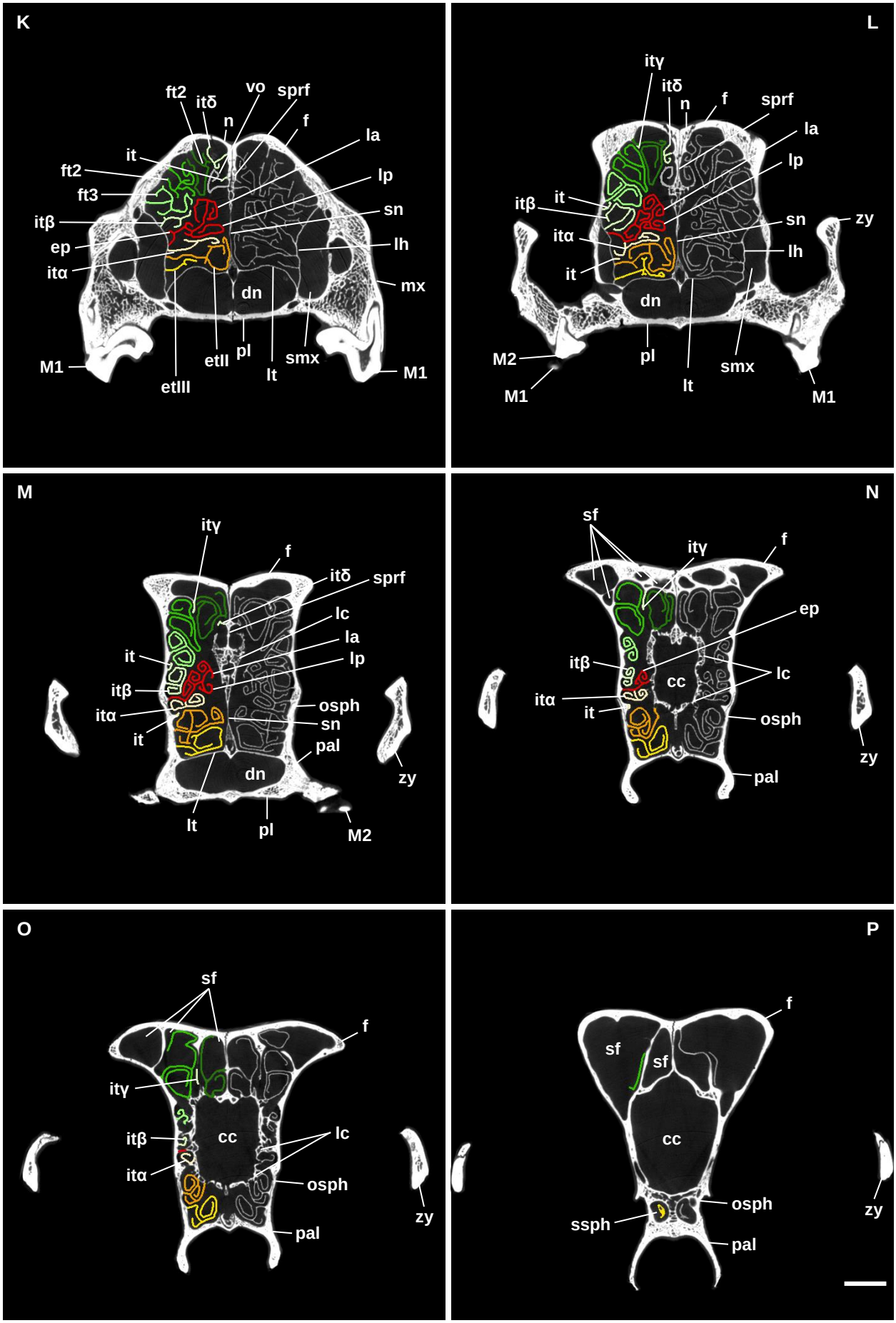

Fig. 16: Adult German shepherd (SMF 93607): **A)** virtual 3D model showing the position of the turbinal skeleton within the transparent nasal cavity in medial view (right side); next to it the skull in lateral view showing the region of interest; **B)** virtual 3D model of the turbinal skeleton in medial and **C)** in lateral view; **D)–P)** µCT cross sections of the ethmoidal region from rostral to caudal in rostral view, the turbinals are highlighted on one side. Scale bars: 10mm; Abbreviations: 1; colors refer to the turbinal color code.

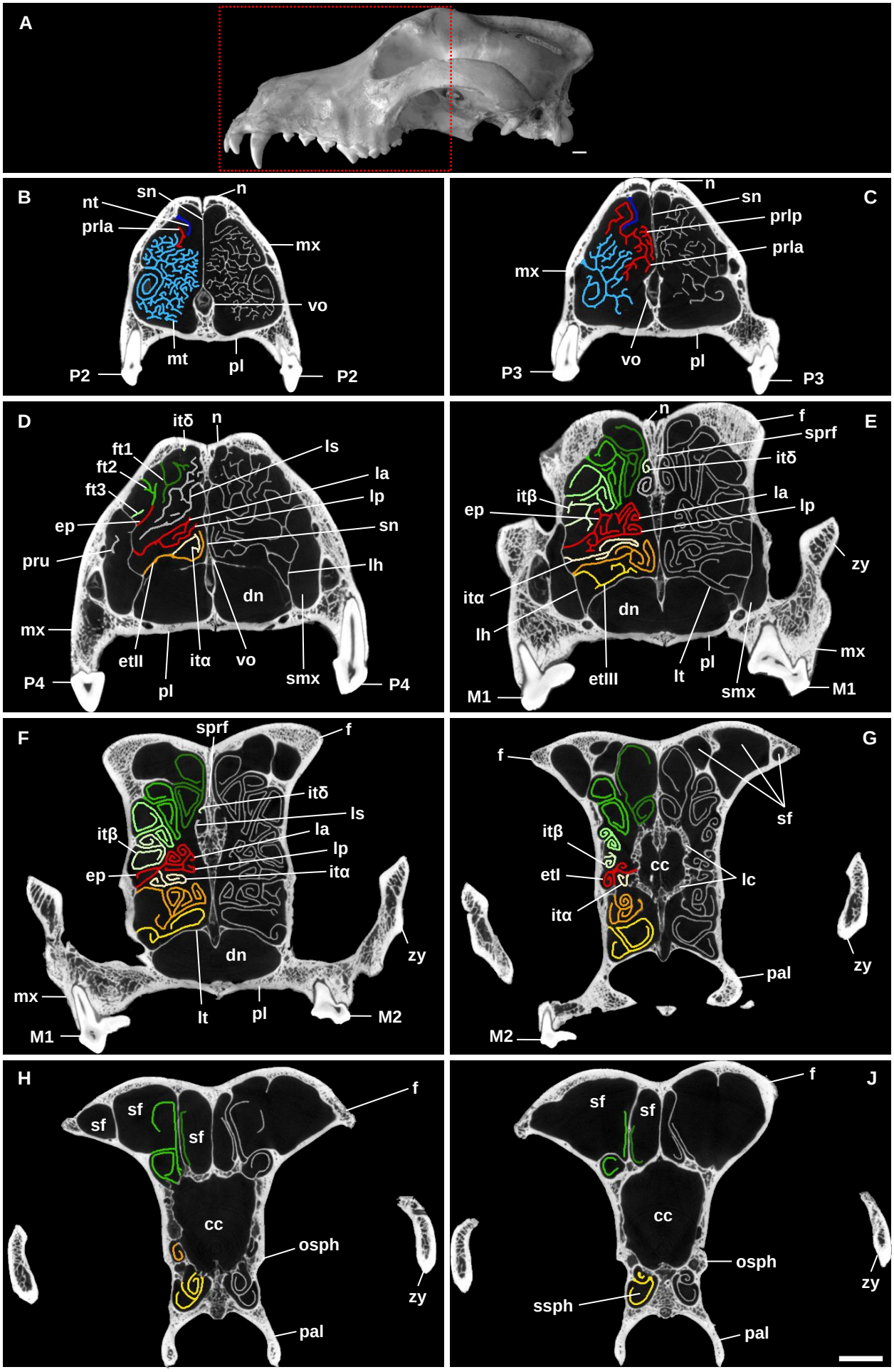

Fig. 17: Groenendael (MNHN 1985-1216): **A)** skull in lateral view showing the region of interest; **B)–J)** µCT cross sections of the ethmoidal region from rostral to caudal in caudal view, the turbinals are highlighted on one side. Scale bars: 10mm; Abbreviations: 1; colors refer to the turbinal color code.

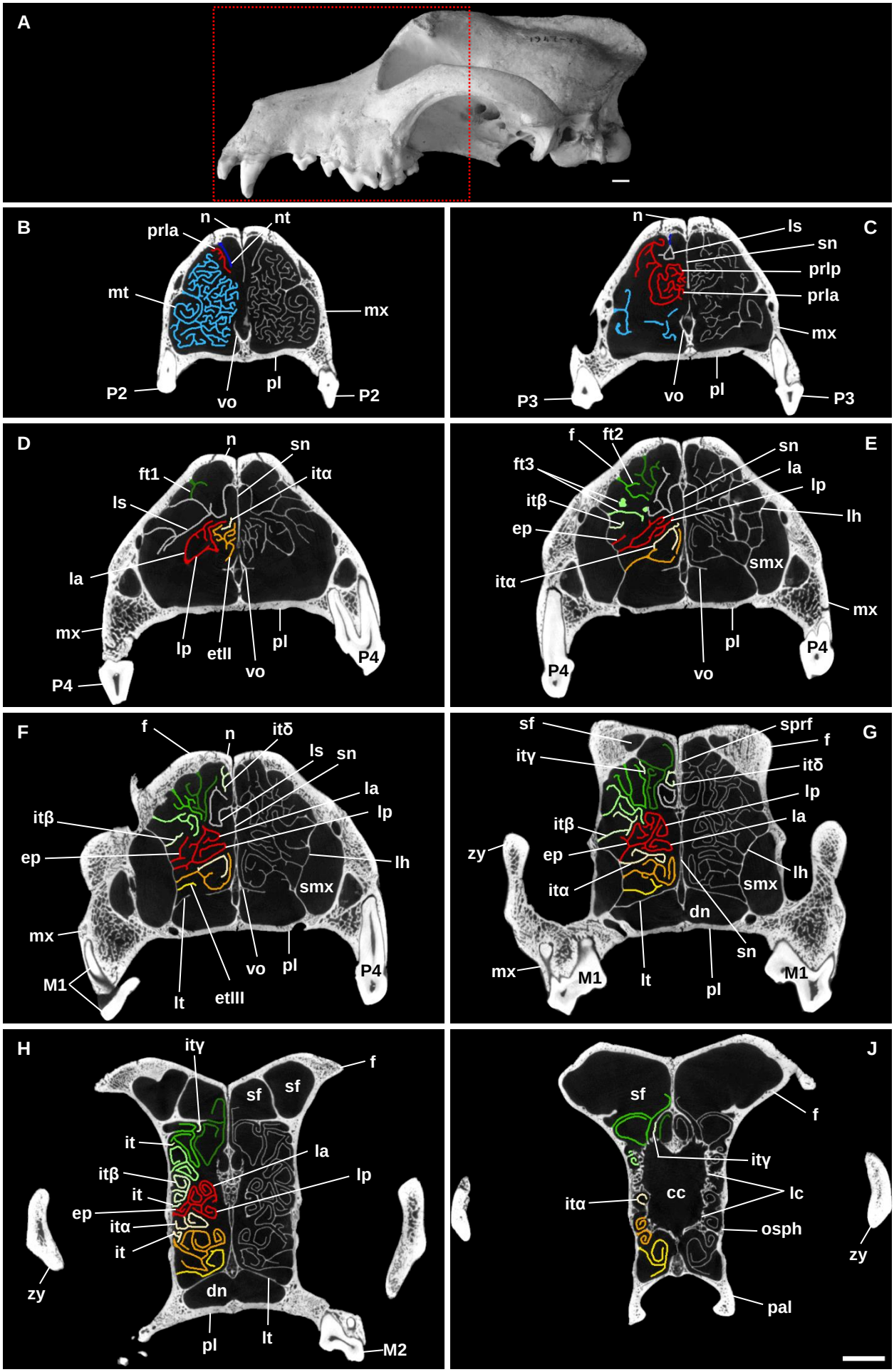

Fig. 18: Greenland dog (MNHN 1947-78): **A)** skull in lateral view showing the region of interest; **B)–J)** µCT cross sections of the ethmoidal region from rostral to caudal in caudal view, the turbinals are highlighted on one side. Scale bars: 10mm; Abbreviations: 1; colors refer to the turbinal color code.

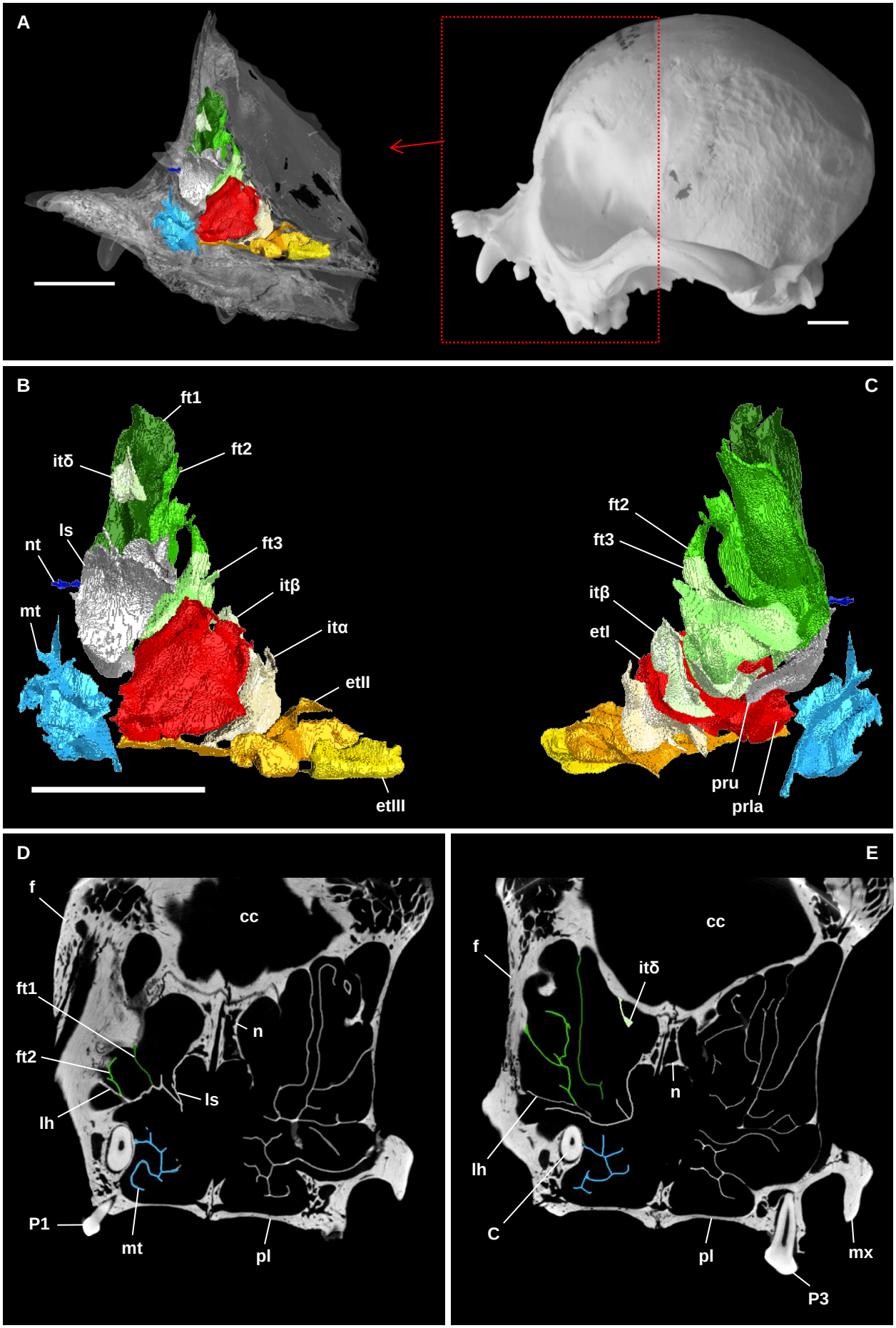

Fig. 19: King spaniel (NMBE 1051945): **A)** virtual 3D model showing the position of the turbinal skeleton within the transparent nasal cavity in medial view (left side, mirrored); next to it the skull in lateral view showing the region of interest; **B)** virtual 3D model of the turbinal skeleton in medial and **C)** in lateral view (both mirrored); **D)–L)** µCT cross sections of the ethmoidal region from rostral to caudal in caudal view, the turbinals are highlighted on one side. Scale bars: 10mm; Abbreviations: 1; colors refer to the turbinal color code.

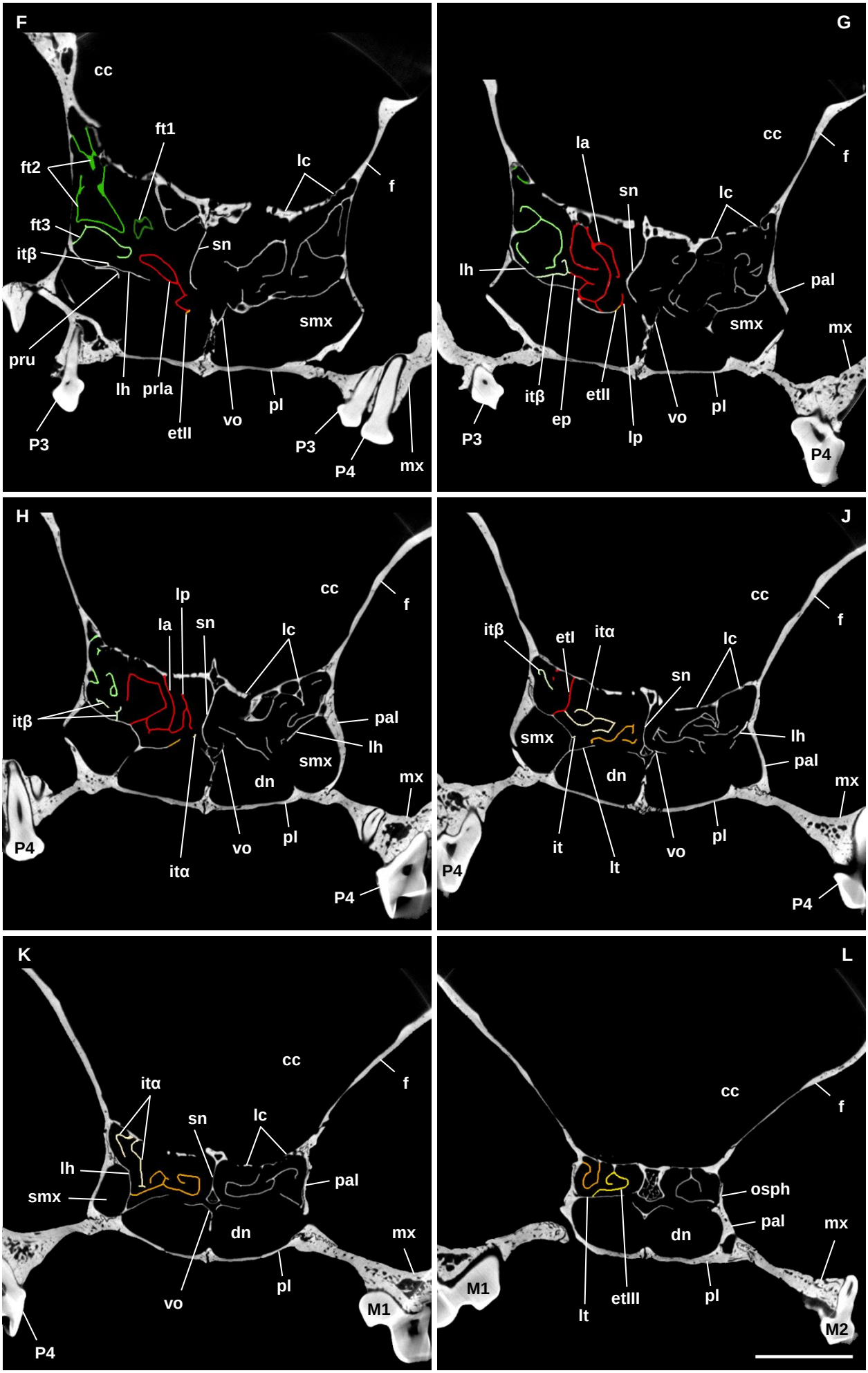

Fig. 19 (continued)

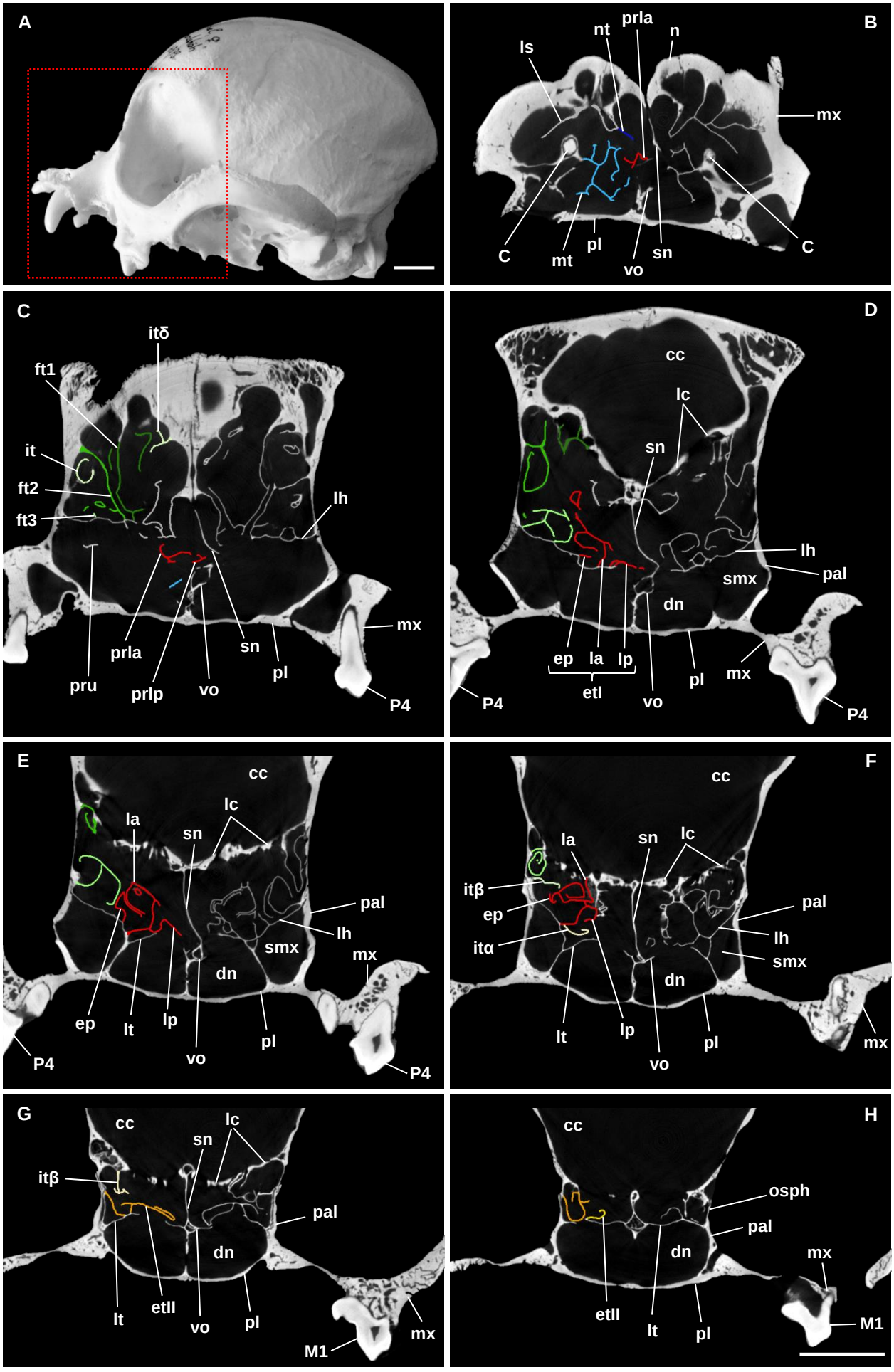

Fig. 20: King spaniel (NMBE 1051948): **A)** skull in lateral view showing the region of interest; **B)–H)** µCT cross sections of the ethmoidal region from rostral to caudal in caudal view, the turbinals are highlighted on one side. Scale bars: 10mm; Abbreviations: 1; colors refer to the turbinal color code.

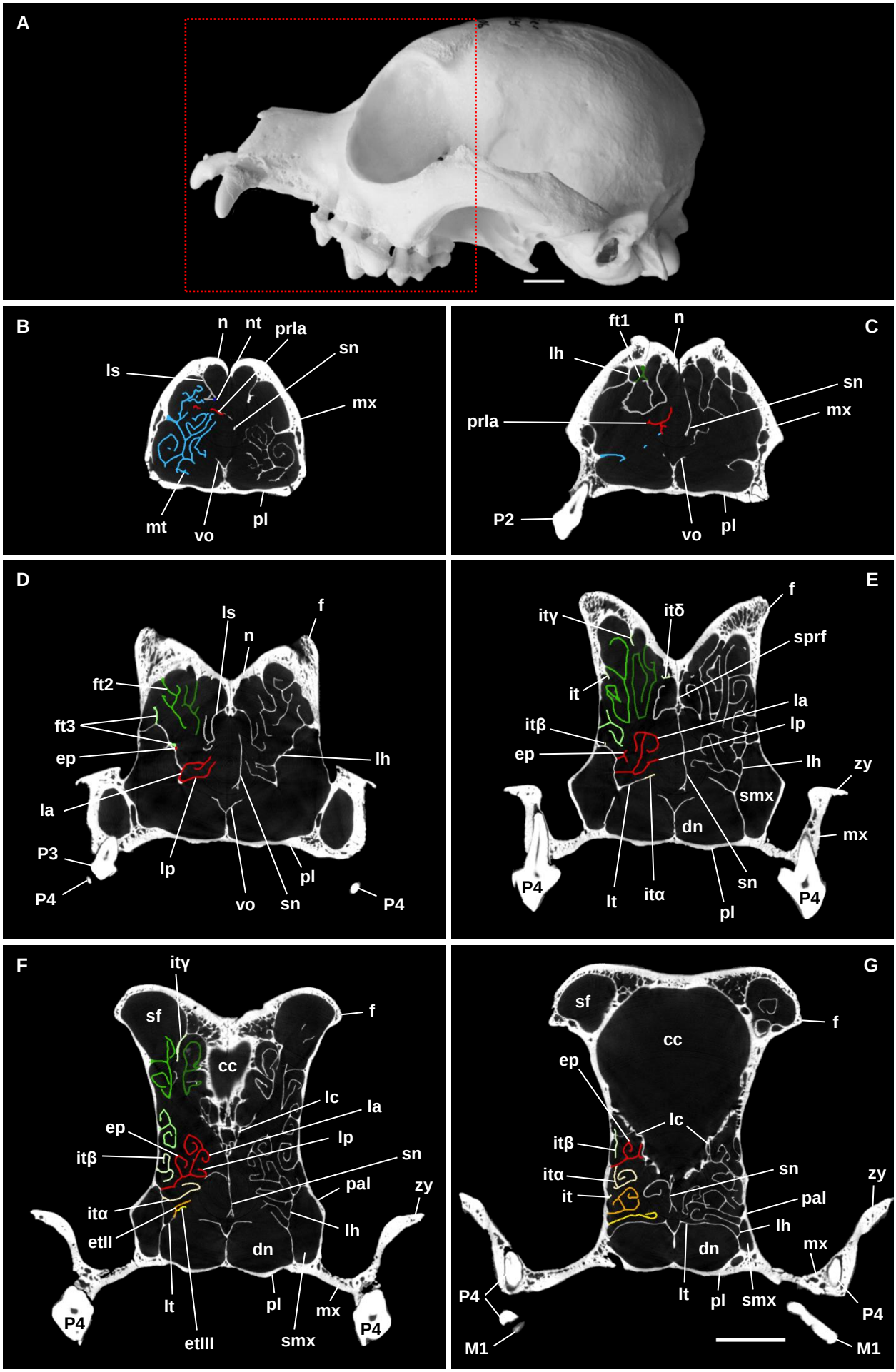

Fig. 21: Cavalier (NMBE 1059207): **A)** skull in lateral view showing the region of interest; **B)–J)** µCT cross sections of the ethmoidal region from rostral to caudal in caudal view, the turbinals are highlighted on one side. Scale bars: 10mm; Abbreviations: 1; colors refer to the turbinal color code.

FIGURES

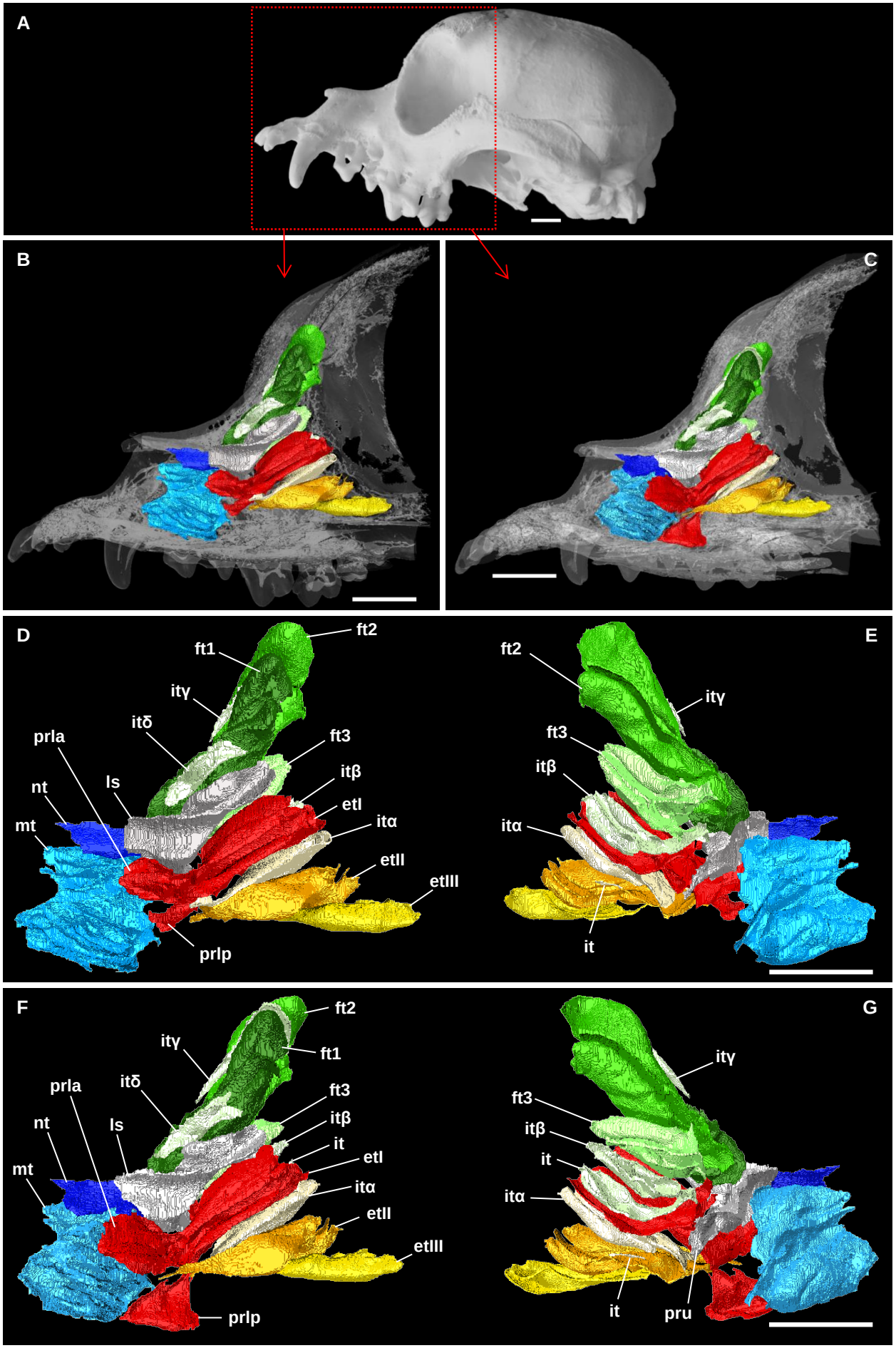

Fig. 22: Cavalier (NMBE 1062998): **A)** skull in lateral view showing the region of interest; **B)** position of the left (mirrored) and **C)** right turbinal skeleton within the transparent nasal cavity, both in medial view; **D)** virtual 3D model of the left turbinal skeleton in medial and **E)** in lateral view (both mirrored); **F)** virtual 3D model of the right turbinal skeleton in medial and **G)** in lateral view;... (continued on next page)

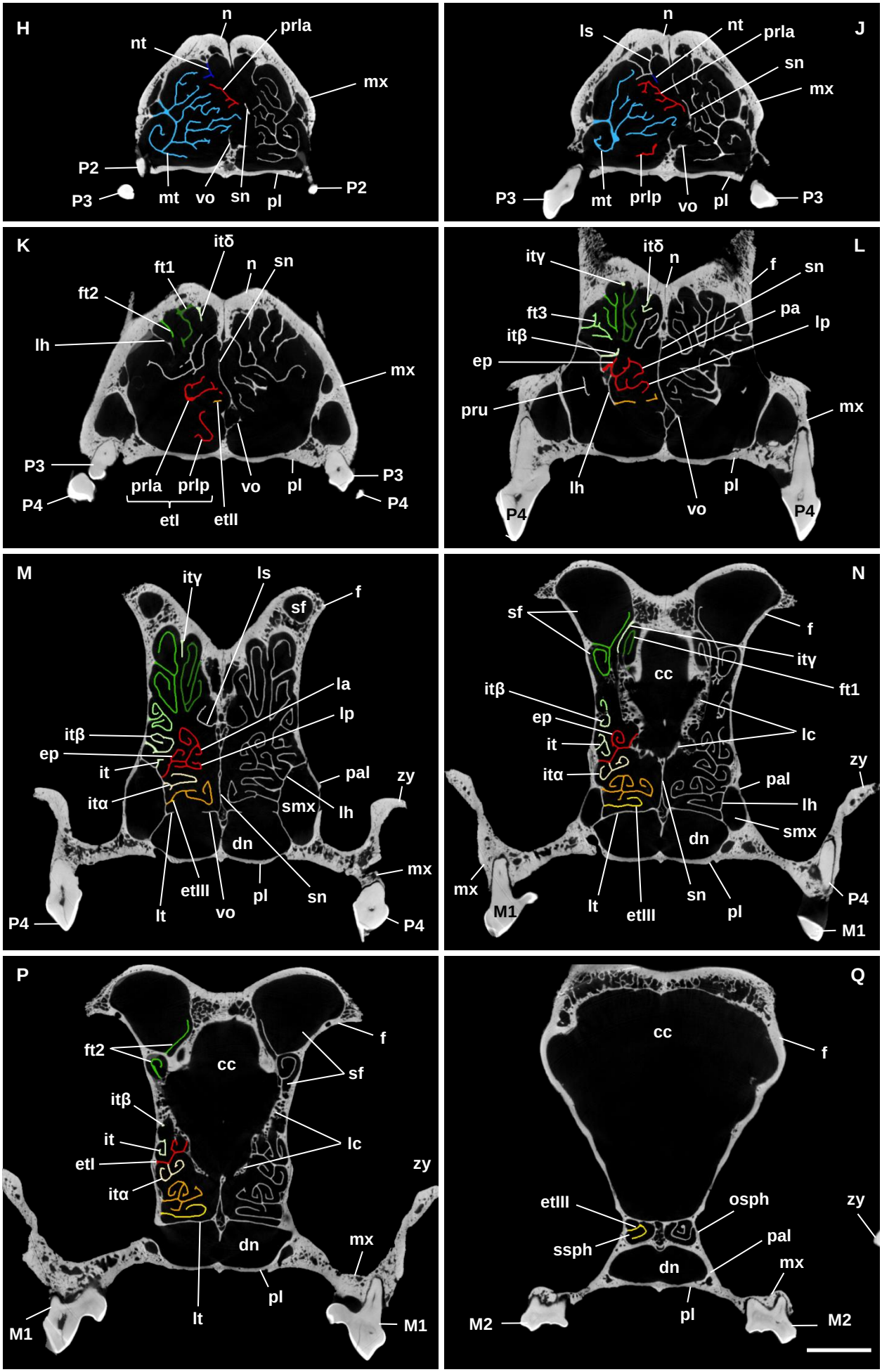

Fig. 22 (continued): ... **H)–Q)** µCT cross sections of the ethmoidal region from rostral to caudal in rostral view, the turbinals are highlighted on one side. Scale bars: 10mm; Abbreviations: 1; colors refer to the turbinal color code.

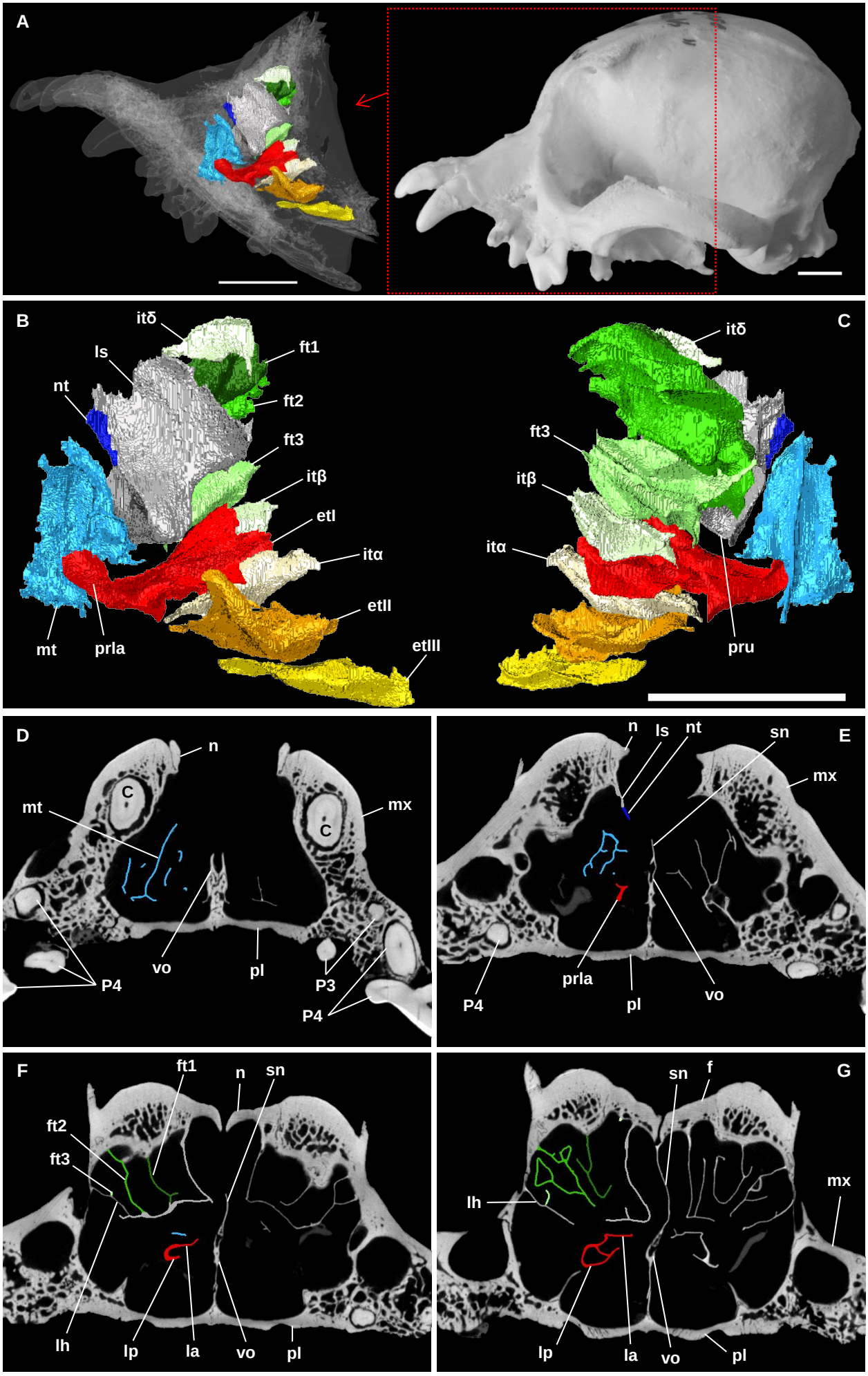

Fig. 23 (description: next page)

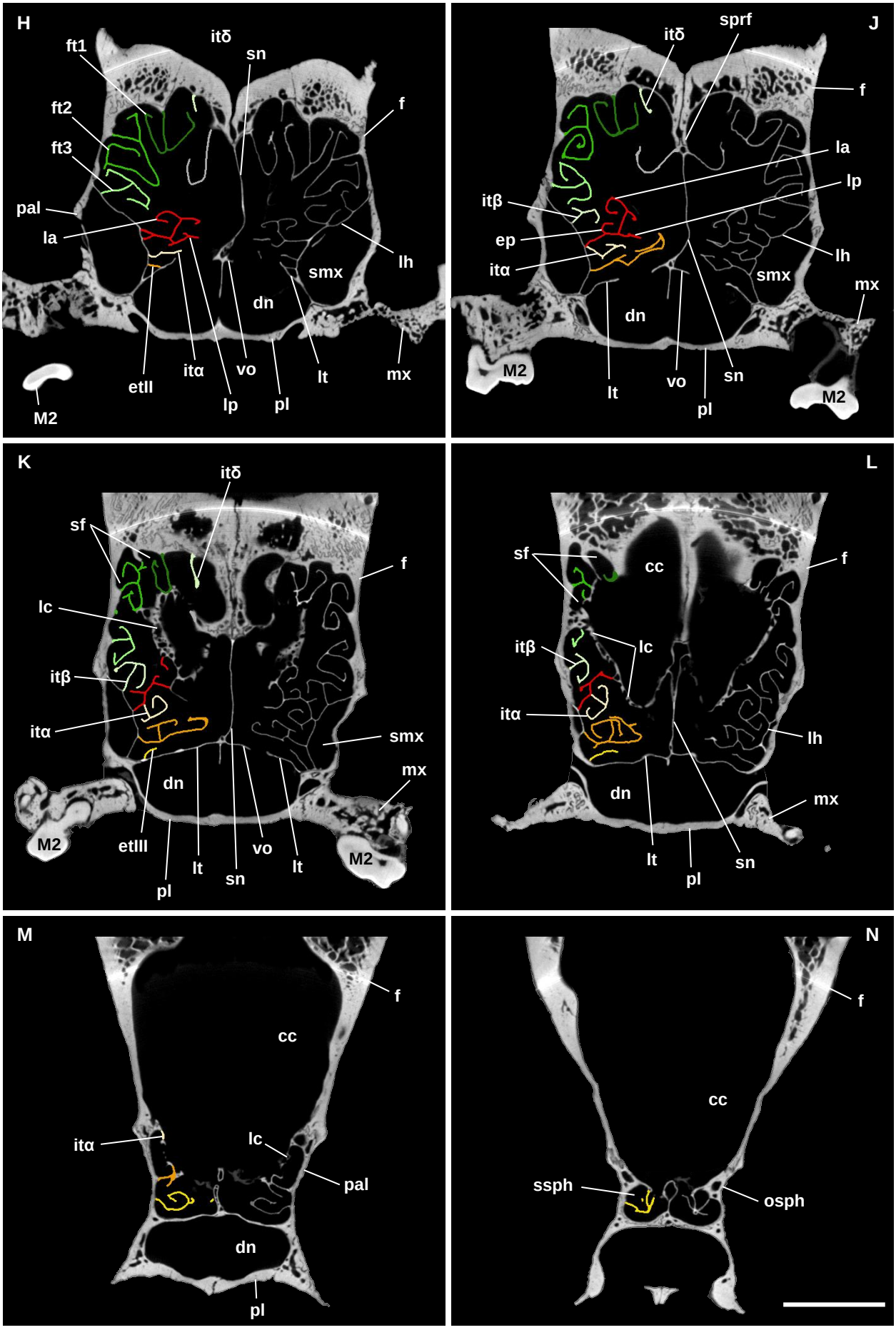

Fig. 23: Pekingese (NMBE 1051962): **A)** virtual 3D model showing the position of the turbinal skeleton within the transparent nasal cavity in medial view (right side); next to it the skull in lateral view showing the region of interest; **B)** virtual 3D model of the turbinal skeleton in medial and **C)** in lateral view; **D)–N)** µCT cross sections of the ethmoidal region from rostral to caudal in rostral view, the turbinals are highlighted on one side. Scale bars: 10mm; Abbreviations: 1; colors refer to the turbinal color code.

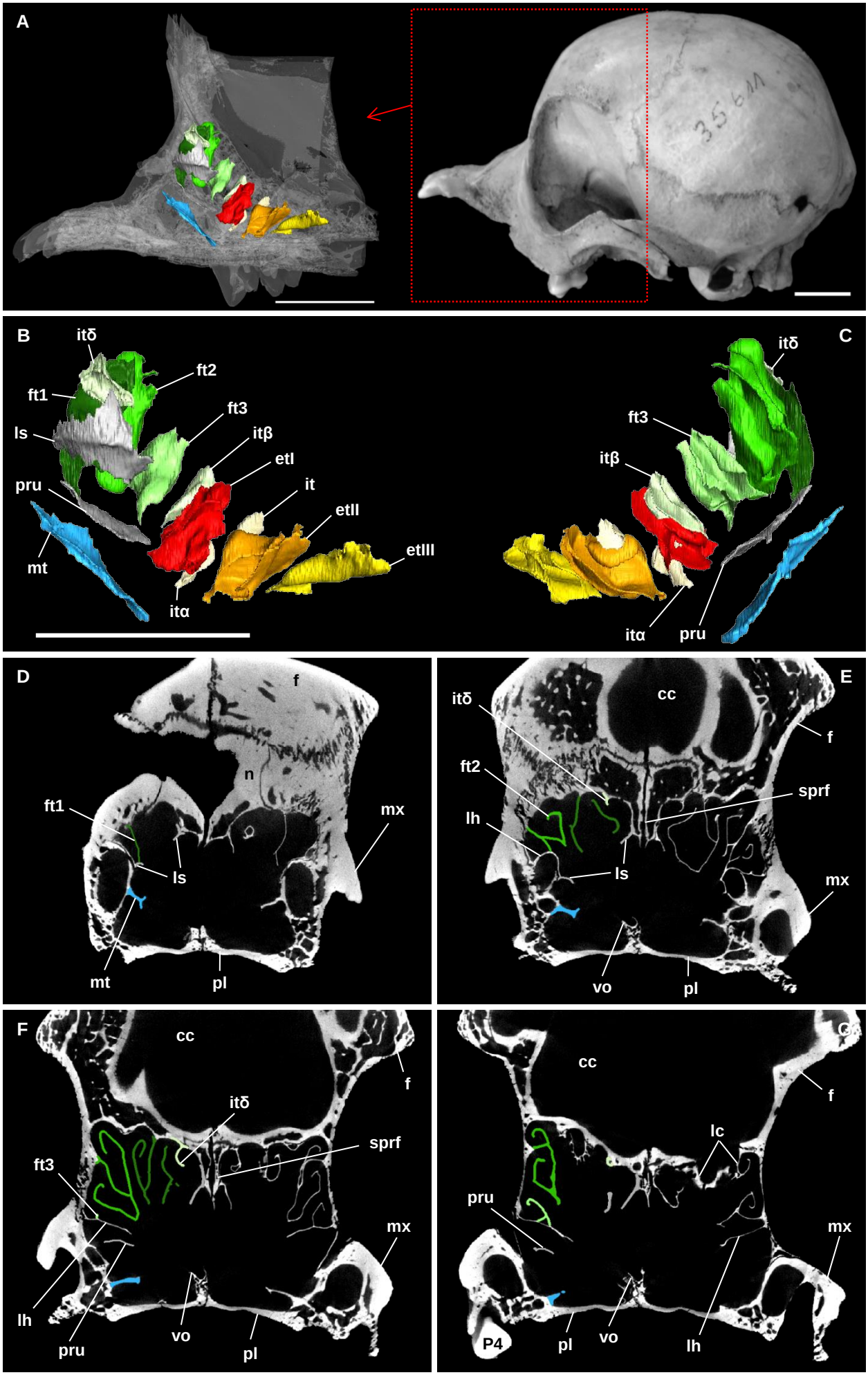

Fig. 24 (description: next page)

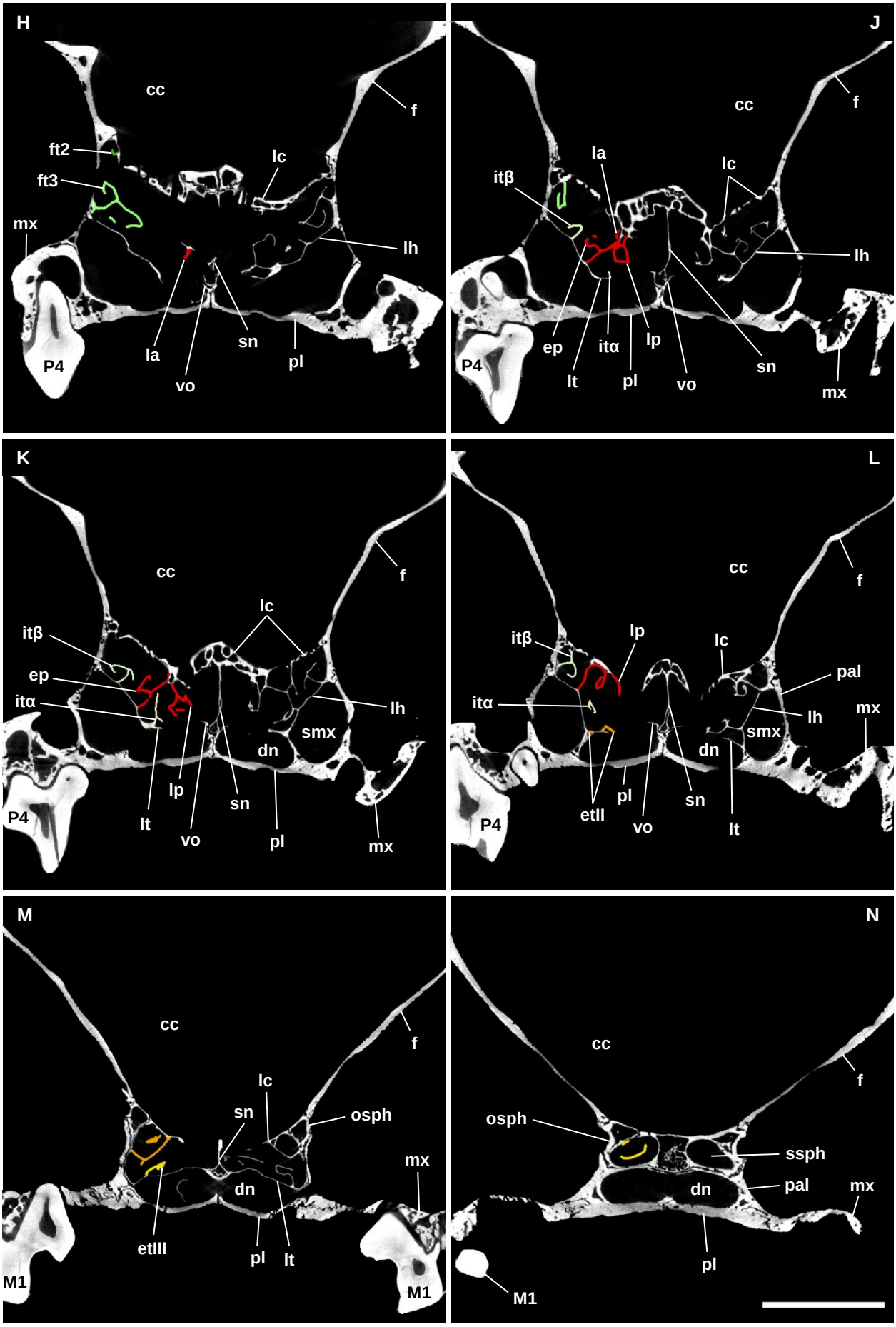

Fig. 24: Pekingese (SMF 35611): **A)** virtual 3D model showing the position of the turbinal skeleton within the transparent nasal cavity in medial view (right side); next to it the skull in lateral view showing the region of interest; **B)** virtual 3D model of the turbinal skeleton in medial and **C)** in lateral view; **D)–N)** µCT cross sections of the ethmoidal region from rostral to caudal in rostral view, the turbinals are highlighted on one side. Scale bars: 10mm; Abbreviations: 1; colors refer to the turbinal color code.

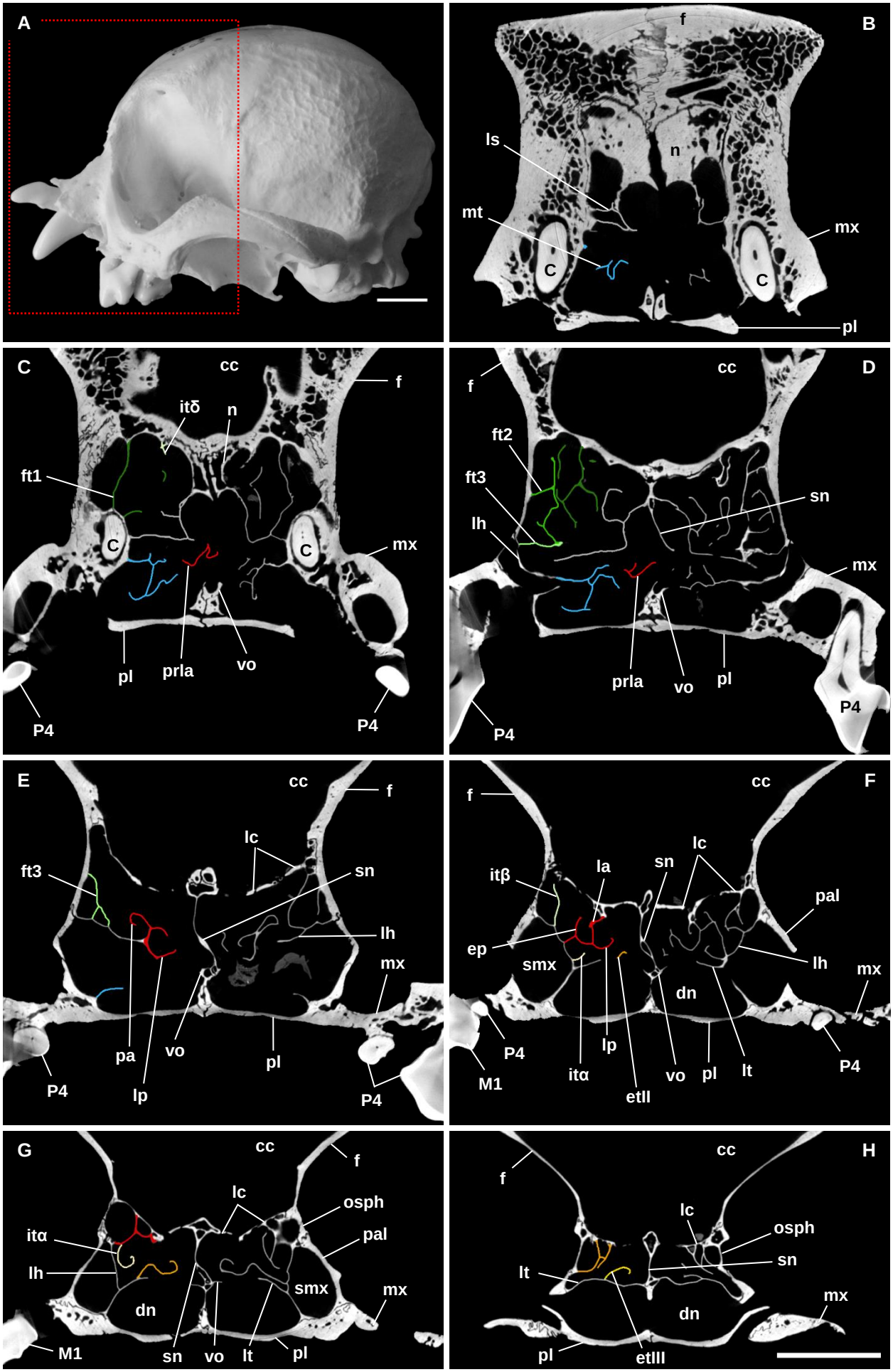

Fig. 25: Pekingese (NMBE 1051965): **A)** skull in lateral view showing the region of interest; **B)–H)** µCT cross sections of the ethmoidal region from rostral to caudal in caudal view, the turbinals are highlighted on one side. Scale bars: 10mm; Abbreviations: 1; colors refer to the turbinal color code.

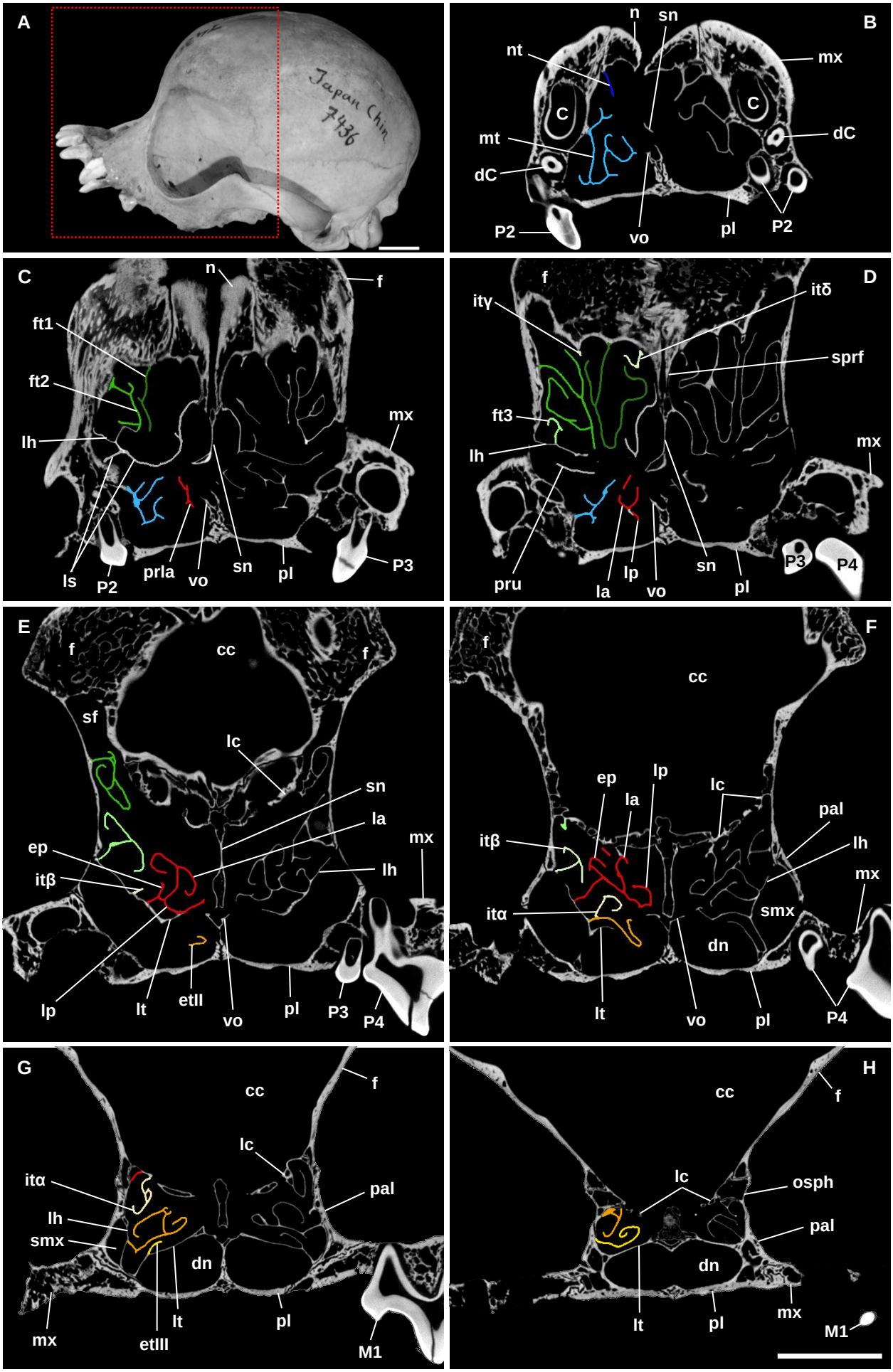

Fig. 26: Chin (ZMB_MAM 7436): **A)** skull in lateral view showing the region of interest; **B)–J)** µCT cross sections of the ethmoidal region from rostral to caudal in caudal view, the turbinals are highlighted on one side. Scale bars: 10mm; Abbreviations: 1; colors refer to the turbinal color code.

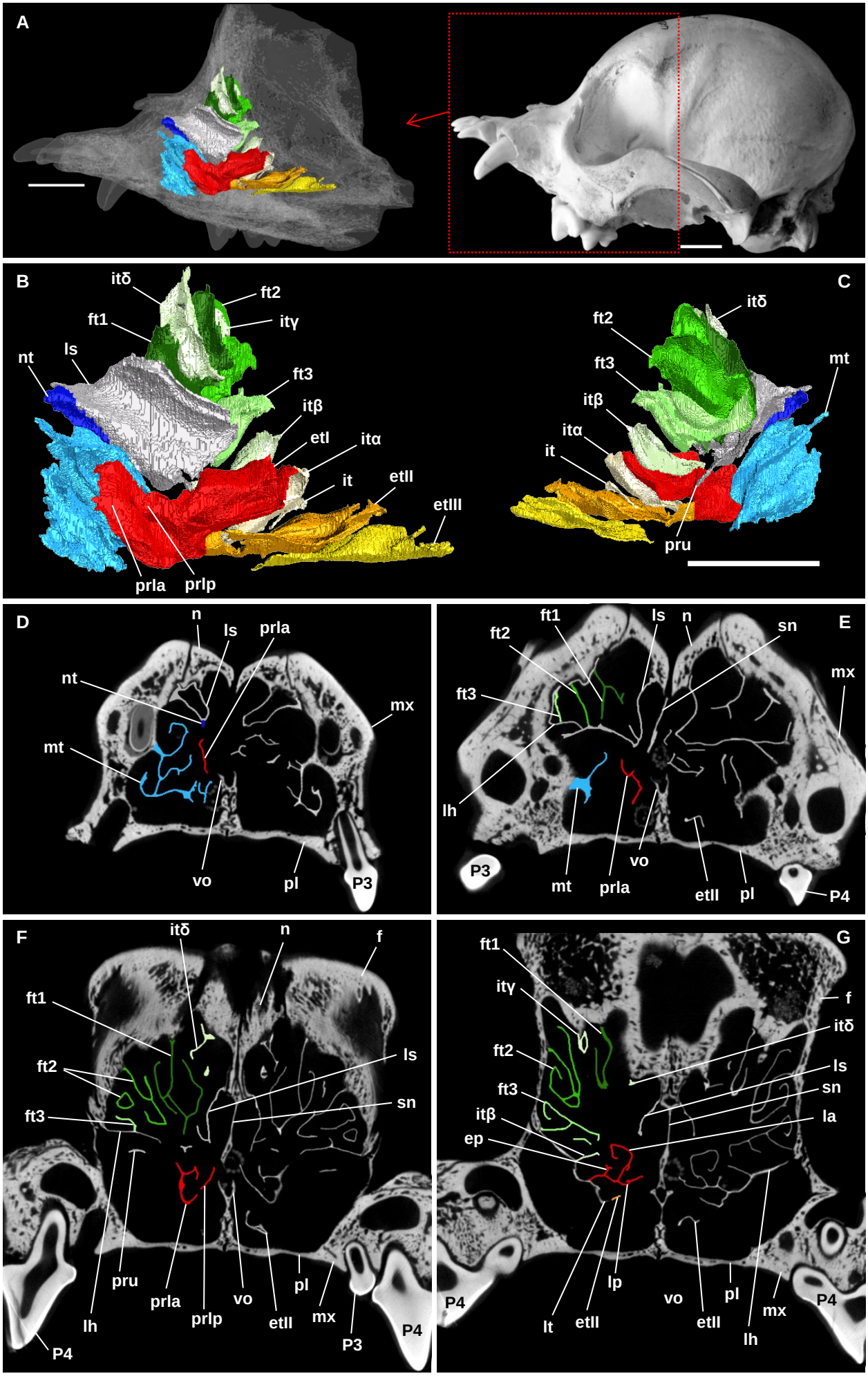

Fig. 27 (description: next page)

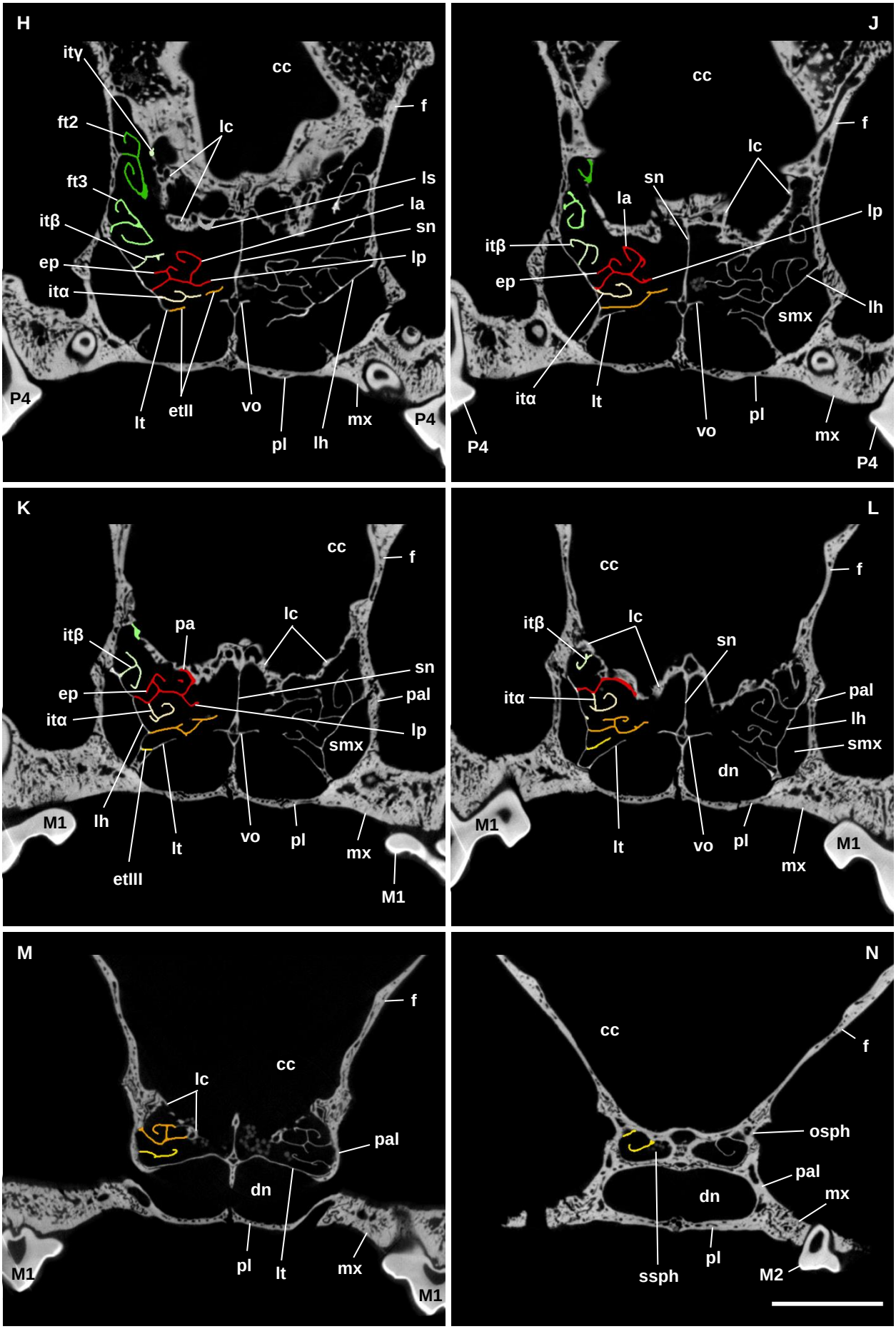

Fig. 27: Chin (NMBE 1051951): **A)** virtual 3D model showing the position of the turbinal skeleton within the transparent nasal cavity in medial view (left side, mirrored); next to it the skull in lateral view showing the region of interest; **B)** virtual 3D model of the turbinal skeleton in medial and **C)** in lateral view (both mirrored); **D)–N)** µCT cross sections of the ethmoidal region from rostral to caudal in caudal view, the turbinals are highlighted on one side. Scale bars: 10mm; Abbreviations: 1; colors refer to the turbinal color code.

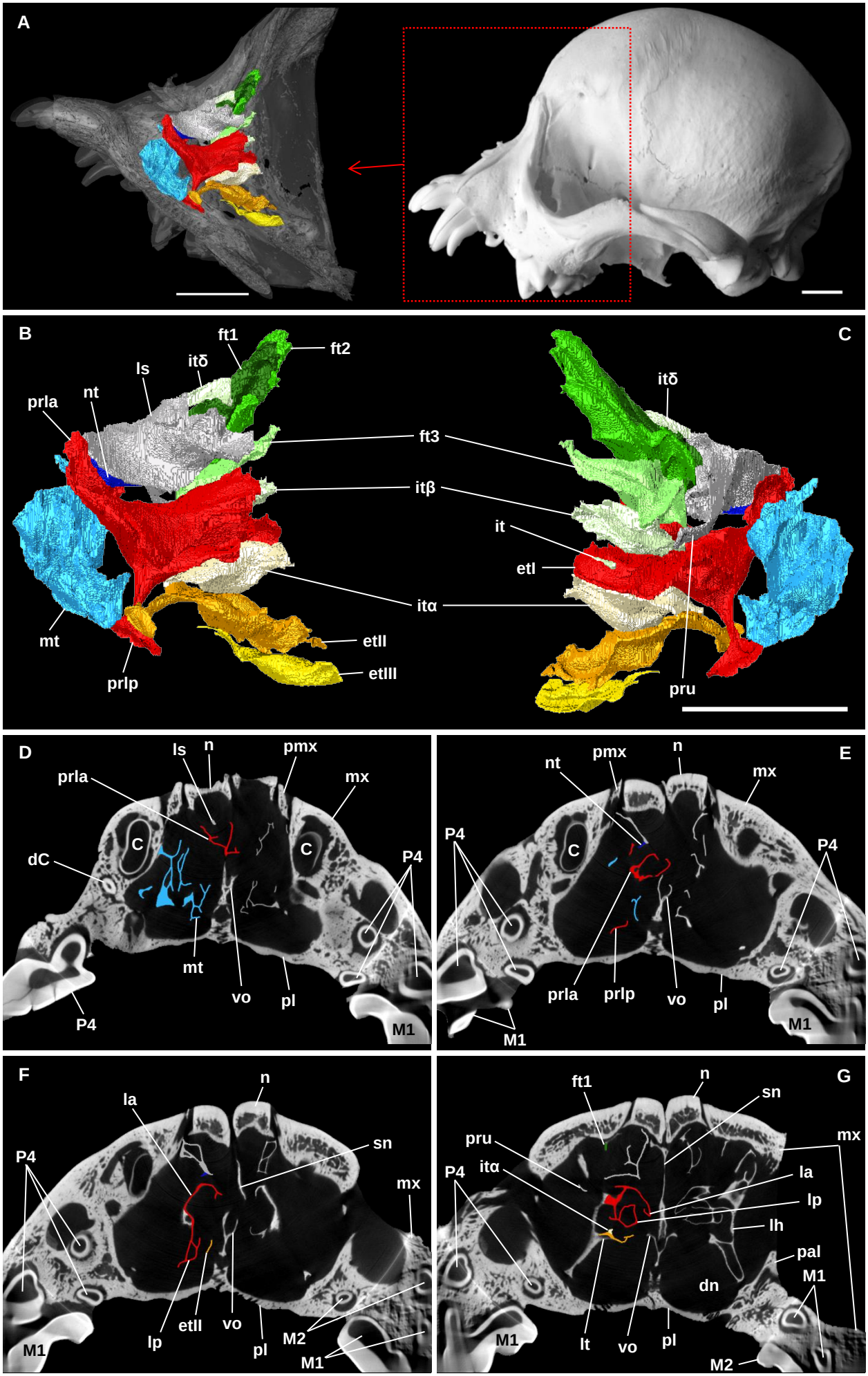

Fig. 28 (description: next page)

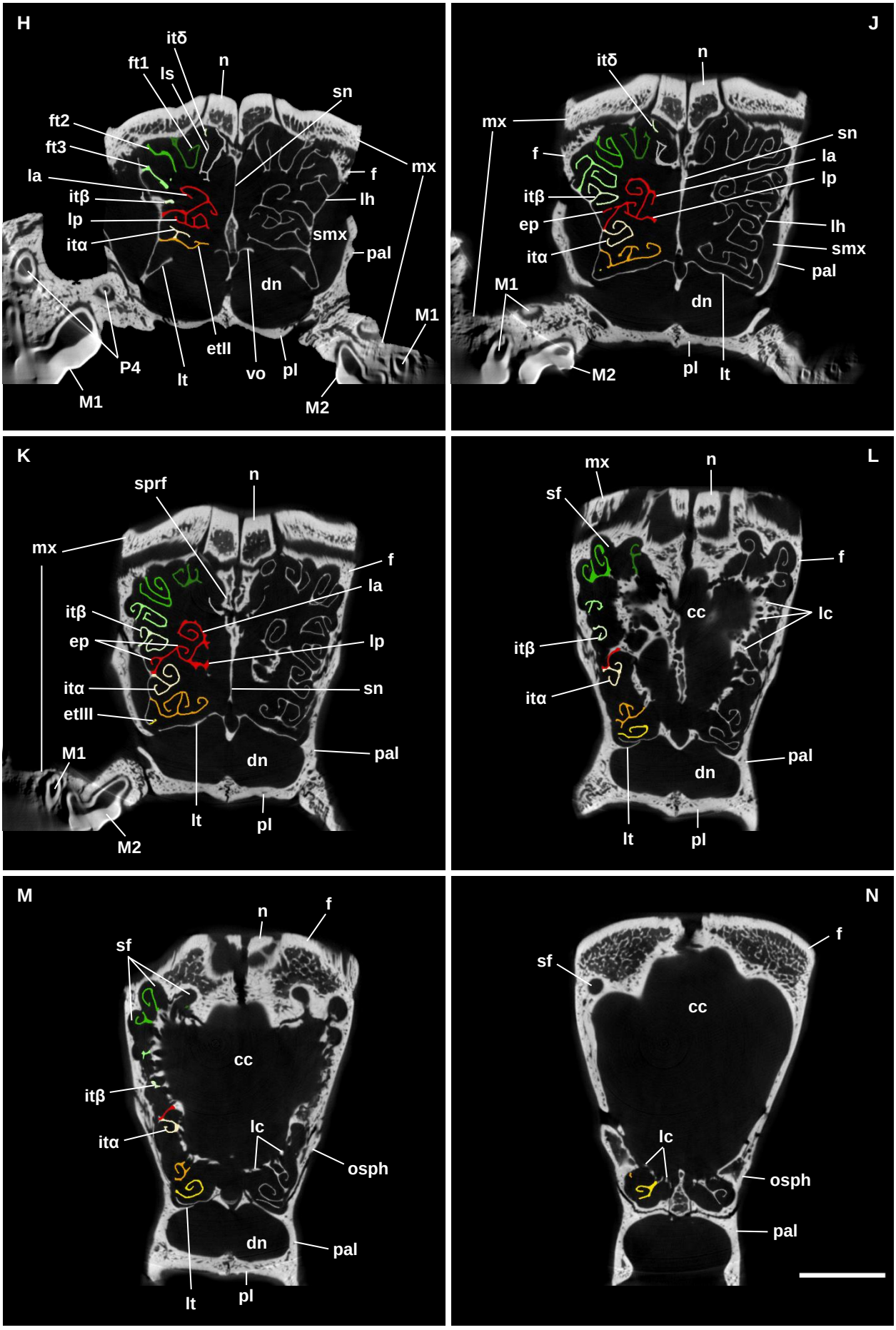

Fig. 28: Adult pug, modern type (NMBE 1051937): **A)** virtual 3D model showing the position of the turbinal skeleton within the transparent nasal cavity in medial view (right side); next to it the skull in lateral view showing the region of interest; **B)** virtual 3D model of the turbinal skeleton in medial and **C)** in lateral view; **D)–N)** µCT cross sections of the ethmoidal region from rostral to caudal in rostral view, the turbinals are highlighted on one side. Scale bars: 10mm; Abbreviations: 1; colors refer to the turbinal color code.

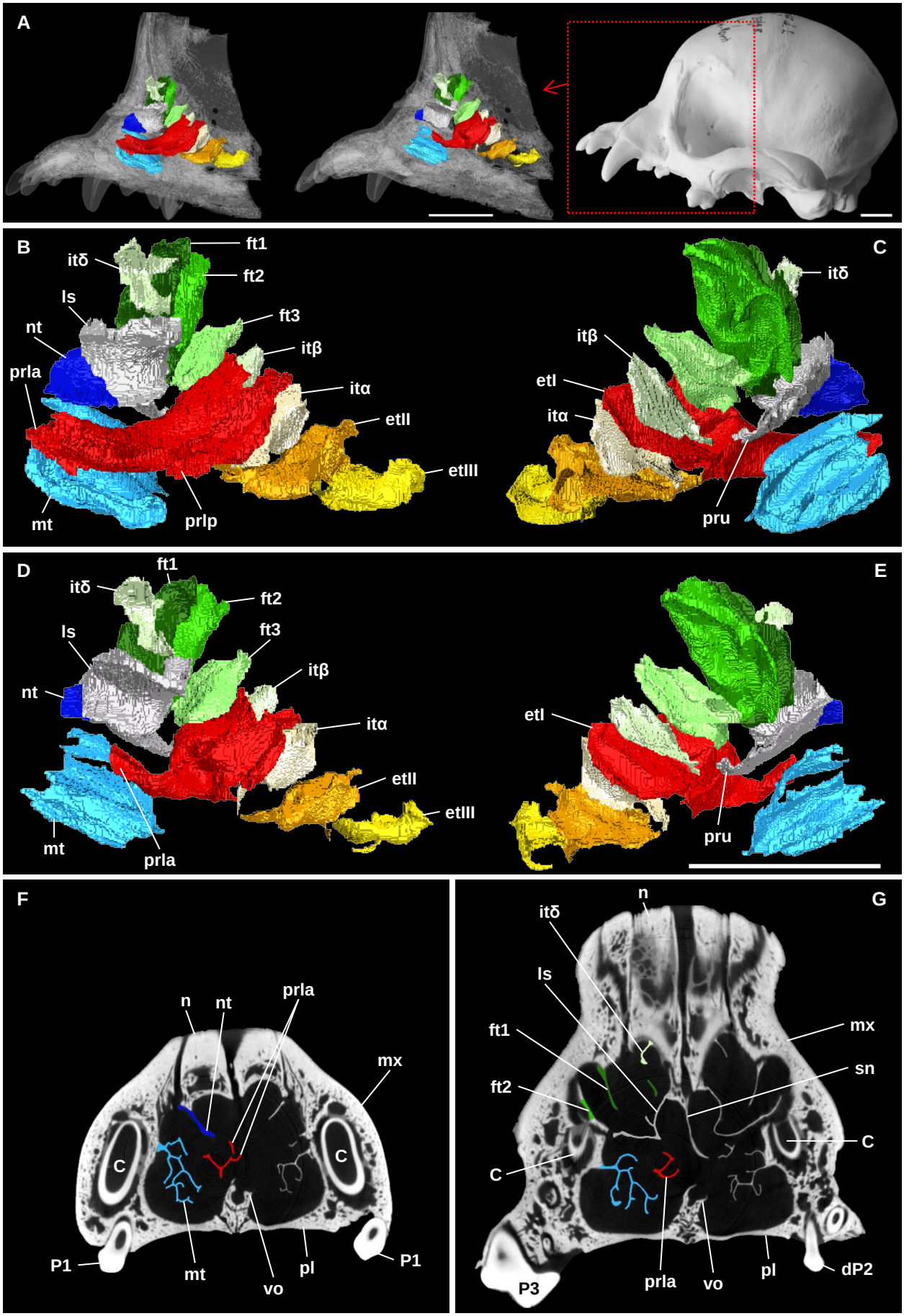

Fig. 29: Adult pug, modern type (NMBE 1052345): **A)** position of the right and left (mirrored) turbinal skeleton within the transparent nasal cavity, both in medial view; next to them the skull in lateral view showing the region of interest; **B)** virtual 3D model of the right turbinal skeleton in medial and **C)** in lateral view; **D)** virtual 3D model of the left turbinal skeleton in medial and **E)** in lateral view (both mirrored); **F)–Q)** µCT cross sections of the ethmoidal region from rostral to caudal in rostral view, the turbinals are highlighted on one side. Scale bars: 10mm; Abbreviations: 1; colors refer to the turbinal color code.

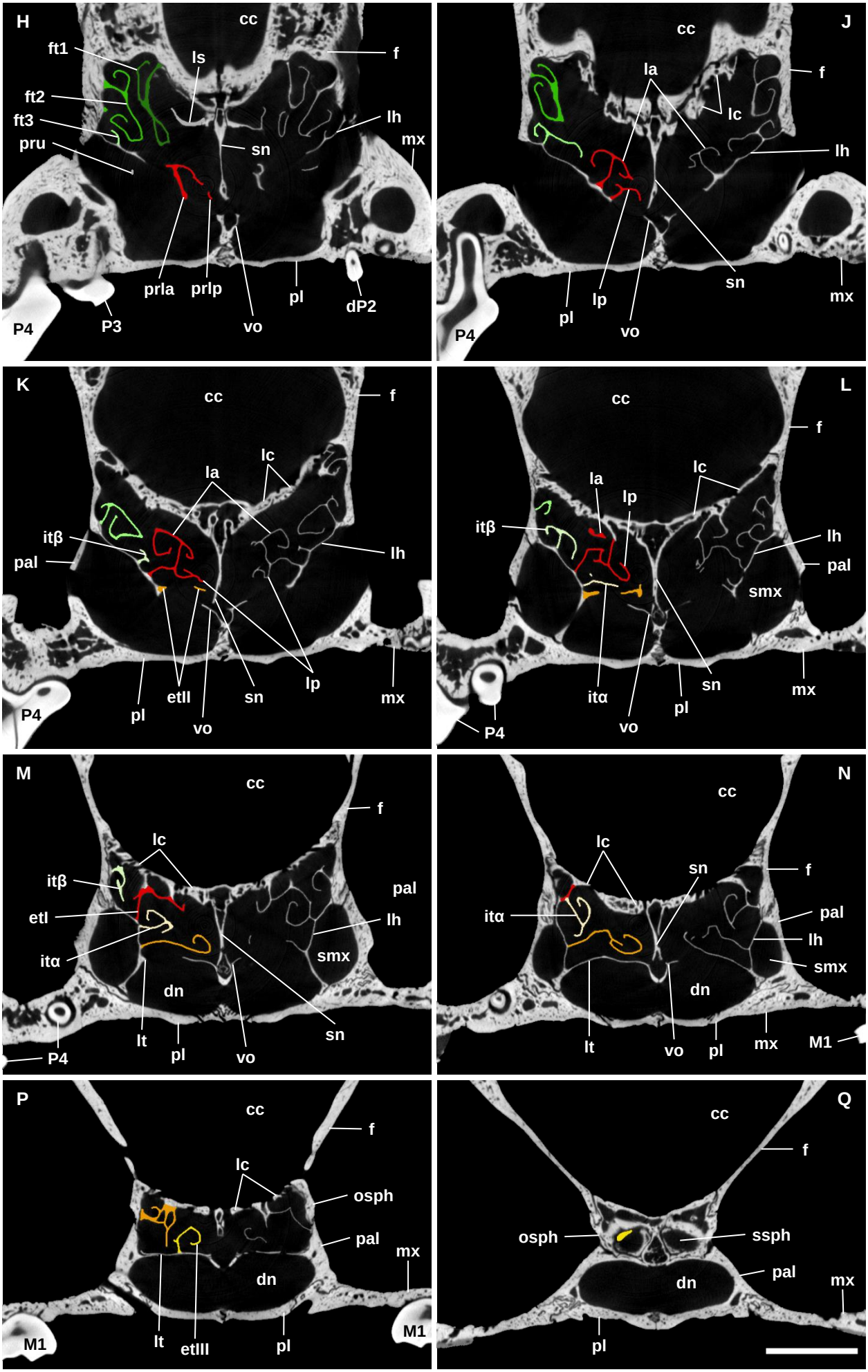

Fig. 29 (continued)

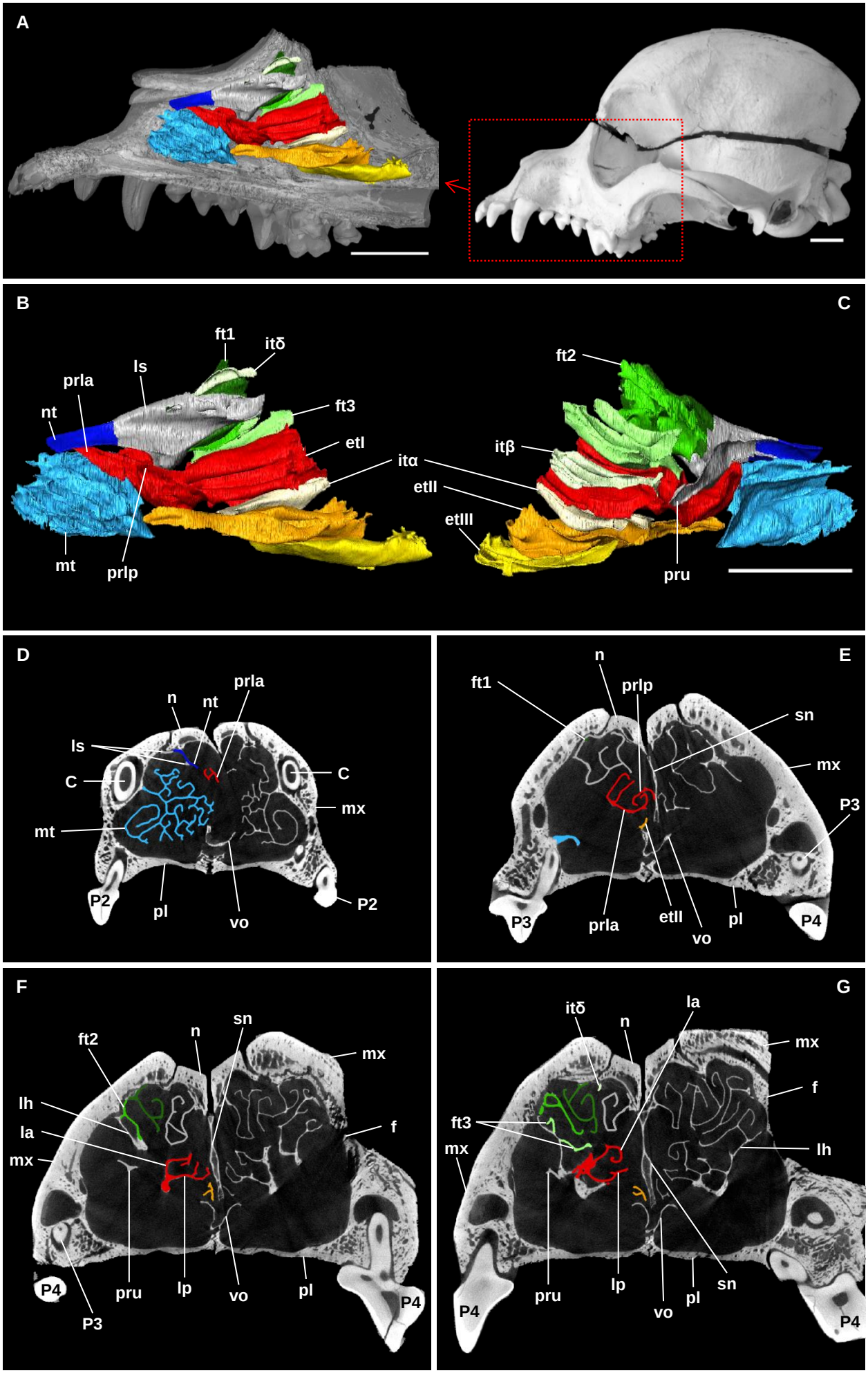

Fig. 30 (description: next page)

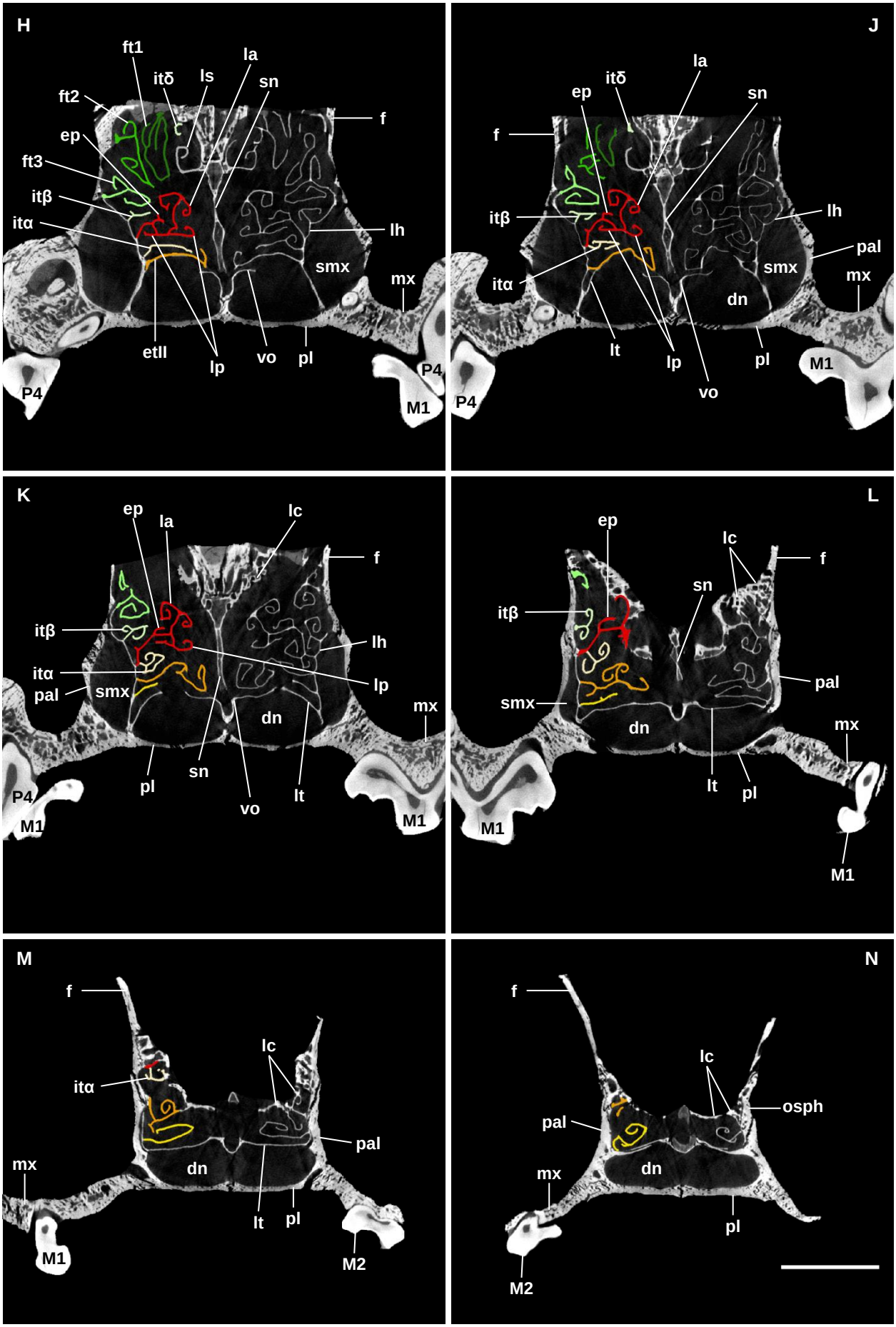

Fig. 30: Adult pug, ancient type (SMF 16284): **A)** virtual 3D model showing the position of the turbinal skeleton within the transparent nasal cavity in medial view (right side); next to it the skull in lateral view showing the region of interest; **B)** virtual 3D model of the turbinal skeleton in medial and **C)** in lateral view; **D)–N)** µCT cross sections of the ethmoidal region from rostral to caudal in rostral view, the turbinals are highlighted on one side. Scale bars: 10mm; Abbreviations: 1; colors refer to the turbinal color code.

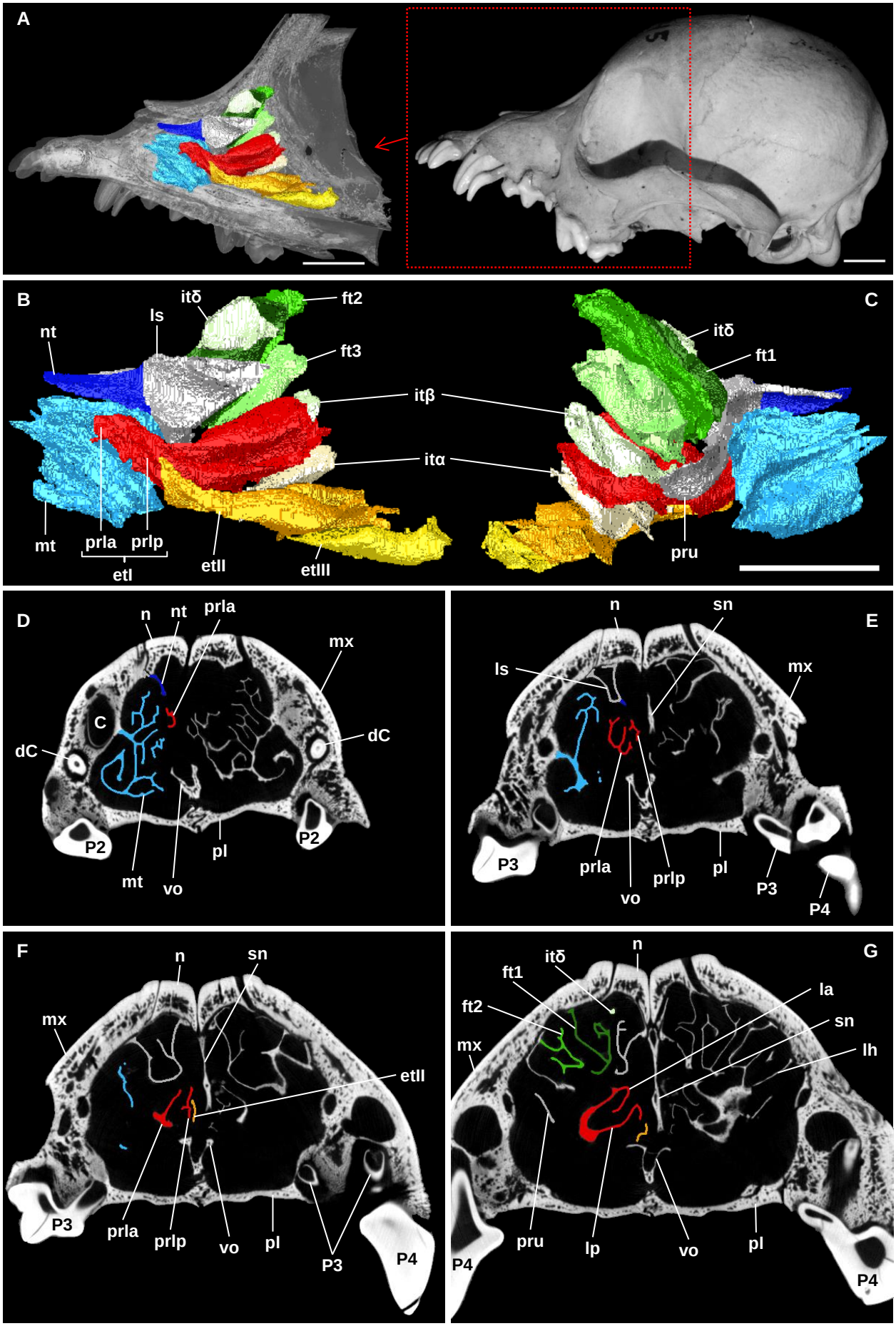

Fig. 31: Adult pug, ancient type ([MfN] 1845): **A)** virtual 3D model showing the position of the turbinal skeleton within the transparent nasal cavity in medial view (right side); next to it the skull in lateral view showing the region of interest; **B)** virtual 3D model of the turbinal skeleton in medial and **C)** in lateral view; **D)–N)** µCT cross sections of the ethmoidal region from rostral to caudal in rostral view, the turbinals are highlighted on one side. Scale bars: 10mm; Abbreviations: 1; colors refer to the turbinal color code.

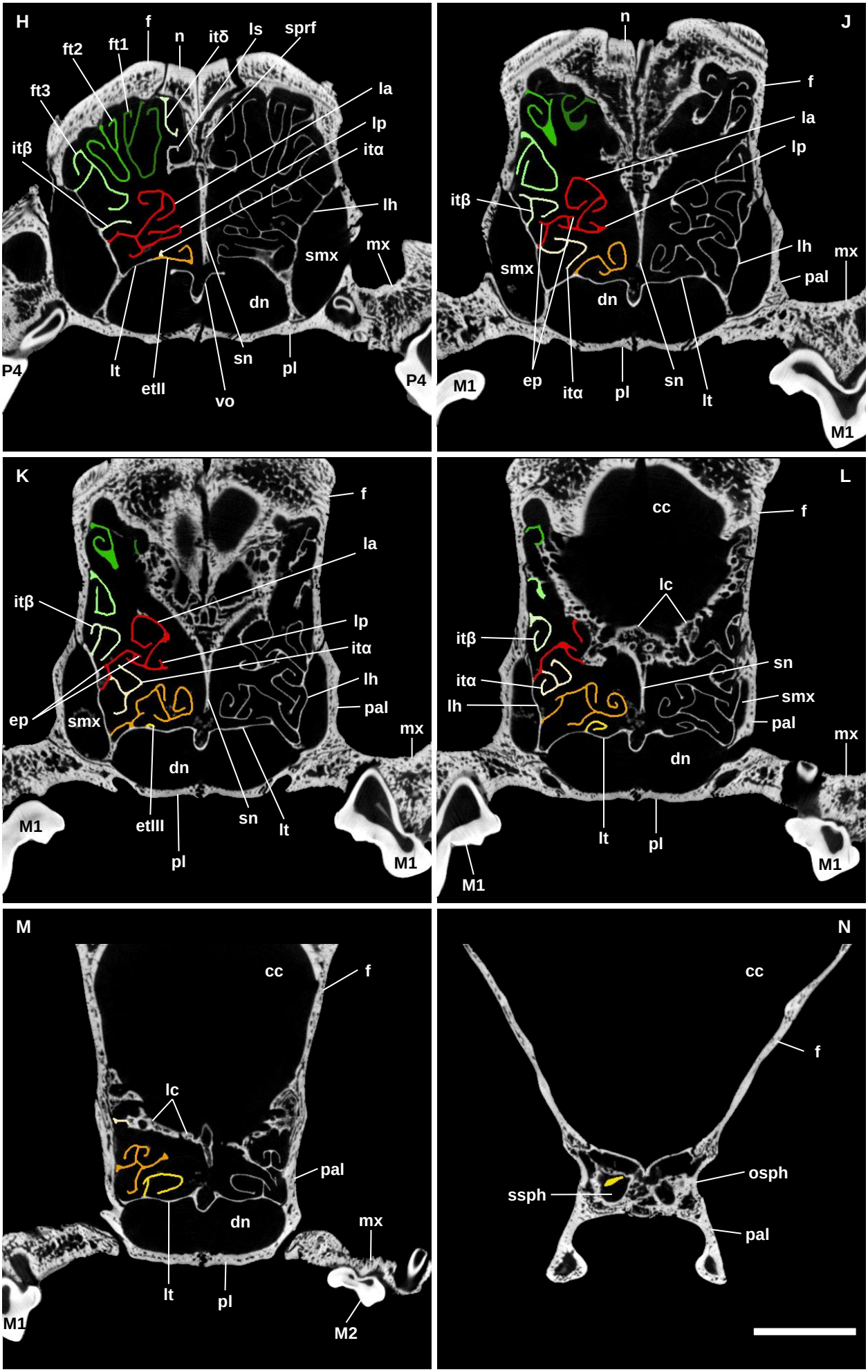

Fig. 31 (continued)

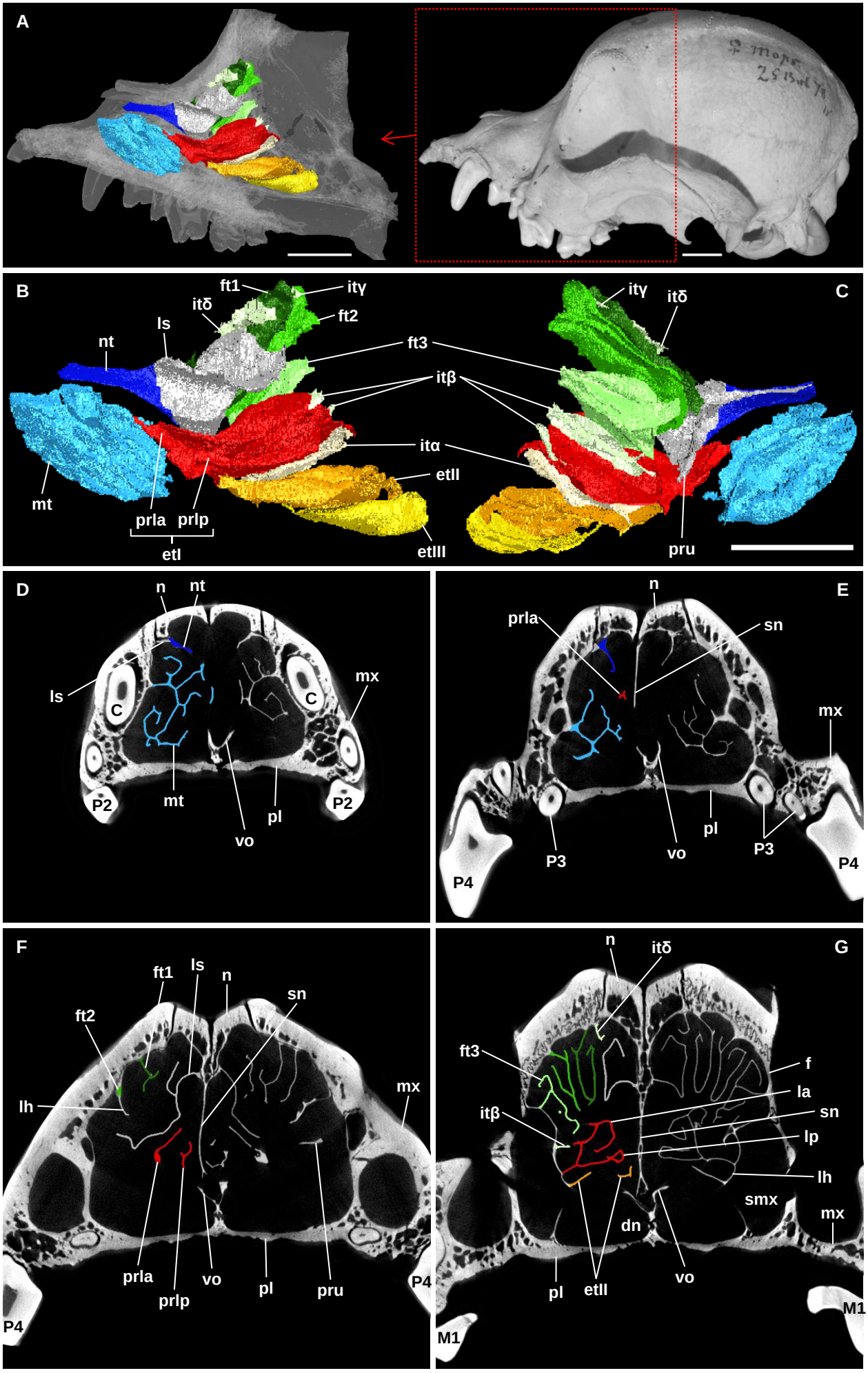

Fig. 32 (description: next page)

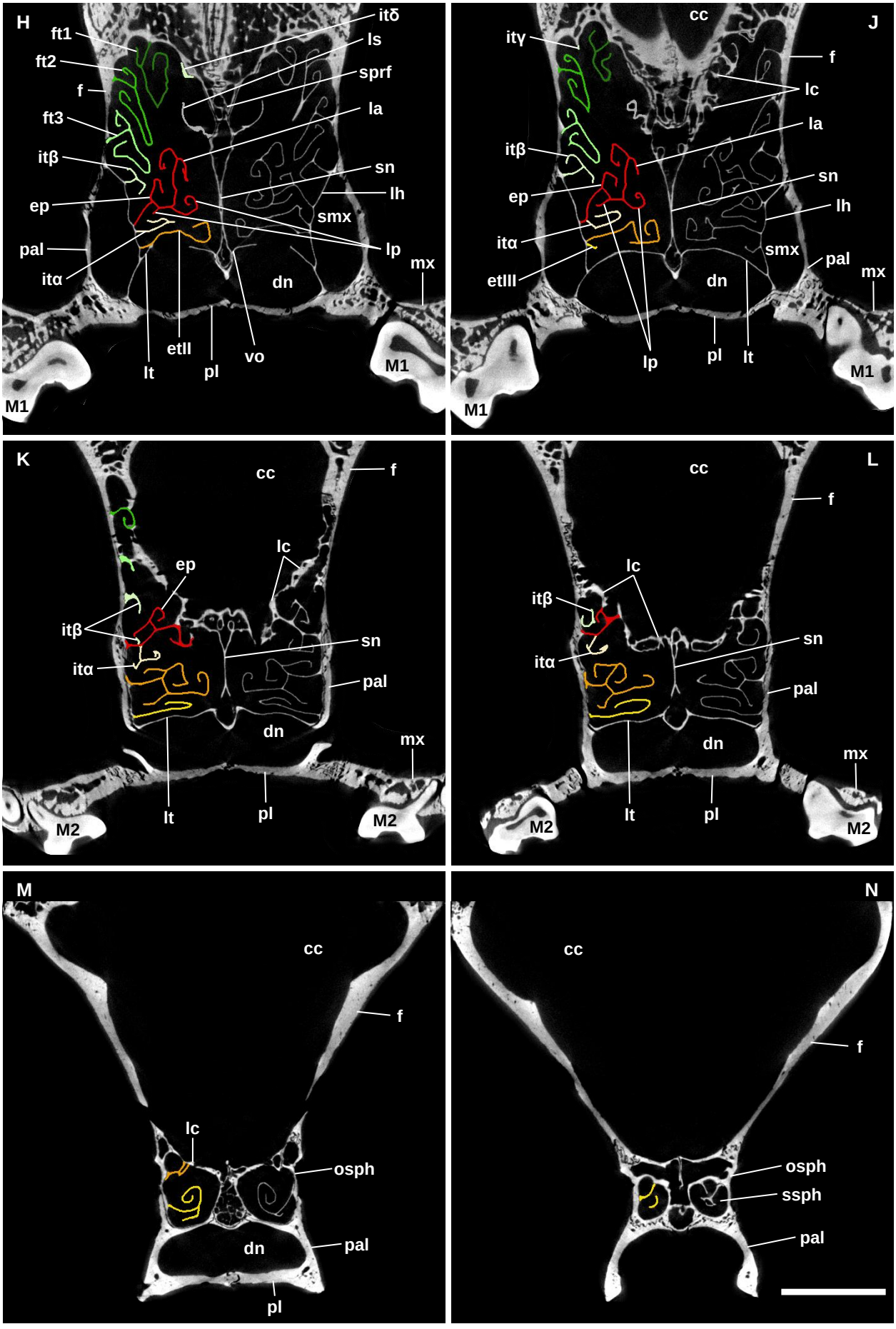

Fig. 32: Adult pug, ancient type ([MfN] 2620): **A)** virtual 3D model showing the position of the turbinal skeleton within the transparent nasal cavity in medial view (left side, mirrored); next to it the skull in lateral view showing the region of interest; **B)** virtual 3D model of the turbinal skeleton in medial and **C)** in lateral view (both mirrored); **D)–N)** µCT cross sections of the ethmoidal region from rostral to caudal in caudal view, the turbinals are highlighted on one side. Scale bars: 10mm; Abbreviations: 1; colors refer to the turbinal color code.

FIGURES

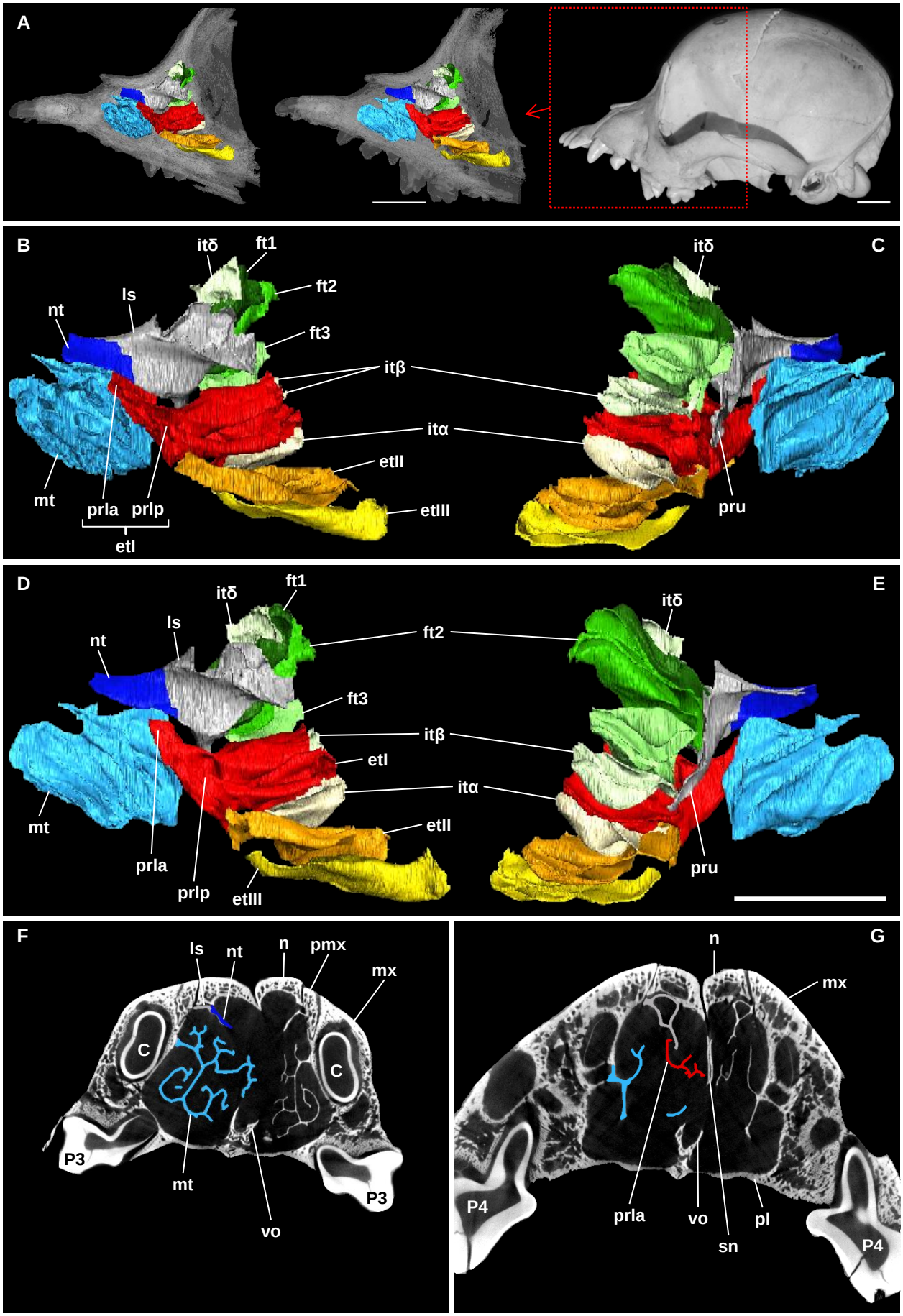

Fig. 33: Adult pug, ancient type ([MfN] 2630): **A)** position of the right and left (mirrored) turbinal skeleton within the transparent nasal cavity, both in medial view; next to them the skull in lateral view showing the region of interest; **B)** virtual 3D model of the right turbinal skeleton in medial and **C)** in lateral view; D**)** virtual 3D model of the left turbinal skeleton in medial and **E)** in lateral view (both mirrored); **F)–N)** µCT cross sections of the ethmoidal region from rostral to caudal in rostral view, the turbinals are highlighted on one side. Scale bars: 10mm; Abbreviations: 1; colors refer to the turbinal color code.

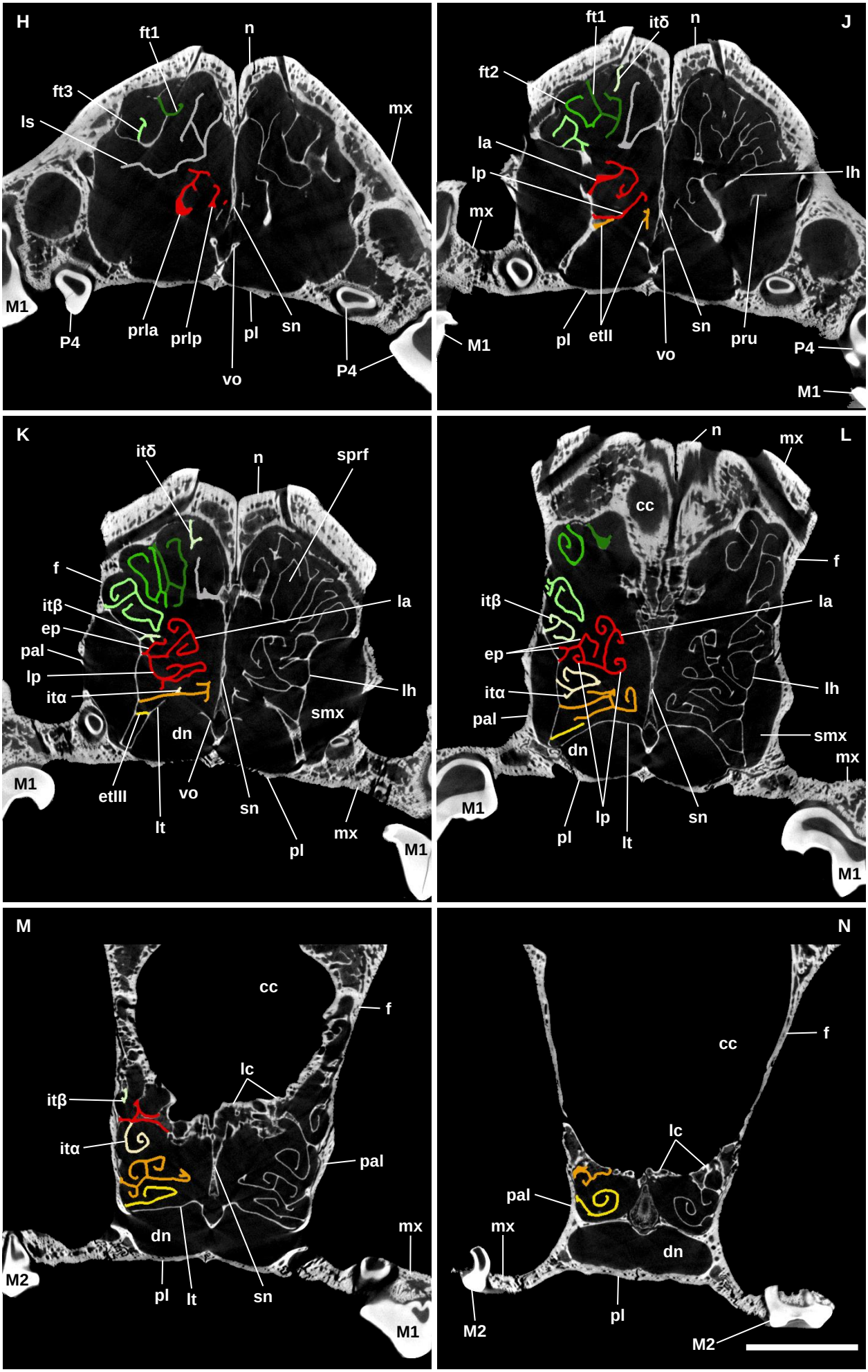

Fig. 33 (continued)

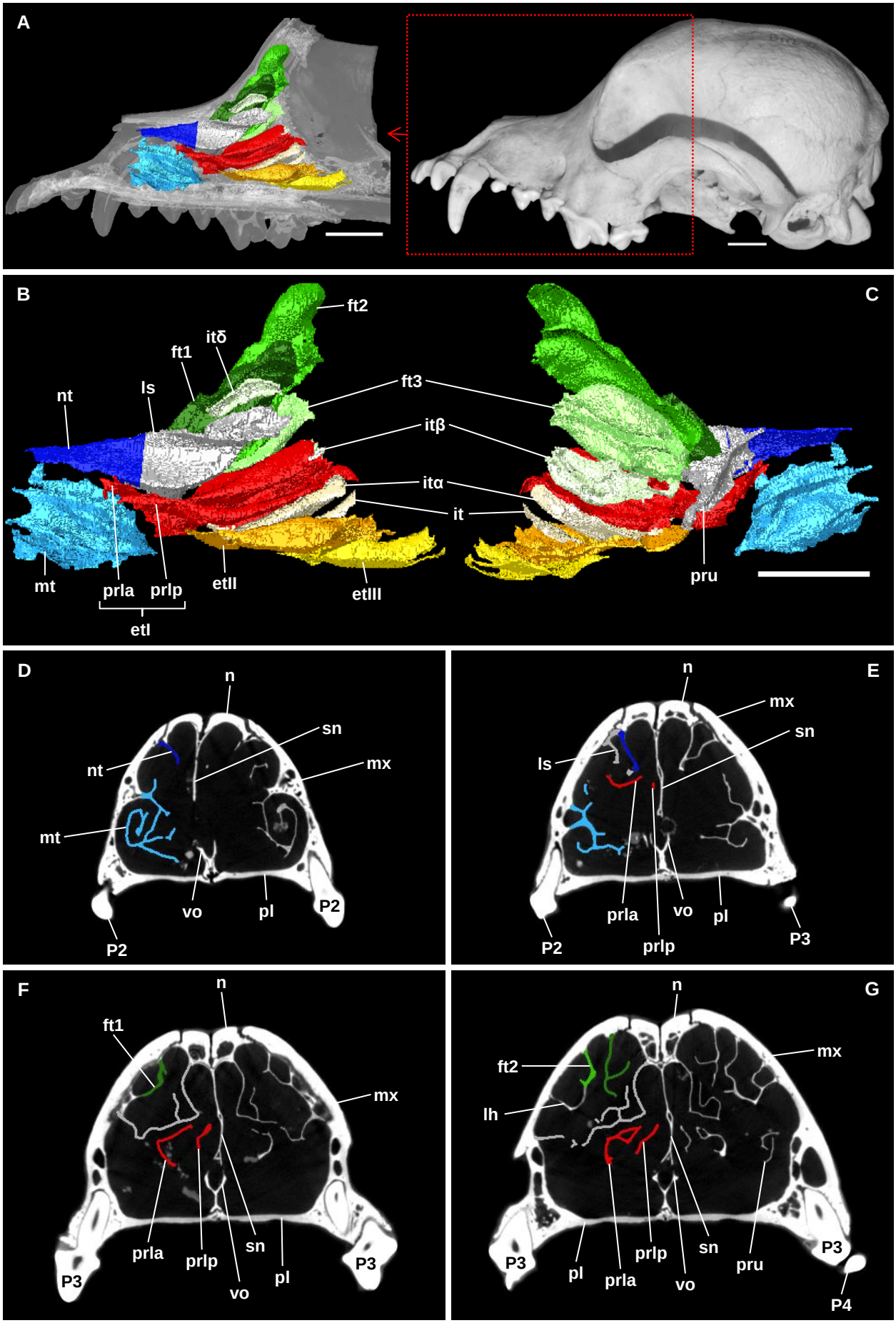

Fig. 34: Adult pug, ancient type ([MfN] 2657): **A)** virtual 3D model showing the position of the turbinal skeleton within the transparent nasal cavity in medial view (right side); next to it the skull in lateral view showing the region of interest; **B)** virtual 3D model of the turbinal skeleton in medial and **C)** in lateral view; **D)–N)** µCT cross sections of the ethmoidal region from rostral to caudal in rostral view, the turbinals are highlighted on one side. Scale bars: 10mm; Abbreviations: 1; colors refer to the turbinal color code.

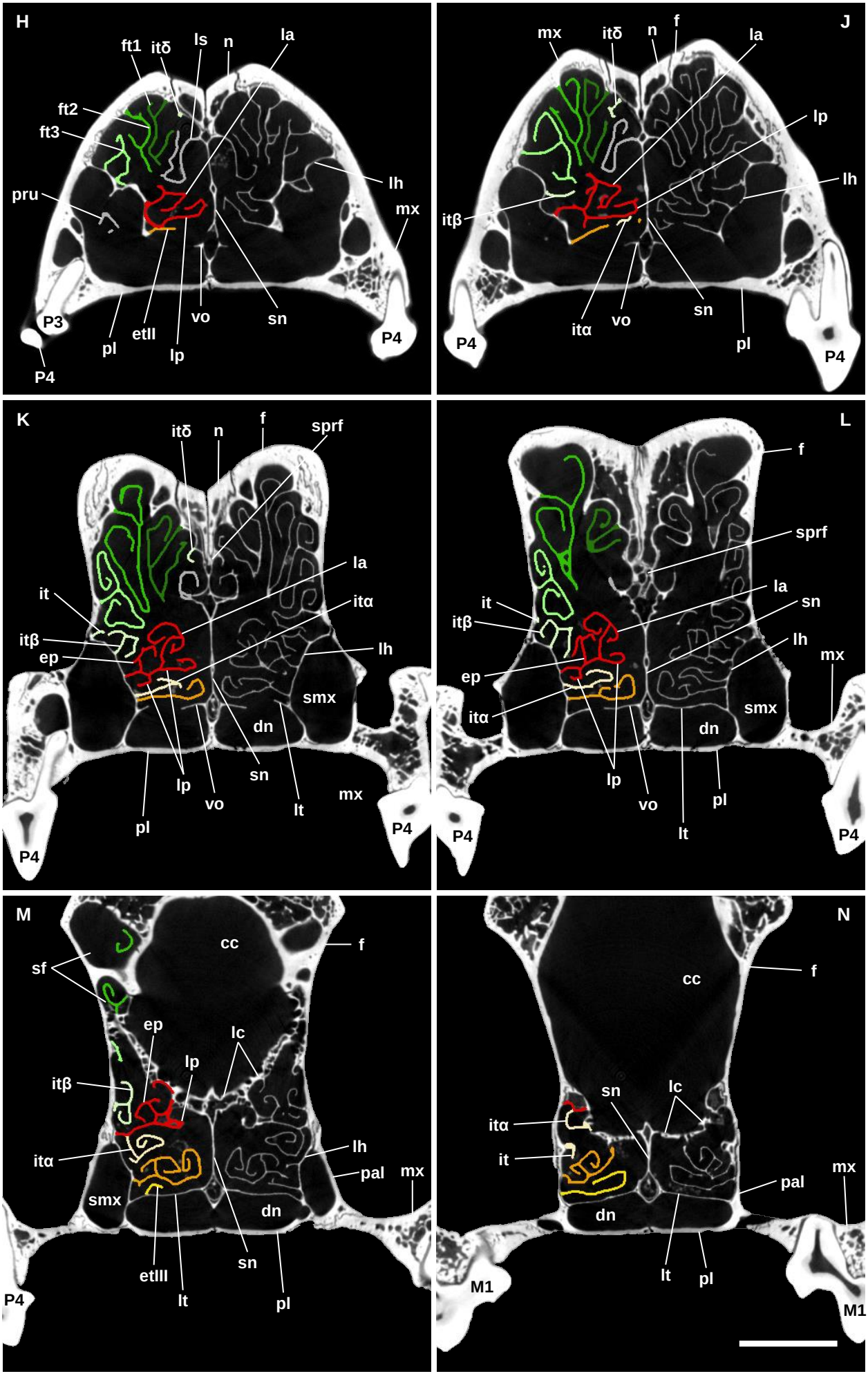

Fig. 34 (continued)

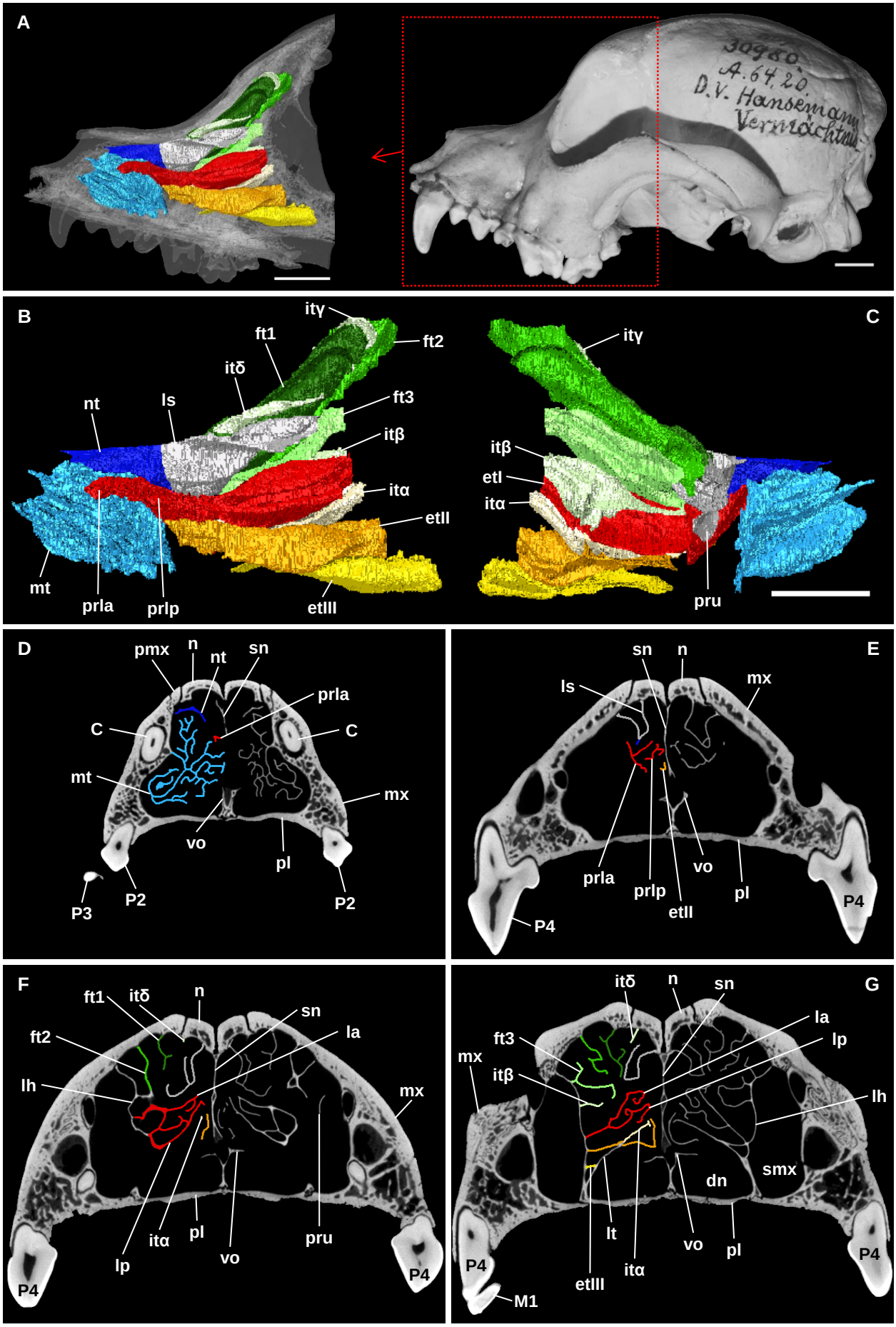

Fig. 35: Adult pug, ancient type (ZMB_MAM 30980): **A)** virtual 3D model showing the position of the turbinal skeleton within the transparent nasal cavity in medial view (right side); next to it the skull in lateral view showing the region of interest; **B)** virtual 3D model of the turbinal skeleton in medial and **C)** in lateral view; **D)–N)** µCT cross sections of the ethmoidal region from rostral to caudal in rostral view, the turbinals are highlighted on one side. Scale bars: 10mm; Abbreviations: 1; colors refer to the turbinal color code.

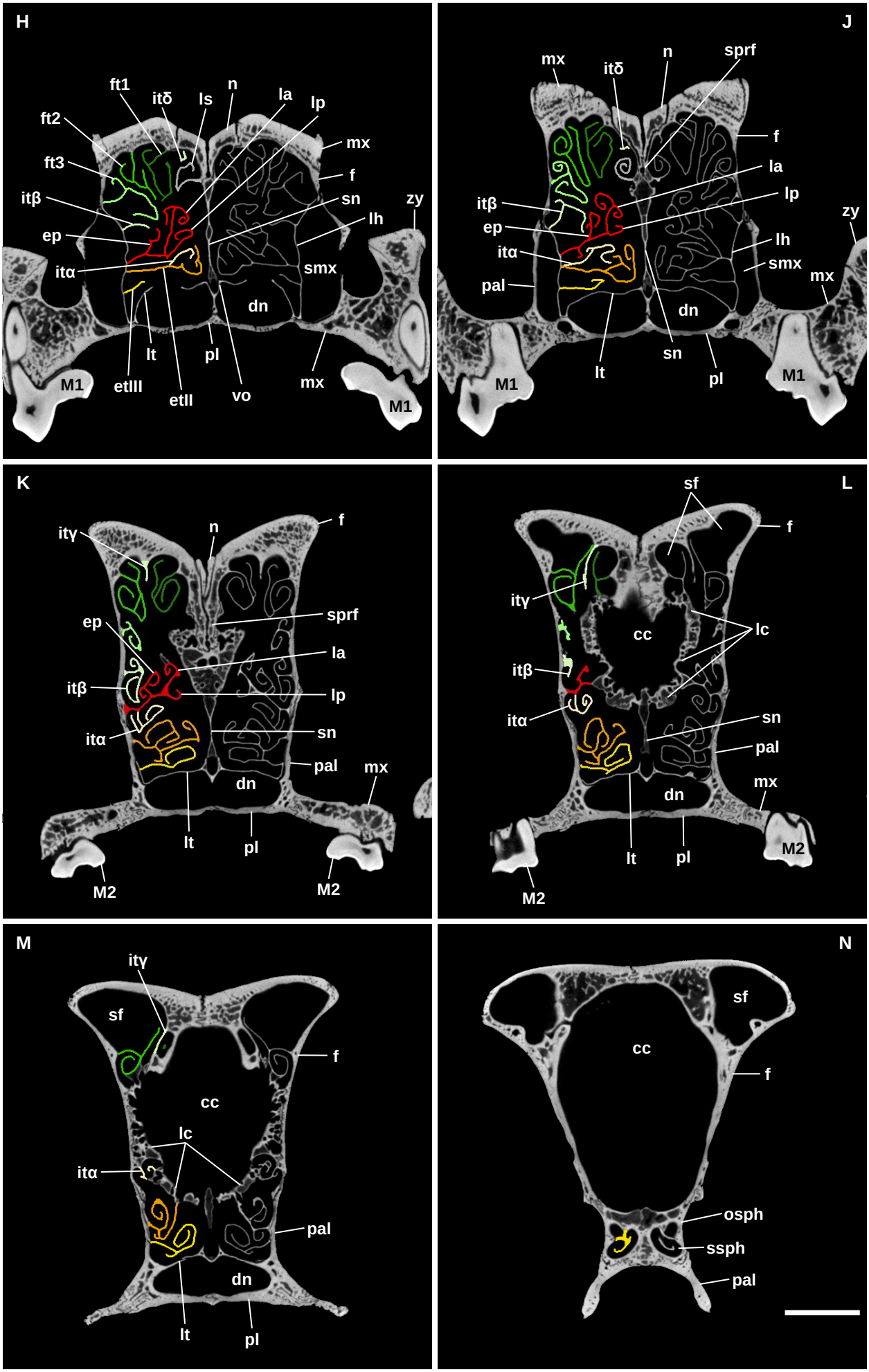

Fig. 35 (continued)

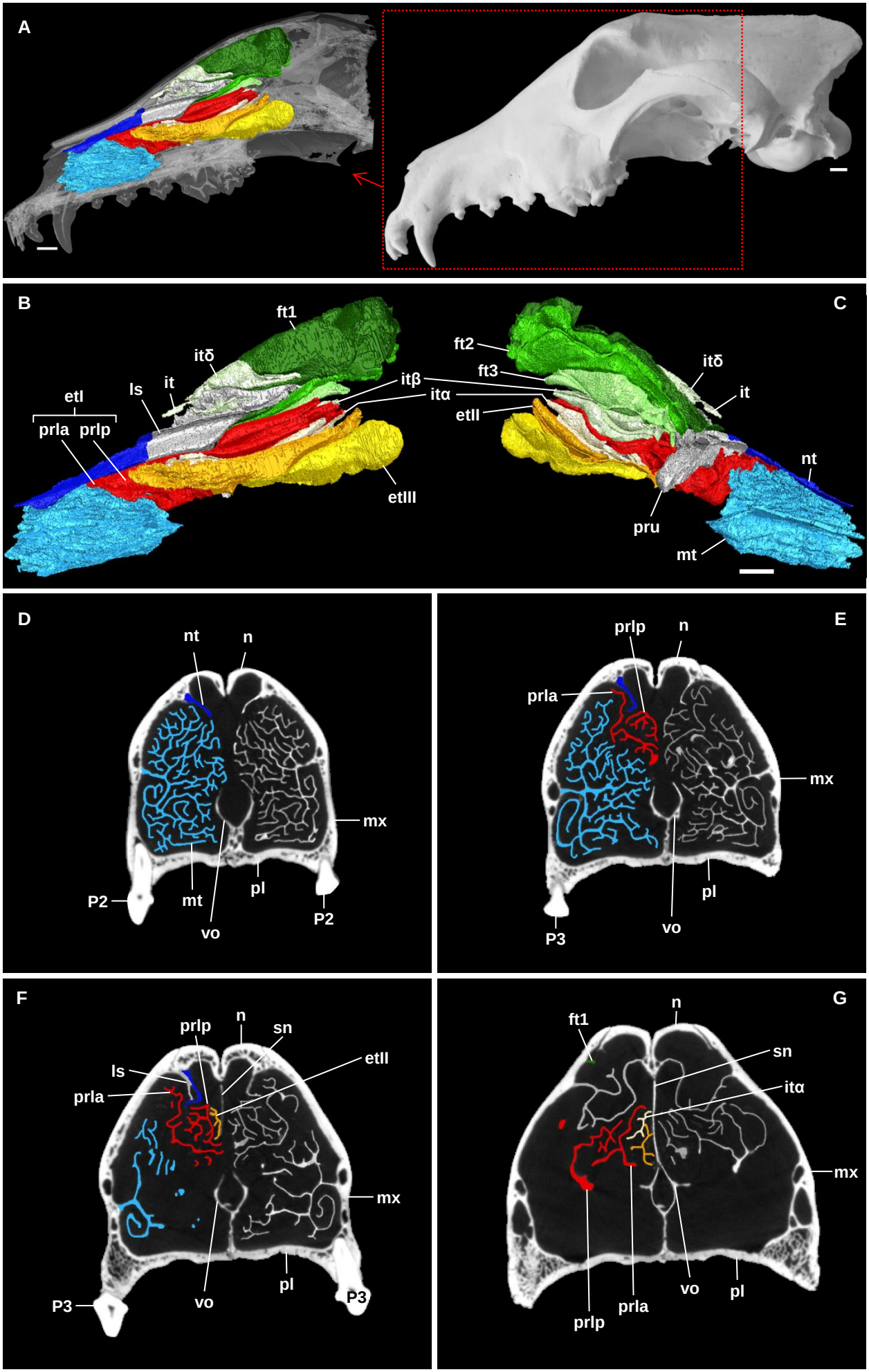

Fig. 36 (description: next page)

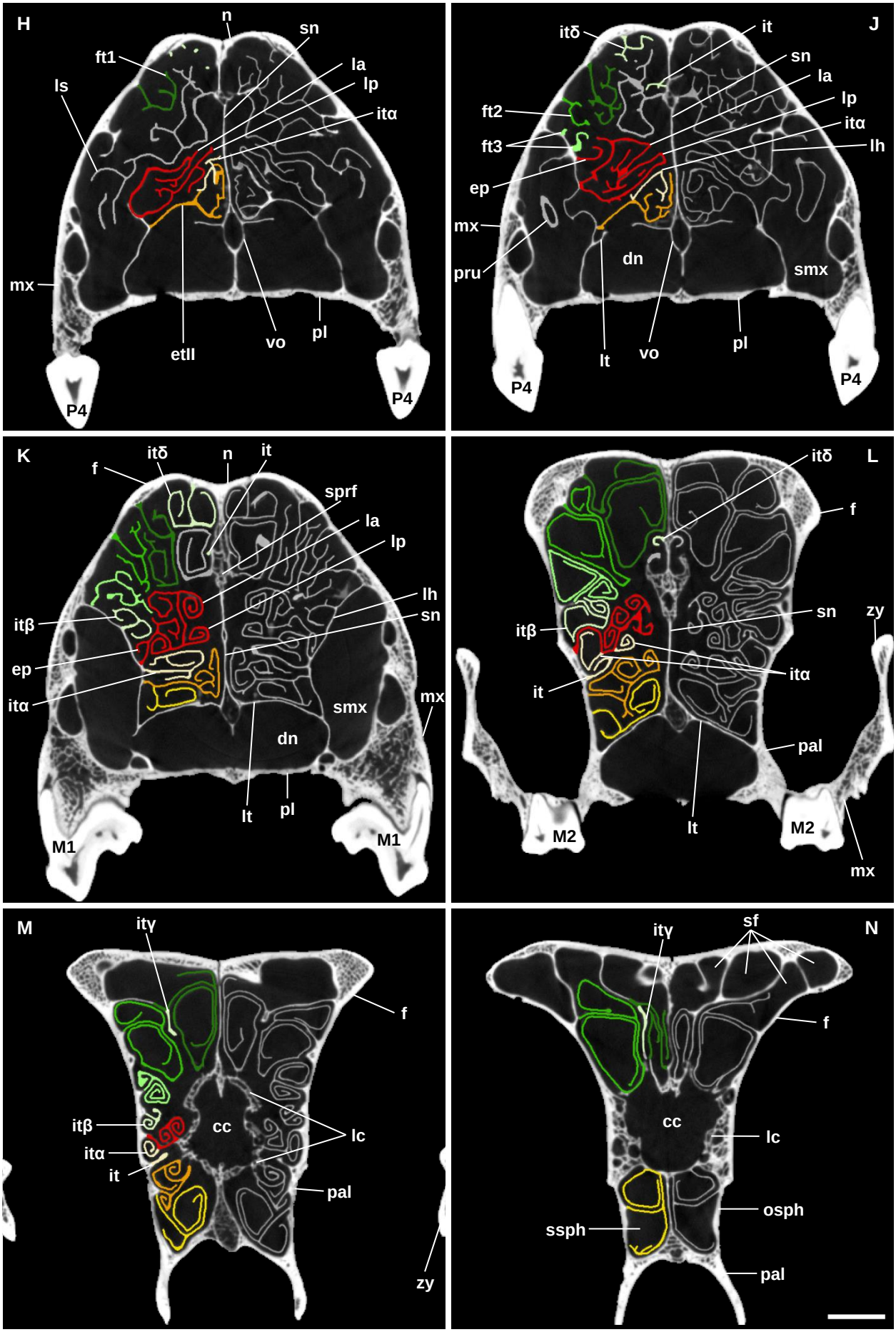

Fig. 36: Borzoi (NMBE 1051164): **A)** virtual 3D model showing the position of the turbinal skeleton within the transparent nasal cavity in medial view (left side, mirrored); next to it the skull in lateral view showing the region of interest; **B)** virtual 3D model of the turbinal skeleton in medial and **C)** in lateral view (both mirrored); **D)–N)** µCT cross sections of the ethmoidal region from rostral to caudal in caudal view, the turbinals are highlighted on one side. Scale bars: 10mm; Abbreviations: 1; colors refer to the turbinal color code.

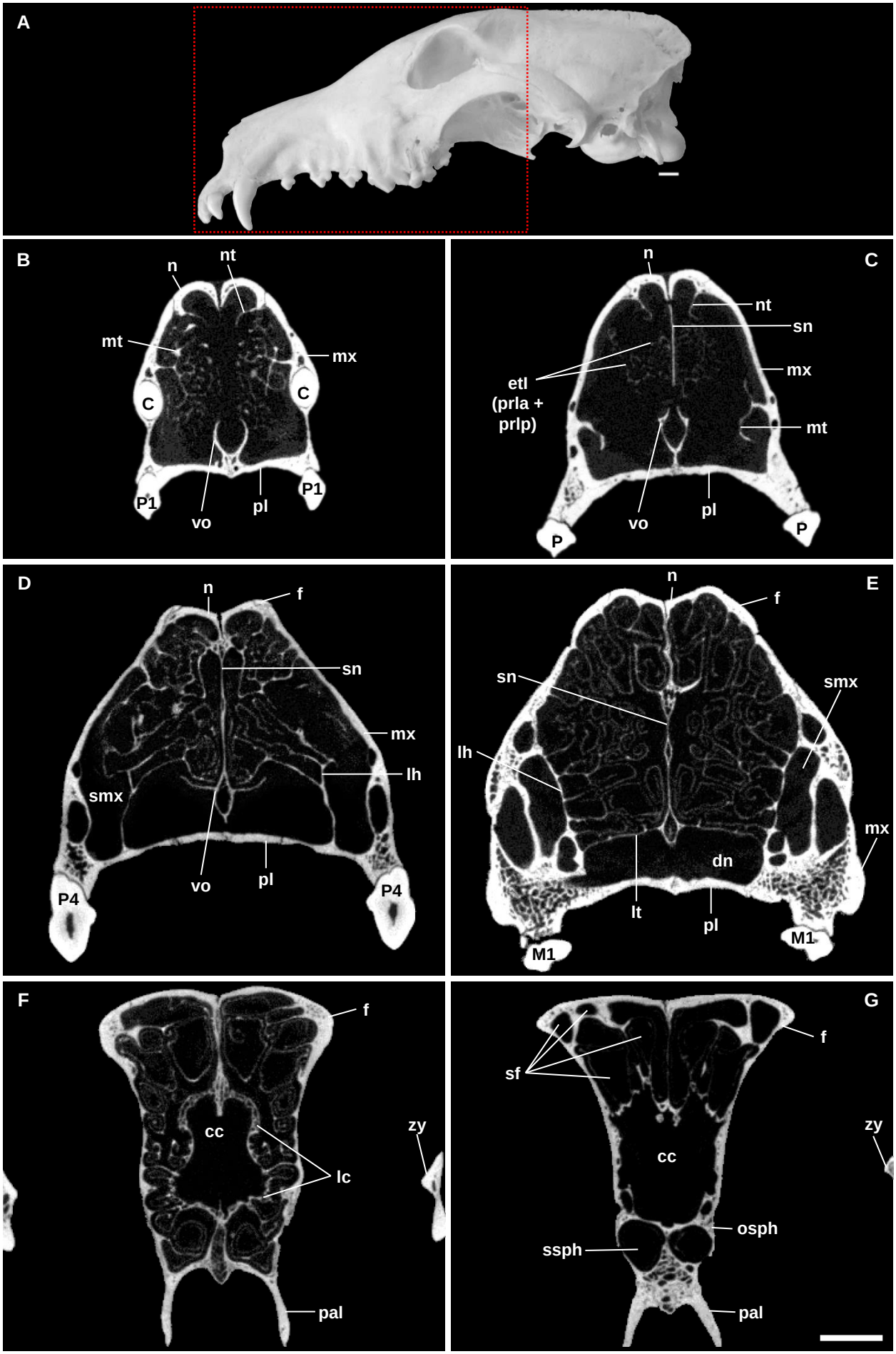

Fig. 37: Adult borzoi (NMBE 1051166): **A)** skull in lateral view showing the region of interest; **B)–G)** µCT cross sections of the ethmoidal region from rostral to caudal in caudal view. The turbinals have not been highlighted due to the low contrast of the scan that could not be digitally enhanced. The lamellae's morphology can be only roughly identified. Scale bars: 10mm; Abbreviations: 1.

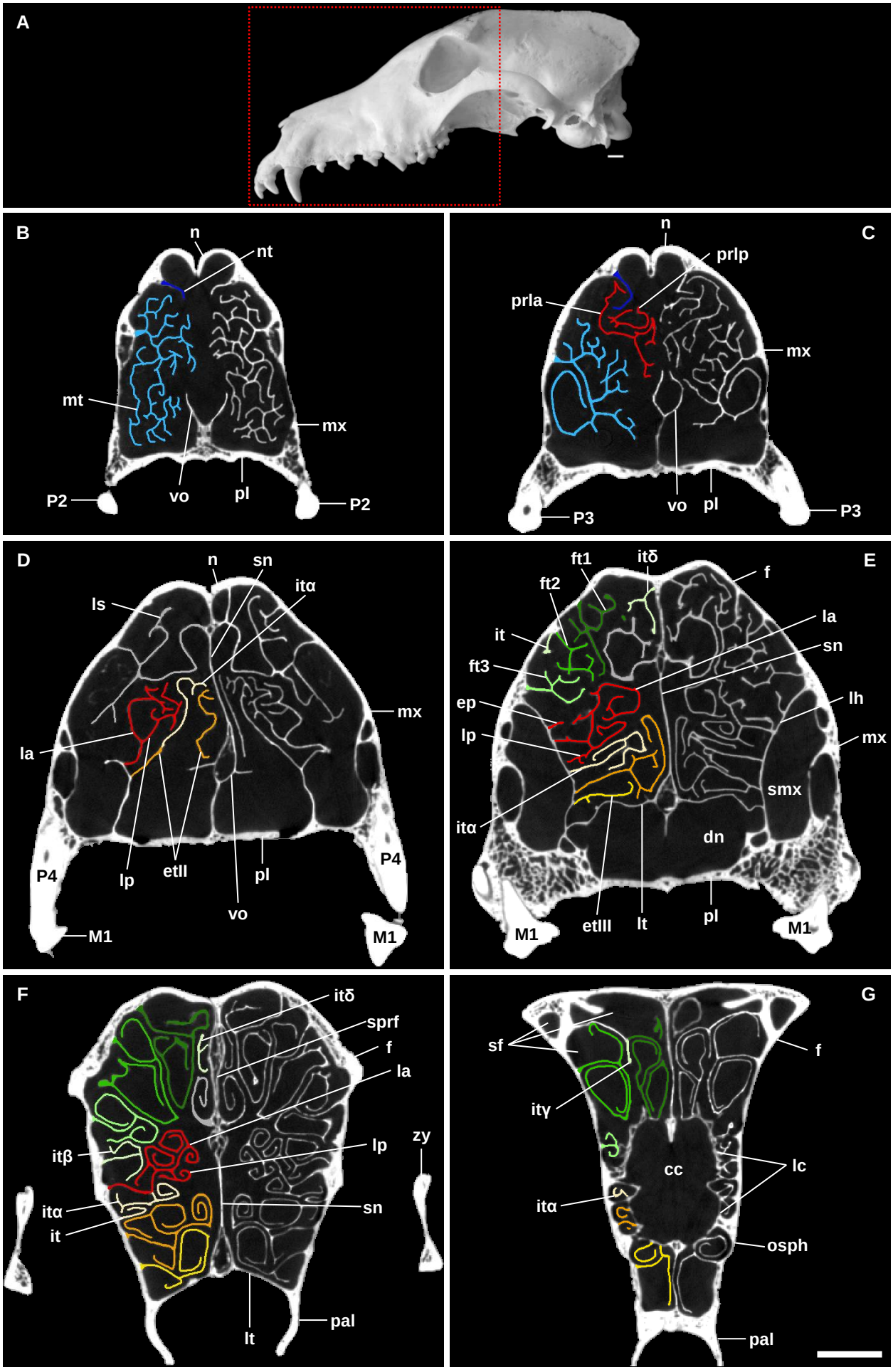

Fig. 38: Adult borzoi (NMBE 1051180): **A)** skull in lateral view showing the region of interest; **B)–G)** µCT cross sections of the ethmoidal region from rostral to caudal in caudal view, the turbinals are highlighted on one side. Scale bars: 10mm; Abbreviations: 1; colors refer to the turbinal color code.

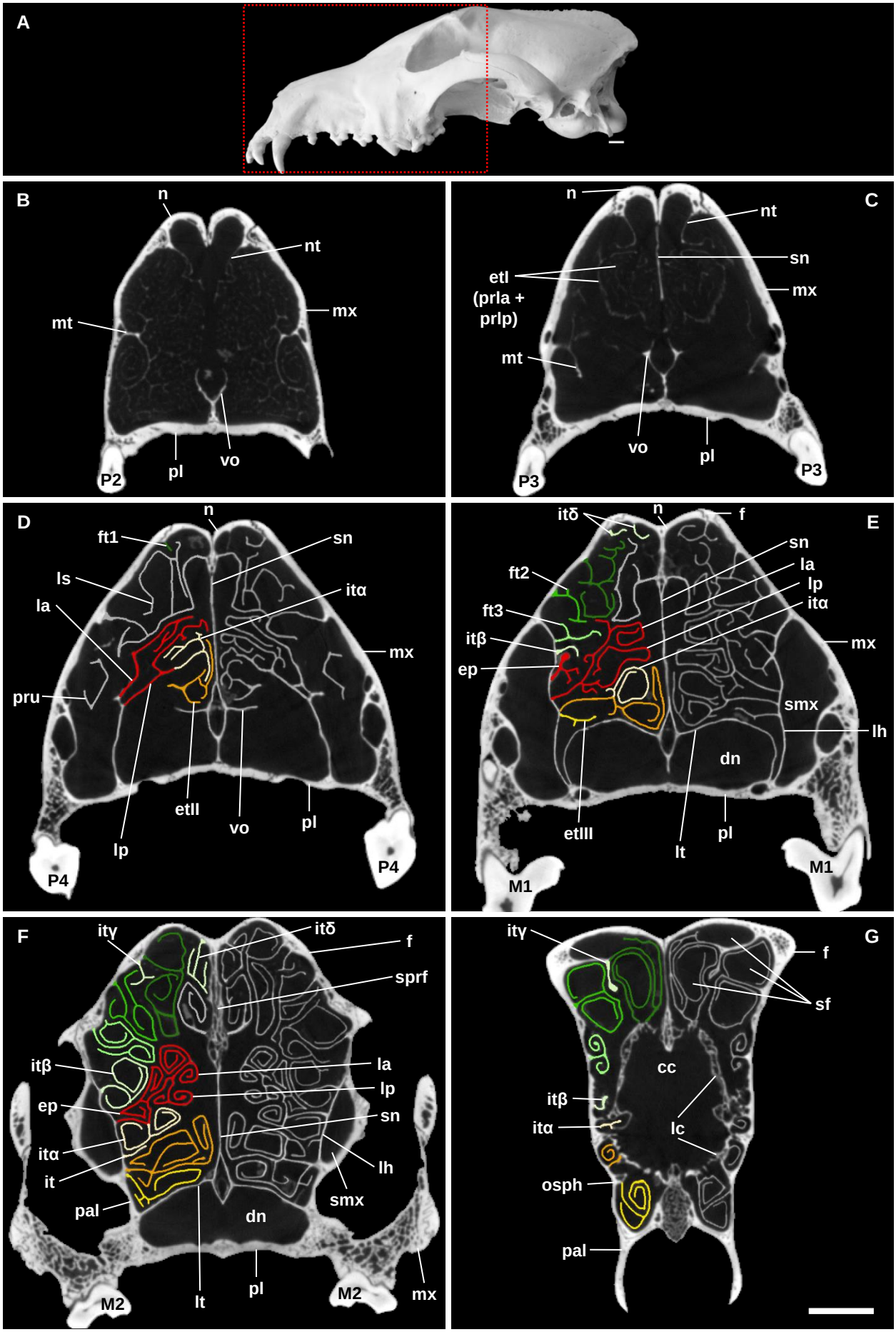

Fig. 39: Adult borzoi (NMBE 1052706): **A)** skull in lateral view showing the region of interest; **B)–G)** µCT cross sections of the ethmoidal region from rostral to caudal in caudal view. In the rostral region (maxilloturbinal, both anterior processes of ethmoturbinal I) the contrast was too low as the lamellae are extremely delicate and perforated in this specimen. Hence, only in the posterior part the turbinals are highlighted on one side. Scale bars: 10mm; Abbreviations: 1; colors refer to the turbinal color code.

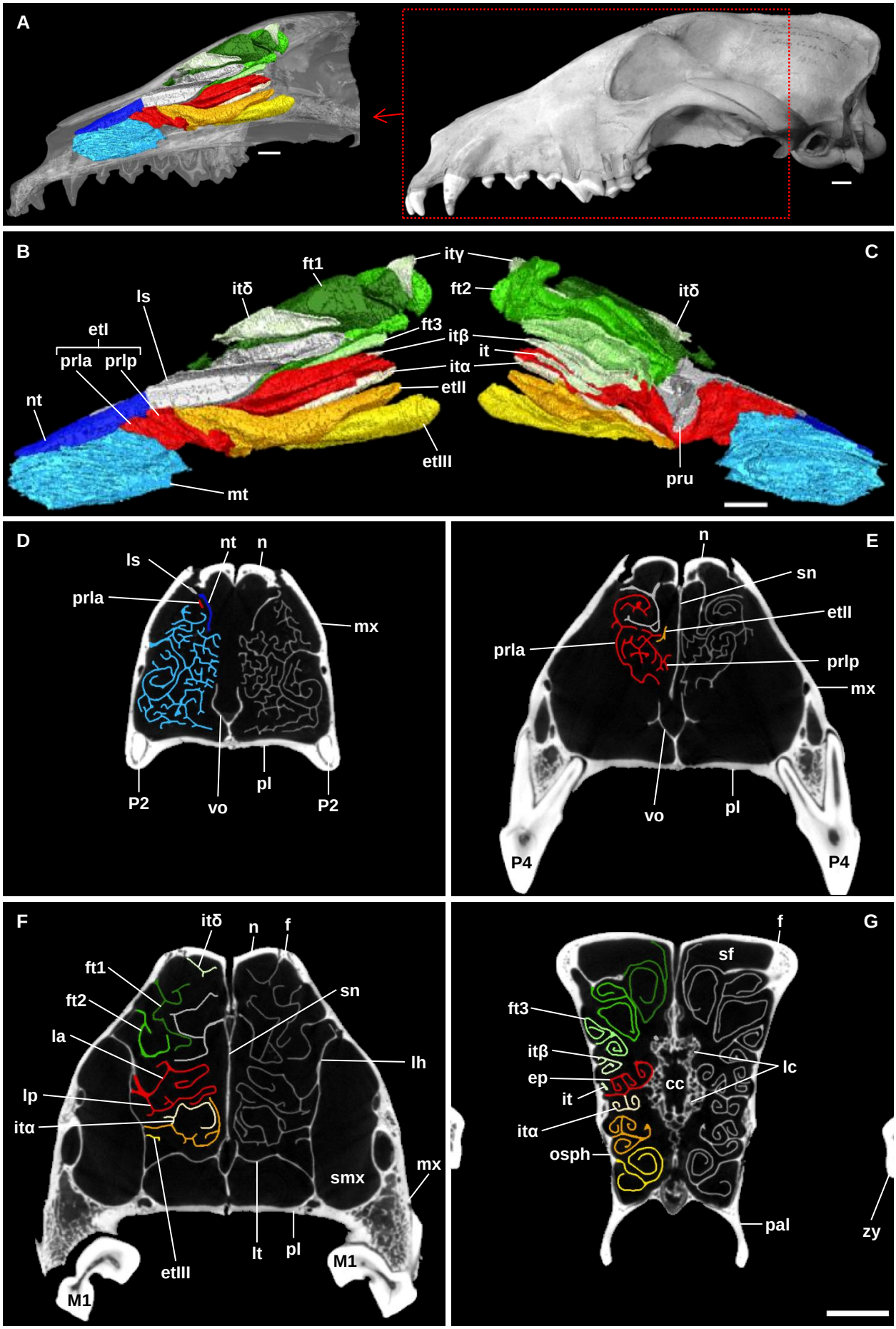

Fig. 40: Adult borzoi ([MfN] 1403): **A)** virtual 3D model showing the position of the turbinal skeleton within the transparent nasal cavity in medial view (left side, mirrored); next to it the skull in lateral view showing the region of interest; **B)** virtual 3D model of the turbinal skeleton in medial and **C)** in lateral view (both mirrored); **D)–G)** µCT cross sections of the ethmoidal region from rostral to caudal in caudal view, the turbinals are highlighted on one side. Scale bars: 10mm; Abbreviations: 1; colors refer to the turbinal color code.

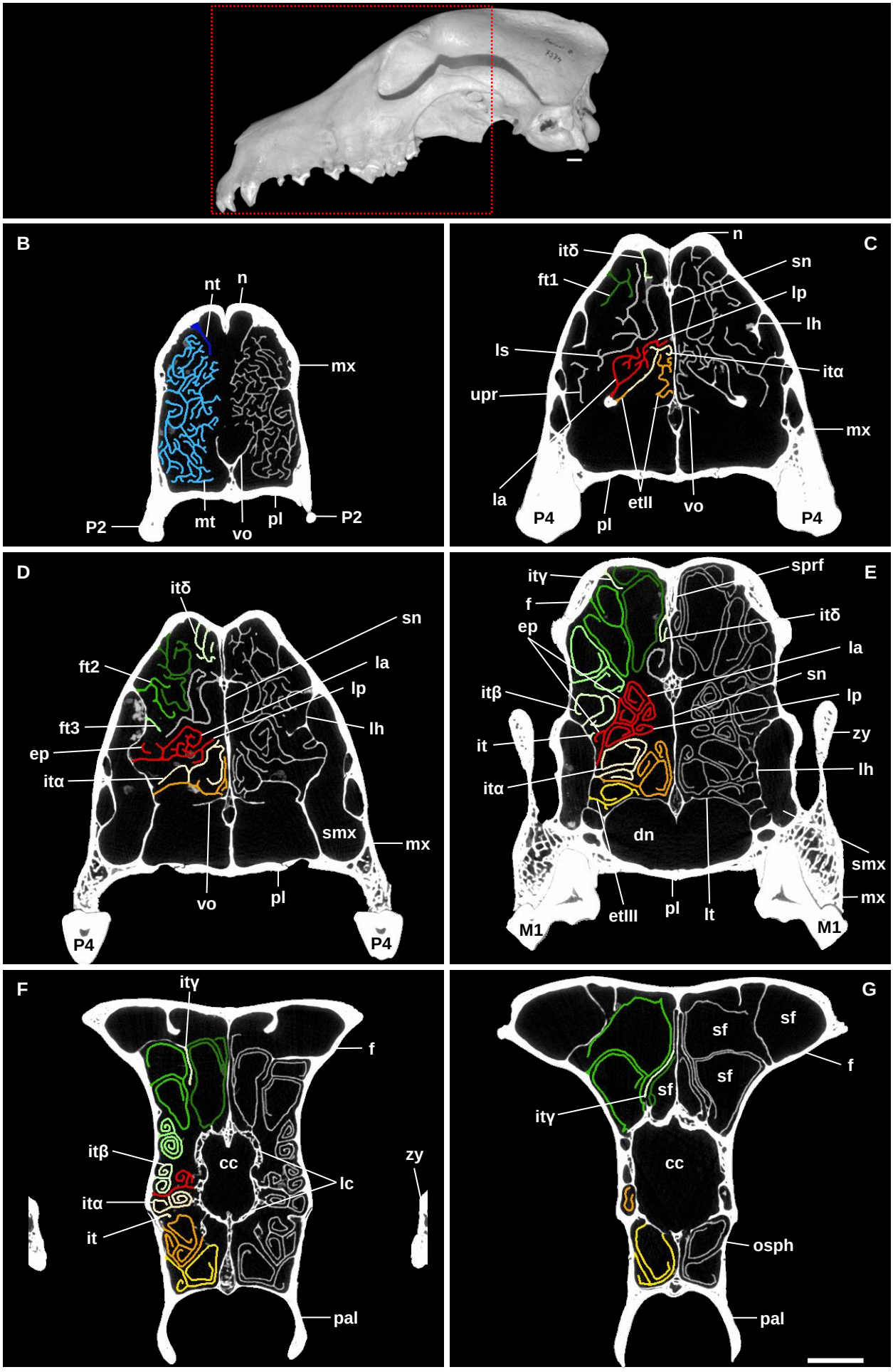

Fig. 41: Adult borzoi ([MfN] 7374): **A)** skull in lateral view showing the region of interest; **B)–G)** µCT cross sections of the ethmoidal region from rostral to caudal in caudal view, the turbinals are highlighted on one side. Scale bars: 10mm; Abbreviations: 1; colors refer to the turbinal color code..

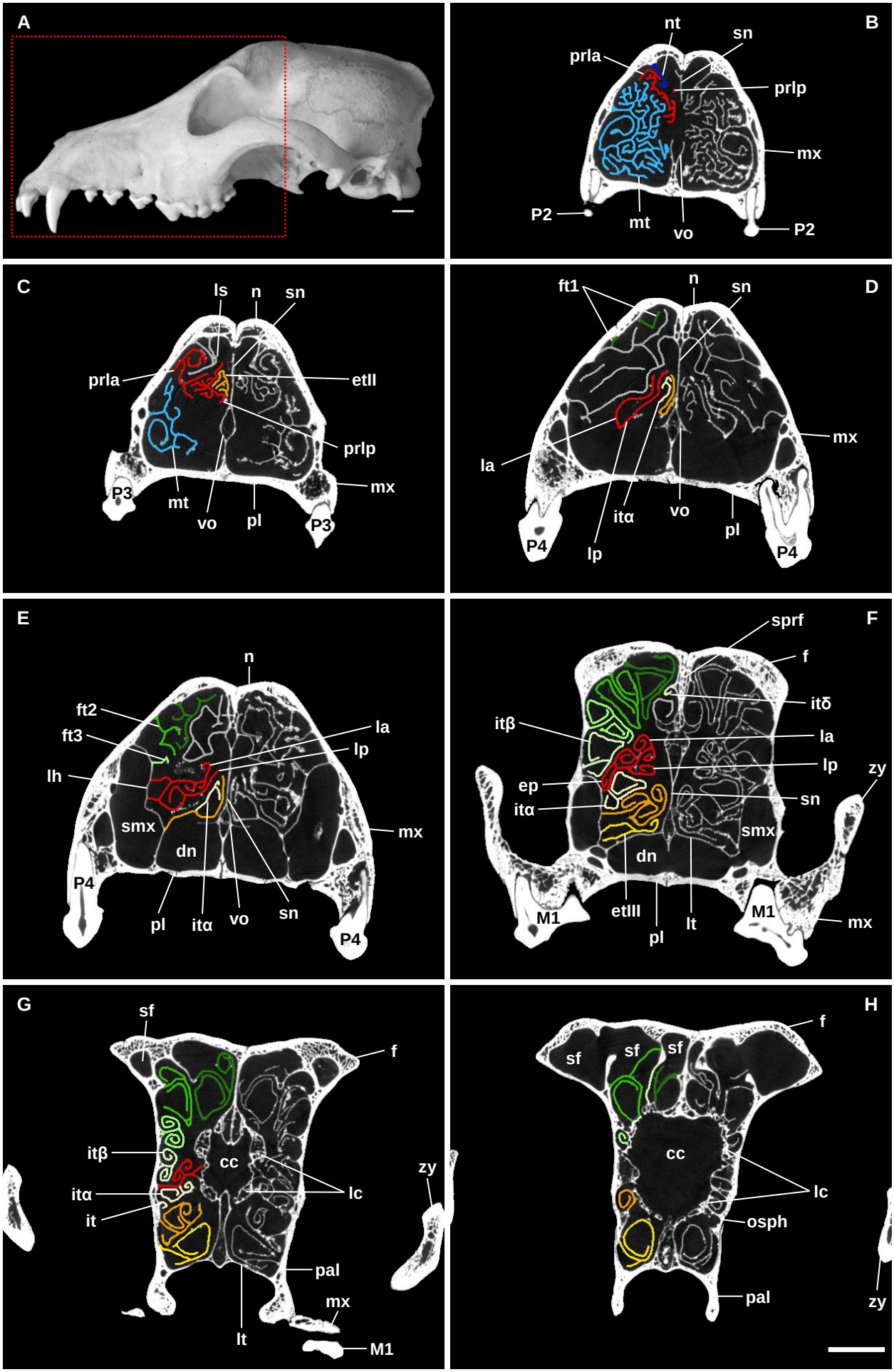

Fig. 42: Saluki ([MfN] 2709): **A)** skull in lateral view showing the region of interest; **B)–H)** µCT cross sections of the ethmoidal region from rostral to caudal in caudal view, the turbinals are highlighted on one side. Scale bars: 10mm; Abbreviations: 1; colors refer to the turbinal color code.

FIGURES

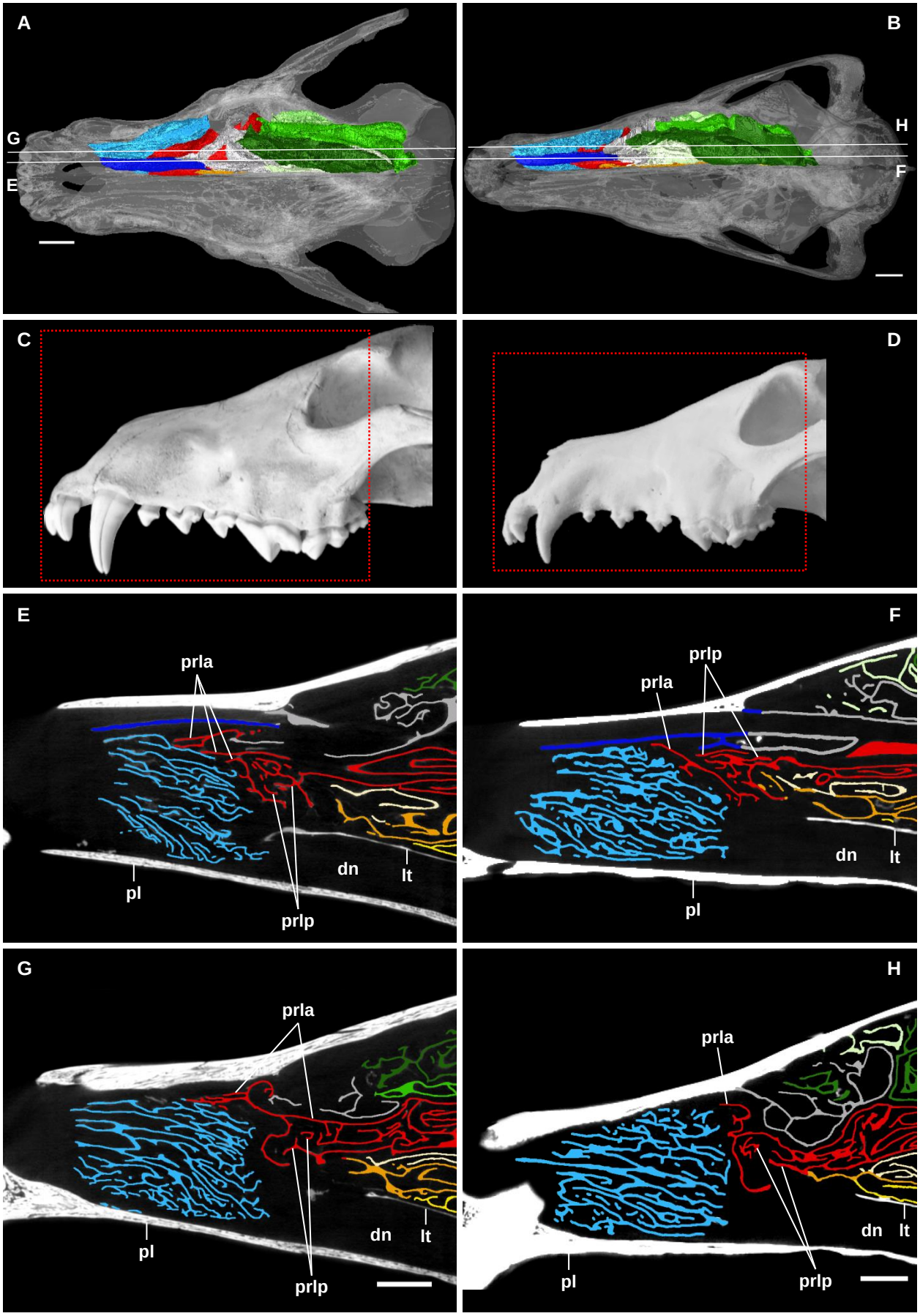

Fig. 43: Comparison of the respiratory pathway in four specimens of *Canis lupus*: **A), C), E), G) Eurasian wolf** (*Canis lupus lupus*, ZMB_MAM 93307, right side); **B), D), F), H) borzoi** (NMBE 1051164, left side, mirrored); **J), L), N), Q) modern pug** (NMBE 1051937, right side); **K), M), P), R) Cavalier** (NMBE 1062998, right side). **A), B), J), K**) virtual 3D models of the transparent skulls in dorsal view showing the position of the µCT sagittal sections; **C), D), L), M)** skulls in lateral view showing the region of interest; **E)-H), N)-R)** µCT sagittal sections in medial view. The displaced turbinals represent *CAT and maybe **RAT. See also Figs. 13 & 36, 28 & 22. Scale bars: 10mm; Abbreviations: 1; colors refer to the turbinal color code.

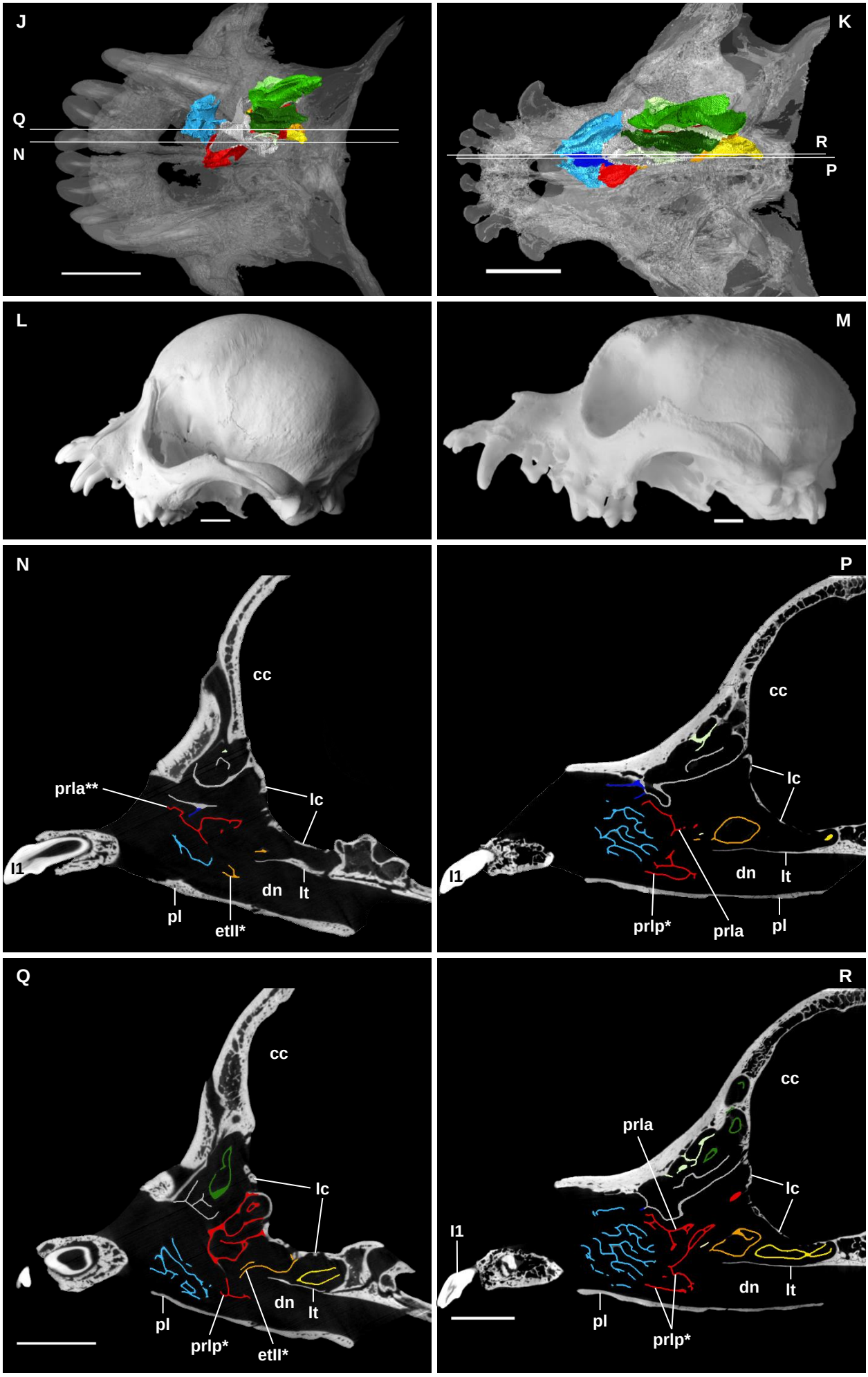

Fig. 43 (continued)

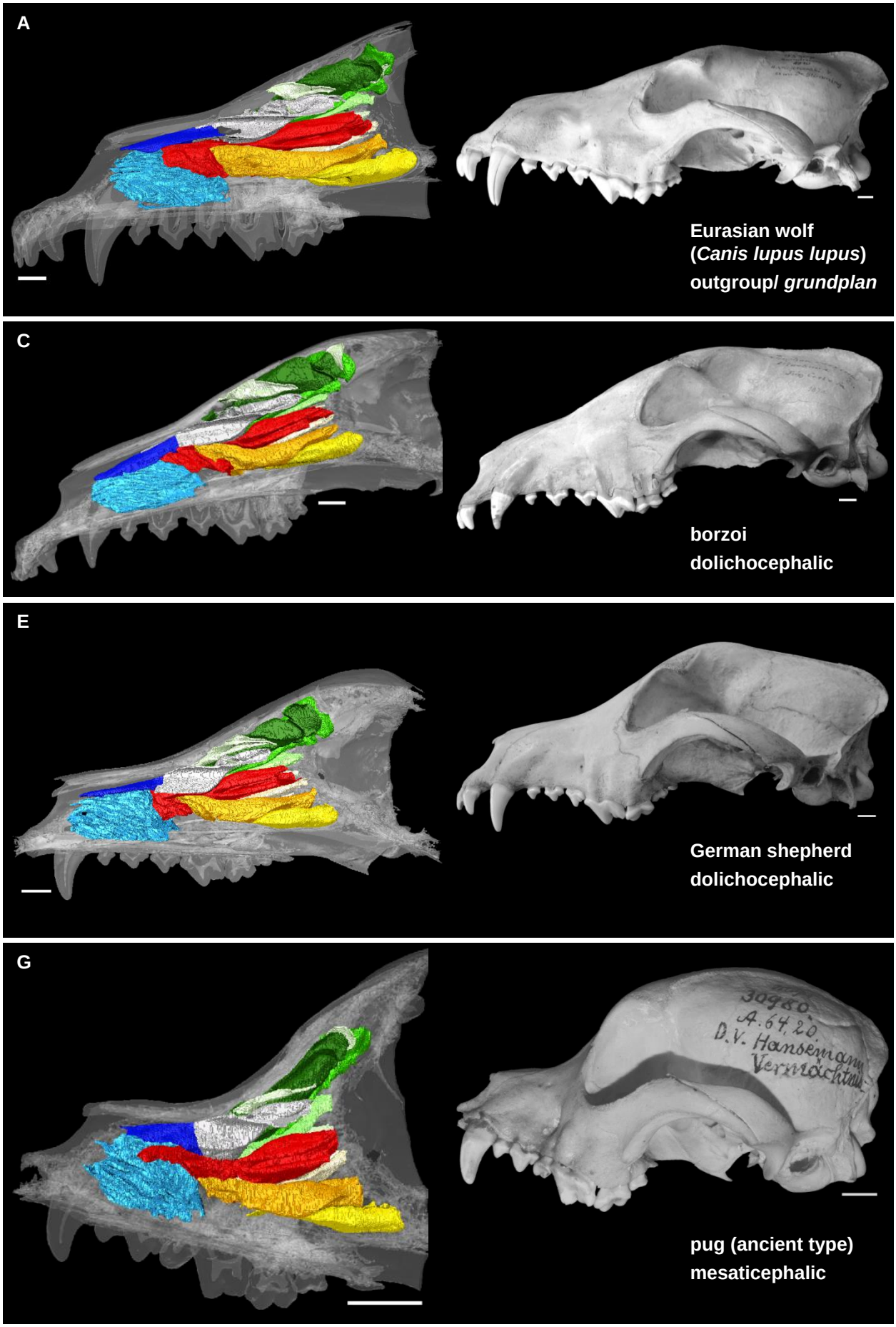

Fig. 44: Virtual 3D models showing the position and shape of the turbinal skeleton within the transparent nasal cavity in medial (A, C, E, G, J, L, N, Q), and dorsal (B, D, F, H, K, M, P, R) view, together with the skulls in lateral and dorsal view, in the different snout length types of *Canis lupus*: **A/B) Eurasian wolf** (*Canis lupus lupus*, ZMB_MAM 93307, right side); **C/D) borzoi** ([MfN] 1403, left side, 3D models mirrored); **E/F) German shepherd** (SMF 93607, right side); **G/H) pug** (ancient type, ZMB_MAM 30980, right side); ... (continued on page after next)

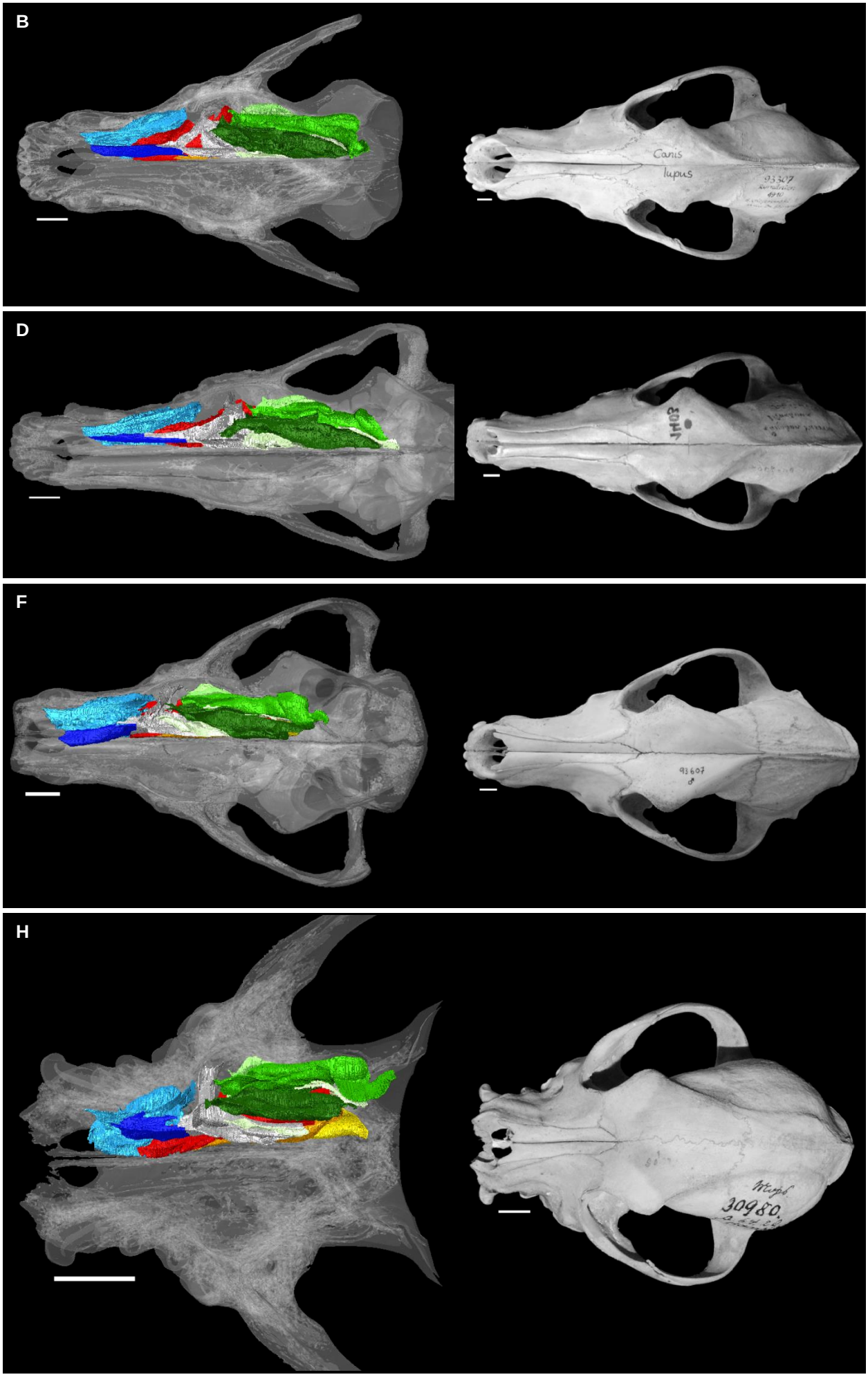

Fig. 44 (continued)

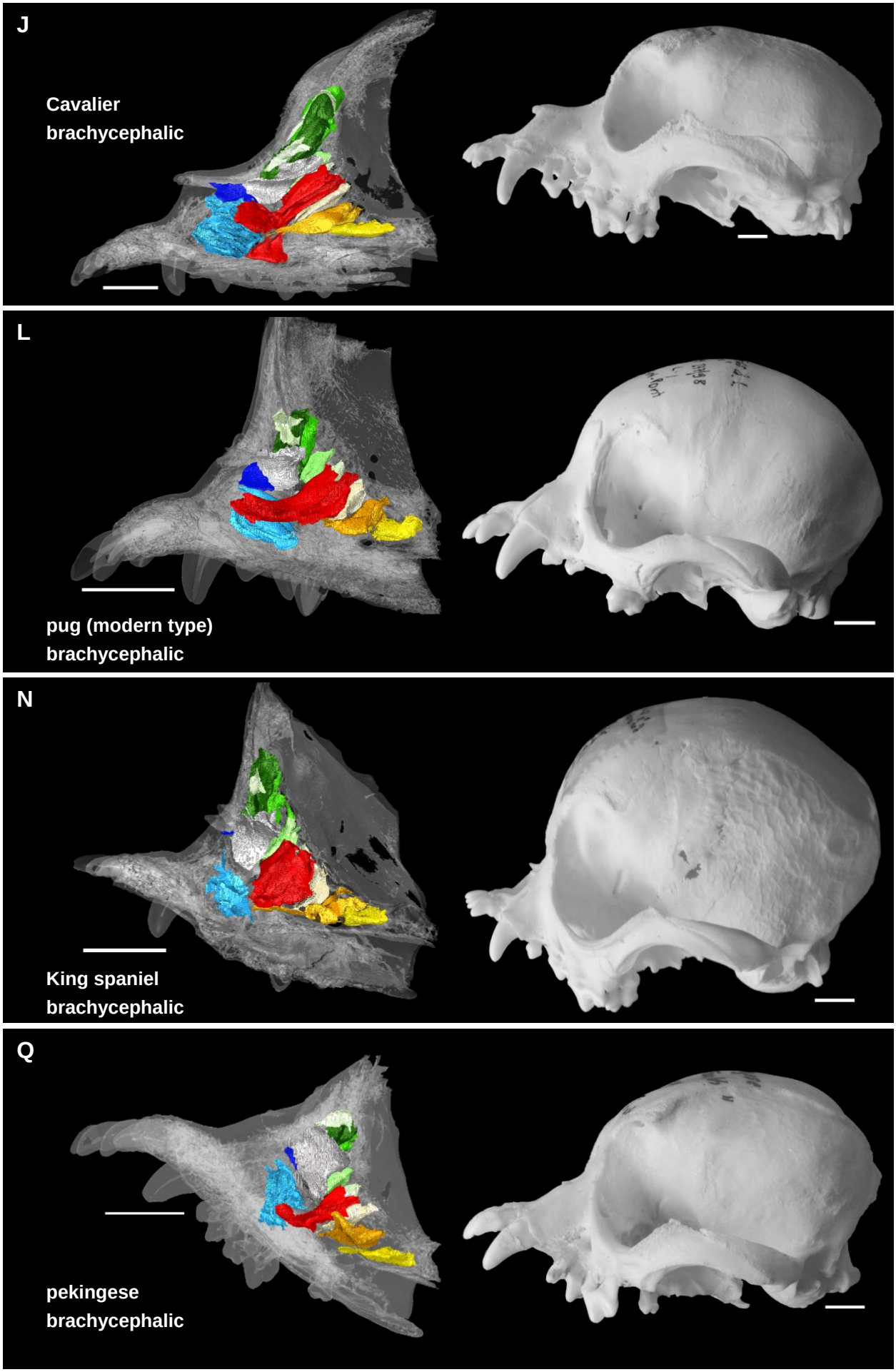

Fig. 44 (continued) ... **J/K) Cavalier** (NMBE 1062998, right side); **L/M) pug** (modern type, NMBE 1052345, right side); **N/P) King spaniel** (NMBE 1051945, left side, 3D models mirrored); **Q/R) pekingese** (NMBE 1051962, right side). Scale bars: 10mm; colors refer to the turbinal color code.

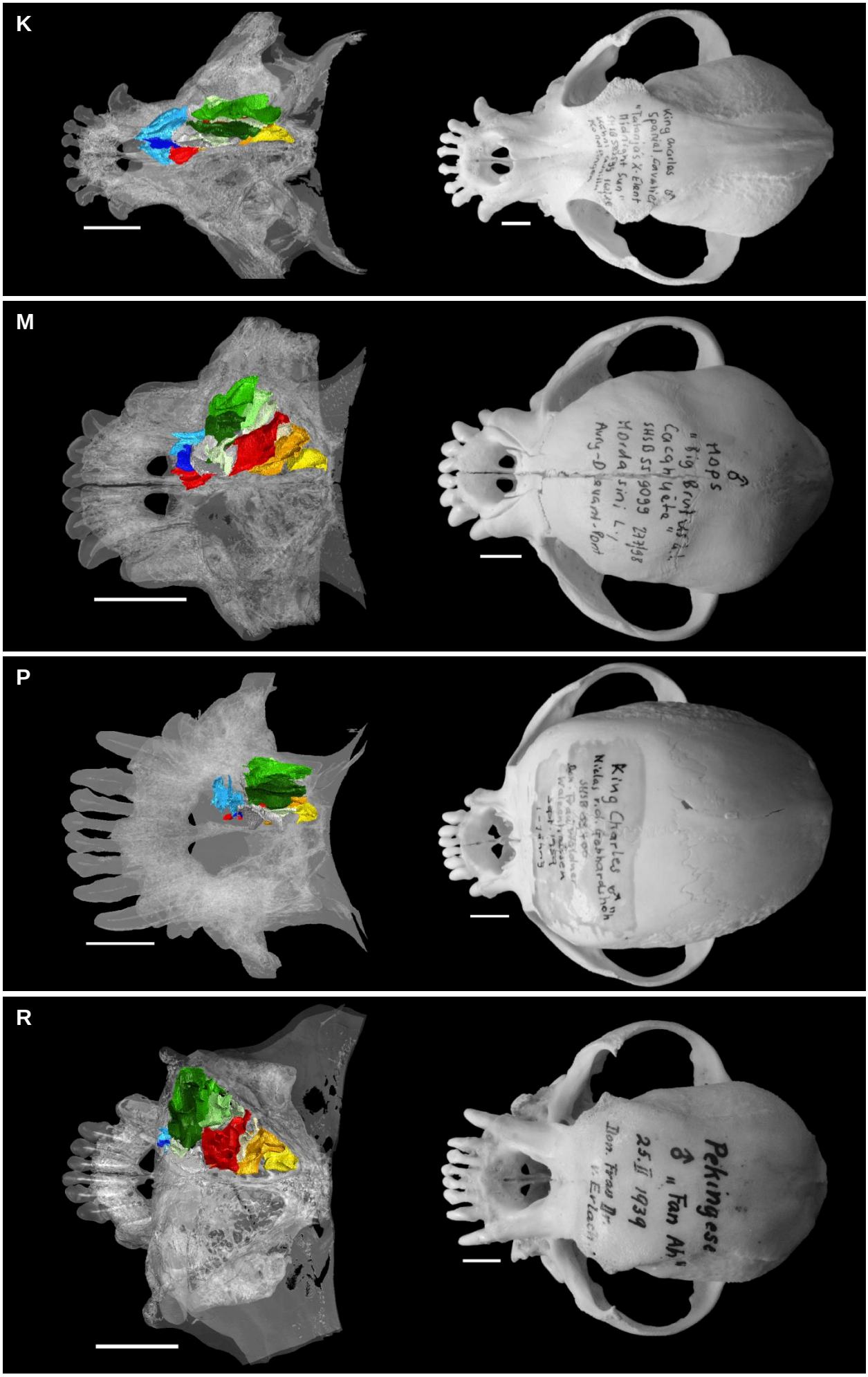

Fig. 44 (continued)

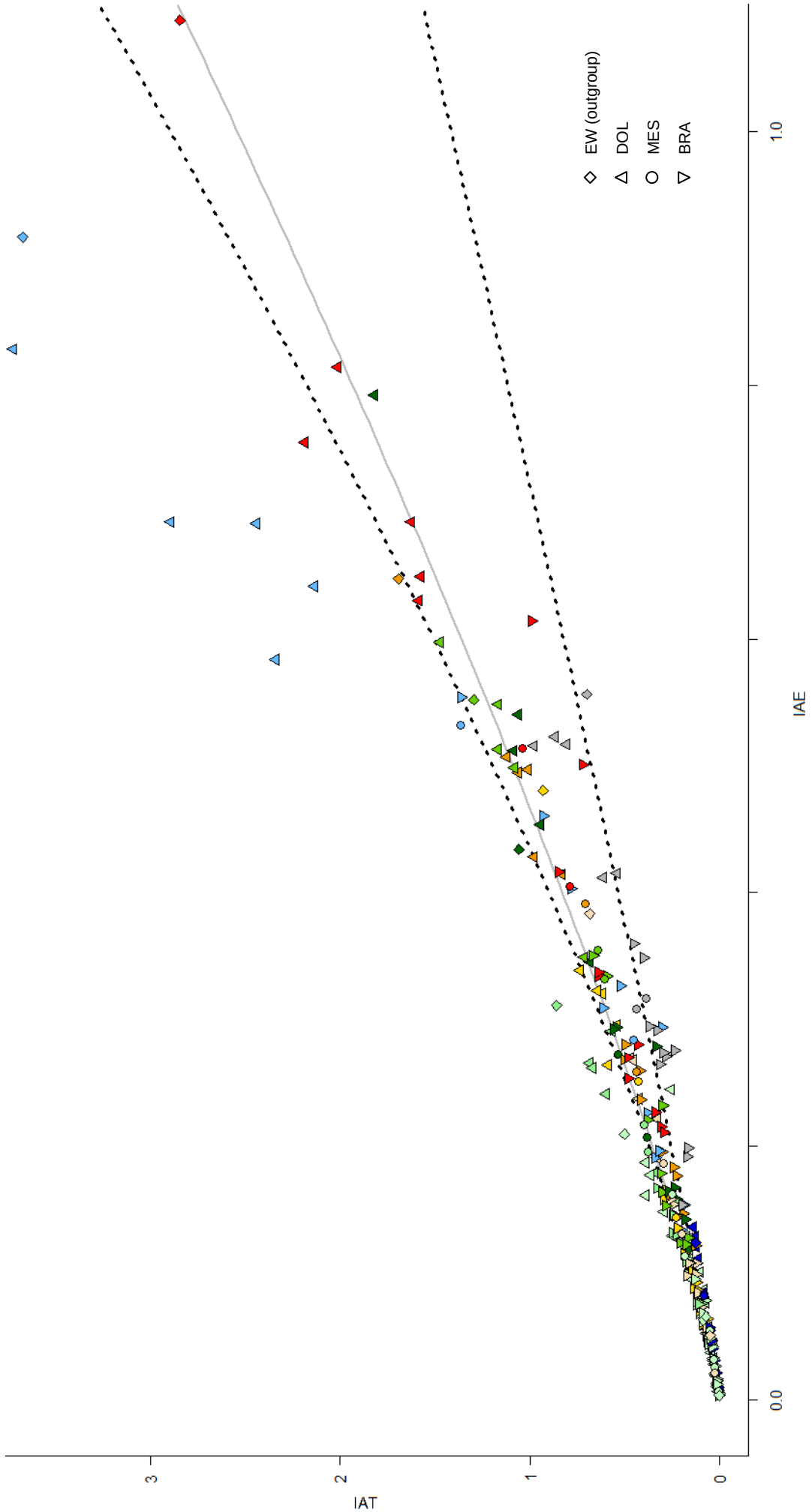

Fig. 45: Correlation between index turbinal surface area (IAT) and index exterior surface area (IAE) in the single turbinals including the lamina semicircularis in the investigated specimens of *Canis lupus familiaris*, grouped into the three snout length types based on IFB (ELLENBERGER & BAUM 1891). To show the spreading between the regression lines the steepest (borzoi NMBE 1051164) and the flattest (pug NMBE 1052345, left side) curve (dashed black lines) as far as of the Eurasian wolf (*Canis lupus lupus*, solid grey line) for outgroup comparison are added. The values of IAT and IAE are listed in Table 4. Abbreviations: 1; colors refer to the turbinal color code.

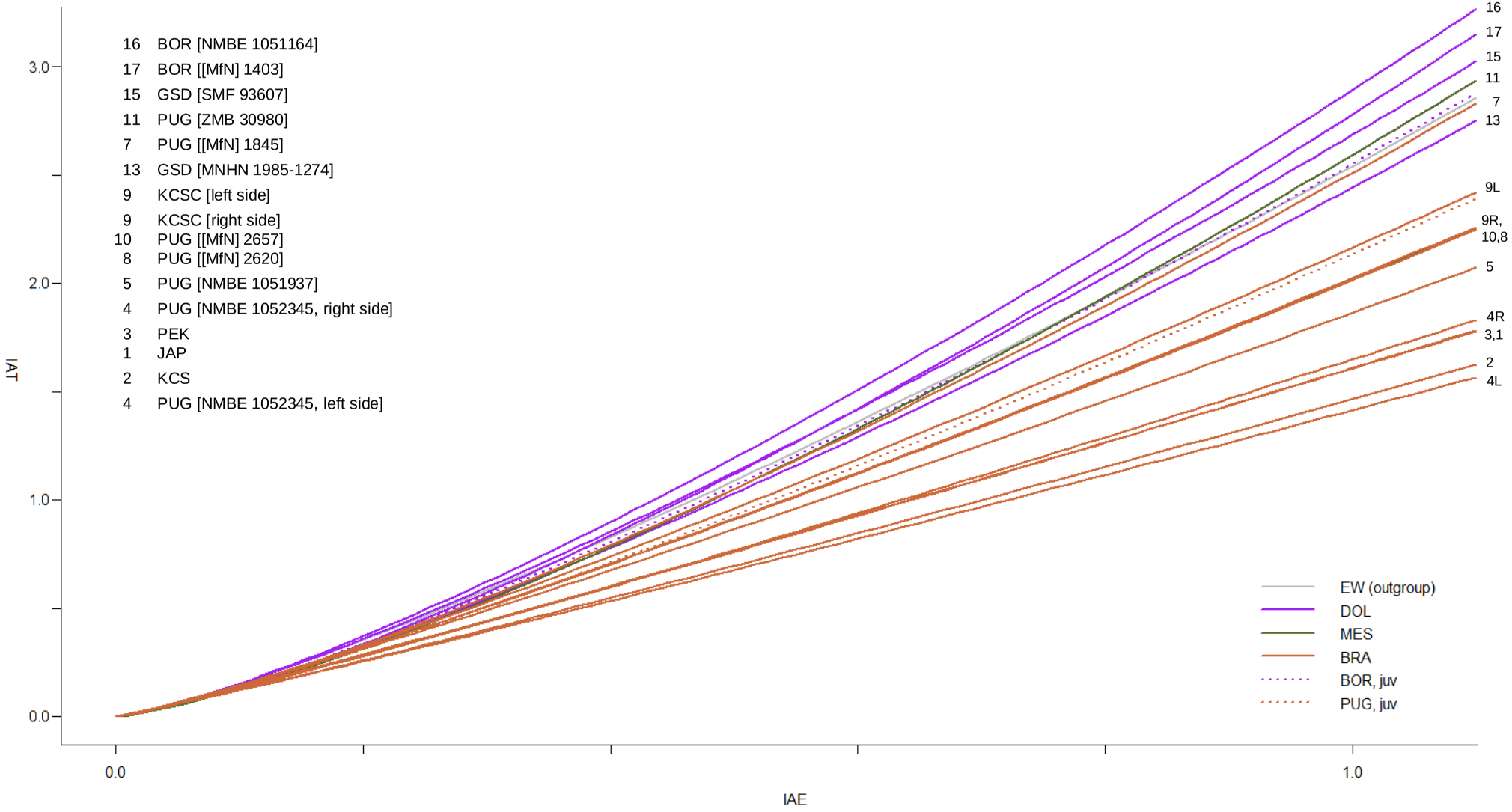

Fig. 46: Regression lines of all specimens of *Canis lupus* from Fig. 5 and Fig. S3 (Supplementary material) and Fig. 45. The specimens of *Canis lupus familiaris* are grouped into the three snout length types based on index facial length to length of braincase (IFB, ELLENBERGER & BAUM 1891); the Eurasian wolf (*Canis lupus lupus*) serves for outgroup comparison. The values of the regression lines (a, m) are listed in Table S5 (Supplementary material). Abbreviations: 1.

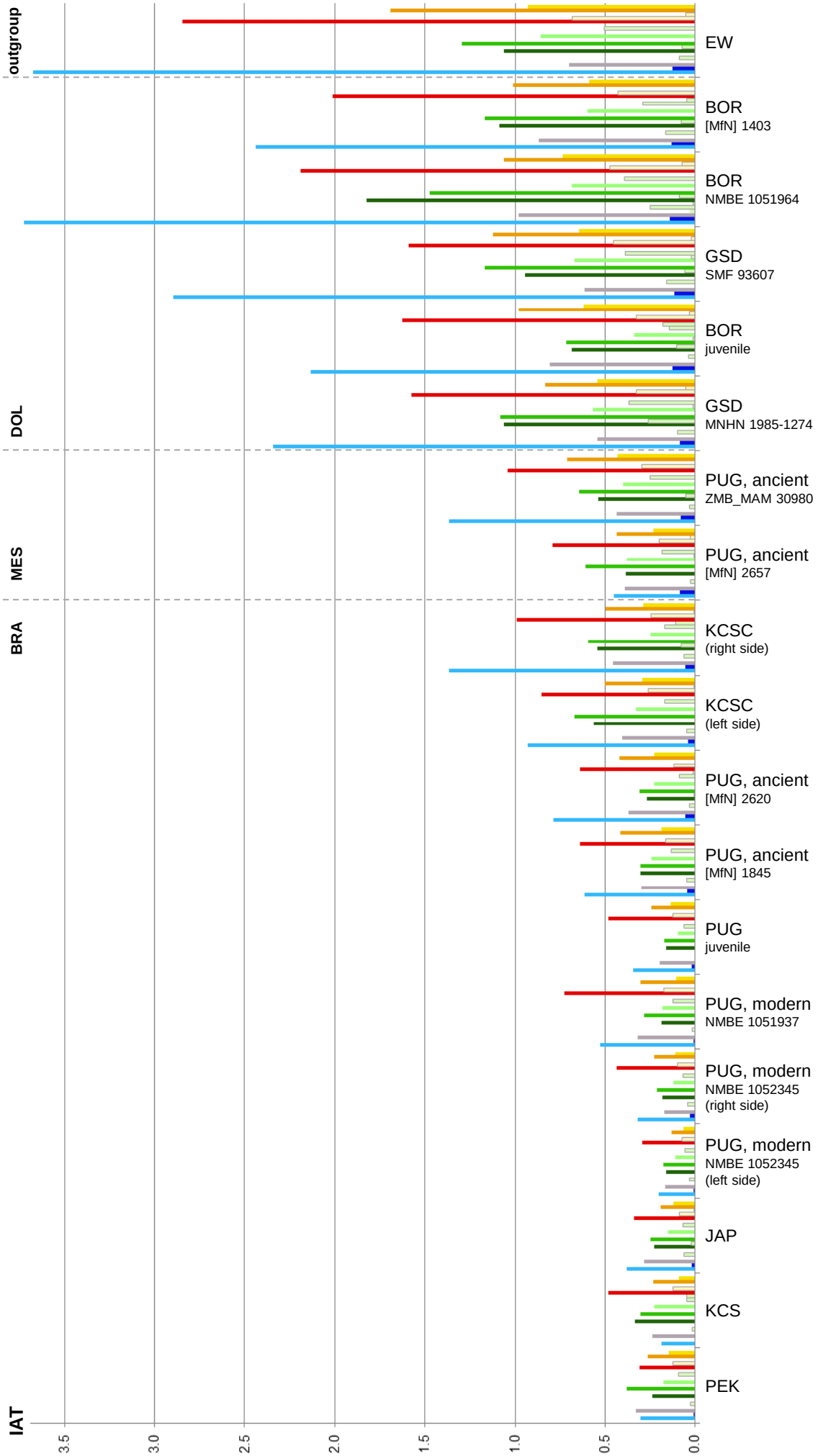

Fig. 47: Index turbinal surface area (IAT) within and between the investigated specimens of *Canis lupus*. The Eurasian wolf (*Canis lupus lupus*) serves for outgroup comparison, whereas the dogs (*Canis lupus familiaris*) are ordered based on index facial length to length of braincase (IFB, ELLENBERGER & BAUM 1891) and grouped into the three snout length types. The values of IAT are listed in Table 4. Abbreviations: 1; colors refer to the turbinal color code.

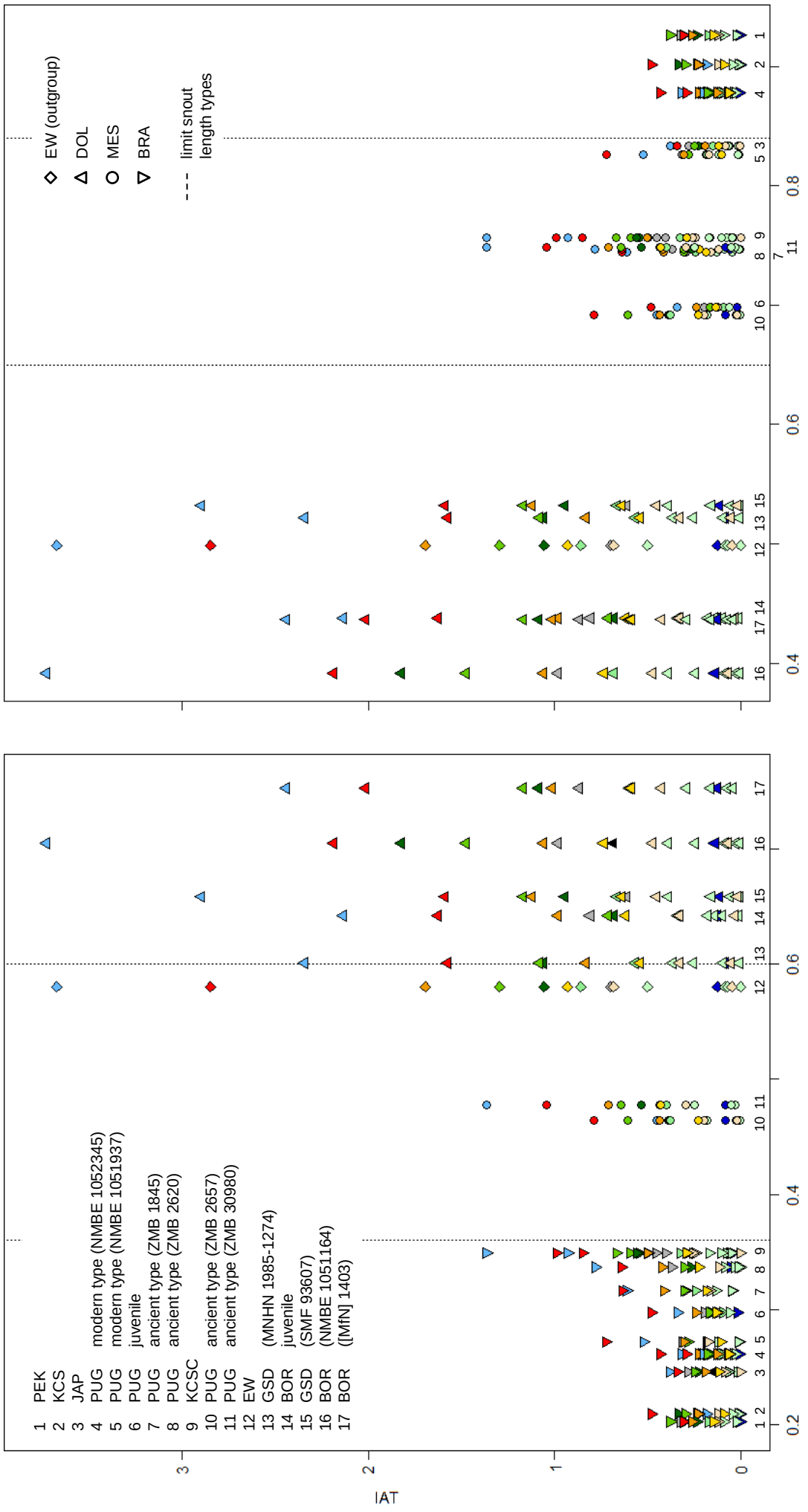

Fig. 48: Index turbinal surface area (IAT) within and between the investigated specimens of *Canis lupus*, plotted against the two snout length indices index facial length to length of braincase (IFB) and index breadth to length of skull (IBL) (ELLENBERGER & BAUM 1891). The Eurasian wolf (*Canis lupus lupus*) serves for outgroup comparison, whereas the dogs (*Canis lupus familiaris*) are grouped into the three snout length types. The values are listed in Table 1 (IFB, IBL) and Table 4 (IAT). Abbreviations: 1; colors refer to the turbinal color code.

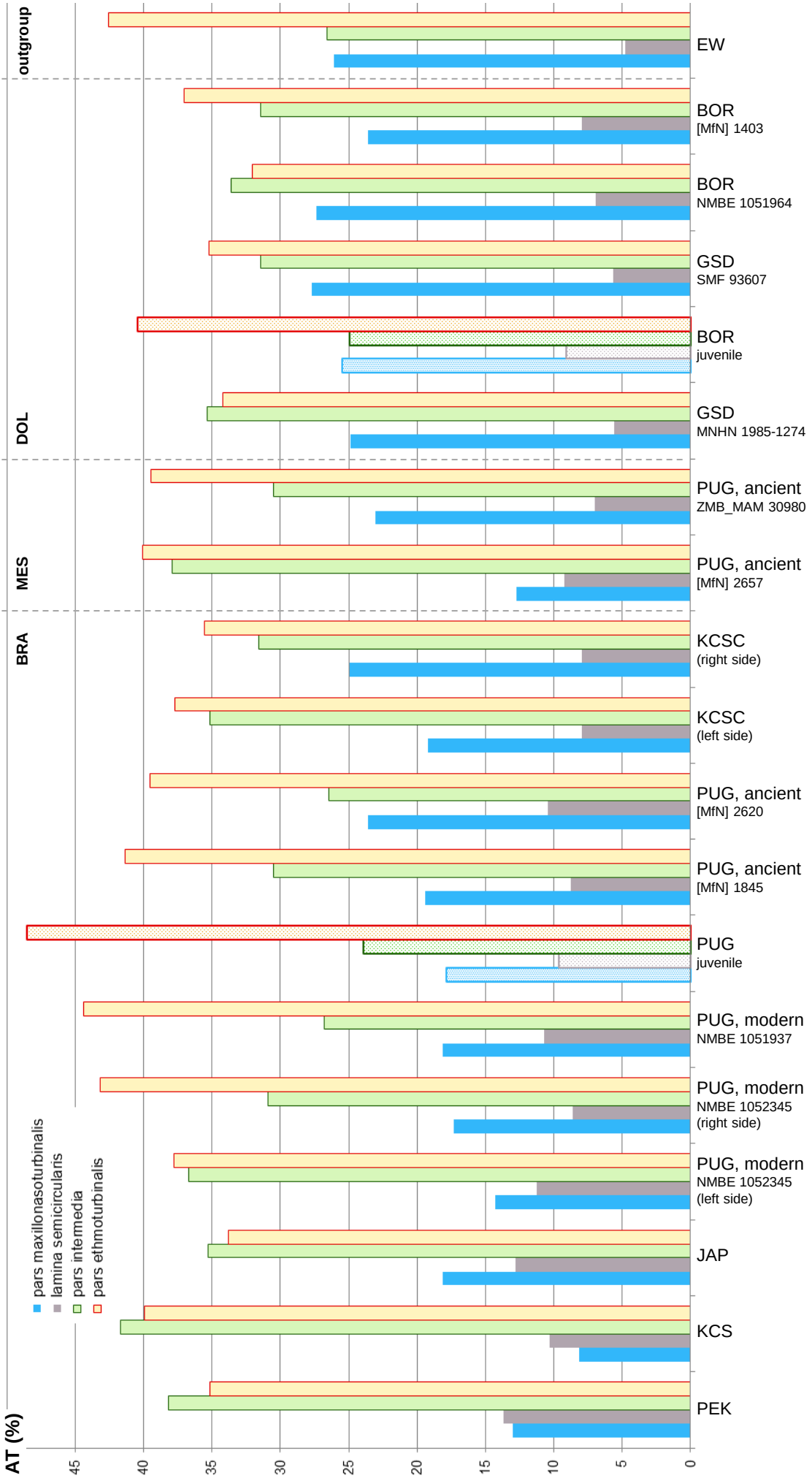

Fig. 49: Distribution of turbinal surface area (AT, %) on the three compartments in the ethmoidal region and the lamina semicircularis in the investigated specimens of *Canis lupus*. The Eurasian wolf (*Canis lupus lupus*) serves for outgroup comparison, whereas the dogs (*Canis lupus familiaris*) are ordered based on index facial length to length of braincase (IFB, ELLENBERGER & BAUM 1891) and grouped into the three snout length types. The bars of the two juveniles are dotted. The values of AT (%) are listed in Table S7 (Supplementary material). Abbreviations: 1.

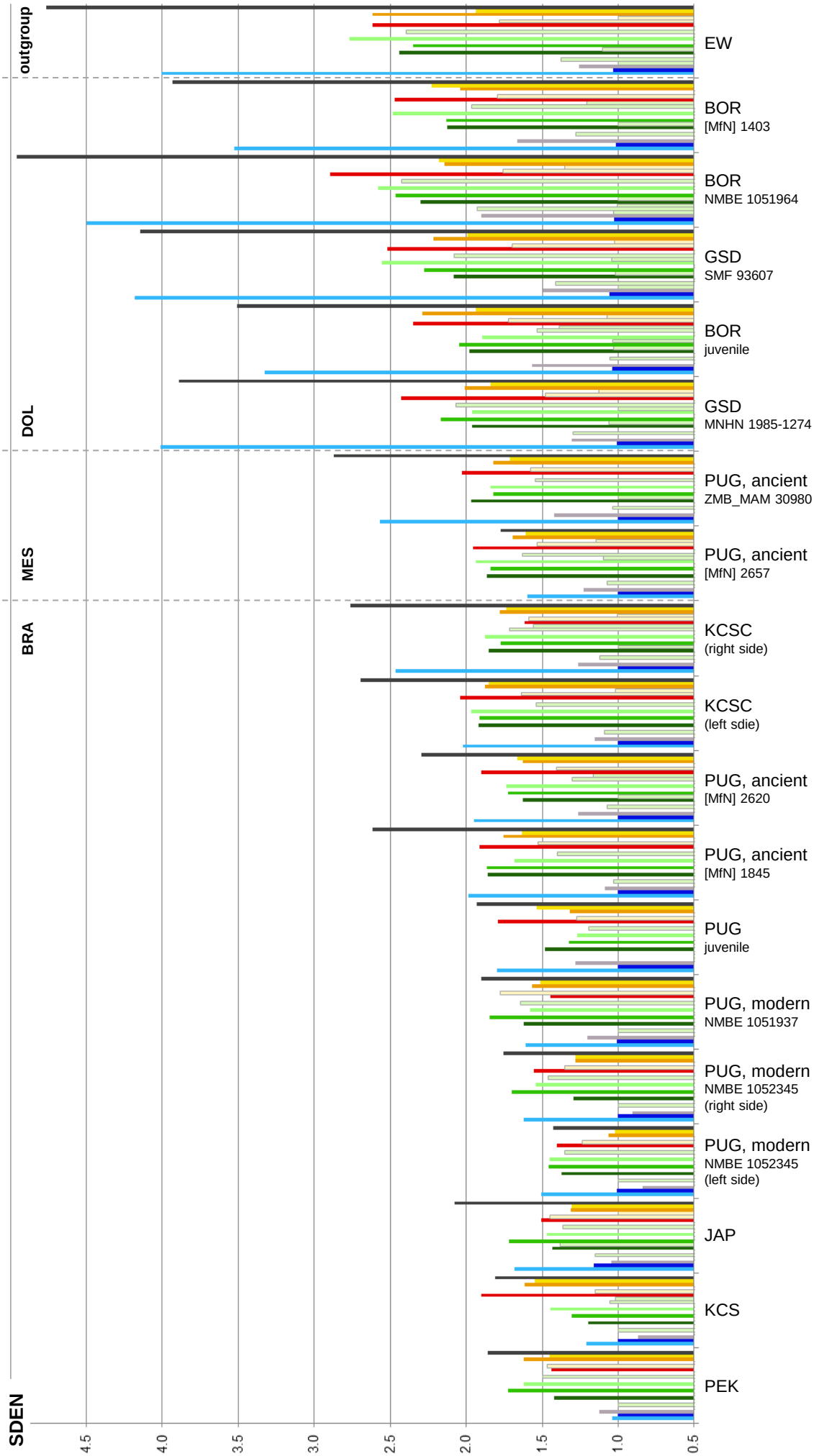

Fig. 50: Turbinal surface density (SDEN) within and between the investigated specimens of *Canis lupus*. The Eurasian wolf (*Canis lupus lupus*) serves for outgroup comparison, whereas the dogs (*Canis lupus familiaris*) are ordered based on index facial length to length of braincase (IFB, ELLENBERGER & BAUM 1891) and grouped into the three snout length types. The values of SDEN are listed in Table S10 (Supplementary material). Abbreviations: 1; colors refer to the turbinal color code, black bar = total SDEN.

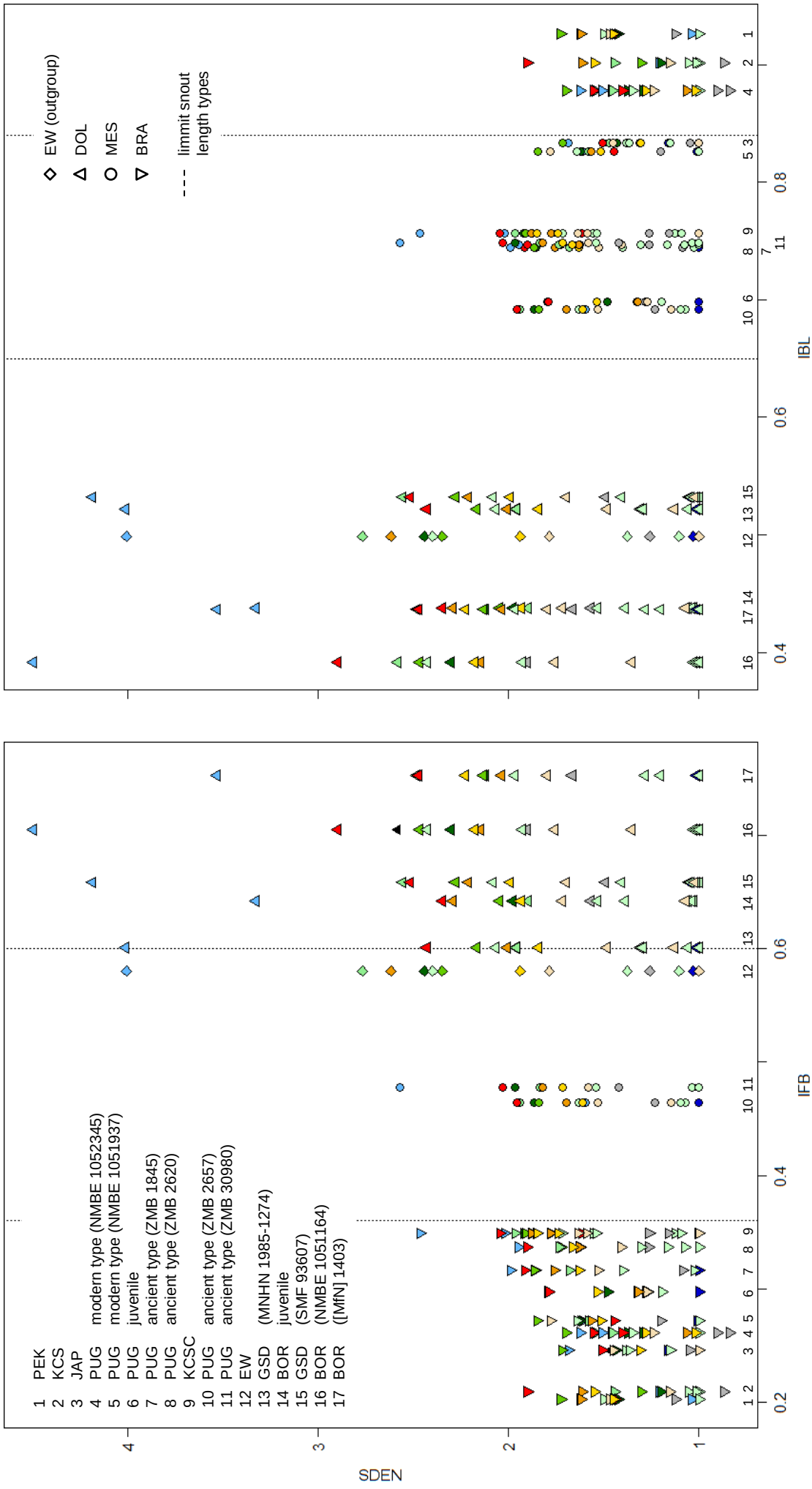

Fig. 51: Turbinal surface density (SDEN) within and between the investigated specimens of *Canis lupus*, plotted against the two snout length indices index facial length to length of braincase (IFB) and index breadth to length of skull (IBL) (ELLENBERGER & BAUM 1891). The Eurasian wolf (*Canis lupus lupus*) serves for outgroup comparison, whereas the dogs (*Canis lupus familiaris*) are grouped into the three snout length types. The values are listed in Table 1 (IFB, IBL) and Table S10 (SDEN; Supplementary material). Abbreviations: 1; colors refer to the turbinal color code.

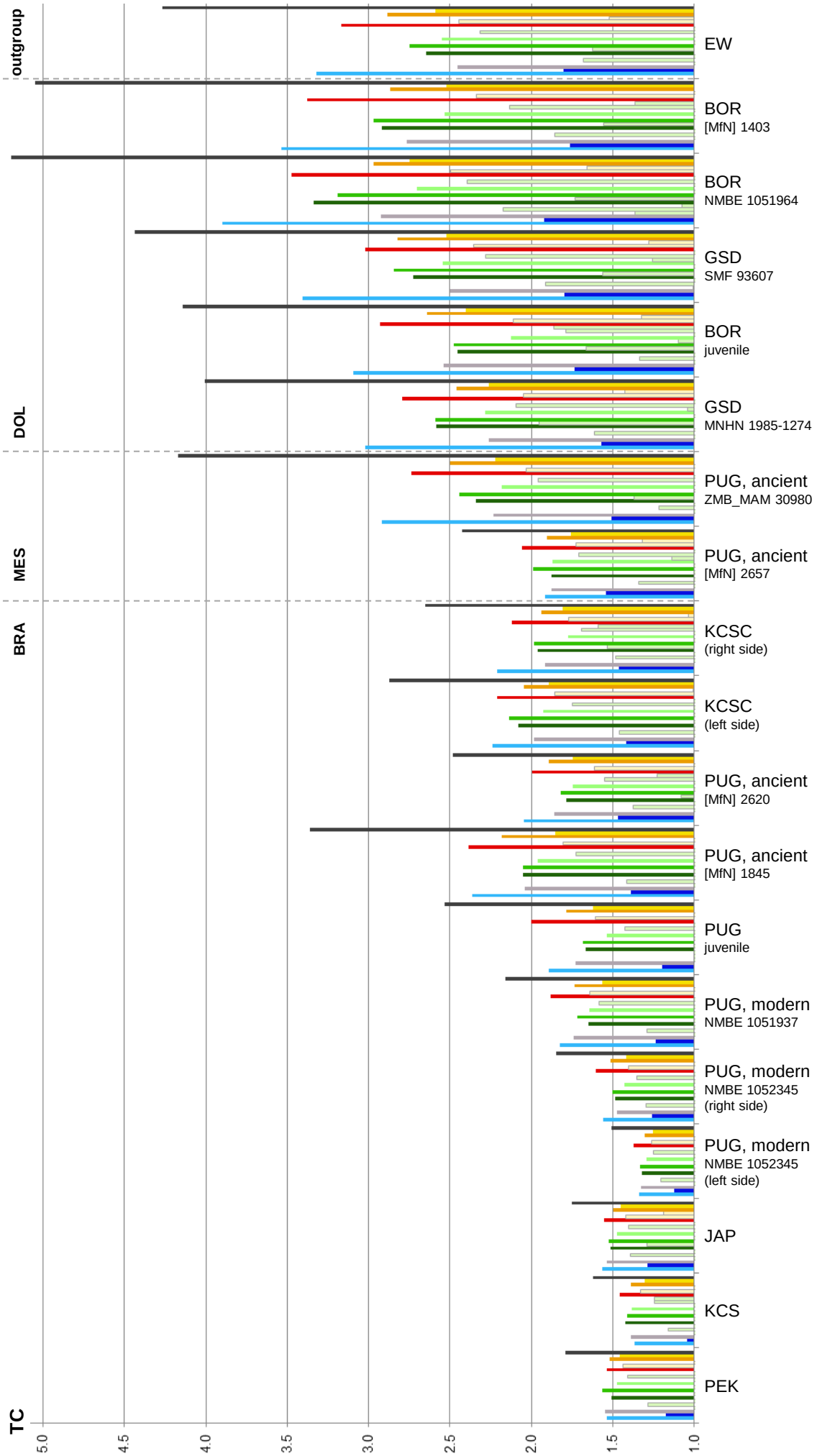

Fig. 52: Turbinal complexity (TC) within and between the investigated specimens of *Canis lupus*. The Eurasian wolf (*Canis lupus lupus*) serves for outgroup comparison, whereas the dogs (*Canis lupus familiaris*) are ordered based on index facial length to length of braincase (IFB, ELLENBERGER & BAUM 1891) and grouped into the three snout length types. The values of TC are listed in Table S11 (Supplementary material). Abbreviations: 1; colors refer to the turbinal color code, black bar = total TC.

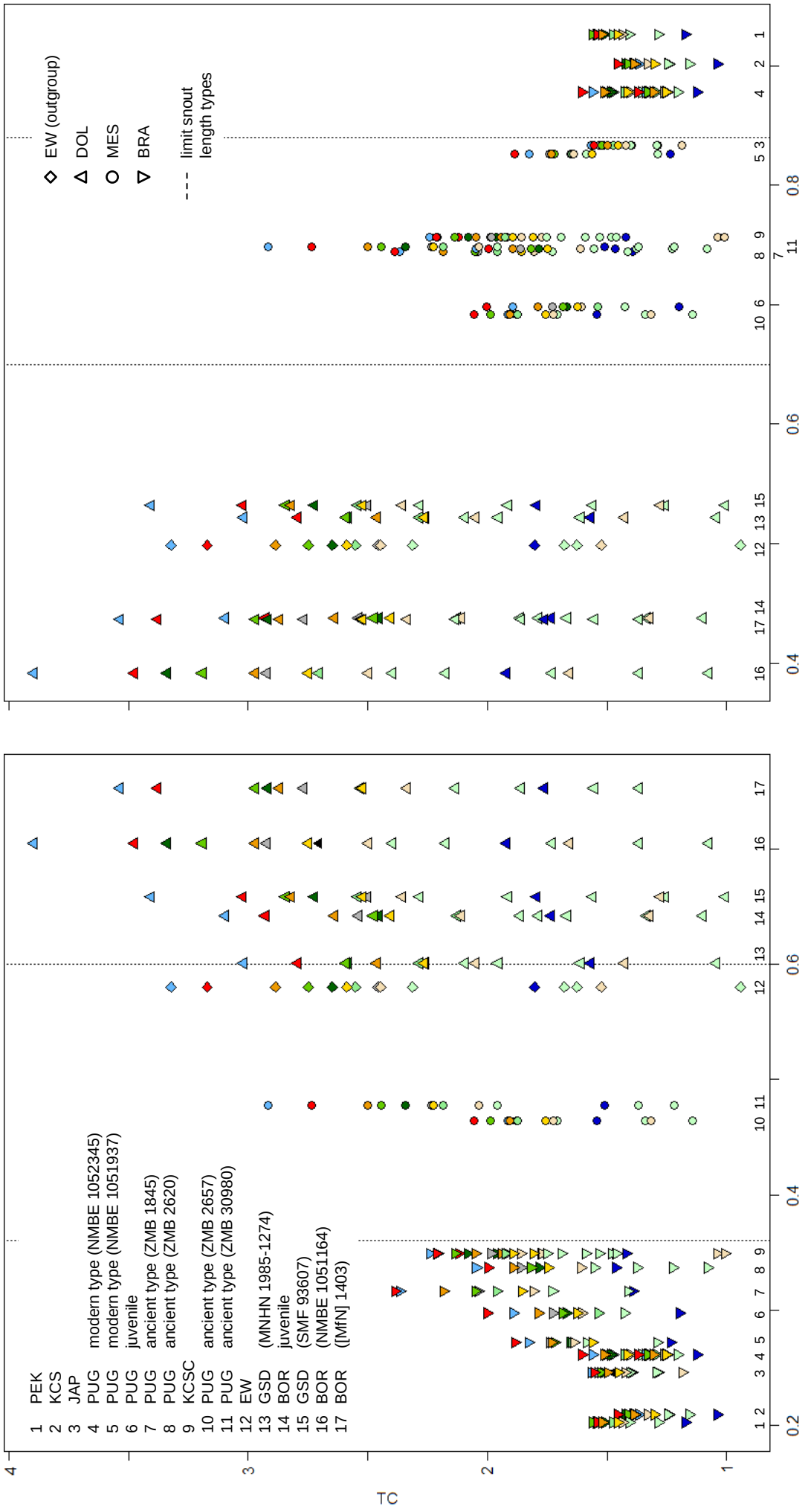

Fig. 53: Turbinal complexity (TC) within and between the investigated specimens of *Canis lupus*, plotted against the two snout length indices index facial length to length of braincase (IFB) and index breadth to length of skull (IBL) (ELLENBERGER & BAUM 1891). The Eurasian wolf (*Canis lupus lupus*) serves for outgroup comparison, whereas the dogs (*Canis lupus familiaris*) are grouped into the three snout length types. The values are listed in Table 1 (IFB, IBL) and Table S11 (TC; Supplementary material). Abbreviations: 1; colors refer to the turbinal color code.

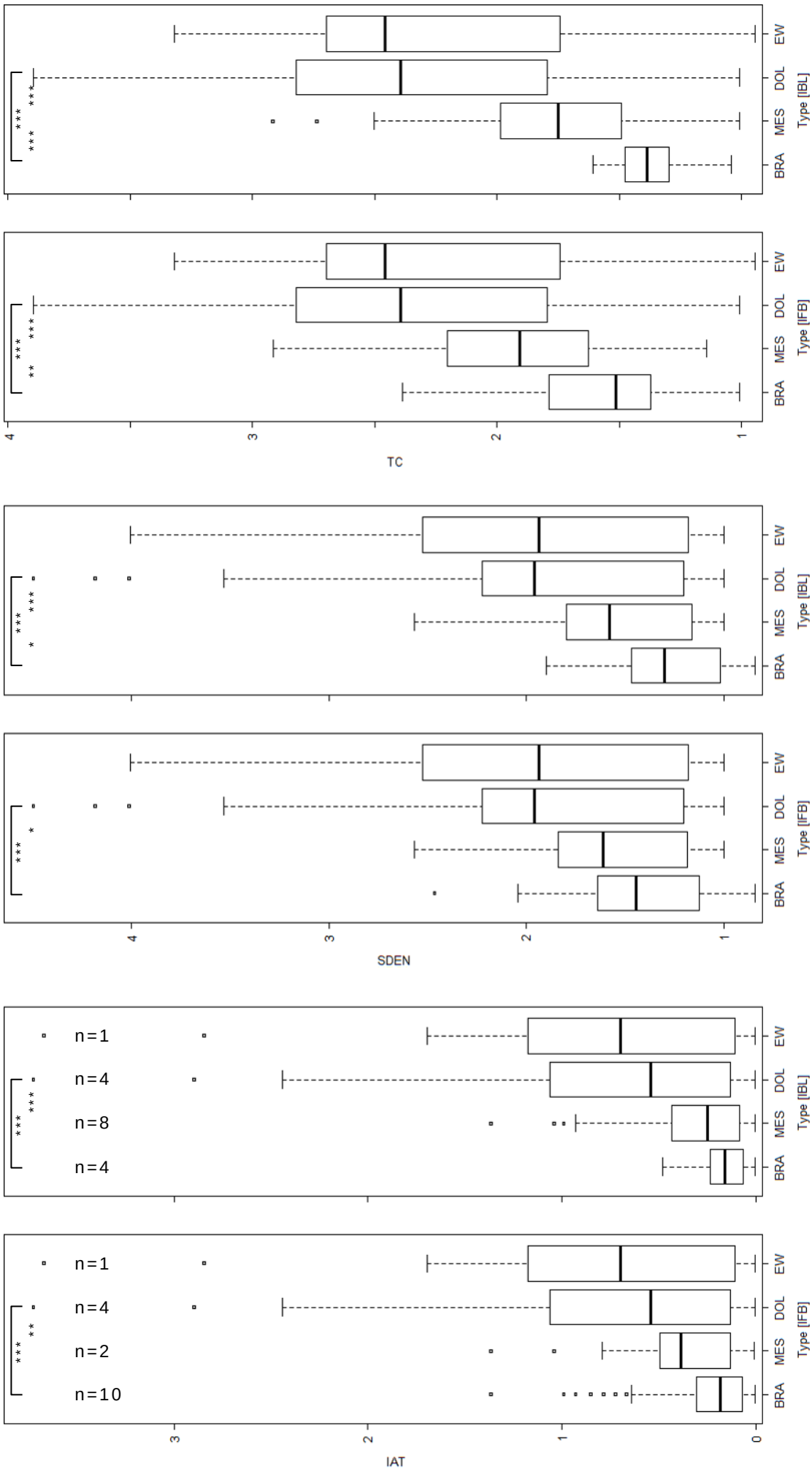

Fig. 54: Comparison of index turbinal surface area (IAT), turbinal surface density (SDEN), and turbinal complexity (TC) between the three snout length types of *Canis lupus familiaris* (n, number of specimens per group), based on the two snout length indices index facial length to length of braincase (IFB) and index breadth to length of skull (IBL) (ELLENBERGER & BAUM 1891). The Eurasian wolf (*Canis lupus lupus*) serves for outgroup comparison. The asterisks indicate the significance based on the TukeyHSD test in R 3.3.0 that is listed in Table S14 (Supplementary material). Abbreviations: 1.

SUPPLEMENTARY MATERIAL – TABLES

Table S1: Measurements with the caliper (mean, mm) on the skulls of *Canis lupus familiaris* and *Canis lupus lupus* in this study. The definitions of the measurements are listed in Table 2 and illustrated in Fig. 3; except the parameter ALB (LPII*IOB, mm^2). Some measurements could not be taken on each skull (NA) e.g., because the structure is broken. The raw data is given in Table eS1 (electronic Supplementary material).

Specimen	Breed	CBL	GLS	BLI	BLII	NLI	NLII	SL	LBC
48.1	GSD	89.7	95.5	84.3	81.2	27.8	25.8	41.3	61.5
MNHN 1881-47	PUG	72.0	78.7	68.5	66.1	19.0	17.2	31.3	57.9
SMF 16303	BOR	171.1	176.3	159.0	153.8	66.8	59.9	91.0	93.3
MNHN 2007-428	PUG	50.7	59.0	NA	NA	NA	NA	NA	NA
ZMB_MAM 815	EW	NA	252.8	226.6	221.0	101.7	90.4	130.0	129.9
ZMB_MAM 93307	EW	225.1	240.5	213.6	208.2	83.1	75.1	117.2	129.5
ZMB_MAM 93308	EW	206.7	223.8	195.0	189.9	84.0	74.9	112.6	118.6
MNHN 1985-1274	GSD	199.0	210.7	187.3	183.6	78.6	68.5	104.7	114.1
SMF 93607	GSD	196.7	208.9	185.9	182.1	82.4	72.7	107.2	110.4
MNHN 1985-1216	GD	205.5	225.6	194.1	189.5	83.7	74.4	115.2	121.0
MNHN 1947-78	GLD	201.1	218.2	190.3	184.8	80.6	70.3	106.4	119.6
NMBE 1051945	KCS	77.4	88.8	74.9	74.2	16.1	15.3	25.6	73.1
NMBE 1051948	KCS	79.7	90.9	79.4	78.6	15.6	13.5	25.8	71.3
NMBE 1059207	KCSC	107.1	111.6	103.0	99.5	39.7	34.2	54.1	64.8
NMBE 1062998	KCSC	110.6	118.0	106.5	104.7	30.4	26.5	45.8	75.8
NMBE 1051962	PEK	83.7	88.5	79.7	77.8	15.0	12.8	29.6	63.4
NMBE 1051965	PEK	68.8	72.1	64.9	62.9	12.0	9.1	18.6	60.2
SMF 35611	PEK	60.9	68.8	57.1	56.0	12.4	11.4	20.2	54.8
NMBE 1051951	JAP	80.1	84.3	75.2	74.4	17.4	14.9	27.5	60.7
ZMB_MAM 7436	JAP	73.3	79.0	67.3	66.7	14.7	12.5	22.2	61.2
NMBE 1051937	PUG	84.2	94.0	77.0	75.3	20.9	19.2	33.3	70.8
NMBE 1052345	PUG	77.5	87.6	72.1	70.5	18.8	17.8	30.9	68.1
SMF 16284	PUG	98.6	NA	93.9	90.4	NA	NA	NA	NA
[MfN] 1845	PUG	95.5	104.0	88.4	86.5	25.1	21.4	39.9	67.7
[MfN] 2620	PUG	97.8	103.0	92.5	89.9	27.1	23.3	40.7	69.0
[MfN] 2630	PUG	87.9	93.0	81.5	79.7	22.2	19.8	35.0	66.8
[MfN] 2657	PUG	106.8	112.2	101.5	99.8	34.7	31.2	50.2	67.3
ZMB_MAM 30980	PUG	109.8	117.1	NA	102.8	38.6	34.4	50.1	72.0
[MfN] 2709	SAL	168.2	180.3	158.9	154.8	70.1	62.8	93.9	96.2
NMBE 1051164	BOR	244.1	269.2	229.0	223.3	111.7	100.2	146.0	142.1
NMBE 1051166	BOR	225.5	239.1	210.4	205.7	97.0	90.6	128.2	126.2
NMBE 1051180	BOR	228.4	247.4	216.5	211.5	97.6	88.1	131.8	130.0
NMBE 1052706	BOR	221.0	237.6	208.4	203.7	96.0	86.5	129.1	121.7
[MfN] 1403	BOR	217.9	226.6	205.1	199.8	96.5	87.0	122.7	115.6
[MfN] 7374	BOR	235.4	255.9	222.2	217.3	104.9	92.4	136.4	136.3

BLI/II, basal length I/II; **BOR**, borzoi; **CBL**, condylobasal length; **EW**, Eurasian wolf; **GD**, Groenendael; **GLD**, Greenland dog; **GLS**, greatest length of skull; **GSD**, German shepherd; **IOB**, interorbital breadth; **JAP**, Japanese chin; **KCS**, King Charles spaniel; **KCSC**, Cavalier King Charles spaniel; **LBC**, length of braincase; **[MfN]**, alternative labeling of mammal collection at Museum für Naturkunde Berlin, Germany; **MNHN**, Museum national d'Histoire naturelle Paris, France; **NLI/II**, nasal length I/II; **NMBE**, Naturhistorisches Museum der Burgergemeinde Bern, Switzerland; **OH**, occipital height; **PEK**, pekingese; **SAL**, saluki; **SL**, skull length; **SMF**, Senckenberg Forschungsinstitut und Naturmuseum Frankfurt am Main, Germany; **ZMB_MAM**, mammal collection of Museum für Naturkunde Berlin, Germany.

Table S1 (continued)

Specimen	Breed	LPI	LPII	LIF	BZB	RB	NB	BIF	IOB
48.1	GSD	50.6	45.4	5.9	57.0	23.8	10.8	2.1	21.5
MNHN 1881-47	PUG	35.3	30.3	4.6	55.0	21.6	9.6	2.1	23.1
SMF 16303	BOR	86.6	77.1	10.4	77.2	31.0	16.4	2.7	26.1
MNHN 2007-428	PUG	NA	NA	NA	46.1	17.3	NA	NA	6.7
ZMB_MAM 815	EW	118.4	104.2	13.4	134.4	47.4	26.5	4.4	42.3
ZMB_MAM 93307	EW	112.1	99.3	15.4	119.9	45.3	24.4	4.8	39.4
ZMB_MAM 93308	EW	103.4	91.5	11.2	125.7	43.0	24.8	3.8	43.5
MNHN 1985-1274	GSD	105.5	92.1	12.9	110.0	38.2	24.5	5.0	42.8
SMF 93607	GSD	103.1	91.7	13.7	111.1	39.6	22.4	4.8	38.7
MNHN 1985-1216	GD	103.5	NA	NA	116.3	41.1	23.4	NA	48.7
MNHN 1947-78	GLD	102.1	90.0	13.6	120.3	42.6	23.9	4.5	42.0
NMBE 1051945	KCS	38.9	31.8	4.8	80.0	27.3	16.4	3.9	34.2
NMBE 1051948	KCS	39.8	32.8	6.2	80.9	27.5	15.7	4.2	32.1
NMBE 1059207	KCSC	53.8	50.0	7.8	78.1	24.9	16.4	3.3	25.8
NMBE 1062998	KCSC	54.7	45.8	7.3	89.3	31.2	15.3	3.5	27.6
NMBE 1051962	PEK	44.9	34.2	5.1	81.9	32.7	14.8	4.2	27.5
NMBE 1051965	PEK	34.5	30.2	5.3	78.8	29.8	13.8	4.3	26.7
SMF 35611	PEK	30.7	25.1	4.5	57.8	20.4	11.1	2.1	23.6
NMBE 1051951	JAP	42.4	34.8	4.5	70.3	26.3	12.3	2.7	28.7
ZMB_MAM 7436	JAP	36.6	29.9	4.8	67.3	24.4	12.5	3.0	27.3
NMBE 1051937	PUG	39.4	32.8	6.2	77.6	32.6	15.9	3.7	27.2
NMBE 1052345	PUG	38.2	31.5	4.9	76.9	30.8	14.1	3.0	28.2
SMF 16284	PUG	49.4	44.5	7.9	78.0	26.2	13.5	2.6	25.5
[MfN] 1845	PUG	48.9	43.5	7.7	77.4	28.3	12.9	2.9	25.8
[MfN] 2620	PUG	47.4	42.8	7.4	76.9	29.4	13.7	3.2	26.0
[MfN] 2630	PUG	43.1	37.4	6.9	70.2	25.8	12.4	3.0	24.0
[MfN] 2657	PUG	54.3	48.3	8.0	77.6	23.8	14.3	3.4	25.0
ZMB_MAM 30980	PUG	55.2	49.3	7.1	87.6	31.1	15.0	3.6	28.9
[MfN] 2709	SAL	85.4	75.0	11.2	96.0	31.5	17.9	3.4	36.1
NMBE 1051164	BOR	125.7	108.3	16.1	105.4	39.6	25.3	6.4	49.2
NMBE 1051166	BOR	117.6	101.8	13.5	94.9	33.1	21.5	5.1	37.8
NMBE 1051180	BOR	122.3	104.5	12.3	93.9	34.7	22.2	3.7	42.3
NMBE 1052706	BOR	115.7	99.7	13.6	99.7	33.8	23.3	5.0	37.5
[MfN] 1403	BOR	112.2	99.3	12.1	99.0	32.9	20.2	4.0	38.6
[MfN] 7374	BOR	122.7	106.8	13.1	99.1	31.9	22.0	4.5	40.5

BIF, breadth of incicive foramina; **BOR**, borzoi; **BZB**, bizygomatic breadth; **EW**, Eurasian wolf; **GD**, Groenendael; **GLD**, Greenland dog; **GSD**, German shepherd; **IOB**, interorbital breadth; **JAP**, Japanese chin; **KCS**, King Charles spaniel; **KCSC**, Cavalier King Charles spaniel; **LIF**, length of incisive foramina; **LPI/II**, length of palate I/II; **[MfN]**, alternative labeling of mammal collection at Museum für Naturkunde Berlin, Germany; **MNHN**, Museum national d'Histoire naturelle Paris, France; **NB**, nasal width; **NMBE**, Naturhistorisches Museum der Burgergemeinde Bern, Switzerland; **PEK**, pekingese; **RB**, rostral breadth; **SAL**, saluki; **SMF**, Senckenberg Forschungsinstitut und Naturmuseum Frankfurt am Main, Germany; **ZMB_MAM**, mammal collection of Museum für Naturkunde Berlin, Germany.

Table S1 (continued)

Specimen	Breed	IOB	POC	BC	OH	NHI	NHII	HC	ALB
48.1	GSD	21.5	NA	9.3	39.2	16.7	9.6	2.5	975.3
MNHN 1881-47	PUG	23.1	40.0	9.8	43.2	13.8	8.1	2.4	700.2
SMF 16303	BOR	26.1	40.1	16.1	51.8	33.9	21.4	13.8	2013.2
MNHN 2007-428	PUG	6.7	NA	NA	34.1	NA	NA	3.4	NA
ZMB_MAM 815	EW	42.3	58.6	19.2	75.9	42.9	28.0	6.0	4409.1
ZMB_MAM 93307	EW	39.4	54.1	20.2	68.9	44.4	26.9	2.9	3911.1
ZMB_MAM 93308	EW	43.5	61.2	20.5	65.3	40.0	23.9	2.1	3978.6
MNHN 1985-1274	GSD	42.8	58.6	19.8	64.2	39.0	23.8	4.1	3940.5
SMF 93607	GSD	38.7	57.0	19.2	60.5	36.4	23.4	13.6	3547.5
MNHN 1985-1216	GD	48.7	70.8	20.7	70.4	43.2	NA	10.2	NA
MNHN 1947-78	GLD	42.0	68.4	16.9	70.8	39.7	23.8	13.7	3775.6
NMBE 1051945	KCS	34.2	53.6	11.9	56.6	13.1	9.5	8.4	1087.6
NMBE 1051948	KCS	32.1	47.2	13.8	52.0	14.6	10.3	13.0	1055.0
NMBE 1059207	KCSC	25.8	36.7	11.1	49.8	17.8	13.9	8.1	1289.2
NMBE 1062998	KCSC	27.6	43.7	12.5	51.5	18.7	13.6	5.4	1266.5
NMBE 1051962	PEK	27.5	43.7	11.6	46.6	19.0	10.5	4.5	940.5
NMBE 1051965	PEK	26.7	42.7	13.5	43.6	11.5	9.5	4.0	806.3
SMF 35611	PEK	23.6	41.6	9.4	41.1	10.4	6.4	4.3	594.0
NMBE 1051951	JAP	28.7	45.3	12.9	45.7	13.2	8.3	3.7	998.8
ZMB_MAM 7436	JAP	27.3	45.6	12.2	46.6	11.5	7.8	5.0	816.4
NMBE 1051937	PUG	27.2	NA	11.6	52.1	15.7	9.7	3.9	893.1
NMBE 1052345	PUG	28.2	42.3	12.5	49.3	15.0	8.4	8.5	887.3
SMF 16284	PUG	25.5	41.1	13.2	47.7	16.3	12.0	8.1	1136.2
[MfN] 1845	PUG	25.8	44.4	10.9	49.0	18.1	12.3	10.9	1122.9
[MfN] 2620	PUG	26.0	42.9	11.4	50.8	17.4	12.7	3.6	1110.5
[MfN] 2630	PUG	24.0	42.9	10.7	46.9	15.7	10.2	6.6	895.6
[MfN] 2657	PUG	25.0	39.2	12.7	47.1	18.9	13.2	4.8	1208.3
ZMB_MAM 30980	PUG	28.9	42.3	13.0	49.3	16.5	10.5	6.4	1425.7
[MfN] 2709	SAL	36.1	51.2	14.9	55.3	32.4	19.6	5.7	2708.7
NMBE 1051164	BOR	49.2	67.5	21.7	71.4	47.9	27.8	6.3	5330.3
NMBE 1051166	BOR	37.8	52.9	19.0	63.8	41.2	25.4	5.9	3843.4
NMBE 1051180	BOR	42.3	59.9	15.7	69.2	46.5	27.3	5.4	4418.3
NMBE 1052706	BOR	37.5	54.5	17.0	65.6	44.5	28.7	9.9	3743.3
[MfN] 1403	BOR	38.6	57.1	20.0	60.4	39.1	23.9	10.3	3835.0
[MfN] 7374	BOR	40.5	63.5	20.0	69.7	47.2	28.5	9.5	4327.6

ALB, area of length and breadth of snout; **BC**, breadth of choanae; **BOR**, borzoi; **EW**, Eurasian wolf; **GD**, Groenendael; **GLD**, Greenland dog; **GSD**, German shepherd; HC, height of choanae; **IOB**, interorbital breadth; **JAP**, Japanese chin; **KCS**, King Charles spaniel; **KCSC**, Cavalier King Charles spaniel; **[MfN]**, alternative labeling of mammal collection at Museum für Naturkunde Berlin, Germany; **MNHN**, Museum national d'Histoire naturelle Paris, France; **NHI/II**, nasal height I/II; **NMBE**, Naturhistorisches Museum der Burgergemeinde Bern, Switzerland; **OH**, occipital height; **PEK**, pekingese; **POC**, postorbital constriction; **SAL**, saluki; **SMF**, Senckenberg Forschungsinstitut und Naturmuseum Frankfurt am Main, Germany; **ZMB_MAM**, mammal collection of Museum für Naturkunde Berlin, Germany.

Table S2: Body size (height at withers) and body mass of the studied breeds, adopted from the American Kennel Club (AKC) breed standards. As some individuals (borzoi and pug; see Table 3) originated from the 19th century, the historical data cited in BECKMANN (1894, 1895) for these two breeds is given as well. The Greenland dog is not a registered breed by the AKC, so alternatively the body mass from the Fédération Cynologique Internationale (FCI) is noted, whereas no data about this breed's body size is given at all (NA).

		AKC breed standards		Converted values		Historical values (BECKMANN 1894, 1895)	
Breed	**Sex**	**Height (in)**	**Body mass (lb)**	**Height (cm)**	**Body mass (g)**	**Height (cm)**	**Body mass (g)**
GSD	m	24-26	65-90	61.0-66.0	29,484-40,823	-	-
	f	22-24	50-70	55.9-61.0	22,680-31,751	-	-
GD	m	24-26	55-75	61.0-66.0	24,948-34,019	-	-
	f	22-24	45-60	55.9-61.0	20,412-27,216	-	-
GLD	m	NA	≥60 [FCI]	NA	≥27,216	-	-
	f	NA	≥55 [FCI]	NA	≥24,948	-	-
KCS	m/f	9-10	8-14	22.9-25.4	3,629-6,350	-	-
KCSC	m/f	12-13	13-18	30.5-33.0	5,897-8,165	-	-
PEK	m/f	6-9	≤ 14	15.2-22.9	≤ 6,350	-	-
JAP	m/f	8-11	7-11	20.3-27.9	3,175-4,990	-	-
PUG	m/f	10-13	14-18	25.4-33.0	6,350-8,165	30	[5,750-] 7,750
SAL	m	23-28	40-65	58.4-71.1	18,144-29,484	-	-
	f	-smaller-	40-65	58.4-71.1	18,144-29,484	-	-
BOR	m	≥28	75-105	≥71.1	34,019-47,627	75-80	41*
	f	≥26	60-85	≥66.0	27,216-38,555	-	-
WH	m	19-22	25-40	48.3-55.9	11,340-18,144	-	-
	f	18-21	25-40	45.7-53.3	11,340-18,144	-	-

f, female; **GSD**, German shepherd dog; **GD**, Groenendael; **GLD**, Greenland dog; **KCS**, King Charles spaniel; **KCSC**, Cavalier King Charles spaniel; **PEK**, pekingese; **JAP**, Japanese chin; **m**, male; **SAL**, saluki, **BOR**, borzoi; **WH**, whippet; *original data in BECKMANN (1894: 373): 100 Russian pound; Beckmann, L (1894/1895), *Geschichte und Beschreibung der Rassen des Hundes* I/II. Braunschweig: Druck und Verlag von Friedrich Bieweg und Sohn.

Table S3: Surface area of the maxilloturbinal (AT_{mt}, mm^2) and averaged body mass (lb, adopted from the American Kennel Club breed standards and from BECKMANN 1894/1895, respectively; see Table S2, Supplementary material) in the adult specimens of *Canis lupus familiaris*.

Specimen	**Breed**	**Sex**	**Type (IFB)**	**AT_{mt} (mm^2)**	**Mass (lb)**
NMBE 1051164	BOR	m	DOL	19857	90
[MfN] 1403	BOR	m	DOL	9356	90
MNHN 1985-1274	GSD	f	DOL	9223	60
SMF 93607	GSD	m	DOL	10272	78
NMBE 1051951	JAP	NA	BRA	381	9
NMBE 1051945	KCS	m	BRA	203	12
NMBE 1062998 [R]	KCSC	m	BRA	1730	16
NMBE 1062998 [L]	KCSC	m	BRA	1179	16
NMBE 1051962	PEK	m	BRA	287	13
[MfN] 1845	PUG (ancient type)	NA	BRA	690	15
[MfN] 2620	PUG (ancient type)	NA	BRA	872	15
[MfN] 2657	PUG (ancient type)	f	MES	548	14
ZMB_MAM 30980	PUG (ancient type)	NA	MES	1949	15
NMBE 1051937	PUG (modern type)	m	BRA	469	16.5
NMBE 1052345[R]	PUG (modern type)	m	BRA	283	16.5
NMBE 1052345[L]	PUG (modern type)	m	BRA	179	16.5

BOR, borzoi; **BRA**, brachycephalic; **DOL**, dolichocephalic; **f**, female; **GSD**, German shepherd dog; **IFB**, index facail length to length of braincase; **JAP**, Japanese chin; **KCS**, King charles spaniel; **KCSC**, Cavalier King Charles spaniel; **[L]**, left side; **m**, male; **MES**, mesaticephalic; **[MfN]**, alternative labeling of mammal collection at Museum für Naturkunde Berlin, Germany; **MNHN**, Museum national d'Histoire naturelle Paris, France; **NA**, data not available; **NMBE**, Naturhistorisches Museum der Burger-gemeinde Bern, Switzerland; **PEK**, pekingese; **[R]**, right side; **SMF**, Senckenberg Forschungsinstitut und Naturmuseum Frankfurt, Germany; **ZMB_MAM**, mammal collection of Museum für Naturkunde Berlin, Germany.

Table S4: ANOVA between the two snout length indices (IFB, IBL; ELLENBERGER & BAUM 1891) in *Canis lupus lupus* (n=3) and the adult specimens of *Canis lupus familiaris* (n=27). The plot is illustrated in Figure S2 (Supplementary material).

	se	**df**	**r^2**	**F**	**p**
IBL~IFB	0.05777	28	0.914	309.3	<10^-16
log(IBL)~IFB	0.1021	28	0.8915	239.2	3*10-15
IBL~log(IFB)	0.06138	28	0.903	270.8	6*10-16
log(IBL)~log(IFB)	0.1208	28	0.8482	163.1	3*10-13

IBL= -0.91543*IFB+1.08786.

IBL, index length to breadth of skull; **IFB**, index facial length to length of braincase; **df**, degrees of freedom; **r^2**, adjusted r^2; **se**, standard error; Ellenberger W, Baum H (1891): *Systematische und topographische Anatomie des Hundes*. Berlin, Hamburg: Paul Parey.

Table S5: ANOVA between index turbinal surface area (IAT) and index exterior turbinal surface area (IAE) (both logarithmized) in the specimens of *Canis lupus lupus* and *Canis lupus familiaris* whose turbinal skeleton has been segmented in AMIRA 5.4.0. a and m have been given in the ANOVA and describe a power function as regression line for every specimen with the formula $IAT=a*IAE^{m}$. The associated plots are illustrated in Fig. 5 and Fig. S3 (Supplementary material).

Specimen	**Breed**	**se**	**df**	**r^2**	**F**	**p**	**a**	**m**
ZMB_MAM 93307	EW	0.13440	13	0.9722	490.3	$\sim10^{-11}$	2.5416160	1.22214
SMF 16303	BOR (juv)	0.08807	14	0.9810	777.2	$<10^{-12}$	2.5548180	1.25715
NMBE 1051164	BOR	0.11590	14	0.9744	571.9	$<10^{-12}$	2.8938770	1.27514
[MfN] 1403	BOR	0.10430	12	0.9610	321.7	$<10^{-9}$	2.7814420	1.31181
MNHN 1985-1274	GSD	0.12250	13	0.9617	352.3	$<10^{-10}$	2.4433180	1.24644
SMF 93607	GSD	0.10730	14	0.9808	767.3	$<10^{-12}$	2.6863960	1.24948
NMBE 1051945	KCS	0.09356	11	0.9764	497.1	$<10^{-9}$	1.4662570	1.07280
NMBE 1062998 [R]	KCSC	0.09011	13	0.9801	690.7	$<10^{-11}$	2.0259560	1.14705
NMBE 1062998 [L]	KCSC	0.08371	12	0.9848	846	$<10^{-11}$	2.1653100	1.17067
NMBE 1051962	PEK	0.08247	10	0.9736	406.7	$<10^{-8}$	1.6102750	1.07928
NMBE 1051951	JAP	0.06290	12	0.9872	1000	$<10^{-12}$	1.6074960	1.06884
MNHN 1881-47	PUG (juv)	0.04769	9	0.9833	589.5	$<10^{-8}$	2.1360920	1.19605
NMBE 1051937	PUG	0.07307	10	0.9833	649.3	$<10^{-9}$	1.8659070	1.10817
NMBE 1052345 [R]	PUG	0.08793	10	0.9344	157.7	$<10^{-6}$	1.6497570	1.10084
NMBE 1052345 [L]	PUG	0.08500	10	0.9561	240.4	$<10^{-7}$	1.4153050	1.06211
[MfN] 1845	PUG	0.08396	10	0.9481	201.9	$<10^{-7}$	2.5111920	1.25779
[MfN] 2620	PUG	0.06581	12	0.9894	1211	$<10^{-12}$	2.0159050	1.14600
[MfN] 2657	PUG	0.07304	12	0.9853	871.9	$\sim10^{-12}$	2.0223670	1.14663
ZMB_MAM 30980	PUG	0.05700	11	0.9865	877	$<10^{-11}$	2.5938810	1.30671
-all adult dogs- [n = 16]		0.09655	215	0.9746	8281	$<10^{-16}$	2.1974550	1.18682

ANOVA: $\log(IAT)\sim\log(IAE) \rightarrow$ regression = power function: $IAT \cong a*IAE^{m}$

BOR, borzoi, **df**, degrees of freedom; **EW**, Eurasian wolf; **GSD**, German shepherd; **JAP**, Japanese chin; **juv**, juvenile; **KCS**, King Charles spaniel; **KCSC**, Cavalier King Charles spaniel; **[L]**, left side; **[MfN]**, alternative labeling of mammal collection at Museum für Naturkunde Berlin, Germany; **MNHN**, Museum national d'Histoire naturelle Paris, France; **NMBE**, Naturhistorisches Museum der Burgergemeinde Bern, Switzerland; **PEK**, pekingese; **[R]**, right side; **r^2**, adjusted r^2; **se**, standard error; **SMF**, Senckenberg Forschungsinstitut und Naturmuseum Frankfurt, Germany; **ZMB_MAM**, mammal collection of Museum für Naturkunde Berlin, Germany.

Table S6: ANOVA between percentage turbinal surface area (AT, %; see Table S7, Supplementary material) of the three compartments in the ethmoidal region plus the lamina semicircularis and the two snout length indices (IFB, IBL; ELLENBERGER & BAUM 1891) in 14 adult specimens of *Canis lupus familiaris* (n=16, as in two individuals both sides have been reconstructed in AMIRA 5.4.0).

	IFB		**IBL**	
	r^2	**p**	**r^2**	**p**
Pars maxillonasoturbinalis	0.4792	0.0018	0.5254	0.0009
Lamina semicircularis	0.5406	0.0007	0.4917	0.0015
Pars intermedia	-0.0364	0.5029	0.1414	0.0836
Pars ethmoturbinalis	-0.0272	0.4506	0.1838	0.0551

IBL, index length to breadth of skull; **IFB**, index facial length to length of braincase; **r^2**, adjusted r^2; Ellenberger W, Baum H (1891): *Systematische und topographische Anatomie des Hundes*. Berlin, Hamburg: Paul Parey.

Table S7: Turbinal surface area (AT, %) of the three compartments of the ethmoidal region and the lamina semicircularis in *Canis lupus familiaris* and *Canis lupus lupus*.

			Pars maxillo-nasoturbinalis	**Lamina semicircularis**	**Pars intermedia**	**Pars ethmo-turbinalis**
NMBE 1051962	PEK	BRA	13.0	13.7	38.2	35.1
NMBE 1051945	KCS	BRA	8.1	10.3	41.7	39.9
NMBE 1051951	JAP	BRA	18.1	12.8	35.3	33.8
NMBE 1052345 [L]	PUG	BRA	14.3	11.3	36.7	37.8
NMBE 1052345 [R]	PUG	BRA	17.3	8.6	30.9	43.2
NMBE 1051937	PUG	BRA	18.1	10.7	26.8	44.4
MNHN 1881-47	PUG (juv)	BRA	17.9	9.7	23.9	48.5
[MfN] 1845	PUG	BRA	19.4	8.7	30.5	41.4
[MfN]2620	PUG	BRA	23.6	10.4	26.5	39.5
NMBE 1062998 [L]	KCSC	BRA	19.2	8.0	35.1	37.7
NMBE 1062998 [R]	KCSC	BRA	24.9	8.0	31.6	35.5
[MfN] 2657	PUG	MES	12.8	9.2	37.9	40.1
ZMB_MAM 30980	PUG	MES	23.1	7.0	30.5	39.4
MNHN 1985-1274	GSD	DOL	24.9	5.6	35.3	34.2
SMF 16303	BOR (juv)	DOL	25.5	9.1	25.0	40.4
SMF 93607	GSD	DOL	27.7	5.7	31.4	35.2
NMBE 1051164	BOR	DOL	27.4	6.9	33.6	32.1
[MfN] 1403	BOR	DOL	23.6	8.0	31.4	37.0
ZMB_MAM 93307	EW	outgroup	26.1	4.8	26.6	42.5

BOR, borzoi; **BRA**, brachycephalic; **EW**, Eurasian wolf; **DOL**, dolichocpehalic; **GSD**, German shepherd; **JAP**, Japanese chin; **juv**, juvenile; **KCS**, King Charles spaniel; **KCSC**, Cavalier King Charles spaniel; **[L]**, left side; **MES**, mesaticpehalic; **[MfN]**, alternative labeling of mammal collection at Museum für Naturkunde Berlin, Germany; **MNHN**, Museum national d'Histoire naturelle Paris, France; **NMBE**, Naturhistorisches Museum der Burgergemeinde Bern, Switzerland; **PEK**, pekingese; **[R]**, right side; **SMF**, Senckenberg Forschungsinstitut und Naturmuseum Frankfurt, Germany; **ZMB_MAM**, mammal collection of Museum für Naturkunde Berlin, Germany.

Table S8: ANOVA between turbinal surface area (AT, total and maxilloturbinal only; mm^2) and facial length (IFB; NLII in mm) in 14 adult specimens of *Canis lupus familiaris* (n=16, as in two individuals both sides have been reconstructed in AMIRA 5.4.0).

		se	**df**	**r^2**	**F**	**p**
IFB	**AT_{total}**	10790	14	0.7507	46.16	$8.7*10^{-6}$
	AT_{mt}	3005	14	0.7156	38.74	$2.2*10^{-5}$
NLII	**AT_{total}**	5469	14	0.9359	220.2	$<10^{-9}$
	AT_{mt}	1710	14	0.9079	148.9	$<10^{-8}$

AT, turbinal surface area; **df**, degrees of freedom; **IFB**, index facial length to length of braincase; **mt**, maxilloturbinal; **NLII**, nasal length II; **r^2**, adjusted r^2; **se**, standard error.

Table S9: ANOVA between maxilloturbinal surface area (AT_{mt}, in mm^2) and body mass (lb, adopted from the American Kennel Club breed standards) in 14 adult specimens of *Canis lupus familiaris* (n=16, as in two individuals both sides have been reconstructed in AMIRA 5.4.0). The associated plot is illustrated in Fig. S4 (Supplementary material). The data used for the ANOVA is listed in Table S3 (Supplementary material).

AT_{mt}	**se**	**df**	**r^2**	**F**	**p**
Body mass	2119	14	0.8586	92.05	1.6*10-7

AT_{mt}=176.17*lb-1830.66

df, degrees of freedom; **r^2**, adjusted r^2; **se**, standard error.

Table S10: Turbinal surface density (SDEN=IAT*IAE^{-1}) of the turbinals and the lamina semicircularis in the specimens of *Canis lupus familiaris* and *Canis lupus lupus* which have been segmented in AMIRA 5.4.0, based on the data given in Table 4.

Specimen	**Breed**	**Type [IFB]**	**mt**	**nt**	**ls**	**it**	**itδ**	**it**	**ft1**	**itγ**	**ft2**
NMBE 1051962	PEK	BRA	1.037	1.000	1.126	-	1.000	-	1.423	-	1.726
NMBE 1051945	KCS	BRA	1.211	1.000	0.870	-	1.000	-	1.200	-	1.304
NMBE 1051951	JAP	BRA	1.685	1.162	1.047	-	1.152	-	1.433	1.384	1.716
NMBE 1052345 [L]	PUG	BRA	1.508	1.007	0.841	-	1.000	-	1.375	-	1.458
NMBE 1052345 [R]	PUG	BRA	1.622	1.000	0.905	-	1.000	-	1.295	-	1.698
NMBE 1051937	PUG	BRA	1.608	1.009	1.200	-	1.000	-	1.620	-	1.847
MNHN 1881-47	PUG (juv)	BRA	1.796	1.000	1.279	-	-	-	1.480	-	1.325
[MfN] 1845	PUG	BRA	1.988	1.000	1.087	-	1.028	-	1.858	-	1.863
[MfN] 2620	PUG	BRA	1.948	1.000	1.263	-	1.075	-	1.626	1.000	1.726
NMBE 1062998 [L]	KCSC	BRA	2.021	1.000	1.157	-	1.091	-	1.918	-	1.910
NMBE 1062998 [R]	KCSC	BRA	2.465	1.000	1.262	-	1.123	-	1.852	1.000	1.775
[MfN] 2657	PUG	MES	1.598	1.000	1.229	-	1.070	-	1.865	-	1.838
ZMB_MAM 30980	PUG	MES	2.569	1.000	1.422	-	1.038	-	1.966	1.000	1.819
MNHN 1985-1274	GSD	BRA	4.011	1.011	1.305	-	1.295	-	1.964	1.059	2.167
SMF 16303	BOR (juv)	BRA	3.327	1.038	1.565	-	1.056	-	1.978	1.027	2.049
SMF 93607	GSD	BRA	4.183	1.055	1.492	1.000	1.410	-	2.083	1.016	2.279
NMBE 1051164	BOR	BRA	4.496	1.030	1.903	1.029	1.926	1.006	2.300	1.000	2.468
[MfN] 1403	BOR	BRA	3.529	1.012	1.664	-	1.280	-	2.124	1.000	2.132
ZMB_MAM 93307	EW	out-group	4.005	1.031	1.257	1.000	1.376	-	2.440	1.103	2.347

BOR, borzoi; **BRA**, brachycephalic; **DOL**, dolichocephalic; **et**, ethmoturbinal; **EW**, Eurasian wolf; **ft**, frontoturbinal; **GSD**, German shepherd; **it**, interturbinal; **JAP**, Japanese chin; **juv**, juvenile; **KCS**, King Charles spaniel; **KCSC**, Cavalier King Charles spaniel; **[L]**, left side; ls, lamina semicircularis; MES, mesaticephalic; [MfN] alternative labeling of mammal collection at Museum für Naturkunde Berlin, Germany; **MNHN**, Museum national d'Histoire naturelle Paris, France; **mt**, maxilloturbinal; **NMBE**, Naturhistorisches Museum der Burgergemeinde Bern, Switzerland; **nt**, nasoturbinal; **PEK**, pekingese; **[R]**, right side; **SMF**, Senckenberg Forschungsinstitut und Naturmuseum Frankfurt, Germany; **ZMB_MAM**, mammal collection of Museum für Naturkunde Berlin, Germany.

Table S10 (continued)

it	ft3	it	itβ	it	etI	itα	it	etII	etIII	Total	Breed	Specimen
-	1.622	-	1.499	-	1.441	1.470	-	1.619	1.451	1.861	PEK	NMBE 1051962
-	1.447	-	1.055	1.016	1.901	1.153	-	1.613	1.550	1.813	KCS	NMBE 1051945
-	1.469	-	1.363	-	1.506	1.450	1.000	1.310	1.309	2.079	JAP	NMBE 1051951
-	1.453	-	1.352	-	1.402	1.238	-	1.065	1.021	1.428	PUG	NMBE 1052345 [L]
-	1.543	-	1.459	-	1.552	1.351	-	1.282	1.280	1.756	PUG	NMBE 1052345 [R]
-	1.580	-	1.640	-	1.446	1.779	-	1.565	1.515	1.899	PUG	NMBE 1051937
-	1.269	-	1.196	-	1.790	1.274	-	1.321	1.535	1.932	PUG (juv)	MNHN 1881-47
-	1.681	-	1.398	-	1.913	1.528	-	1.757	1.631	2.619	PUG	[MfN] 1845
-	1.735	-	1.305	1.164	1.903	1.408	-	1.631	1.666	2.298	PUG	[MfN] 2620
-	1.966	-	1.538	-	2.043	1.635	1.018	1.878	1.851	2.698	KCSC	NMBE 1062998 [L]
-	1.875	-	1.717	1.555	1.614	1.587	1.008	1.777	1.739	2.763	KCSC	NMBE 1062998 [R]
-	1.939	1.096	1.630	-	1.956	1.532	1.144	1.695	1.611	1.774	PUG	[MfN] 2657
-	1.837	-	1.543	-	2.028	1.579	-	1.819	1.715	2.870	PUG	ZMB_MAM 30980
-	1.959	1.000	2.066	-	2.429	1.482	1.129	2.008	1.843	3.893	GSD	MNHN 1985-1274
1.038	1.895	-	1.531	1.388	2.347	1.719	1.073	2.292	1.935	3.508	BOR (juv)	SMF 16303
-	2.557	1.043	2.083	-	2.518	1.698	1.022	2.213	1.990	4.143	GSD	SMF 93607
-	2.581	-	2.423	-	2.898	1.758	1.351	2.145	2.177	4.959	BOR	NMBE 1051164
-	2.480	-	1.965	1.206	2.472	1.797	-	2.038	2.226	3.935	BOR	[MfN] 1403
-	2.766	-	2.398	-	2.617	1.785	1.000	2.615	1.939	4.765	EW	ZMB_MAM 93307

BOR, borzoi; **BRA**, brachycephalic; **DOL**, dolichocephalic; **et**, ethmoturbinal; **EW**, Eurasian wolf; **ft**, frontoturbinal; **GSD**, German shepherd; **it**, interturbinal; **JAP**, Japanese chin; **juv**, juvenile; **KCS**, King Charles spaniel; **KCSC**, Cavalier King Charles spaniel; **[L]**, left side; **ls**, lamina semicircularis; **MES**, mesaticephalic; **[MfN]**, alternative labeling of mammal collection at Museum für Naturkunde Berlin, Germany; **MNHN**, Museum national d'Histoire naturelle Paris, France; **mt**, maxilloturbinal; **NMBE**, Naturhistorisches Museum der Burgergemeinde Bern, Switzerland; **nt**, nasoturbinal; **PEK**, pekingese; **[R]**, right side; **SMF**, Senckenberg Forschungsinstitut und Naturmuseum Frankfurt, Germany; **ZMB_MAM**, mammal collection of Museum für Naturkunde Berlin, Germany.

Table S11: Turbinal complexity ($TC=am*(IAT*a^{-1})^{-(1/m)+1}$) of the turbinals and the lamina semicircularis in the specimens of *Canis lupus familiaris* and *Canis lupus lupus* segmented in AMIRA 5.4.0, based on the data given in Table S5 (a, m; Supplementary material) and Table 4 (IAT).

Specimen	**Breed**	**Type [IFB]**	**mt**	**nt**	**ls**	**it**	**itδ**	**it**	**ft1**	**itγ**	**ft2**
NMBE 1051962	PEK	BRA	1.538	1.174	1.546	-	1.286	-	1.510	-	1.563
NMBE 1051945	KCS	BRA	1.367	1.043	1.391	-	1.160	-	1.423	-	1.413
NMBE 1051951	JAP	BRA	1.566	1.289	1.536	-	1.396	-	1.515	1.293	1.524
NMBE 1052345 [L]	PUG	BRA	1.341	1.125	1.327	-	1.207	-	1.325	-	1.332
NMBE 1052345 [R]	PUG	BRA	1.562	1.263	1.478	-	1.296	-	1.486	-	1.504
NMBE 1051937	PUG	BRA	1.827	1.236	1.739	-	1.291	-	1.653	-	1.720
MNHN 1881-47	PUG (juv)	BRA	1.893	1.199	1.728	-	-	-	1.670	-	1.686
[MfN] 1845	PUG	BRA	2.367	1.393	2.040	-	1.414	-	2.051	-	2.051
[MfN] 2620	PUG	BRA	2.049	1.467	1.863	-	1.376	-	1.786	1.080	1.819
NMBE 1062998 [L]	KCSC	BRA	2.241	1.420	1.984	-	1.460	-	2.082	-	2.136
NMBE 1062998 [R]	KCSC	BRA	2.209	1.463	1.918	-	1.482	-	1.964	1.532	1.985
[MfN] 2657	PUG	MES	1.915	1.543	1.878	-	1.339	-	1.876	-	1.989
ZMB_MAM 30980	PUG	MES	2.916	1.509	2.233	-	1.220	-	2.341	1.368	2.445
MNHN 1985-1274	GSD	DOL	3.020	1.569	2.261	-	1.611	-	2.582	1.954	2.592
SMF 16303	BOR (juv)	DOL	3.096	1.734	2.539	-	1.334	-	2.453	1.668	2.475
SMF 93607	GSD	DOL	3.407	1.796	2.500	1.008	1.914	-	2.724	1.561	2.843
NMBE 1051164	BOR	DOL	3.897	1.921	2.922	1.366	2.174	1.076	3.340	1.730	3.191
[MfN] 1403	BOR	DOL	3.537	1.763	2.768	-	1.859	-	2.918	1.555	2.969
ZMB_MAM 93307	EW	out-group	3.321	1.803	2.457	0.942	1.680	-	2.649	1.627	2.748

BOR, borzoi; **BRA**, brachycephalic; **DOL**, dolichocephalic; **et**, ethmoturbinal; **EW**, Eurasian wolf; **ft**, frontoturbinal; **GSD**, German shepherd; **it**, interturbinal; **JAP**, Japanese chin; **juv**, juvenile; **KCS**, King Charles spaniel; **KCSC**, Cavalier King Charles spaniel; **[L]**, left side; **ls**, lamina semicircularis; **MES**, mesaticephalic; **[MfN]** alternative labeling of mammal collection at Museum für Naturkunde Berlin, Germany; **MNHN**, Museum national d'Histoire naturelle Paris, France; **mt**, maxilloturbinal; **NMBE**, Naturhistorisches Museum der Burgergemeinde Bern, Switzerland; **nt**, nasoturbinal; **PEK**, pekingese; **[R]**, right side; **SMF**, Senckenberg Forschungsinstitut und Naturmuseum Frankfurt, Germany; **ZMB_MAM**, mammal collection of Museum für Naturkunde Berlin, Germany.

Table S11 (continued)

it	ft3	it	itβ	it	etI	itα	it	etII	etIII	Total	Breed	Specimen
-	1.478	-	1.409	-	1.540	1.438	-	1.521	1.458	1.790	PEK	NMBE 1051962
-	1.385	-	1.243	1.248	1.458	1.330	-	1.389	1.304	1.623	KCS	NMBE 1051945
-	1.475	-	1.403	-	1.555	1.423	1.186	1.498	1.455	1.754	JAP	NMBE 1051951
-	1.295	-	1.249	-	1.372	1.262	-	1.307	1.255	1.507	PUG	NMBE 1052345 [L]
-	1.428	-	1.356	-	1.607	1.404	-	1.514	1.418	1.850	PUG	NMBE 1052345 [R]
-	1.647	-	1.586	-	1.885	1.640	-	1.733	1.563	2.163	PUG	NMBE 1051937
-	1.538	-	1.427	-	2.002	1.606	-	1.788	1.625	2.534	PUG (juv)	MNHN 1881-47
-	1.961	-	1.730	-	2.386	1.807	-	2.185	1.857	3.362	PUG	[MfN] 1845
-	1.748	-	1.554	1.227	1.997	1.611	-	1.894	1.748	2.485	PUG	[MfN] 2620
-	1.925	-	1.751	-	2.212	1.859	1.011	2.050	1.894	2.872	KCSC	NMBE 1062998 [L]
-	1.775	-	1.691	1.592	2.120	1.772	1.039	1.941	1.809	2.653	KCSC	NMBE 1062998 [R]
-	1.872	1.140	1.708	-	2.057	1.725	1.318	1.907	1.758	2.425	PUG	[MfN] 2657
-	2.184	-	1.958	-	2.736	2.035	-	2.502	2.224	4.172	PUG	ZMB_MAM 30980
-	2.284	1.044	2.093	-	2.793	2.048	1.427	2.461	2.263	4.004	GSD	MNHN 1985-1274
1.098	2.126	-	1.787	1.864	2.928	2.111	1.324	2.641	2.404	4.143	BOR (juv)	SMF 16303
-	2.543	1.258	2.283	-	3.022	2.355	1.279	2.820	2.522	4.438	GSD	SMF 93607
-	2.704	-	2.396	-	3.474	2.497	1.658	2.972	2.747	5.195	BOR	NMBE 1051164
-	2.532	-	2.135	1.367	3.379	2.337	-	2.870	2.522	5.049	BOR	[MfN] 1403
-	2.551	-	2.314	-	3.171	2.447	1.524	2.885	2.588	4.267	EW	ZMB_MAM 93307

BOR, borzoi; **BRA**, brachycephalic; **DOL**, dolichocephalic; **et**, ethmoturbinal; **EW**, Eurasian wolf; **ft**, frontoturbinal; **GSD**, German shepherd; **it**, interturbinal; **JAP**, Japanese chin; **juv**, juvenile; **KCS**, King Charles spaniel; **KCSC**, Cavalier King Charles spaniel; **[L]**, left side; **ls**, lamina semicircularis; **MES**, mesaticephalic; **[MfN]** alternative labeling of mammal collection at Museum für Naturkunde Berlin, Germany; **MNHN**, Museum national d'Histoire naturelle Paris, France; **mt**, maxilloturbinal; **NMBE**, Naturhistorisches Museum der Burgergemeinde Bern, Switzerland; **nt**, nasoturbinal; **PEK**, pekingese; **[R]**, right side; **SMF**, Senckenberg Forschungsinstitut und Naturmuseum Frankfurt, Germany; **ZMB_MAM**, mammal collection of Museum für Naturkunde Berlin, Germany.

Table S12: ANOVA between the morphometric parameters (IAT, SDEN, and TC) of the turbinals plus the lamina semicircularis and the two snout length indices (IFB, IBL; ELLENBERGER & BAUM 1891) in 14 adult specimens of *Canis lupus familiaris* (n=16, as in two individuals both sides have been reconstructed in AMIRA 5.4.0). The detailed p-values for the single turbinals and the lamina semicircularis are listed in Table S13 (Supplementary material).

		se	**df**	**r^2**	**F**	**p**
IAT	**IFB**	0.4613	215	0.1960	53.65	$<10^{-11}$
	IBL	0.4614	215	0.1957	53.56	$<10^{-11}$
SDEN	**IFB**	0.5032	215	0.1596	42.01	$<10^{-9}$
	IBL	0.5015	215	0.1650	43.69	$<10^{-9}$
TC	**IFB**	0.4358	215	0.4062	148.7	0
	IBL	0.4370	215	0.4031	146.8	0

df, degrees of freedom; **IAT**, standardized turbinal surface area; **IBL**, index breadth to length of skull; **IFB**, index facial length to length of braincase; **r^2**, adjusted r^2; **SDEN**, surface density; **se**, standard error; **TC**, turbinal complexity; Ellenberger W, Baum H (1891): *Systematische und topographische Anatomie des Hundes*. Berlin, Hamburg: Paul Parey.

Table S13: ANOVA of the single turbinals plus the lamina semicircularis between the morphometric parameters (IAT, SDEN, TC) and the two snout length indices (IFB, IBL; ELLENBERGER & BAUM 1891) in 14 adult specimens of *Canis lupus familiaris* (n=16, as in two individuals both sides have been reconstructed in AMIRA 5.4.0). The data of the summarized turbinal skeleton is given in Table S12 (Supplementary material).

	IAT		**SDEN**		**TC**	
	IFB	IBL	IFB	IBL	IFB	IBL
mt	$<10^{-6}$	$<10^{-6}$	$<10^{-6}$	$<10^{-6}$	$<10^{-7}$	$<10^{-7}$
nt	$<10^{-9}$	$<10^{-7}$	0.9594	0.822	$<10^{-7}$	$<10^{-7}$
ls	$<10^{-5}$	$<10^{-6}$	$<10^{-5}$	$<10^{-5}$	$<10^{-7}$	$<10^{-7}$
itδ	$<10^{-4}$	$<10^{-5}$	$<10^{-3}$	$<10^{-4}$	$<10^{-4}$	$<10^{-6}$
ft1	$<10^{-5}$	$<10^{-6}$	$<10^{-5}$	$<10^{-5}$	$<10^{-7}$	$<10^{-8}$
ft2	$<10^{-7}$	$<10^{-7}$	$<10^{-4}$	$<10^{-5}$	$<10^{-8}$	$<10^{-7}$
ft3	$<10^{-8}$	$<10^{-7}$	$<10^{-6}$	$<10^{-6}$	$<10^{-7}$	$<10^{-7}$
itβ	$<10^{-6}$	$<10^{-6}$	$<10^{-4}$	$<10^{-5}$	$<10^{-7}$	$<10^{-7}$
etI	$<10^{-8}$	$<10^{-8}$	$<10^{-5}$	$<10^{-6}$	$<10^{-7}$	$<10^{-7}$
itα	$<10^{-7}$	$<10^{-6}$	0.0055	0.0067	$<10^{-7}$	$<10^{-6}$
etII	$<10^{-8}$	$<10^{-6}$	$<10^{-3}$	$<10^{-3}$	$<10^{-7}$	$<10^{-6}$
etIII	$<10^{-8}$	$<10^{-7}$	$<10^{-4}$	$<10^{-4}$	$<10^{-7}$	$<10^{-7}$
Total	$<10^{-7}$	$<10^{-8}$	$<10^{-5}$	$<10^{-6}$	$<10^{-6}$	$<10^{-6}$

et, ethmoturbinal; **ft**, frontoturbinal; **IAT**, index turbinal surface area; **IBL**, index length to breadth of skull; **IFB**, index facial length to length of braincase; **it**, interturbinal; **ls**, lamina semicircularis; **mt**, maxilloturbinal; **nt**, nasoturbinal; **SDEN**, surface density; **TC**, turbinal complexity; Ellenberger W, Baum H (1891): *Systematische und topographische Anatomie des Hundes*. Berlin, Hamburg: Paul Parey.

Table S14: TukeyHSD test between the morphometric parameters (IAT, SDEN, TC) and the three snout length types (BRA, MES, DOL) in 14 adult specimens of *Canis lupus familiaris* (n=16, as in two individuals both sides have been reconstructed in AMIRA 5.4.0). The associated boxplot is illustrated in Fig. 54.

		BRA	MES	DOL
IAT	BRA		**0.29672** [IFB]	**<10^{-5}** [IFB]
	MES	**0.17379** [IBL]		**0.00284** [IFB]
	DOL	**<10^{-5}** [IBL]	**<10^{-5}** [IBL]	
SDEN	BRA		**0.34414** [IFB]	**<10^{-5}** [IFB]
	MES	**0.02587** [IBL]		**0.01853** [IFB]
	DOL	**<10^{-5}** [IBL]	**0.00002** [IBL]	
TC	BRA		**0.00198** [IFB]	**<10^{-5}** [IFB]
	MES	**<10^{-5}** [IBL]		**0.00031** [IFB]
	DOL	**<10^{-5}** [IBL]	**<10^{-5}** [IBL]	

BRA, brachycephalic; **DOL**, dolichocephalic; **IAT**, index turbinal surface area; **IBL**, index breadth to length of skull; **IFB**, index facial length to length of braincase; **MES**, mesaticephalic; **SDEN**, surface density; **TC**, turbinal complexity.

SUPPLEMENTARY MATERIAL – FIGURES

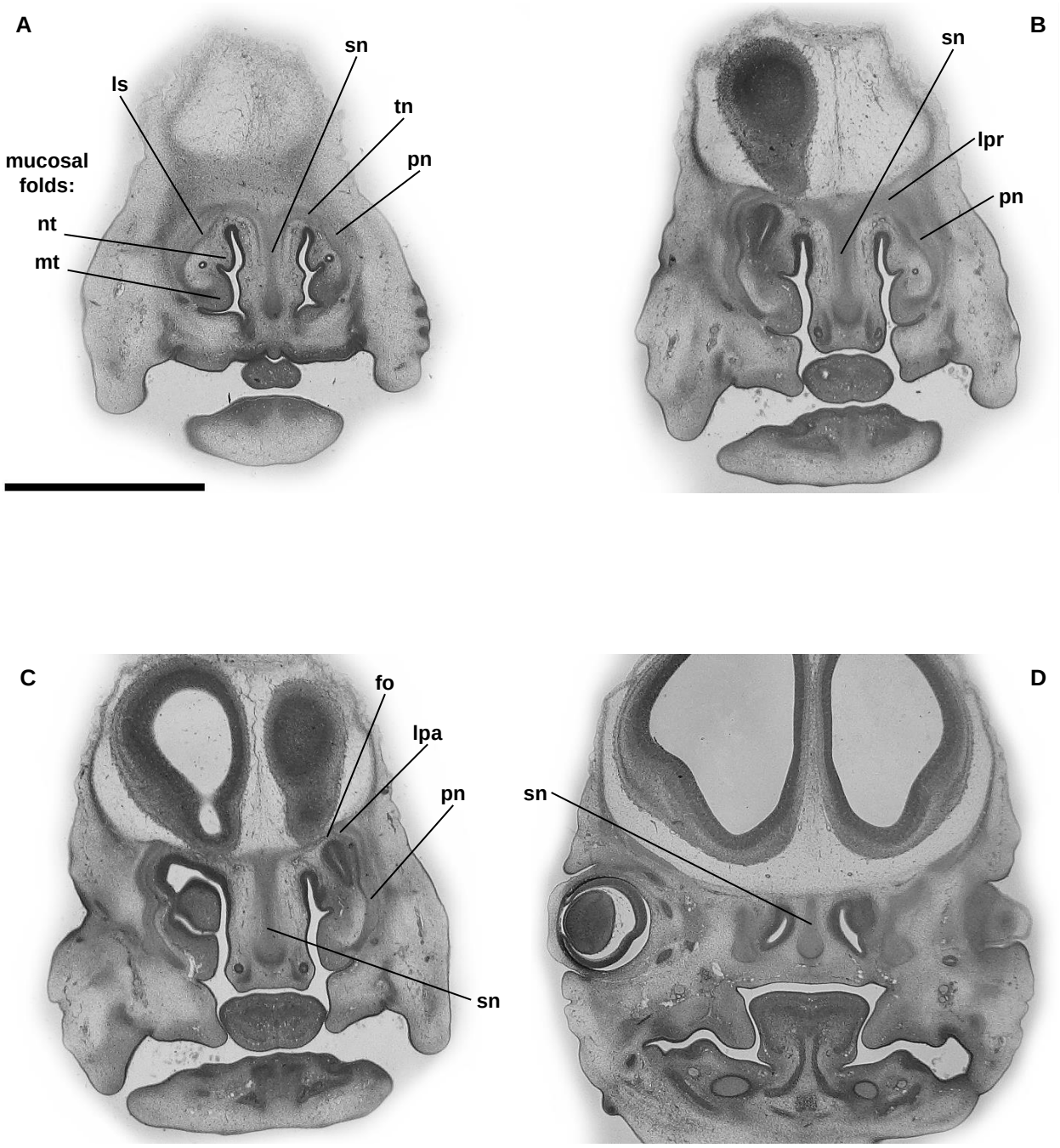

Fig. S1: Histological serial sections of the ethmoidal region of the prenatal 'whippet A' (*Canis lupus* familiaris; SCHLIEMANN 1966) from roastral to caudal in coronal view. In this fetal stage the tripartite character of the nasal capsule has developed, but no turbinals are present yet. **A)** pars maxillonasiturbinalis, the maxilloturbinal and the nasoturbinal are visible as mucosal folds and the lamina semicircularis is starting to separate from the nasal side wall; **B, C)** pars ethmoturbialis and pars intermedia; **D)** pars ethmoturbinalis. Scale bar: 2mm. **fo**, fenestra olfactoria; **lpa**, limbus paracribrosus; **lpr**, imbus praecribrosus; **ls**, lamina semicircularis; **mt**, maxilloturbinal; **nt**, nasoturbinal; **pn**, paries nasi; **sn**, septum nasi; **tn**, tectum nasi.

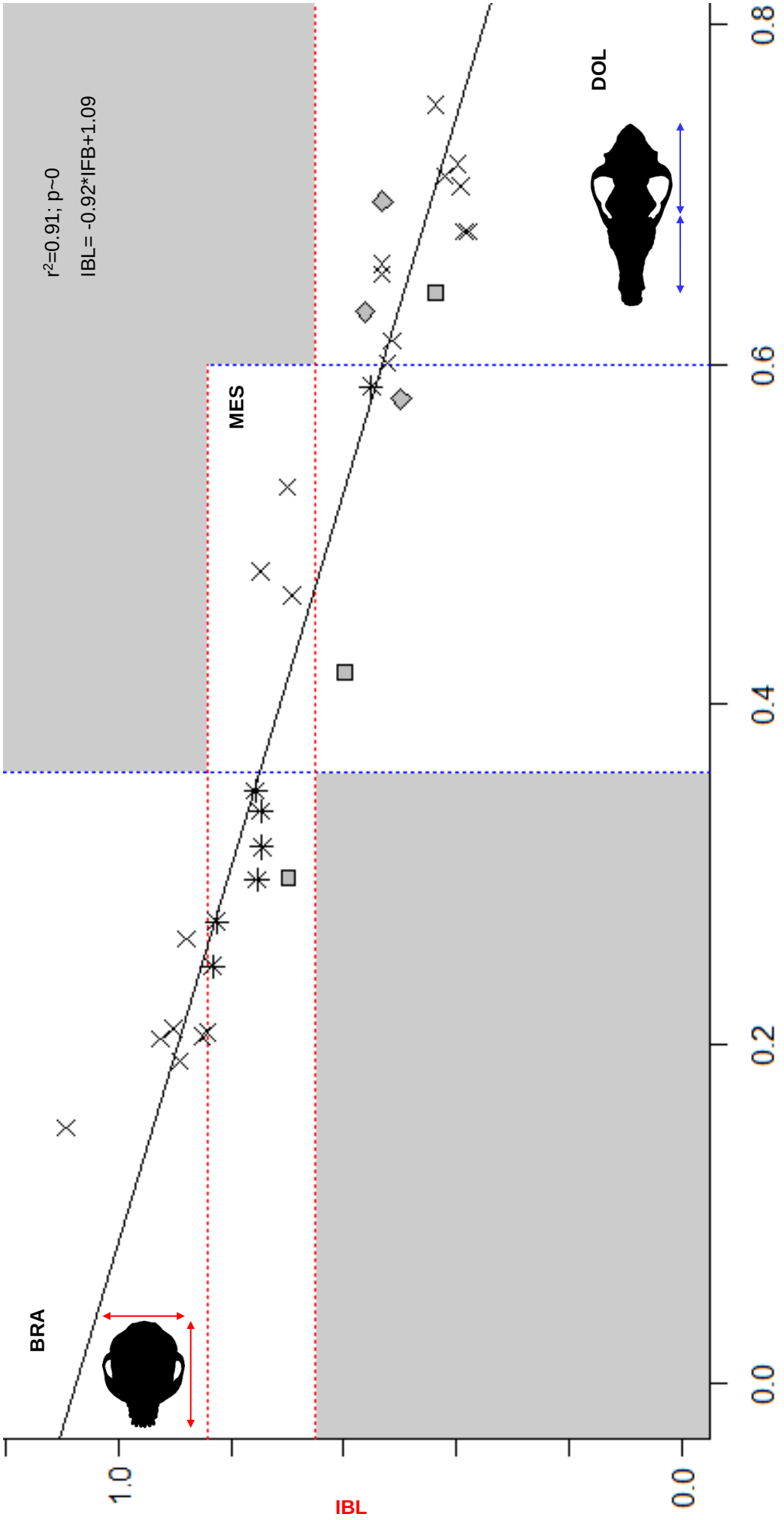

Fig. S2: Grouping of all specimens of *Canis lupus lupus* (◇, n=3) and *Canis lupus familiaris* (n=30) into the two snout length indices index facial length to length of braincase (IFB) and index length to breadth of skull (IBL) (ELLENBERGER & BAUM 1891). The adult dog specimens are either homogeneously (✕, n=20) or heterogeneously (✳, n=7) grouped; the separately plotted juveniles (□, n=3) are not included into the ANOVA and the resulting abline (see Table S4, Supplementary material). The values of IFB and IBL are listed in Table 1. **BRA**, brachycephalic; **DOL**, dolichocephalic; **MES**, mesaticephalic, $\mathbf{r^2}$, adjusted r^2.

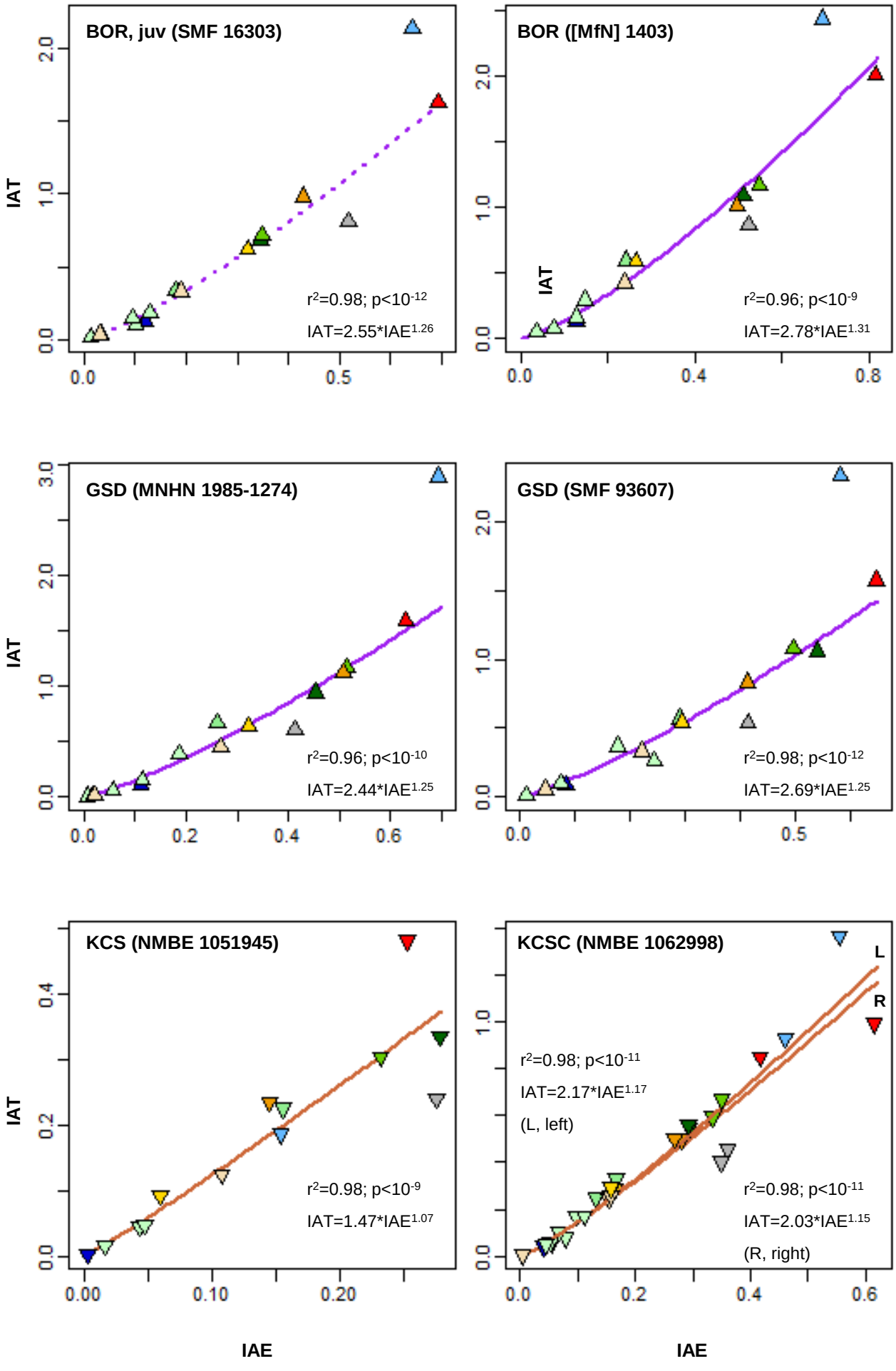

Fig. S3 (description: page after next)

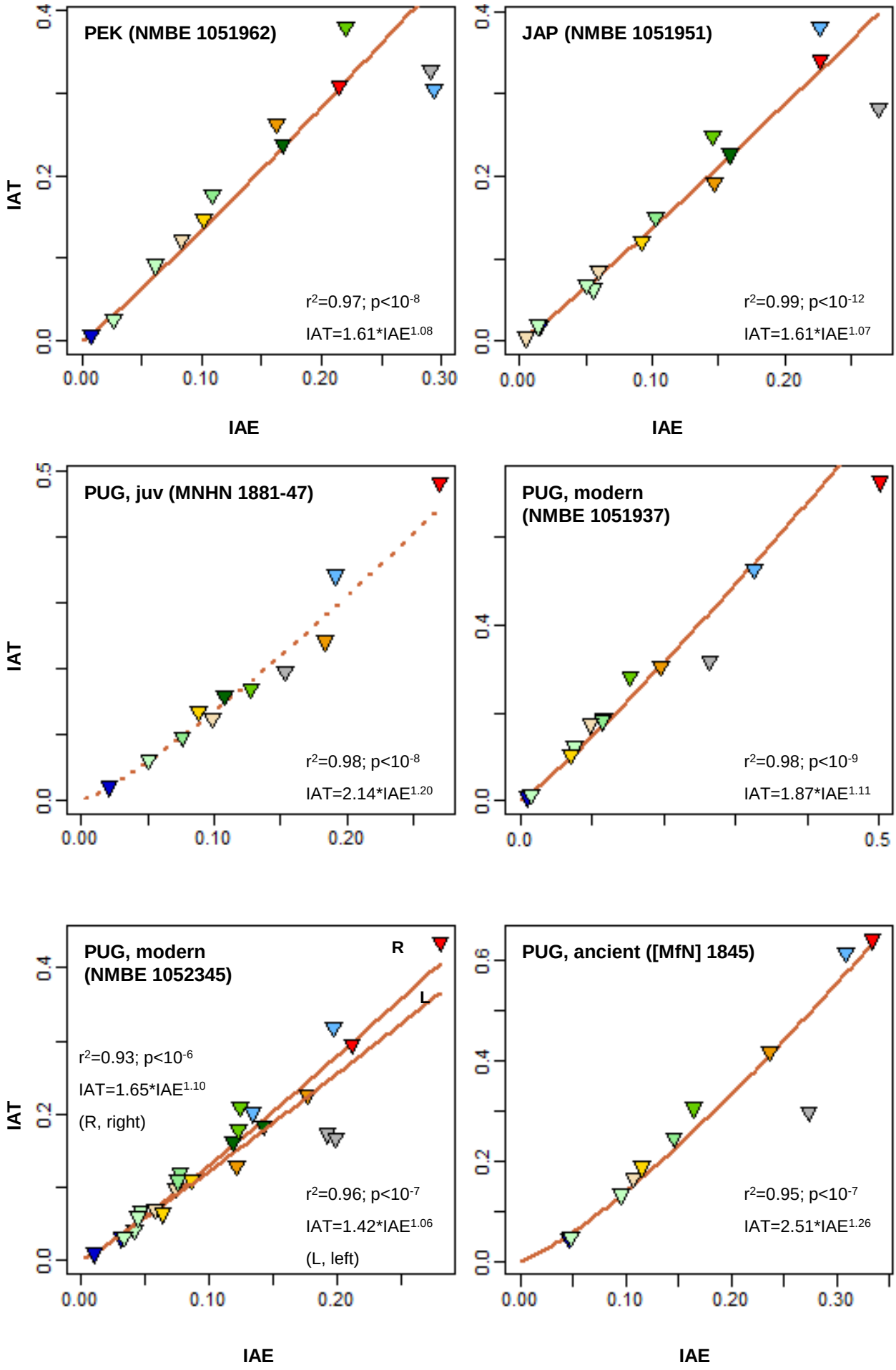

Fig. S3 (description: next page)

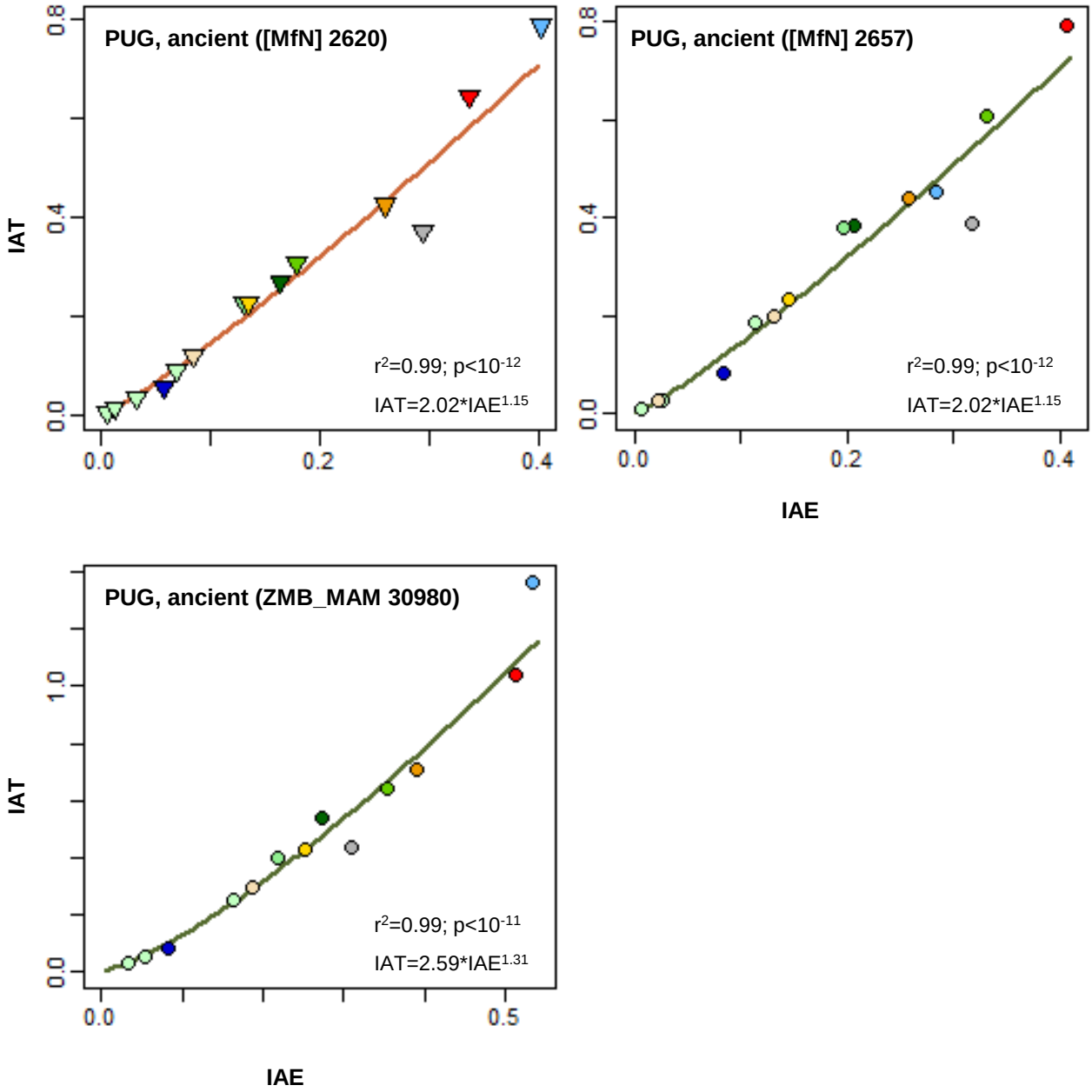

Fig. S3: Correlation between index turbinal surface area (IAT) and index exterior surface area (IAE) between the turbinals plus the lamina semicircularis in the single specimens of *Canis lupus familiaris*. The positive correlation describes a power function given in the plot, as far as the adjusted r^2- and the p-value resulting from the ANOVA in R 3.3.0. The detailed values are listed in Table S5 (Supplementary material). The colors of the ablines refer to their summarized illustration in Fig. 46. The plots of three further specimens (Eurasian wolf, borzoi, pekingese) are separately illustrated in Fig. 5. Colors of the points refer to the turbinal color code. **BOR**, borzoi; **GSD**, German shepherd; **JAP**, Japanaese chin; **juv**, juvenile; **KCS**, King Charles spaniel; **KCSC**, CavalierKing Charles Spaniel; **[MfN]**, alternative labelling of mammal collection at Museum für Naturkunde Berlin, Germany; **MNHN** Muséum national d'Histoire naturelle Paris, France; **NMBE**, Naturhistorisches Museum der Burgergemeinde Bern, Switzerland; **PEK**, pekingese; **SMF**, Senckenberg Forschungsinstitut und Naturmuseum Frankfurt, Germany; **ZMB_MAM**, mammal collection of Museum für Naturkunde Berlin, Germany.

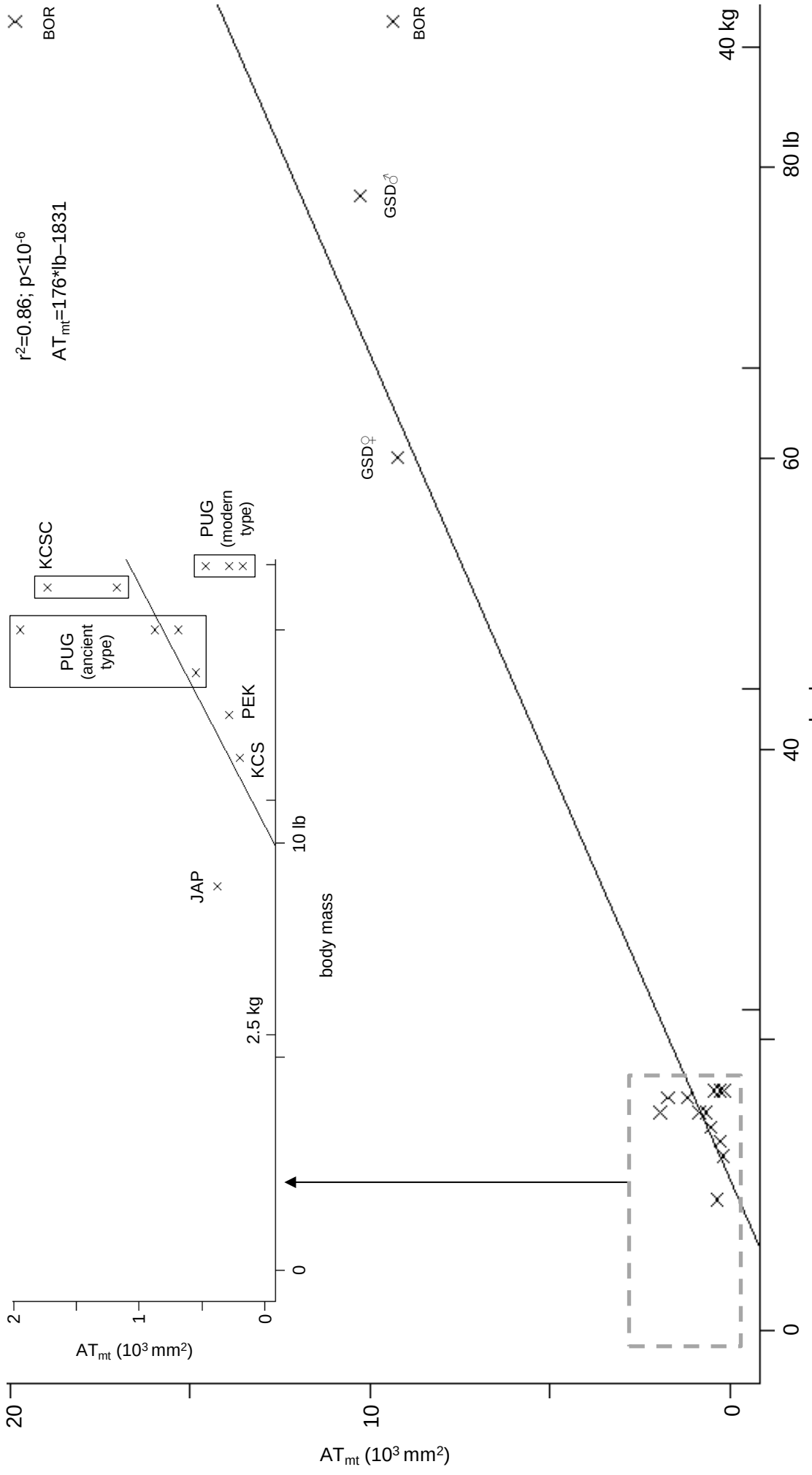

Fig. S4: Correlation between the surface area of the maxilloturbinal (AT_{mt}, mm^2) and body mass (lb/kg) in 14 segmented adult specimens of *Canis lupus familiaris*. The body mass (original data in lb) was adopted from the American Kennel Club (Table S2 and S3; Supplementary material). The values of the ANOVA are listed in Table S9 (Supplementary material). **BOR**, borzoi; **GSD**, German shepherd; **JAP**, Japanese chin; **KCS**, King Charles spaniel; **KCSC**, Cavalier King Charles spaniel; **PEK**, pekingese; $\mathbf{r^2}$, adjusted r^2.

ELECTRONIC SUPPLEMENTARY MATERIAL – TABLES

Table eS1: Raw data of the linear measurements (in mm) on the skulls of *Canis lupus lupus* and *Canis lupus familiaris* which have been chosen for the present study. For the definitions of the measurements see Table 2 and the illustrations in Fig. 3. Some measurements could not be taken e.g., because the structure is broken (NA). The measurements were taken three times; the mean is given in Table S1 (Supplementary material). The left and the right incisive foramen were measured separately in length and breadth (LIFl/LIFr, BIFl/BIFr) and then both sides were averaged (LIF, BIF, see Table S1, Supplementary material). Additionally, the standard deviation is given.

Table eS2: Raw data of the turbinal surface area (AT, mm^2) and the exterior turbinal surface area (AE, mm^2) of the single turbinals and the lamina semicircularis measured in AMIRA 5.4.0 in the virtually reconstructed specimens of *Canis lupus lupus* and *Canis lupus familiaris*. '-' refers to turbinals which are absent in a specimen.

ELECTRONIC SUPPLEMENTARY MATERIAL – FIGURES

Histological serial sections of the ethmoidal region of the three prenatal whippets and the neonate whippet which are housed at the Centrum für Naturkunde, Universität Hamburg, Germany. The slides have been studied and photographed at the institute with the KEYENCE VHX-5000 digital microscope. All four specimens are sectioned coronally and in rostral to caudal view. As a morphological description does not require the complete series, selected slices have been photographed. For further information about the material see Table 3. Scale bars: 2000µ.

File name	# slices	Labeling of selected sections
Whippet-A__CeNat_HH	18	Fig. S1 (Supplementary material)
Whippet-B__CeNat_HH	65	Fig. 6
Whippet-C__CeNat_HH	172	Fig. 6
Whippet-neonatus-I__ CeNat_HH	242	Fig. 7

µCT cross sections and virtual 3D models of the specimens of *Canis lupus lupus* and *Canis lupus familiaris* which have been segmented in AMIRA 5.4.0 and AVIZO 9.0.1. On the selected µCT cross sections the turbinals are highlighted. The sections proceed from rostral to caudal, but in contrast to the text-figures, the sections are all in caudal view. The virtual 3D models are not mirrored either. They show the turbinal skeleton within the transparent nasal cavity in lateral, medial, and dorsal view. Scale bars: 10mm.

File name	#sections	reconstructed side	Labeling of selected sections
Canis-lupus-familiaris_Borzoi_-MfN-1403	25	left	Fig. 40
Canis-lupus-familiaris_Borzoi_NMBE1051164	28	left, right	Fig. 36
Canis-lupus-familiaris_Borzoi_SMF16303	24	left	Fig. 10
Canis-lupus-familiaris_Cavalier_NMBE1062998	28	left, right	Fig. 22
Canis-lupus-familiaris_Chin_NMBE1051951	24	left	Fig. 27
Canis-lupus-familiaris_GermanShepherd_48-1	43	left	Fig. 8
Canis-lupus-familiaris_GermanShepherd_MNHN1985-1274	28	right	Fig. 15
Canis-lupus-familiaris_GermanShepherd_SMF93607	27	right	Fig. 16
Canis-lupus-familiaris_KingSpaniel_NMBE1051945	21	left	Fig. 19
Canis-lupus-familiaris_Pekingese_NMBE1051962	14	right	Fig. 23
Canis-lupus-familiaris_Pekingese_SMF35611	31	left, right	Fig. 24
Canis-lupus-familiaris_Pug_-MfN-1845	24	right	Fig. 31
Canis-lupus-familiaris_Pug_-MfN-2620	23	left	Fig. 32
Canis-lupus-familiaris_Pug_-MfN-2630	22	left, right	Fig. 33
Canis-lupus-familiaris_Pug_-MfN-2657	24	right	Fig. 34
Canis-lupus-familiaris_Pug_MNHN1881-47	20	left	Fig. 9
Canis-lupus-familiaris_Pug_NMBE1051937	20	right	Fig. 28
Canis-lupus-familiaris_Pug_NMBE1052345	17	left, right	Fig. 29
Canis-lupus-familiaris_Pug_SMF16284	53	right	Fig. 30
Canis-lupus-familiaris_Pug_ZMB_MAM30980	21	right	Fig. 35
Canis-lupus-lupus_ZMB_MAM93307	24	right	Fig. 13